GEOTECHNOLOGIES AND THE ENVIRONMENT

Pamela S. Showalter · Yongmei Lu (Eds.)

Geospatial Techniques in Urban Hazard and Disaster Analysis

Geotechnologies and the Environment

Volume 2

Series Editors:

Jay D. Gatrell, *School of Graduate Studies and Department of Geography, Geology, and Anthropology, Indiana State University, Terre Haute, IN, USA*

Ryan R. Jensen, *Department of Geography, Brigham Young University, Provo, UT, USA*

The "Geotechnologies and the Environment" series is intended to provide specialists in the geotechnologies and academics who utilize these technologies, with an opportunity to share novel approaches, present interesting (sometimes counter-intuitive) case studies, and most importantly to situate GIS, remote sensing, GPS, the internet, new technologies, and methodological advances in a real world context. In doing so, the books in the series will be inherently applied and reflect the rich variety of research performed by geographers and allied professionals.

Beyond the applied nature of many of the papers and individual contributions, the series interrogates the dynamic relationship between nature and society. For this reason, many contributors focus on human-environment interactions. The series are not limited to an interpretation of the environment as nature per se. Rather, the series "places" people and social forces in context and thus explore the many socio-spatial environments humans construct for themselves as they settle the landscape. Consequently, contributions will use geotechnologies to examine both urban and rural landscapes.

For further volumes:
http://www.springer.com/series/8088

Pamela S. Showalter · Yongmei Lu
Editors

Geospatial Techniques in Urban Hazard and Disaster Analysis

Springer

Editors
Dr. Pamela S. Showalter
Texas State University
Department of Geography
San Marcos TX 78666-4616
USA
ps15@txstate.edu

Dr. Yongmei Lu
Texas State University
Department of Geography
San Marcos TX 78666-4616
USA
yl10@txstate.edu

ISBN 978-90-481-2237-0 e-ISBN 978-90-481-2238-7
DOI 10.1007/978-90-481-2238-7
Springer Dordrecht Heidelberg London New York

Library of Congress Control Number: 200992683

Cover image: Diamondhead Debris Sites-Post-Kalrina Imagery and Parcels, photo courtesy of Federal Emergency Management Agency, USA.

Printed on acid-free paper

Springer is part of Springer Science+Business Media (www.springer.com)

Preface

This book is the second in a series that examines how geographic information technologies (GIT) are being implemented to improve our understanding of a variety of hazard and disaster situations. The main types of technologies covered under the umbrella of GIT, as used in this volume, are geographic information systems, remote sensing (not including ground-penetrating or underwater systems), and global positioning systems. Our focus is on urban areas, broadly defined in order to encompass rapidly growing and densely populated areas that may not be considered "urban" in the conventional sense.

The material presented here is also unabashedly applied – our goal is to provide GIT tools to those seeking more efficient ways to respond to, recover from, mitigate, prevent, and/or model hazard and disaster events in urban settings. Therefore, this book was created not only with our colleagues in the academic world in mind, but also for hazards professionals and practitioners. We also believe graduate students will find the material presented here of interest, as may upper division undergraduate students.

Pamela S. Showalter
San Marcos, Texas Yongmei Lu

Acknowledgments

We are very grateful for the support of our colleagues, friends, and family members during the many months spent laboring on this book. Special thanks go to the following individuals (listed alphabetically), whose thoughtful suggestions vastly improved the effort presented here: Stephen D. Ambrose, Applied Sciences Program, NASA Headquarters; Lindsey Barnes, University of Colorado-Colorado Springs; Sally Caldwell, Texas State University-San Marcos; Richard Campanella, Tulane University; Xuwei Chen, Northern Illinois University; Thomas Cova, University of Utah; Ellen K. Cromley, The Institute for Community Research; Timothy J. Dolney, The Pennsylvania State University–Altoona College; David L. Eslinger, NOAA Coastal Services Center; Andrew Graettinger, University of Alabama; Ron Hagelman, Texas State University-San Marcos; Alisa Holloway, University of Cape Town; Mark W. Horner, Florida State University; Bo Huang, The Chinese University of Hong Kong; Chris J. Johannsen, Purdue University; Norman Kerle, International Institute for Geoinformation Science and Earth Observation (ITC), Enschede, the Netherlands; Michael Kevany, PlanGraphics, Inc.; Poh-Chin Lai, The University of Hong Kong; Jonathan Li, University of Waterloo, Canada; Ge Lin, University of Nebraska Medical Center; Susan Macey, Texas State University-San Marcos; Jeremy Mennis, Temple University; Robert J. Nicholls, University of Southampton; John Pine, Louisiana State University; Kathleen L. Purvis-Roberts, Claremont McKenna, Pitzer, and Scripps Colleges; Lynn M. Resler, Virginia Polytechnic Institute and State University (Virginia Tech); Jose L. Silván-Cárdenas, Texas State University-San Marcos; Susan I. Stewart, Northern Research Station, U.S. Forest Service; Jeannette Sutton, University of Colorado at Boulder; Lisa A. Taylor, NOAA National Geophysical Data Center; Jean-Claude Thill, University of North Carolina at Charlotte; Deborah S.K. Thomas, University of Colorado-Denver; Stefan Voigt, German Aerospace Center (DLR); William A. Wallace, Rensselaer Polytechnic Institute; Thomas J. Wilbanks, Oak Ridge National Laboratory; Olga Wilhelmi, National Center for Atmospheric Research (NCAR); F. Benjamin Zhan, Texas State University-San Marcos; and Sisi Zlatanova, Delft University of Technology, Delft, The Netherlands. Two additions to the above list are also the individuals responsible for instigating the entire enterprise: Jay D. Gatrell (Indiana State University) and Ryan R. Jensen (Brigham Young University) – thank you for encouraging us to take part in this venture.

We also wish to express our gratitude to the guidance of our sincere friends at Springer-Verlag. Special thanks go to Nina Bennink, Earth Sciences Publishing Assistant, and Robert K. Doe, Earth Sciences Publishing Editor, whose help and patience allowed us the time necessary to navigate the nuances of producing this book.

We are especially indebted to our loved ones. Pamela S. Showalter's deepest thanks go to her partner, Raylene, whose boundless support was offered from the moment the project was tackled. Yongmei Lu is in debt to her dearest husband, Shuwei, and her most lovely angels, Katie and Jeffrey, for their endless support and understanding during and beyond this book project. Both editors also wish to express their appreciation to Texas State University–San Marcos. Dr. Lu particularly appreciates the faculty development leave provided by Texas State University as well as the Visiting Professorship provided by Beijing Normal University, both of which greatly supported the second stage of her work on this project.

Finally, we acknowledge that no book is without its shortcomings – while we have attempted to keep errors of commission and omission to a minimum, we accept full responsibility for those that eluded us.

Contents

Contributors

Beverley J. Adams ImageCat Ltd., Communications House, Surrey, KT21 2BT, United Kingdom, bja@imagecatinc.com

Joshua S. Belhadj School of Planning, University of Cincinnati, Cincinnati, OH 45221-0016, USA, jsbelhadj@hotmail.com

Jean Pierre Bizimana Department of Geography, Faculty of Sciences, National University of Rwanda, Rwanda, Africa, bizijp@yahoo.fr

Molly E. Brown NASA Goddard Space Flight Center, Greenbelt, MD, USA, molly.brown@nasa.gov

Alexander Buyantuyev Sino-US Center for Conservation, Energy and Sustainability Science (SUCCESS), Inner Mongolia University, Inner Mongolia 010021, P.R. China, alexander.buyantuyev@asu.edu

Fernando López-Caloca Centro de Investigación en Geografía y Geomática "Ing. Jorge L. Tamayo A.C., Contoy 137 Lomas de Padierna Tlalpan 14240 México D.F., ferlopez@centrogeo.org.mx.

Lori Carter Malcom Pirnie, Inc., Austin, TX 78701, USA, lcarter@pirnie.com

Christopher Chamberlin NOAA/PMEL/NCTR/JISAO, Seattle, WA 98115 USA, Chris.Chamberlin@noaa.gov

Yunhao Chen College of Resources, Beijing Normal University, Beijing 100875, China, cyh@ires.cn

Jinmu Choi Department of Geosciences, Mississippi State University, MS 39762-5448, USA, jc778@msstate.edu

Gretchen Culp Earth and Environmental Sciences Program, City University of New York Graduate Center, New York, NY 10016, USA, gculp@gc.cuny.edu

Andrew J. Curtis Department of Geography, University of Southern California, Kaprielian Hall (KAP), Los Angeles, CA 90089-0255, USA, ajcurtis@usc.edu

Bruce A. Davis Infrastructure and Geophysical Division, Science and Technology Directorate, Department of Homeland Security, Washington, DC 20528, bruce.a.davis@dhs.gov

Philippe De Maeyer Department of Geography, Faculty of Sciences, Ghent University, 9000 Gent, Belgium, philippe.demaeyer@ugent.be

Pieter Deckers Department of Geography, Faculty of Sciences, Ghent University, 9000 Gent, Belgium, pieter.deckers@ugent.be

Ronald T. Eguchi ImageCat, Inc., Long Beach, CA 90802, USA, rte@imagecatinc.com

William F. Fagan Disaster Science and Management Program, CADGIS Research Laboratory, Louisiana State University, Baton Rouge, LA 70806, USA, fagan.brla@gmail.com

Yvette C. Feliberty Department of Geography, Northern Illinois University, DeKalb, IL 60115, USA, yvette.c.feliberty@monsanto.com

Michael P. Finn US Geological Survey, Rolla, MO 65401, USA, mfinn@usgs.gov

A. Stewart Fotheringham National Centre for Geocomputation, National University of Ireland, Maynooth, Co. Kildare, Ireland, stewart.fotheringham@nuim.ie

Christopher C. Funk University of California, Santa Barbara, CA, 93106, chris@geog.ucsb.edu

Shubharoop Ghosh ImageCat, Inc., Long Beach, CA 90802, USA, sg@imagecatinc.com

A-du Gong Academy of Disaster Reduction and Emergency Management, Beijing Normal University, Beijing 100875, China, gad@ires.cn

Susanne Grossman-Clarke Global Institute of Sustainability, Arizona State University, Tempe, AZ 85287-3211, USA, sg.clarke@asu.edu

Sharon L. Harlan School of Human Evolution and Social Change, Arizona State University, Tempe, AZ 85287-2402, USA, sharon.harlan@asu.edu

Michael E. Hodgson Department of Geography, University of South Carolina, Columbia, SC 29208, USA, hodgsonm@sc.edu

Charles K. Huyck ImageCat, Inc., Long Beach, CA 90802, USA, ckh@imagecatinc.com

Weiguo Jiang Academy of Disaster Reduction and Emergency Management, Beijing Normal University, Beijing 100875, China, jwg@ires.cn

Wim Kellens Department of Geography, Faculty of Sciences, Ghent University, 9000 Gent, Belgium, wim.kellens@ugent.be

Jitka Kotelenska CH2M HILL, WA 98004, USA, jitka.kotelenska@CH2M.com

Jiyeong Lee Department of Geoinfomatics, University of Seoul, Korea; Dongdaemun-gu, Seoul 130-743, Korea, jlee@uos.ac.kr

Michael Leitner Department of Geography and Anthropology, Louisiana State University, Baton Rouge, LA 70803, USA, mleitne@lsu.edu

Jing Li Academy of Disaster Reduction and Emergency Management, Beijing Normal University, Beijing 100875, China, lijing@ires.cn

Yongmei Lu Department of Geography, Texas State University-San Marcos, San Marcos, TX 78666, USA, yl10@txstate.edu

Juliana Maantay Environmental, Geographic, and Geological Sciences Department, Lehman College, City University of New York, NY 10468, USA, juliana.maantay@lehman.cuny.edu

Susan M. Macey James and Marilyn Lovell Center for Environmental Geography and Hazards Research, Department of Geography, Texas State University-San Marcos, San Marcos, TX, USA, sm07@txstate.edu

Andrew Maroko Environmental, Geographic, and Geological Sciences Department, Lehman College, City University of New York, NY 10468, USA, andrew.maroko@lehman.cuny.edu

Timothy McCarthy National Centre for Geocomputation, National University of Ireland, Maynooth, Co. Kildare, Ireland, tim.mccarthy@nuim.ie

Anneley McMillan ImageCat Ltd., Communications House, Surrey KT21 2BT, UK, am@imagecatinc.com

Nazila Merati NOAA/PMEL/NCTR/JISAO, Seattle, WA 98115, USA, nazila.merati@noaa.gov

Jacqueline W. Mills Department of Geography, California State University, Long Beach CA 90840-1101, USA, jacquelinewmills@gmail.com

Christopher Moore PMEL/NCTR/JISAO, Seattle, WA 98115 USA, Christopher.Moore@noaa.gov

Melany Noltenius Department of Geography, University of Tennessee, Knoxville, TN 37996-0925, USA, mnolteni@yahoo.com

Firooza Pavri Department of Geography-Anthropology, University of Southern Maine, Gorham, ME 04038, USA, fpavri@usm.maine.edu

John Pine Research Institute for Environment, Energy and Economics, Appalachian State University, Boone, NC 28608, USA, pinejc@appstate.edu

Bruce A. Ralston Department of Geography, University of Tennessee, Knoxville, TN 37996-0925, USA, bralston@utk.edu

Johan Reyns Department of Geography, Faculty of Sciences, Ghent University, 9000 Gent, Belgium, johan.reyns@ugent.be

Darren M. Ruddell School of Geographical Sciences, Arizona State University, Tempe, AZ 85287-0104, USA, darren.ruddell@asu.edu

Michele Schilling Chemin des Clotts, 05 160 Saint Apollinaire, France, schilligmichele@gmail.com

Pamela S. Showalter James and Marilyn Lovell Center for Environmental Geography and Hazards Research, Department of Geography, Texas State University-San Marcos, TX 78666, USA, ps15@txstate.edu

Vasily Titov PMEL/NCTR/JISAO, Seattle, WA 98115 USA, vasily.titov@noaa.gov

E. Lynn Usery U.S. Geological Survey, Rolla, MO 65401, USA, usery@usgs.gov

Tiffany C. Vance NOAA/NMFS/RACE, Seattle, WA 98115, USA, tiffany.c.vance@noaa.gov

Wouter Vanneuville Flanders Hydraulics Research, Antwerpen, Belgium, wouter.vanneuville@mow.vlaanderen.be

Elvia Martínez-Viveros Centro de Investigación en Geografía y Geomática “Ing. Jorge L. Tamayo A.C., Contoy 137 Lomas de Padierna Tlalpan 14240 México D.F., emartinez@centrogeo.org.mx

Fahui Wang Department of Geography and Anthropology, Louisiana State University, Baton Rouge, LA 70803, USA, fwang@lsu.edu

Xinhao Wang School of Planning, University of Cincinnati, Cincinnati, OH 45221-0016, USA, xinhao.wang@uc.edu

Steven M. Ward Department of Geography and Anthropology, Louisiana State University, Baton Rouge, LA 70803, USA, sward2@lsu.edu

Heng Wei Department of Civil and Environmental Engineering, University of Cincinnati, Cincinnati, OH 45221-0071, USA, heng.wei@uc.edu

Chapter 1
Introduction

Pamela S. Showalter and Yongmei Lu

1.1 Overview

This volume is a compilation of recent research using geographic information systems (GIS), remote sensing (RS), and other technologies such as global positioning systems (GPS) to examine urban hazard and disaster issues. The goal is to improve and advance the use of such technologies during the four classic phases of hazard and disaster research: response, recovery, preparation, and mitigation. Reflecting what has become common practice, the above technologies have been folded into a single term, "geographic information technology" (GIT), along with other spatial-technical aids that appear later in the book. We use GIT interchangeably, regardless of the number of technologies employed in any given study, or whether one or more is given primacy in the work. Chapters were solicited using a broad multidisciplinary call resulting in contributions from scholars representing Africa, Asia, Europe, Latin America and North America. All of the chapters underwent a double-blind peer-review process. It is every author's goal in this book to reduce the impact of future extreme events in urban environments by improving understanding of GIT and expanding its role at the local, regional, state, and federal levels.

The discipline of geography has developed broadly accepted meanings for the words "hazard", "disaster", and "urban", which we have expanded somewhat in order to embrace the range of work presented here. For example, a hazard is generally considered to be a component of the landscape that creates risk when it intersects with human activities. One example is a floodplain—unoccupied, it presents no risk; occupied it presents the risk of flooding and the potential for disaster. Conversely, terrorism is spatially indistinct because it can occur anywhere, any time, and is a direct result of human activities. An occupied floodplain and a terrorist

P.S. Showalter (✉)
James and Marilyn Lovell Center for Environmental Geography and Hazards Research, Department of Geography, Texas State University-San Marcos, San Marcos, TX 78666, USA
e-mail: ps15@txstate.edu

P.S. Showalter, Y. Lu (eds.), *Geospatial Techniques in Urban Hazard and Disaster Analysis*, Geotechnologies and the Environment 2, DOI 10.1007/978-90-481-2238-7_1,

represent potential problems. A disaster, however, is the embodiment of a real situation that must be addressed immediately (Tobin and Montz 1997) because it represents an event of such magnitude that it disrupts the social fabric (Stallings 2002).

An in-depth discussion of the many scholarly definitions of "urban" is far beyond the scope of this book. While Westerners have a tendency to associate the term "urban" with areas replete with high-rise building or skyscrapers, such is not the case in some rapidly expanding cities of the developing world. There, large numbers of people are urbanizing areas poorly equipped to absorb them, often resulting in the creation of "informal settlements". For our purposes, Hartshorn's (1992) concept that "urban" includes areas within or near a city (as opposed to a village, town, or hamlet) is appropriate, as well as the idea that cities, and/or areas considered to be urban, share broad characteristics such as population concentration; shared and distinctive employment patterns, lifestyle and land use; and the existence of a variety of institutions that coordinate the use of public facilities. The use of a broader definition allows the incorporation of studies that include extra-urban areas (e.g., stands of coastal mangroves) because there can be a direct relationship between the health of such ecosystems and the survival of nearby urban areas in the wake of a natural disaster such as a hurricane or tropical cyclone.

Due to the technical nature of this book, certain assumptions are made regarding the reader's familiarity with common GIT terminology and acronyms. For those readers unfamiliar with such terms, we recommend the glossaries and related chapters found in textbooks we have employed in our classrooms, such as DeMers (2008), Jensen (2000), Lillesand et al. (2008), and Longley et al. (2005).

The book is organized into five parts: sea level rise and flood analysis; metropolitan case studies; earthquakes, tsunamis, and international applications; hurricane response/recovery; and evacuation studies. The rationale for the book's organization is twofold. The first part addresses flooding because it is the most commonly experienced problem across the globe, both in terms of its frequency and spatial distribution. Not surprisingly, flood-related studies represented the largest number of submissions we received, resulting in that part containing the largest number of chapters in the book. Second, the book's focus on applied work led us to organize subsequent parts in such a manner that readers seeking specific guidance on, say, the use of GIT to address hurricane issues, would quickly be able to locate the majority of that material. However, we encourage such readers to look closely at the chapters in other parts because there is some "cross-over" work—for example, a chapter in the evacuation studies part is based on the scenario of a hurricane occurring in Key West, Florida while two in the flood analysis part address issues occurring in metropolitan locations.

Some readers may wish to quickly locate information regarding the basic contents of each chapter. Therefore, a brief description of each chapter follows describing the type of GIT employed (including new tools offered to advance our understanding of risk and vulnerability), as well as the spatial focus of the work.

1.2 Part Descriptions

1.2.1 Part I—Sea Level Rise and Flood Analysis

This part contains five chapters, beginning with Usery, Choi, and Finn's global animation of sea level rise. Their work is offered not as a predictive model but to demonstrate a methodology for using GIS data layers to create models, animate data, and provide the basis for more detailed modeling which can lead to improved coastal policy-making. In keeping with the theme of sea level rise but focusing on a more specific area, Pavri follows with an examination of sea level rise related flood vulnerability for Mumbai (Bombay), India using remote sensing. Through the use of readily available RS data and commonly employed classification methods, the author demonstrates that a relatively "low tech" approach yields results that can support the need for more aggressive flood control activities. Chapter 4 uses GIS to address the risk of flooding in Flanders, Belgium, a coastal area susceptible to sea-level rise as well as riverine floods. The team of Deckers, Kellens, Reyns, Vanneuville, and Maeyer developed a flood risk assessment tool (LATIS) to assess flood risk based on hydrologic models, land use information and socio-economic data with the goal of performing risk analysis quickly and effectively. Their chapter is followed by Maantay, Maroko, and Culp's examination of the flood risk in New York City. These authors developed the Cadastral-based Expert Dasymetric System (CEDS) and the New York City Hazard Vulnerability Index (NYCHVI) in order to more accurately estimate vulnerable populations in densely developed mega-cities, characterizing those populations based on measures of social, physical, and health vulnerability. The final chapter in this part presents the research of Bizimana and Schilling, who combined GIS, Quickbird imagery, GPS, and surveys to perform flood risk analysis for informal settlements in the Nyabugogo flood plain of Kigali City in Rwanda. Their work impacted local policy, resulting in the relocation of a major market and development restrictions within the flood plain.

1.2.2 Part II—Metropolitan Case Studies

Composed of five chapters, this part represents our "least traditional" portion of the book, describing the use of GIT in studying atmospheric pollutants, wild fire, and agriculture (vis a vis food security). Leading off is Chapter 7, where Macey uses GIS to examine the "respiratory riskscape" of five major metropolitan areas in Texas. The study utilizes readily available "criteria air pollution data" from federal government sources to determine the spatial pattern of urban air pollutants and combines this information with respiratory and nonrespiratory decedents' demographic characteristics to identify levels of variation between urban areas' pollution data and mortality rates. In a similar vein, Wang and Feliberty examine the spatial distribution of Chicago's toxic release inventory sites in an effort to identify whether environmental inequity exists in the area. The authors incorporate

data from the census and the Environmental Protection Agency's Toxic Release Inventory into a GIS to examine whether or not minority and low-income groups are disproportionately exposed to environmental hazards. Next, Ruddell, Harlan, Grossman-Clarke, and Buyantuyev examine risk and exposure to extreme heat in the semi-arid city of Phoenix, Arizona. The authors used the Weather Research and Forecasting (WRF) model to simulate air temperature variability throughout the region, and studied 40 diverse neighborhoods through survey analysis to better understand perceived temperatures and heat-related health problems during the summer of 2005. In keeping with the theme of heat, Lu, Carter, and Showalter follow with a wildfire risk analysis of Travis County's Wildland-Urban Interface (WUI). The authors combined historic wildfire records, land cover types, topographical characteristics, and housing density information into a GIS to create a wildfire risk profile and identified the need for expanded fire control and fire regulations in the WUI. The part closes with a chapter by Brown and Funk that details their use of GIT to investigate the growing food security crisis in Harare, Zimbabwe. Using MODIS NDVI data to estimate corn production shortfalls enabled early and decisive resource distribution by humanitarian groups to forestall a food crisis in 2007.

1.2.3 Part III—Earthquakes, Tsunamis, and International Applications

This part begins with a timely chapter by Li, Chen, Gong, and Jiang who studied the recent (May 2008) Wenchuan Earthquake in China. Beginning with a discussion of China's disaster management and emergency management systems, the authors relate how GIT was applied as a disaster relief tool following the earthquake, and conclude with a description of China's new "Small Satellite Constellation for Environment and Disaster Monitoring and Forecasting". The next chapter's focus is Mexico City, where Martínez Viveros and López Caloca discuss development of "Geodisplat"—an interactive, computerized tool that fuses data from multiple sources and models systems that interact during the disaster cycle. The goal of the tool is to efficiently support decision makers' information needs during all stages of the disaster cycle. Tsuami research is the focus of the next chapter, where Merati, Chamberlin, Moore, Titov, and Vance use geospatial data and GIS to build a tsunami forecasting system for US Tsunami Warning Centers. The authors discuss the use of open source and commercially available GIT to improve tsunami research and hazard mitigation as well as how they coupled tsunami model results with coastal risk, vulnerability, and evacuation models. The part concludes with a more general discussion of the use of GIT in managing hazards and disasters. Eguchi, Huyck, Ghosh, Adams, and McMillan pooled their efforts to introduce new and emerging technologies that have either proven effective in disaster management or show future promise. The authors conclude by addressing research/implementation issues as well as problems related to real-time event monitoring, privacy protection, information sharing, and trust management.

1.2.4 Part IV—Hurricane Response/Recovery

The fourth part of the book addresses hurricanes, and begins with a contribution by Hodgson, Davis, and Kotelenska who describe the use of GIT—with a focus on remote sensing—during the response and recovery phases of the disaster cycle. Analyzing three major hurricanes that impacted the US, they conclude GIT is still not uniformly implemented during those phases and work needs to be done to increase its use and acceptance by potential users. Hurricane Katrina's impact on the US Gulf Coast created the next two studies found in this part. Ward, Leitner, and Pine utilize GIT in New Orleans to assess the level of recovery, determine the most appropriate scale to use for studying the spatial aspects of recovery, and to identify spatial indicators of recovery. Curtis, Mills, McCarthy, Fotheringham, and Fagan follow with another New Orleans study that produced a Spatial Video Acquisition System. This system improved the collection of post-disaster geospatial damage assessment data in the spatially and temporally dynamic urban environment of a post-disaster neighborhood.

1.2.5 Part V—Evacuation Studies

The final part of the book contains three efforts to improve evacuation. Noltinius and Ralston test evacuation time estimates in Key West, Florida and found that there are three important aspects of pre-evacuation trip making behavior that run counter to common evacuation modeling assumptions. Incorporating these findings into future evacuation models will improve efforts to remove populations from harm's way. Choi and Lee create a 3D geometric network and agent-based evacuation model at the "micro-level"—buildings—in which they incorporate models of human behavior when attempts are made to exit the building. They found that the rate of building evacuation is greatly influenced by jamming situations, which are not uncommon under such circumstances. And, finally, Wang, Belhadj, and Wei developed a Community Evacuation Planning Support System (CE-PSS) to aid urban communities tasked with identifying likely terrorist targets as well as the optimum location for shelters following an attack. Developed with a GIS, the goal of the CE-PSS is to assist planners, citizens, and community leaders in their efforts to plan for possible terrorist attacks.

1.3 Closing Remarks

The maturity of GIT in hazards and disaster analysis is becoming more evident. As recently as six years ago, a book describing different methods applied to disaster research (Stallings 2002) devoted one chapter to the use of a single type of geographic technology, GIS (Dash 2002). Happily, there have been recent notable additions to the literature regarding the use of GIS, remote sensing, and other GIT in hazards and disaster analysis, e.g., Laben (2002), Cutter (2003), Mansor et al.

(2004), Van Oosterom et al. (2005), Adams and Huyck (2005), Li et al. (2007), National Research Council (2007), Shailesh and Zlatanova (2008), and Zlatanova and Li (2008). It is our hope that this volume makes a modest contribution to this growing body of literature, specifically through its focus on the application of GIT to urban hazard and disaster studies.

The chapters in this volume present a broad spectrum of applications of geographic information technologies to studies of various types of hazards and disasters in different urban settings. Our reading of the material has led us to conclude that there are several issues that warrant additional scrutiny by the community of hazards professionals. The first of these relates to the creation and dissemination of geographic information data that can be incorporated into GIT to reduce losses from urban hazards and disasters. This problem is twofold. On the one hand, in some urban areas (especially in the developing world) there is a lack of available information critical for understanding and preparing for hazard situations. This data shortage represents the major barrier to GIT's ability to contribute to urban hazard and disaster management in those locales. On the other hand, there is "an embarrassment of riches" in other parts of the world, where the amount of information is so great that there exists an urgent need to better oversee its proper dissemination and usage. How to ensure that appropriate geographic information and technologies are properly used in a proper manner at a proper time for a proper hazard and disaster reduction purpose? As we wrote in a recent column (Showalter and Lu 2009), we again urge the GIT community to address issues related to ready access to GIT information and how GIT is being used to communicate risk and other disaster-related data to non-professionals and members of the general public.

The second issue relates to urban hazard/disaster modeling that uses GIT. The combination of rapid development of computing power, richer data sets, and more efficient data collection/processing technologies, has led to models that tend to be more sophisticated, based on algorithms that can be extremely complicated, creating sometimes enormous data input demands, and perhaps hard-to-intepret results. While all of the above have the potential to advance scientific understanding of the specific disaster or hazard being investigated, we wish to reaffirm the applied nature of urban hazard and disaster analysis. Efforts linking advances in research labs with real-world hazardous event prediction, preparation, response, recovery, and overall loss reduction are encouraged. Some chapters in this book provide good examples of such efforts. We applaud research that both advances our scientific understanding of urban hazards and disasters, and attempts to determine the best manner of putting those scientific tools into public use to solve an actual problem. Significant contributions to urban hazard and disaster studies occur not only from the advancement of complicated models but also from their simplification and operationalization.

Last, GIT has helped, and will continue to help, strengthen the interdisciplinary nature of the study of urban hazards and disasters. As can be seen from the wide array of disciplines that form the roots of our chapter authors, the application of GIT to urban hazard and disaster analysis brings together social and physical scientists, engineers and planners, geographers and hydrologists, federal/regional/local public servants and the private sector, as well as many others not listed here. This

disciplinary "soup" not only has significant implications for education and training programs for specialists in urban hazard and disaster studies; it also signifies the importance of cross-disciplinary collaboration. In a sense, GIT's ability to absorb and massage data representing a variety of instruments, formats, scales, and levels of accuracy mirrors the field of urban hazard and disaster analysis, which absorbs input from a host of disciplines but has a singular two-pronged goal: saving lives and reducing losses.

References

Adams B.J. and Huyck C.K. 2005. The Emerging Role of Remote Sensing Technology in Emergency Management. In: C. Taylor and E. VanMarcke (eds.) *Infrastructure Risk Management Processes: Natural, Accidental, and Deliberate Hazards* (Monograph 1). Reston, VA: American Society of Civil Engineers, pp. 95–117.

Cutter S.L. 2003. GI Science, Disasters, and Emergency Management. Transactions in GIS 7(4): 439–446.

Dash N. 2002. The Use of Geographic Information Systems in Disaster Research. In: Robert A. Stallings (ed.) *Methods of Disaster Research*, pp. 320–333. International Research Committee on Disasters Bloomington, IN: Xlibris Corporation.

DeMers M. 2008. *Fundamentals of Geographic Information Systems* (4th edition). New York: John Wiley and Sons, Inc.

Hartshorn T.A. 1992. *Interpreting the City: An Urban Geography* (2nd edition). New York: John Wiley and Sons, Inc.

Jensen J. 2000. *Remote Sensing of the Environment: An Earth Resource Perspective*. New Jersey: Prentice Hall.

Laben C. 2002. Integration of Remote Sensing Data and Geographic Information System Technology for Emergency Management and Their Applications at the Pacific Disaster Center. Optical Engineering 41(9): 2129–2136.

Li J., Zlatanova S., and Fabbri A. 2007. *Geomantics Solutions for Disaster Management*. Berlin/Heidelberg: Springer-Verlag.

Lillesand T.M., Kiefer R.W., and Chipman J.W. 2008. *Remote Sensing and Image Interpretation* (6th edition). New Jersey: John Wiley and Sons, Inc.

Longley P., Goodchild M., Maguire D., and Rhind D. 2005. *Geographic Information Systems and Science*. New York: John Wiley and Sons, Inc.

Mansor S., Abu Shariah M., Billa L., Setiawan I., and Jabar F. 2004. Spatial Technology for Natural Risk Management. Disaster Prevention and Management 13(5): 364–373.

National Research Council (2007). *Successful Response Starts with a Map: Improving Geospatial Support for Disaster Management.* Committee on Planning for Catastrophe, Washington, DC: National Academies Press, 184p.

Shailesh N. and Zlatanova S. 2008. *Remote Sensing and GIS Technologies for Monitoring and Prediction of Disasters*. Berlin/Heidelberg: Springer-Verlag.

Showalter P., and Lu Y. 2009. Techno-Hyperactivity. GIM International. 23(1). http:www.gim-international.com/issues/articles/id1238-Technohyperactivity.htm. Last updated January 12.

Stallings R.A. (ed). 2002. *Methods of Disaster Research* (Volume Two). International Research Committee on Disasters Monograph Series. Bloomington, IN: Xlibris Corporation.

Tobin G.A., and Montz B.E. 1997. *Natural Hazards: Explanation and Integration*. New York/London: The Guilford Press.

Van Oosterom P., Zlatanova S., and Fendel E. 2005. *Geo-Information for Disaster Management*. Berlin/Heidelberg: Springer.

Zlatanova S. and Li J. 2008. *Geospatial Information Technology for Emergency Response*. London: Taylor and Francis Group.

Part I
Sea Level Rise and Flood Analysis

Chapter 2
Modeling Sea-Level Rise and Surge in Low-Lying Urban Areas Using Spatial Data, Geographic Information Systems, and Animation Methods

E. Lynn Usery, Jinmu Choi, and Michael P. Finn

Abstract Spatial datasets including elevation, land cover, and population of urban areas provide a basis for modeling and animating sea-level rise and surges resulting from storms and other catastrophic events. With a geographic information system (GIS), elevation data can be used to determine urban areas with large population numbers and densities in low-lying areas subject to inundation from rising water. This chapter provides details of the analysis and modeling procedure, as well as animations for specific areas of the world that are at risk from inundation from moderate rises or surges of sea level. The work is not an attempt to predict sea-level rise, but rather a methodological study of how to use GIS data layers to create the models and animations. Whereas global sea level rise is currently measured by millimeters per year, this work examines theoretical rise measured in meters as well as coastal threats posed by tsunamis, such as occurred in the Indian Ocean in 2004. Global, regional, and local animations can be created using widely available elevation, land cover, and population data. The models and animations provide a basis for determining areas with large population numbers in relatively low-lying areas and potentially subject to inundation risk, as was the case when Hurricane Katrina devastated New Orleans. This determination can provide a basis for more detailed modeling and policy planning such as development and evacuation.

Keywords Map projection · Global GIS data · Urban GIS data · Sea level rise · Modeling · Animation

2.1 Introduction

The development of high resolution geographical data (e.g., elevation, population, land cover) and geographical modeling and animation capabilities makes it possible to develop comprehensive spatial models of the effects of high surges and moderate

E.L. Usery (✉)
US Geological Survey, Rolla, MO 65401, USA
e-mail: usery@usgs.gov

P.S. Showalter, Y. Lu (eds.), *Geospatial Techniques in Urban Hazard and Disaster Analysis*, Geotechnologies and the Environment 2, DOI 10.1007/978-90-481-2238-7_2,

rises of sea level on human populations in areas of risk. This chapter makes no attempt to predict sea level rise, but rather provides a methodology for combining GIS data layers in a simulation and animation that reveals low-lying areas with large population numbers that may be subject to inundation and thus require evacuation planning. For global modeling, 30 arc-second resolution equiangular grid data from the US Geological Survey for elevation (GTopo30) and land cover (Global Land Cover), and population (Landscan 2005) from the Oak Ridge National Laboratory provide a basis for determining areas of land cover types and numbers of people below specific elevations that are subject to inundation. For regional areas outside the United States (US), 90-m resolution Shuttle Radar Topographic Mission (SRTM) elevation data are used and for US coasts, 30 m resolution elevation and land cover data are used with population converted to 30 m raster cells from the vector polygons of US Census block data. Whereas such global and regional datasets can be used to model sea-level rise, the resolution prohibits illustrating small increases as are now occurring. An extreme upper limit of 80 m, the approximate theoretical maximum rise in sea level if all icecaps and glaciers melt, is used for some of the global simulations because of resolution limitations. A limit of 30 m is used for the local and urban area simulations. The model of rising water is based only on elevation and does not attempt to account for tidal changes or the way a tidal wave would actually interact with coastal features.

The approaches discussed in this paper are most appropriate simulating large surges of sea water, such as the 30 m wave that occurred during the Indian Ocean Tsunami in 2004 and the 4 m inundation from hurricanes Katrina and Rita in 2005. With higher resolution data, for example a 10 cm resolution elevation grid from LIDAR data, the same methods can be used to model small rises of a few millimeters, as are now occurring each year. It is the purpose of this paper to present these global and regional modeling techniques and methods of animating the results of the models as potential tools for risk assessment, development, and evacuation planning.[1]

The next section of this chapter provides a motivation for the work and a brief discussion of the history and potential heights of sea-level rise. The third section provides information regarding storm surge and potential surge levels. Section 2.4 of the chapter discusses data preparation methods, particularly projection and resampling of raster data. The fifth section examines the multiscale modeling approach and includes discussion of the visualization and animation methods. A final section draws conclusions, discusses limitations, and provides recommendations for future research.

2.2 History and Potential Heights of Sea-Level Rise

Global sea level and the Earth's climate are intricately linked. With the consistent trend towards higher temperatures, conditions are less icy in the Artic regions as seen in increasing melt areas over the Greenland ice sheet, retreating glaciers,

[1] Animations are available at http://cegis.usgs.gov/sea_level_rise.html.

reduced sea ice coverage, and permafrost thawing (Arctic Climate Impact Assessment 2005). Comiso et al. (2008) determined that the extent of Arctic sea ice coverage was 24 percent lower in September 2007 than September 2005, the previous record low.

The Intergovernmental Panel on Climate Change (IPCC) Fourth Assessment Report (IPCC 2007) estimates of sea-level rise range from 0.18 to 0.59 m by the 2090s from the average level between 1980 and 2000. The Greenland and West Antarctica ice sheets may be collectively adding 0.35 mm/yr to sea-level rise in recent years (Shepherd and Wingham 2007). Because it is unknown how these ice sheets may respond to the increased polar temperatures expected during this century, it is essential that ice sheet monitoring be expanded (Horton et al. 2008).

Estimates of current (2008) rates of global sea-level rise vary from 1.0 to 3.1 mm/yr (Douglas et al. 2001; Miller and Douglas 2004; Wadhams and Munk 2004; Church and White 2006; Holgate 2007; IPCC 2007). The 20th century acceleration of sea-level rise appears to be a global phenomenon (Gehrels et al. 2008). This rise is likely associated with the concurrent upsurge in global temperatures and is demonstrated by Gehrels et al. (2008) by the rate of sea-level rise in New Zealand, which was determined as approximately 2.8 mm/yr. In the Mediterranean Sea and Atlantic Ocean, Marcos and Tsimplis (2007) determined that the residual sea-level rise corrected for post-glacial rebound processes were 0.9 and 1.3 mm/yr, respectively.

Research by Beckley et al. (2007) determined a global sea-level rise rate of 3.36 $\pm$ 0.41 mm/yr during 14 years from 1993 to 2007, whereas Chao et al. (2008) show an essentially constant rate of rise for global sea level of +2.46 mm/yr during at least the past 80 years. Chambers (2008) provides a description of methods for measuring global sea-level rise using satellite altimetry and reports that a rise of 3.5 $\pm$ 0.5 mm is the average for the entire ocean. Chambers (2006) indicates that the rise rate is not constant across the oceans, but is affected by temperature and salinity, that affect gravity measurements.

One of the most important consequences of diminishing mountain glacier cover is rising sea level (Arendt et al. 2002). Schiefer et al. (2007) determined that between 1985 and 1999 the rate of glacier loss in the Coast Mountains of British Columbia approximately doubled that observed for the previous two decades and could account for about 8.3 percent of the contribution from mountain glaciers and ice caps. For example, the retreat of the Grinnell Glacier since the early 1900s is shown in Fig. 2.1. The images show the former extent of the glacier in 1938, 1981, 1978, and 2006. Mountain glaciers are excellent monitors of climate change; the worldwide shrinkage of mountain glaciers is thought to be caused by a combination of a temperature increase from the Little Ice Age (which ended in the latter half of the 19th century) and increased greenhouse-gas emissions (Poore et al. 2000).

Small magnitude changes in the rate at which sea level is observed to rise enhance the ability to monitor sea level and predict its change (Cazenave and Nerem 2004). Jenkins and Holland (2007) put bounds on potential sea-level rise associated with ice shelf melting, icebergs, and sea ice currently afloat in the world's oceans.

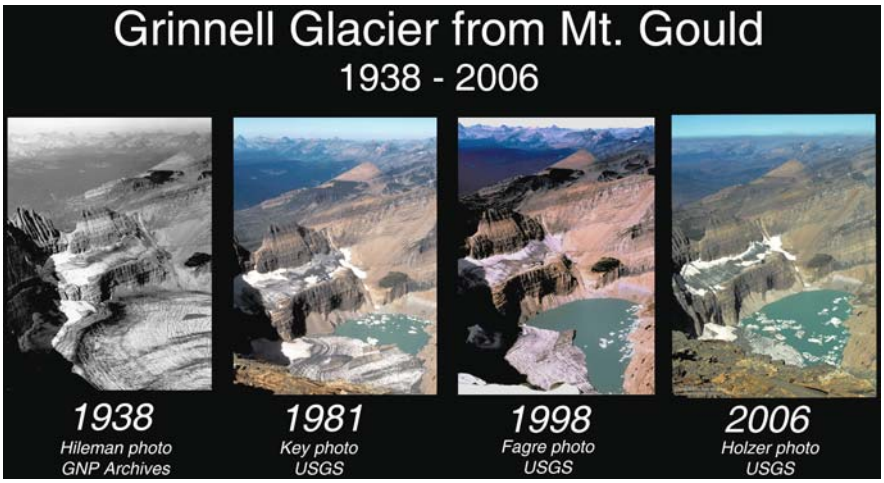

Fig. 2.1 The melting of the Grinnell Glacier from 1938 to 2006 in Glacier National Park (USGS)

Kolker and Hameed (2007) also find that beyond broad climatologic data there is a meteorological driver of sea-level trends through atmospheric centers of action that have some affect on winds, pressure, and sea-surface temperatures, thereby influencing sea level via a suite of oceanographic processes.

Most current (2008) global land ice mass is in the Antarctic and Greenland ice sheets (Fig. 2.2). Complete melting of these ice sheets would cause a maximum sea-level rise of 80 m (Table 2.1). Whereas today's rates of sea-level rise are only a few millimeters per year, the geological record shows a 20 m rise over a 500 year period, resulting from Meltwater Pulse 1A during the collapse of Earth's former ice sheets (Weaver et al. 2003).

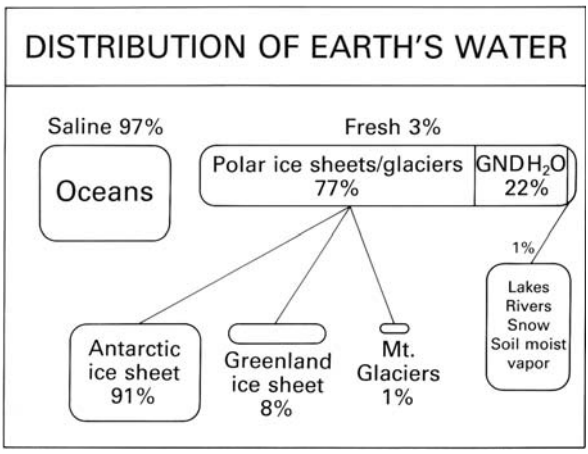

Fig. 2.2 Distribution of Earth's water showing most of the freshwater is in the Antarctic and Greenland ice sheets (Thomas, 1993)

Table 2.1 Potential sea-level rise from the Earth's ice sheets

Location	Volume	Potential sea-level rise (m)
East Antarctic Ice Sheet	26,039,200	64.80
West Antarctic Ice Sheet	3,262,000	8.06
Antarctic peninsula	227,100	0.46
Greenland	2,620,000	6.55
Other ice caps, fields, glaciers	180,000	0.45
Total	32,328,300	80.32

Source: Thomas (1993).

Ice sheets are composed of a largely homogeneous material and move so slowly that turbulence, Coriolis, and other inertial effects can be ignored by climate modelers; yet rooted within ice sheets are outlet glaciers (Vaughan and Arthen 2007). These glaciers, for example, those flowing from the Greenland Ice Sheet, discharge ice directly into the ocean at 200 to 12,000 mm/yr (Joughin et al. 2008). Recent reports record the rapidly escalating discharge of Greenland's outlet glaciers (Joughin et al. 2004; Rignot and Kanagaratnam 2006; Truffer and Fahnestock 2007). Data indicate summer increases of 50 to 100 percent of the volume of surface meltwater reaching the ice-bedrock interface of the ice sheet (Joughin et al. 2008). Current (2008) observations demonstrate that the ice flow all along western fringe of Greenland's ice sheet accelerates all through the summer as surface meltwater lubricates sliding at the interface (Zwally et al. 1998; Joughin et al. 2008). Das et al. (2008) described the swift drainage of a 5.6 km^2 supraglacial lake on the Greenland Ice Sheet signifying that an efficient drainage system dispersed the meltwater subglacially. Such findings can clarify calculations regarding observed net regional summer ice flow increase by incorporating the impact from multiple lake drainages. Variation on the Antarctic Ice Sheet surface noted from satellite observations also seems to indicate moving subglacial water under a huge ice stream (Fricker et al. 2007).

2.3 Storm Surge and Effects: Tsunamis and Hurricanes

Across our planet, civilization is vulnerable to disaster events that can annihilate because they catch individuals by surprise. Sea waves act to dissipate concentrations of energy in the Earth's dynamic systems that stem from various meteorological or geophysical sources, and can sometimes result in a natural disaster (Zebrowski 1999). Tsunamis are seismic sea waves generated spontaneously by a rapid release of energy from submarine earthquakes, explosions of sea-level volcanoes, and by undersea landslides along the continental shelves. Tsunamis have long wavelengths and periods, i.e., the time for passage of one wavelength, and the first wave peak hitting land is not necessarily the largest (Zebrowski 1999). These long periods often cause unexpected wavefronts to hit local populations.

In 2004, a massive tsunami occurred in the Indian Ocean. Coastal areas in Indonesia, Thailand, India and surrounding locations received significant inundation including a 30 m wave that hit Banda Aceh on the northwestern tip of the island of Sumatra in Indonesia. In Sri Lanka and other locations the wave heights crested 10 m or more. Wave heights at these levels can inundate large coastal areas causing significant loss of life and damage to property and infrastructure (as of this writing, a selection of before/after images of the tsunami's impact on Banda Aceh were available on the World Wide Web at http://homepage.mac.com/demark/tsunami/9.html; Demark 2005).

While tsunamis are particularly devastating with high surges of sea water, hurricanes occur more frequently, in more world locations, and can also cause high water surges. The 1900 Galveston hurricane is on record as the worst natural disaster in US history with an estimated loss of life of between 6000 and 12,000 persons (McGee 1900; Zebrowski 1999). Barrier islands, similar to the one on which Galveston is built, are found along the coasts of the US Atlantic Ocean and Gulf of Mexico, and are areas most prone to hammering by high-energy waves and storm surges (Zebrowski 1999).

On August 28, 2005, Hurricane Katrina passed across the Gulf of Mexico and became a Category 5 storm on the Saffir-Simpson hurricane scale, with winds estimated at 175 miles per hour (NOAA 2007). Hurricane Katrina devastated New Orleans and other Gulf Coast areas destroying lives, homes, and city infrastructure. As of this writing, many people are still coping with Katrina's devastation. The storm surge was particularly destructive (see http://www.snopes.com/katrina/photos/surge.asp), flooding a large area around New Orleans. Coastal storm surge flooding was 7 to 10 m (20 to 30 feet) above normal tide levels (FEMA 2007). In the same year that Katrina hit the Gulf Coast, Hurricane Rita caused a second wave of devastation a few months later. A series of before and after maps and images of the effects of Katrina and Rita are available from the USGS (2008a).

The potential for damage from hurricanes and tsunamis becomes apparent from these few examples. To better perform risk assessment, understand development opportunities and challenges, and improve evacuation routing, it is necessary to develop methods to model areas subject to inundation that include the number of persons who could be affected, various land covers (that can impede or exacerbate the movement of coastal surges), and infrastructure at risk. Following is a description of methods employed for global, regional, and local areas.

2.4 Global, Regional, and Local Modeling of Sea-Level Rise

The availability of global elevation, land cover, and population datasets at 30 arcsec (approximately 1 km at the Equator) resolution have made it possible to model inundation effects globally and regionally. The SRTM elevation data are available at 90 m resolution for much of the world, and provide a basis for more accurate modeling in regional areas. In the US, higher resolution 30 m elevation and land-cover data can be augmented with population numbers from the US Census block converted to 30 m raster cells (Table 2.2).

Table 2.2 Datasets used in models and animations

Area	Elevation	Land cover	Population
Global	Gtopo30 30 arc-sec	USGS Global Land Cover 30 arc-sec	LandScan 2005 30 arc-sec
Regional	SRTM 90 m	USGS Global Land Cover Resampled to 90 m	LandScan 2005 Resampled to 90 m
US Coasts/ Local	National Elevation Dataset 30 m	National land Cover Dataset 30 m	US Census Block Numbers Converted to 30 m

2.4.1 Problems and Solutions for Global Projection and Resampling

In order for global, regional, and local models to be created, the data used in these models must be resampled to a standard projection. Whereas elevation data can be resampled with an averaging resampler (e.g., bilinear interpolation), land cover and population data require different methods. Categorical (land cover) data must be resampled with a nearest neighbor algorithm causing significant pixel gain/loss in some locations (Seong and Usery 2001; Seong et al. 2002). Population data (numbers of people in each raster cell) cannot be resampled with averaging or nearest neighbor methods, but instead require an additive resampler. In the additive resampler, the output pixel value is a result of combination of multiple input pixel values. The software adds all complete input pixels that map to the area covered by a single output pixel. We proportionally assign input pixels that are split across output pixel boundaries. Thus, each output pixel has a unique value (number of people) that results from the additive combination of the appropriate set of input pixels. We validate the process by checking the total number of people in the output image against the total number from the input image. These must exactly match so we do not loose or gain people in the resampling process.

For global projections, significant problems were encountered with commercial software when attempting to resample and project the 2 Gb elevation and 1 Gb land cover/population raster files. Software problems included unreliable global projections, inability to account for singularities such as the North and South Poles, and specific projections unable to process to completion (aborting before the plane representation is complete). Inverse projection results moved North America across the Atlantic to the Greenwich meridian, increased file sizes by orders of magnitude, and repeated areas at edges of a global projection (i.e., caused both Alaska and Siberia to appear on both edges of the map). Computation time was also an issue because it can be extensive, lasting up to 200 hours or more on high-end desktop computers (Usery and Seong 2001; Usery et al. 2003).

To solve such problems, a USGS software package called mapIMG was used (available from http://carto-research.er.usgs.gov/projection/acc_proj_data.html). To account for pixel loss and gain in categorical data, the resampling method uses a statistical strategy, such as the modal category or some other user-defined strategy.

For example, to down-sample the data from a 30 arc-sec to an 8 × 8 km pixel, 64 input values are used to determine a single output value. The mapIMG software examines the 64 values and tabulates the number of values in each category. The user can then assign the modal category (the value that occurs the highest number of times) to the output cell. The result is a smoother image of categorical data with a reduction in pixel loss and gain (Steinwand 2003). For population data, an additive resampler was used. Using the above example of 64 input pixels to one output pixel, the mapIMG software adds the values of the 64 pixels to create one output value. MapIMG, is available for various computing platforms and can be downloaded without charge.

2.4.2 Multi-Scale Modeling Approach

Global and regional effects of rising sea level are modeled using elevation, population, and land cover data at 30 arc-sec spatial resolution projected and resampled to 1 km cells as described in the previous section. The datasets were transformed to the Mollweide projection to provide a global view with equal areas of land cover (Fig. 2.3), using a decision support system for map projection selection that is freely available to users of global and regional raster/vector datasets (USGS 2008b).

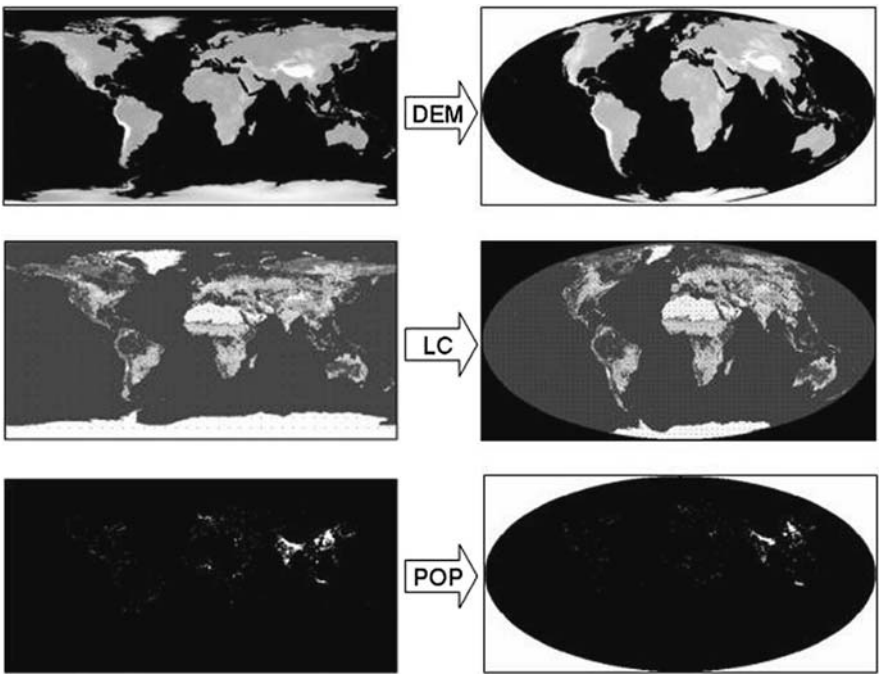

Fig. 2.3 Transformation of the global datasets for elevation, land cover, and population from geographic coordinates to the Mollweide projection

The subsequent modeling effort utilizes statistical summaries and animations. Statistical summaries show sea-level rise effects at global and regional scales, as well as surge effects in low-lying urban areas at local scales and in relation to affected populations and land cover loss. Animations are used to illustrate the locations of affected areas; a blue mask aids the visualization of rising water as it "inundates" existing land cover. One caveat regarding the simulations, animations, and statistical models presented here is that their accuracy is dependent on the resolution and accuracy of the elevation data. Determining the extent of land classes and numbers of people affected depends on the resolution and accuracy of the land cover and population data. As with all models, any errors in these data will be propagated throughout the models, and may invalidate the results.

To determine areas of inundation and affected land cover types, and to extract the number of people in inundation areas of specific levels of rise, a conditional overlay and global summation operation are used (Fig. 2.4). The model is established to operate on intervals of sea-level rise and create an output map for each interval. For example, on a 1 m interval, individual maps are created for 1, 2, 3, 4, 5 m and so forth. To extract the number of people residing in the inundation area, the first conditional overlay uses population and elevation data. A population value is assigned to an output pixel only when the location is at an elevation equal to, or lower than, the specified elevation in the condition. Otherwise, a 0 value is assigned to the pixel. The second conditional overlay considers both elevation and land cover type from the 25 land cover categories in the Global Land Cover dataset as listed

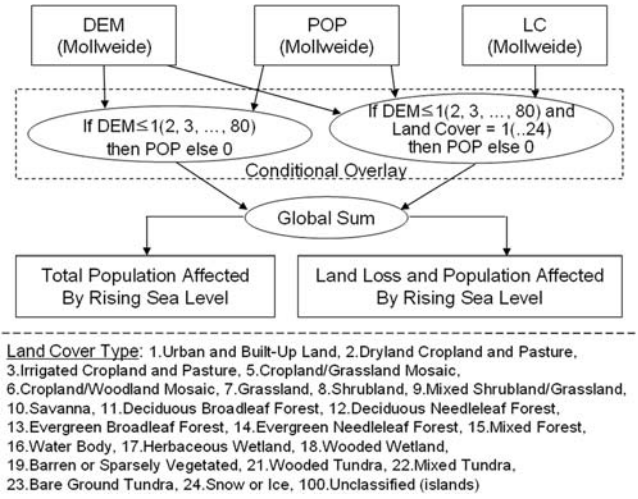

Fig. 2.4 A schematic of the conditional model used to determine areas of land cover and numbers of people in areas of inundation. The if-then conditional on the *left side* of the figure assigns population numbers as pixel values when the elevation of the pixel is below a specified value or a 0 otherwise. The conditional on the *right side* assigns land cover values if the elevation is above a specified value, otherwise a 0 is assigned. The global summation function tabulates numbers of people and total areas of each land cover category at below specified elevations

in the figure. If a pixel value is a specified land cover type and meets the elevation condition, the overlay assigns the population value at the location in the result data. Otherwise, a 0 is also assigned. The population in the area that is inundated, assigned a blue mask color, is totaled and shown in the running counter and the land cover categories outside the inundation area are used to set colors for the remainder of the map in the animations.

2.5 Sea-Level Rise Effects at Global and Regional Scales

Approximately 11 percent of the world's population lives in areas subject to a 5 m rise in sea level (Table 2.3). Nearly 1.5 billion people, or approximately 23 percent of the world's population, live in areas that would be inundated area in the event of a 30 m rise in sea level. The model used in this study indicates that there is a linear relationship between rising sea level and the number of people affected by that rise. As people become affected, so too will be their surroundings, including homes, infrastructure, critical facilities (e.g., hospitals), and schools. Community cohesion may be ruptured as relocation becomes necessary, and social stressors may increase as cities attempt to absorb the displaced.

Rising sea level impact on people and land cover was examined by exploring the 25 land-cover categories of the Global Land Cover dataset shown in Fig. 2.4. Among these categories, urban and built-up areas contain the highest population densities (about 3600 people per km^2); over 960 million people (about 16 percent of the world's population) live in those areas (Table 2.4). With a 5 m rise in sea level, 125 million people (about 2 percent of world population) living in urban and built-up areas are affected, or approximately 13 percent of the total urban population. Other land cover categories with high population densities include three cropland areas, Dry Land Cropland and Pasture, Irrigated Cropland and Pasture, and Crop Land/Woodland Mosaic, that are residence to more than 50 percent of the world's population. While population densities are not as high in these areas as in the Urban and Built-up Land, more land falls into this category. Therefore, should sea levels rise 5 m in these three cropland areas, over 250 million people would be affected.

Table 2.3 Population affected by rising sea level

Water level increase (m)	Area of land loss (km^2)	Number of people affected (percent)
5	5,431,902	669,739,183 (10.8)
10	6,308,676	870,751,960 (14.0)
20	7,888,233	1,176,709,476 (18.9)
30	9,459,562	1,405,824,876 (22.6)
Total world population		6,228,997,089 (100)

Table 2.4 Population affected with major land cover types by rising sea level

Land cover	Total land area (km^2)	POP density (per km^2)	Total population (percent)*	Population affected by rising sea level		
				5 m (percent)	10 m (percent)	20 m (percent)
Urban and Built-up land	3,100,287	3629	966,920,555 (15.5)	125,426,492 (2.0)	167,534,955 (2.7)	225,034,603 (3.6)
Irrigated Cropland and Pasture	3,811,178	392	1,285,065,525 (20.6)	146,650,929 (2.3)	231,800,008 (3.7)	353,447,741 (5.7)
Dryland Cropland and Pasture	14,141,964	121	1,480,209,129 (23.8)	90,514,229 (1.4)	117,463,463 (1.9)	169,232,478 (2.7)
Cropland/ Woodland Mosaic	5,086,575	90	394,546,228 (6.3)	18,977,528 (0.3)	28,429,804 (0.5)	46,827,725 (0.8)
Total			6,228,997,089(100)	669,739,138 (10.8)	870,751,960 (14.0)	1,176,709,476 (18.9)

*Percentage of total population residing in this land cover type.

2.5.1 Surge Effects at Local and Urban Scales

The impacts of 2004's Indian Ocean Tsunami and 2005's Hurricanes Katrina and Rita indicate the importance of local flood simulation. From the model, estimates of the number of people affected by 1−30 m flooding in the Los Angeles, Washington, DC, and New York areas are shown in Tables 2.5, 2.6, and 2.7, respectively (note that the numbers reflect the areas selected for modeling and do not apply to urban areas as defined by the US Census or other spatially defined boundaries). The highest surge flooding from Hurricane Katrina was 13 feet (approximately 4 m) along the coasts of Louisiana and Mississippi. Using 4 m as a "design surge" in Los Angeles produces an impact on about 276,000 people; in Washington, DC on about 1,500,000; and in the New York area on about 1,300,000. If the flooding is increased to 30 m, the approximate number of people living in these areas that would be affected is 3,600,000; 7,000,000; and 12,000,000, respectively.

Table 2.5 Population affected by urban flooding in the Los Angeles area

Flooding height (m)	Population affected	Percent of total population*
1	95,443	0.79
2	114,583	0.94
3	198,879	1.64
4	276,014	2.28
5	350,898	2.89
6	433,352	3.57
8	602,799	4.97
10	851,246	7.02
12	1,117,857	9.22
14	1,379.794	11.38
16	1,668,664	13.76
18	1,956,670	16.16
20	2,218,638	18.29
22	2,497,027	20.59
24	2,844,003	23.45
26	3,126,605	25.78
28	3,380,608	27.87
30	3,677,386	30.32
Total population*	12,128,147	100.00

* Total number of people in the area used for the model and animation

2.5.2 Visualization with Animation

Animations can be created using elevation and land cover data by taking "snapshots" of inundated land cover at particular elevations/water levels. The snapshot images are imported into animation software such as Macromedia® Flash® or Microsoft®

Table 2.6 Population affected by urban flooding in the Washington, DC area (including Baltimore, Philadelphia, Richmond)

Flooding height (m)	Population affected	Percent of total population*
1	220,811	1.22
2	542,712	3.00
3	1,042,825	5.76
4	1,503,203	8.30
5	1,907,150	10.53
6	2,376,907	13.12
8	2,901,938	16.02
10	3,395,204	18.75
12	3,917,752	21.63
14	4,322,253	23.86
16	4,676,841	25.82
18	5,041,001	27.83
20	5,399,400	29.81
22	5,750,108	31.75
24	6,092,345	33.64
26	6,458,236	35.66
28	6,781,498	37.44
30	7,095,692	39.18
Total population*	18,112,065	100.00

* Total number of people in the area used for the model and animation

Table 2.7 Population affected by urban flooding in the New York area

Flooding height (m)	Population affected	Percent of total population*
1	240,798	1.17
2	478,033	2.32
3	963,085	4.67
4	1,344,586	6.52
5	1,832,608	8.89
6	2,502,664	12.14
8	3,497,555	16.96
10	4,652,513	22.57
12	5,655,103	27.43
14	6,477,280	31.42
16	7,376,777	35.78
18	8,256,420	40.05
20	9,022,190	43.76
22	9,816,514	47.62
24	10,466,181	50.77
26	11,103,041	53.86
28	11,672,852	56.62
30	12,184,647	59.10
Total Population*	20,616,311	100.00

* Total number of people in the area used for the model and animation

Powerpoint®. The images are arranged sequentially to simulate the rise of sea level from 1−30 m (or, 80 m in the case of some of the global and regional animations). Finally, the sequential images are exported to an animation file such as .avi or .wmv to create a flipbook animation.

Figure 2.5 illustrates land covered by rising sea levels of 5, 10, 20, and 30 m in several areas including Florida in the US, the Netherlands in Europe, and China in East Asia. The figure includes the number of people worldwide who would be affected by each level of rise. Most areas in Florida would be flooded by a 30-m rise in sea level. Beijing and Shanghai, the two largest cities in China, would be flooded by 10−20 m rises. And, in Europe, the western one-half of the Netherlands would be flooded by a 5-m rise in sea level.

More moderate rises were also modeled to examine localized results. Although the western coast of the US does not normally experience hurricanes, severe storms can occur in the area, including tropical cyclones and tsunamis (Butler 2005). Figure 2.6 displays simulated storm surge flooding in Los Angeles, California. As flood levels increase, the southern part of the city is increasingly flooded. With 30 m flooding, about half the city is inundated.

Simulations for Washington, DC (Fig. 2.7) and New York (Fig. 2.8) show significantly larger land areas affected by sea level rise. Examining these figures with Tables 2.6 and 2.7 demonstrates how low east coast elevations expose more people to inundation at low levels of rise.

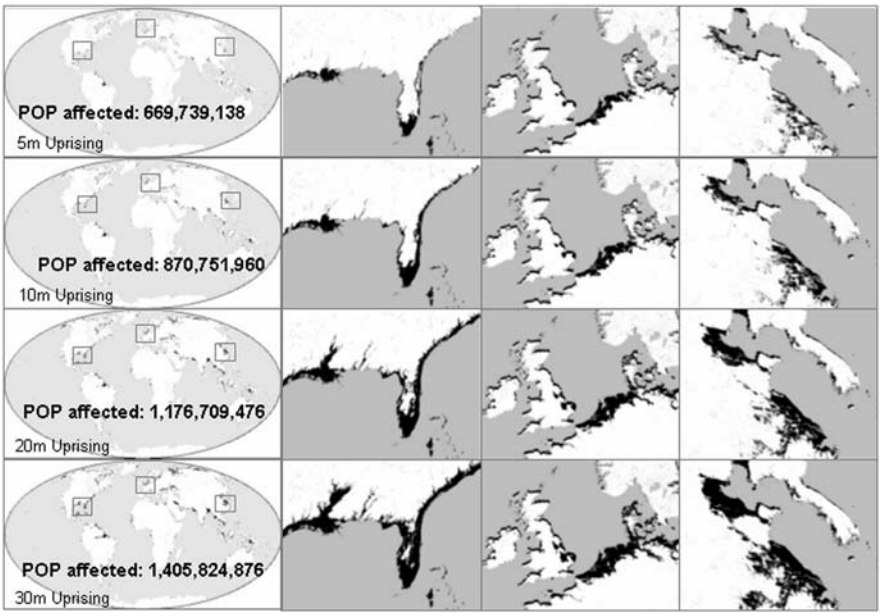

Fig. 2.5 Land loss in selected areas and global population affected

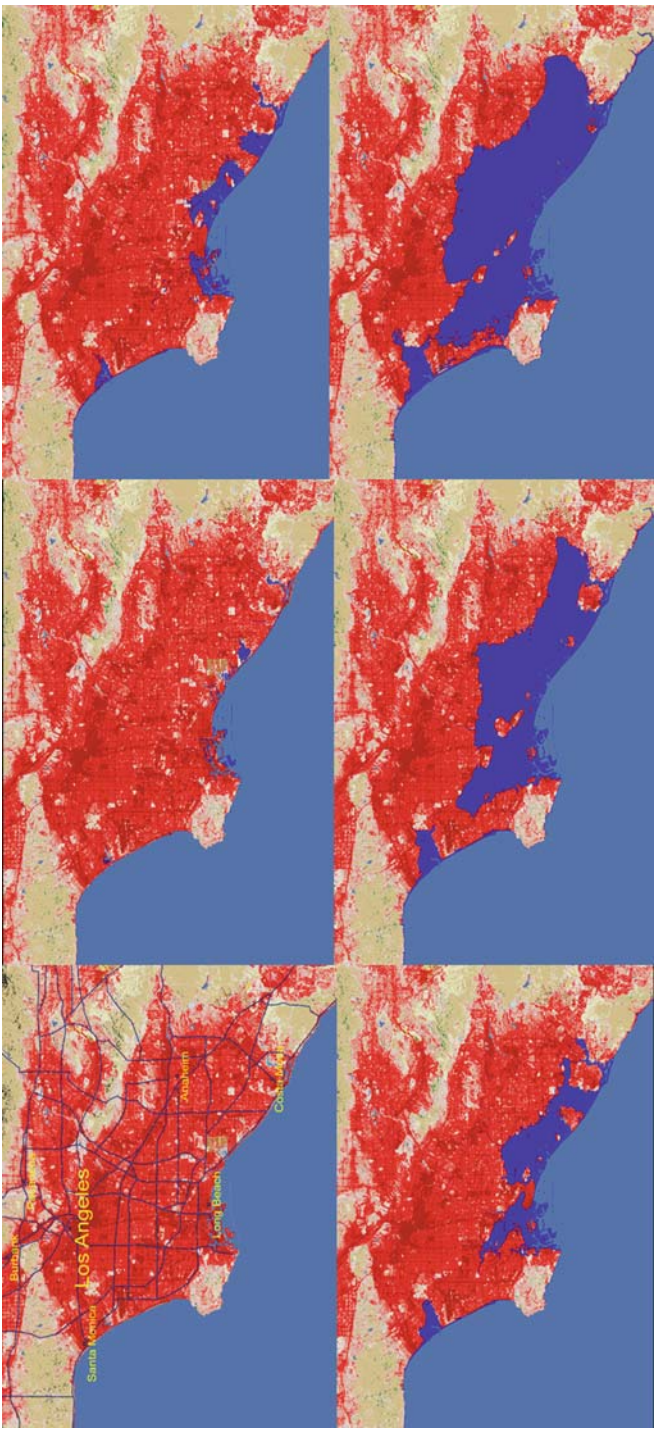

Fig. 2.6 Storm surge flooding simulation in the Los Angeles, California area

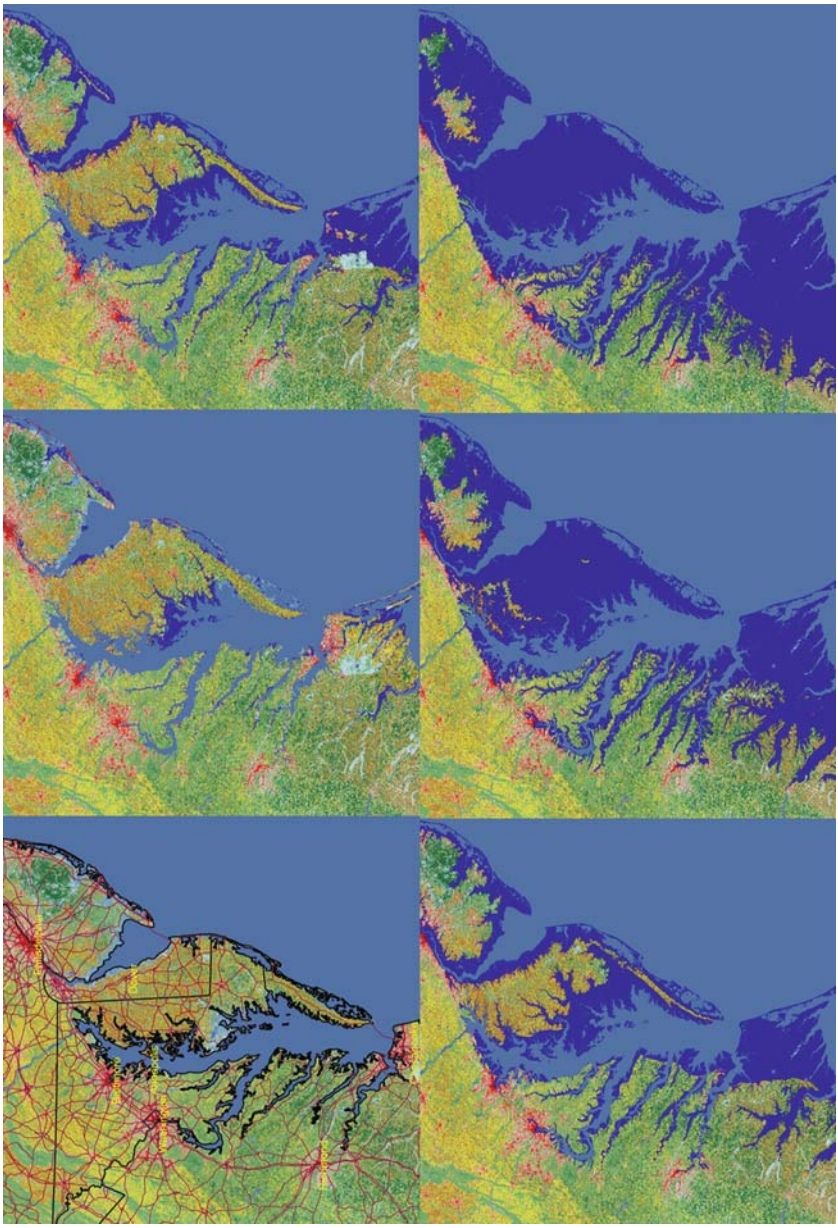

Fig. 2.7 Storm surge flooding simulation in the Washington, DC area

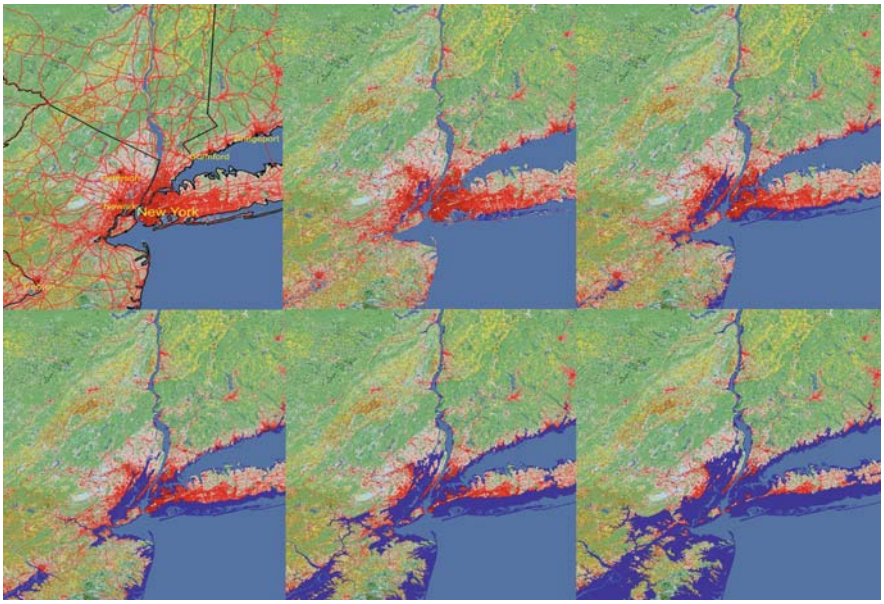

Fig. 2.8 Storm surge flooding simulation in the New York area

Flood simulations such as those shown in Figs. 2.6, 2.7, and 2.8 can help planners focus on areas that may experience inundation, plan evacuation routes, and undertake appropriate mitigation measures. The US Geological Survey is currently producing flood simulation animation files for all US coastal areas using 30 m elevation, land cover, and population data. The 90 m SRTM data are being used to produce animations for major urban areas along the world's coasts. These global animations with regional enlargements have been created with data at 30 arc-sec resolution for elevation, land cover, and population. All of these animations are available at http://cegis.usgs.gov/sea_level_rise.html.

2.6 Conclusion

Large numbers of people living in rural and urban coastal areas are at risk from sea-level rise and storm surge. Using a multi-scale approach, sea-level rise at global and regional scales and storm surge effects at local and urban scales were modeled. Modeling sea-level rise effects across the globe utilized land cover, elevation, and population at 30 arc-sec resolution projected and resampled to 1 km raster cells. Results show that a 5 m rise in sea level would potentially affect about 700 million people; of these, 125 million live in urban and built-up areas. A 30 m rise places 1.4 billion, or 23 percent, of the world's people in areas of risk.

Storm surge modeling for Los Angeles, Washington, DC, and New York is based on 30 m resolution data for land cover, elevation, and population. Southern Los

Angeles has relatively low elevation so that area is easily flooded. Raising sea level 1 m in the Los Angeles area would inundate locations occupied by over 95,000 people; a 1 m rise in Washington, DC and New York will affect over 220,000 and 240,000 people, respectively. In Los Angeles, a 5 m rise would affect over 350,000 people, whereas, in Washington, DC and New York, a similar rise inundates over 1,900,000 and 1,800,000 people, respectively. And a 10 m rise in global sea level would affect more than 8 million people in these three urban areas.

The methods presented in this chapter are used with available global and regional datasets, limiting the ability to model small sea level change, such as the 3.5 mm that is now occurring each year. Higher resolution datasets, such as elevation data from LIDAR placed on a 10 cm grid, can be used to model small rises in sea level using the same methods outlined here. These methods provide a basis for visualizing risk and can help guide urban planning, development and evacuation decisions.

Future research includes the development of complete datasets at 30 m resolution for the United States and at 90 m for selected parts of the world where large coastal populations are found. An interactive capability allowing users to access these datasets on the World Wide Web to conduct user-selected area of interest simulations is also being developed. Such an interactive capability will permit GIS laymen and the general public to educate themselves and others to the potential harm of global warming through "playing" with the website with different simulations, adjusting areas to those of immediate interest. Additionally, simulations incorporating high resolution LIDAR data are being created and further refinements are being added, such as data layers containing boundaries and place names.

References

Arctic Climate Impact Assessment. (2005). *Arctic Climate Impact Assessment*. Cambridge: Cambridge University Press, 1042.

Arendt, A.A., Echelmeyer, K.A., Harrison, W.D., Lingle, C.S., and Valentine, V.B. (2002). Rapid wastage of Alaska glaciers and their contribution to rising sea level. *Science*, Volume 297. no. 5580, 382–386.

Beckley, B.D., Lemoine, F.G., Luthecke, S.B., Ray, R.D., and Zelensky, N.P. (2007). A reassessment of global and regional mean sea level trends from TOPEX and Jason-1 altimetry based on revised reference frame and orbits. *Geophysical Research Letters*, Volume 34, L14608.

Butler, R. (2005). Hurricane could hit San Diego. Web document. mongabay.com. http://news.mongabay.com/2005/0908-san_diego.html.

Cazenave, A., and Nerem, R.S. (2004). Present-day sea level change: Observations and causes. *Reviews of Geophysics*, Volume 42, RG3001.

Chambers, D. (2008). Causes and effects of sea-level rise. Presentation to the National Research Council Mapping Sciences Committee, April 24, 2008.

Chambers, D.P. (2006). Observing seasonal steric sea level variations with GRACE and satellite altimetry. *Journal of Geophysical Research*, Volume 111, C03010.

Chao, B.F., Wu, Y.H., and Li, Y.S. (2008). Impact of artificial reservoir water impoundment on global sea level. *Science*, Volume 320, 212–214, 11 April.

Church, J.A., and White, N.J. (2006). A 20th century acceleration in global sea-level rise. *Geophysical Research Letters*, Volume 33, L01602.

Comiso, J.C., Parkinson, C.L., Gersten, R., and Stock, L. (2008). Accelerated decline in the Arctic sea ice cover. *Geophysical Research Letters*, Volume 35, L01703.

Das, S.B., Joughin, I., Hehn, M.D., Howat, I.M., King, M.A., Lizarralde, D., and Bhatia, M.P. (2008). Fracture propagation to the base of the Greenland ice sheet during Supraglacial Lake drainage. *Science*, Volume 320, 778–781, 9 May.

Demark, T. (2005). Before and after images of areas affected by the Indian Ocean Tsunami, Web document. http://homepage.mac.com/demark/tsunami/9.html.

Douglas, B.C., Kearney, M.S., and Leatherman, S.P. (2001). *Sea-level rise: History and consequences*. New York: Academic Press.

FEMA. (2007). About Louisiana Katrina flood recovery maps. Web document. FEMA. http://fema.gov/hazard/flood/recoverydata/katrina/katrina_la_index.shtm.

Fricker, H.A., Scambos, T., Bindschadler, R., and Padman, L. (2007). An active subglacial water system in West Antarctica mapped from space. *Science*, Volume 315, 1544–1548, 16 March.

Gehrels, W.R., Hayward, B.W., Newnham, R.M., and Southall, K.E. (2008). A 20th century acceleration of sea-level rise in New Zealand. *Geophysical Research Letters*, Volume 35, L02717.

Holgate, S.J. (2007). On the decadal rates of sea level change during the twentieth century. *Geophysical Research Letters*, Volume 34, L01602.

Horton, R., Herweijer, C., Rozenzweig, C., Liu, J., Gormitz, V., and Ruane, A.C. (2008). Sea-level rise predictions for current generation CGCMd based on the semi-empirical method. *Geophysical Research Letters*, Volume 35, L02715.

Intergovernmental Panel on Climate Change (IPCC). (2007). *Climate change 2007: The physical science basis*. In S. Solomon, D. Qin, M. Manning, M. Marquis, K. Averyt, M. Tignor, H.L. Miller, Jr., and Z. Chen (Eds.). Cambridge: Cambridge University Press. Web document. http://ipcc-wg1.ucar.edu/wg1/wg1-report.html. Accessed 10 May 2008.

Jenkins, A., and Holland, D. (2007). Melting of floating ice and sea-level rise. *Geophysical Research Letters*, Volume 34, L16609.

Joughin, I., Abdalati, W., and Fahnestock, M. (2004). Large fluctuations in speed on Greenland's Jakobshavn Isbræ glacier. *Nature,* Volume 432, 608–610, 2 December 2004.

Joughin, I., Das, S.B., King, M.A., Smith, D.E., Howat, I.M., and Moon, T. (2008). Seasonal speedup along the western flank of the Greenland ice sheet. *Science*, Volume 320, 781–783, 9 May.

Kolker, A.S., and Hameed, S. (2007). Meteorological driven trends in sea level rise. *Geophysical Research Letters*, Volume 34, L23616.

Landscan. (2005). 2005 Global Population Database Release, Web document. http://www.ornl.gov/sci/landscan/landscanCommon/landscan05_release.html. Accessed 8 December 2008.

Marcos, M., and M. N. Tsimplis (2007). Forcing of coastal sea level rise patterns in the North Atlantic and the Mediterranean Sea. *Geophysical Research Letters*, Volume 34, L18604.

McGee, W.J. (1900). The lessons of Galveston. *National Geographic*, October, 377–378.

Miller, L., and Douglas, B.C. (2004). Mass and volume contributions to twentieth-century global sea-level rise. *Nature*, Volume 428, 406–409, 25 March.

NOAA. (2007). Hurricane Katrina—Most destructive hurricane ever to strike the US Web document, NOAA. http://www.katrina.noaa.gov.

Poore, R.Z., Williams, R.S., Jr., and Tracey, C. (2000). Sea level and climate. *USGS Fact Sheet 002–00*.

Rignot, E., and Kanagaratnam, P. (2006). Changes in the velocity structure of the Greenland ice sheet. *Science*, Volume 311, 986–990, 17 February.

Schiefer, E., Menous, B., and Wheate, R. (2007). Recent volume loss of British Columbian glaciers, Canada. *Geophysical Research Letters*, Volume 34, L16503.

Seong, J.C., and Usery, E.L. (2001). Modeling raster representation accuracy using a scale factor model. *Photogrammetric Engineering and Remote Sensing*, Volume. 67, no. 10, 1185–1191.

Seong, J.C., Mulcahy, K.A., and Usery, E.L. (2002). The Sinusoidal Projection: A new meaning for Global Image Data. *The Professional Geographer*, Volume 54, no. 2, 218–225.

Shepherd, A., and Wingham, D. (2007). Recent sea-level contributions of Antarctic and Greenland ice sheets. *Science*, Volume 315, 1529–1532, 16 March.

Steinwand, D. (2003). A new approach to categorical resampling, Proceedings. American Congress on Surveying and Mapping Annual Convention, Phoenix, AZ. Web document. http://www.acsm.net/sessions03/NewMethodologies41.pdf. Accessed April 2007.

Thomas, R.H. (1993). Ice Sheets. In R.J. Gurney, J.L. Foster, C.L., and Parkinson (Eds.), *Atlas of Satellite Observations Related to Global Change*. Cambridge, UK: Cambridge University Press, 385–400.

Truffer, Martin and Mark Fahnestock. (2007). Rethinking ice sheet time scales. *Science*, Volume 315, 1508–1510, 16 March.

Usery, E.L., and Seong, J.C. (2001). All equal area map projections are created equal, but some are more equal than others. *Cartography and Geographic Information Science,* Volume 28, no. 3, 183–193.

Usery, E.L., Finn, M.P., Cox, J.D., Beard, T., Ruhl, S., and Bearden, M. (2003). Projecting global datasets to achieve equal areas. *Cartography and Geographic Information Science*, Volume 30, no. 1, 69–79.

USGS. (2008a). Products related to Hurricanes Katrina and Rita. Web document. http://store.usgs.gov/mod/HurricaneAreas.html.

USGS. (2008b). Decision support system for map projections of small scale data. US Geological Survey. Web document. http://mcmcweb.er.usgs.gov/DSS/, Accessed May.

Vaughan, D.C., and Arthern, R. (2007). Why is it hard to predict the future of ice sheets? *Science*, Volume 315, 503–1504, 16 March.

Wadhams, P., and Munk, W. (2004). Ocean freshening, sea level rising, sea ice melting. *Geophysical Research Letters*, Volume 31, L11311.

Weaver, A.J., Saenko, O.A., Clark, P.U., and Mitrovica, J.X. (2003). Meltwater pulse 1A from Antarctica as a trigger of the Bølling-Allerød warm interval. *Science*, Volume 299, no. 5613, 1709–1713.

Zebrowski, E., Jr. (1999). *Perils of a Restless Planet: Scientific Perspectives on Natural Disasters*. Cambridge: Cambridge University Press (First paperback edition).

Zwally, H.J., Brenner, A.C., and DiMarzio, J.P. (1998). Growth of the southern Greenland Ice Sheet. *Science*, Volume 281, 1251a, 28 August.

Chapter 3
Urban Expansion and Sea-Level Rise Related Flood Vulnerability for Mumbai (Bombay), India Using Remotely Sensed Data

Firooza Pavri

Abstract Rapid growth and expansion of the developing world's urban areas has both social and biophysical consequences such as increased population density, inadequate infrastructure and services, the expansion of impermeable surfaces, and habitat fragmentation with a loss of green space. Data from NASA's Landsat and Shuttle Radar Topography Mission (SRTM) programs are employed to examine urban patterns between 1973 and 2004 for the coastal mega-city of Mumbai (formerly Bombay), India. By 2015 Mumbai is expected to be the world's second largest city containing 22.6 million people with one of the highest population densities (UN Population Division 2006). This chapter considers the city's ongoing and future vulnerability to flood hazards in the light of climate change models predicting an increased intensity of monsoonal storms, as well as a 0.38−0.59 m sea level rise by the end of the 21st century. Landsat MSS and ETM+ data are used to map change in urban patterns, while an unsupervised classification produces a land use map for the city and its environs. SRTM data are used to build an elevation model which is analyzed in conjunction with the land use map. Zones of vulnerability to floods are identified for the city and its environs. The results suggest that the predicted consequences of climate change will exacerbate the city's ongoing vulnerability to flooding if urgent measures are not taken to improve storm water drainage systems and shore up other flood control defenses.

Keywords Urban expansion · Vulnerability · Sea-level rise · Satellite data · Mumbai (Bombay) · India

3.1 Introduction

On July 26, 2005 a severe 24-hour monsoon event resulted in close to 965 mm of rain falling in the city of Mumbai (formerly Bombay), the commercial and financial

F. Pavri (✉)
Department of Geography-Anthropology, University of Southern Maine, Gorham, ME 04038, USA
e-mail: fpavri@usm.maine.edu

P.S. Showalter, Y. Lu (eds.), *Geospatial Techniques in Urban Hazard and Disaster Analysis*, Geotechnologies and the Environment 2, DOI 10.1007/978-90-481-2238-7_3,

capital of India. The ensuing disastrous flooding led to loss of life, property damage that rose into the millions, epidemic threats, and the city coming to a grinding halt for days (TNN 2005a). While the monsoonal event was unusual in its severity and was coupled with astronomical high tides, the vulnerability of the city to climate hazards is not new. The city has long struggled with regular monsoon-related floods owing to antiquated sewer and flood control infrastructure, now clearly unable to cope with the level of population explosion and development witnessed over the past 50 years.

The most recent and definitive (to date) report by the Intergovernmental Panel on Climate Change (IPCC) has confirmed the global threat of rising sea levels and extreme weather patterns to coastal regions (Nicholls et al. 2007). Across South Asia, research suggests that sea level rise will test the coping capacity of coastal cities to their limits, while a study ranking India's coastal zones by their vulnerability found Mumbai to be the most likely to experience considerable damage from sea level rise (Nicholls 1995; Nicholls et al. 2007; TERI 1996; Wilbanks et al. 2007). A recent United Nations' report on World Urbanization Prospects has projected that by 2015 the Mumbai Metropolitan region of India will be the world's second largest urban agglomeration with 22.6 million people, up from its current 18 million residents (UN Population Division 2006). This increase will only add to already overburdened city services and result in predictable demands on housing, infrastructure and transportation. Added to this, Mumbai's island orientation, high population density, lack of suitable housing for a vast section of its population, and its vulnerability to persistent flooding will further complicate planning efforts.

The growth and expansion of urban areas creates a variety of impacts with both social and biophysical consequences. In the 21st century, the mega cities of the world will be primarily concentrated in developing nations where resources are limited and the ability of local governments to provide services are already stretched to their breaking point (UN Population Division 2006). Population density is particularly high in the developing world's cities and can be problematic on a number of fronts. Governments often fall short in providing infrastructure and services, preserving intra-city green space, and crafting adequate disaster management plans (Demographia 2007). Furthermore, urban sprawl leads to leapfrog development as the growth of satellite towns and bedroom communities expand into the rural hinterlands, consuming essential agricultural land. The expansion of urban surfaces also reduces ground permeability and increases runoff and the risk for flooding. The semi-variable predictability of seasonal rainfall like the monsoon, while providing residents with some opportunity for preparation, can still have very different impacts even within neighborhoods and households based on housing structure, the floor a resident occupies, and socio-economic status.

Historically, hazards researchers have sought to identify and provide practical risk reduction alternatives to perilous environmental conditions including severe meteorological, hydrological or geological events and their consequences. This work commonly provided human-engineered solutions to minimize threats faced by populations (Barrows 1923; White 1964). The now well established field of vulnerability research traces its roots back to this earlier hazards work. Vulnerability

research recognizes that human systems are inextricably linked to understanding the variable impact of hazards on individuals and their abilities to cope, resist and recover from these hazards (Blaikie et al. 1994, p. 9; Burton et al. 1993; Cutter 1996; Cutter et al. 2000; Few 2003; Hewitt 1997; Kasperson et al. 1995; Smith 1992).

More generally, vulnerability research helps clarify and make explicit the connections between hazard events and their impact on the coping capacity of populations based on their socio-economic and demographic characteristics. Hazard events have traditionally been considered momentous events such as earthquakes and tsunamis or extreme weather related occurrences such as hurricanes. Recent vulnerability research has expanded the definition of hazard to include longer term evolving conditions such as drought, desertification, pollution, deforestation, and more recently conditions related to climate change such as sea level rise and changing precipitation patterns. Vulnerability research has much to contribute in terms of assessing the impact of a changing environment on affected populations. Furthermore, the focus on coping capacities and adaptations to these changing conditions offers important policy prescriptions to help tackle this situation.

The use of satellite imaging technology to monitor urban environments in the developing world is rapidly expanding (Alrababah and Alhamad 2006; Al Rawashdeh and Saleh 2006; Ji et al. 2001; Kaya 2007; Kwarteng and Chavez 1998; Maktav and Erbek 2005; Mundia and Aniya 2005; Weber et al. 2005; Zhang et al. 2002). Remote sensing technology can be particularly useful given the paucity and limited accessibility of data from some parts of the developing world. Vulnerability research, in particular, has been hindered by the dearth of reliable data to feed its data rich models. Analysis of satellite imagery provides one step toward filling this data void. This technology also allows for quick assessments and hence can be practical for post-hazards adaptation and rescue and recovery operations. Thus far, systematic studies using satellite imagery to monitor urban growth patterns and map flood vulnerability zones for Mumbai and its immediate surrounding are largely lacking (TNN 2005b). As researchers have suggested, such assessments provide necessary information for decision-makers and are an important first step to identifying effective urban planning options in the face of hazard events (Maktav et al. 2005). Mumbai is often promoted as the financial and commercial capital of one of the world's fastest growing economies. If the city is to sustain such growth and provide an acceptable quality of life for its citizens, its planners, as a first step, will need to monitor existing sprawl patterns and their impact on habitat fragmentation, flood vulnerability and the population's ability to cope with changing environmental conditions.

3.2 Background

Located on the west coast of India by the Arabian Sea, Mumbai's history can be traced back to seven original islands reclaimed and filled-in over centuries. The seven original islands currently contain most of the older part of the city and its central business district (CBD). Ruled by various regional Hindu and Muslim rulers,

it was not until the landing of Francis Almeida and the Portuguese take-over in 1534 that this deep natural harbor was named *Bom Bahia* (the Good Bay). In 1668 the islands were acquired by the British East India Company, who later shortened the name to Bombay, and made it their Company headquarters. This marked the turning point in Bombay's history. Thereafter the city grew in size from 13,726 in 1780 to 977,822 by 1906, fed largely by early merchant migrants and those interested in commerce (TIFR 1999a). Post-independence expansion and the large influx of rural migrants contributed to the current approximate size of 18 million (MMRDA 2003). In 2001, population density for the Greater Mumbai Metropolitan region was reportedly at 27,715 people per square kilometer, and second only to Hong Kong, China (Demographia 2007; MMRDA 2003).

Today, Mumbai is a microcosm of larger India. It has an ethnically and religiously diverse population, tens of different languages spoken by its newer migrants, and citizenry living at the extremes of staggering wealth or abject poverty typical of the developing world. Aptly named "Maximum City" in a recent account of the metropolis, the city's "larger than life" aura is apparent to even the most casual visitor (Mehta 2004). Geographically, the greater metropolitan region of Mumbai spans approximately 482 km^2 with much of the city's coastline at or just above sea level. The island of Mumbai has an average elevation ranging between 10 and 15 m with the highest point found in the city's northern section at 460 m. Mumbai experiences southwest monsoons between the months of June through September, with an average rainfall of 1800 mm (TIFR 1999b).

The rapid urbanization experienced by the city and its environs over the past four decades has left planners struggling to cope. Development is often unplanned with once small suburbs and neighboring towns becoming overnight bedroom communities and cities in their own right with minimal improvements in infrastructure and amenities. Recent data indicate that the rate of growth in the outlying suburbs and satellite towns has far outpaced that observed within the city (MMRDA 2003). For example, Navi Mumbai (formerly New Bombay), conceived in 1971, is one of the largest planned cities in the world and was designed to accommodate approximately 2 million residents and alleviate some of the population pressures experienced by Mumbai (MMRDA 2003). Today, however, it is widely recognized that even though the planned city contained approximately 704,000 residents in 2001, it failed to draw some of the more important business and employment opportunities away from Mumbai (MMRDA 2003). For the most part, Navi Mumbai serves as a bedroom community to its larger neighbor across the creek. On the other hand, Mumbai's shanty town or slum population has steadily increased to a staggering 50% of the city's population (MMRDA 2003). These densely packed parcels of land contain makeshift huts and inadequate infrastructure (Leahy 2008). One example is Dharavi, also infamously known as Asia's largest slum, which houses approximately 60,000 families and is located in a low lying district close to the center of the city (Leahy 2008). For the most part, slums are interspersed on open land throughout the city and abut high rise apartments, which themselves command astronomical prices comparable to many of the developed world's megalopolises.

The island orientation of the main city of Mumbai, with limited space for expansion, has led to a steady destruction of green space and fringing coastal wetlands, compounding the effects of habitat fragmentation and stretching ecosystem resources and services to their breaking point. Despite this, Mumbai is one of the few mega cities of the world with a National Park within its geographic boundaries. Besides being the largest park in the world within a metropolitan city, the Sanjay Gandhi National Park (SGNP) occupies a vast section of the north-central portion of the city and houses three important water reservoirs specifically for the city's populace. However, the encroachment of shanty towns and housing developments within and along the park boundary has been steady and unabated, spurred on by strong development pressures (Zerah 2007). Likewise, fringing coastal mangroves on both the eastern and western coasts of the city, while theoretically protected by coastal zone development moratoriums, face constant development and encroachment pressures.

The Mumbai Metropolitan Region Development Authority (MMRDA) is responsible for the planning goals of the city. The Authority includes an Emergency Operations Center and develops emergency management and hazard response plans. This agency also assesses risk and vulnerability to a myriad of hazards including cyclones, earthquakes, epidemics, and industrial disasters and outlines response scenarios (MMRDA 1999). Even with these agencies in place, inadequate response during the catastrophic flooding of July 2005 made obvious the deficiencies in the city's emergency response infrastructure (TNN 2005c). Basic emergency response systems such as ambulance, fire and rescue services were unable to operate; rail and other transport links stalled, and electricity for vast sections of the city was not restored for days. Despite India having much past experience coping with natural disasters, researchers have puzzled over the weak response of the Indian government to hazard events in general (Ray-Bennett 2007).

This chapter uses data from the US National Aeronautics and Space Administration's (NASA) Landsat and Shuttle Radar Topography Mission (SRTM) programs to analyze urban sprawl patterns for Mumbai city and its surroundings from 1973 through 2004. Particular attention is given to the contraction of green space due to sprawl, in-filling of open city space, leapfrog urban development patterns, and identifying flood vulnerable zones. Recent climate models predict a global sea level rise of anywhere between a 0.38 and 0.59 m by the end of the 21st century with significant local variations (Meehl et al. 2007). In the case of Mumbai not only would sea level rise have a very significant impact, but additionally, more severe monsoonal activity and increased precipitation as also predicted by general circulation climate models would compound its vulnerability (Meehl et al. 2007). By using readily downloadable multispectral data through NASA's Landsat mission and merging these with elevation data through the SRTM program, this chapter employs methods tested and accepted in the conventional literature to assess the potential impact of predicted sea-level rise for the greater Mumbai Metropolitan region. In so doing, it provides a template for similar such studies for the developing world's coastal cities.

3.3 Data and Methods

Data used for this study were derived from the Landsat program's long historical archive of multispectral imagery. The first image is a Multispectral Scanner (MSS) four band dataset from 9 January 1973 at 79 m spatial resolution and obtained through the Earth Science Data Interface (ESDI) at the Global Land Cover Facility website supported by NASA (GLCF 1997). This image is used primarily to assess the city's urban extent in 1973. The image is one of the earliest cloud-free and downloadable images of the city available from the Landsat archive and provides an important glimpse of the city's geographical extent prior to the recent exponential growth in population. The coarse spatial and spectral resolution of these data, however, limits detailed analyses. Additionally, the lack of data in the region of 400−500 nm limits its use for urban applications.

The second image is a 17 October 2004 gap-filled six band dataset from the Enhanced Thematic Mapper + (ETM+) sensor at 30 m spatial resolution obtained from the Earth Resources Observation and Science (EROS) Data Center (USGS EROS 2006). These data were captured after the ETM+ sensor developed the Scan Line Corrector (SLC) problem, which compensated for the forward movement of the satellite. To correct this problem, the US Geological Survey (USGS) now provides ETM+ gap filled data products using an average DN from previous passes over the same area. In this case, values from a previous pass were used to fill in the SLC missing data. However, filling in these data sometimes causes striping to occur and this is evident on the 2004 ETM+ image. While data from both time periods (1973 and 2004) are not captured during the same time of year, they are acceptable because both were obtained during the dry season. However, because the ETM+ image was acquired in October, it should be noted that the recent end of the monsoons in September of that year will significantly influence the vegetation signal. Given the mismatch in terms of time of capture and the lack of any sensor calibration data for the MSS image, the two images were only visually compared to assess obvious changes in the spatial extent of the city. Most analytical efforts focused on the 2004 ETM+ image to map land use and identify zones of vulnerability.

In addition to the imagery, an SRTM elevation dataset also obtained via the USGS EROS website at 3 arcsec (90 m spatial resolution) is used to construct a digital elevation model for the city and aid in identifying zones of vulnerability to sea level rise and flood events (SRTM 2006). At present, these elevation data are only available at 1 m z-value increments. Consequently, mapping fine-scale vulnerability zones is limited by the dataset and to 1 m increments. While some issues have been raised about the accuracy of the SRTM dataset (Rabus et al. 2003), SRTM are the *only* systematic elevation dataset freely downloadable for most of the globe and as such provide an enormously rich source of information for data poor regions across the developing world. Given the 90 m spatial resolution for these data, they are coarser than that captured by ETM+ and the dataset does contain a few gaps in terms of dropped pixels. However, for the study site, these gaps are minimal and appeared mostly in non-urban areas. Reference data for ground control points

and for accuracy assessments were obtained through a topographic map and high resolution Google Earth™ imagery. All image processing and analysis was conducted using ERDAS® Imagine® software and ESRI's ArcGIS™ was used for an overlay analysis and to produce vulnerability data.

The paper uses existing methodologies and analytical tools established in the literature (Auch et al. 2004; Jensen et al. 2005). False color composites (FCC) for both the 1973 and 2004 datasets using standard stretching and contrast techniques are examined and findings reported. An unsupervised classification procedure is used to build a land use map from the 2004 ETM+ dataset. The Iterative Self Organizing Data Analysis (ISODATA) algorithm in ERDAS®, which uses a minimum distance function to assign pixels to a cluster, is employed (Lillesand et al. 2008). To appropriately capture land surface variability, selecting a suitable number of clusters is an important parameter to take into account when running the ISODATA routine (Mundia and Aniya 2005). After experimentation, 15 clusters were determined to be the most appropriate number for the ETM+ image. After visually inspecting and naming the clusters, the 15 were further reclassed into eight clusters. Accuracy assessments were performed on the ETM+ classified dataset using 256 points generated using a stratified random sample, while high spatial resolution Google Earth™ imagery, local knowledge, and topographic maps of the area were used for verification. The final unsupervised classification results were imported into ArcGIS™ to be analyzed in conjunction with the SRTM elevation dataset. ArcGIS's Spatial Analyst module was used to overlay the SRTM elevation data with land use classes to map and examine vulnerability zones to sea level rise across the city and its environs. Attention was focused on simulating flood vulnerability zones from 1 to 4 m above sea level. While the predicted rise in sea level is less than 1 m over the next 100 years, the ensuing vulnerability to flooding will likely spread across low lying regions. Spatial Analyst's raster calculator functionality is used to calculate land use impacted within the flood vulnerable zones and the areas are mapped to assess their spatial distribution across the city.

3.4 Analysis and Results

The data analysis proceeds in four stages. First, a visual assessment of the 1973 MSS and 2004 ETM+ false color composites are presented, focusing in particular on deciphering urban patterns and changes therein. Next, results of the unsupervised classification and accuracy assessments for the 2004 ETM+ image are discussed. Third, an SRTM elevation model is constructed for the greater metropolitan area. Finally, results from the land use analysis and the SRTM elevation model are combined in ArcGIS's Spatial Analyst to assess the impact of potential climate change on land use activities across the region and identify zones of flood risk.

3.4.1 False Color Composites for 1973 and 2004

A visual assessment of the 1973 MSS false color composite (FCC) of Bands 1, 2, 3 (Fig. 3.1) shows most of the city of Bombay contained within the southern portion of

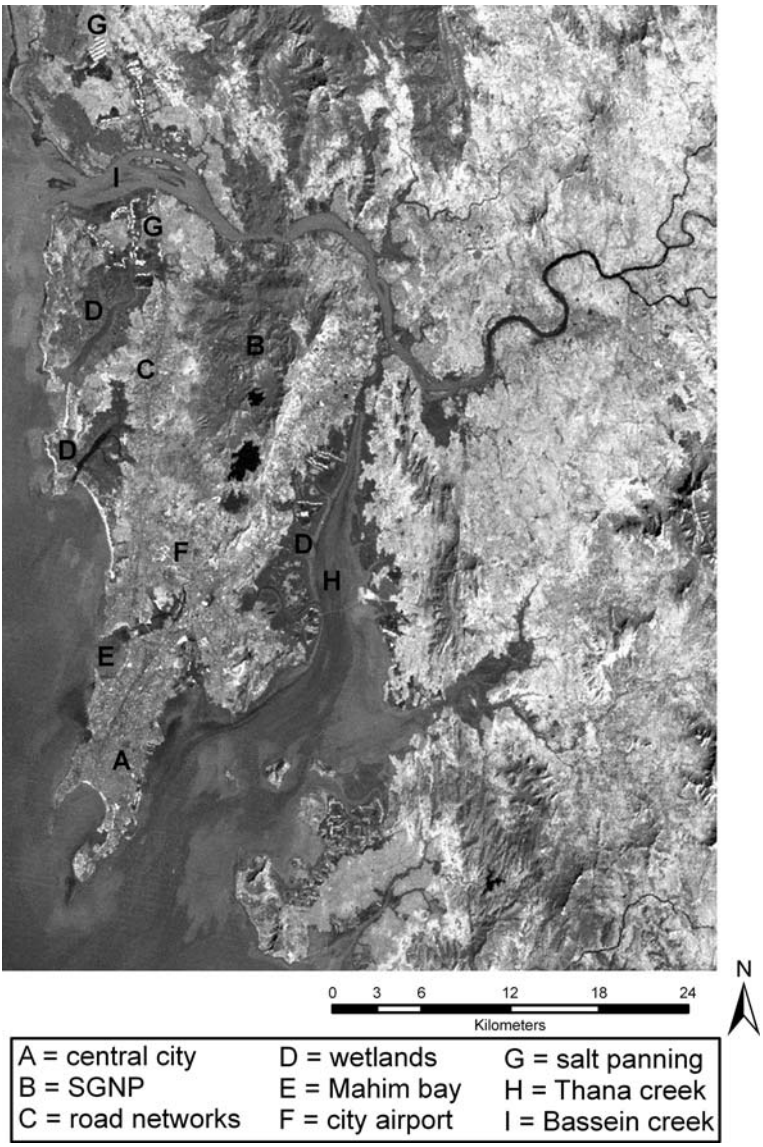

Fig. 3.1 Landsat MSS false color composite for the Greater Mumbai Metropolitan region and surrounding, 1973

the island peninsula ("A" on the bottom left of the figure). Key arterial expressways can be seen extending out from the city center into the northern suburban sections of the island on either side of the Sanjay Gandhi National Park (SGNP; "B"), with some suburban development along either side of these expressways (C). The image shows green space interspersed throughout the city. The SGNP covers a vast section

of the north-central portion of the image. Taken in the month of January, the image displays some mixed tropical deciduous tree cover with leaf-off conditions. Development activities, including cleared tracks, are seen interspersed within and adjacent to the park's boundaries. Also noteworthy are the robust coastal mangroves and estuarine wetlands that border the northeastern and northwestern sections of the island city (D). These habitats are an essential and important protective buffer from tidal surges and cyclonic activity and appear relatively healthy. Extensive mudflats appearing during low tide conditions are also apparent along the eastern coast of the island.

The southern end of the island, south of Mahim bay (E), contains the city's core central business district and original residential areas. It is also in the south end of the island that most reclamation activities were undertaken, and where the original seven islands of Bombay were eventually joined together. In this case, the FCC suggests a fairly dense urban landscape. Urban density declines north of the city's airport (F), which is typified by greater expanses of green space.

Overall, the MSS image from 1973 suggests that the densest concentration of urban activity was largely limited to the southern section of the island. While development is clearly expanding outward from the core old city, it is mostly restricted to areas along the western and eastern expressways that make their way out of the central city and into the island's suburban northern reaches. The mainland to the north of Bassein creek (I) and east of Thana creek (H) is typified by the city's rural hinterland. Agricultural activities dominate here, but for the most part, the data indicate fallow agricultural fields yet to be planted with the winter crop. At this spatial resolution, smaller towns in the rural hinterland are difficult to distinguish. The city of Navi Mumbai across the harbor to the east of the island has not yet been developed. Urban development on the mainland north of the city is also largely absent. For the most part, this land is used for salt panning activities (G). In 1971 the Mumbai Metropolitan Region's population stood at approximately 7.8 million with an annual growth rate of 3.7%, the highest it had seen in its history (MMRDA 2003).

A cursory visual comparison between in the 1973 MSS (Fig. 3.1) and the 2004 ETM+ false color composite (Fig. 3.2) reveals dramatic shifts in land cover over the 30 year period. The obvious changes are in the expansion and intensification of developed land surface across the city and its outlying townships. Also observed is an ensuing contraction of the city's green space. As indicated earlier, the vegetation signal is quite strong because the 2004 image was taken at the end of the monsoon season where almost every non-paved surface is taken over by ephemeral shrubs and grasses. The 2004 image also indicates that the vital coastal mangroves along the main island have are encroached upon by development activities since the time of the 1973 image.

By 2004 the city of Mumbai has seen a tremendous boom in suburbs on the island itself, now occupying virtually all of the open space on the island with the exception of the SGNP. Moreover, the larger region has also witnessed an expansion of new suburbs and satellite towns on the mainland. The cities of Navi Mumbai (A), Thane (B), Kalyan (C), Dombivili (D), Bhiwandi (E) and Panvel (F) on the mainland to the northeast of the city and Mira (G) and Nalasopara (H) to the north of the

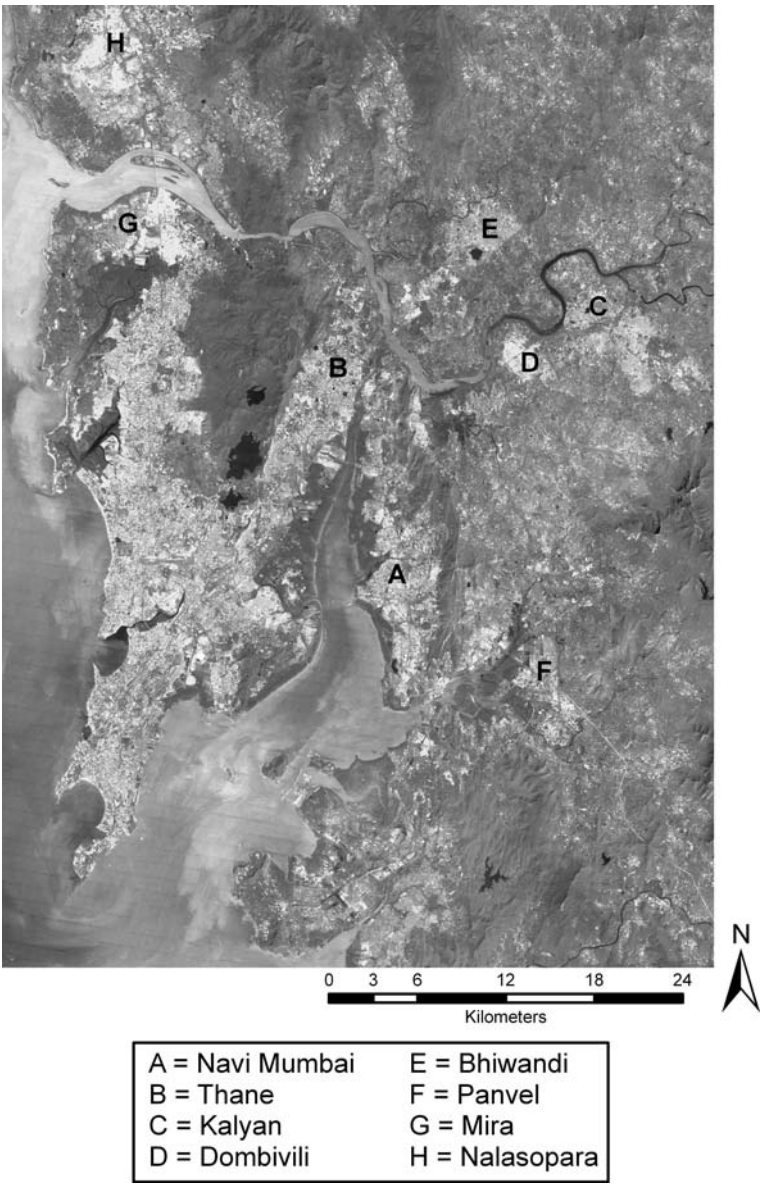

Fig. 3.2 Landsat ETM+ false color composite for the Greater Mumbai Metropolitan region and surrounding, 2004

city were small towns in the 1973 image. Today, they all contain populations of over 100,000 residents, with Thane and Kalyan containing over 1 million residents each (MMRDA 2003). A visual analysis of the changes between 1973 and 2004 indicates these dramatic shifts. Urban expansion for the city and its environs has

been typified by intensification across the island, encroachment into open space along coastal mangroves and green pockets across the city, expansion into outlying suburban areas, and leapfrog development into the rural hinterland especially across the mainland east of the island.

3.4.2 Land Use Classification

Land use classification maps are an effective way to observe spatial patterns. In this case, an ISODATA routine is employed to arrive at a land use map for the city and its surroundings using the 2004 ETM+ dataset. The routine was originally run with a large number of clusters and later collapsed into eight classes representing land use patterns for the city (Fig. 3.3).

Quantifying the accuracy of any classification routine is a necessary step toward building confidence in the results. For the accuracy assessment, a stratified random sample of 256 pixels with a minimum of 20 pixels per class was generated to ensure coverage of all eight cover classes and to minimize bias. These reference pixels are checked against 3 m high spatial resolution Google Earth^{TM} imagery and substantiated by extensive local knowledge and topographic maps. The results of the error matrix generated indicate an overall classification accuracy of 83.5% (Table 3.1). The overall Kappa index of agreement, which indicates the extent to which the assignment of pixels in the error matrix were due to "true" versus "chance" agreement, was reported at 0.81 (Lillesand et al. 2008). In terms of Producer's Accuracy all classes were above 70% with the exception of the Encroaching Development class at 60.71%. All classes were above 70% in terms of User's Accuracy. The important Urban/Developed class was at 81.25 and 72.22% for Producer's and User's Accuracy respectively. Overall, the ISODATA routine, a simple yet powerful algorithm, provided better than expected results in terms of producing a final land cover map. The map was exported into ArcGIS's Spatial Analyst for further analysis.

3.4.3 SRTM Elevation Model

SRTM data were downloaded and imported into ArcMap for further analysis (Fig. 3.4). Figure 3.4 uses a color palette to distinguish elevation above sea level, and large expanses of land can be seen at or just above sea level for the greater metropolitan region of Mumbai.

Table 3.2 reports the spatial coverage of elevation zones across the image. Particularly noteworthy is the extent of land under a 4 m elevation cut-off. On the main island of Mumbai, these areas are also some of the more densely packed sections of the city and with low to middle income housing. Strikingly, this section of the island city was particularly impacted by the severe monsoon event and flooding of 2005 referenced at the beginning of this chapter. Low lying areas across the city

Fig. 3.3 Land use map using ETM+ data for the Greater Mumbai Metropolitan region and surrounding, 2004

are already prone to flooding. In many cases, this area houses some of the city's poorer shanty town residents who are already economically vulnerable and whose ability to cope with and recover from hazard events is very limited. The flood of 2005 produced large numbers of fatalities from these areas (TNN 2005d).

Table 3.1 Error matrix for the Greater Mumbai Metropolitan region land use map derived from Landsat ETM+ data

Land-use class	1	2	3	4	5	6	7	8	Total	Producer's accuracy	User's accuracy	Kappa statistic
1	*38*	0	0	0	0	0	0	0	38	100.00	100.00	1
2	0	*20*	0	0	0	0	0	0	20	100.00	100.00	1
3	0	0	*18*	0	2	1	0	0	21	81.82	85.71	.84
4	0	0	0	*23*	1	1	3	2	30	92.00	76.67	.74
5	0	0	2	0	*26*	6	2	0	36	81.25	72.22	.68
6	0	0	1	0	3	*17*	3	0	24	60.71	70.83	.67
7	0	0	1	1	0	0	*36*	2	40	70.59	90.00	.87
8	0	0	0	1	0	3	7	*36*	47	90.00	76.60	.72
Total	38	20	22	25	32	28	51	40	–	–	–	–

Overall classification accuracy = 83.5%
Kappa Index of Agreement = 0.81

Land Use Class Index: 1 Water; 2 Inland Waterways; 3 Mud flat/urban surface; 4 Coastal/ Riverine marsh/Green cover; 5 Urban/Developed; 6 Encroaching Development; 7 Agricultural Land/Undeveloped Urban; 8 Green space

3.4.4 Land Use and SRTM Overlay Analysis

The SRTM elevation model is used in conjunction with the land use map to calculate the areal size of each of the land use classes contained within 0−1 m, 1−2 m, 2−3 m and 3−4 m elevation zones (Table 3.3). These are identified as critical, severe, high and moderate risk zones for flooding, respectively.

Given the predicted 0.38−0.59 m rise in sea level over the next 100 years and increased severity of storms, these zones will be subject to the most hazardous flood conditions. It is here that efforts need to be focused to build more effective flood control measures, redesign housing structures, or perhaps even resettle populations and development activities over the next 50–100 years. While the total amount the of Urban/Developed land use class within the 0−1 m critical flood vulnerability zone comprises a relatively small area of 3.05 km^2, when one considers the high population density for the metropolitan region at 27,715 km^2 reported in 2001 (Demographia, 2007), that area could amount to as many as approximately 83,000 affected people (see Table 3.3). Additionally, vulnerability will not just be contained to the predicted approximate 0.58 m sea level rise zone – its effects would permeate across most low lying areas of the city, with its impact compounded in economically poor neighborhoods.

The two land uses affected the most significantly between 0 and 4 m in elevation vulnerability zones include the Coastal/Riverine marsh/Green cover class for a total of 12.7 km^2 and the Urban/Developed class for a total of 11.6 km^2 (see Table 3.3). This finding suggests that mangrove areas already under pressure from present development will face additional pressures from sea level rise and flood vulnerability and perhaps, as observed elsewhere, will affect the configurations of

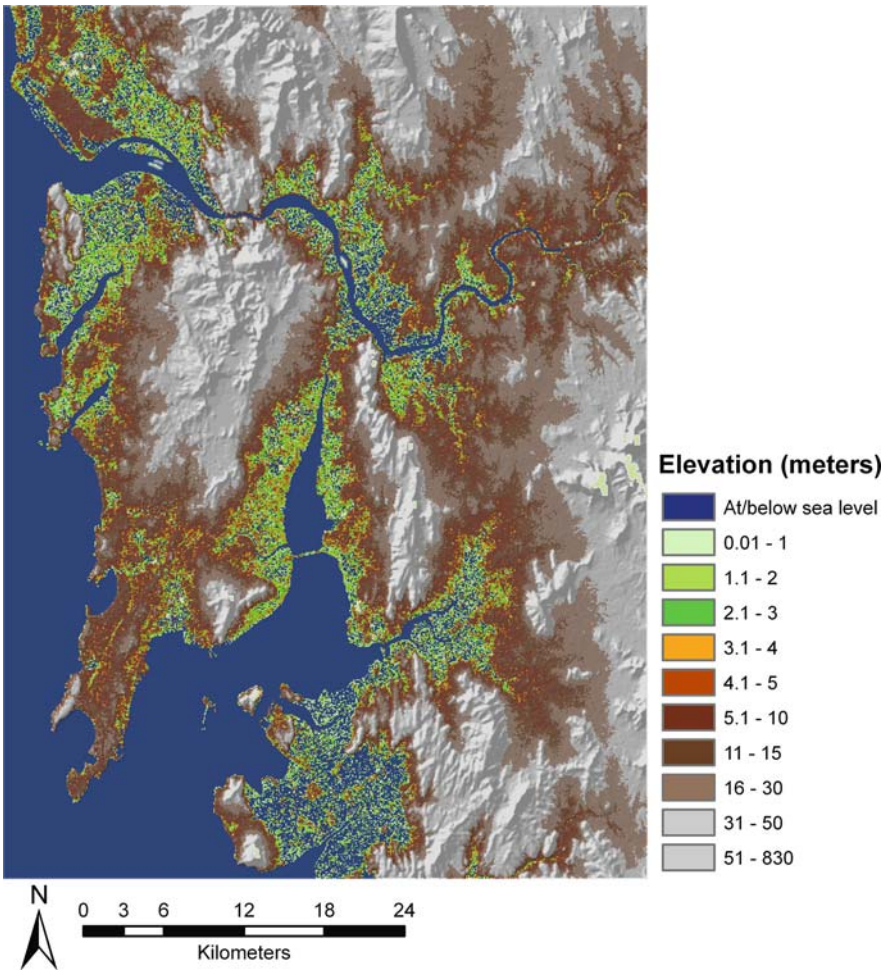

Fig. 3.4 SRTM elevation model for the Greater Mumbai Metropolitan region and surrounding

wetland species. Of more concern would be the area of the Urban/Developed class that falls within the 4 m vulnerability zone. The coping strategies and local response to these conditions at present involve ad-hoc household level adaptations and a reliance on kinship networks to survive periodic flood conditions. However, with the increased severity and frequency of these conditions, longer term response measures will need to be developed. The data from this analysis suggest that a very significant proportion of the city and its suburbs will be subject to more persistent hazardous conditions based on climate predictions for the next 50–100 years.

To date, Mumbai has utilized large World Bank loans for piecemeal improvements in potable water and drainage infrastructure. However, as most citizens will attest, these improvements are short lived as population densities increase and sheer numbers of people overwhelm city services. To have more long lasting benefits,

Table 3.2 Land area at or above sea level for the Greater Mumbai Metropolitan region using SRTM data

Elevation (m)	Area coverage (in km^2)
0–1	101.5
1–2	95.5
2–3	85.3
3–4	74.7
4–5	67.8
5–10	320.8
10–15	276.0
15–30	495.3
30–50	275.9
50–150	375.0
50–830	181.6

Table 3.3 Extent of land use (in square kilometers) within flood vulnerability risk zone

Land use	0−1 m (critical)	1−2 m (severe)	2−3 m (high)	3−4 m (moderate)
Mud flat/urban surface	1.28	1.01	0.82	0.61
Coastal/Riverine marsh/Green cover	3.79	3.40	2.73	1.87
Urban/Developed	3.05	3.05	2.82	2.69
Encroaching Development	0.75	0.81	0.97	0.76
Agricultural Land/Undeveloped Urban surfaces	1.09	1.21	1.34	1.50
Green space	0.37	0.45	0.45	0.47

efforts to tackle flood vulnerability need to be considered from several angles. The city's planners and governance bodies need to give more serious consideration to updating and expanding storm drainage systems and flood control barriers and defenses, protect the city's natural mangrove defenses from development activities and expand mangrove coverage, engage in politically charged slum redevelopment schemes to provide adequate housing, and shore up the city's disaster response systems, all of which have been promised for decades. Perhaps the information from recent climate models suggesting higher sea levels and the increased intensity and frequency of storms, coupled with the results of studies such as the present one, will provide the impetus to address, with some urgency, the city's vulnerability to persistent flood events.

3.5 Conclusion and Future Recommendations

The analysis conducted for this study provides a synoptic view of a developing world city and its environs. Such an approach to understanding the landscape can be useful as it offers a comprehensive look at the interconnection of systems within

an urban environment, helps identify areas that require quick attention or target others for further analysis. Classification techniques, such as the one used in this study, form an important aspect of image interpretation and pattern recognition. Such analyses provide quantifiable information on land use activities and provide planners with essential data when crafting development plans. Regional or urban land use planning is a multi-faceted process that requires economic, social, demographic and spatial data to inform the planning process. The application of remote sensing data as demonstrated in this chapter provides one approach to analyze urban systems, illustrating its usefulness for planners, environmentalists, developers, and even non-government groups engaged in improving land use conditions in urban areas.

There is much scope for future remote sensing applications research on hazards and vulnerability for the city of Mumbai. With over 50% of the city's population living in shanty towns lacking basic infrastructure, future efforts must focus on more detailed analyses of these zones. As was pointed out in this chapter, shanty towns often occupy the city's low lying regions and face the persistent threat of monsoonal flooding. As a start, these areas need more fine scale mapping using high resolution imagery. Likewise, the city's few remaining green spaces require protection from development activities. Intra-urban green space is fundamental to the health of urban ecosystems and must be paid more attention by planning efforts. In the case of Mumbai, fringing coastal wetlands will serve as important natural barriers as the city copes with rising sea levels over the next century. City planners must not only protect remaining coastal marshes, but also engage in active wetland regeneration activities where encroachment has caused losses. Finally, as planning efforts focus on the city, satellite towns must not be inadvertently overlooked, as these are the growth areas of the 21st century. Planning lessons learned for the metropolis should be heeded and transferred as attention shifts to these newer cities.

Remote sensing technology has revolutionized the way we can assess change in land use and land cover over time. Imagery has provided scientists with a data rich environment to examine parts of the world that have heretofore been overlooked. Data scarcity is particularly problematic in the developing world and as a result, until very recently, vulnerability and hazards studies were mostly focused on the developed world. This chapter demonstrates that the use of readily available remotely sensed data coupled with conventional techniques can prove informative. Today, the proliferation of high spatial resolution data makes it possible to engage in analyses at higher levels of detail that enhance our ability to decipher fine-scale patterns and thereby improve policy recommendations. While the costs associated with such data are still high, increased future competition in the private remote sensing sphere and increased demand for such products will undoubtedly reduce prices. The limited number of spectral bands available through commercial enterprises, however, still provides an essential role for Landsat data. Moreover, the recent USGS announcement to make all of its Landsat data archive available free of cost to users, now makes virtually every part of the globe accessible to those with the necessary theoretical and technical skills to contribute to Land Use and Land Cover Change science in general and hazard vulnerability research in particular.

References

Alrababah, M. A. and M. N. Alhamad. (2006). Land use/cover classification of arid and semi-arid Mediterranean landscapes using Landsat ETM. *International Journal of Remote Sensing*, 27(13), 2703–2718.

Al Rawashdeh, S. and B. Saleh. (2006). Satellite Monitoring of urban spatial growth in the Amman area, Jordan. *Journal of Urban Planning and Development*, 132(4), 211–216.

Auch, R., J. Taylor and W. Acevedo. (2004). *Urban Growth in American Cities: Glimpses of US Urbanization*. USGS Circular 1252: US Department of the Interior.

Barrows, H. (1923). Geography as human ecology. *Annals of the Association of American Geographers*, 13, 1–14.

Blaikie, R., T. Cannon, I. Davis and B. Wisner. (1994). *At Risk: Natural Hazards, People's Vulnerability and Disasters*. London: Routledge.

Burton, I., R. W. Kates and G. F. White. (1993). *The Environment as Hazard.* New York: Guilford Press, p. 240.

Cutter, S. L. (1996). Vulnerability to environmental hazards. *Progress in Human Geography*, 20, 529–539.

Cutter, S. L., J. T. Mitchell, and M. S. Scott. (2000). Revealing the vulnerability of people and places: A case study of georgetown county, south carolina. *Annals of the Association of American Geographers*, 90(4), 713–737.

Demographia. (2007). *World Urban Areas*. http://www.demographia.com/db-worldua.pdf Accessed April 24, 2008.

Few, R. (2003). Flooding, vulnerability and coping strategies: local responses to a global threat. *Progress in Development Studies*, 3(1), 43–58.

GLCF (Global Land Cover Facility) (1997). *Data and Products.* http://glcf.umiacs.umd.edu/data/ Accessed November 6, 2007.

Hewitt, K. (1997). *Regions of Risk: A Geographical Introduction to Disasters.* Essex: Longman.

Jensen, R., J. Gatrell and D. McLean (eds.). (2005). *Geo-Spatial Technologies in Urban Environments.* Heidelberg: Springer Verlag.

Ji, C. Y., Q. Liu, D. Sun, S. Wang, P. Lin, and X. Li. (2001). Monitoring urban expansion with remote sensing in China. *International Journal of Remote Sensing*, 22(8), 1441–1455.

Kasperson, J. X., R. E. Kasperson and B. L. Turner II. (1995). *Regions at Risk: Comparisons of Threatened Environments.* Tokyo: United Nations University Press.

Kaya, S. (2007). Multitemporal analysis of rapid urban growth in Istanbul using remotely sensed data. *Environmental Engineering Science*, 24(2), 228–233.

Kwarteng, A. Y. and P. S. Chavez, Jr. (1998). Change detection study of Kuwait City and environs using multi-temporal Landsat Thematic Mapper data. *International Journal of Remote Sensing*, 19(9), 1651–1662.

Leahy, J. (2008). Riches rise from Mumbai slum clearance. *Financial Times*, May 6, 2008.

Lillesand, T. M., R. W. Kiefer, and J. W. Chipman. (2008). *Remote Sensing and Image Interpretation*. 6th edition. New York: Wiley.

Maktav, D., F. S. Erbek, and C. Jurgens. (2005). Remote sensing of urban area. *International Journal of Remote Sensing*, 26(4), 655–659.

Maktav, D. and F. S. Erbek. (2005). Analysis of urban growth using multi-temporal satellite data in Istanbul, Turkey. *International Journal of Remote Sensing*, 26(4), 797–810.

Mehta, S. (2004). *Maximum City: Bombay Lost and Found*. New York: Alfred A. Knopf.

Meehl, G. A., T. F. Stocker, W. D. Collins, P. Fiedlingstein, A. T. Gaye, J. M. Gregory, A. Kitoh, R. Knutti, J. M. Murphy, A. Noda, S. C. B. Raper, I. G. Watterson, A. J. Weaver and Z. C. Zhao. (2007). Global climate projections. In Solomon, S., D. Qin, M. Manning, Z. Chen, M. Marquis, K. B. Averyt, M. Tignor and H. L. Miller (eds.), *Climate Change 2007: The Physical Science Basis. Contribution of Working Group I to the Fourth Assessment Report of the Intergovernmental Panel on Climate Change.* Cambridge University Press, Cambridge, United Kingdom and New York, USA.

Mundia, C. N. and M. Aniya. (2005). Analysis of land use/cover changes and urban expansion of Nairobi city using remote sensing and GIS. *International Journal of Remote Sensing*, 26(13), 2831–2849.

MMRDA (Mumbai Metropolitan Region Development Authority). (1999). *Regional Plan for Mumbai Metropolitan Region, 1996–2011.* http://www.regionalplan-mmrda.org / Accessed May 1, 2008.

MMRDA (Mumbai Metropolitan Region Development Authority). (2003). *Population and Employment Profile of Mumbai Metropolitan Region*. http://www.mmrdamumbai.org/docs/Population%20and%20Employment%20profile%20of%20MMR.pdf Accessed May 1, 2008.

Nicholls, R. (1995). Coastal megacities and climate change. *GeoJournal*, 37(3), 369–379.

Nicholls, R. J., P. P. Wong, V. R. Burkett, J. O. Codignotto, J. E. Hay, R. F. McLean, S. Ragoonaden and C. D. Woodroffe. (2007). Coastal systems and low-lying areas. In M. L. Parry, O. F. Canziani, J. P. Palutikof, P. J. van der Linden and C. E. Hanson (eds.), *Climate Change 2007: Impacts, Adaptation and Vulnerability. Contribution of Working Group II to the Fourth Assessment Report of the Intergovernmental Panel on Climate Change*, Cambridge University Press, Cambridge, United Kingdom and New York, USA.

Rabus, B., M. Eineder, A. Roth, and R. Bamler. (2003). The shuttle radar topography mission – a new class of digital elevation models acquired by spaceborne radar. *ISPRS Journal of Photogrammetry and Remote Sensing*, 57, 241–262.

Ray-Bennett, N. S. (2007). Environmental disasters and disastrous policies: An overview from India. *Social Policy and Administration*, 41(4), 419–424.

SRTM (Shuttle Radar Topography Mission). (2006). *Shuttle Radar Topography Mission – Finished.* http://edc.usgs.gov/products/elevation/srtmbil.html Accessed November 22, 2007.

Smith, K. (1992). *Environmental Hazards: Assessing Risk and Reducing Disaster*. London: Routledge, p. 324.

TERI (Tata Energy Research Institute). (1996). *The Economic Impact of a One Meter Sea Level Rise on the Indian Coastline: Method and Case Studies.* Report submitted to the Ford Foundation.

TIFR (Tata Institute for Fundamental Research). (1999a). *The History of Mumbai.* http://theory.tifr.res.in/bombay/history /Accessed May 4, 2008.

TIFR (Tata Institute for Fundamental Research). (1999b). *The Geography of Mumbai.* http://theory.tifr.res.in/bombay/physical /Accessed May 4, 2008.

TNN (Times News Network). (2005a). Mumbai is down under. *The Times of India*, Thursday July 28, 2005, p. 1.

TNN (Times News Network). (2005b). Could technology have stemmed the tide of Mumbai's misery? *The Times of India*, Thursday July 28, 2005, p. 6.

TNN (Times News Network). (2005c). Where's the government? Public rage against administration spills onto streets. *The Times of India*, Sunday July 31, 2005, p. 1.

TNN (Times News Network). (2005d). Island city, for real. *The Times of India*, Thursday July 28, 2005, p. 6.

United Nations, Population Division, Department of Economic and Social Affairs. (2006). *World Urbanization Prospects: The 2005 Revision*. CD-ROM Edition data in digital form POP/DB/WUP/Rev.2005. http://www.un.org/esa/population/publications/WUP2005/2005wup.htm Accessed April 24, 2008.

USGS EROS (United States Geological Survey – Earth Resources Observation Science). (2006). *Satellite Products*. http://eros.usgs.gov/products/satellite.html Accessed February 4, 2007.

Weber, C., C. Petropoulou and J. Hirsch. (2005). Urban development in the Athens metropolitan area using remote sensing data with supervised analysis and GIS. *International Journal of Remote Sensing*, 26(4), 785–796.

White, G. F. (1964). *Choice of Adjustment to Floods*. Department of Geography Research Paper No. 93. Chicago: University of Chicago Press, p. 149.

Wilbanks, T. J., J. T. Ensminger, and C. K. Rajan (2007). Climate change vulnerabilities and responses in a developing country city: Lessons from Cochin, India. *Environment*, 49(5), 22–33.

Zhang, Q., J. Wang, X. Peng, P. Gong, and P. Shi. (2002). Urban built-up land change detection with road density and spectral information from multi-temporal Landsat TM data. *International Journal of Remote Sensing*, 23(15), 3057–3078.

Zerah, M.-H. (2007). Conflict between green space preservation and housing needs: The case of the Sanjay Gandhi National Park in Mumbai. *Cities*, 24(2), 122–132.

Chapter 4
A GIS for Flood Risk Management in Flanders

Pieter Deckers, Wim Kellens, Johan Reyns, Wouter Vanneuville, and Philippe De Maeyer

Abstract In the past decades, Flanders, a region of north Belgium that extends from the coastline inland (in northwest Europe), has suffered several serious riverine floods that caused substantial property damage. As Flanders is one of the most densely populated regions in the world, a solid water management policy is needed in order to mitigate the effects of this type of calamity. In the past, Flemish water managers chose to drain off river water as quickly as possible by heightening the dikes along the rivers. However, this method leads to a higher flood probability further downstream. Moreover, water defence infrastructure can always suffer from technical failures (e.g., breaching) creating even more damage than would have occurred if no defences were in place. In a search for a better solution to this recurring problem, the Flemish administration proposed a new approach in the 1990s. This approach focuses on minimizing the consequences of flooding instead of attempting to prevent floods. To implement this approach, large amounts of data were gathered for the Flemish Region. Using a Geographic Information System (GIS), a risk-based methodology was created to quantitatively assess flood risk based on hydrologic models, land use information and socio-economic data. Recently, this methodology was implemented in a specifically designed GIS-based flood risk assessment tool called *LATIS*. By estimating the potential damage and number of casualties during a flood event, *LATIS* offers the possibility to perform risk analysis quickly and effectively. This chapter presents a concise overview of *LATIS*' methodology and its implementation for flood risk management in Flanders.

Keywords Floods · Damage · Risk · Flanders · GIS · Modeling

P. Deckers (✉)
Department of Geography, Faculty of Sciences, Ghent University,
Krijgslaan 281, 9000 Gent, Belgium
e-mail: pieter.deckers@ugent.be

P.S. Showalter, Y. Lu (eds.), *Geospatial Techniques in Urban Hazard and Disaster Analysis*, Geotechnologies and the Environment 2, DOI 10.1007/978-90-481-2238-7_4,

4.1 Introduction

Flanders is located in the centre of northwest Europe, in the low-lying northern part of Belgium, bordering the North Sea (Fig. 4.1). The region is characterised by a number of river valleys with moderate slopes and minor elevation differences. During heavy torrents or long-lasting rainy weather, parts of Flanders are regularly flooded due to overflow (and in rare occasions by breaching) of river dikes. For example, the Dender catchment (the dark grey region west of Brussels indicated by the "D" in Fig. 4.1) suffered heavy floods in 1995, 1999 and 2002–2003.

As Flanders is one of the most densely populated and industrialised regions in the world, adequate flood risk management is necessary. In the past, the solution of the Flemish administration to the flood problem was to drain the water downstream as quickly as possible by heightening the dikes along the river banks. However, experience showed that this was far from an ideal solution. It has become clear that this method leads to higher water levels and a higher flood risk downstream. Moreover, water defence infrastructure can collapse due to technical failure such as breaching, often creating more damage than would have occurred if no flood defence infrastructure had existed.

The Flemish minister responsible for addressing these types of issues launched a new approach in the governmental note, "Mobility and Public Works 2000−2004" (Vanneuville et al. 2003). The new idea was a paradigm shift away from attempting to protect against high water levels to reducing damages caused by the water. This

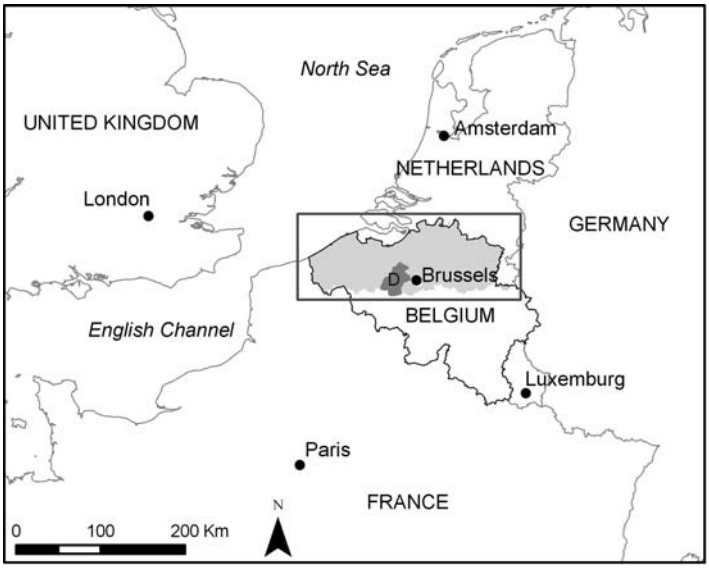

Fig. 4.1 Situation of the region of Flanders (the *gray* region in the *rectangle*) in northwest Europe Source: Vector versie van het "Voorlopig Referentiebestand Gemeentegrenzen", AGIV, toestand 22/05/2003 (GIS-Vlaanderen) and – Vectoriële versie van de "VHA-waterlopen and –zones", Vlaamse Milieumaatschappij – Afdeling Operationeel Waterbeheer (AGIV)

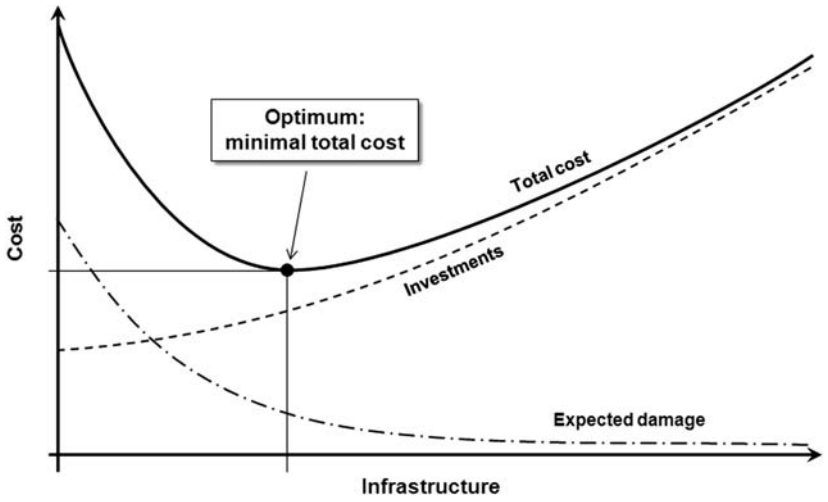

Fig. 4.2 Economic optimum in a cost benefit analysis for water infrastructure

shift created the need to identify the level of investment represented on the landscape (e.g., buildings, infrastructure) and the cost of repairing those investments following a flood. Figure 4.2 provides a graph of this cost benefit analysis, where a point has been placed on the "Total cost" to illustrate the "Optimum minimal total cost". The lower the investment in flood defence infrastructure, the higher the expected costs for damage. As investments in infrastructure increase, expected damage decreases as does the total cost. At a certain point, higher investments no longer lead to major decreases in expected damages and the total cost begins to increase again. At this point, the total cost of investments and expected damage is minimal (De Nocker et al. 2004).

In agricultural areas, the impacts of floods are limited due to low population density, fewer buildings, and reduced amounts of infrastructure. In other areas (e.g., nature conservation zones), flooding can even have positive effects. The opposite is true in densely populated areas or in areas with important industrial activities. In these areas, extra effort and investment must be made to try to reduce the effects of flooding, such as delineating controlled inundation areas to provide short term storage for large volumes of water. In order to estimate and compare the benefits from each of different types of measures, a uniform risk analysis approach is necessary. In this context, several objectives were set by policy makers in the governmental note described earlier (Vanneuville et al. 2003):

- The development of a methodology for the uniform calculation of damage and risk for the whole of Flanders;
- Use of this methodology to calculate change in flood risk and damage due to change in local infrastructure works and/or land use; and,
- A definition of data and software necessary for running the equations in a geographic information technology (GIT) environment.

To meet these goals, Flanders Hydraulics Research,[1] in cooperation with the Department of Geography at Ghent University, developed a risk-based methodology to assess potential flood damage. This chapter describes how the risk-based methodology was implemented via the assessment tool *LATIS*, providing an overview of the input data, chosen assumptions, and different calculations performed. The methodological framework is provided, as well as how flow velocity was modeled as a damage factor and how flood casualties are calculated. Because there is a need for more effective and adaptable tools, *LATIS* is offered as a substitute for earlier GIS-based models. The capability of using *LATIS* to calculate flood risk scenarios with regard to climate change is also demonstrated. The chapter concludes by discussing methodological issues and future research.

4.2 Overview of the Risk-Based Methodology

Generally, risk is defined by the probability of an event (e.g., a flood) and the magnitude of its consequences (Jacobs and Worthley 1999). These consequences can be measured in terms such as buildings damaged or lives lost (Ahola et al. 2007). Although some researchers have added additional criteria to the definition of risk, flood risk studies in European countries are usually performed using the combination of probability and consequences (Verwaest et al. 2008). The methodology described in this chapter follows this general definition.

Several steps are required to calculate damage and risk (Vanneuville et al. 2005), as is shown in Fig. 4.3. The first step requires the generation of a set of flood maps, each representing the extent of a flood with a certain return period, using hydrological, hydraulic, and digital elevation models. Second, different land use maps are combined with a variety of socio-economic data resulting in a maximum damage map. This maximum damage map is subsequently combined with the different flood maps to create damage maps for each return period. In the final phase, these damage maps are combined into a single risk map.

4.2.1 Flood Map Calculations

Before calculating damage and risk, it is necessary to estimate an area's flooding probability through statistical analysis of past water levels and flow rates. First, the return period, or average period of time in which a particular maximum water level and discharge may occur, is calculated. Higher water levels and discharge volumes correspond to longer return periods of occurrence. Calculating probability of occurrence is performed using composite hydrographs, which are synthetic hydrographs integrated from Quantity/Duration/Frequency (QDF)-relationships. These

[1] Flanders Hydraulics Research is part of the Department of Mobility and Public Works of the Flemish Government and is responsible for the navigable waterways in Flanders.

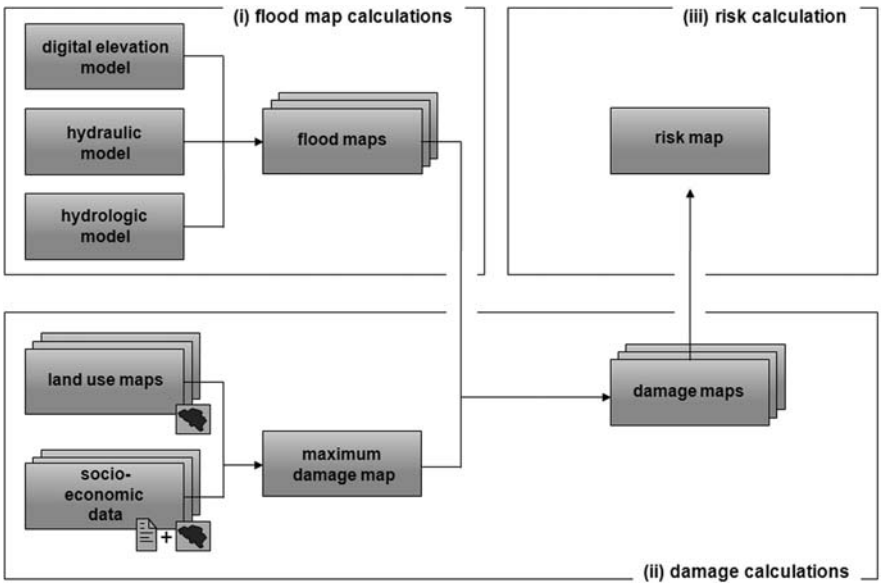

Fig. 4.3 Framework for risk mapping (to be read counterclockwise, starting at *upper left*)

QDF-relationships statistically link every river discharge with its duration and return period. Composite hydrographs have the advantage that in every point along the waterway (and in the flood zones) the calculated water levels have the same return period. Only one calculation is required for every return period, resulting in more rapid risk calculation models (Vaes et al. 2002).

As stated above, flood maps are created using hydrological, hydraulic, and digital elevation models. These maps show maximum water levels and flooding extent. Additional information such as flow velocity and the "rise velocity" of water (especially important for casualty assessment) can also be obtained. Thus for each return period, a set of maps is available indicating flood extent, flow velocity and rise velocity. Since creating and validating composite hydrographs is time-consuming, only a discrete set of flood maps was created (e.g., 1, 2, 5, 10, 25, 50, 100, 250 years for the Dender catchment). If more historical data are available, flood maps for even longer return periods can be calculated.

4.2.2 Damage Calculations

In this step, land use information and socio-economic data are used to produce a maximum damage map. This maximum damage map contains the potential damage value per surface area, where maximal damage can occur from a hazardous event. Put differently, this map indicates the cost value for a virtual scenario in which everything is destroyed by a (flood) event. By combining the maximum damage map with the flood maps, expected damage for a given inundation can be calculated.

4.2.2.1 Different Types of Damage

Numerous definitions of damage can be found in the disaster literature (e.g., Cochrane 2004). However, a number of distinctions are common with regard to flooding (De Maeyer et al. 2003). Financially, damage can be split into monetary (tangible) and non-monetary (intangible – including emotional) damage. A second classification can be made between internal and external damage. Internal damage is damage caused in the inundated zone itself, external damage occurs outside the inundated area. An example of the latter is production loss due to economic dependence on customers and/or suppliers located in the flooded area. A third classification is between direct and indirect damage. The first refers to damage affecting buildings, furniture, stocks, crops, and the like while the second refers to production losses and clean-up costs.

The risk methodology used here only considers monetary, internal, and direct/indirect damage. Although several authors have performed flood risk assessment including non-monetary (Yates 1992; Lekuthai and Vongvisessomjai 2001; Simonovic and Carson 2003) and external damage (Penning-Rowsell et al. 2003; Van der Veen and Logtmeijer 2005), these criteria were beyond the scope of this study.

4.2.2.2 Maximum Damage Map

Different land use categories have different potential maximum damage values. Damage values for completely destroyed cropland are less when compared to the total destruction of a factory. Therefore, land use information is needed to create a maximum damage map. Two major resources were used to create an overall land use map of Flanders: CORINE Land Cover (a classified land use map that covers all European member states) and the Small Scale Land Use map of Flanders and Brussels.[2] The combination of these data makes it possible to classify land use into different categories such as built-up areas, industrial grounds, crop lands, pastures, transport infrastructure and airports (Vanneuville et al. 2003). Both CORINE Land Cover and the Small Scale Land Use Map are based on LANDSAT images with a resolution of 30 m per pixel. As this resolution was insufficient to fulfill all needs, vector-based land use information such as road and railroad networks, and locations of highly valued buildings (e.g., hospitals, fire stations, schools, churches, electricity and communication infrastructure) was added to the database.

Once land use information is available, the maximum damage values have to be linked to the land use categories. To perform this task, socio-economic data is gathered. As it is difficult[3] to incorporate the individual value of each household, factory

[2]Both land use maps are included for two reasons: (i) the combination provides additional land use information unavailable when using only one data source, and (ii) each data set has a different renewal period, so the most recent land use map can be used when required.

[3]Insurance companies possess information on the monetary value of individual households, but are generally unwilling to disclose such private information. For croplands, another problem arises

or cropland, aggregated spatial data was used (e.g., mean housing value per statistical area, average value of crops per agricultural area, average value of factories per industrial sector). This approach causes every house in a particular statistical area to have the identical maximum damage value, but homes in residential areas will have higher values than those found in areas that are economically disadvantaged. Similarly, croplands in agricultural areas where fruits and vegetables are most important will carry a higher maximum damage value than croplands in agricultural areas where potatoes and cereals are more common. Data was gathered and grouped for each land use category (for a detailed description, see Vanneuville et al. 2003). After combining the land use map with the damage values, a maximum damage map can be produced.

4.2.2.3 Calculating Damage Maps

The next step combines the maximum damage map with the different flood maps to create maps of real flood damage suffered during each return period. Floods rarely lead to total destruction. The extent of damage depends on water depth because all land use categories have different relationships between the amount of damage that occurs and water depth. These relationships are defined by damage functions or α-factors (Penning-Rowsell et al. 2003). To illustrate, five different damage functions are shown in Fig. 4.4. The quantitative relationship reflected in these functions

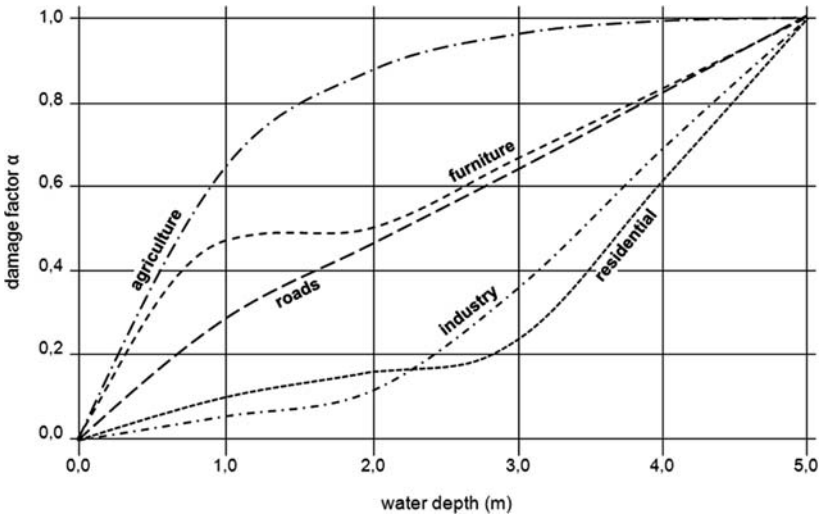

Fig. 4.4 Damage functions: real damage as a function of water depth

because of regular shifts in cultivation. For example, one year potatoes may be cultivated and the next corn; the gathering of such information is very intensive, time-consuming and sometimes impossible (due to privacy reasons).

are based on Van de Sande and Corné (2001) and Vanneuville et al. (2003). Each damage function represents a relationship between a given water depth (X-axis) and the dependent damage factor (Y-axis) that can be expected for that land use category. For example, a water depth of 3 m equals a damage factor of approximately 0.36 (36%) for industry. The same water depth causes nearly 100% damage to agriculture. The odd shape of the furniture curve is caused by the assumption that all homes and offices have a "ground floor" containing furniture and the slightest amount of water depth can cause substantial damage. A water depth of 2 m or higher corresponds to an increasing damage factor caused by the appearance of furniture installed on higher floors of a building.

Another important concept in our approach is the "doorstep level" (Vanneuville et al. 2003), or the height above ground level that defines the "zero" level for damage. For industry and housing the "doorstep level" is a physical reality; the concept is based on calibration methods performed in the Netherlands, by which people were asked to indicate the water height above their doorsteps (Vrisou Van Eck et al. 1999). Water levels were conservatively grouped into 25 cm increments, with all water levels in the flood map rounded to the next multiple of 25 cm. Below the "doorstep level", damage is set to zero. For housing, the doorstep level is 25 cm, whereas for roads and industry the doorstep is 50 cm (for roads, the assumption is that low water heights do not cause any damage in the short term). For all other classes of land use, the doorstep level is 0 cm, meaning that damage occurs the moment there is water.

In a flood zone the real damage caused by inundation at a certain water height can be calculated by summing all unique surface entities (i.e., discrete land use categories) and combining the water depth (translated to the corresponding α-factor, the parameter that is represented in Fig. 4.4) with the maximum damage of that land use category. Mathematically, this is described as:

$$S_w = \sum_{landusei} \alpha_i \times S_{i,\max} \tag{4.1}$$

Where

S_w : real damage in a zone
$S_{i,max}$: maximal damage in a land use class *i*
α_i : coefficient expressing the relationship between water depth and damage for land use class *i*

4.2.3 Risk Calculation

In the final step, the different damage maps for each return period are combined into one risk map. As stated above, risk is defined as the probability of a certain event multiplied by the damage caused by that event. The risk (expressed as the mean annual damage per surface unit per year) is then equal to the damage caused by

an event with a 1-year return period, plus half of the damage difference between a 2-year flood and a 1-year flood, plus one-third of the damage difference between a 3-year flood and a 2-year flood, and so forth. The mathematical explanation of this procedure is explained in Equations 4.2 and 4.3:

$$R = \sum_{i=1}^{n} \frac{1}{i}(S_i - S_{i-1}) \tag{4.2}$$

Or

$$R = \frac{1}{1}S_1 + \frac{1}{2}(S_2 - S_1) + \frac{1}{3}(S_3 - S_2) + ... + \frac{1}{n}(S_n - S_{n-1}) \tag{4.3}$$

Where

R risk
S_i the damages related to a flood with a return period of i years
n the highest return period

As explained above, the creation and validation of flood maps is time-consuming, so only a few have been created. To calculate risk in practice, it is assumed that linear interpolation of the flood damage between two return periods is valid, so the formula (in the case of return periods of 1, 2, 5, 10, 25, 50 and 100 years) can be simplified to (Vanneuville et al. 2003):

$$R = \frac{1}{1}S_1 + \frac{1}{2}(S_2 - S_1) + \frac{\frac{1}{3} + \frac{1}{4} + \frac{1}{5}}{5 - 2}(S_5 - S_2) + \frac{\frac{1}{6} + \frac{1}{7} + \frac{1}{8} + \frac{1}{9} + \frac{1}{10}}{10 - 5}(S_{10} - S_5) + ... \tag{4.4}$$

Equation 4.4 can be further simplified to:

$$\begin{aligned} R = {} & 0.5 \times S_1 + 0.2389 \times S_2 + 0.132 \times S_5 + 0.07 \times S_{10} + 0.0318 \\ & \times S_{25} + 0.0135 \times S_{50} + 0.0138 \times S_{100} \end{aligned} \tag{4.5}$$

4.3 Flow Velocity

Until recently, damage and risk calculations were performed only for flood events caused by the overflow of dikes, restricting the main cause of damage to water depth. However, overflow is not the only failure mechanism. Technical failures caused by dike/dune breaching may inflict damage to built-up areas that is much greater than that caused by overflow. In the vicinity of a breach, high flow velocities can even cause total collapse of buildings (Jonkman et al. 2008). Therefore, the potential for flow velocity damage needs to be incorporated into damage calculations based purely on depth. This additional damage cannot be greater than the difference

between maximum damage and damage caused by water depth. Based on Vrisou Van Eck et al. (1999), new damage functions were developed combining levels of water depth with flow velocity (Verwaest et al. 2008).

In cases of breaching, flow velocity at a certain location is a function of three parameters: (i) distance to the breach, (ii) bottom shear, and (iii) the presence of obstacles in the inundated area (e.g., a road above ground level). The approach differs depending on whether a 1-D or 2-D hydraulic model is available.

In cases where hydrodynamic boundary conditions are known only from a 1-D model, no detailed information on depth or velocity in the inundated area is available. This limitation necessitates a conceptual approach (Kellens and Vanneuville 2007), which is schematically depicted in Fig. 4.5 and which represents a dike breach along a river. Around the breach, three concentric zones (A, B, C) are defined according to expected amounts of property damage. In Zone A, closest to

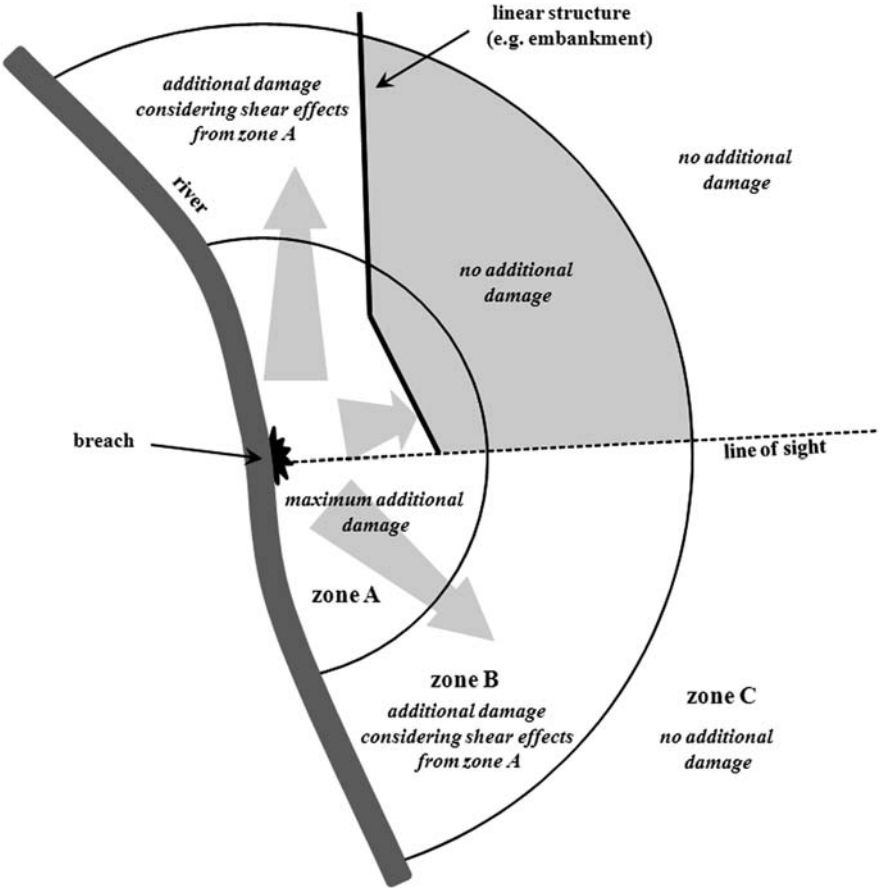

Fig. 4.5 Summary of the conceptual approach (Kellens and Vanneuville, 2007)

the breach, maximum additional loss is expected. Traveling away from the breach, flow velocities and damage decline because of shear and directional spreading of the water. The influence of shear depends on the land use in Zone A, as the water has to travel through this zone before it reaches Zone B; the influence of land use on flow resistance is based on Maijala (2001). The radii of Zones A and B are a function of the maximum discharge through the breach. The influence of barriers is also included; based on available vector data, possible obstructions for the traveling water are identified within the inundated area. Behind embankments no additional damage is expected provided there are no culverts or under-passes. The zone of influence of these barriers is determined by a line-of-sight analysis. Zone C sustains no additional damage.

In cases where water levels and velocity output are available from 2-D hydrodynamic models, Vrisou Van Eck et al. (1999) proposed combining flow velocity and water depth to determine maximum additional damage to construction due to breaching. Those authors considered a velocity of 3 m/s and a water depth of at least 0.5 m as necessary thresholds for buildings to collapse. For combinations of velocity and water depths lower than these values, continuous functions were constructed. The shape of the functions reflects the nature of the damage sustained: at low values for both parameters, losses are expected to be small. If either flow velocity or water depth increases, damage will increase dramatically until maximum additional losses occur.

4.4 Casualties

Besides material damage, floods cause human casualties due to the instability of people in rapidly flowing water and from building collapse (Jonkman et al. 2008). Although some have attempted to place a monetary value on human life (Card and Mooney 1977; Breyer and Felder 2005), a similar undertaking was not part of this study. Ramsbottom et al. (2003) and Jonkman and Vrijling (2008) denote the importance of water depth, rise velocity and flow velocity with regard to calculating loss of life caused by floods. The combination of great water depths and the rapid rise of water creates hazardous situations. People have limited time to reach higher floors or shelters and they may be trapped inside buildings. Consequently, the number of victims is calculated as the number of inhabitants multiplied by two proportionality factors, one for water depth and a second for rise velocity. Based on the findings of Jonkman et al. (2008), the model assumes 100% casualties if the water depth is higher than 6 m or if the rise velocity exceeds 3 m/h. For values lower than these thresholds, casualty functions were taken from Vrisou Van Eck et al. (1999).

An additional factor was added in the case of coastal inundations, where wave overtopping of coastal defense structures can create a substantial number of victims. Based on the work of Verhaeghe (2002) and Allsop (2005), an overtopping discharge of 0.095 l/m/s was set as the threshold value above which the maximum of casualties can be expected.

4.5 Implementation of the Methodology in a GIS

4.5.1 Early GIS-Model

The development of the risk-based methodology described above is insufficient, of itself, to perform risk analysis. The method needs to be translated into a useful model that executes all necessary steps in a pre-programmed chain of actions. Starting with land use maps and flood maps, all steps to create risk maps are separated into submodels based on a raster GIS approach. To determine whether to use raster or vector GIS, a preliminary study was performed (Vanneuville et al. 2003). While the tests did not produce large differences in precision nor accuracy, calculation times in raster GIS occur much more quickly than in vector GIS; 90% of the over 400 computations were more optimally performed in a raster-based GIS (Burrough and McDonnel 1998). One disadvantage of raster-based GIS is that the required storage capacities are much higher than for vector data; however, this is regarded as a minor issue (Eastman 2006).

The model was initially implemented in IDRISI® software (developed by Clark Labs, Clark University, Massachusetts) for raster GIS calculations. All operations were implemented using the software's model builder, which enables implementation of the different steps (as outlined above) within different submodels to reduce complexity. Unfortunately, the design of the software did not produce satisfactory results. As one example, it was necessary to perform time-consuming preprocessing of all necessary input layers and an intensive start-up procedure for each risk computation. The intensive start-up procedure made it difficult for other users in the organization who are unfamiliar with the methodology or IDRISI, to independently compute damage and risk maps.

Although the IDRISI model had possibilities (optimal computing capacities and built-in standard modules), its disadvantages led to the development of *LATIS*. *LATIS* is a GIS application that guides the user through each step of the different damage and risk calculations with a user-friendly interface.

4.5.2 Development of a Flood Risk Assessment Tool: LATIS

In 2007, Flanders Hydraulics Research, in cooperation with the Department of Geography at Ghent University developed a GIS tool named *LATIS* as a substitute for the model structure described above. One of the main prerequisites for the development of the tool was a user-friendly and easy accessible Graphical User Interface (GUI). Therefore, the GUI of *LATIS* (the "Client Application" in Fig. 4.6) is built in the C#.NET programming language. The interface of *LATIS* is a simple windows application, hiding the complexity of professional GIS software. The algorithms of the methodology are also implemented in C#.NET, but for the execution of the geospatial operations, *LATIS* still uses the optimal computing capacity and built-in standard modules (which perform the geospatial operations) of IDRISI. The .NET technology enables the use and execution (in the background)

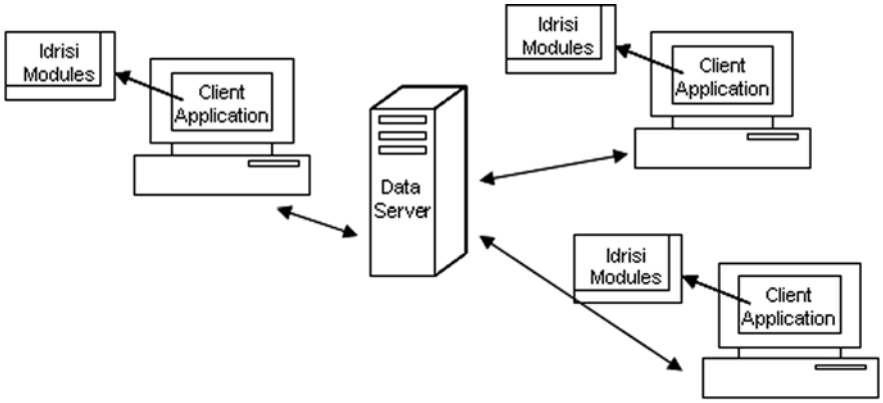

Fig. 4.6 Overview of the *LATIS* structure

of those IDRISI modules (Fig. 4.6, where the single-headed arrows represent the relationships between the client applications and the IDRISI modules), which are stand-alone executable files. The tool performs all necessary actions with the corresponding parameters in the background of the application so the user only has to input data that affect the risk calculations (i.e., the flood and land use maps and the socio-economic data).[4]

LATIS was also designed to address data management by developing a system that allows administrators to easily manage basic land use maps and socio-economic data. These maps and data are uniformly gathered for the extent of Flanders and are centrally managed on a data server. The manipulation of these base data is possible via the *LATIS* application of an administrator (shown in Fig. 4.6 by the arrows in the direction of the data server). When a user runs a damage and risk assessment, the application selects and extracts the necessary data (the standard is to select the most recent data) for the extent of a certain flooding scenario from the data server (shown in Fig. 4.6 by the arrows in the direction of the applications). Consequently, the application performs the preprocessing of land use and socio-economic data and the user only has to input the flood maps. The data management system also records what data is used in an assessment so a specific risk calculation can easily be repeated. Development of *LATIS* now allows damage and risk maps in Flanders to be calculated in an efficient, uniform, and reproducible manner.

4.6 LATIS in Action: Impact of Climate Change on Risk

The calculation of climate change scenarios in Flanders is one of the first projects for which the *LATIS* tool has been used. These climate change scenarios are based on regional climate models for different levels of CO_2 emissions. Based on potential

[4] *LATIS* is not an acronym – it is the Celtic goddess of water (and beer).

change in rainfall and evaporation rates, a high, mean and low scenario was defined for the summer and winter period in Flanders. In general, the potential for drought is expected to increase during the summer, while changes that may occur during the winter are highly uncertain (represented by a strong increase in flooding in the high scenario to a slight decrease in flooding in the low scenario).

The runs of the hydraulic model were executed based on the climate change scenarios and the available measurement series for water level, discharge and evaporation in order to derive catchment flood maps with different return periods. Both flood extent and water depth were used as the main factors influencing damage. Flood maps were used to recalculate damage and risk maps with the most recent socio-economic data available. These maps were used as references and compared with the flood risk maps produced under the climate change scenarios. For all four scenarios (current, low, mean and high), the flood risk is based on the same series of return periods as are used for flood map calculations (1, 50, 100 and 500 years).

A relatively small increase or decrease in water level can cause large differences in damage and risk. Vulnerable sites that are flooded once a century (on average) can be flooded more frequently, causing the risk to increase significantly. On the other hand, a large increase in water depth on agricultural land does not lead to a large increase in damage and risk because once crops are rotten, water depth is no longer important.

Economic damages are generally calculated for such features as housing, industry, and agricultural land. However, special attention is given to local features that are: (1) sensitive to extreme high damage values (e.g., power supply installations, museums), (2) important in case of an emergency (e.g., fire brigades, police stations) and (3) problematic due to evacuation reasons (e.g., hospitals, retirement homes).

Interpretation of the results of the damage and risk maps from the climate change scenarios is done (as for all flood risk assessments) in a relative manner. Because many generalizations are incorporated into the model, the risk values are not used as absolute stand-alone values – risk values of one scenario have to be compared with the risk values of other scenarios. Consequently, risk values between the scenarios are not compared on a pixel by pixel basis. Instead, the individual risk values in zones are grouped in order to evaluate scenarios. In the example of the Dender catchment (Table 4.1) the values are summarized in eight zones between two successive sluices and locks (Fig. 4.7).

As Table 4.1 indicates, the high scenario lead to a serious increase in monetary risk for the Dender catchment. In the master plan for this catchment – for which studies are already on-going – the location and dimensioning of the sluices will be evaluated and adapted. The proposed measures also have to be sustainable under conditions of climate change, so that the evaluated scenarios can be reused.

Figures 4.8 and 4.9 illustrate risk maps for part of the Dender catchment (the area covered by the rectangle in Fig. 4.7) representing the low (Fig. 4.8) and high (Fig. 4.9) climate change scenarios. These figures show a much larger spatial extent for risk in the high than the low scenario. For example, the factory at the south of the image is nearly 100% flooded in the high scenario compared to the low.

Table 4.1 Risk calculation for different climate change scenarios, Dender catchment (1000 euro/year)

Zone	Present	Low	Mean	High
1	806	148	445	1558
2	441	89	337	793
3	186	63	278	543
4	759	115	944	2426
5	257	126	320	1835
6	10	0	2	45
7	45	5086	5754	5933
8	720	276	374	423
Sum	3224	5902	8455	13,556

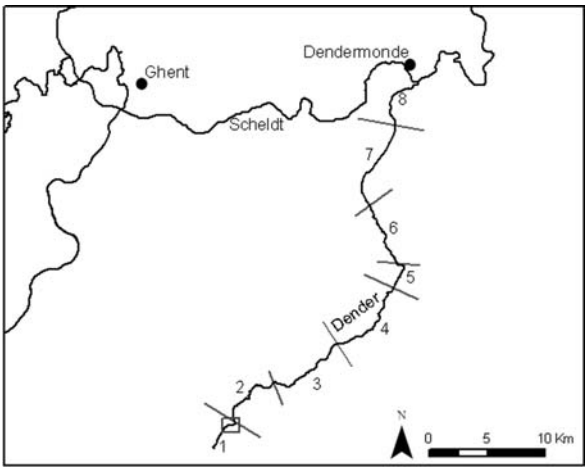

Fig. 4.7 Overview of the different zones in the Dender catchment (the *small rectangle* at the bottom of the figure indicates the location of the area shown in Figs. 4.8 and 4.9)
Source: Vectoriële versie van de "VHA-waterlopen & -zones", Vlaamse Milieumaatschappij – Afdeling Operationeel Waterbeheer (AGIV)

4.7 Conclusions and Further Developments

LATIS, a GIS application for assessing flood risk in Flanders, Belgium has been described, including an overview of the underlying risk methodology, which incorporates hydrologic and hydraulic models, land use information and socio-economic data. Presently, *LATIS* is being used as part of social cost-benefit analyses for estimating the effects of flood mitigation measures. These analyses are being performed in support of several riverine and coastal management plans, including studies on the widening and deepening of waterways, the construction of controlled flood zones, and proposed improvements in the coastal defense infrastructure. These plans not

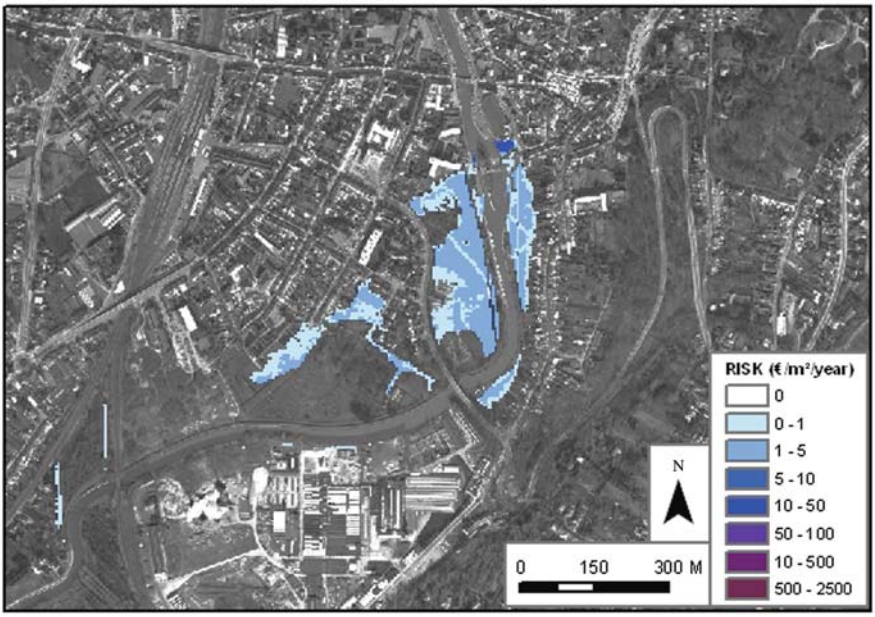

Fig. 4.8 Flood risk under the low climate change scenario in part of the Dender catchment Source of background map: Digitale versie van Orthofoto's, middenschalig, kleur, provincie Oost-Vlaanderen, AGIV en Provincie Oost-Vlaanderen, opname 2006 [GIS-Vlaanderen]

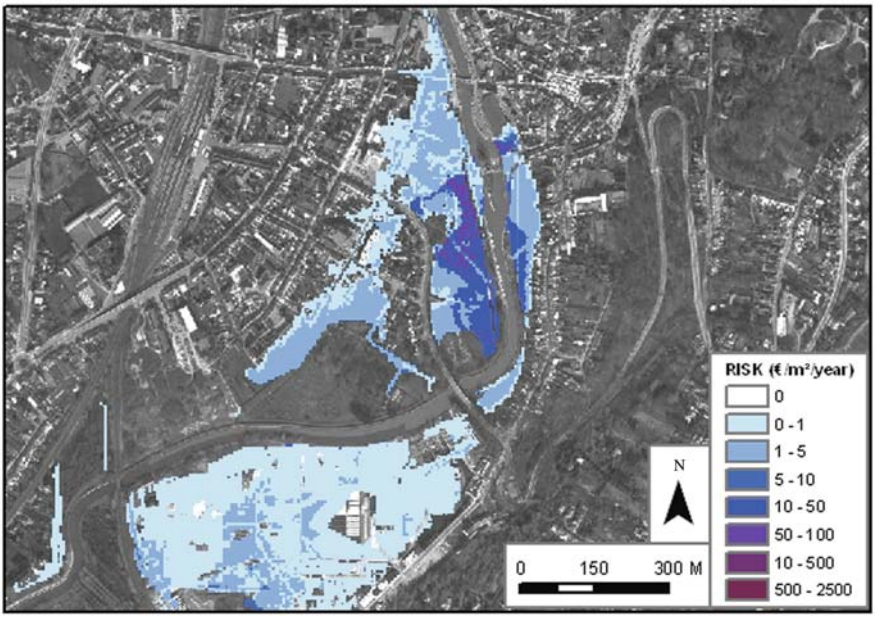

Fig. 4.9 Flood risk under the high climate change scenario in part of the Dender catchment Source of background map: Digitale versie van Orthofoto's, middenschalig, kleur, provincie Oost-Vlaanderen, AGIV en Provincie Oost-Vlaanderen, opname 2006 (GIS-Vlaanderen)

only seek to protect against current flood risk conditions but also to incorporate adjustments to deal with possible climate changes.

Currently, *LATIS* is limited to only four types of damage: monetary, internal, and direct/indirect. Future improvements to the methodology could include adding external and non-monetary damage to the model.

The model could be further improved with the use of more detailed base data. The main reason the current methodology uses aggregated data is pragmatic: data gathering is a time-consuming and costly job and processing time becomes longer with more detailed data. Therefore, the decision was made to work with generalized spatial data and to proceed gradually to more detailed data when more time and resources become available. This future work is important because estimating the number of people who could be afflicted directly impacts evacuation needs. Fortunately, although Flanders' flood plains are densely populated, it boasts a dense road network that is expected to support substantial evacuation numbers in the event of a calamity.

While flow velocity and the calculation of casualties due to floods were attempted, certain assumptions and simplifications were necessary for the present study. However, as these knowledge gaps are filled, more robust results could be produced. *LATIS* has proven its usefulness for calculating flood risk scenarios in Flanders. However, the real challenge lies in the near future, when European standards have to be met with respect to flood risk management. In 2007, the European Union released its European Flood Directive (2007/60/EC). In the next few years, all European member states have to comply with the demands described in that directive, most of which involve creating an inventory of objects in flood zones. Concurrent with that effort, potential flood damage and its likelihood will be evaluated, and necessary modifications made to improve the model. This on-going work will continue to strengthen *LATIS'* ability to function as an efficient data integration and data management system combined with a user friendly interface to improve flood risk management.

Acknowledgments The authors wish to acknowledge the financial support by the Flemish Government under contract WL16EB/06/07.

References

Ahola, T., Virrantaus, K., Krisp, J. M., Hunter, G. J. (2007). A spatio-temporal population model to support risk assessment and damage analysis for decision-making. *International Journal of Geographical Information Science*, 21(8), 935–953.

Allsop, N.W.H. (2005). D38: *Report on Hazard Analysis*. Report CLASH WP6, Coordinator HR Wallingford, 28p.

Breyer, F., Felder, S. (2005). *Mortality Risk and the Value of a Statistical Life: The Dead-Anyway Effect Revis(it)ed.* Geneva Risk and Insurance Review, 30(1), 41–55.

Burrough, P.A., McDonnel R.A. (1998). *Principles of Geographical Information Systems*, Oxford University Press, Oxford, p. 333.

Card W.I., Mooney G.H. (1977). What is the monetary value of a human life? *British Medical Journal*, 2, 1627–1629.

Cochrane, H.C. (2004). Indirect losses from natural disasters: measurement and myth. In: Okuyama, Y., Chang, S.E. (Eds.), *Modelling Spatial and Economic Impacts of Disasters*. Springer-Verlag, Berlin Heidelberg New York.

De Maeyer Ph., Vanneuville W., Maeghe K., Mostaert F. (2003). *Modélisation des effets de crue dans le bassin de la Dendre, basée sur une méthodologie de risqué* (Modelling the Effects of Flooding in the Dender Catchment based on a Risk Methodology), Le Geo Evenement, 4–6 march 2003, Paris, Actes des conférences sur Cd-rom, p. 7.

De Nocker, L., Broekx, S., Liekens, I. (2004). *Social Cost Benefit Analysis on Safety against Flooding in the River Scheldt Estuary – Conclusions on the Outlines*. VITO in cooperation with RA-IMDC, s.l., 92pp.

Eastman J.R. (2006). *Idrisi Andes, Guide to GIS and Image Processing*, Clark Labs – Clark University, Worchester, USA.

European Flood Directive. (2007). Directive 2007/60/EC of the European Parliament and of the Council, 23 October 2007. *Official Journal of the European Union*, L 288, 27–34.

Kellens, W., Vanneuville, W. (2007). *Damage and Risk Calculations, Report of Action 3b of the Interreg IIIB Project SAFECoast*, Ghent University and Flanders Hydraulics Research, Antwerp, Belgium, p. 41.

Jacobs, L., Worthley, R. (1999). A comparative study of risk appraisal: A new look at risk assessment in different countries. *Environmental Monitoring and Assessment*, 59(2), 225–247.

Jonkman, S. N., Vrijling, J. K. (2008). Loss of Life due to Floods. *Journal of Flood Risk Management*, 1(1), 43–56.

Jonkman, S.N., Vrijling, J.K., Vrouwenvelder, A.C.W.M. (2008). Methods for the estimation of loss of life due to floods: A literature review and a proposal for a new method. *Natural Hazards*, 46(3), 353–389.

Lekuthai, A., Vongvisessomjai, S. (2001). Intangible flood damage quantification. *Water Resources Management*, 15(5), 343–362.

Maijala M. (2001). *RESCDAM: Development of Rescue Actions Based on Dam-Break Flood Analysis.* Final Report June 1999–March 2001, p. 48.

Penning-Rowsell E., Johnson C., Tunstall S., Tapsell S., Morris J., Chatterton J., Coker A., Green C. (2003). *The Benefits of Flood and Coastal Defence: Techniques and Data for 2003*. Flood Hazard Research Centre, Middlesex University (book + CD-ROM with damage data).

Ramsbottom D., Floyd P., Penning-Rowsell E. (2003). *Flood Risks to People – Phase 1*. R&D Technical Report FD2317TR.

Simonovic, S.P., Carson, R.W. (2003). Flooding in the Red River Basin – Lessons from post flood activities. *Natural Hazards*, 28(2–3), 345–365.

Vaes, G., Willems P., Berlamont J. (2002). *Selectie en compositie van representatieve hydrogrammen voor riviermodellering.* Water, May 2002, p. 8.

Van de Sande, Corné (2001). *River Flood Damage Assessment using IKONOS Imagery*. In cooperation with the European Commission, Joint Research Centre, Space Applications Institute, EGEO Unit, Natural Hazards Project, Flood Damage and Flood Hazard assessment.

Van der Veen, A., Logtmeijer, C. (2005). Economic hotspots: Visualizing vulnerability to flooding. *Natural Hazards*, 36(1–2), 65–80.

Vanneuville W., De Maeyer Ph., Maeghe K., Mostaert F. (2003) Model the Effects of a Flood in the Dender Catchment, Based on a Risk Methodology. *Society of Cartography Bulletin*, 37(2), 59–64.

Vanneuville W., De Rouck K., Maeghe K., Deschamps M., De Maeyer Ph., Mostaert F. (2005). *Spatial Calculation of Flood Damage and Risk Ranking*, In: Conference Proceedings of Agile 2005, 8th Conference on Geographic Information Science, pp. 549–556.

Verhaeghe, H. (2002). *Toelaatbare Golfoverslag Over Zeeweringen: Literatuuroverzicht*. Universiteit Gent, vakgroep Civiele Techniek, Afdeling Weg- en Waterbouwkunde, intern rapport, p. 23.

Verwaest, T., Van Poucke, Ph., Reyns, J., Van der Biest, K., Vanderkimpen, P., Peeters, P., Kellens, W., Vanneuville, W (2008). *SAFECoast: Comparison Between Different Flood Risk Method-*

ologies: action 3B report, SAFECoast Interreg IIIb NorthSea project, Flanders Hydraulics Research, Belgium.

Vrisou Van Eck, N., Kok, M., Vrouwenvelder, A.C.W.M. (1999). *Standaardmethode Schade & Slachtoffers als gevolg van overstromingen – deel 2: Achtergronden*, HKV-Lijn in Water en TNO Bouw in opdracht van RWS-DWW.

Yates, S. (1992). Lay attributions about distress after a natural disaster. *Personality and Social Psychology Bulletin*, 18(2), 217–222.

Chapter 5
Using Geographic Information Science to Estimate Vulnerable Urban Populations for Flood Hazard and Risk Assessment in New York City

Juliana Maantay, Andrew Maroko, and Gretchen Culp

Abstract The research presented in this chapter seeks to demonstrate a new method to more accurately estimate populations vulnerable to hazards, especially in densely developed mega-cities, and to characterize at-risk populations based on measures of social, physical, and health vulnerability. Emergency management and disaster preparation, planning, mitigation, and recovery requires accurate estimation of potentially at-risk populations and sub-populations. Census data alone, however, cannot provide sufficiently detailed knowledge of population location and distribution, particularly in large, hyper-heterogeneous urban areas like New York City. Additionally, specific sub-populations (i.e., racial/ethnic minorities) may be at higher risk, yet under-counted by existing methods of calculating potentially exposed or impacted populations. We discuss two new inter-related methods that employ Geographic Information Science (GISc) to assess and quantify risk and vulnerability: the Cadastral-based Expert Dasymetric System (CEDS) and the New York City Hazard Vulnerability Index (NYCHVI). CEDS uses an expert system and dasymetric mapping to disaggregate population and sub-population data to the property tax lot level. The analysis shows that compared to CEDS, conventional areal weighting of census data and centroid-containment selection methods under count at-risk population for floods by 37 and 72%, respectively. We found that minorities and other vulnerable sub-populations are disproportionately underestimated using traditional methods, which impairs preparedness and relief efforts. NYCHVI provides a straightforward way of assigning a vulnerability rating to populations in potentially impacted areas, and incorporates locally significant factors that are not captured using national models. Used in tandem, CEDS and NYCHVI are effective in characterizing the vulnerable populations and areas subject to flooding and other hazards, enabling significant improvements in estimating vulnerability over prevailing methods.

J. Maantay (✉)
GISc Program and the Urban GISc Lab, Environmental, Geographic, and Geological Sciences Department, Lehman College, City University of New York, Bronx, NY 10468, USA
e-mail: juliana.maantay@lehman.cuny.edu

P.S. Showalter, Y. Lu (eds.), *Geospatial Techniques in Urban Hazard and Disaster Analysis*, Geotechnologies and the Environment 2, DOI 10.1007/978-90-481-2238-7_5,

Keywords Flood hazard · Dasymetric mapping · CEDS · Vulnerability · Cadastral · NYCHVI · HVA

5.1 Flood Hazard and Vulnerable Populations in New York City

Emergency management and disaster preparation, planning, mitigation, and recovery require accurate estimation of potentially at-risk populations and sub-populations, yet census data alone do not necessarily yield sufficiently detailed knowledge of population location and distribution, particularly in large, hyper-heterogeneous urban areas like New York City (NYC). Additionally, specific sub-populations (i.e., racial/ethnic minorities) may be at higher risk (Blaikie et al. 1994; Cutter 2006; Fielding and Burningham 2005; Fothergill et al. 1999; Mitchell 1999), yet minority sub-populations remain under-counted by existing methods of calculating potentially exposed or impacted populations. New York City, most of which is at or only slightly above sea-level, is at risk from flooding due to storm surge from hurricanes, "nor'easters," and the effects of sea-level rise from global warming, as well as from other natural and technological disasters (Bloomfield et al. 1999; Coch 1994; Gornitz et al. 2002).

This chapter demonstrates the benefits of developing new geomatic methods to more accurately estimate populations vulnerable to hazards, especially in densely developed mega-cities, and to characterize the at-risk populations based on measures of social, physical, and health vulnerability. Geomatics (geospatial technologies) is the discipline of gathering, storing, processing, and delivering of geographic information, or spatially referenced information, and it encompasses the tools and techniques used in land surveying, remote sensing, geographic information systems (GIS), photogrammetry, geodesy, global navigation satellite systems, and related forms of earth mapping. We introduce two new geomatic methods that employ Geographic Information Science (GISc) and models loosely-coupled with the GIS. These two methods, the Cadastral-based Expert Dasymetric System (CEDS) and the New York City Hazard Vulnerability Index (NYCHVI), represent inter-related ways to assess and quantify risk and vulnerability.

5.1.1 FEMA 100-Year Floodplain

Flooding has been, and continues to be, a concern not only in the New York City region, but across the country. Nationally, according to the United States Geological Survey, floods annually average 140 deaths and $6 billion in property damage.

A common way to delineate the extent of the flood hazard is with what is termed the "100-year floodplain." This designation represents areas with a 1-percent-annual-chance for flooding and was created as a standardized measure among federal, state, and local agencies involved with floodplain management. The Federal Emergency Management Agency (FEMA) estimates that nearly 150,000 square miles of the United States (over 4% of the total area) are within the 100-year

Fig. 5.1 FEMA Q3 100-year floodplain in New York City Source: FEMA 1996

floodplain (FEMA 1983). Approximately 15% of NYC's land area is within this floodplain. As one of the nation's most densely populated metropolitan regions susceptible to flood hazards, the City would be particularly difficult to evacuate because it is a city of islands surrounded by water – oceans, rivers, tidal straits, estuaries, and bays – with nearly 600 miles of coastline and numerous inland waterbodies (Bloomfield et al. 1999; Fig. 5.1).

Given the high density of NYC's built environment, encompassing both residential and commercial development, there is enormous potential for damage to life and property from flooding. New York City experiences frequent and destructive "nor'easters", and the occasional hurricane, and the storms' strength and potential for devastation are magnified by the unique configuration of Long Island's land mass in relation to the mainland – it sits at nearly a 90-degree angle to the eastern seaboard of the US. Hurricane experts state that even a Category 3 hurricane here could have devastating consequences (Coch 1994).

Further exacerbating the situation, it is predicted that global warming and accelerated sea level rise could greatly increase flood risk. Gornitz (2000) claims that the ". . .vulnerability of the Metropolitan East Coast Region to coastal hazards, such as more frequent storm flooding, beach erosion, submergence of coastal wetlands, and saltwater intrusion, will intensify as sea level rises" (p. 45) and that due to accelerated sea level rise ". . .the return period of the 100-year storm flood could be reduced to 19–68 years, on average, by the 2050s, and 4–60 years by the 2080s" (p. 61).

5.1.2 Vulnerable Populations

It is of particular importance in risk assessment of floods and other natural and technological disasters to determine what portion of the population is vulnerable, and

more specifically, the location of these potentially vulnerable populations. Vulnerability may be defined using several criteria, each of which serves as a "vulnerability indicator" that can contribute to a person's or a community's overall vulnerability potential.

Certain people may be disproportionately exposed to hazards not only due to physical factors (i.e., living in poor quality housing that inadequately withstands hazard events), but also due to lack of access to strong social, financial, or political support structures. Such individuals thus suffer greater relative loss and experience a longer recovery time after a disaster than those populations considered affluent, mainstream, or socially supported (Mitchell 1999; Marandola and Hogan 2007). Consequently, identical physical phenomena can have dramatically different impacts on those who are socially and economically vulnerable, and/or whose access to a social support structure is limited (Blaikie et al. 1994).

Previous research in the United States has demonstrated increased disaster risk and vulnerability for communities of color (Fothergill et al. 1999). Additional factors, such as an individual's health status, can also result in increased vulnerability. People with reduced mobility, or who suffer from conditions such as heart disease, emphysema, asthma, AIDS, or cancer, as well as those who are blind or deaf tend to be more vulnerable and at increased risk from flooding (Kilbourne 1997; Sanderson 1997; Etzel and French 1997). Young children and the elderly are also considered to be more vulnerable than other age cohorts (Noji 1997).

Negri et al. (2005) note that by,

> analyzing census data with GIS tools, we can identify specific areas where people are at risk for floods and landslides. Some factors further increase social vulnerability, such as limited access to political power and representation, lack of access to resources (including information and technology), lack of social capital (like social networks), and poor health. Beliefs and customs, and the age, type, and density of infrastructure, buildings, and lifelines are also factors that affect risk and potential losses (p. 1245)

Different populations represent differing demographics, socio-economic characteristics, and health conditions for those at risk from floods, and therefore may require different strategies and approaches to disaster preparedness, emergency response, and disaster relief. In order to design appropriate warning communications, mitigation, and recovery planning efforts for implementation prior to or in the aftermath of a flood, it is not only necessary to determine the size and location of potentially affected populations, but also to know exactly which members of those populations are most vulnerable to a major natural disaster.

5.2 GeoTechnical Contributions to Flood Hazard Assessment: CEDS and NYCHVI

Geographic Information Science is a discipline which employs geomatic technologies such as Geographic Information Systems (GIS), remote sensing, Global Positioning Systems (GPS), geo-statistical analysis, and environmental modeling, to

examine research issues. The technologies are used to assemble, create, store, display, analyze, edit, and map spatial and attribute data. GIS can convert "real world" information into constituent elements, creating data layers or themes, which can then be re-combined within the GIS to yield information that was unavailable when the data were separate. GIS, which combines specialized mapping software, spatial and attribute databases, is a powerful tool in the hands of the analyst/user who makes decisions about and interprets the datasets, the methodologies employed, the analyses, the output, and the results (Maantay and Ziegler 2006).

We developed two geographic information system tools to determine the "who" and "where" regarding the potentially most impacted and vulnerable populations. The first of the two tools is the Cadastral-based Expert Dasymetric System (CEDS), which is described in Section 5.2.1. The second tool is the New York City Hazard Vulnerability Index (NYCHVI) based on the Human Vulnerability Assessment (HVA) model, and is described in Section 5.2.2. Each data layer of vulnerability indicators can also be utilized independently of the compiled index, which can be very useful for many planning and management needs.

5.2.1 Disaggregating Population Data Using CEDS

The Cadastral-based Expert Dasymetric System (CEDS) is a model that uses both an expert system and dasymetric mapping to disaggregate population data (e.g., from the census) into much higher resolution data, giving a more realistic depiction of population locations and densities (Maantay et al. 2007). Dasymetric mapping uses ancillary datasets to refine and redistribute the locations of some phenomena (e.g., population) to reflect its distribution more accurately. CEDS, for instance, uses data sets that mask off the areas where people tend not to live (such as parks and waterbodies), then re-distributes the census populations throughout only the known inhabited areas, rather than throughout the entirety of the census unit area. CEDS then uses tax-lot (cadastral) data, which in NYC is on average 150 times finer resolution than the census block group data, to further disaggregate the census population data, as described below.

The expert system is a computerized decision-making program, which has been instructed to "decide", based on heuristic rules and expert judgment, which among several variables in the tax-lot data set to use for disaggregating the census data to calculate the optimally accurate tax-lot level population. Total populations, as well as sub-populations such as racial/ethnic groups, age cohorts, income/poverty status, and educational attainment levels, can be reliably disaggregated with CEDS.

5.2.1.1 Comparison of Three Methods: CEDS, FAW, and CCM

There are a few commonly-used methods to estimate at-risk populations. The Federal Emergency Management Agency (FEMA) uses a model called HAZUS (FEMA 2006). HAZUS employs the centroid containment method (CCM) to select only the

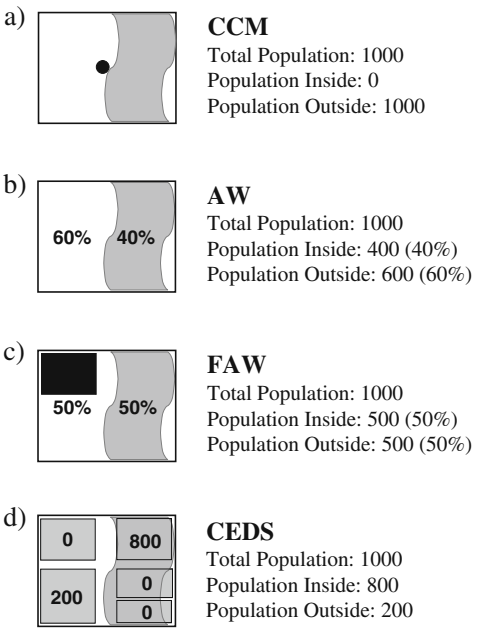

Fig. 5.2 Methodological differences and potential improvement of population estimation of the CEDS method (**d**), over the CCM – Centroid Containment method (**a**); AW – Areal Weighting (**b**); and FAW – Filtered Areal Weighting (**c**). Note that the *light grey* curved area represents a hazard area (e.g. floodplain) and the *black rectangle* in figure (**c**) represents an unpopulated area (e.g. park)

tract or block group polygons whose geometric centroids fall within the boundaries of interest, e.g., the floodplain (Fig. 5.2a).

Unfortunately, difficulties are encountered when trying to estimate population data within areas that do not coincide with the boundaries of census units. For instance, the boundaries of the floodplain are rarely, if ever, spatially coincident with the boundaries of census tracts, making it difficult to determine how many people are within the floodplain that intersects the census unit. This problem is commonly addressed by using areal weighting (AW), which is a spatial interpolation method that assumes a population is distributed homogeneously throughout a unit (Wu et al. 2005). This assumption also creates errors when trying to establish accurate counts for analyses that rely on a smaller, or different spatial unit of analysis than the original (Eicher and Brewer 2001; Holt et al. 2004).

With AW, if the boundaries of the phenomena of interest (e.g., floodplain) intersect a census unit a ratio based on areal proportions is applied to the population. If a quarter of an area is within the zone, one quarter of the population is assumed to be within the zone (Fig. 5.2b). Of course, in the real world, this assumption is a gross generalization and in hyper-heterogeneous urban areas like NYC can lead to incorrect estimation of the distribution of population in terms of both number and rate. Within census tracts and even block groups and blocks in NYC, there are very often enormous variations in land uses and population locations.

Areal weighting does not capture the nuances of complex urban areas. Filtered areal weighting (FAW) is an attempt to refine AW by using an ancillary data set to mask out uninhabited areas. The purpose is to redistribute the population only within

inhabited areas, but its accuracy is still insufficient for performing environmental, health, or risk analyses in a city such as NYC (Fig. 5.2c).

Due to the inexact results of the previous three approaches, we needed an improved method to estimate population within impact zones. CEDS has provided superior results by disaggregating data to the tax lot level (Fig. 5.2d). One of the main benefits of using CEDS is that it can estimate population data within areas that do not coincide with the boundaries of census units, for instance, floodplain boundaries. Figure 5.3 illustrates the necessity for a finer-grained method such as CEDS in a hyper-heterogeneous setting. The figure shows a typical New York City block, illustrating that even within the relatively small geographic unit of a census block there is considerable variation in population density and land use types (Fig. 5.3).

5.2.1.2 CEDS Methodology

The Cadastral-based Expert Dasymetric system relies primarily upon two proxies for population distribution – residential area (RA), which is the amount of square feet designated for residential use in the tax lot, and number of residential units (RU), which is the number of individual dwellings in the tax-lot (LotInfo 2003). Both of these are proxies for the population in each tax lot, and are therefore inexact. The tax lot data do not reveal how many people live within each lot or within each residential unit on the lot, nor how many square feet of residential area exist for each person, therefore one must estimate the population by disaggregating from the census data using RA or RU as proxies.

CEDS-derived population estimates were calculated in a two-step process, with each step occurring at different scales. Step 1, which informs the expert system, disaggregates the census tract population (from the US Bureau of the Census) to the tax-lot level based on either the ratio of RA in the tax lot versus the RA in the entire census tract or the ratio of the number of RU in the tax-lot versus the RU of the tract. Tax-lots that contain a greater proportion of proxy units are assumed to have an equally greater proportion of the population. The estimated tax-lot level populations are then re-aggregated up to the census block group level and compared with the block group population data as reported by the US Census Bureau. The absolute difference between the CEDS-estimated population, for both RA and RU, is then assessed and summed over each block group in the tract. The ancillary dataset that functioned better (i.e., lower absolute difference) is then chosen to be used as the proxy data for the geographic sub-groups contained within that particular census tract during Step 2. Step 1 was repeated for each of NYC's census tracts. These data not only inform the expert system but also act as validation by comparing its performance with data disaggregated by different, more common, techniques such as filtered areal weighting, as shown in Fig. 5.4a and b. The figures, which compare scatterplots of CEDS and FAW NYC block group population estimates, reveal that CEDS produces a superior output.

Step 2 calculates the final CEDS-derived population. Each census block group, rather than census tract, is disaggregated to the tax-lot level using the higher functioning proxy unit (RA or RU), as determined in Step 1 by the expert system. The

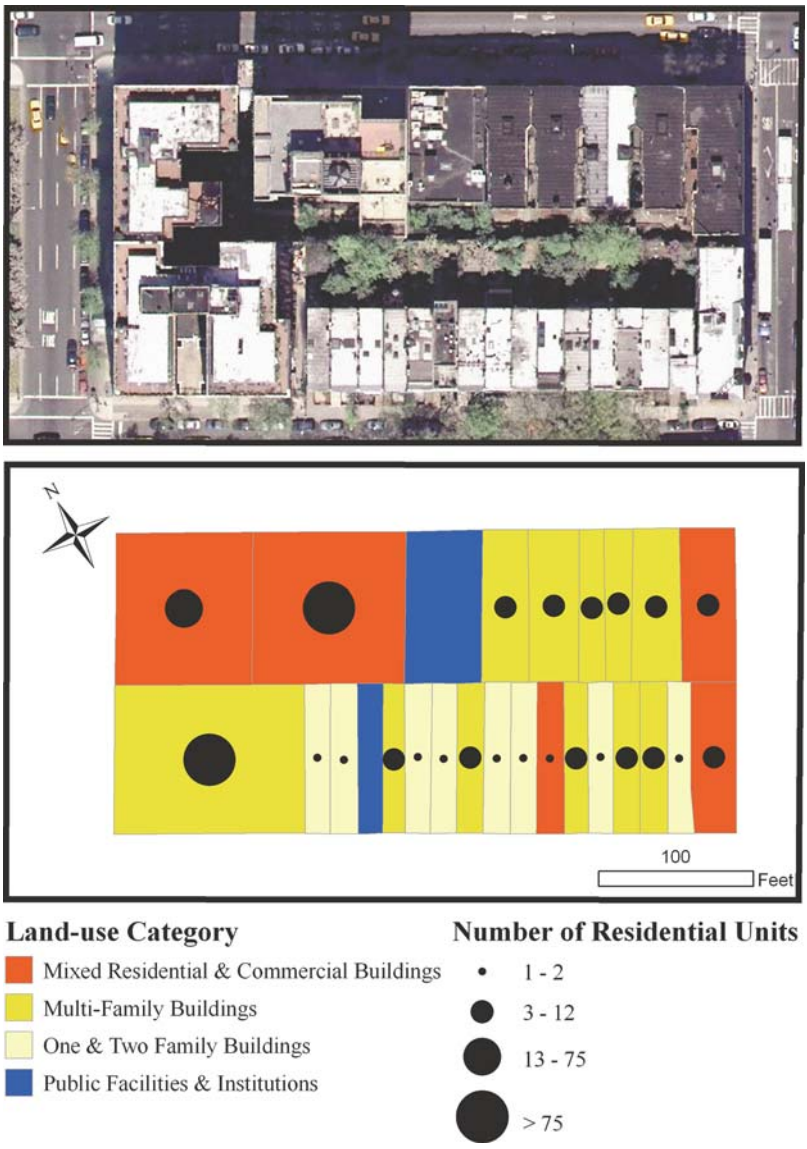

Fig. 5.3 Heterogeneity of a Manhattan city block. The orthophoto (*above*) and the cadastral map show the uneven distribution of land use categories and residential units at the tax-lot level even when examining only one city block. (There are, on average, more than 16 city blocks in a New York City census tract)
Source: NYCMap 2004; LotInfo 2003

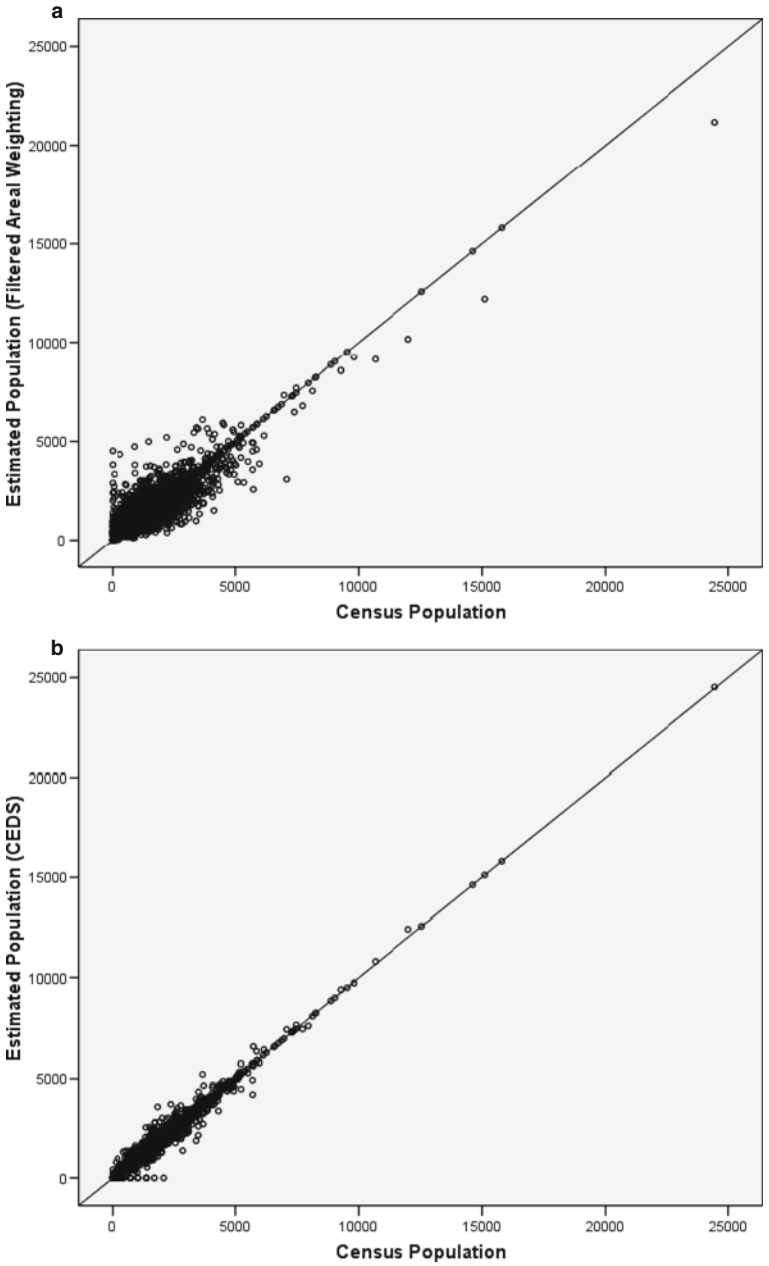

Fig. 5.4 Scatterplots of population estimations in New York City as compared to Census block group data using (**a**) Filtered Areal Weighting (FAW); and (**b**) CEDS

assumption is that when the source data is at a finer spatial resolution (census block groups are smaller than census tracts) there is less error in the system since CEDS is by nature a pycnophylactic process where mass is preserved (population numbers remain constant within the boundaries of each block group).

In this study, CEDS has been applied not only to the total population of NYC and specific racial and ethnic groups, but also to other census-based variables which are particularly important when assessing vulnerability, such as income (poverty status); educational attainment (persons 25 years and older without a high school diploma); age (persons 10 years and younger, and 65 and above); linguistic ability (persons 5 and older who speak English either 'not well' or 'not at all'); and disability (a self reported variable based on non-institutionalized individuals five years old and older). Although the sub-population estimations tend to be distributed similarly to the CEDS-derived total population, the expert system still functions independently for each variable. As such, the resulting estimates are distinct and vary in terms of redistribution ratios across the datasets. The census-based vulnerability variables have been disaggregated by CEDS, FAW, and CCM, and the resulting estimations of populations and sub-populations within the floodplain compared.

5.2.1.3 CEDS Results Versus Other Methods

In addition to total population numbers, ethnic and racial sub-populations were also spatially disaggregated to the property tax lot in this study to determine if there are any environmental justice impacts associated with flood risk in NYC (Fig. 5.4). Compared to the CEDS method, there are 37% (overall) fewer people estimated to be at risk from floods using the conventional areal weighting of census data and 72% fewer people at risk using the centroid containment selection method (Fig. 5.5). While minority populations city-wide do not disproportionately live within the floodplain, they are disproportionately undercounted by the traditional methods of population estimation. For example, in the floodplain, Non-Hispanic Blacks are undercounted at twice the rate of Non-Hispanic Whites.

The utility of CEDS for estimating potentially impacted vulnerable populations is illustrated by the case study of Brighton Beach, Brooklyn, New York. Brighton Beach is a community on the peninsula of Coney Island, which is joined by an isthmus to the rest of the borough of Brooklyn (Fig. 5.6). The community is a fairly dense residential neighborhood with a large population of immigrants and residents of Russian and Ukrainian descent. A considerable portion of Brighton Beach is also within the FEMA 100-year floodplain.

Population within the floodplain was estimated using the centroid containment method, filtered areal weighting, and CEDS (Fig. 5.7). Of the just over 35,000 residents in Brighton Beach, CCM estimates 4661 (13.2%) are in the floodplain, FAW estimates 9487 (26.9%) are in the floodplain, while CEDS estimates 11,798 (33.5%) are in the floodplain.

The markedly different estimates for this neighborhood indicate that the centroid containment method yields the least satisfactory results, FAW is an improvement, and CEDS provides the most precise estimates for total population as well as for

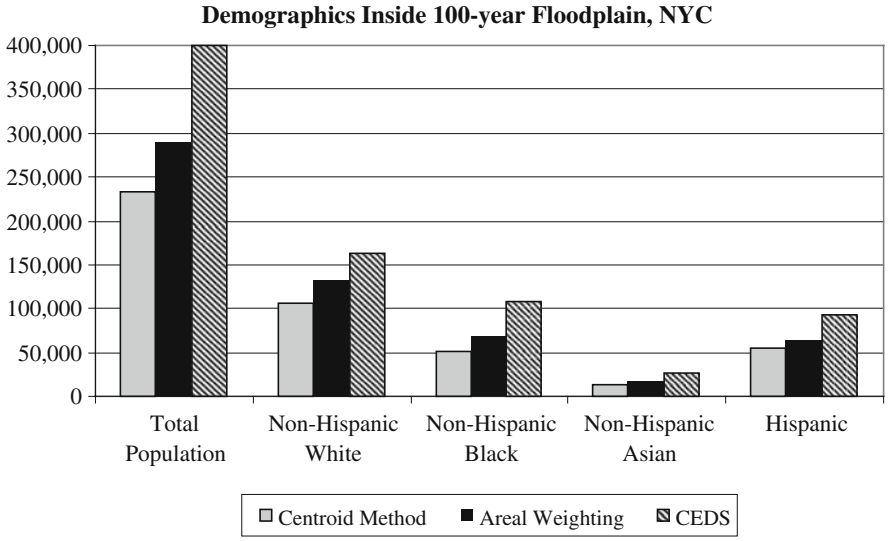

Fig. 5.5 Estimated populations and sub-populations within the 100-year floodplain in NYC comparing CEDS, FAW and CCM

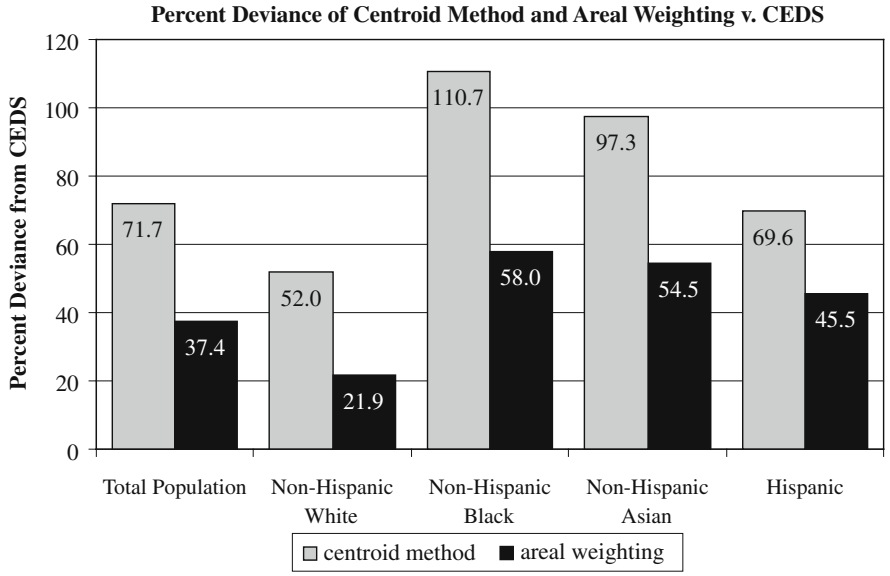

Fig. 5.6 Percent deviance of the Centroid Containment Method and AW vs. CEDS regarding undercounting of racial/ethnic groups

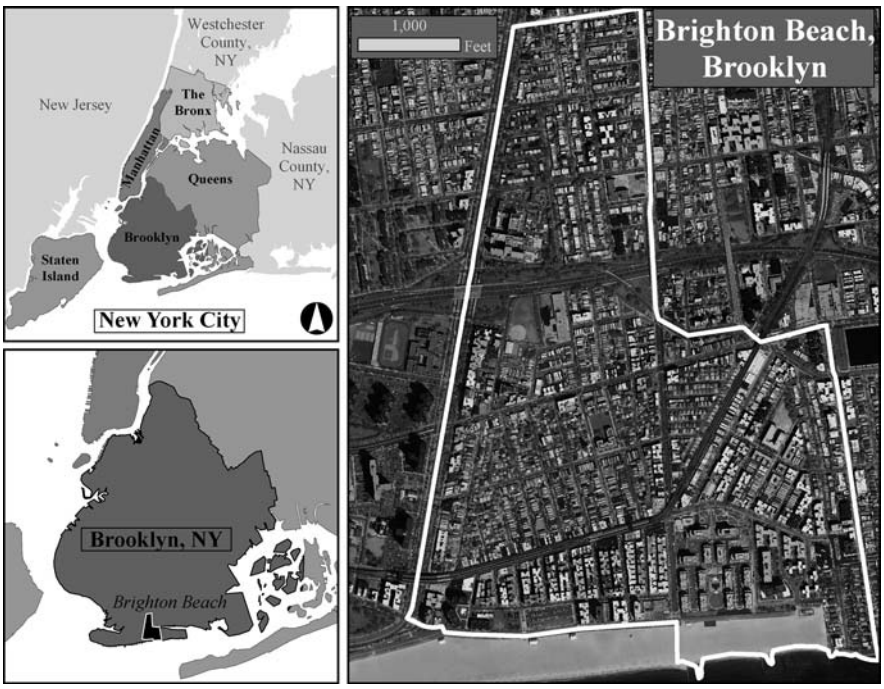

Fig. 5.7 Locator map of Brighton Beach community in Brooklyn, New York

all the sub-populations examined in the case study (Figs. 5.7, 5.8, and 5.9). Some populations estimated by the centroid containment method are undercounted by 200% or more (e.g., elderly 65 years and older; non-Hispanic black; and Hispanic) when compared against the estimates derived from CEDS. This undercounting of vulnerable populations can have serious ramifications for disaster planning, management, and mitigation.

5.2.2 New York City Human Vulnerability Index (NYCHVI) Model

The New York City Human Vulnerability Index (NYCHVI) is a user-driven hazard-of-place model based on the Human Vulnerability Assessment (HVA), a qualitative risk analysis tool created by the Geospatial Research, Analysis, and Services Program (GRASP) at the Centers for Disease Control and Prevention (CDC). The HVA is an application composed of an ArcObjects® MXD project, as well as data layers crafted from US Census and ESRI® Data and Maps (ESRI®, Inc.).

Conventionally, in times of disaster, attention was focused on property loss rather than estimation of human casualties (Cutter et al. 2000). Disaster epidemiologists, however, are tasked with measuring and describing adverse health effects, and factors contributing to those effects, that result from natural and human disasters in

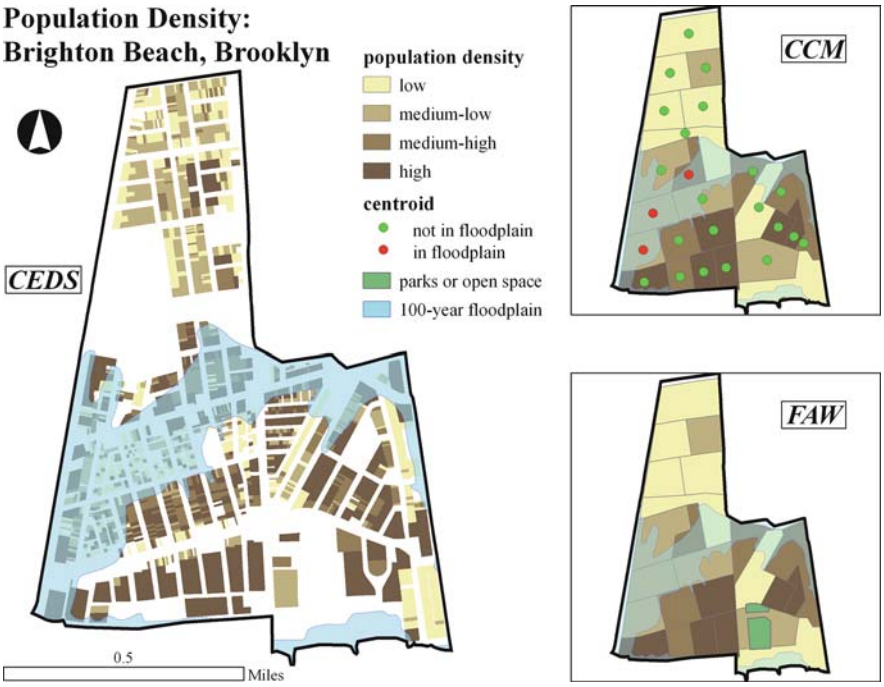

Fig. 5.8 Estimated total population densities in the case study area of Brighton Beach, Brooklyn, comparing CEDS, FAW and CCM. CEDS is aggregated to the tax lot, whereas FAW and CCM are at the census block group level. Population densities are shown in quartiles based on each dataset individually since the denominator (area) is not consistent across datasets (CEDS only accounts for the tax lot areas, whereas FAW and CCM utilize the entire census block group area)
Source: US Census 2000; LotInfo 2003; NYC Parks and Recreation Dept.; FEMA, Q3 2006

order to assess and meet the needs of disaster-affected populations. The HVA produces map-based reports "on-the-fly", allowing for the identification of populations potentially at risk of higher morbidity or mortality during a disaster. This model is intended to assist state and local decision-makers in targeting populations vulnerable to natural and man-made disasters. At this point in time, HVA is available only as a beta version, thus, its map reports may be subject to incompleteness or various inconsistencies.

5.2.2.1 Constructing the NYCHVI Model

In order to construct a locationally-relevant vulnerability index, it was necessary to modify and augment the national-level HVA by incorporating geographically specific datasets. The HVA model employs fifteen US Census variables at the census tract level. The model calculates the percentile rank of ninety or higher (PRC90) for each variable. If a variable is within the ninetieth percentile, it receives a PRC90 score of one. The overall vulnerability is determined by summing the

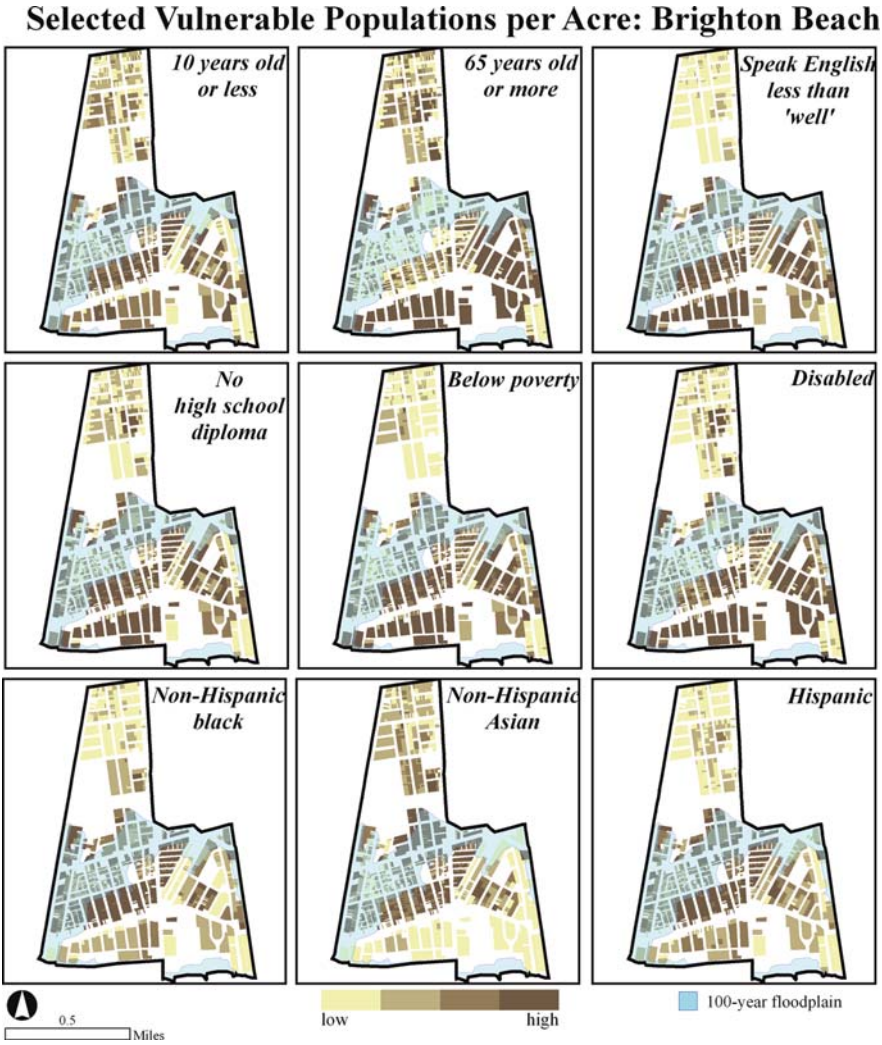

Fig. 5.9 Selected vulnerability variables – Persons per Acre. Each map represents a CEDS-derived variable at the tax lot level whose individual data range has been classified by quartiles
Source: US Census 2000; LotInfo 2003; NYC Parks and Recreation Dept.; FEMA, Q3 2006

PRC90 for all variables, which are not standardized and are weighted equally. The HVA overall vulnerability score can range from zero (very low vulnerability) to fifteen (extremely vulnerable). In addition, these fifteen variables can be organized into four indicator groups that measure the source of social vulnerability: *Socio-Economic* (income, poverty, employment, and education); *Household Structure and Disability* (age, dependency, disability, and single-parenting); *Race and Ethnicity* (minority status and non-English speaking); and *Housing and Transportation* (urban/rural housing, crowding, and transportation) (Table 5.1). These indicator

Table 5.1 HVA Variables (adapted from CDC 2008)

Variable	Data source*	Additional description
Group A. Socio-economic status		
1. Percent individuals below poverty	2000 US Census, Summary File 3, Population for Whom Poverty Status is Determined, Table P88. Ratio of Income in 1999 to Poverty Level	Individuals below poverty = "Under 0.50" + "0.50 to 0.74" + "0.75 to 0.99". Percent of persons below federally-defined poverty line, a threshold that varies by the size and age composition of the household. Denominator is total population where poverty status is checked.
2. Percent civilian unemployed	2000 US Census, Summary File 3, Population 16 years and Over, Table P43. Sex by Employment Status	Based on total population 16+. Civilian persons unemployed divided by total civilian population. Unemployed persons actively seeking work.
3. Per Capita Income in 1999	2000 US Census, Summary File 3, Total Population, Table P82. Per Capita Income in 1999	The mean income computed for every person in the census tract.
4. Percent persons with no high school diploma	2000 US Census, Summary File 3, Population 25 Years and Over, Table P37. Sex by Educational Attainment	Percent of persons 25 years of age and older, with less than a 12th grade education (including individuals with 12 grades but no diploma).
Group B. Household structure and disability		
5. Percent persons 65 years of age or older	2000 US Census, Summary File 3, Total Population, Table P8. Sex by Age	Percent persons 65 years of age or older.
6. Percent persons 17 years of age or younger	2000 US Census, Summary File 3, Total Population, Table P8. Sex by Age	Percent persons 17 years of age or younger.
7. Percent persons more than 5 years old with a disability	2000 US Census, Summary File 3, Civilian non Institutionalized Population 5 Years and Over, Table P42. Sex by Age by Disability Status by Employment Status	Percent civilian population not in an institution that are 5 years of age and older with a disability.
8. Percent male or fe-male householder, no spouse present, with children under 18	2000 US Census, Summary File 3, Households, Table P10. Household Size by Household Type by Presence of Own Children Under 18 Years	Other Family: Male Householder, no wife present, with own children under 18 years + Other Family: Female Householder, no husband present, with own children under 18 years.

Table 5.1 (continued)

Variable	Data source*	Additional description
Group C. Minority status and language		
9. Percent Minority	2000 US Census, Summary File 3, Total Population, Table P6. Race and Table P7. Hispanic or Latino by Race	Total of the following: "Black or African American alone" + "American Indian and Alaska Native alone" + "Asian alone" + "Native Hawaiian and Other Pacific Islander alone" + "Some Other race alone" + "Two or more races" + "Hispanic or Latino – White alone".
10. Percent persons 5 years of age or older who speak English less than "well"	2000 US Census, Summary File 3, Population 5 Years and Over, Table P19. Age by Language Spoken at Home by Ability to Speak English	For all age groups and all languages – the total of persons who speak English "not well" or "not at all".
Group D. Housing and transportation		
11. Percent multi-unit structure	2000 US Census, Summary File 3, Housing Units, Table H30. Units in Structure	Percent housing units with 10 or more units in structure
12. Crowding	2000 US Census, Summary File 3, Housing Units, Table H30. Units in Structure	At household level, more people than rooms. Percent total occupied housing units (i.e., households) with >1 person per room
13. No vehicle available	2000 US Census, Summary File 3, Occupied Housing Units, Table H44. Tenure by Vehicles Available	Percent households with no vehicle available.
14. Percent of persons in group quarters	2000 US Census, Summary File 3, Total Population, Table P9. Household Type by Relationship	Percent of persons who are in institutionalized group quarters (e.g., correctional institutions, nursing homes) and non-institutionalized group quarters (e.g., college dormitories, military quarters).
15. Percent mobile homes	2000 US Census, Summary File 3, Housing Units, Table H30. Units in Structure	Percent housing units which are mobile homes

*Beginning in 1790, the United States Census Bureau has conducted a decennial count of everyone living in the United States and its territories. In-depth population and housing data collected on a sample basis from the Census 2000 long form survey in addition to topics from the short form 100-percent data (age, race, sex, and vacancy status) are presented in Summary File 3. This includes population totals for ancestry groups as well as selected characteristics for a limited number of race and Hispanic or Latino categories. For more information on the United States Census, please refer to http://www.census.gov/.

groups are based on eleven factors devised by Cutter et al. (2003) to distinguish US counties according to level of social vulnerability in relation to environmental hazards. The HVA presents this information in a dynamic letter-sized cartographic report that includes six maps: one for each indicator group, an overall index and a reference map. The HVA model is national in scope and generates user-driven reports by county (e.g., Kings) or region (e.g., New York, NY – Northeastern New Jersey). This coarse scale may not provide adequate detail for local jurisdictions (CDC/ATSDR 2008). In addition, the HVA contains variables that are geared toward suburban or rural areas (number of mobile homes, for instance) and is therefore inappropriate for an urban hazard-of-place model.

The HVA variables are selected to serve as a broad overview and are considered a guide for potential indicators of vulnerability. A good vulnerability index emphasizes hazards that could potentially impact a community, indicates possible locations of hazard-related damage, and identifies those community elements that should be addressed to lessen exposure. NYCHVI (Table 5.2) is intended to enhance the HVA for New York City, not only by using locationally-specific data, but also by

Table 5.2 NYCHVI variables

Variable	Data source*	Additional description
Group A. Socio-economic status		
1. Percent individuals below poverty	Same as HVA (Table 5.1).	Same as HVA.
2. Percent civilian unemployed	Same as HVA.	Same as HVA.
3. Per Capita Income in 1999	Same as HVA.	Same as HVA.
4. Percent persons with no high school diploma	Same as HVA.	Same as HVA.
Group B. Household structure and disability		
5. Percent persons 65 years of age or older	Same as HVA.	Same as HVA.
6. Percent persons 10 years of age or younger	2000 US Census, Summary File 3, Total Population, Table P8. Sex by Age	Percent persons 10 years of age or younger
7. Percent persons more than 5 years old with a disability	Same as HVA.	Same as HVA.
8. Percent male or female house-holder, no spouse present, with children under 18	Same as HVA.	Same as HVA.
Group C. Minority status and language		
9. Percent Minority	Same as HVA.	Same as HVA.

Table 5.2 (continued)

Variable	Data source*	Additional description
10. Percent persons 5 years of age or older who speak English less than "well"	Same as HVA.	Same as HVA.
Group D. Housing and transportation		
11. Percent multi-unit structure	Same as HVA.	Same as HVA.
12. Crowding	Same as HVA.	Same as HVA.
13. No vehicle available	Same as HVA.	Same as HVA.
14. Percent of persons in group quarters	Same as HVA.	Same as HVA.
Group E. Public health		
15. AIDS	New York State Department of Health SPARCS – 2006 Persons, ICD-9: 042–044	Percent of population that underwent an AIDS-related hospitalization
16. Asthma	New York State Department of Health SPARCS – 2006 Persons, ICD-9: 493	Percent of population that underwent an asthma-related hospitalization
17. Cancer	New York State Department of Health SPARCS – 2006 Persons, ICD-9: 140–208	Percent of population that underwent a cancer-related hospitalization
18. Diabetes	New York State Department of Health SPARCS – 2006 Persons, ICD-9: 250	Percent of population that underwent a diabetes-related hospitalization
19. Heart Condition	New York State Department of Health SPARCS – 2006 Persons, ICD-9: 390–429	Percent of population that underwent a heart condition-related hospitalization

*Established in 1979, the Statewide Planning and Research Cooperative System (SPARCS), a comprehensive data reporting system, is the result of cooperation between the health care industry and government. While SPARCS was initially created to gather information on hospital discharges, it currently collects patient level data on patient characteristics, diagnoses and treatments, services, and charges for every hospital discharge, ambulatory surgery patient, and emergency department admission in New York State. The World Health Organization′s International Classification of Diseases Ninth Revision (ICD-9) is designed to facilitate international comparability in the collection, processing, classification, and presentation of mortality and morbidity statistics. In SPARCS, all hospital discharges are assigned an ICD-9 code based on the disease or condition associated with the hospitalization. For more information on the SPARCS dataset, please refer to http://www.health.state.ny.us/statistics/sparcs/.

expanding the model to take additional factors such as biophysical information into account – the HVA currently does not include a biophysical vulnerability component. Thorough vulnerability indices provide analysis of all critical public and private facilities and infrastructure (CDC/ATSDR 2008). For example, "special needs" facilities (i.e., health care facilities, schools, day care centers, and senior centers) are at higher risk because their occupants are dependent on others for their well being (Cutter et al. 2000). Proximity to "lifeline" resources including key infrastructure (e.g., public transit) and emergency response facilities (e.g., fire houses) may provide valuable information for mitigation planning. Capability of structures and lifeline systems to withstand past disasters is yet another consideration (Noji 1992). A comprehensive vulnerability index must also contain spatial information regarding areas prone to natural hazards (e.g., floodplain) (Cutter et al. 2000; Fedeski and Gwilliam 2007). Thus, important elements that (ideally) should be included in a hazard vulnerability index model include hazard-specific layers such as floodplain, hazardous waste facilities, building data, special needs facilities (e.g., hospitals, schools, eldercare centers), infrastructure (e.g., bridges, transportation, utilities), and public health data (e.g., hospitalization records regarding medically vulnerable individuals) other than the limited disability fields of the 2000 Census Survey (Table 5.3).

Elements should be symbolized employing a standard set of symbols developed for Emergency Management and First Responder agencies at the National, State, Local and Incident level that provide immediate and general understanding of the event (Homeland Security Working Group 2005).

The NYCHVI examines areas (ranging from borough to tax lot) within New York City's boundaries. This index can aid disaster preparation, management, mitigation, and recovery by identifying the locations of specific sub-populations that are at increased risk in a natural disaster.

5.2.2.2 NYCHVI Methods and Results

NYCHVI's (Table 5.2) variables for *Socio-economic Status* (Group A), and *Minority Status and Language* (Group C) are identical to those of HVA (Table 5.1). NYCHVI's *Household Structure and Disability* (Group B) category differs from that of HVA by the replacement of the original variable "Percent persons 17 years of age or younger" with "Percent persons 10 years of age or younger." Epidemiological literature suggests that younger children are more vulnerable to hazards than teenage adolescents and adults (Noji 1997). For the *Housing and Transportation* (Group D), the metric "Percent mobile homes" was removed because very few (~0.07%) of New Yorkers reside in mobile homes. NYCHVI's main departure from HVA is found with the addition of a new group of variables examining public health indicators (Group E). These data originated from New York State's Department of Health, Statewide Planning and Research Cooperative System (SPARCS), which estimates vulnerability based on pre-existing medical conditions (i.e., heart condition, AIDS, asthma, diabetes, and cancer).

Table 5.3 NYCHVI natural hazard and spatial layers

Spatial sector	Layer file	Source
Infrastructure	Subways	New York City Transit (NYCT)
	NYC streets (Linear Integrated Ordered Network – LION streets)	City of New York Department of City Planning (DCP)
	Property tax lot data – (Planning Primary Land Use Tax Lot Output – PLUTO)	City of New York Department of City Planning (DCP)
	Buildings footprints	New York City Department of Information Technology and Telecommunications (DoITT)
Biophysical	100-floodplain	Federal Emergency Management Agency (FEMA)
Lifeline	Police stations	City of New York Police Department (NYPD)
	Fire houses	New York City Fire Department (FDNY)
Special needs	Senior centers	New York City Department for the Aging (DFTA)
	Senior facilities	New York City Department for the Aging (DFTA)
	Charter schools	New York City Department of Education (DOE)
	Day care centers	City of New York Department of City Planning (DCP)
	Institutional housing	City of New York Department of City Planning (DCP)
	Hospitals	New York City Office of Emergency Management (OEM)
	Special education	New York City Department of Education (DOE)
	Regional schools	New York City Department of Education (DOE)

These pre-existing medical conditions are also used to create the New York City Department of Health and Mental Hygiene's Community Health Profiles, annual reports that address the health status and vulnerability of NYC neighborhoods (NYC-DOHMH 2006).

As with HVA, NYCHVI overall vulnerability is determined by summing the PRC90 for all variables featured in Table 5.2 (which are not standardized and are weighted equally), with an overall vulnerability score that can range from zero (very low vulnerability) to nineteen (extremely vulnerable). While HVA calculates the PRC90 on a national level, NYCHVI determines PRC90 on a city level. In other words, HVA compares a census tract to all other census tracts within the United States while NYCHVI compares a census tract to all other census tracts within

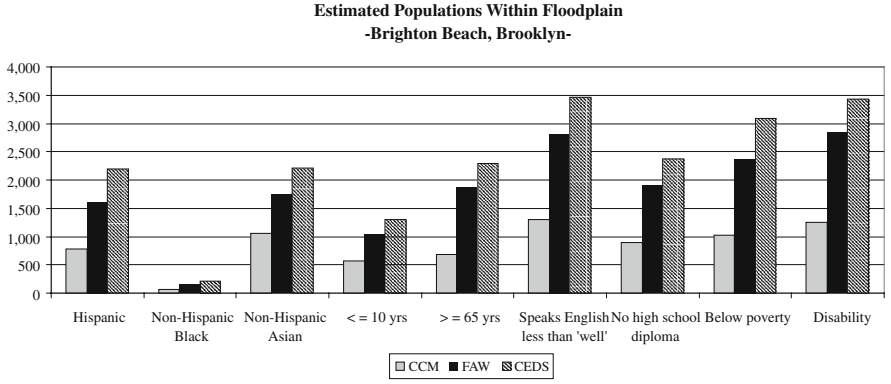

Fig. 5.10 Estimated total and sub-populations within the 100-year floodplain in the case study area of Brighton Beach, Brooklyn, comparing CEDS, FAW and CCM

New York City. A user-driven NYCHVI report for the Brooklyn neighborhood of Brighton Beach is shown in Fig. 5.10.

The "Special Needs" dataset (Table 5.3) was created to account for the facilities where particularly vulnerable populations gather, including hospitals, day care facilities, schools, institutions and senior housing. "Lifeline" and "Infrastructure" datasets incorporate data regarding transportation, residential (tax) lots, building footprints and emergency responder location (e.g., fire, police). Finally, a biophysical vulnerability component (FEMA's 100-year floodplain) was added. Where feasible, overlays were symbolized using the Homeland Security Emergency Management Symbol set. Figures 5.11 and 5.12 depict user-driven NYCHVI letter size (11″ X 8.5″) reports featuring a finely detailed map for the Brighton Beach area of Brooklyn (Please note, these reports are for illustrative purposes and have been reduced to fit the pages of this book). These figures depict neighborhood level maps of the same extent and are meant to be viewed as a set. Figure 5.11 plots the hazard vulnerability variables while Fig. 5.12 is a block level detail of Fig. 5.11 showing important features such as building level data as well as the floodplain.

5.3 Discussion

CEDS and NYCHVI can work in tandem, yet independently, as illustrated in Figs. 5.7, 5.8, 5.9, 5.10, 5.11, 5.12, and 5.13. As an example, we introduce the case study area of Brighton Beach, Brooklyn. NYCHVI can be used to quickly and efficiently disseminate crucial information to decision-makers and field personnel via an easily understood and interpreted dynamic user-driven and interactive cartographic product. For instance, the NYCHVI tool can be utilized to site critical care facilities (e.g., temporary housing, triage units, morgues) as well as expedite flexible

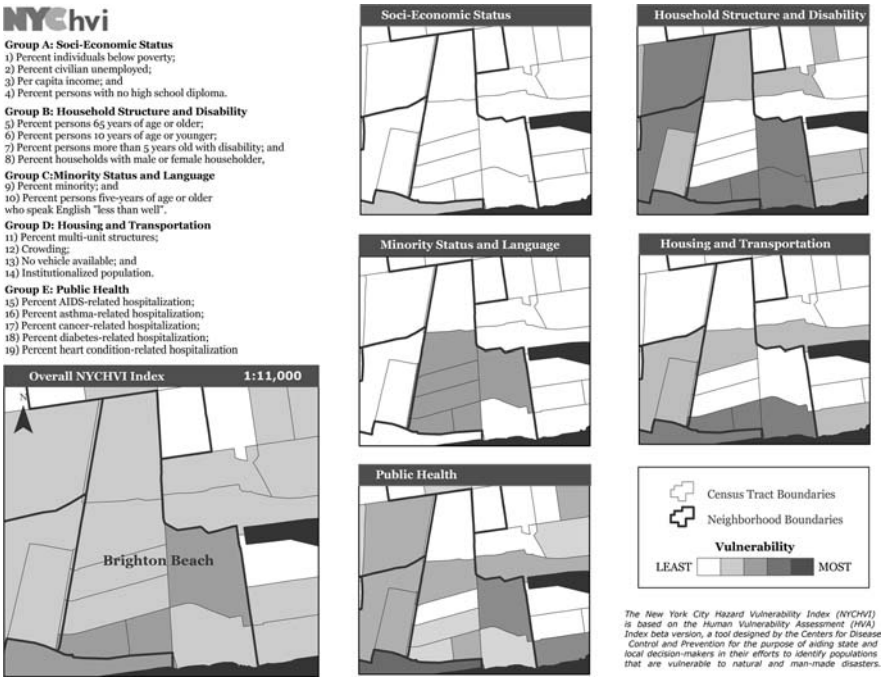

Fig. 5.11 NYCHVI print-out depicting five indicator groups and resulting overall index for the neighborhood of Brighton Beach, Brooklyn, NY at a scale of 1:40,000
Source: Tables 5.1, 5.2 and 5.3

planning for evacuation routes as information about the areal extent and magnitude of the disaster becomes available. For pre-disaster planning and mitigation, the NYCHVI model can be used to identify communities most vulnerable to flood hazards based on various socio-demographic factors. This ability enables more effective educational outreach, including the ability to create and distribute linguistically- and culturally-appropriate bulletins and publications. NYCHVI can also be employed to target specific at-risk communities for pre- and post-disaster resource allocation, based on socio-economic need and the particular health concerns of their residents.

Figure 5.11, for example, illustrates the potentially devastating effects of a flood on both special needs facilities and transportation systems. Several schools, childcare and eldercare institutions are either within the floodplain or are cut off from the main landmass by the floodplain's extent. The same situation holds true for the subway lines servicing the neighborhood as well as for a network of major and minor roadways. Figure 5.12 displays a specific grade school and neighboring residential buildings that are at risk of from the flood hazard.

CEDS provides more precise estimates of populations and sub-populations that could be directly affected by flooding, enabling efficient pre-disaster evacuation planning and allocation of post-disaster emergency resources. Used in tandem with

Fig. 5.12 NYCHVI user-driven report featuring overlay of lifeline and special needs facilities affected by a FEMA 100-year floodplain for the neighborhood of Brighton Beach, Brooklyn, NY at a scale of 1:10,000
Source: See Tables 5.1, 5.2 and 5.3

NYCHVI, the information is even more compelling. For instance, by examining the easternmost census tract in Brighton Beach (Fig. 5.10), NYCHVI reveals a comparatively high level of vulnerability mainly due to public health concerns, linguistically ability, and preponderance of specific age cohorts. Simultaneously, CEDS (Fig. 5.8) reinforces this impression by providing the absolute numbers and concentrations of vulnerable populations in categories such as disabled, elderly, children, limited English-speaking ability, lower-income, and racial/ethnic minorities.

5.4 Conclusion

The purpose of this chapter is to demonstrate the utility of two new complementary geomatic techniques: CEDS and NYCHVI. Using cadastral-based dasymetric disaggregation of census data, as well as the creation of vulnerability indices, more accurate and nuanced information is made available for emergency response and disaster planning.

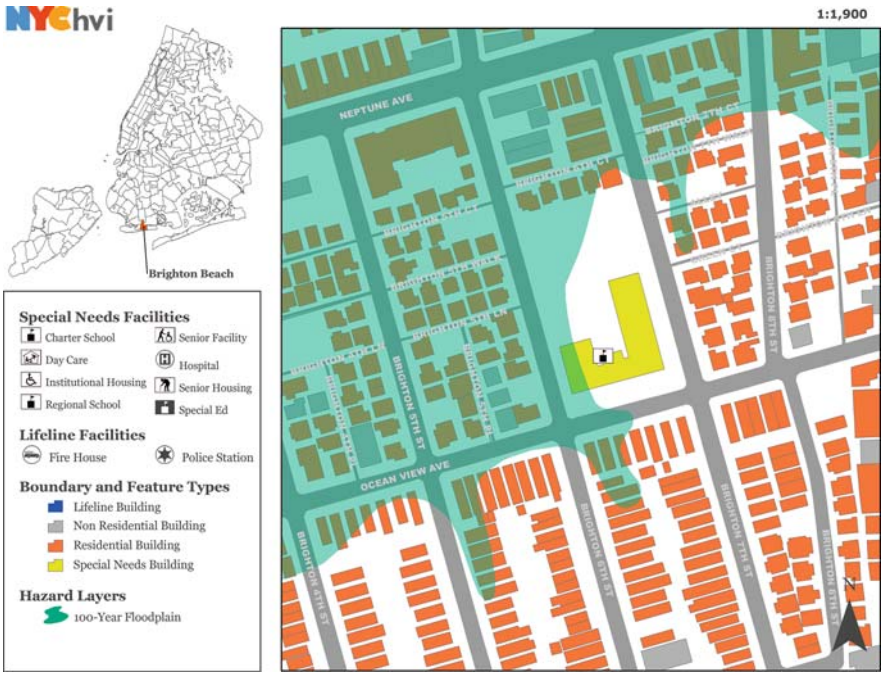

Fig. 5.13 NYCHVI user-driven report showing life line, special needs and residential buildings affected by FEMA 100-year floodplain for the neighborhood of Brighton Beach, Brooklyn, NY at a scale of 1:1900
Sources: Tables 5.1, 5.2 and 5.3

Both CEDS and NYCHVI enhance understanding of the geographic extent and magnitude of vulnerability to the flood hazard in New York City, providing significantly improved vulnerability estimates over previous methods. Through the addition of important elements, the manipulation of existing variables, and the incorporation of particularized spatial data layers and supplementary indicator data, the resulting NYCHVI is an overall vulnerability index based on potentially exposed population and population density, salient population indicators, and social and biophysical vulnerability. The disaggregation of census data with the CEDS technique results in a more precise way to delineate the boundaries containing populations potentially impacted by hazards.

The CEDS and NYCHVI methods are complementary but not duplicative, and each has specific purposes. CEDS provides general and sub-population density information revealing those who are especially vulnerable to hazards. NYCHVI examines relative quantities (e.g., rates, percentages) of vulnerable populations' potential exposure to flood risk in order to assist with resource allocation and plans for the provision of emergency services. Together, CEDS and NYCHVI provide a more comprehensive and accurate estimate than would be obtained using either method individually because they are taking into account different factors at different spatial scales.

While there is a benefit to examining vulnerability at different scales, inherent difficulties arise if one wishes to devise a single standard metric for a combined vulnerability index. NYCHVI works with census tract level data (e.g., health data), which is unlikely to be available at a finer resolution. CEDS performs at the tax lot level. While it might be possible to integrate CEDS and NYCHVI into a single index in the future, it currently seems more useful to retain them as separate indices since they are measuring different aspects of vulnerability.

There are substantial policy implications if CEDS and NYCHVI are used to estimate and identify populations at risk. These tools can more accurately determine the number of people at risk, as well as provide a more realistic indication of their socio-demographic characteristics. This knowledge can support planning efforts for emergency management, preparation, prevention, mitigation, and recovery planning, as well as encourage planning and response activities be crafted to address the specific needs of the populations involved. Culturally- and linguistically-appropriate materials can be developed to improve disaster preparation by better informing potentially affected communities, and also to better serve specific populations in a disaster's aftermath. Having precise knowledge of a at-risk populations' general health conditions (e.g., disabilities, mobility issues) that might complicate preparation or response activities (e.g., evacuation) could be critical in the event of a disaster. Such access also facilitates sending aid targeted to areas most in need of immediate help, for instance, areas with a high proportion of the elderly, disabled, or young. Since it has been shown that traditional methods of estimation significantly undercount populations of non-Hispanic Blacks, Hispanics, and those 65-years old or older that are located in NYC's flood hazard zones, these and similar populations will also benefit from these new models.

CEDS and NYCHVA can serve as a model to help other municipalities develop customized methods to estimate vulnerability to hazards, tailored to the specific conditions and characteristics of their locales. While this study focused on the flood threat, the models can estimate vulnerability and exposure to other types of hazards such as earthquakes, extreme weather events, and technological disasters (e.g., chemical spills, nuclear/toxic releases). By improving on past methods, CEDS and NYCHVA provide a robust visualization of biophysical and social vulnerability with more precise quantification of potential exposure.

Acknowledgments This research was partially supported by the National Oceanic and Atmospheric Administration's Cooperative Remote Sensing Science and Technology Center (NOAA-CREST) under NOAA grant number NA17AE162. The National Institute of Environmental Health Sciences of the National Institutes of Health also provided critical support for this project under NIEHS grant number 2 R25 ES01185-05. The statements contained within this paper are not the opinions of the funding agencies or the US government, but reflect the authors' opinions. This research was also supported by a Faculty Research Award from the Professional Staff Congress of the City University of New York (PSC-CUNY), Awards # 69372-0038, "Perfecting the Denominator: Developing a Cadastral-based Expert Dasymetric System in New York City."

List of Acronyms

ATSDR	Agency for Toxic Substances and Disease Registry
AW	Areal weighting
CCM	Centroid Containment Method
CDC	Centers for Disease Control and Prevention (US)
CEDS	Cadastral-based Dasymetric Expert System
FAW	Filtered Areal Weighting
FEMA	Federal Emergency Management Agency
GIS	Geographic Information System
GISc	Geographic Information Science
GPS	Global Positioning Systems
GRASP	Geospatial Research, Analysis, and Services Program
HAZUS	Hazards US
HVA	Human Vulnerability Assessment
NYC	New York City
NYCHVI	New York City Hazards Vulnerability Index
RA	Residential Area
RU	Residential Units
SPARCS	Statewide Planning and Research Cooperative System (New York State Department of Health)

References

Blaikie, P., Cannon, T., Davis, I., and Wisner, B. (1994). *At Risk: Natural Hazards, People's Vulnerability, and Disasters.* London, UK: Routledge.

Bloomfield, J., Smith, M., and Thompson, N. (1999). *Hot Nights in the City: Global Warming, Sea-Level Rise and the New York Metropolitan Region.* Washington, DC: Environmental Defense Fund.

Centers for Disease Control and Prevention/Agency for Toxic Substances and Disease Registry (CDC/ATSDR). (2008). *The CDC/ATSDR Public Health Vulnerability Mapping.*

Coch, N.K. (1994). Hurricane hazards in the Northeast US. *Journal of Coastal Research, Special Issue*, 12:115–147.

Cutter, S.L. (Ed.) (2006). *Hazards, Vulnerability and Environmental Justice.* London, UK: Earthscan.

Cutter S.L., Boruff B.J., and Shirley W.L. (2003). Social vulnerability to environmental hazards. *Social Science Quarterly*, 84(2):242–261.

Cutter, S.L., Mitchell, J.T., and Scott, M.S. (2000). Revealing the Vulnerability of People and Places: A Case Study of Georgetown County, South Carolina. *Annals of the Association of American Geographers*, 90(4):s713–737.

Eicher, C., and Brewer, C. (2001). Dasymetric mapping and areal interpolation: implementation and evaluation. *Cartography and Geographic Information Science*, 28:125–138.

Etzel, R.A., and French. J.G. (1997). Chapter 16: Air Pollution. In Noji, E.K. editor. *The Public Health Consequences of Disasters*. 1st ed. New York: Oxford University Press, pp. 336–353.

Federal Emergency Management Agency (FEMA) (1983). *The 100-year Base Flood Standard and the Floodplain Management Executive Order: A Review.* Prepared for the Office of Management and Budget. Washington DC: US Printing Office.

Federal Emergency Management Agency (FEMA) (2006). *HAZUS: FEMA's Software Program for Estimating Potential Losses from Disasters*, FAQ; www.fema.gov/plan/prevent/hazus/.

Fedeski, M., and Gwilliam, J. (2007). Urban Sustainability in the presence of flood and geological hazards: The development of a GIS-based vulnerability and risk assessment methodology. *Landscape and Urban Planning*, 83:50–61.

Fielding, J, and Burningham, K. (2005). Environmental inequality and flood hazard. *Local Environment*, 10(4):379–395.

Fothergill, A., Maestas, E.G.M., and Darlington, J. (1999). Race, ethnicity and disasters in the United States: A review of the literature. *Disasters*, 23(2):156–173.

Gornitz, V. (2000). *Climate Change and a Global City: An Assessment of the Metropolitan East Coast (MEC) Region Coastal Zone Sector Report: Sea Level Rise and Coastal Hazards*. (June 8, 2000). http://metroeast_climate.ciesin.columbia.edu/.

Gornitz, V., Couch, S., and Hartig, E. (2002). Impacts of sea level rise in the New York City metropolitan area. *Global and Planetary Changes*, 32:61–88.

Holt, J. B., Lo, C.P., and Hodler, T. W. (2004). Dasymetric estimation of population density and areal interpolation of census data. *Cartography and Geographic Information Science*, 31:103–121.

Homeland Security Working Group. (14 Sept. 2005). *Homeland Security Working Group Symbology Reference*. 28 Apr 2008 http://www.fgdc.gov/HSWG/index.html.

Kilbourne, E.M. (1997). Chapter 12: Heat waves and hot environments. In: Noji, E.K. (ed.) *The Public Health Consequences of Disasters*. 1st ed. New York: Oxford University Press, pp. 245–269.

LotInfo, LLC. (2003). *LotInfo*. SpaceTrack, Inc. 304 Park Ave, 11th Floor New York, NY 10010.

Maantay, J.A., Maroko, A., and Herrmann, C. (2007). Mapping population distribution in the urban environment: The cadastral-based expert dasymetric system (CEDS). *Cartography and Geographic Information Science*, 34(2):77–102.

Maantay, J.A., and Ziegler, J. (2006). *GIS for the Urban Environment*. Redlands, CA: Environmental Systems Research Institute (ESRI) Press.

Marandola Jr., E. and Hogan, D.J. (2007). Vulnerabilities and risks in population and environmental studies. *Population and Environment*, 28(2):83–112.

Mitchell, J.K. (1999). *Crucibles of Hazard: Megacities and Disasters in Transition*. Tokyo: United Nations University Press.

Negri, A., Burkardt, N., Golden, J., Halverson, J., Huffman, G., Larsen, M., McGinley, J., Updike, R., Verdin, J., and Wieczorek, G. (2005). The hurricane–flood–landslide continuum. *Bulletin of the American Meteorological Society*, 86(9):1241–1247.

New York Coty Department of Health and Mental Hygiene [DOHMH]. (2006). *Community Health Profiles: Southern Brooklyn.*

Noji, E.K. (1992). Disaster epidemiology: Challenges for public health action. *Journal of Public Health Policy*, 13(3):332–340.

Noji, E.K. (1997). Chapter 8: Earthquakes. In: Noji, E.K. (ed.) *The Public Health Consequences of Disasters*. 1st ed. New York: Oxford University Press, pp. 135–178.

Sanderson, L.M. (1997). Chapter 18: Fires. In Noji, E.K. editor. *The Public Health Consequences of Disasters*. 1st ed. New York: Oxford University Press, pp. 373–396.

Wu, S., Qiu, X., and Wang, L. (2005). Population estimation methods in GIS and remote sensing: A review. *GIScience and Remote Sensing*, 42(1):80–96.

Chapter 6
Geo-Information Technology for Infrastructural Flood Risk Analysis in Unplanned Settlements: A Case Study of Informal Settlement Flood Risk in the Nyabugogo Flood Plain, Kigali City, Rwanda

Jean Pierre Bizimana and Michele Schilling

Abstract The main objective of this research was to improve flood mitigation within Rwanda's rapidly growing Kigali City using Geo-Information Technology (GIT) to identify flood hazard zones, analyze flood exposure and vulnerability, and suggest planning interventions. Multiple sources of data and methods were utilized including a very high resolution Quickbird image, Global Positioning Systems, interviews and a survey that aided flood hazard zone delineation, flood depth interpolation and mapping. The flood exposure analysis incorporated vulnerable infrastructure, buildings, population and economic activities and revealed that 27% of buildings were located in flood prone areas. Additionally, two sensitive sectors of infrastructure, four sensitive economic sectors and approximately 500 people were identified as vulnerable. The results influenced policy because Kiruhura's major market was relocated to a new site and new urban developments were restricted from building within the flood way. The study developed a model for flood risk analysis adapted to the specificity of Kigali City, demonstrating the need to explicitly incorporate these risks into the recently developed Kigali City Master Plan. The research stresses the importance of the integration of flood risks (and natural risks, in general) into major national development strategies, policies and laws related to Rwanda's urbanization.

Keywords Rwanda · Flood modeling · Flood management · Developing country · Africa

---

J.P. Bizimana (✉)
Geography Department, Faculty of Sciences, National University of Rwanda,
Affiliated Researcher at CGIS-NUR Butare, Rwanda
e-mail: bizijp@yahoo.fr

At the time of writing, Dr. Michele A. Schilling was a Senior Lecturer in the Geography Department, Faculty of Sciences, and an Affiliated Researcher in the Geographic Information Systems and Remote Sensing Centre of the National University of Rwanda. As founder and Director of the Center (2001-2007), Schilling was instrumental in the development of a GISc-based Education and Research program at the University and in Rwanda.

P.S. Showalter, Y. Lu (eds.), *Geospatial Techniques in Urban Hazard and Disaster Analysis*,
Geotechnologies and the Environment 2, DOI 10.1007/978-90-481-2238-7_6,

6.1 Introduction

Urbanization in flood hazard zones creates a challenge as urban areas accommodate higher concentrations of people, buildings and infrastructure (Wamsler 2004). Despite increasing flood risk awareness, human settlements continue to develop in flood-prone areas due to the need for land, and poverty (Gupta 1994). These conditions reflect reality for the urban poor who are faced with little option other than to illegally occupy public land or purchase affordable land in hazard zones (Montoya 2006).

Recently, this general relationship between urbanisation and informal settlement growth in flood-prone areas has been observed in Kigali, capital of Rwanda (MINITERE/Rwanda 2004). Rwanda, known as the "Country of a Thousand Hills", has a topography characterized by steep hills and mountains. While these characteristics generate landscapes of exceptional beauty, they also pose serious challenges for urban planning in Kigali.

Kigali City, which is located on interlocking hills separated by valleys and swampy areas, has little land for urban development. According to the recent Kigali City Master Plan, most informal developments in the city are located in wetlands or on steep slopes where 12% of the built-up areas are already located on land unsuitable for development (MININFRA/Rwanda 2006). This situation is aggravated by cumbersome legal procedures that discourage access to land by the urban poor. As noted by Duran Lasserve (2005), the urban poor (such as those in Kigali) cannot comply with construction standards and regulations, so find themselves living in slums.

Recognition of the increased vulnerability of people and infrastructure to the threat of flood loss in Kigali stimulated the need for a robust assessment of risks in flood-exposed informal settlements, and the complexity of the problem called for the application and adaptation of contemporary Geo-Information Technologies (GIT). The research applied existing GIT-based approaches for flood risk analysis of rapidly growing and unplanned settlements in Kigali City to improve urban planning and policy formulation by decision makers. Table 6.1 provides the sub-objectives and research questions defined for the study.

Table 6.1 Objectives and research questions

Sub-objectives	Research questions
Identify the flood zones in the study area.	■ What locally measurable indicators can be used to identify flood hazards? ■ What is the extent of flood hazards in the study area?
Analyze flood exposure and identify elements that are highly exposed to flooding	■ What indicators can be used to analyze exposure to flooding? ■ What elements are exposed to flooding?
Analyse flood vulnerability	■ What are suitable indicators for identifying vulnerability to flooding? ■ What was the impact of the last flood event on buildings, infrastructure, population, and economy in the study area?

Table 6.1 (continued)

Sub-objectives	Research questions
Suggest effective planning strategies to mitigate the risks of flooding along the Nyabugogo River	■ What are the expected losses or damage to property when the next flood occurs? ■ What are the implications for future policy development for areas along the Nyabugogo River? ■ What policy is needed to prevent urban expansion in flood-prone areas along the Nyabugogo River?

6.2 Flood Risks

6.2.1 Urban Flooding: The Global Context

Dartmouth University's flood database reveals that flooding has killed about 300,000 people between 1985 and 2006. From January to October 2006 alone, more than 6790 people died while 17,336,000 people were displaced around the world due to floods (University of Dartmouth 2006). A single event, a tropical cyclone flood in 1991, killed 138,000 people in Bangladesh. In Africa, approximately 980 people died and more than 500,000 were displaced by floods in 2006 (University of Dartmouth 2006).

Asian countries are more affected by floods due to monsoonal rain, high population density in the cities, and lack of planning regulations and flood controls (Nelson 2006). However, the West is not immune to the problem, as was dramatically illustrated by the flooding of New Orleans in 2005 – 80% of the city was inundated, mainly due to the breaching of 53 different levees. And, in view of the recent damages caused by successive hurricanes worldwide in 2008, the threat of flooding seems to be on the increase (Dartmouth Flood Observatory).

In general, flood losses have greatly increased over the years due to land-use change, urbanization of flood-prone areas, sub-standard construction, and high population density (Guarin et al. 2004). Cities are more affected by floods than rural areas due to high population densities and concentration of economic activities (Merson et al. 2004; Montoya 2003). Urban floods are intensified by impermeable surfaces and runoff concentration, and by buildings that obstruct water flow. Mendel (2006) describes four types of urban flood: (1) localized – occurs many times a year especially due to increased runoff and poor drainage conditions; (2) small stream – water rises quickly with high flows that exceed drainage capacity if channels are not regularly maintained; (3) river – results from upstream land use change and engineering works when dams and levees break, leading to sudden flooding downstream (urbanization of flood plains also impacts the natural river overflow and increases the possibility of flooding); (4) seasonal – when rain and river water combine to elevate water levels at certain times of the year. Urban areas in developing countries are at greater risk due to high population growth and rapid urbanization caused by rural-

to-urban migration. Large numbers of urban immigrants find themselves in fragile economic circumstances, which lead to the creation/expansion of informal settlements in high risk zones. Therefore, urban flooding increases with urbanization in flood-prone areas (Alkema 2003).

Fortunately, the United Nations Development Program's global report (UNEP 2004) states that urbanization doe not necessarily have to lead to an increased disaster risk and can, if properly managed, contribute to disaster reduction. When urban growth in flood hazard-prone locations is accompanied by proper building standards and planning considerations, the flood risk can be managed or even reduced. However, the complexity of the flood risk in urban areas suggests that high resolution data collection systems are required in order to identify patterns of flood hazard, vulnerability and exposure. Where the required data and information are lacking, urban flood risk assessment and monitoring poses a wide range of conceptual, methodological, and implementation challenges. Such is the case in Rwanda, and especially in Kigali City, where rapid urban development spreads out on steep slopes and in flood-prone locations where flood information is not regularly recorded.

6.2.2 Kigali City: Urban Growth and Rainfall Exposure

Kigali is the only official city in Rwanda. It is located in the central part of the country (Fig. 6.1).

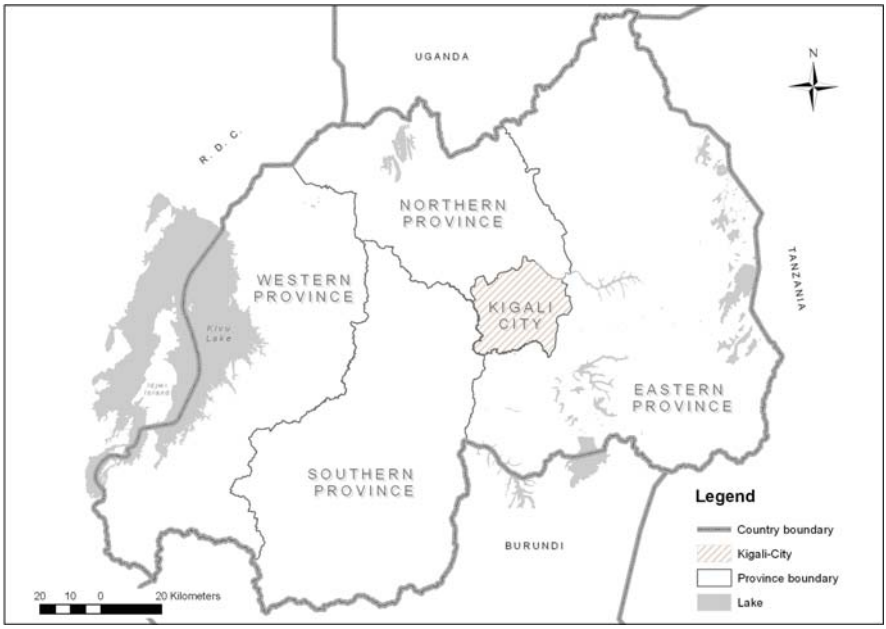

Fig. 6.1 Location of Kigali City in Rwanda.
Source: MINITRACO/CGIS-NUR, 2001 and NISR, 2006

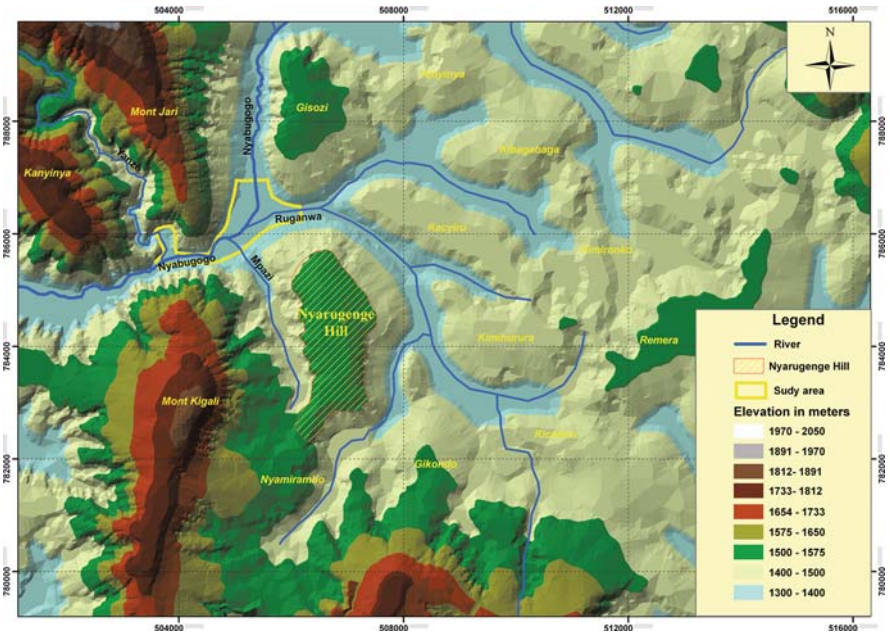

Fig. 6.2 Location of the study site
Source: Topographic map of Rwanda, 1988

The new administrative region of Kigali City is large and dominated by rural land use but also encompasses a mix of urbanized and urbanizing areas. The growth of Kigali City during the colonial period (from 1909 to 1962) was very slow and limited to the Nyarugenge hill (Fig. 6.2). Soon after independence, when all administrative functions were relocated to Kigali, the city extended beyond Nyarugenge hill to neighboring hills such as Nyamirambo, Gikondo, Kimihurura and Kacyiru (MININFRA 2006).

The study area (Fig. 6.2) lies near the original hill of Nyarugenge along Nyabugogo River, between the steep hills of Gisozi, Mont Jari and Kanyinya, Mont Kigali and Nyarugenge. Due to the steepness of relief and intense rainfall, the swampy valleys constitute hazardous locations for settlements and a drainage challenge, especially along Nyabugogo River.

From 1996 to 2002, Kigali City's population increased from 350,000 to 603,000, an increase of 42% (MINECOFIN 2002; MININFRAST 2004); the average annual growth rate is 2.6%. The current urban population is more than one million, located within a "built-up" area estimated to be 65.6 km^2 in size. Urban development is characterized by the coexistence of formal and informal growth, with the majority of people (83–85%) living in informal settlements (Aibinu 2001).

As Kigali City urbanized, people began occupying the Nyabugogo River's flood plains, raising the issue of flood exposure. Figure 6.3 illustrates this issue by showing the proximity of the Kiruhura Market to the river's waterway.

Fig. 6.3 Location of Kiruhura Market near Nyabugogo River Source: Photo Tordjeman, April 2003

Data from the closest weather stations to Kigali City show that the annual rainfall between 1992 and 2006 ranges from 900 to 1600 mm. The total annual rainfall within the city of Kigali averaged just over 900 mm (MININFRA 2006; MININFRAST 2004). Figure 6.4 illustrates that the western highlands and north-western parts of Kigali are receiving higher rainfall than regions further east. In the Nyabugogo River plain, the highest average annual rainfall varies from 1100 to 1600 mm.

The combination of intense rainfall, wetland areas, and steep slopes make the areas around Kigali City highly susceptible to risk of flooding.

6.2.3 Kigali: Recent Flood History

Due to the steepness of its terrain, intense rainfall (Sirven et al. 1974; Verdoodt 2003), and population pressure on land, many areas of Rwanda have been flooded in the last twenty years. In May 1988, a flood occurred in former Ruhengeri Province

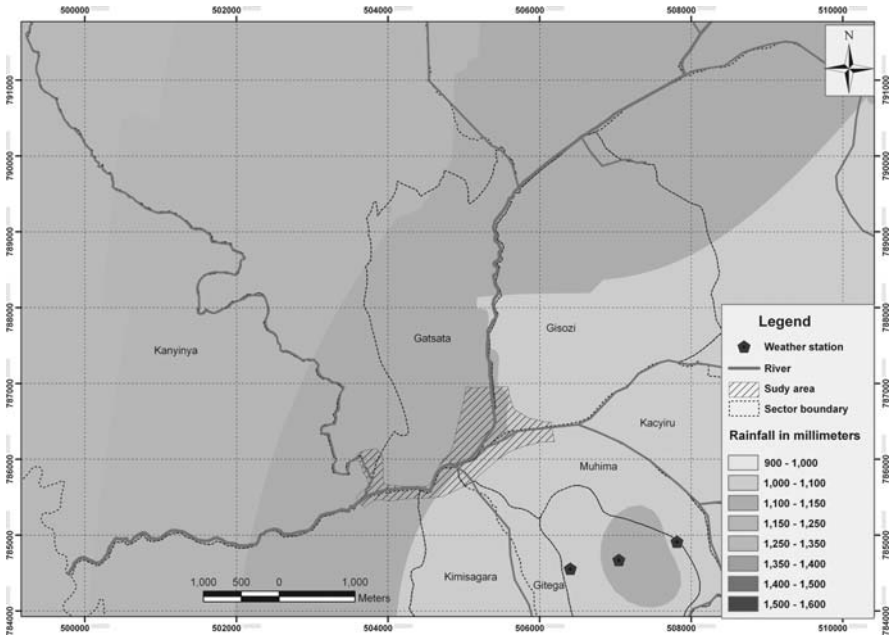

Fig. 6.4 Average rainfalls distribution for the study area from 1992 to 2006
Source: Rwanda Meteorological Services, MININFRA, 2006

(Byers 1992), during September and December 2001 floods damaged infrastructure and crops in west Rwanda (MININFRA/Rwanda 2004b) and another flood occurred that November in Kijote settlement (formerly Gisenyi Province) (University of Dartmouth 2006; USAID 2001). Recently, on 28 November 2006, 25 people died in Rulindo district when the Base River burst its banks and swamped a village. Similarly in Rubavu District (Western Province) during a flood in September 2007, houses were flooded and people died (New Times[1]).

In April 2002, the main road connecting traffic between Rwanda's two major cities (Kigali and Butare, now Huye) was cut off at Nyabarongo Bridge and became temporarily impassible. This situation created traffic congestion. More recently, a flood in April 2006 destroyed 40 houses and resulted in two deaths (New Times,10 April 2006). The Kiruhura market in the Nyabugogo River plain (Fig. 6.3) is located in a narrow valley between two steep mountainous areas and the river overflowed into the shops reaching 1.5 m in height. The 132 small shops had to be temporarily relocated upstream. In May 2006, the Kigali City council decided to relocate the market to a new site free of flood hazard risks. Similarly, the RWANTEXICO factory was flooded to 1.5 m and ceased functioning (Fig. 6.5).

The cases described above show that repeated flooding is becoming a serious problem and challenge for urban and regional planners in the City. The flood chal-

[1]New Times, Rwanda daily newspaper (www.newtimes.co.rw)

Fig. 6.5 Flood level observed in RWANTEXICO floods of April 2006
Source: Photo taken by Jean Pierre Bizimana, September 2006

lenge requires that new strategies and mitigation measures be implemented in areas identified as being at risk of floods.

6.3 Flood Risk Analysis: Conceptual Frame and Analytic Steps

6.3.1 Analytic Components of Flood Risk Analysis

The key concepts underpinning this research are flood hazard, flood exposure, flood vulnerability and flood risk. Although often used interchangeably, these terms have meanings that communicate slightly different ideas (Zeigler et al. 1983). The flood hazard denotes the probability and severity of occurrence of a flood of a certain magnitude (Alkema 2003). The flood exposure refers to the extent to which property, buildings, economic activities, infrastructure and population are located in relationship to a flood hazard (Barroca et al. 2006; McEwen et al. 2002). Flood vulnerability encompasses physical, social, economic and environmental factors which increase susceptibility to the flood hazard (UN/ISDR 2004a). Flood risk represents expected loss or damage to property, loss of human life, and interruption of economic activities due to flooding. Flood risk depends on flood hazard, exposure and vulnerability (Davidson 1997). For example, if buildings are located in a flood plain, both hazard and exposure are present, but if the buildings are perfectly resistant to floods, vulnerability is absent, so there is no flood risk. As another example, consider an empty plot of land within the flood plain – the hazard is present but both exposure and vulnerability are absent, so there is no flood risk for that property (Fedeski and Gwilliam 2007).

When analyzing flood risks, some basic questions flood analysts might ask are: What can go wrong in the case of flooding? How likely is it that it will happen? If it does happen, what may be the consequences? What can be done to eliminate flood occurrence or reduce the risk of flooding? (Zeigler et al. 1983). Geographers are interested in spatial questions such as: Where will the flood occur? How likely is it that a flood hazard will happen at this place? If it is flooding, what will be the event's geographical extent and impact? How can the space be managed to reduce flood risks? Answering these questions can help identify effective planning strategies to mitigate the risks of flooding.

Different frameworks have been developed to identify flood hazards and risks (Barredo et al. 2005; Davidson 1997). One such study used the flood hazard, exposure, vulnerability and capacity indicators to analyse the flood risk in the Volga River Basin, Russia (UNU-IEHS and NNSUACE 2006; Fig. 6.6). But this proposed framework does not contain suitable indicators for flood risk analysis in Kigali City. The capacity component can not be assessed for this research as the necessary data are lacking or difficult to acquire in the study area. Consequently, the framework has been altered, as shown in Fig. 6.7.

The framework in Fig. 6.7 is instructive but highly generalized. Therefore, a clearer explanation of flood risk indicators is necessary. The next section of this chapter discusses our attempt to identify indicators for each component and describes how these components can be analyzed.

6.3.2 Flood Hazard Identification and Mapping

Various definitions of flood hazard have been provided. According to Alkema (2003), flood hazard represents the probability of occurrence at a certain level

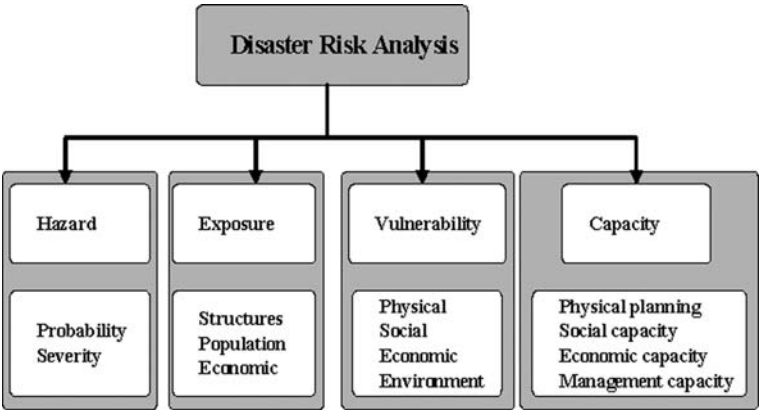

Fig. 6.6 Framework for flood risk analysis
Source: Modified from UNU-IEHS and NNSUACE, 2006

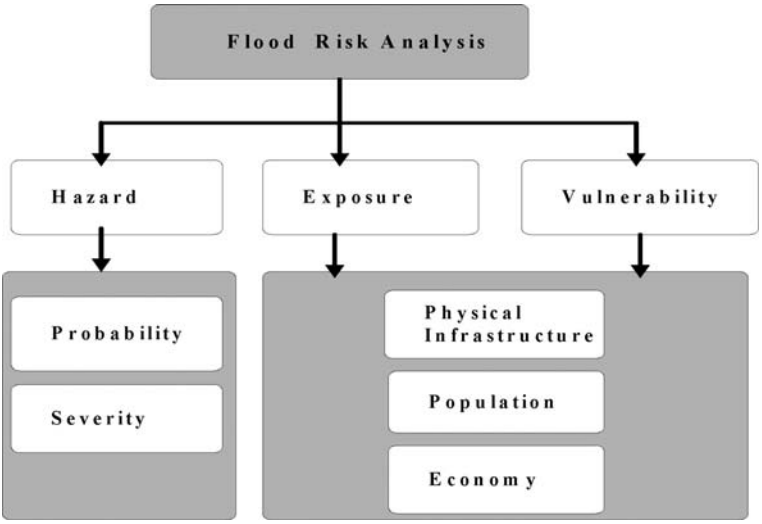

Fig. 6.7 Modified framework for flood risk analysis
Source: Modified from Davidson 1997 and UNU-IEHS/ NNSUACE, 2006

of severity. Flood severity is characterized by water level, flood duration and velocity, while probability refers to flood frequency (Alkema 2003; Barroca et al. 2006). Other authors add to the definition warning time, the rate at which the water rises, accessibility to flooded areas, and level of development (which may impede or improve access) to characterize flood hazards (New South Wales 2005). Similarly, the Disaster Management Programme of the United Nations Commission for Human Settlement has recommended consideration of the following indicators: flood rate, load sediments, volume of water, duration and area affected (UNCHS-Habitat 2001). As can be seen by the above, one approach to flood analysis is largely based on physical characteristics (depth, duration, velocity, frequency, extent, flood size, and load sediments), and another approach on response variables (warning time, readiness, rate of rise and access). This research emphasizes the physical characteristics with a focus on measurable indicators such as flood depth, frequency, and duration.

When a flood hazard is identified, the next step may be flood mapping. This step identifies and displays the spatial variation and extent of the flood (Noson 2002). To fulfill this step, one approach is based on historical records of flood characteristics where flood depth is the main indicator (Islam and Sado 2002). Sanyal and Lu (2005) argue that a higher flood depth is associated with a higher discharge of water which determines the extent of flood-induced flood damages. The flood level is defined as the highest level reached by water above the local height datum. The flood extent map defines how far a given water level will locally extend. Based on flood level, different methodologies have been developed to generate flood extent maps. MacKinnon (2004) derived flood extent from a digital elevation model (DEM) by separating pixel values into areas below and above the high

flood level, thereby delineating areas that would or would not be flooded. To assess potential flood damage, flood depth and extent were modeled by giving pixels at water level values of zero to enable pixels below water level to have positive values depending on their "depth". Then, using the flood extent map, the flood depth raster map was clipped to display flood depth values solely within the extent of the flood (MacKinnon 2004). Tennakoon (2004) reclassified the flood depth pixel values into different flood hazard zones, with 0.8 and 1.2 m representing the upper limits of low and medium flood, respectively. The present research is based on MacKinnon's and Tennakoon's approach.

While spatial extent and flood depth are commonly used for flood mapping, it is also quite useful to integrate flood duration and velocity (Tennakoon 2004) to help evaluate flood severity. However, duration has not been integrated into many flood hazard studies due to the data and expertise cost of its estimation (Tennakoon 2004), which requires hydrologic modeling. These constraints, as well as the lack of reliable hydrological records for the study area, preclude the use of flood duration data in this research.

When there are no flood records, remote sensing technology can be used to map flooded areas if satellite images have been acquired during the flood's peak (Prathumcha and Samarakoon 2005). While estimating flood depth from remote sensing images is very difficult, indirect methods based on the amount of energy reflected by water have been developed (Sanyal and Lu 2005). However, such estimates require advanced satellite image processing capability utilizing radar (e.g., Synthetic Aperture Radar). Although radar imagery can penetrate cloud cover, its use in developing countries such as Rwanda is constrained by its high price and limited spatial and temporal coverage due to the lack of ground receiving stations.

6.3.3 Flood Exposure

Flood exposure is the extent to which properties, houses, economic activities and infrastructure are geographically situated in flood-prone areas (Barroca et al. 2006; McEwen et al. 2002). Exposure relates the floodplain, people's location and closeness to the area of inundation, and housing/property characteristics to one another. The relationship between flood exposure and vulnerability of exposed elements is directly proportional: as exposure increases, vulnerability increases. Accordingly, there is no vulnerability to flooding where there is no flood and there is no vulnerability if no elements are exposed (Goosby et al. 2005).

Flood exposure analysis identifies flood-prone areas and the elements within them that are exposed to flooding. The physical characteristics of the flood are examined and information about exposed elements (proximity to river, location in or closeness to flood plain) provided. In urban areas, elements at risk may include properties, buildings, infrastructure, population, environment, cultural assets and economic activities (Messner and Meyer 2006). To document exposure requires knowledge about the number of people, buildings, critical facilities and infrastructure (e.g., roads, bridges), and land use types (e.g., residential, commercial, industrial, agricultural) within flood prone areas (Barredo et al. 2005).

6.3.4 Flood Vulnerability Assessment

There are three main approaches to assess flood vulnerability: physical, social context, and combined (or global). The physical approach focuses on human occupancy of flood zones, degree of loss, flood characteristics, and flood impacts (Messner and Meyer 2006). This approach determines how exposed people, physical objects and activities may be affected (Davidson 1997). Physical vulnerability can be assessed through examining infrastructure, housing, economic activities, geographic location and population density. Exposed elements (e.g., residential houses, infrastructure, industrial or commercial activity, health services) have different degrees of vulnerability when located in the same flood-prone area (Barroca et al. 2006). Some mechanisms such as location of structures, structure types, their ability to resist flood damage, and tendency to flood can turn a mundane flood into disaster by increasing physical vulnerability to the flood (Blaikie et al. 1994).

Social vulnerability approaches examine the social context of floods as it relates to the coping response of communities (Messner and Meyer 2006). In this context, flood vulnerability analysis examines how well prepared and equipped a community is to avoid or cope with floods (Etkin et al. 20043). Coping includes the adaptive capacity of a system or people to deal with floods or reduce flood risk. Another aspect relates to the knowledge of exposed people as is studied by examining awareness and perception. When aware of the flood risk, individuals or societies are able to adapt. They may modify urban development plans or change building techniques (Barroca et al. 2006). Flood vulnerability can also be assessed by documenting the lack of ability or unwillingness of planning authorities to reduce the flood risk (Messner and Meyer 2006).

The global approach combines the physical and social approaches by including physical, social, economic and environmental factors (UN/ISDR 2004a). According to Barroca et al. (2006), this approach is gaining increasing significance in scientific research. This research sees flood vulnerability as a combination of the characteristics and location of properties, buildings, housing, infrastructure, population, and economic activities in terms of their capacity to anticipate, cope with or resist floods. Identifying the strengths and weaknesses of the exposed elements and relevant stakeholders allows decision makers to effectively allocate limited resources to prevent or mitigate the effects of the floods (UN-Habitat and UNEP 2001).

6.3.5 Flood Risk Indicators

Following the above description of the main aspects in flood risk analysis, the analytical framework and the associated indicators for this urban flood research is presented in Fig. 6.8. This framework considers three main components of flood risks and corresponding indicators. If data are locally available, they can help identify flood-prone areas, determine exposed elements, and analyze vulnerability to flooding. Unfortunately, reliable, timely data are difficult to obtain in developing

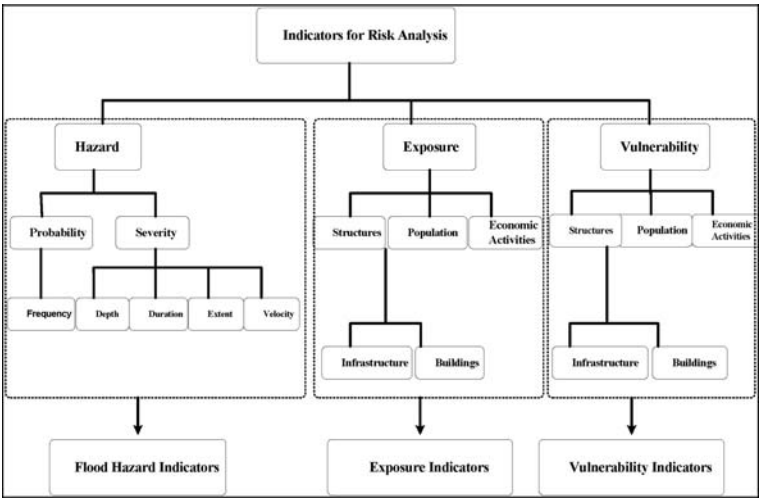

Fig. 6.8 Indicators for flood risk analysis
Source: Adapted from Davidson 1997 and UNU-IEHS and NNSUACE, 2006

countries; in some cases, the information may be known but not adequately communicated to, or perceived by decision makers (Bacic-Ivan et al. 2006) who seek to formulate flood risk reduction strategies. In this study, GIT is utilized as most of the data are spatial in nature (Beerens 2006; Montoya 2006). Using GIS and remote sensing to identify and help visualize flood risks can improve understanding and therefore help reduce the impact of flooding.

6.4 Research Methods and Findings

6.4.1 Data Collection

This research has been guided by an extensive literature review of research articles, government reports and policy documents analysis. Secondary data and primary data were both used. Secondary spatial datasets consist of a Quickbird multispectral satellite image acquired on 26 December 2004 with a resolution of 2.82 m (available from CGIS-NUR[2]), aerial photos taken in 2003 above Kiruhura market, existing spatial datasets (boundaries, roads network, river streams) derived from topographical maps of Rwanda (1:50,000 sheet, Kigali 1988), and meteorological data linked to the weather stations. Primary data consist of field observations, photography, interviews with urban planning authorities at sector, district and city levels and a household survey (including GPS location data of housing

[2] *Geographic Information Systems and Remote Sensing Training and Research Center of National University of Rwanda.*

units). This survey was conducted during September 2006 with 120 households. The survey sample was selected within or along the Nyabugogo flood plain in areas that experienced the April 2006 flooding and within a distance of 20 m from the flood plain (the distance was chosen because construction is not allowed in closer proximity to the floodplain) (Primature-Rwanda 2005). Sampling was based on proximity to the riverbank or flood plain, experience with floods, and occupation by infrastructure, properties, housing or settlements. In collaboration with community leaders, flooded areas were delineated using the Quickbird satellite image aided by local knowledge about flood extent in the study area. To generate building footprints and other critical land uses in the study area, the Quickbird image was georeferenced and digitized on a computer screen using ArcGIS® 9.2 software.

6.5 Flood Risk Analysis: Identifying and Mapping Flood Hazard-Prone Areas

As discussed earlier, the flood hazard consists of probability and severity. Because of data limitation, the analysis focused on severity. Flood severity was assessed using flood depth and flood extent. To identify the flood hazard areas, the flowchart in Fig. 6.9 illustrates the methodology used to generate the flood map. The input data were contour lines, the Quickbird image, and flood depth information from the household surveys. The flood hazard map was generated through the delineation of the flood plain extent using information from local experts at the district level, Digital Elevation Model (DEM) quality improvement, extraction of elevation information at the houses (point location of flood depth), subdivision of the study area into two zones, flood depth interpolation and flood depth mapping based on average house elevation in each zone.

6.5.1 Data Quality Control and Preparation

As the study area occupies a narrow valley between two highlands, the lowest elevation was not shown by the lowest contour line of 1375 m. However, most of the household samples were located below 1375 m. Therefore, an alternative approach was needed to improve the low resolution DEM. Based on methodology developed by Hengl et al. (2004), the resolution was improved by digitizing a supplementary contour line and interpolating other intermediate contour lines that indicate small morphologies not indicated on the topographic map. The new value of the digitized contour line was assigned using spot height values of the river in the topographic map. The final DEM was generated using an Inverse Distance Weighted Interpolation technique that calculates height value for any point that falls between two contour lines. The result is an improved DEM with new elevation contour lines in the flood plain, providing more topographical information regarding variation in elevation.

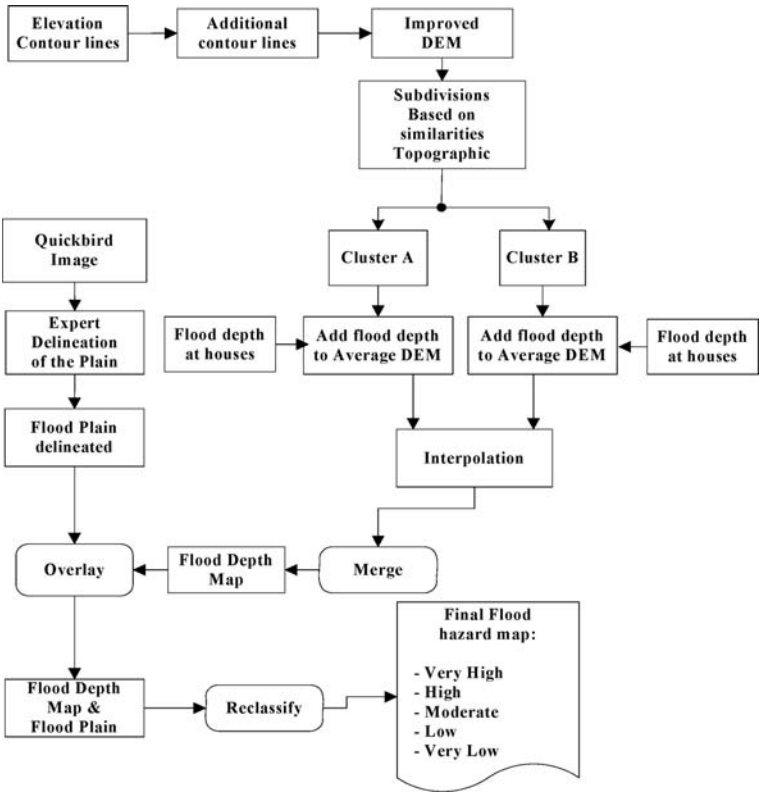

Fig. 6.9 Flowchart process for flood hazard mapping

Once the DEM was improved, a triangulated irregular network (TIN) was generated at 10 m pixel size. The 10 m pixel size was chosen because it illustrates more details in the valley. To obtain topographic information at each house, the household sample points digitized from the Quickbird image were superimposed on the TIN and elevation was extracted for each house's location (Fig. 6.10). This way, the resolution of the DEM was improved to help extract topographic information needed for flood hazard mapping.

6.5.2 Mapping Flood Extent and Depth

The data used for flood extent mapping were obtained from official interviews at the district level. To identify the flood extent, the flood plain was delineated by local experts and digitized from the Quickbird image. The flood depth from household surveys was estimated based on watermarks found on the houses with reference to the ground. To obtain data of flood depth, the observed flood depth at a house

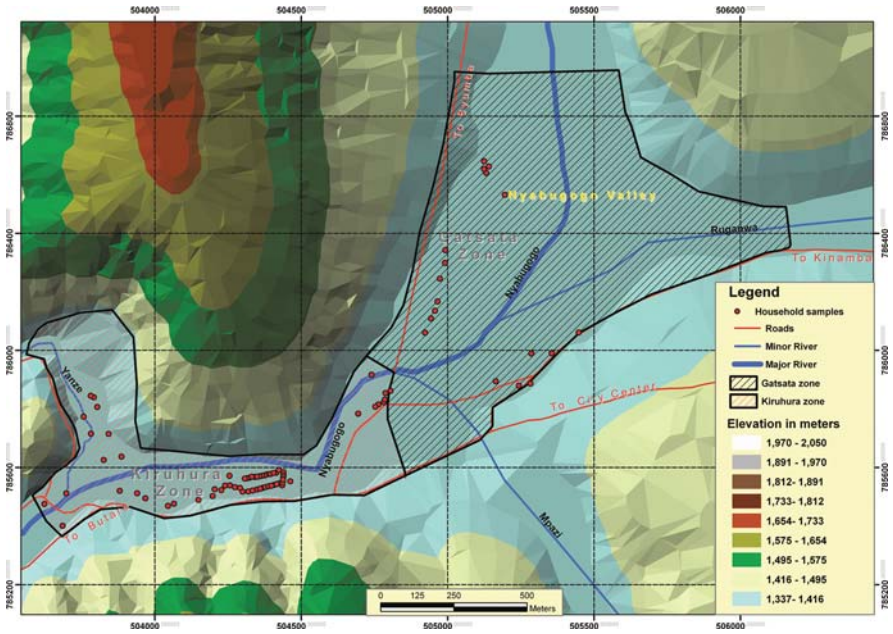

Fig. 6.10 Topography and location of surveyed houses
Source: Topographic map of Rwanda, 1988

location was first added to the corresponding elevation value from the DEM; interpolation was then conducted to generate a flood depth surface. However, the elevation of the study area varied greatly (from 1368 to 1377 m) within a very small area and flooding is strongly influenced by flatness or steepness of topography. For example, different houses experienced the same degree of flooding (1.00 m of flood depth) while being located in areas of great difference in elevation (4 m of elevation difference). Thus, interpolating flood depth based on elevation would not produce an accurate result. To solve this issue, it was decided to analyze flood depth extent in two subdivisions based on the topographic similarities of the house samples (zones with almost the same altitudes and slopes). Figure 6.10 illustrates that the two flood zones are largely separated by the paved road to Byumba.

Data for a runoff flood were not integrated because that type of flood is very localized. The flood map was generated by interpolating flood elevation values based on average elevation of flooded houses and presents the spatial distribution of flood level, from a very low to a very high flood. The corresponding flood class values are listed as: very low (0−0.30 m), low (0.30−0.60 m), moderate (0.60−0.90 m), high (0.90−1.20 m) and very high (1.20−1.50 m). Based on flood depth distribution, three high flood zones are distinguished (Fig. 6.11). The first zone in the southwest lies near the confluence of the Yanze and Nyabugogo Rivers. The second zone is located near the Kiruhura market where buildings obstruct the flood ways and delay or hold back water flow. The third zone (northeast) is on very flat

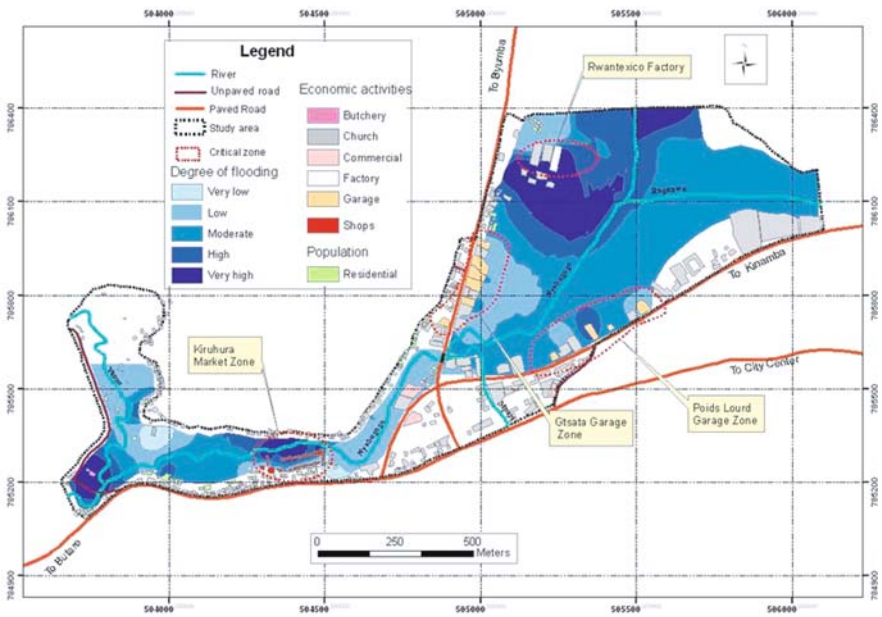

Fig. 6.11 Flood exposed economic activities in Nyabugogo valley

terrain where Nyabugogo valley is located. This zone is swampy and acts to store large amounts of water during the rainy season. Interestingly, a runoff flood was located in the Gatsata zone caused by poor drainage infrastructure (an inadequate bridge and closed culverts). Nevertheless, this finding was not incorporated into the analysis because it is much localized and strongly dependent on topography and/or drainage infrastructure.

6.6 Flood Risk Analysis: Analyzing Flood Exposure

After mapping the flood depth, information about elements at risk (e.g., buildings, roads, bridges, water supply, population, economic activities) were overlaid on the flood zones. Figure 6.12 presents a flowchart that describes the methodology used to estimate the exposed elements in each flood zone.

The flood exposure analysis was performed by locating exposed elements in relation to flooding. The result of the analysis revealed that 27% of buildings were located in flood prone areas in addition to two sensitive zones of infrastructure, and approximately 500 people. Four sensitive economic zones were also identified as exposed: Kiruhura Market, Gatsata Garage, Poids Lourd Garage and Rwantexico factory (Fig. 6.12). The Kiruhura market is located in a high flood zone, in the flood way of Nyabugogo valley. The market's location makes it prone to seasonal river flooding. Moreover, the concentrations of buildings (mainly shops) are not only

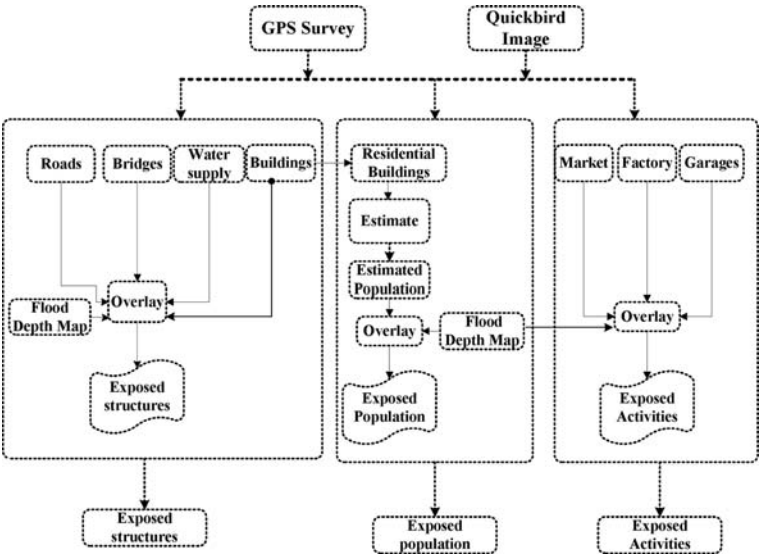

Fig. 6.12 Flowchart process for flood exposure analysis

exposed to flood, but also contribute to flooding by blocking water flow. In the Gatsata and Poids Lourd Garage zones, the flood exposure is related to their location in flood storage areas. Some buildings are located in a swamp so they are exposed to seasonal floods and groundwater movements. Finally, the Rwantexico factory zone is located in a high flood risk zone within the Nyabugogo floodplain. Due to the flooding, this factory stops functioning during rainy season.

It was not feasible, within the scope of this research, to conduct an analysis for every type of infrastructure. Therefore, the analysis focused on those parts of the physical infrastructures considered important by local authorities at the district and sector levels. These types of infrastructure include roads, bridges and water supply lines. Bridges and water supply lines were visited and located using GPS during field observation, while roads were digitized from the Quickbird image. Subsequently, the roads, bridges, water supply lines, and buildings were overlaid on the flood hazard zone map for exposure analysis. The flood depth values used in this analysis are based on watermarks left on houses after the flood of April 2006.

Figure 6.13 displays the distribution of exposed infrastructure relative to the flood zone. For example, in the southwest, the Yanze Bridge is located in a high flood zone near the confluence of the Yanze and Nyabugogo Rivers. At this location, a bridge and a water supply line for Kigali City are regularly swept away by overflows during the rainy season. The heavy load of sediment carried by flash floods from mountainous areas cut the water supply lines resulting in drinking water contamination (MININFRA/Rwanda 2006). In the central part of the study area, the Nyabugogo Bridge on the Kigali-Gatuna asphalt road is a piece of critical infrastructure that, even though located outside the high flood zone, is affected by overflow at the

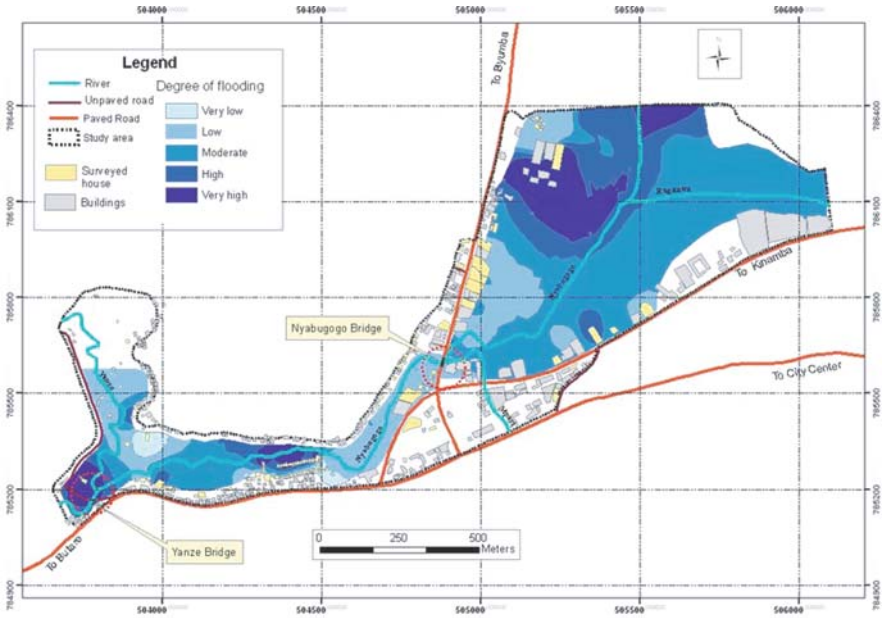

Fig. 6.13 Buildings and infrastructures in flood-prone areas

confluence of Nyabugogo and Mpazi Rivers. The problem is aggravated by the fact that the natural flow of the river was changed to create plots for new houses. The road and bridge are being eroded by water from the Nyabugogo River, which has been redirected from its natural flow.

6.7 Flood Risk Analysis: Analyzing Flood Vulnerability

Figure 6.14 summarizes the framework used for flood vulnerability analysis in the study area. Housing vulnerability was estimated by recording three variables: type of wall material, foundation, and vulnerability of the water supply line. Analysis of population vulnerability was based on the level of flood protection and flood mitigation activities. Lastly, vulnerability of critical economic activities (e.g., market, factory) located in the flood prone areas were estimated.

The general trend shows a higher proportion of collapsed buildings in the high flood zone (62.5%) than in the low flood zone (37.5%). Figure 6.15 shows the vulnerability of buildings by virtue of their location.

Masonry and wood houses constituted 31% of the total sample of visited houses (120). Of the masonry houses, severe building damage was observed in 87% of the cases while only 13% of the wood houses suffered the same level of damage. The three types of foundation found in the study area were stone in mortar (57%), stone

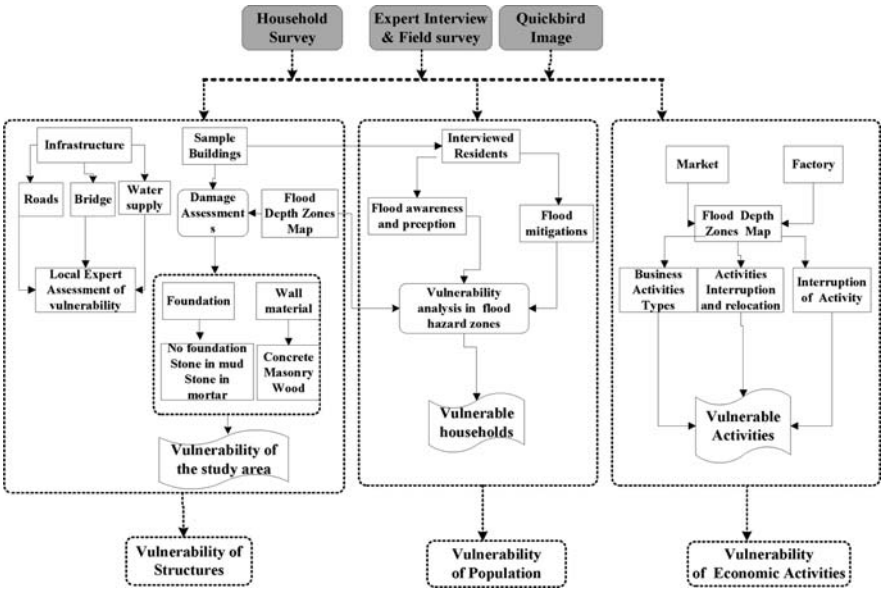

Fig. 6.14 Flowchart process for flood vulnerability analysis

Fig. 6.15 Vulnerability of housing by location. Collapsed house in swampy area; A house near the river stream
Source: Photo taken by Bizimana, September 2006

in mud (21%), and buildings without a foundation (22%). Interestingly, the quality of foundation did not reveal a clear difference as related to flood damages.

As for the recovery of the buildings following the flood, few buildings (16%) were repaired. The main reasons people did not pursue repairs were regulatory constraints from district authorities and the ongoing relocation process.

Fig. 6.16 Inadequate flood protection measure
Source: Photo taken by Jean Pierre Bizimana, September 2006

Unfortunately, damaged buildings that remain un-repaired are more vulnerable to the next flood.

Flood protection measures (as applied by respondents) were also examined in an effort to better understand vulnerability. Sixty percent of the respondents did not attempt to implement flood protection measures (e.g., open up drainages, raising the parcel's elevation, water proofing, sandbags, relocation). Some measures (e.g., sand bagging) cannot efficiently deal with the magnitude of flooding (Fig. 6.16). Due to poverty, many owners can only use sandbags in an attempt to prevent water from entering their houses. The fact that houses occupy the flood zone implies inadequate flood mitigation planning to protect vulnerable groups in the Nyabugogo flood plains within Kigali City.

Another situation that exacerbates flooding is the poor drainage system. Figure 6.17 shows efforts to open closed culverts on the former drainage channel of Mpazi River before its confluence with Nyabugogo River. Simultaneously, other people were attempting to excavate the river stream by removing solid wastes dumped into the river near the Gatsata garage zone. These local initiatives to improve the drainage conditions are having limited success, however, because other people continue to dump solid wastes into the river stream, even though such activity is strictly forbidden by existing environmental law. Therefore, to improve flood protection measures, assistance is needed for environmental law enforcement at the neighborhood level.

Fig. 6.17 Local initiatives to improve drainage conditions: (**a**) opening up of closed culvert; (**b**) excavation of Nyabugogo River
Source: Photo taken by Bizimana, September 2006

6.8 Flood Risk Management and its Implications for Kigali City Planning

The research performed in this study indicates a direct correlation between risk of flooding and inadequate planning and control. Most of the recently constructed buildings have no building permit or land registration ownership; some (especially the garage and shops) were officially located in the swamp lands by municipal planning authorities.[3] The location of the Kiruhura Market, started in 1998 by shoe traders on a small scale, was purposely chosen in the flood plain because there the traders were less likely to be forcefully evicted by authorities.[4] Over time, the market attracted more and more people who then settled in the nearby flood-prone areas and on steep slopes. The new settlements and mixed shops increase the flood risk along the Nyabugogo River, and the situation is aggravated by illegal dumping of solid waste in the river (Primature-Rwanda 2005).

Planning interventions within Kigali City suffer from inadequate legislative sanctions on those who illegally occupy the flood plain and a lack of planning capacity to cope with rapid urban growth (Aibinu 2001). As a consequence, local authorities are now facing the challenge of demolition, relocation, and resettlement of exposed households and properties to reduce the risk of flooding. Future plans should include the prohibition of new urban developments in high flood-prone areas and the relocation of the buildings within highly flooded zones (approximately 110 buildings).

[3]Interview with local authority at sector level.

[4]Interview with traders in the former Kiruhura market.

6.9 Conclusion

The main objective of this research was to develop a GIT-based approach using locally available data to identify flood hazard zones, analyze flood exposure and vulnerability, and use the findings to suggest possible strategies for flood mitigation in unplanned settlements along the Nyabugogo River in Kigali City, Rwanda. GI Technology proves to be a necessary tool to locate the household samples and calibrate the flood depth by interpolation and delineate the flood plain extent. Associated with local perceptions about floods and very high resolution satellite imagery, the flood zone and exposure maps were produced.

While the research confirms the usefulness of GIT for flood risk analysis, it also reveals constraints associated with the availability of base data (e.g., topographic information). Very high resolution satellite imagery combined with GPS field survey data can be utilized for delineating flood plains and analysing flood risk for properties and infrastructure in a developing-world urban setting when other data are not readily available. Participatory GIS could also be explored as a method to improve flood vulnerability assessments by incorporating local population's knowledge into the database and, hence into flood risk models.

For planning and decision making purposes, this research revealed a number of constraints that increase the vulnerability of properties along the Nyabugogo River that are in need of adequate flood migration measures. First, the lack of reliable flood records makes it difficult to prevent urban development in flood risk zones. Second, there is a lack of awareness about construction techniques that can improve housing resistance to floods. Third, the majority of the residents are not using any flood protection measures. Fourth, there is inadequate intervention by urban authorities to improve and regularly maintain drainage along the Nyabugogo River, where most of the urban development is informal.

As an immediate strategy to reduce the risk of flooding within the Nyabugogo flood plain, Kigali City Planning needs to improve the poor drainage infrastructure which has been identified as the main cause of flooding. As mid- and long-term strategies, proper construction standards should be carefully designed and implemented and guidance provided regarding where urban development takes place and levels of infrastructure needed to reduce the impact of future floods. Such initiatives require a level of land use management that influences land availability and encourages those struggling with poverty to avoid living in hazardous locations. Finally, to minimize financial loss and to avoid the situation of having to relocate or resettle those living in the flood plain, a technical flood risk assessment should first be required during the land allocation process. Ultimately, this study highlights the need to further explore the potential of GIT to assist urban planners and decision-makers with formulating appropriate planning and policy strategies in order to limit flood losses in developing countries.

References

Aibinu, A., 2001. GIS Application in Urban Planning and Urban Management: Utilizing GIS in Kigali Urban Planning and City Management, CORP 2001, Vienna University of Technology.

Alkema, D., 2003. Flood risk assessment for EIA: Environmental impact assessment, an example of a motorway near Trento, Italy. In: Studi Trentini di Scienze Naturali: Acta Geologica, 78: 147–154.

Bacic-Ivan, L.Z., Rossiter, D.G. and Bregt, A.K., 2006. Using spatial information to improve collective understanding of shared environmental problems at watershed level. Landscape and Urban Planning, 77: 54–66.

Barredo, J.I., Lavalle, C. and Ad De Roo, 2005. European flood risk mapping; EC DG JRC – Weather Driven Natural Hazards, Joint Research Center, European Commussion.

Barroca, B., Bernardara, P., Mouchel, J.M. and Hubert, G., 2006. Indicators for identification of urban flood vulnerability. Natural Hazards and Earth System Sciences, 6: 553–561.

Beerens, S.J.J., 2006. Facing disasters with geo-information and earth observation: the UNU – ITC programme for disaster geo-information management: Keynote. Presented at ICAST 2006: 17th International Conference on Advances in Space Technologies, 2–3 September 2006 Islamabad, Pakistan, P. 7.

Blaikie, P., Cannon, T., Davis, I. and Wisner, B., 1994. At Risk, Natural Hazards, People's Vulnerability, and Disasters. Routledge, London.

Byers, A.C., 1992. Soil loss and sediment transport during the storms and landslides of May 1988 in Ruhengeri prefecture. Rwanda Natural Hazards, 5(3): 279–292.

Davidson, R., 1997. A multidisciplinary urban earthquake disaster risk index: EERI annual student paper award. Earthquake Spectra, 13(2): 211–223.

Duran Lasserve, A., 2005. Dealing with market eviction processes in the context of developing cities, Third World Bank Urban Research Symposium on Land Development, Urban Policy and Poverty Reduction, Brasilia, April 2005.

Etkin, D., Haque, E., Bellisario, L. and Burton, I., 2004. An Assessment of Natural Hazards and Disasters in Canada: A Report for Decision-Makers and Practitioners. The Canadian Natural Hazards Assessment Project.

Fedeski, M., and Gwilliam, J., 2007, Urban sustainability in the presence of flood and geological hazards: The development of a GIS-based vulnerability and risk assessment methodology. Landscape and Urban Planning, 83: 50–61.

Goosby, S., Chiesa, C., Mielbrecht, S. and Bosse, T., 2005. Assessing and reducing the impacts of disasters in the Asia Pacific Region, Pacific Disaster Center, First International Conference on Urban Disaster Reduction, Kobe, Japan.

Guarin, G.P., Westen, C.J. and Montoya, L., 2004. Community-Based Flood Risk Assessment Using GIS for the Town of San Sebastián, Guatemala. International Institute for Geo-information Science and Earth Observation (ITC).

Gupta, T.N., 1994. Vulnerability of Houses in hazard Prone Areas, The World Conference on the International Decade for Natural Disaster Reduction (IDNDR), Yokohama, Japan; May 23–27, 1994.

Hengl, T., Gruber, S. and Shrestha, D.P., 2004. Reduction of error in digital terrain parameters used in soil-landscape modelling. International Journal of Applied Earth Observation and Geoinformation, 5: 97–112.

Islam, M.M. and Sado, K., 2002. Development priority map for flood countermeasures by remote sensing data with geographic information system. Journal of Hydrologic Engineering, 7(5): 346–355.

MacKinnon, E., 2004. Three Dimensional Flood Modeling with High Resolution LIDAR; Applied Geomatics Research Group/Center of Geographic Sciences. Nova Scotia Community College (NSCC), Middleton, NS.

McEwen, L., Hall, T., Hunt, J., Dempsey, M. and Harrison, M., 2002. Flood warning, warning response and planning control issues associated with caravan parks: the April 1998 floods on the lower Avon floodplain, Midlands region, UK. Applied Geography, 22: 271–305.

Mendel, G., 2006. Climate Change, Urban Flooding and the Rights of the Urban Poor in Africa: Key Findings from Six African Cities, Action Aid International, London -Johannesburg.

Merson, M.E., Montoya, L. and Paresi, C., 2004. Manage data – manage hazards: development of urban hazard information infrastructure for the city of Windhoek Namibia. Management of Environmental Quality: An International Journal, 15(3): 276–293.

Messner, F. and Meyer, V., 2006. Flood damage, vulnerability and risk perception-challenges of damage research. In: Schanze, J., Zeman, E. and Marsalek, J. (Editors), Flood Risk Management-Hazards Vulnerability and Mitigation Measures, Leipzig.

MINECOFIN, 2002. The 3rd General Census of Population and Housing in Rwanda, Kigali.

MININFRA, 2006. Document de politique nationale d'urbanisation, Kigali, Rwanda.

MININFRA/Rwanda, 2004b. Generation and Application of Climate Information, Products and Services for Disaster Preparedness and Sustainable Development in Rwanda; Ministry of Infrastructure. Rwanda Meteorological Service.

MININFRA/Rwanda, 2006. Kigali City Master Plan: Existing Condition Analysis; Prepared by the Master Plan Team for the Ministry of Infrastructure; Kigali.

MININFRAST, 2004. National Human Settlement Policy in Rwanda, Ministry of Infrastructure, Kigali.

MINITERE/Rwanda, 2004. Sectorial Policy on Water and Sanitation; Ministry of Lands, Environment, Forestry, Water and Mines; Kigali.

Montoya, A., 2003. Geo-data acquisition through mobile GIS and digital video: an urban disaster management perspective. Environmental Modeling & Software, 18: 869–876.

Montoya, L., 2006. Disaster Management. In: Hofstee;P (ed.), GIS for urban planning in developing world, International Institute for Geo-Information Science for Earth Observation (ITC), Enschede, Lecture Note.

Nelson, S.A., 2006. River Systems and Causes of Flooding. http://www.tulane.edu/˜sanelson/geol204/riversystems.pdf.Last updated on 27 March 2006.

Noson, L., 2002. Hazard mapping and risk assessment, Regional Workshop on Best Practices in Disaster Mitigation, Bali, Indonesia; 24–26 September 2002.

Prathumcha, K. and Samarakoon, L., 2005. Application of Remote Sensing and GIS Techniques for Flood Vulnerability and Mitigation Planning in Munshiganj District of Bangladesh. www.geoinfo.ait.ac.th/publications/ACRS2005_Prathumchai_K.pdf

Primature-Rwanda, 2005. Organic law determining the modalities of protection, conservation and promotion of environment in Rwanda. Official gazette of the Republic of Rwanda, 44(9): 22–42.

Sanyal, J. and Lu, X.X., 2005. Remote sensing and GIS-based flood vulnerability assessment of human settlement, A case study of Gangetic West Bengal, India. Hydrological Processes, 19(18): 3699–3716.

Sirven, P., Gotanegre, J.F. and Prioul, C., 1974. Geographie du Rwanda, Editions A. De Boeck., Bruxelles.

Tennakoon, K.B.M., 2004. Parameterization of 2D Hydrodynamic Models and Flood Hazard Mapping for Naga City, Philippines, ITC, Enschede, 101pp.

UN-Habitat and UNEP, 2001. Vulnerability Assessment: Tools to Support Participatory Urban Decision Making Process. United Nations Human Settlements Programme and United Nations Environment Programme.

UN/ISDR, 2004a. Terminology: Basic terms for disaster risk reduction. United Nations International Strategy for Disaster Reduction (UN/ISDR), Palais des Nations, Switzerland. http://www.unisdr.org/eng/library/lib-terminology-eng%20home.htm.Updated 31 March 2004.

UNCHS-Habitat, 2001. Assessment of vulnerability to flood impacts and damages, Disaster Management Programme, Nairobi, Kenya.

University of Dartmouth, 2006. Global Active Archive of Large Flood Events, Dartmouth Flood Observatory.

UNEP, 2004, Reducing Disaster Risk: A Challenge for Development, United Nations Development Programme, Bureau for Crisis Prevention and Recovery, New York, NY 10017, USA www.undp.org/bcpr.

UNU-IEHS and NNSUACE, 2006. Indicator design for flood vulnerability assessment; United Nations University-Institute for Environment and Human Security, Germany/Nizhny Novgorod State University of Architecture and Civil Engineering, Russia. http://www.cabri-volga.org/DOC/D3 CaseStudies/CaseStudyIndicatorDesign.doc. Last accessed 23 January 2007.

USAID, 2001. Monthly Report on Food Security in Rwanda; PASAR-SISA Project, Agricultural Engineering Department of MINAGRI, Famine Early Warning System Network, November 7, 2001.

Verdoodt, A., 2003. Elaboration and Application of an Adjusted Agricultural Land Evaluation Model for Rwanda, PhD Thesis, University of Gent, Belgium.

Wamsler, C., 2004. Managing Urban Risk: Perceptions of Housing and Planning as a Tool for Reducing Disaster Risk. GBER, 4(2): 11–28.

Zeigler, D.J., Jonhson, J.H. and Brunn, S.D. 1983. Technological Hazards. Association of American Geographers; Washington, D.C.

Part II
Metropolitan Case Studies

Chapter 7
A Respiratory Riskscape for Texas Cities: A Spatial Analysis of Air Pollution, Demographic Attributes and Deaths from 2000 Through 2004

Susan M. Macey

Abstract This study utilizes readily available criteria air pollution data from federal government sources to determine the spatial pattern of urban air pollutants. Using both geographic information systems spatial processing functions and statistical analysis, these data are then combined with respiratory and nonrespiratory decedents' demographic characteristics (including age, race/ethnicity, and gender). Respiratory diseases, including asthma, chronic bronchitis and emphysema, are a leading cause of illness and death in the United States. The areas studied include the major Texas cities of Austin, Dallas-Fort Worth, El Paso, Houston and San Antonio. The purpose of this research is to develop a "respiratory riskscape" in two steps. First, a spatial model of air pollutants for major urban areas in Texas is created. Second, the spatial pattern revealed by that model is analyzed for any significant relationships between specific pollutant sources/emissions and decedent's demographic characteristics, and mortality rates where respiratory disease is a primary or contributing cause of death. Results show variations among urban areas, and a complex interaction between pollution data and mortality rates based on demographic attributes.

Keywords Air pollution · Respiratory disease · Public health · Mortality rates · Texas

7.1 Introduction

Air pollution is a leading urban hazard. The highly variable nature of this hazard along with its numerous origins makes its study a major challenge. While air quality has improved, concerns for human health, particularly among more susceptible subgroups, remains (US Environmental Protection Agency 2006). Geospatial

S.M. Macey (✉)
James and Marilyn Lovell Center for Environmental Geography and Hazards Research, Department of Geography, Texas State University-San Marcos, San Marcos, TX, USA
e-mail: sm07@txstate.edu

P.S. Showalter, Y. Lu (eds.), *Geospatial Techniques in Urban Hazard and Disaster Analysis*, Geotechnologies and the Environment 2, DOI 10.1007/978-90-481-2238-7_7,

information technologies have great potential to aid in identifying areas most at risk and to evaluate the potential impact of this hazard on populations residing in those areas.

Studies dating back to the mid-1980s have linked air pollution, a common technological hazard in urban areas, with negative health consequences (Goldberg et al. 2001; Kim et al. 2004; Schwartz 1991a, b; Schwartz and Dockery 1992a, b), and it is generally agreed that long term health risks from exposure to outdoor air pollution are likely underestimated (Adgate et al. 2004). Numerous epidemiological studies have documented consistent associations between specific ambient air pollution components, specifically the criteria air pollutants (CAPs) including carbon monoxide (CO), nitrous oxide (NO_x), particulate matter (PM_{10} and $PM_{2.5}$), sulfur dioxide (SO_2), and volatile organic compounds (VOC), with various adverse health conditions. These studies have found significant negative impacts on health at levels below the national air quality standards set by the 1990 Clean Air Act. While emissions have been reduced, concern remains as studies continue to show adverse health impacts.

This study utilizes criteria air pollution data from several public sources to determine the spatial pattern of urban air pollutants in the major urban areas of Texas for the period 2000–2004. These data are then combined with the demographic characteristics of the proximate population and data regarding respiratory deaths, most notably chronic obstructive pulmonary diseases (COPD). As defined by the American Thoracic Society (1995), COPD is a disease that is characterized by decreased expiratory flow in the airways of the lungs. COPD consists of three related diseases: asthma, chronic bronchitis and emphysema. As one of the leading causes of illness and death in the United States, COPD causes a substantial economic burden on individuals and society. The purpose of this research is twofold: (1) to create a spatial model of air pollutants for the major urban areas in Texas, and (2) to analyze the spatial pattern for any significant relationships between specific pollutants and pollution levels, decedent's demographic characteristics (including age, race/ethnicity, and gender), and mortality rates where respiratory disease is a primary or contributing cause of death. The goal of the research is to develop a respiratory riskscape for Texas' urban areas.

7.2 Literature Review

Studies dating back to the mid-1980s have linked air pollution with negative consequences for children's health (Erbas et al. 2005; Kim et al. 2004; Lin et al. 2002; Norris et al. 1999; Pouliou et al. 2008; Schenker et al. 1986). Asthma is a chronic condition that occurs when the main air passages of the lungs become inflamed and narrowed and breathing becomes difficult; it is one of the most frequent reasons for hospital admissions among children. Children are particularly susceptible to air pollution related attacks (Erbas et al. 2005). Daily ambient exposure to CAPs has been implicated in increased attacks or worsening of

the condition. In part, the problem has been linked to a larger deficit in lung function growth rate for children exposed to outdoor nitrogen dioxide (NO_2), $PM_{2.5}$, and PM_{10}(Gauderman et al. 2000, 2002). A recent study by Islam et al. (2007) noted that exposure to high levels of $PM_{2.5}$ attenuated the effect of better lung function against new onset asthma. Karr et al. (2007) suggest that infant bronchiolitis may be added to the list of adverse effects of $PM_{2.5}$ exposure. Several studies have also linked childhood asthma exacerbation to levels of ozone (Gent et al. 2003; McConnell et al. 2002; Thurston et al. 1997). Ozone was implicated in hospitalization for acute respiratory diseases for children under two years of age in a study by Burnett et al. (2001). Particulate matter in the form of PM_{10}(Timonen and Pekkanen 1997; Tolbert et al. 2000) or PM_{10} in combination with ozone (Gielen et al. 1997), and $PM_{2.5}$ have also been implicated even when levels were below annual National Ambient Air Quality Standard (NAAQS) levels (Norris et al. 1999). Indeed, recent studies suggest that the role of such pollutants as organic carbon and NO_2 as potential causes of chronic symptoms of bronchitis, decreased lung function and asthma in children may have been underestimated (Gauderman et al. 2002, 2004; McConnell et al. 2003). The prevalence of asthma among children under 18 years has increased from 3.6% of all children in 1980 to 8.9% in 2005 (Mitka 2008). Nitrogen oxides and VOCs, two major power plant emissions, are precursors of ozone.

The probability of asthma occurrence is also generally greater among minority children (Evans 1992). Elevated asthma levels for Hispanic children, especially those of Cuban and Puerto Rican extraction have been noted in several recent studies (Davis et al. 2006; Delfino et al. 2003a). Metzer and Delgado (1995) suggest that higher risk for Hispanic and other minority groups may be partly related to their disproportionate representation in areas failing to meet one or more National Ambient Air Quality Standards (NAAQS). While an early study of children with asthma in the vicinity of coal-fired power stations found occurrence of symptoms not to be associated with measurements of SO_2 and NO_x (Henry et al. 1991), recent studies have provided convincing evidence of an association even at distances of over 60 miles (Levy et al. 2002). Chestnut and Mills (2005) conclude that human health would benefit from further reductions in SO_2 and NO_x emissions from power plants beyond those currently required by Title IV, and that such reductions are clearly warranted.

Outdoor air pollution studies have also linked increased mortality rates, especially among infants, to CAP levels. For example, two studies have shown evidence of a link between sudden infant death syndrome (SIDS) with increases in levels of NO_2 (Ritz et al. 2006) and PM (Glinianaia et al. 2004). Kaiser et al. (2004) have called for further studies to quantify the relationship between infant mortality and air pollution. Other studies indicating a spatial connection between demographics and air pollution have found links with educational level (Levy et al. 2002), and income (O'Neill et al. 2003).

Traffic emissions have been a particular focus of study throughout the last 20 years (Tonne et al. 2007; Watson et al. 1988). Pollutants from traffic exposure have been associated with childhood asthma by several authors

(Gauderman et al. 2005; Kim et al. 2004; Lin et al. 2002). Some recent articles have focused on the use of geographic information systems (GIS) to analyze the distribution and impact of air pollution. Jerrett et al. (2001) compared the relative value of several criteria in modeling the relationship between socioeconomic status and exposure to suspended particles in the air. Chakraborty (2001) analyzed exposure of school children to accidental releases of hazardous substances.

While fewer studies have been published on the impact of air pollution on older persons' health, the heightened susceptibility of the elderly subpopulation along with their growing numbers warrants increased investigation. In the early and mid 1990s, studies by Schwartz and his colleagues (Schwartz and Dockery 1992a, b; Schwartz and Morris 1994; Schwartz and Morris 1995) found increases in ischemic heart disease among the elderly population associated with PM_{10} exposure. More recently, several studies have found a significant association between elderly health problems and levels of air pollution (Tonn et al. 2001), particularly particulate matter (Dominici et al. 2006; Hartog et al. 2003; Pope et al. 2004; Schwartz 1994a, b, c; Williams et al. 2000a, b; Zanobetti et al. 2000). Filleul et al. (2004) found a significant relationship between air pollution levels and elderly respiratory mortality. Just as asthmatic children have been found to be particularly vulnerable to ozone, adult asthma symptoms have also been associated with this pollutant (Eiswerth et al. 2005), and both respiratory and coronary deaths among the elderly population have been associated with ozone (Goldberg et al. 2001). Of particular note is the national study by Samet et al. (2000) which found an association between hospitalization, pneumonia and COPD, and PM_{10} for those 65 years and older.

The impact of air pollution on cardiovascular disease represents a further serious public health problem. Mann et al. (2002) found hospital admissions for ischemic heart disease were associated with levels of CO and NO_2. Creason et al. (2001) linked $PM_{2.5}$with heart rate variability in elderly individuals. Pope et al. (2006) also found short term exposure to ambient $PM_{2.5}$ to be associated with ischemic heart disease. Brook et al. (2004) noted a consistent increased risk for cardiovascular events in relation to present-day concentrations of ambient PM, particularly in certain at-risk subsets of the population. Hospital admissions for cardiovascular and respiratory diseases have also been linked to $PM_{2.5}$ Medicare patients (Peng et al. 2008). As in studies on children, this increased risk has been noted even when levels are within current air quality standards (Peters et al. 2001; Pope et al. 2002).

In sum, numerous studies have found significant negative health impacts of air pollutants even at levels below the NAAQS set by the 1990 Clean Air Act (Peters et al. 2001; Pope et al. 2002; Schwartz 1993). While emissions have been reduced, concern remains as studies continue to show adverse health impacts. Respiratory morbidity and mortality show consistent links to emission levels of CAPs. In light of these findings, this study evaluates the spatial aspects of the emission of criteria air pollutants (CAPs) from various sources and respiratory mortality in five major Texas urban areas.

7.3 Methodology

7.3.1 Study Area, CAP Emissions, and Demographic Data

Chronic obstructive pulmonary disease (COPD) was one of the ten most frequent causes of hospitalizations in Texas (Texas Department of State Health Services 2006), accounting for approximately 33,000 hospitalizations in 2002 (Texas Health Care Information Council 2005). Sixteen of the state's 254 counties had risk-adjusted admission rates for this indicator that were more than twice the state average, with one-third of these being in the eastern part of the state. Pediatric asthma hospitalizations were more significant in southern and western counties with 31 counties reporting significantly higher admission rates than the state average.

In Texas, nearly 51% of the state's population lives in counties that do not meet federal ozone standards (US Environmental Protection Agency 2006). The worst areas are coincident with major urban areas found around Austin, Dallas-Fort Worth, Houston, El Paso, and San Antonio (Fig. 7.1).

These five urban areas form the basis for this study. Houston, the largest city, lies adjacent to the Gulf of Mexico. There is a major industrial and port area in the southeastern sector of the city which contributes to Houston ranking first in emissions from all sources (Table 7.1). As may be expected from the size and spatial extent of the Dallas-Fort Worth metroplex, this conurbation ranks second in mobile pollution sources, but ranks third overall behind San Antonio where utility power plants contribute a greater share of the emissions. Austin, where the state's capital

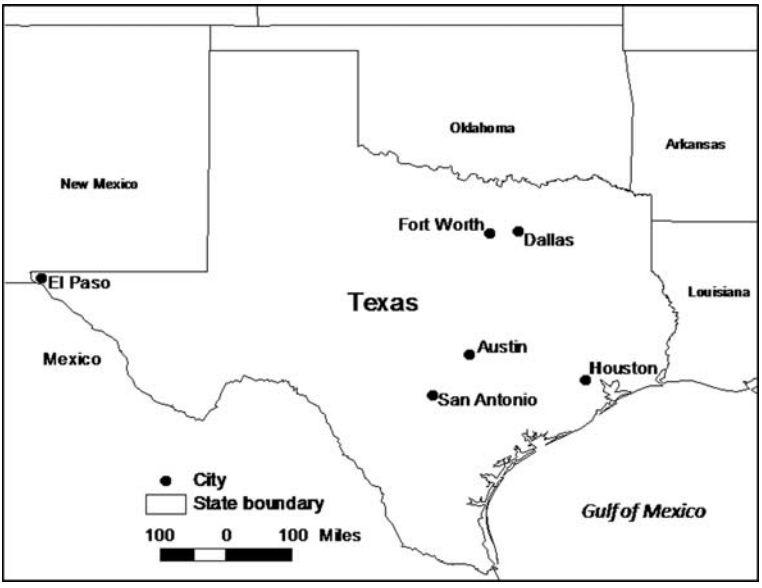

Fig. 7.1 Study area showing city locations

Table 7.1 Urban area rank* for criteria air pollutants by pollution source

	Austin	Dallas-Fort Worth	El Paso	Houston	San Antonio
Utility power plant	4	3	5	1	2
Nonpoint source	2	3	5	1	4
Nonroad mobile	4	2	5	1	3
Onroad mobile	4	2	5	1	3
Area source	4	3	5	1	2
Nonutility point source	3	4	2	1	5
Total – all sources	4	3	5	1	2

*Rank: 1 highest.

is located, ranks fourth, while El Paso, a much smaller city than the other four, consistently ranks lowest in emissions.

In Texas, electric utilities are the leaders in the volume of CAP emissions produced, including carbon monoxide (CO), nitrous oxide (NO_x), particulate matter (PM_{10} and $PM_{2.5}$), sulfur dioxide (SO_2), and volatile organic compounds (VOC). This situation is due in large part to the fact that two-thirds of the electric power plants were built or were under construction before 1971 and are therefore exempt from the tougher clean air standards and permit requirements of the Clean Air Act. Despite additional state legislation in 1999 aimed specifically at reducing emissions from these "grandfathered" electric generating facilities, problems persist. The Voluntary Emissions Reduction Permit (VERP) program under then Governor Bush was a failure – only one plant applied. One significant exempted facility emitted approximately 35% of the total air emissions in Texas in 1999 (Huston et al. 2001). In 1998, Texas led the nation in nitrous oxide production and was second nationally in releases of carbon monoxide and volatile organic compounds (US Energy Information Administration 2003). The state also led the nation in carbon dioxide emissions from electric power plants in 2001. Smog reduction is characteristically focused on three primary sources – automobiles, heavy industry, and power plants. Grandfathered industries and power plants produced as much nitrous oxides in 1997 as 18 million automobiles (US Environmental Protection Agency 1997) making these facilities prime targets for study.

Coal (bituminous, lignite, sub-bituminous, and petroleum coke), biomass and wood products are more commonly used as utility energy sources in Texas. The Texas Natural Resource Conservation Commission's 1997 Emissions Inventory confirmed the extent of the contribution of these facilities by documenting that grandfathered plants accounted for 900,000 tons of pollution annually – 36% of the state total (Huston et al. 2001). One response to these emissions was Bernsen's amendment to state HB 2912 (introduced at the end of 2001) that requires all grandfathered facilities in Texas to apply for permits by September 1, 2003 if the facility is located in East Texas, and by September 1, 2004 if located in West Texas. Grandfathered facilities have been ordered to comply with all conditions of the permits, including installation of emissions controls or reductions of emissions of air

contaminants, by March 1, 2007 for facilities in the East of the state and by March 1, 2008 in the West.

The Clear Skies Act of 2003 set a new emissions reduction goal of 40% less SO_2 for Texas (US Environmental Protection Agency 2006). A reduction in NO_x of 22% is also expected by 2020, with associated reductions in premature deaths, hospitalizations/emergency room visits for asthma and chronic bronchitis, and fewer nonfatal heart attacks. Since their introduction over the last 18 years existing Clean Air Act regulations have resulted in CAP level reductions. The primary focus of the Clear Skies Act is to further reduce power plant emissions, including those from 13 units spread throughout Texas. In all, 27% of Texas' facilities would install Selective Catalytic Reduction (SCR) devices while 24% of plants would install scrubbers.

The two demographic groups considered most at risk from CAPs are the young and the elderly population. Consequently, Texas' demographic composition makes it a good candidate for study because 28% of the population is under 18 years of age and approximately 10% is aged 65 years or older (Table 7.2) (US Bureau of the Census 2000). The proportion of senior citizens is also growing, particularly with the influx of 'snowbirds' (elderly, seasonal inmigrants) to southern parts of the state. In terms of other demographic variables, Texas has a large and growing Hispanic population, currently comprising approximately one-third of the state's total population. Blacks represent a smaller proportion of the total mix (approximately 12%) having higher representation in the northern and eastern counties. In the five study cities, the populations in Austin and El Paso are slightly younger than those of the others. Houston and Dallas-Fort Worth have a higher proportional representation of Blacks while San Antonio and El Paso outrank the others in the proportions of Hispanics, where they comprise more than half of the total population.

Table 7.2 Demographic characteristics of Texas and the five urban study areas

	Texas	Austin	Dallas-Fort Worth	El Paso	Houston	San Antonio
Total population	20,851,820	901,920	4,145,659	674,801	3,822,509	1,327,554
Median age (years)	32.3	30.1	31.7	30.0	31.4	32.0
Percent < 18 years	28.2	24.9	28.1	32.0	29.2	28.4
Percent 18–64 years	61.9	69.0	64.2	58.2	63.5	61.2
Percent 65 and older	9.9	6.1	7.8	9.8	7.3	10.4
Percent White	71.0	69.3	65.5	73.5	59.1	68.5
Percent Black	11.5	9.0	15.9	3.0	18.2	7.5
Percent Hispanic	32.0	26.8	24.0	78.8	31.6	54.5
Percent male	49.6	51.0	49.8	48.2	49.8	48.5

Source: US Bureau of the Census (2000)

7.3.2 Data Sources and Analysis Techniques

To meet the objective of creating a respiratory riskscape for the five major urban areas in Texas, the best available public data on the sources and types of air pollution emissions was used. Specific air pollutants studied here are those designated as criteria air pollutants (CAPs), and include carbon monoxide, nitrogen oxides, particulate matter (PM_{10} and $PM_{2.5}$), sulfur dioxide, and volatile organic compounds recorded in the National Emissions Inventory (NEI) database. As discussed above, these pollutants have been repeatedly implicated in studies of respiratory illnesses. Data on air pollution sources and emissions for Texas were downloaded from two existing Environmental Protection Agency (EPA) databases and served as the environmental predictors in this study.

The NEI data for CAPs in 2002 breaks sources down by nonpoint, area, non-road and on-road mobile sources, and nonutility point sources including heavy industry (US Environmental Protection Agency 2008b). NEI 'onroad mobile', 'nonroad mobile', 'nonpoint' and 'area' source data are only available at the county level. Studies have shown traffic related emissions to be a factor in childhood asthma hospitalization up to 200 or 300 m from the source (Hoffman et al. 2007; Lin et al. 2002; Kim et al. 2004). Therefore, in order to provide a more realistic view of their potential impact, a 250 m buffer was created around major roadways and onroad sources. County information was subsequently attached to these buffers. County-level values for nonroad mobile emissions were also attached to their potential sources (e.g., airports, railroads) to derive a potentially more accurate definition for such emissions. Each of these features was extracted from the ESRI® data sets provided with the software and a 500 m buffer attached to each feature to account for the potential extent of exposure from each source.

Nonpoint and area sources are more problematic as they may include any source that individually does not produce sufficient emissions to qualify as a point source, but collectively may be significant (US Environmental Protection Agency 2008b). These sources may range from home or office buildings to diffuse stationary sources such as agricultural tilling and wildfires. Therefore, the data on specific pollutants for these county based sources were first joined into one table. Then the county value was assigned to tracts so that a composite total emission value was calculable. Unfortunately, the county level nature of the emission information remains a primary limitation when examining contribution from nonpoint and area sources.

These data were supplemented with the location of electric power plants and their emission data for four pollutants: nitrous oxide, ozone, sulfur dioxide and carbon dioxide emissions using the EPA's emission and generation resource integrated database (e-GRID) (US Environmental Protection Agency 2008a). These emissions are all listed in the NAAQS as CAPs. The eGRID database is a comprehensive source of data on the environmental characteristics of all electric power generated in the United States from 1997 through 2002. The database's attributes include primary fuel type, plant age and the last year the plant added production capacity, plant efficiency, production, air pollutant emissions, allowances, resource mix for

individual plants, and the compliance methods employed by the plants (US Environmental Protection Agency 2008a).

In order to evaluate the health impacts of the pollutants emanating from these sources, mortality data from the individual mortality files compiled by the Texas Department of State Health Services (2006) were downloaded for the years 2000–2004, the latest year currently available. Additional attributes were created to separate cases where deaths associated with COPD were listed as the primary cause of death or as a contributing cause under the International Classification of Diseases (ICD-10) (such causes include bronchitis, emphysema, chronic obstructive pulmonary disease and asthma, using codes J40–J47).

Finally, demographic tract level data from the US 2000 Census (US Bureau of the Census 2000) for the attributes of age, race/ethnicity and gender were extracted for the five major urban areas. Tract level data were used because block group number of deaths were too low to allow meaningful rates to be calculated for each demographic category. The 2000 Census was selected as more closely correlated to the years available for the mortality data being studied (2000–2004), as well as the time frame for which the pollution data were available. The mortality records were aggregated to the tract level and these data were then combined with the census data to calculate mortality rates for respiratory disease as the primary or contributing cause of death. Nonrespiratory-related death rates were also calculated to serve as a benchmark against which to compare the respiratory death rates.

ArcView® GIS 3.3, a desktop GIS software package, was used to create the GIS layers for the spatial dimensions of the respiratory riskscape in this research. Preliminary processing of the emissions data included matching the NEI power plant data with the corresponding plants in eGRID to produce a composite layer with both plant and emission characteristics for each of the datasets. As studies have shown adverse health effects from exposure to air pollutants at a variety of distances from utility sources including from 6 to 60 miles from power plants (Henry et al. 1991; Levy et al. 2002; Levy et al. 2003), a conservative buffer corresponding to a distance of 6 miles from each plant was created to serve as the basis for analyzing the effect of their impact on death rates over space. Nonutility point sources can be anything from a recycling facility or a dry cleaning shop to a chemical plant. The disparate nature of these points precludes their being considered as part of a surface where pollution values might be interpolated. Therefore, they were retained as points to maintain their integrity.

Several GIS functions were then used to create a composite layer containing source emissions and demographic attributes. Emissions for the point and mobile sources were combined with the buffered features that represent their spatial location. Census areas within the urban area boundary for the cities included in the study were then extracted and the emissions data were combined with the census data. Point locations of decedents from the Texas DSHS were joined to the emissions and census data to identify corresponding attributes in the latter for the residence location of each decedent. Mortality rates were calculated by summing the number of individual decedents in each census tract; rates per 1000 population were then

calculated. This level of specificity was necessitated by the low frequency of cases in each block group making rates at a finer spatial resolution meaningless. Maximum emission levels for each pollutant from all sources found in each tract were also calculated.

Following the spatial processing of the data, statistical analysis was undertaken using the Statistical Package for the Social Sciences (SPSS) software. First, cases were examined for annual and seasonal trends. Then a comparison of decedent characteristics was made among the five urban areas. Decedent's demographic characteristics (age, race, ethnicity, gender) were evaluated in relationship to respiratory disease being listed as a primary or contributing cause of death. Nonrespiratory decedent characteristics were also examined for comparative purposes. Finally, death rates were calculated at the tract level and these rates were evaluated for their association with specific sources and types of pollutants. Nonparametric tests including Spearman's rank order correlation and chi-square statistics were used to test for associations or differences. As the number of cases was large, a more conservative probability level of 0.01 was set as the minimum level for significance throughout the analysis.

7.4 Discussion of Results

7.4.1 Spatial Pattern of Air Pollution Sources

The spatial pattern of urban air pollutant sources detailed below identifies the areas of greatest potential respiratory health risk within each of the major urban areas. As noted above, Houston consistently had the highest levels of emissions for all sources among all urban areas studied (Table 7.1). Six electric power plants are inside the urban boundary while five impinge on the southern and eastern sides of the city (Fig. 7.2). The map of the Houston urban area shows radial and radiating sources of nonroad and onroad mobile sources, plus numerous nonutility point sources which tend to coincide with transportation routes particularly on the eastern side of the city.

The Dallas-Fort Worth metroplex also presents a tangle of onroad and nonroad sources (Fig. 7.3), and ranks second for emissions from both these sources (Table 7.1). Eight electric power plants are within the urban area while the six mile buffer for three more overlap parts on the northern side of the metroplex. Dallas-Fort Worth ranks third behind San Antonio in electric power plant and area emissions, and third behind Austin for nonpoint source emissions. While dotted with nonutility point sources, emissions from these sources contributed the least to air pollution in the Dallas-Fort Worth area.

Taking all sources into consideration, emissions in San Antonio elevate this urban area to the second highest ranking in terms of total amount of pollution. While fewer in number than in Houston and Dallas-Fort Worth, electric power plants, along with area sources contribute more than other sources for this city (Fig. 7.4).

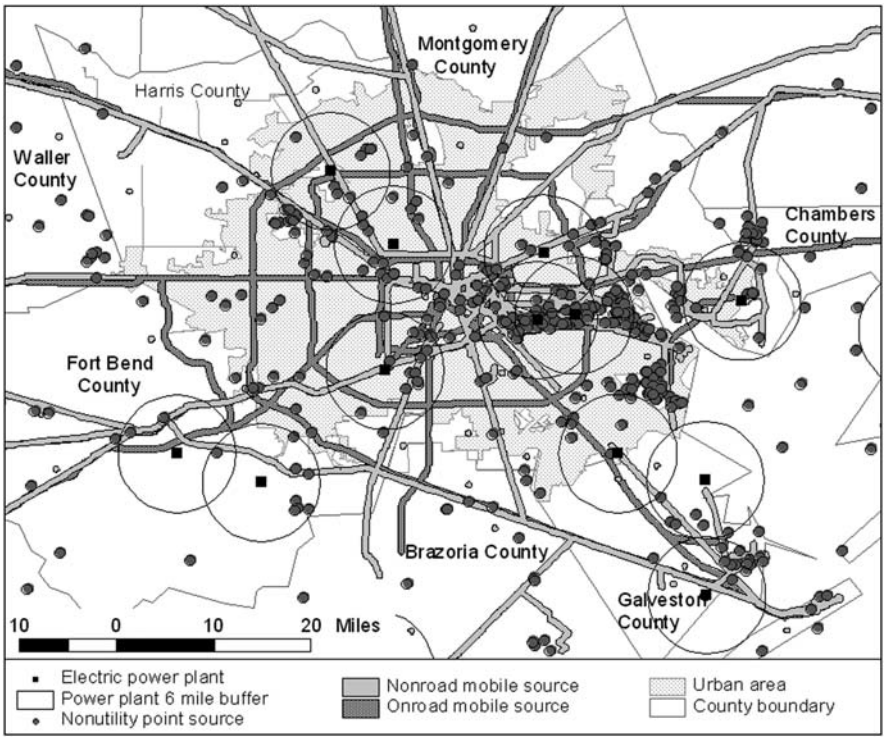

Fig. 7.2 Houston urban area air pollution sources

Nonutility point sources are also fewer in the Austin urban area. Austin's emissions ranked fourth overall and for most of the emission sources. Only three electric power plants are located in the city, which also has far fewer nonutility point sources listed (Fig. 7.5).

El Paso ranked consistently lowest for all but nonutility point sources. The city has only one electric power plant within the urban area and one whose buffer overlaps a northern section of the urban area (Fig. 7.6). One caveat regarding the accuracy of observations for El Paso is that it lies adjacent to the Mexican border. No data on emissions from the adjacent area in Mexico that could potentially contribute to air pollution levels in the El Paso area is available. However, it is suspected that air pollution from south of the border confounds the situation.

By far the largest quantity of emissions was recorded for carbon monoxide (Fig. 7.7) followed by PM_{10}, NO_x, SO_2 and VOC (US Environmental Protection Agency 2008b). Nitrous oxides noted in several studies (Chestnut and Mills 2005; Gauderman et al. 2000, 2002; Henry et al. 1991; Mann et al. 2002) came from a variety of sources including (in order of importance) onroad mobile, nonroad mobile, electric utility plants and nonutility point sources. The largest contribution of PM_{10}, cited as having a negative impact on health in numerous studies (Dominici et al.

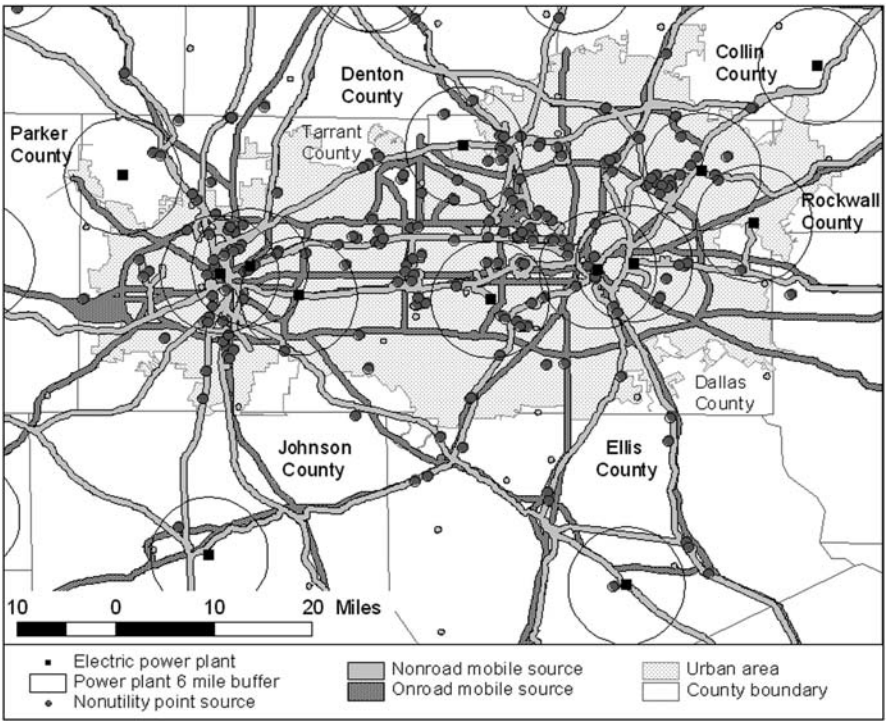

Fig. 7.3 Dallas-Fort Worth urban area air pollution sources

2006; Hartog et al. 2003; Pope et al. 2004; Samet et al. 2000; Schwartz 1994a, b, c; Williams et al. 2000a, b; Zanobetti et al. 2000) came predominantly from area sources. $PM_{2.5}$ which has received much attention in recent years (Islam et al. 2007; Karr et al. 2007; Peng et al. 2008) was present in the lowest levels and also came mainly from area sources. The makeup of sources and their contribution for VOC particularly linked to asthma in children (Delfino 2003b) reflected those of NO_x, though area sources contributed more to VOC.

The largest proportion of emissions came from onroad mobile sources which in addition to their large emission of CO, added to the levels of NO_x and VOC (Fig. 7.8) (US Environmental Protection Agency 2008b). Area sources, the greatest source of PM_{10}, contributed the second largest amount of pollutants, primarily being the major source of PM_{10} and $PM_{2.5}$, as well as a primary source of VOC. Nonroad mobile sources such as airports and railroad lines are notable for their CO, and to a lesser extent, NO_x and VOC contributions. Point sources, both from electric utility power plants and nonutility point sources add a lesser amount of air pollution than the other four sources noted, but combined contribute the most SO_2 which has been cited in studies by Chestnut and Mills (2005), Henry et al. (1991), and Levy et al. (2002). Carbon dioxide and ozone data were only available for electric utility power plants and are therefore not shown. The average level of power plant CO_2 emissions

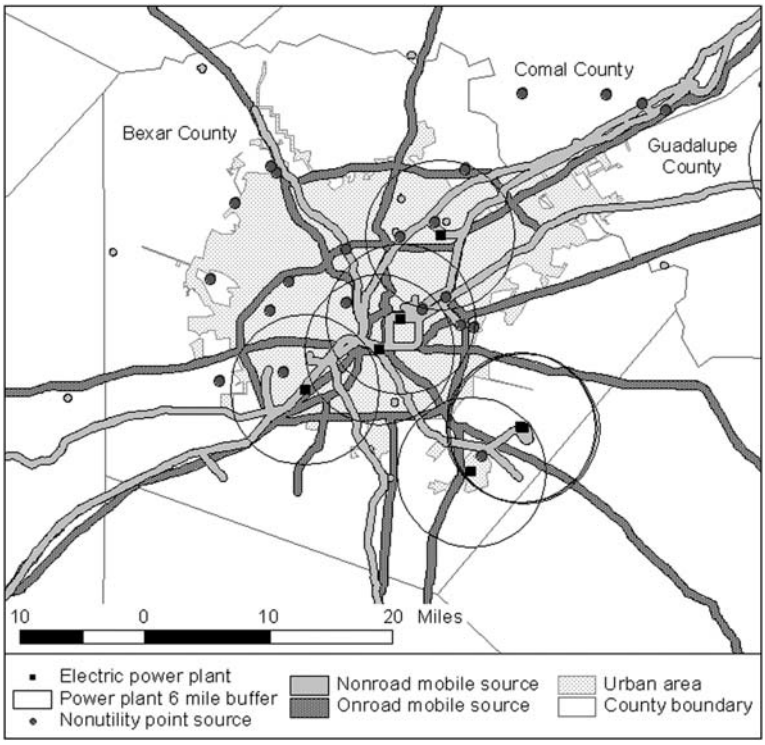

Fig. 7.4 San Antonio urban area air pollution sources

recorded was five times that for CO from onroad mobile sources while mean levels of ozone ranked between power plant emissions of NO_x and SO_2. Ozone has been implicated as a factor contributing to asthma in children by a number of studies (Burnett et al. 2001; Eiswerth et al. 2005; Gent et al. 2003). It must be remembered that NO_x and VOC are precursors of ozone and therefore, while ozone is not specifically recorded for all sources, any source of these pollutants could contribute to the problem.

7.4.2 Decedent Attributes

Turning to the cause of death, cases were first examined to establish the relative proportion of deaths where respiratory disease was listed as the primary cause or a contributing cause. Respiratory causes include bronchitis, emphysema, chronic obstructive pulmonary disease and asthma and are denoted by the ICD-10 codes, J40–J47. Where respiratory disease was listed as a contributing cause of death, the major primary causes noted here were chronic ischemic heart disease (ICD-10 code I25) listed for 23.2%, lung cancer (ICD-10 code C34) at 15.2%, heart failure

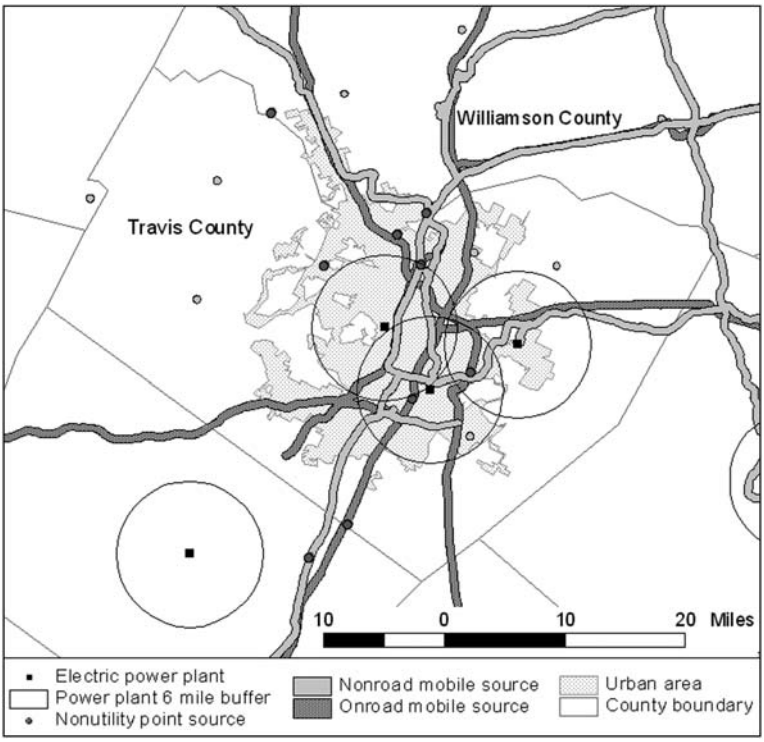

Fig. 7.5 Austin urban area air pollution sources

(ICD-10 code I50) in 3.9%, and stroke (ICD-10 code I64) for 2.1% of cases. The breakdown of deaths in each category by urban area is listed in Table 7.3.

By far the greatest proportion of respiratory deaths was cited as COPD, accounting for nearly 80% or more of all primary respiratory deaths for each area. The highest level was observed in San Antonio (85.3% of all respiratory primary cause deaths) and the lowest one in Houston (78.1%). Emphysema was the second highest proportion in all areas with the largest percent being recorded in Houston (16.0% of primary causes) and the lowest in San Antonio (9.6%), the reverse of the COPD pattern. Asthma shows much lower fatality proportions, accounting for between 2.9% at the low end for Austin to a high of 3.8% for Houston. In all instances, the percentages for respiratory disease as a contributing cause of death were slightly higher than those for primary cause percentages ranging from 4.2% for Houston to 5.5% for El Paso.

An examination of the characteristics of decedents in each respiratory category gives a more complete view of the relative contribution of respiratory disease versus nonrespiratory related causes for mortality. Minority group status, especially Hispanic ethnicity has been evaluated as a risk factor with studies particularly focusing on Hispanic children (Evans 1992; Davis et al. 2006; Delfino et al. 2003a; Metzer and Delgado 1995). The proportion of respiratory related deaths (primary

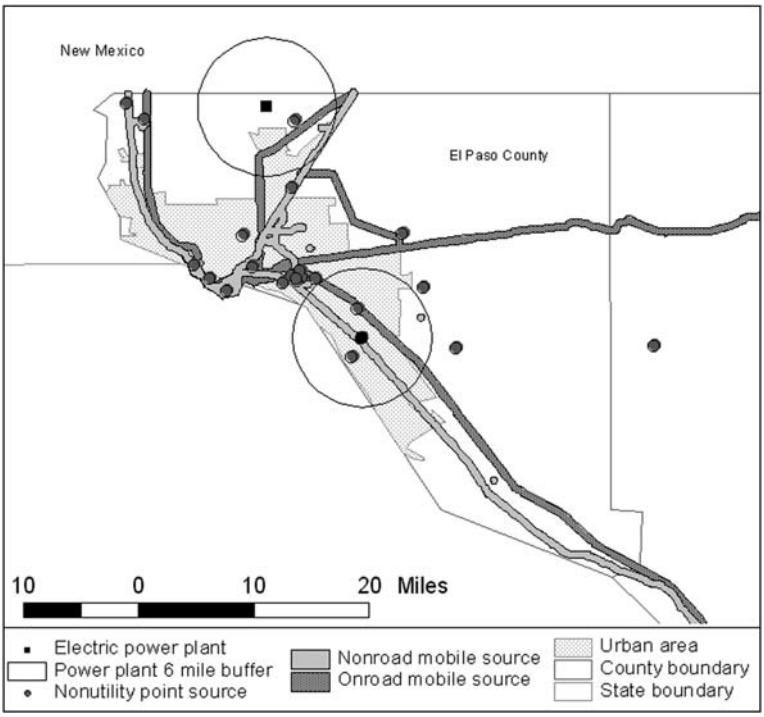

Fig. 7.6 El Paso urban area air pollution sources

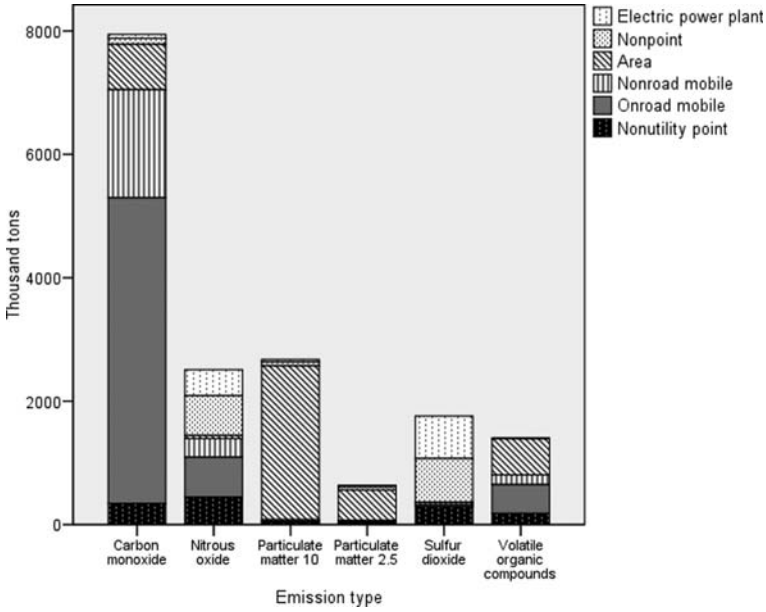

Fig. 7.7 Air pollution emission type by source

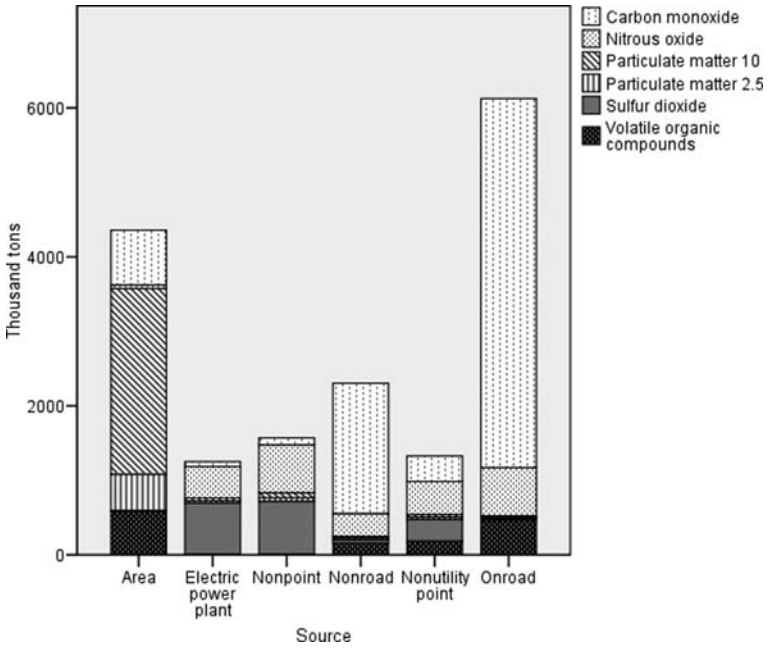

Fig. 7.8 Air pollution source contributions to emission total

and contributing) for Hispanics was highest in El Paso and San Antonio (Table 7.4), though the percentage was lower than for Hispanic nonrespiratory caused deaths. Black proportions were highest in the largest urban areas, Houston and Dallas-Fort Worth and again were lower than percentages for nonrespiratory deaths. The percentage of male respiratory decedents was highest in El Paso (51.8%) and lowest in Austin (42.7%). This pattern reflects that for nonrespiratory decedents more closely than for any other demographic category. While mean age in years shows little variation among urban areas, respiratory (both as a primary and contributing cause) decedents were older than nonrespiratory decedents. In order to examine the two primary respiratory risk groups based on age noted in the literature, children (Adgate et al. 2004; Gauderman et al. 2000, 2002; Pouliou et al. 2008) and the elderly population (Filleul et al. 2004; Goldberg et al. 2001; Samet et al. 2000; Tonn et al. 2001), those less than 18 years of age were grouped to represent children in the mortality data, and those 65 years and older were grouped to represent elderly decedents. The percentage of children dying from respiratory related diseases or having one as a contributing cause was very low across all locations and was considerably lower than nonrespiratory percentages. The situation for elderly decedents showed the reverse pattern with the respiratory primary and contributing cause categories being 15–20 percentage points higher than for nonrespiratory deaths.

These results support findings in previous studies. Elderly individuals have been cited as being at greater risk in numerous studies (Dominici et al. 2006; Hartog

Table 7.3 Cause of death for urban areas

	All areas	Austin	Dallas-Fort Worth	El Paso	Houston	San Antonio
Respiratory primary cause						
Number of cases	12,654	769	5609	772	3539	1965
Percent for urban area						
Bronchitis	0.4	0.5	0.4	0.4	0.5	0.4
Chronic bronchitis	0.4	0.5	0.4	0.6	0.4	0.5
Emphysema	14.3	14.3	14.9	14.0	16.0	9.6
COPD	80.2	79.2	79.7	80.6	78.1	85.3
Asthma	3.5	2.9	3.5	3.0	3.8	3.1
Status asthmaticus	0.4	1.2	0.3	1.2	0.5	0.1
Bronchiectasis	0.8	1.4	0.7	.3	0.8	1.2
Percent of primary cause deaths by area	100	6.1	44.3	6.1	28.0	15.5
Respiratory contributing cause						
Number of cases	14,399	754	6224	983	4117	2321
Percent of contributing cause deaths by area	100	5.2	43.2	6.8	28.6	16.1
Nonrespiratory cause						
Number of cases	270,837	15,735	106,126	16,166	90,714	42,096
Percent of nonrespiratory deaths by area	100	5.8	39.2	6.0	33.5	15.1
All cases						
Percent						
Respiratory primary	4.2	4.5	4.8	4.3	3.6	4.2
Respiratory contributing	4.8	4.4	5.3	5.5	4.2	5.0
Nonrespiratory	90.9	91.2	90.0	90.2	92.2	90.8

et al. 2003; Pope et al. 2004; Schwartz 1994a, b, c; Tonn et al. 2001; Williams et al. 2000a, b; Zanobetti et al. 2000). They need to be considered as at higher risk as their representation in both respiratory primary and contributing cause categories are almost uniformly 20 percentage points above their proportional representation in the nonrespiratory deaths category. Those individuals with heart conditions need to be particularly vigilant as they comprise the largest group (approximately 25%) of the contributing cause category, and the association between respiratory and cardiovascular disease is well documented (Schwartz and Dockery 1992a, b; Schwartz and Morris 1994, 1995) especially for elderly individuals (Creason et al. 2001; Hartog et al. 2003; Pope et al. 2004). The under-18 years of age category shows the reverse pattern in all areas, perhaps reflecting the low respiratory mortality versus morbidity for children. Several studies have addressed childhood morbidity, especially related to asthma (Burnett et al. 2001; Delfino et al. 2003a; Erbas et al. 2005; Gauderman et al. 2000 and 2002; Gent et al. 2003; Lin et al. 2002).

Table 7.4 Urban area decedent demographic characteristics by cause of death

	All areas	Austin	Dallas-Fort Worth	El Paso	Houston	San Antonio
Respiratory primary cause						
Number of cases	12,654	769	5609	772	3539	1965
Mean age (years)	76.0	76.5	75.6	78.2	75.5	77.5
Percent < 18 years	0.3	0.4	0.4	0.4	0.3	0.2
Percent 18–64 years	13.7	12.6	15.1	9.2	14.7	10.6
Percent 65 and older	85.9	87.4	84.5	90.4	85.0	89.2
Percent White	80.3	87.9	86.5	59.8	77.2	73.3
Percent Black	10.7	7.5	10.3	2.2	16.1	6.6
Percent Hispanic	8.0	3.6	2.4	37.0	5.3	19.5
Percent male	46.6	42.7	45.7	51.8	47.6	46.9
Respiratory contributing cause						
Number of cases	14,399	754	6224	983	4117	2321
Mean age (years)	75.6	77.5	74.7	78.8	74.6	77.7
Percent < 18 years	0.3	0.0	0.3	0.2	0.2	0.2
Percent 18–64 years	16.4	11.4	18.5	8.2	18.9	11.6
Percent 65 and older	83.3	88.6	81.2	91.6	80.9	88.2
Percent White	75.6	83.8	82.1	54.9	75.2	65.1
Percent Black	13.1	9.3	14.5	2.2	16.9	13.1
Percent Hispanic	10.4	6.2	2.8	41.8	6.2	26.3
Percent male	52.4	48.5	51.0	52.2	54.0	54.8
Nonrespiratory cause						
Number of cases	270,837	15,735	106,126	16,166	90,714	42,096
Mean age (years)	68.4	68.9	68.3	70.6	67.0	70.5
Percent < 18 years	3.2	3.3	3.4	2.6	3.4	2.7
Percent 18–64 years	32.2	31.7	32.3	26.9	35.1	30.0
Percent 65 and older	64.6	65.0	64.3	70.5	61.5	69.4
Percent White	59.6	69.1	69.2	32.8	56.8	48.2
Percent Black	18.5	13.9	19.6	2.8	25.6	8.5
Percent Hispanic	20.0	15.7	9.4	63.7	14.9	42.9
Percent male	49.8	49.3	49.1	50.8	50.7	49.6

7.4.3 Association of Mortality Rates with Air Pollution Sources and Types

While the number and percentage of deaths is instructive in terms of the absolute magnitude of the potential problem, in order to discern any disproportional risk, rates must be evaluated. The mortality records were aggregated to census tract level. Rates per thousand were then calculated using census tract values for each demographic attribute. For the under-18 year old age category, values were too low to be meaningful, and so this category was dropped from further analysis. The mean rates for all other demographic attributes under study are displayed in Table 7.5.

Table 7.5 Average death rates per thousand at the tract level by urban area

	Austin	Dallas-Fort Worth	El Paso	Houston	San Antonio
Respiratory primary cause rate					
All case**	4.75	7.28	6.43	12.71	7.41
Aged 65 years or older*	2.87	1.88	0.78	1.20	1.88
White**	5.83	10.18	5.47	6.92	7.72
Black[1]	2.96	3.16	4.21	3.44	5.14
Hispanic**	0.73	0.68	2.68	0.95	2.15
Male**	4.15	6.94	7.01	4.99	6.92
Female**	5.38	7.64	5.91	5.30	7.86
Respiratory contributing cause rate					
All case**	4.59	8.22	7.94	6.25	9.11
Aged 65 years or older[1]	1.52	1.62	2.64	1.18	1.19
White**	5.59	10.75	6.28	8.12	8.59
Black*	2.91	5.38	4.81	3.86	8.32
Hispanic**	1.13	1.12	3.83	1.13	3.68
Male**	4.42	8.65	8.76	6.86	10.04
Female**	4.78	7.85	7.19	5.58	8.24
Nonrespiratory cause rate					
All case**	103.48	160.75	138.56	155.86	171.46
Aged 65 years or older**	35.71	29.79	22.50	22.59	25.60
White**	99.80	153.50	69.21	133.27	116.75
Black*	112.10	132.19	126.21	140.61	158.30
Hispanic**	50.17	55.89	103.55	61.61	107.91
Male**	101.43	147.35	146.81	145.61	176.46
Female**	105.86	145.17	131.37	135.93	162.69

[1]Difference among areas not significant
*Difference significant at $p < 0.01$
**Difference significant at $p < 0.001$

In the case of respiratory as primary cause deaths, Houston topped the list when all cases were considered together and the rate exceeded those for all other urban areas by nearly two to one over Dallas-Fort Worth, El Paso, and San Antonio, or more in the case of Austin (Table 7.5). This result could be expected given that Houston ranked first for all air pollution sources (Table 7.1). The overall rates for the other urban areas also reflect their overall air pollution ranking. All group rates except for Black decedents also showed significant differences among urban areas. White rates were highest in Dallas-Fort Worth, Black rates highest in San Antonio, and Hispanic rates higher in El Paso and San Antonio than in the other three areas. In all cases, rates for Whites were higher than for Blacks, with Hispanics exhibiting the lowest rates. In the case of gender, male and female rates differed among the urban areas. El Paso, Dallas-Fort Worth and San Antonio exhibit higher values than Houston and Austin for both genders. San Antonio has the highest female rates and El Paso the highest male rates. Female rates exceeded male rates in all cities

except El Paso. The single category where Austin exceeded all other areas was for individuals aged 65 years and older. In general, elderly rates were lower than for all other categories except Hispanics who had the lowest respiratory-related death rates of all race/ethnicity groups in this study. The latter finding somewhat contradicts the literature which suggests that Hispanics are at higher risk than other racial or ethnic groups (Davis et al. 2006; Delfino et al. 2003a; Metzer and Delgado 1995). However, these previous studies examined morbidity rather than mortality. Thus, while Hispanics comprise a larger proportion of the population than Blacks in Texas, Blacks experience a higher death rate suggesting the need for further research. The higher rates for White decedents may reflect the influence of economic status whereby access to health professionals improves the accuracy of information found on death certificates while the Hispanic death rate may be underreported due to the opposite.

Where respiratory disease was a contributing cause, the differences among group rates generally reflect those for primary cause with three exceptions: the variation in the rate for Blacks was significantly different among urban areas while the rate for the elderly group was not. San Antonio rates for all cases also exceeded those for the other urban areas, and for males as well as Blacks. For nonrespiratory cases, rates differed on all attributes among the urban areas. Unlike the comparable rates for respiratory-primary and respiratory-contributing related deaths, rates for Blacks exceeded those for Whites, and, with the exception of EI Paso where the White rate was lower than that for Hispanics, rates for Hispanics were the lowest in all categories except for elderly deaths.

When mortality rates were tested for association with pollution emission levels for all urban tracts, only weak relationships were observed (all Spearman rank order correlation values were below 0.23.). All cause categories were positively associated with emissions from electric utility power plants, nonpoint, and nonroad mobile sources (Table 7.6), with the strength of correlations for electric power plants being the highest. As noted above, pollution from power plants in Texas has long been a source of contention. The findings here reinforce the greater contribution of this source to mortality not just for respiratory but also for nonrespiratory causes.

No association was noted between primary or contributing rates and onroad source emissions. Area sources did not register as significant in overall respiratory rates, though three of the pollutants from this source (CO, NO_x and VOC) were positively associated with contributing rates. When the total from all sources was examined, the same three pollutants showed a positive association with both primary and contributing rates, while total emissions of $PM_{2.5}$ also showed a positive association with contributing rates. The overall lack of association between total emissions for particulate matter pollutants and primary rates suggests that studies that focus solely on these pollutants, while valuable in establishing specific levels for PM, may miss the broader sweep of the influence of complex pollution mixes.

When race rates were considered, power plant and nonpoint source pollutants were associated with death rates for all groups, though the associations were weak (Table 7.7). The Black primary and contributing rates were also associated with nonroad and onroad mobile sources. White contributing rates also showed a weak association with onroad sources, while Hispanic rates showed no association with any of these sources. Respiratory as the primary cause and nonrespiratory rates for

Table 7.6 Death rates by source and type of pollution

	Respiratory primary cause rate	Respiratory contributing cause rate	Nonrespiratory cause rate
Electric power plant			
Nitrous oxide	0.15*	0.20*	0.23*
Ozone	0.15*	0.20*	0.23*
Sulfur dioxide	0.13*	0.19*	0.20*
Carbon dioxide	0.13*	0.19*	0.21*
Nonpoint source			
Carbon monoxide	0.09**	0.15**	0.12**
Nitrous oxide	0.10**	0.15**	0.13**
Particulate matter 10	0.08**	0.14**	0.12**
Particulate matter 2.5	0.08**	0.14**	0.11**
Sulfur dioxide	0.07**	0.13**	0.11**
Volatile organic compounds	0.09**	0.15**	0.12**
Area source			
Carbon monoxide	ns	0.06*	0.17**
Nitrous oxide	ns	0.07**	0.15**
Particulate matter 10	ns	ns	0.14**
Particulate matter 2.5	ns	ns	0.15**
Sulfur dioxide	ns	ns	0.11**
Volatile organic compounds	ns	0.07**	0.18**
Nonroad mobile source			
Carbon monoxide	0.07*	0.07*	0.13**
Nitrous oxide	0.07*	0.07*	0.13**
Particulate matter 10	0.07*	0.07*	0.13**
Particulate matter 2.5	0.07*	0.07*	0.13**
Sulfur dioxide	0.06*	0.06*	0.13**
Volatile organic compounds	0.07*	0.07*	0.13**
Onroad mobile source			
Carbon monoxide	ns	ns	0.09**
Nitrous oxide	ns	ns	0.09**
Particulate matter 10	ns	ns	0.09**
Particulate matter 2.5	ns	ns	0.09**
Sulfur dioxide	ns	ns	0.09**
Volatile organic compounds	ns	ns	0.09**
Nonutility point source			
Carbon monoxide	−0.08**	ns	−0.06*
Nitrous oxide	−0.08**	ns	−0.06*
Particulate matter 10	−0.08**	ns	−0.06*
Particulate matter 2.5	−0.07**	ns	−0.06*
Sulfur dioxide	−0.09**	ns	−0.07**
Volatile organic compounds	−0.06*	ns	ns
Total – all sources			
Carbon monoxide	0.07**	0.09**	0.16**
Nitrous oxide	0.08**	0.09**	0.16**
Particulate matter 10	ns	ns	0.16**
Particulate matter 2.5	ns	ns	0.16**
Sulfur dioxide	ns	0.09**	0.20**
Volatile organic compounds	0.09**	0.11**	0.19**

ns Difference among areas not significant
*Significant at $p < 0.01$
**Significant at $p < 0.001$

Table 7.7 Race/ethnicity death rates by source and type of pollution*

	Respiratory primary cause rate			Respiratory contributing cause rate			Nonrespiratory cause rate		
	White	Black	Hispanic	White	Black	Hispanic	White	Black	Hispanic
Electric power plant									
Nitrous oxide	0.11	0.11	0.14	0.15	0.13	0.16	0.14	0.20	0.17
Ozone	0.11	0.11	0.14	0.15	0.13	0.16	0.15	0.20	0.16
Sulfur dioxide	0.10	0.10	0.13	0.14	0.13	0.14	0.13	0.19	0.15
Carbon dioxide	0.10	0.10	0.12	0.15	0.12	0.15	0.14	0.19	0.15
Nonpoint source									
Carbon monoxide	0.08	0.07	0.07	0.11	0.10	0.10	0.08	0.10	0.09
Nitrous oxide	0.09	0.07	0.07	0.12	0.10	0.11	0.09	0.11	0.10
Particulate matter 10	0.07	0.07	0.08	0.10	0.10	0.11	0.07	0.10	0.10
Particulate matter 2.5	0.07	0.07	0.08	0.10	0.10	0.11	0.07	0.10	0.10
Sulfur dioxide	0.07	0.06	0.06	0.10	0.09	0.10	0.08	0.09	0.08
Volatile organic compounds	0.10	0.08	ns	0.13	0.12	0.07	0.11	0.11	0.06
Area source									
Carbon monoxide	ns	0.08	ns	0.06	ns	ns	0.14	0.12	0.13
Nitrous oxide	0.09	0.11	−0.12	0.11	0.07	−0.09	0.22	0.15	ns
Particulate matter 10	ns	0.08	ns	ns	ns	0.06	0.10	0.12	0.13
Particulate matter 2.5	0.06	0.10	−0.08	0.08	0.06	ns	0.19	0.15	0.06
Sulfur dioxide	ns	ns	0.15	ns	ns	0.19	ns	0.07	0.19
Volatile organic compounds	ns	0.09	ns	0.06	ns	0.07	0.13	0.14	0.15
Nonroad mobile source									
Carbon monoxide	ns	0.10	ns	ns	0.10	ns	ns	0.15	0.08
Nitrous oxide	ns	0.09	ns	ns	0.10	ns	ns	0.15	0.08
Particulate matter 10	ns	0.09	ns	ns	0.10	ns	ns	0.15	0.07
Particulate matter 2.5	ns	0.09	ns	ns	0.10	ns	ns	0.15	0.07
Sulfur dioxide	ns	0.09	ns	ns	0.10	ns	ns	0.15	0.07
Volatile organic compounds	ns	0.10	ns	ns	0.10	ns	ns	0.15	0.07

Table 7.7 (continued)

	Respiratory primary cause rate			Respiratory contributing cause rate			Nonrespiratory cause rate		
	White	Black	Hispanic	White	Black	Hispanic	White	Black	Hispanic
Onroad mobile source									
Carbon monoxide	ns	0.09	ns	0.06	0.09	ns	0.06	0.12	0.04
Nitrous oxide	ns	0.09	ns	0.07	0.09	ns	0.09	0.12	ns
Particulate matter 10	ns	0.09	ns	0.07	0.09	ns	0.08	0.12	ns
Particulate matter 2.5	ns	0.09	ns	0.07	0.09	ns	0.08	0.12	ns
Sulfur dioxide	ns	0.09	ns	0.07	0.09	ns	0.09	0.12	ns
Volatile organic compounds	ns	0.09	ns	0.07	0.09	ns	0.09	0.12	ns
Nonutility point source									
Carbon monoxide	−0.06	ns	ns	ns	ns	ns	−0.06	ns	ns
Nitrous oxide	−0.06	ns	ns	ns	ns	ns	−0.06	ns	ns
Particulate matter 10	ns	ns	ns	ns	ns	ns	−0.06	ns	ns
Particulate matter 2.5	ns	ns	ns	ns	ns	ns	−0.06	ns	ns
Sulfur dioxide	−0.07	ns	ns	ns	ns	ns	−0.07	ns	−0.06
Volatile organic compounds	ns	ns	ns	ns	ns	ns	−0.06	ns	ns
Total – all sources									
Carbon monoxide	0.08	0.12	ns	0.09	0.12	ns	0.12	0.17	0.07
Nitrous oxide	0.09	0.13	ns	0.10	0.12	ns	0.15	0.18	ns
Particulate matter 10	ns	0.10	0.07	ns	0.07	0.10	0.11	0.16	0.17
Particulate matter 2.5	ns	0.11	ns	0.07	0.08	ns	0.16	0.17	0.08
Sulfur dioxide	ns	0.11	ns	0.07	0.08	ns	0.16	0.17	0.08
Volatile organic compounds	0.10	0.13	ns	0.11	0.11	ns	0.16	0.18	0.10

ns Difference among areas not significant
* Significant at $p < 0.01$

Whites were negatively associated with nonutility point source emissions. As these sources vary greatly in type, ranging from dry cleaning stores to chemical plants, it was not possible to capture the spatial extent of each facility's potential influence. However, the negative association may reflect the "not-in-my-backyard" effect of the more visible sources, such that the residents try to avoid proximity to such facilities.

7.5 Conclusion

While air pollution emissions have been reduced across the United States, concern for public health remains as studies continue to show the negative impact of emissions at levels below those set by national air quality standards. This study sought to evaluate the spatial aspects of the emission of criteria air pollutants from various sources on respiratory mortality in the five major Texas urban areas of Austin, Dallas-Fort Worth, El Paso, Houston and San Antonio. Using GIS spatial processing functions, a spatial picture of air pollution sources was created and joined to individual level mortality data to allow a comparison of the association of pollution sources and types with deaths where respiratory disease was listed as either the primary or as a contributing cause. It is clear from this analysis that the urban areas differ not only in pollution sources and levels, but also in the composition of the population affected as characterized by age, race/ethnicity and gender. As would be expected, Houston has both the highest rank for emissions, and the highest rate of respiratory primary cause mortality. Race/ethnicity appears to be a more defining attribute than gender or age in identifying the subgroup in the population with the highest risk. While Hispanics have been the focus of much research, findings here show that White and Black primary and contributing rates were higher for the five urban areas in this study. The respiratory related rate of mortality for those aged 65 years or older did not show elevated levels when compared to the elderly group's nonrespiratory rate.

The associations between pollution sources and mortality rates examined here showed only weak positive associations overall. The weak strength of these associations may reflect methodological limitations, as this study sought to use readily available government pollution data that were largely limited in spatial resolution, the complex nature of exposure, and factors that predispose individuals to be at risk for respiratory diseases. In addition, the decedent's work location and mode of transportation for any work commute was not available. Therefore, only residential exposure was able to be identified. Similarly, the emission data only represent outdoor exposure. However, because several studies have found indoor and outdoor pollution concentrations to be associated, this limitation was not deemed to be major (Delfino 2002; Koenig et al. 2005; Rodes et al. 2001; Rojas-Bracho et al. 2000; Williams et al. 2000a).

However, two findings stand out as noteworthy. First, electric power plant pollutants showed the strongest association with all mortality rates, while nonutility point source pollution exhibited negative relationships with all rates. In the case of the former, there has been considerable public pressure resulting in policy that should

reduce future power plant emissions. It is suggested that the negative association for rates and nonutility point sources may reflect the effectiveness of public avoidance of the larger facilities in this category. Second, the complex variation in associations between the different pollution sources and types and the demographic attributes suggest that additional evaluation is needed to find specific reasons for such variations. Overall, this research provides a benchmark for further air quality investigations related to emissions reduction from specific sources. As such, the work may facilitate future efforts to spatially evaluate the impact of facilities that produce air pollution, leading to the improvement of public health and resulting in measurable health benefits.

References

Adgate, J. L., Church, T. R., Ryan, A. D., Ramachandran, G., Fredrickson, A. L., Stock, T. H., Morandi, M. T., and Sexton, K. (2004). Outdoor, indoor, and personal exposure to VOCs in children. *Environmental Health Perspectives, 112*(14), 1386–1392.

American Thoracic Society. (1995). Standards for the diagnosis and care of patients with chronic obstructive pulmonary disease. *American Journal of Respiratory and Critical Care Medicine, 152*(5), S77–S121.

Brook, R. D., Franklin, B., Cascio, W., Hong, Y., Howard, G., Lipsett, M., Luepker, R., Mittleman, M., Samet, J., Smith, S. C., Jr, and Tager, I. (2004). Air pollution and cardiovascular disease: a statement for healthcare professionals from the expert panel on population and prevention science of the American heart association. *Circulation, 109*(21), 2655–2671.

Burnett, R. T., Smith-Doiron, M., Stieb, D., Raizenne, M. E., Brook, J. R., Dales, R. E., Leech, J. A., Cakmak, S., and Krewski, D. (2001). Association between ozone and hospitalization for acute respiratory diseases in children less than 2 years of age. *American Journal of Epidemiology, 153*(5), 444–452.

Chakraborty, J. (2001). Analyzing exposure of school children to accidental releases of hazardous substances. *Journal of Exposure Analysis and Environmental Epidemiology, 11*(4), 269–278.

Chestnut, L. G., and Mills, D. M. (2005). A fresh look at the benefits and costs of the US acid rain program. *Journal of Environmental Management, 77*(3), 252–266.

Creason, J., Neas, L., Walsh, D., Williams, R., Sheldon, L., Liao, D., and Shy, C. (2001). Particulate matter and heart rate variability among elderly retirees: the Baltimore 1998 PM study. *Journal of Exposure Analysis and Environmental Epidemiology, 11*, 116–122.

Davis, A. M., Kreutzer, R., Lipsett, M., King, G., and Shaikh, N. (2006). Asthma prevalence in Hispanic and Asian American ethnic subgroups: ressults from the California Healthy Kids Survey. *Pediatrics, 118*(2), 363–370.

Delfino, R. J. (2002). Epidemiologic evidence for asthma and exposure to air toxics: Linkages between occupational, indoor, and community air pollution research. *Environmental Health Perspectives, 110*(Supplement 4), 573–589.

Delfino, R. J., Gong Jr., H., Linn, W. S., Pellizzari, E. D., and Hu, Y. (2003a). Asthma symptoms in Hispanic children and daily ambient exposures to toxic and criteria air pollutants. *Environmental Health Perspectives, 111*(4), 647–656.

Delfino, R. J., Gong, H., Linn, W. S., Hu, Y., and Pellizzari, E. D. (2003b). Respiratory symptoms and peak expiratory flow in children with asthma in relation to volatile organic compounds in exhaled breath and ambient air. *Journal of Exposure Analysis & Environmental Epidemiology, 13*(5), 348–363.

Dominici, F., Peng, R. D., Bell, M. L., Pham, L., McDermott, A., Zeger, S. L., and Samet, J. M. (2006). Fine particulate air pollution and hospital admission for cardiovascular and respiratory diseases. *Journal of the American Medical Association, 295*(10), 1127–1134.

Eiswerth, M. E., Shaw, W. D., and Yen, S. T. (2005). Impacts of ozone on the activities of asthmatics: revisiting the data. *Journal of Environmental Management, 77*(1), 56–63.

Erbas, B., Kelly, A.-M., Physick, B., Code, C., and Edwards, M. (2005). Air pollution and childhood asthma emergency hospital admissions: Estimating intra-city regional variations. *International Journal of Environmental Health Research, 15*(1), 11–20.

Evans, R. (1992). Asthma among minority children: a growing problem. *Chest, 101*(6), 368S–371S.

Filleul, L., Tertre, A. L., Baldi, I., and Tessier, J.-F. (2004). Difference in the relation between daily mortality and air pollution among elderly and all-ages populations in southwestern France. *Environmental Research, 94*(3), 249–253.

Gauderman, W. J., McConnell, R., Gilliland, F., London, S., Thomas, D., Avol, E., Vora, H., Berhane, K., Rappaport, E. B., Lurmann, F., Margolis, H. G., and Peters, J. (2000). Association between air pollution and lung function growth in southern California children. *American Journal of Respiratory and Critical Care Medicine, 162*, 1383–90.

Gauderman, W. J., Gilliland, G. F., Vora, H., Avol, E., Stram, D., McConnell, R., Thomas, D., Lurmann, F., Margolis, H. G., Rappaport, E. B., Berhane, K., and Peters, J. M. (2002). Association between air pollution and lung function growth in southern California children: results from a second cohort. *American Journal of Respiratory and Critical Care Medicine, 166*, 76–84.

Gauderman, W. J., Avol, E., Gilliland, F., Vora, H., Thomas, D., Berhane, K., McConnell, R., Kuenzli, N., Lurmann, F., Rappaport, E., Margolis, H., Bates, D., and Peters, J. (2004). The effect of air pollution on lung development from 10 to 18 years of age. *The New England Journal of Medicine, 351*(11), 1057–1067.

Gauderman, W. J., Avol, E., Lurmann, F., Kuenzli, N., Gilliland, F., Peters, J., and McConnell, R. (2005). Childhood asthma and exposure to traffic and nitrogen dioxide. *Epidemiology, 16*(6), 737–743.

Gent, J. F., Triche, E. W., Holford, T. R., Belanger, K., Bracken, M. B., Beckett, W. S., and Leaderer, B. P. (2003). Association of low-level ozone and fine particles with respiratory symptoms in children with asthma. *Journal of the American Medical Association, 290*(14), 1859–1867.

Gielen, M. H., van der Zee, S. C., van Wijnen, J. H., and van Steen, C. J. (1997). Acute effects of summer air pollution on respiratory health of asthmatic children. *American Journal of Respiratory and Critical Care Medicine, 155*, 2105–2108.

Glinianaia, S. V., Rankin, J., Bell, R., Pless-Mulloli, T., and Howel, D. (2004). Does particulate air pollution contribute to infant death? A systematic review. *Environmental Health Perspectives, 112*(14), 1365–1370.

Goldberg, M. S., Burnett, R. T., Brook, J., III, J. C. B., Valois, M.-F., and Vincent, R. (2001). Associations between daily cause-specific mortality and concentrations of ground-level ozone in Montreal, Quebec. *American Journal of Epidemiology, 154*(9), 817–826.

Hartog, J. J. d., Hoek, G., Peters, A., Timonen, K. L., Ibald-Mulli, A., Brunekreef, B., Heinrich, J., Tiittanen, P., Wijnen, J. H. v., Kreyling, W., Kulmala, M., and Pekkanen, J. (2003). Effects of fine and ultrafine particles on cardiorespiratory symptoms in elderly subjects with coronary heart disease: the ULTRA Study. *American Journal of Epidemiology, 157*(7), 613–623.

Henry, R. L., Bridgman, H. A., Wlodarczyk, J., Abramson, R., Adler, J. A., and Hensley, M. J. (1991). Asthma in the vicinity of power stations: II. Outdoor air quality and symptoms. *Pediatric Pulmonology, 11*, 134–140.

Hoffmann, B., Moebus, S., Mohlenkamp, S., Stang, A., Lehmann, N., Dragano, N., Schmermund, A., Memmesheimer, M., Mann, K., Erbel, R., Jockel, K.-H., and for the Heinz Nixdorf Recall Study Investigative Group. (2007). Residential exposure to traffic is associated with coronary atherosclerosis. *Circulation, 116*(5), 489–496.

Huston, R. J., Marquez, R. B. R., Baker, J. M., and Saitas, J. A. (2001). *Grandfathered Facilities Report* (SFR-071). Austin: Office of Permitting, Remediation and Registration Texas Natural Resource Conservation Commission.

Islam, T., Gauderman, W. J., Berhane, K., McConnell, R., Avol, E., Peters, J. M., and Gilliland, F. D. (2007). Relationship between air pollution, lung function and asthma in adolescents. *Thorax, 62*(11), 957–963.

Jerrett, M., Burnett, R. T., Kanaroglou, P., Eyles, J., Finkelstein, N., Giovis, C., and Brook, J. R. (2001). A GIS – environmental justice analysis of particulate air pollution in Hamilton, Canada. *Environment and Planning A, 33*(6), 955–973.

Kaiser, R., Romieu, I., Medina, S., Schwartz, J., Krzyzanowski, M., and Künzli, N. (2004). Air pollution attributable postneonatal infant mortality in US metropolitan areas: a risk assessment study. *Environmental Health: A Global Access Science Source, 3*(1), 1–6.

Karr, C., Lumley, T., Schreuder, A., Davis, R., Larson, T., Ritz, B., and Kaufman, J. (2007). Effects of subchronic and chronic exposure to ambient air pollutants on infant bronchiolitis. *American Journal of Epidemiology, 165*(5), 553–560.

Kim, J. J., Smorodinsky, S., Lipsett, M., Singer, B. C., Hodgson, A. T., and Ostro, B. (2004). Traffic-related air pollution near busy roads. *American Journal of Respiratory and Critical Care Medicine, 170*(5), 520–526.

Koenig, J. Q., Mar, T. F., Allen, R. W., Jansen, K., Lumley, T., Sullivan, J. H., Trenga, C. A., Larson, T. V., and Liu, L.-J. S. (2005). Pulmonary Effects of Indoor– and Outdoor-Generated Particles in Children with Asthma. *Environmental Health Perspectives, 113*(4), 499–503.

Levy, J. I., Greco, S. L., and Spengler, J. D. (2002). The importance of population susceptibility for air pollution risk assessment: a case study of power plants near Washington, DC. *Environmental Health Perspectives, 110*(12), 1253–1260.

Levy, J. I., Wilson, A. M., Evans, J. S., and Spengler, J. D. (2003). Estimation of primary and secondary particulate matter intake fractions for power plants in Georgia. *Environmental Science and Technology, 37*(24), 5528–5536.

Lin, S., Munsie, J. P., Hwang, S.-A., Fitzgerald, E., and Cayo, M. R. (2002). Childhood asthma hospitalization and residential exposure to state route traffic. *Environmental Research Section A, 88*(2), 73–81.

Mann, J. K., Tager, I. B., Lurmann, F., Segal, M., Queensberry, C. P., Lugg, M. M., Shan, J., and Van Eeden, S. K. (2002). Air pollution and hospital admissions for ischemic heart disease in persons with congestive heart failure or arrhythmia. *Environmental Health Perspectives, 110*(12), 1247.

McConnell, R., Berhane, K., Gilliland, F., London, S. J., Islam, T., Gauderman, W. J., Avol, E., Margoli, H. G., and Peters, J. M. (2002). Asthma in exercising children exposed to ozone: a cohort study. *The Lancet, 359*, 386–391.

McConnell, R., Berhane, K., Gilliland, F., Molitor, J., Thomas, D., Lurmann, F., Avol, E., Gauderman, W. J., and Peters, J. M. (2003). Prospective study of air pollution and bronchitic symptoms in children with asthma. *American Journal of Respiratory and Critical Care Medicine, 168*, 790–97.

Metzer, R., and Delgado, J. L. (1995). Environmental health and Hispanic children. *Environmental Health Perspectives Supplements, 103*(Supplement 6), 25–32.

Mitka, M. (2008). New evidence-based guidelines focus on treatment of children with asthma. *Journal of the American Medical Association, 299*(10), 1122–1123.

Norris, G., YoungPong, S. N., Koenig, J. Q., Larson, T. V., Sheppard, L., and Stout, J. W. (1999). An association between fine particles and asthma emergency department visits for children in Seattle. *Environmental Health Perspectives, 107*(6), 489–493.

O'Neill, M. S., Jerrett, M., Kawachi, I., Levy, J. I., Cohen, A. J., Gouveia, N., Wilkinson, P., Fletcher, T., Cifuentes, L., and Schwartz, J. (2003). Health, wealth, and air pollution: advancing theory and methods. *Environmental Health Perspectives, 111*(16), 1861–1870.

Peng, R. D., Chang, H. H., Bell, M. L., McDermott, A., Zeger, S. L., Samet, J. M., and Dominici, F. (2008). Coarse particulate matter air pollution and hospital admissions for cardiovascular and respiratory diseases among medicare patients. *Journal of the American Medical Association, 299*(18), 2172–2179.

Peters, A., Dockery, D. W., Muller, J. E., and Mittleman, M. A. (2001). Increased particulate air pollution and the triggering of myocardial infarction. *Circulation, 103*(23), 2810–2815.

Pope III, C. A., Burnett, R. T., Thun, M. J., Calle, E. E., Krewski, D., Ito, K., and Thurston, G. D. (2002). Lung cancer, cardiopulmonary mortality, and long-term exposure to fine particulate air pollution. *Journal of the American Medical Association, 287*(9), 1132–1141.

Pope III, C. A., Hansen, M. L., Long, R. W., Nielsen, K. R., Eatough, N. L., Wilson, W. E., and Eatough, D. J. (2004). Ambient particulate air pollution, heart rate variability, and blood markers of inflammation in a panel of elderly subjects. *Environmental Health Perspectives, 112*(3), 339–345.

Pope III, C. A., Muhlestein, J. B., May, H. T., Renlund, D. G., Anderson, J. L., and Horne, B. D. (2006). Ischemic heart disease events triggered by short-term exposure to fine particulate air pollution. *Circulation, 114*(23), 2443–2448.

Pouliou, T., Kanaroglou, P. S., Elliott, S. J., and Pengelly, L. D. (2008). Assessing the health impacts of air pollution: a re-analysis of the Hamilton children′s cohort data using a spatial analytic approach. *International Journal of Environmental Health Research, 18*(1), 17–35.

Ritz, B., Wilhelm, M., and Zhao, Y. (2006). Air pollution and infant death in Southern California, 1989–2000. *Pediatrics, 118*(2), 493–502.

Rodes, C. E., Lawless, P. A., Evans, G. F., Sheldon, L. S., Williams, R. W., Vette, A. F., Creason, J. P., and Walsh, D. (2001). The relationships between personal PM exposures for elderly populations and indoor and outdoor concentrations for three retirement center scenarios. *Journal of Exposure Analysis & Environmental Epidemiology, 11*(2), 103–115.

Rojas-Bracho, L., Suh, H. H., and Koutrakis, P. (2000). Relationships among personal, indoor, and outdoor fine and coarse particle concentrations for individuals with COPD. *Journal of Exposure Analysis and Environmental Epidemiology, 10*(3), 294–306.

Samet, J. M., Dominici, F., Curriero, F. C., Coursac, I., and Zeger, S. L. (2000). Fine particulate air pollution and mortality in 20 US cities 1987–1994. *The New England Journal of Medicine, 343*(24), 1742–1749.

Schenker, M. B., Vedal, S., Batterman, S., Samet, J., and Speizer, F. E. (1986). Health effects of air pollution due to coal combustion in the Chestnut Ridge region of Pennsylvania: cross-section survey of children. *Archives of Environmental Health, 41*(2), 104–108.

Schwartz, J. (1991a). Particulate air pollution and daily mortality: a synthesis. *Public Health Review, 19*, 39–60.

Schwartz, J. (1991b). Particulate air pollution and daily mortality in Detroit. *Environmental Research, 56*, 204–213.

Schwartz, J. (1993). Air pollution and daily mortality in Birmingham, Alabama. *American Journal of Epidemiology, 137*(10), 1136–47.

Schwartz, J. (1994a). Air pollution and daily mortality: a review and meta-analysis. *Environmental Research, 64*, 36–52.

Schwartz, J. (1994b). Air pollution and hospital admissions for the elderly in Birmingham, Alabama. *American Journal of Epidemiology, 139*(6), 589–598.

Schwartz, J. (1994c). What are people dying of on high air pollution days? *Environmental Research, 64*, 26–35.

Schwartz, J., and Dockery, D. W. (1992a). Increased mortality in Philadelphia associated with daily air pollution concentrations. *American Review of Respiratory Disease, 145*, 600–604.

Schwartz, J., and Dockery, D. W. (1992b). Particulate air pollution and daily mortality in Steubenville, Ohio. *American Journal of Epidemiology, 135*(1), 12–19.

Schwartz, J., and Morris, R. (1994). Air pollution and hospital admissions for the elderly in Detroit, Michigan. *American Journal of Respiratory and Critical Care Medicine, 150*, 648–655.

Schwartz, J., and Morris, R. (1995). Air pollution and hospital admissions for cardiovascular disease in Detroit, Michigan. *American Journal of Epidemiology, 142*(1), 23–35.

Texas Department of State Health Services. (2006). *2002 Health Facts for Texas*. Texas Department of State Health Services. Available: http://www.dshs.state.tx.us/chs/cfs/cshdpa02.shtm [December 9].

Texas Health Care Information Council. (2005). *Preventable Hospitalizations, 2002*. Texas Department of State Health Services. Available: http://www.dshs.state.tx.us/THCIC/Publications/Hospitals/PQIReport2002/PreventableHospitalizations2002.shtm [2008, April 22].

Thurston, G. D., Lippmann, M., Scott, M. B., and Fine, J. M. (1997). Summertime haze air pollution and children with asthma. *American Journal of Respiratory and Critical Care Medicine, 155*, 654–660.

Timonen, K. L., and Pekkanen, J. (1997). Air pollution and respiratory health among children with asthmatic or cough symptoms. *American Journal of Respiratory and Critical Care Medicine, 156*(2), 546–552.

Tolbert, P. E., Mulholland, J. A., MacIntosh, D. L., Xu, F., Daniels, D., Devine, O. J., Carlin, B. P., Klein, M., Dorley, J., Butler, A. J., Nordenberg, D. F., Frumkin, H., Ryan, P. B., and White, M. C. (2000). Air quality and pediatric emergency room visits for asthma in Atlanta, Georgia, USA. *American Journal of Epidemiology, 151*(8), 798–810.

Tonn, B. E., Waidley, G., and Petrich, C. (2001). The ageing US population and environmental policy. *Journal of Environmental Planning and Management, 44*(6), 851–876.

Tonne, C., Melly, S., Mittleman, M., Coull, B., Goldberg, R., and Schwartz, J. (2007). A case–control analysis of exposure to traffic and acute myocardial infarction. *Environmental Health Perspectives, 115*(1), 53–57.

US Bureau of the Census. (2000). *Census of Population and Housing, Summary Tape File 3a*. Washington, DC: Department of Commerce.

US Energy Information Administration. (2003). *State Electricity Profiles* (DOE/EIA-0348(01)/2). Washington, DC: US Department of Energy.

US Environmental Protection Agency. (1997). *National Air Quality and Emissions Trends Report, 1997*. Available: http://www.epa.gov/air/ airtrends/aqtrnd97/ [2008, April 22].

US Environmental Protection Agency. (2006). *Clear Skies in Texas*. Available: http://www.epa.gov/air/clearskies/state/tx.html [2008, April 22].

US Environmental Protection Agency. (2008a). *eGRID 2002 Archive*. Available: http://www.epa.gov/cleanenergy/energy-resources/egrid/archive.html [2008, April 22].

US Environmental Protection Agency. (2008b). *National Emissions Inventories for the US*. US Environmental Protection Agency. Available: http://www.epa.gov/ttn/chief/net/ [2008, April 22].

Watson, A. Y., Bates, R. R., and Kennedy, D. (1988). *Air Pollution, the Automobile, and Public Health*. Washington, DC: National Academies Press.

Williams, R., Suggs, J., Zweidinger, R., Evans, G., Creason, J., Kwok, R., Rodes, C., Lawless, P., and Sheldon, L. (2000a). The 1998 Baltimore particulate matter epidemiology–exposure study: part 1. Comparison of ambient, residential outdoor, indoor and apartment particulate matter monitoring. *Journal of Exposure Analysis and Environmental Epidemiology, 10*(6), 518–532.

Williams, R., Suggs, J., Creason, J., Rodes, C., Lawless, P., Kwok, R., Zweidinger, R., and Sheldon, L. (2000b). The 1998 Baltimore particulate matter epidemiology–exposure study: part 2. Personal exposure assessment associated with an elderly study population. *Journal of Exposure Analysis and Environmental Epidemiology, 10*(6), 533–543.

Zanobetti, A., Schwartz, J., and Gold, D. (2000). Are there sensitive subgroups for the effects of airborne particles? *Environmental Health Perspectives, 108*(9), 841–845.

Chapter 8
Spatial Distribution of Toxic Release Inventory Sites in Chicago Area: Is There Environmental Inequity?

Fahui Wang and Yvette C. Feliberty

Abstract The purpose of this study is to determine if "environmental inequity" can be associated with the spatial distribution of Toxic Release Inventory (TRI) facilities in the Chicago area. The chapter examines whether neighborhoods with minority concentrations or lower-income residents experience disproportionate exposure to facilities that release toxic emissions into the environment. Demographic information is extracted from 2000 Census data, and facility data are based on the 2004 Environmental Protection Agency's Toxic Release Inventory. Geographic Information Systems (GIS) is used to create "buffers" of various spatial extent around the facilities. Statistical analysis (including *t*-tests and regressions) is conducted to examine whether areas within the buffers are significantly more likely to consist of minority and low-income residents and households than areas outside the buffers. Results indicate that at both the census tract and block group levels, Hispanic and non-white classes as well as low-income residents are more likely to be located within the buffers. Therefore, this study corroborates earlier research findings that minority and low-income groups are disproportionately exposed to environmental hazards.

Keywords GIS · Toxic Release Inventory (TRI) sites · *t*-Test · Environmental inequity · Chicago area · Minority

8.1 Introduction

Since the early 1980s, there has been mounting interest in *environmental equity* in relation to the distribution of environmental hazards in neighborhoods predominantly inhabited by low-income residents and/or minority background. This interest was codified in July 1990 by the Environmental Protection Agency's (EPA)

F. Wang (✉)
Department of Geography and Anthropology, Louisiana State University, Baton Rouge, LA 70803, USA
e-mail: fwang@lsu.edu

P.S. Showalter, Y. Lu (eds.), *Geospatial Techniques in Urban Hazard and Disaster Analysis*, Geotechnologies and the Environment 2, DOI 10.1007/978-90-481-2238-7_8,

Environmental Equity Workgroup, which began to examine (and, ultimately confirmed in 1992) the allegation that racial minorities and low-income populations were at higher environmental risk than others (EPA 2008a). Within their definition of "environmental justice", the EPA states that, "Fair Treatment means that no group of people, including racial, ethnic, or socioeconomic groups, should bear a disproportionate share of the negative environmental consequences resulting from industrial, municipal, and commercial operations ..." (EPA 2008b). Examples of such operations include polluting industries, landfills, incinerators, and illegal dumps (Pellow 2004).

In many studies, environmental equity has been treated as a "chicken and egg" situation due to the question of what came first, the residents or the facility. Essentially, those engaged in answering these questions seek to ascertain whether the residents of a particular area are exposed to environmental hazards due to circumstance (i.e., they moved into an area where environmental hazards pre-existed), or because environmentally hazardous facilities have been purposely located in areas largely occupied by low-income and/or minority residents. If the former is the case, the issue is one of housing availability or housing choice. Either there is a lack of affordable housing elsewhere, or people are making a conscious choice to expose themselves to environmental risk so they can reside in a more convenient location and/or enjoy better housing amenities (Pastor et al. 2001). The policy implication under such circumstances is to address issues pertaining to discrimination in the housing and/or job markets. If the latter is the case, "unfair treatment," and therefore environmental inequity, can be alleged. However, even in cases where environmental inequity seems evident, claims of discrimination cannot automatically be inferred due to community growth and change as well as the complex public processes governing the placement of industrial sites. Consequently, causal statements trying to establish environmental inequity are not fully warranted on scientific grounds (Bowen and Wells 2002).

This study examines possible environmental inequity in the spatial distribution of Toxic Release Inventory (TRI) facilities in the Chicago area, specifically Cook County, Illinois. Cook County is an appropriate study area for several reasons. First, the county is predominantly urban (it includes the City of Chicago), containing large populations of various racial/ethnic and economic backgrounds. Second, the county contains a large number of TRI facilities. Third, the time required to geocode the TRI facilities (a significant number of which required manual geocoding) was offset by the large sample size available for use. Finally, our understanding of the study area's historical development, acquired via an extensive literature review, raises our confidence in the interpretation of our findings.

This study examines whether the neighborhoods containing minority concentrations or low-income residents experience disproportionate exposure to facilities releasing toxic emissions into the environment. Demographic information is extracted from 2000 Census data at two data aggregation levels (census tract and block group). The EPA's 2004 TRI provides the location data for environmentally hazardous sites. Statistical analyses, including regressions and *t*-tests, examine whether residents within specified distances from the facilities have significantly

higher ratios of minorities or lower income residents than areas at further distances. If proximity to hazardous sites by disadvantaged population groups is confirmed, policy implications arise in terms of the vulnerability of such residents to disaster events (whether natural or technological in nature) that could cause releases impacting those neighborhoods.

The remainder of this chapter is organized as follows. Section 8.2 provides a literature review of environmental justice and a brief history of Cook County, Illinois. Section 8.3 explains the data used in this study. Section 8.4 addresses the methodological process employed. Section 8.5 presents and discusses the study results. And, Section 8.6 provides concluding comments on the study's major findings and limitations.

8.2 Background and Literature Review

8.2.1 The Environmental Justice Movement

The Environmental Justice Movement rose to prominence in the early 1980s in response to the growing awareness of the unequal distribution of waste sites, other hazards, and overall environmental degradation prominent in many minority and low-income communities throughout the country. Cole and Foster (2001) identified six major benchmarks in the environmental justice movement that helped shape the future of those involved and of the movement itself: civil rights; grassroots anti-toxics movements; academics; labor movements, such as the farm worker movement of the 1960s; traditional environmentalism; and finally, the struggles of indigenous groups across the United States. Together, these causes helped create a unified front struggling for social justice with regard to the physical environment where low-income and minority groups lived and raised their families.

The First National People of Color Environmental Leadership Summit in Washington, DC, held in 1991, is considered the most important event in the movement's history. The summit broadened the movement's goals beyond that of focusing on anti-toxics to include issues such as public health, worker safety, land use, transportation, housing, resource allocation, and community empowerment (Bullard and Johnson 2000). The movement led to important public policy initiatives such as the 1994 Executive Order 12898 (Federal Actions to Address Environmental Justice in Minority Populations and Low-Income Populations) and the subsequent founding of the EPA's National Environmental Justice Advisory Council (NEJAC) (Bolin et al. 2000; Faber and McCarthy 2001).

8.2.2 Studies on Environmental Justice

Most studies on environmental equity have concluded that minorities and the poor are disproportionately exposed to various types of waste sites in the United States (e.g., Bowen et al. 1995; Pinderhughes, 1996; Towers 2000). Five major works are

credited with publicizing environmental equity issues (Hunter 2000; Pellow et al. 2001). The first was by the US General Accounting Office (USGAO 1983), and revealed that three out of four commercial hazardous waste landfills were located in predominantly African American communities. Another prominent work by the United Church of Christ Commission for Racial Justice (UCCCRJ 1987) found that there were a disproportionate number of waste facilities situated in areas with high rates of poverty and minority habitation throughout the United States. Bullard (1990) compiled a series of case studies that documented methods of resistance to waste sites in the communities of color along with issues regarding environmental racism. Lavelle and Coyle (1992) discussed the roles that government and private corporations played in environmental inequities against minorities of all economic backgrounds. And finally, the Committee on Environmental Justice at the Institute of Medicine (CEJ 1999) concluded that the fields of medicine and science must concentrate on the problems and concerns of non-white communities with regard to environmental health.

Research closely related to our work is a study by Baden and Coursey (2002) on the City of Chicago. Using 1960 and 1990 census data, they performed various regressions at the census tract level to test whether the distribution of waste sites was correlated to populations of minorities and the poor and whether there was any historical pattern to that distribution. They concluded that in 1960 more waste sites were located in poor, non-African American neighborhoods, and that in 1990 Hispanic but not African American neighborhoods were disproportionately represented. They also found that, historically, Hispanics were disproportionately exposed to waste sites. Our study builds on their work by using newer data, an expanded study area, multiple geographic levels and a series of distance ranges from waste sites to revisit the issues they identified, with the goal of obtaining more robust results.

8.2.3 Causes for Environmental Inequity

As explained earlier, an important aspect regarding the discourse in relation to environmental justice is the "chicken and egg" dilemma. In addition, researchers disagree about whether the occupancy of residences close to waste sites is voluntary or forced. Some studies support the idea that poor and minority residents often have environmental disamenities thrust upon them. Hite (2000) posits that personal choice is a key factor in the decision-making process to reside in proximity to a waste site. This selective behavior may cause a person to trade the environmental quality of a neighborhood for other housing desires (e.g., number of rooms) and/or location characteristics (e.g., school districts, or accessible transportation) that are personally appealing. Other studies have concentrated on the powerlessness of poor and minority communities in contending with environmental inequity issues. Glasmeier and Farrigan (2003, 132) state that poor communities are often located in unacceptable areas due to "economic forces" (e.g., more affordable housing prices in undesirable areas).

Others contend that people living in these areas have not been made aware of the consequences and dangers of living in neighborhoods blighted by waste sites (Baden and Coursey 2002). Hunter's (2000) study analyzed the dissemination of information throughout a community from the perspective of linguistic isolation in immigrant households. This "environmental unawareness" causes a lack of public participation in the decision-making process of the community (Laurian 2003). Participation of citizens and community-based organizations in the policy process rests upon equitable access to agency-generated environmental information and effective use of that information by citizens (Kellogg and Mathur 2003). Without adequate knowledge and awareness of issues surrounding proposed planning objectives, residents tend not to engage themselves in public discourse because they are not fully aware of the gravity of the situation (Rast 2006; Ross and Leigh 2000). Public disclosure of information can help stimulate effective and informed participation, and can increase pressure on facilities to reduce their impact on the environment (Arora and Cason 1999). Other researchers (Boone and Modarres 1999; Hunter 2000; Talih and Fricker 2002) find that the poor and minority groups are taken advantage of and deprived of appropriate access to resources.

Zoning laws are often cited as the foundation for the disproportionate distribution of toxic sites in poor and minority neighborhoods (Boone and Modarres 1999; Fricker and Hengartner 2001; Ross and Leigh 2000). The purpose of zoning is to restrict the entry of industrial facilities into residential areas, thereby protecting neighborhoods from the detrimental effects of such facilities. However, some believe that some zoning ordinances (labeled "expulsive zoning") are written as a mechanism to use minority neighborhoods as dumping sites for landfills or other unwanted residential uses (Ross and Leigh 2000).

8.2.4 Brief History of Cook County

Knowledge of the demographic, economic, environmental, and industrial history of the study area allows us to fully understand the "chicken and egg" dilemma surrounding environmental justice discourse. In other words, it is important to know whether the residents or the hazardous sites were the first occupants of an area.

Cook County, comprised of the City of Chicago and its suburbs, is the hub of all major economic activities in Illinois. Located along the western banks of Lake Michigan, Chicago has historically been a key port city, providing explorers and merchants with access to the central United States. The city gained this reputation in the middle of the 19th century when it became a hub for "trade, transportation, and the processing of raw materials from the Midwest" (Baden and Coursey 2002: 65). At this time, businesses were developed along the banks of the rivers stretching out of the lake, such as the Chicago River. Such businesses included "a tannery, a meat packing plant, a soap factory, and a brick yard . . . mainly on the North Side" of the city (Hoyt 1933: 19). The West Side saw the advent of lumberyards, breweries, woodworking shops, foundries, and metal-smithing firms (Baden and Coursey 2002). As industry boomed throughout the city, pollution and waste increased. Lake

Michigan, the Chicago River, Lake Calumet, and other waterways were used as dumping grounds for the waste created, and dumping into these Chicago waterways stretched well into the 20th century. Waste dredged from the Calumet and Chicago Rivers was also dumped into Lake Michigan until these actions were banned by the federal government in 1967 (Colten 1985). In fact, the river flows were reversed to limit the inflows of pollution into the lake.

The construction of the first railroads during the late 1800s provided another mode of transportation and opened up many more opportunities for the expansion of industry further into the state and away from waterways. As Cronon (1991: 74) states, the railroad "would rapidly emerge as the chief link connecting Chicago with the towns and rural lands around it, so the city came finally to seem like an artificial spider suspended at the center of a great steel web." After World War II, it was the advent of the highway system that further changed the methods used in siting industrial and commercial businesses and that introduced commercial and industrial decentralization into the suburbs surrounding the city. As the population living in the city increased, so did the amount of household waste. In the late 1940s, residents of the city began utilizing city dumps, or city-owned sanitary landfills, for the majority of their waste although private lots and dumps continued receiving refuse after this time. Following the Solid Waste Disposal Act of 1965, open dumping and burning was prohibited by city officials (Colten 1985).

Race has also played an integral role in shaping the history of Chicago and the Cook County area. Historically, Hispanics and African Americans have been the two most significant ethnic groups in Chicago. The African American population was typically concentrated in urban ghettoes. The practice of "redlining", which began with the National Housing Act of 1934, prohibited many minority neighborhoods from receiving housing loans. The subsidization of suburbanization during the New Deal era further diverted attention from minority neighborhoods. The Urban Renewal era (1950–1970) produced high-rise public housing buildings within urban ghettoes that further isolated low income, minority residents from surrounding areas. Hispanic residents of Chicago have also faced isolation, although not as much as African Americans. Most residents who identify themselves as Hispanic are first, second, or third generation immigrants from Mexico or Puerto Rico. Mexican migrants began settling in Chicago in 1910, with a significant increase between 1960 and 1980 (Baden and Coursey 2002). Puerto Ricans entered the city after World War II, and their numbers increased from 32,371 in 1960 to 112,074 in 1980 (Black et al. 1983). Both ethnic groups migrated to Chicago in search of work in the unskilled labor sector, and have settled in a few highly concentrated areas such as Humboldt Park, West Town, and Logan Square.

To summarize this section, the environmental justice movement grew out of a joint effort by different parties. Their goal was the same, however, to educate the public about environmental inequality issues and thus begin bringing about change. Many studies, including Baden and Coursey's (2002) on the City of Chicago, generated evidence that minorities and the poor are disproportionately exposed to waste facilities. A common dilemma is determining whether residents or waste facilities occupied an area first. Several theories propose reasons for the cause of such

environmental inequity including a lack of public participation, lack of information, language barriers, zoning laws, and the powerlessness of disadvantaged groups. Cook County has been shaped mostly by its location on the banks of Lake Michigan where the Chicago and Calumet Rivers once flowed. This location provided many with access to the interior of the country as well as with a location for depositing refuse. Railroad construction improved communications and increased the area allotted for industry and commerce. And, as in many US cities, Hispanics and African Americans have historically been segregated and isolated in Chicago, a circumstance that spurs concern whether environmental inequality is disproportionately present in the areas in which they reside.

8.3 Data Sources

Toxic Release Inventory (TRI) data are extracted from the *TRI Explorer*, a database provided by EPA (EPA 2008c). This data became available under the Emergency Planning and Community Right-to-Know Act of 1986 and was later expanded under the Pollution Prevention Act of 1990. Information listed in the TRI database is publicly available and contains data on toxic chemical releases and other waste management activities reported annually by certain covered industry groups as well as federal facilities. Covered industry groups are those facilities with ten or more full-time employees that process 25,000 pounds or more or use 10,000 pounds or more of any one specific TRI chemical (Dolinoy and Miranda 2004). The TRI facility data used in this study were for the year 2004, the most current TRI information available at the time this research began.

The TRI facilities analyzed in this study include all listed TRI facilities for Cook County for the year 2004, and we encountered several issues when using these data. First, the data are self-reported emissions estimates, not actual measures of release (Pastor et al. 2004). Second, some of the geographic coordinates provided by the TRI database were incorrect or missing – we found 122 facilities with missing coordinates. Consequently, verification of coordinate locations is necessary when working with EPA databases, as the data are self-reported to state agencies by the facilities and later passed on to the EPA (Scott et al. 1997). The problem was resolved by cross-referencing the TRI data with the EPA's Resource Conservation and Recovery Act list and correcting any coordinate discrepancies. Based on the addresses provided by the EPA, we used a web-based service provided by Steve Morse (stevemorse.org/jcal/latlon.php) to manually geocode the facilities one by one. Third, the TRI data do not include releases from mobile sources and smaller emissions facilities, both of which are known to contribute to pollution levels and health risks (Pastor et al. 2004). Ultimately, a total of 428 TRI facilities were accessible for use in this study.

In an effort to address the *modifiable areal unit problem* (MAUP; Fotheringham and Wong 1991; Anderton et al. 1994; Bolin et al. 2000; Mennis 2002), this study performs analysis at the census tract and block group levels to determine whether the results are consistent across differently sized units of analysis. Block groups are

the smallest unit for which the Census Bureau ordinarily reports economic information pertinent for the study (Harner et al. 2002). Census tract and block group level data were retrieved from the US Census Bureau website for the year 2000 (US Census Bureau 2008b). The following variables summarize the racial and ethnic composition of the geographic areas involved in this study: White, African American, Hispanic, Native American, Asian, Hawaiian/Pacific Islander, and Other. Additional variables include total population and median income.

It is important to note that these categories of race and ethnicity underwent a revision since the previous census. In 1977, the Office of Management and Budget (OMB) issued Statistical Policy Directive Number 15, "Race and Ethnic Standards for Federal Statistics and Administrative Reporting" (US Census Bureau 2008a). This directive established four main racial categories: American Indian or Alaskan Native, Asian or Pacific Islander, African American, and White. It also established two ethnic categories: Hispanic and Non-Hispanic. Due to the changing racial and ethnic structure of the country since 1977, the Census Bureau determined that these classifications were no longer accurate. Therefore, in 1997, the OMB revealed its new racial and ethnic categories, which include: American Indian or Alaska Native, Asian, African American, Native Hawaiian or Other Pacific Islander, and White. It also includes the category Some Other Race, which is intended to capture ethnicities such as Mulatto, Mestizo, and Creole.

Figure 8.1 illustrates the locations of the 428 facilities throughout Cook County with census tracts as the background. The majority of the facilities are located in the central portion of the county, with many other facilities spreading out towards the northwestern and southern suburbs. The spread may be a result of the post-war decentralization of commerce and industry.

8.3.1 Analysis Methods

The purpose of this study is to determine whether there is evidence of environmental inequity for different racial/ethnic and income groups in Cook County. Environmental inequity will be measured based on whether there is a disproportionate distribution of TRI facilities in areas inhabited by minority groups or residents with low median incomes throughout the county. Mapping the distribution of TRI sites against demographic and socioeconomic backgrounds gives us a visual representation of the relationship. However, statistical analysis is needed to rigorously test the hypothesis.

8.3.1.1 Data Preparation and Mapping

Two aggregation levels of data were used in this study, census tracts, and block groups. Table 8.1 presents the basic statistics for various racial/ethnic group ratios in Cook County at both levels. This study considers four minority groups – African American, Hispanic, Asian and Other – comprising an average of more than four percent of population across census tracts or block groups in the study area.

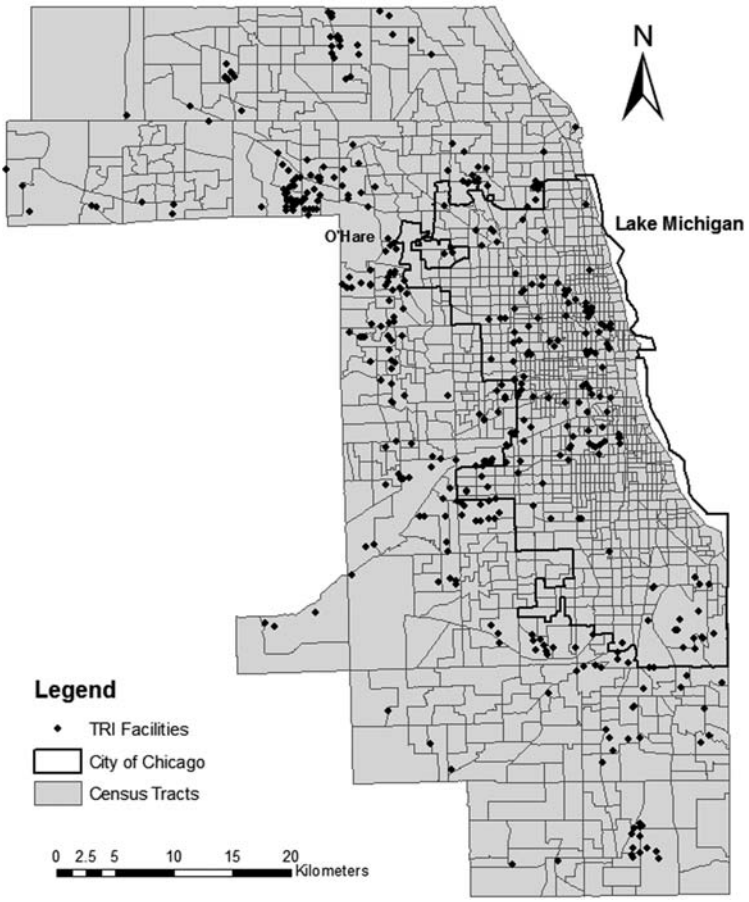

Fig. 8.1 Toxic release inventory (TRI) sites in cook county, 2004

American Indians/Eskimo and Hawaiian/Pacific Islanders are not included because their percentages are considered too low to be significant for this study.

Three distances – 500, 1000 and 1500 m – were used to define proximity to the TRI facilities. Glickman (2004) points out that in urban areas, neighborhoods (and any hazards present within them) typically do not extend further than a mile. If the centroid of a tract or block group falls within one of the aforementioned distances from any TRI facility, it is grouped as "within the proximity," otherwise it is grouped as "outside". A binary variable is created to flag whether a tract or block group is within (=1) or outside (=0) proximity to a TRI site in each of the three distance scenarios. A tract (block group) may be partially within and partially outside the distance described. One may use a spatial interpolation method to allocate population between the split portions. However, by assuming a uniform distribution of attributes within an areal unit, it would create two samples with identical attributes

Table 8.1 Basic statistics for proportions of racial/ethnic groups in cook county 2000

	Census tracts (n = 1337)			Census block groups (n = 4219)		
Variable	Mean	Std dev	Max*	Mean	Std dev	Max*
African Am.	0.33	0.40	1	0.31	0.40	1
Hispanic	0.19	0.25	0.97	0.18	0.25	1
White	0.51	0.35	1	0.54	0.36	1
Am. Indian/Esk.	0.003	0.004	0.05	0.002	0.01	0.57
Asian	0.04	0.08	0.86	0.04	0.08	0.90
Hawaiian/P.I.	0.0005	0.001	0.01	0	0.001	0.05
Other	0.09	0.15	0.68	0.09	0.14	0.74

Note: * Minimum value in all cases is 0.

(i.e., ethnic group ratios or income): one inside and another outside of the range. This does not contribute to the statistical test power. Some population assignment methods using additional information (e.g., Wu 2006) may be also used. Given time constraints and data availability, such approaches were not feasible for this study.

A series of maps were created to examine the relationship between TRI sites and demographic (income) distributions, three of which are included, here. Figures 8.2 and 8.3 illustrate the distribution of African American and Hispanic populations respectively. In Fig. 8.2, African Americans were mainly concentrated in the south of Cook County (where some TRI sites can be found), in another area at the southwest corner, and in the middle of the county, but very few in the area near downtown Chicago. In Fig. 8.3, one cluster of Hispanic population was on the north side by the lake, one was to the southwest of the downtown area, and another band around O'Hare International Airport. All three areas indicate the presence of TRI sites.

Figure 8.4 illustrates the geographic pattern of median income in the study area. The greatest concentration of the highest median income bracket is seen in the northwestern and southwestern suburbs of the county. There are also areas of high median income located within the Loop area of Chicago extending north along the coast of Lake Michigan. One can also see a general absence/lack of TRI facilities in these high income areas, with the exception of a few located near the north and southwestern suburbs.

8.3.1.2 Pooled *t*-Test

Evidence of disproportionate exposure throughout minority areas is supported when the values of the ethnicity ratio of the tracts within the specified distance are larger than the values of the tracts found outside the distance. Given the nature of aggregated data from the census, our hypothesis for testing environmental justice with regard to racial/ethnic groups is structured as:

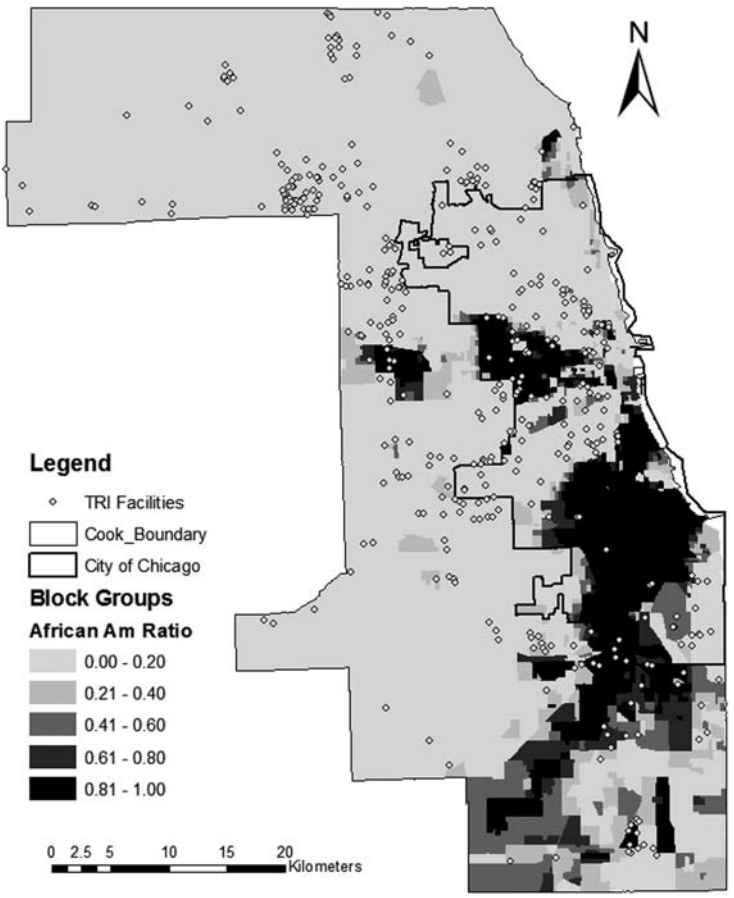

Fig. 8.2 African American population ratios across block groups in cook county, 2000

H_0 (null hypothesis): the ratios of a minority in areas within the proximity of TRI facilities are not different from those outside.

Evidence of disproportionate exposure determined by median income is supported when the values of the median income of the tracts within the specified distance are less than that of the tracts found outside of the distance. Our hypothesis for testing environmental justice with regard to income distribution is:

H_0 (null hypothesis): median incomes in areas within proximity of TRI facilities are not different from those outside.

A pooled *t*-test was used to compare the sample mean of those tracts (block groups) within a specified distance from a TRI facility and the sample mean of those located outside the distance. In this study, Statistical Analysis Software (SAS®; specifically, the "TTEST" procedure) was used to implement the *t*-test.

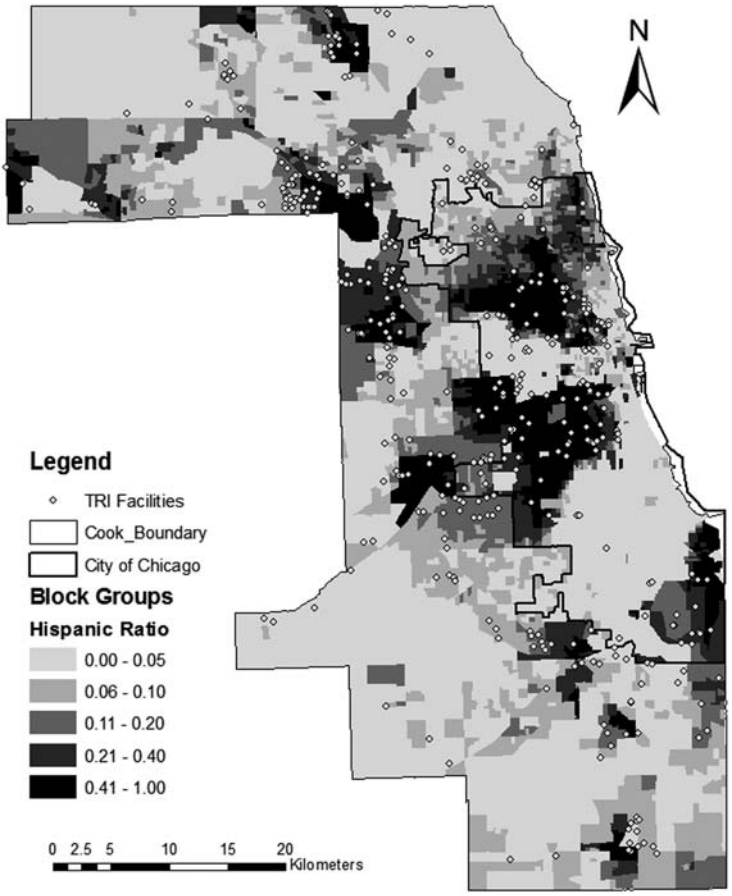

Fig. 8.3 Hispanic population ratios across block groups in cook county, 2000

Table 8.2 presents the results of the *t*-test on Hispanic ratios at the census tract level in Cook County. The sample mean of Hispanic ratios in 979 tracts within 1500 m was 0.2349, and the sample mean of the Hispanic ratios in 358 tracts outside 1500 m was 0.0647. On average, Hispanic ratios within the proximity of TRI sites were 0.1702 higher than outside of the range. Given the sample sizes, means and standard deviations, the t-statistic was calculated to be 11.42, much larger than the critical value of 3.29 at the 0.001 (two-tailed test) level. The hypothesis of no difference in Hispanic ratios between tracts within and outside the proximity of TRI sites is rejected. Similar conclusions can be drawn from Table 8.2 based on the distance ranges of 1000 and 500 m.

Regression with a binary independent variable The pooled *t*-test can be also implemented in a commonly-used regression model. From the above example, the regression model is constructed as

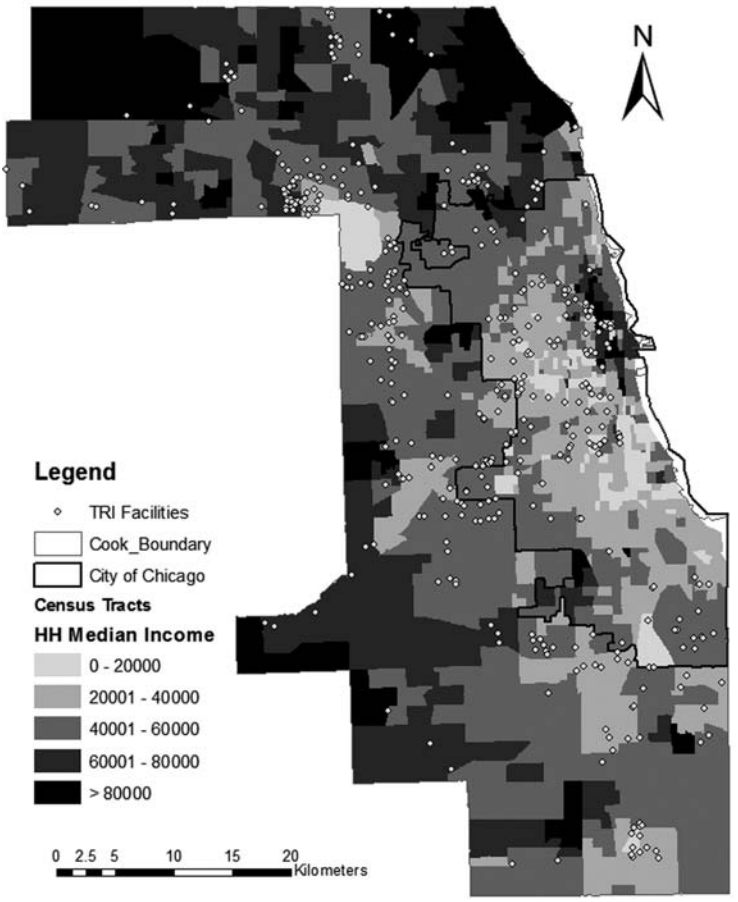

Fig. 8.4 Household median income across census tracts in cook county, 2000

$$Y = a + b * Flag \tag{8.1}$$

where the dependent variable Y is Hispanic ratios in various census tracts, the independent variable *Flag* is a binary dummy variable coded to identify whether a tract was within the proximity of any TRI facilities (=0) or outside (=1), and a and b are parameters to be estimated.

For instance, using 1500 m as the distance range at the census tract level, the regression result for Hispanics (see Table 8.3) is

$$Y = 0.2349 - 0.1702\, Flag$$
$$(30.47)\ (-11.42)$$

Table 8.2 Pooled *t*-Test for Hispanics in census tracts in cook county

	n	Mean	Standard deviation	t-value
All	1337	0.1893	0.2527	
Within 1500 m	979	0.2349	0.2744	11.42
Outside of 1500 m	358	0.0647	0.1065	
Within 1000 m	793	0.2600	0.2877	13.11
Outside of 1000 m	544	0.0864	0.1356	
Within 500 m	552	0.2835	0.2966	12.03
Outside of 500 m	785	0.1231	0.1906	

Table 8.3 Regression results on ethnicity ratios across cook county census tracts (n = 1337)

Minority group	Distance	Variable	Parameter	Std. error	*t* value
Afr. American	1500 m	*a*	0.2836	0.0127	22.42
		b	0.1743	0.0244	7.13
	1000 m	*a*	0.2611	0.0140	18.64
		b	0.1700	0.0220	7.74
	500 m	*a*	0.2323	0.0168	13.83
		b	0.1668	0.0219	7.61
Hispanic	1500 m	*a*	0.2349	0.0077	30.47
		b	−0.1702	0.0149	−11.42
	1000 m	*a*	0.2600	0.0085	30.77
		b	−0.1736	0.0132	−13.11
	500 m	*a*	0.2835	0.0102	27.75
		b	−0.1604	0.0133	−12.03
Asian	1500 m	*a*	0.0445	0.0026	17.45
		b	−0.0054	0.0049	−1.10
	1000 m	*a*	0.0438	0.0028	15.47
		b	−0.0019	0.0044	−0.43
	500 m	*a*	0.0430	0.0034	12.66
		b	0.0001	0.0044	0.02
Other	1500 m	*a*	0.1192	0.0045	26.46
		b	−0.0922	0.0087	−10.58
	1000 m	*a*	0.1333	0.0049	26.98
		b	−0.0952	0.0077	−12.30
	500 m	*a*	0.1462	0.0060	24.49
		b	−0.0879	0.0078	−11.29

The corresponding t values for the intercept a and slope b are in parentheses underneath the equation. Based on the regression result, if $Flag = 0$, then $Y = 0.2349$, which is the intercept, i.e., the sample mean of Hispanic ratios for tracts *within* the distance range (1500 m) from the TRI sites. If $Flag = 1$, then $Y = 0.2349 - 0.1702 = 0.0647$, which is the sample mean of Hispanic ratios for tracts *outside* the distance range. The slope $b = -0.1702$ indicating the difference between

the two sample means, and its corresponding t value (-11.42) is the same as the t value in the pooled-t test (the negative sign indicating a lower sample mean for tracts identified by $Flag = 1$).

In summary, the regression is completely equivalent to the pooled-t test. In the next section, only the regression results are presented. Our primary interest from the regression is on the t value for the slope b, indicating whether and how statistically significant the difference is between the two samples. Since the model is not designed to explain the variation of Y by explanatory variables, the R^2 value, which can be derived from the t value in any bivariate regression (as is the case here), is redundant and thus not presented.

8.4 Results and Discussion

8.4.1 Analyzing Race and Ethnicity

Table 8.3 presents regression results for four racial/ethnic minority groups in Cook County at the census tract level. Table 8.4 shows the results at the block group level. In the tables, the intercept a represents the average ratio of a minority group in tracts within the given distance, and the slope b is the difference of the ratios between those tracts within and outside the distance. A *positive b* indicates a higher average minority ratio *outside than inside* the distance range from TRI sites; and a negative b indicates otherwise. Whether the difference is statistically significant is reflected by the corresponding t value (as well as by the significance level Pr>| t |).

The regression results in Tables 8.3 and 8.4 suggest evidence of environmental inequity for the Hispanic population and those classified as "Other" at each of the three distances (500, 1000, and 1500 m). For Hispanics, as illustrated in the previous section, the average percentage across census tracts inside the given distances from the TRI sites was 23−28% in contrast to 6−12% outside the distance ranges. For "Other", the difference in percentages was about 9%. All are highly significant statistically. However, the results also show that the percentage of African American population living within proximity to TRI facilities was *lower* than those outside, and the difference was statistically significant. This result is surprising because it was expected that the African American population would exhibit some sign of being disproportionately exposed to these facilities. At the census tract level, the percentage of African Americans outside the distance ranges was about 17% higher than the percentage inside the ranges; and at the block group level, the difference was also above 10%. The difference for Asian Americans was not statistically significant.

For comparison, we also tested the model on the white population at both geographic levels and found no evidence of environmental inequity with respect to proximity to TRI facilities. Although there is no evidence of disproportionate exposure with respect to the White population, it must be noted that income plays a role in environmental justice discourse. Because the White population is not devoid of

Table 8.4 Regression results on ethnicity ratios across cook county block groups (n = 4219)

Minority Group	Distance	Variable	Parameter	Std. error	*t* value
Afr. American	1500 m	*a*	0.2666	0.0076	34.88
		b	0.1143	0.0128	8.92
	1000 m	*a*	0.2544	0.0088	28.70
		b	0.1016	0.0123	8.27
	500 m	*a*	0.229	0.0118	19.42
		b	0.1074	0.0138	7.77
Hispanic	1500 m	*a*	0.2383	0.0045	52.93
		b	−0.1617	0.0075	−21.42
	1000 m	*a*	0.2626	0.0052	50.43
		b	−0.1573	0.0072	−21.79
	500 m	*a*	0.2836	0.0070	40.17
		b	−0.1412	0.0082	−17.07
Asian	1500 m	*a*	0.0428	0.0014	28.94
		b	−0.0035	0.0024	−1.41
	1000 m	*a*	0.0426	0.0017	24.89
		b	−0.0020	0.0023	−0.88
	500 m	*a*	0.0419	0.0022	18.42
		b	−0.0005	0.0026	−0.21
Other	1500 m	*a*	0.1199	0.0026	45.78
		b	−0.0873	0.0043	−19.90
	1000 m	*a*	0.1338	0.0030	44.27
		b	−0.0866	0.0041	−20.66
	500 m	*a*	0.1439	0.0041	35.10
		b	−0.0756	0.0048	−15.75

low-income residents, those in the white population that do not have high median incomes may also be affected by disproportionate exposure to TRI facilities and other environmental hazards. This issue will be analyzed in the next subsection.

A census tract covers a larger area, and is made up of a number of block groups, and therefore contains generalized information that may not clearly capture the differences in its resident population. Therefore, block groups are more likely to exhibit variations in data across the study area. The statistics displayed in Tables 8.3 and 8.4 are highly consistent, indicating the robustness of the results and therefore providing little evidence of the Modifiable Area Unit Problem (MAUP).

8.4.2 Analyzing Income Distribution

Median income was only available at the census tract level, therefore the analysis is limited to that level. As described earlier, the regression model in Equation (8.1) is used, with Y as income, to examine the difference in median income between the census tracts inside and outside the distance ranges. Table 8.5 presents the regression results. In the tracts inside 1500 m from the TRI facilities, the average median

income was $44,135. In tracts outside the range, the average median income was $3298 higher. The difference was statistically significant at the 0.05 level. When the distance range is defined as 1000 m, the result is similar with a higher statistical significance (i.e., at the 0.01 level). The difference is no longer significant when using the 500 m distance range. In other words, there is evidence that residents closer to the TRI sites had lower median income than those farther away. The only exception is when using a short distance such as 500 m to define proximity. Note that census tracts are much larger than block groups. By representing an area by its centroid, the result from census tracts is not as reliable as that from block groups; therefore the results obtained at a shorter distance are less reliable than a longer distance.

Table 8.5 Regression results on median income across cook county census tracts (n = 1337)

Distance	Variable	Parameter	Std. error	*t* value
1500 m	*a*	44,135.00	733.85	60.14
	b	3298.24	1419.90	2.32
1000 m	*a*	43,378.00	813.41	53.33
	b	4040.03	1277.35	3.16
500 m	*a*	43,895.00	978.79	44.85
	b	1910.36	1277.47	1.50

8.5 Concluding Comments

The purpose of this study is to determine if there is disproportionate exposure to environmental hazards in areas occupied predominantly by minority groups or those of low median incomes. Three characteristics differentiate this study from previous work on environmental justice research, particularly the one by Baden and Coursey (2002) that is closely related to ours. First, GIS techniques are used in this study in order to determine the proximity of the nearest TRI facility to a census tract or block group more accurately. Second, geocoding the TRI data set with a combination of automatic and manual procedures ensures a maximum matching ratio. Therefore, nearly all the TRI sites are included in the study. Third, data analysis at different aggregation levels helps determine the effects of the Modifiable Area Unit Problem in the study. Consistent results across different areal units demonstrate the robustness of the conclusions drawn from the analysis.

Environmental inequity is a complicated situation that has affected many minority and low-income residents throughout the United States. Cook County, which contains the City of Chicago, has long been highly industrialized and those industrial activities play an integral role in determining who has been exposed to industrial waste products. Some studies find that race is often a better predictor of exposure to environmental hazards than income (e.g., Cole and Foster 2001). The results of the study suggest that both race and income seem to be relevant to

the environmental inequity issue. Evidence of environmental inequity was found for the Hispanic population and those classified as "Other", but not for Asian Americans. As discussed earlier, this finding does not necessarily suggest that TRI facilities were purposely sited where there were higher concentrations of Hispanics or other minorities. Because the Hispanic population developed relatively recently, it is likely that they moved close to industrial areas where many could find jobs and where housing was relatively inexpensive. The surprising result is that the percentage of the African American population living within proximity to TRI facilities was *lower* than those outside, and that the difference was statistically significant. Finally, there is evidence that residents closer to TRI sites have lower median income than those farther away.

Several limitations of the data used in this study need to be pointed out. The data set only contains those facilities listed on the EPA's Toxic Release Inventory Site and does not include those that may not meet the requirements for federally mandated reporting of the facility. The data also exclude noxious facilities such as landfills, underground storage tanks, brownfield areas, or other areas that pose environmental risks and hazards for those living in their proximity. Another aspect of these hazardous sites that was not examined in this study is the type of toxins released, their mode of release (i.e., air, ground, water), and the amounts released. These three characteristics also play a role in determining the level of risk and method of transmission to those residing near release sites. Toxins released by air may travel further and at a different rate than those that are waterborne. Once released from confinement, their chemical structure may be altered when combined with the chemical structure of molecules found in the air, land, and water. All are important issues that may be addressed in future research when better data become available. In terms of methodology, two directions may be pursued to expand or improve the study. This study considers race and income separately. However, the two factors can be correlated with each other as well as other socioeconomic variables, such as poverty levels, ownership status of the residence, and owner and rental cost characteristics. Future work may consolidate these variables into a compound factor (for instance, labeled as "concentrated disadvantages") using factor analysis. Another minor issue is the so-called "edge effect". Residents near the border of the county may be also exposed to TRI facilities of adjacent counties. Inclusion of those TRI facilities within a buffer distance from the county boundary will enhance the value of the work. Finally, this study uses aggregated demographic data at the block group and census tract levels from the census. The analysis is generally adequate for public policy purposes within regulatory agencies, but is not appropriate for environmental epidemiology studies.

References

Anderton, D.L., Anderson, A.B., Oakes, J.M., and Fraser, M.R. (1994). Environmental equity: The demographics of dumping. *Demography 31*: 229–248.

Arora, S. and Cason, N. (1999). Do community characteristics influence environmental outcomes? Evidence from the toxics release inventory. *Southern Economic Journal 65*: 691–716.

Baden, B.M., and Coursey, D.L. (2002). The locality of waste sites within the City of Chicago: A demographic, social, and economic analysis. *Resource and Energy Economics 24*: 53–93.

Black, S.A., Eichenthal, D.R., Espinosa, R., Heidinger, T.E., Hogan III, W.C., Levin, M.R., Maude, J.L., Niemi, P., O'Donnell, M., and Wolfberg, M.L. (1983). *Latinos in Metropolitan Chicago: A Study of Housing and Employment*. Chicago: Latino Institute.

Bolin, B, Matranga, E., Hackett, E.J. Sadalla, E.K., Pijawka, K.D., Brewer, D., and Sicotte, D. (2000). Environmental equity in a sunbelt city: The spatial distribution of toxic hazards in Phoenix, Arizona. *Environmental Hazards 2*: 11–24.

Boone, C.G. and Modarres, A. (1999). Creating a toxic neighborhood in Los Angeles county: A historical examination of environmental inequity. *Urban Affairs Review 35*: 163–187.

Bowen, W.A., Salling, M.J., Haynes, K.E. and Cyran, EJ. (1995). Toward environmental justice: Spatial equity in Ohio and Cleveland. *Annals of the Association of American Geographers 85*: 641–663.

Bowen, W.M. and Wells, M.V. (2002). The politics and reality of environmental justice: A history and considerations for public administrators and policy makers. *Public Administration Review*: *62*: 688–698.

Bullard, R.D. (1990). *Dumping in Dixie: Race, Class, and Environmental Quality.* Boulder, Co: Westview Press.

Bullard, R.D. and Johnson, G.S. (2000). Environmental justice: Grassroots activism and its impact on public policy decision making. *Journal of Social Issues*, *56*: 555–578.

Cole, L.W. and Foster, S.R. (2001). *From the Ground Up: Environmental Racism and the Rise of the Environmental Justice Movement.* New York: New York University Press.

Colten, C.E. (1985). *Industrial wastes in the Calumet area, 1869 – 1970: An historical geography*. Champaign, IL: Hazardous Waste Research and Information Center.

Committee on Environmental Justice, Institute of Medicine (CEJ). (1999). *Toward Environmental Justice: Research, Education, and Health Policy Needs*. Washington, DC: National Academy Press.

Cronon, W. (1991). *Nature's metropolis: Chicago and the Great West*. New York: W.W. Norton and Company.

Dolinoy, D.C. and Miranda, M.L. (2004). GIS modeling of air toxics releases from TRI reporting and non-TRI-reporting facilities: Impacts for environmental justice. *Environmental Health Perspectives 112*: 1717–1724.

Environmental Protection Agency (EPA) 2008a. "What is the Origin of Environmental Justice at EPA?" Environmental Justice: Frequently Asked Questions, http://www.epa.gov/compliance/resources/faqs/ej/index.html, last updated February 5. Accessed September 6, 2008.

Environmental Protection Agency (EPA) 2008b. "How Does EPA Define Environmental Justice?" Environmental Justice: Frequently Asked Questions, http://www.epa.gov/compliance/resources/faqs/ej/index.html, last updated February 5. Accessed September 6, 2008.

Environmental Protection Agency (EPA) 2008c. TRI Explorer. Chemical Report. http://www.epa.gov/triexplorer/, last updated July 23. Accessed September 6, 2008.

Faber, D. and McCarthy, D. (2001). The evolving structure of the environmental justice movement in the United States: New models for democratic decision-making. *Social Justice Research 14*: 405–421.

Fotheringham, A.S. and Wong, D.W.S. (1991). The modifiable areal unit problem in multivariate statistical analysis. *Environment and Planning A 23*: 1025–1044.

Fricker, Jr., R.D. and Hengartner, N.W. (2001). Environmental equity and the distribution of toxic release inventory and other environmentally undesirable sites in metropolitan New York City. *Environmental and Ecological Statistics 8*: 33–52.

Glasmeier, A.K. and Farrigan, T.L. (November 2003). Poverty, sustainability, and the culture of despair: Can sustainable development strategies support poverty alleviation in America's most environmentally challenged communities? *The Annals of the American Academy of Political and Social Science 590*: 131–149.

Glickman, T.S. (2004). *Evaluating equity in Alleghany County*. New York: Program for the Human Environment, Rockefeller University. Available at http://phe.rockefeller.edu/comm_risk/commrsk3.html [accessed May 2, 2007]

Harner, J., Warner, K., Pierce, J., and Huber, T. (2002). Urban environmental justice indices. *The Professional Geographer 54*: 318–331.

Hite, D. (2000). A random utility model of environmental equity. *Growth and Change 31*: 40–58.

Hoyt, H. (1933). *One Hundred Years of Land Values in Chicago*. Chicago: University of Chicago Press.

Hunter, L.M. (2000). The spatial association between US immigrant residential concentration and environmental hazards. *International Migration Review 34*: 460–488.

Kellogg, W.A. and Mathur, A. (2003). Environmental justice and information technologies: Overcoming the information-access paradox in urban communities. *Public Administration Review 63*: 573–585.

Lavelle, M. and Coyle, M. (1992). Unequal protection: The racial divide in environmental law. *National Law Journal 15*: S1–S12.

Laurian, L. (2003). A prerequisite for participation: Environmental knowledge and what residents know about local toxic sites. *Journal of Planning Education and Research 22*: 257–269.

Mennis, J. (2002). Using geographic information systems to create and analyze statistical surfaces of population and risk for environmental justice analysis. *Social Science Quarterly 83*: 281–297.

Pastor, Jr., M., Sadd, J., and Hipp, J. (2001). Which came first? Toxic facilities, minority move-in, and environmental justice. *Journal of Urban Affairs 23*: 1–21.

Pastor, Jr., M., Sadd, J.L., and Morello-Frosch, R. (2004). Waiting to exhale: The demographics of toxic air release facilities in 21st century California. *Social Science Quarterly 85*: 420–440.

Pellow, D.N. (2004). The politics of illegal dumping: An environmental justice framework. *Qualitative Sociology 27*: 511–525.

Pellow, D.N., Weinberg, A., and Schnaiberg, A. (2001). The environmental justice movement: Equitable allocation of the costs and benefits of environmental management outcomes. *Social Justice Research 14*: 423–439.

Pinderhughes, R. (1996). The Impact of Race on Environmental Quality: An Empirical and Theoretical Discussion. *Sociological Perspectives 39*: 231–248.

Rast, J. (2006). Environmental justice and the new regionalism. *Journal of Planning Education and Research 25*: 249–263.

Ross, C.L. and Leigh, N.G. (2000). Planning, urban revitalization, and the inner city: An exploration of structural racism. *Journal of Planning Literature 14*: 367–380.

Scott, M., Cutter, S.L., Menzel, C., and Ji, M. (1997). Spatial accuracy of the EPA's environmental hazards databases and their use in environmental equity analysis. *Applied Geographic Studies 1*: 45–61.

Talih, M. and Fricker, Jr., R.D. (2002). Effects of neighborhood demographic shifts on findings of environmental injustice: A New York City case study. *Journal of the Royal Statistical Society: Series A (Statistics in Society) 165*: 375–397.

Towers, G. (2000). Applying the political geography of scale: Grassroots strategies and environmental justice. *Professional Geographer 52*: 23–36.

United Church of Christ Commission for Racial Justice (UCCCRJ). (1987). *Toxic Wastes and Race in the United States: A National Report on the Racial and Socio-Economic Characteristics of Communities with Hazardous Waste Sites.* New York: United Church of Christ.

US Census Bureau (2008a). Race Data. *Recommendations from the Interagency Committee for the Review of the Racial and Ethnic Standards to the Office of Management and Budget Concerning Changes to the Standards for the Classification of Federal Data on Race and Ethnicity*. http://www.census.gov/population/www/socdemo/race/Directive_15.html last updated April 10. Accessed March 24, 2008.

US Census Bureau (2008b). United States Census 2000. *Your Gateway to Census 2000*. http://www.census.gov/main/www/cen2000.html, last updated April 24. Accessed September 6, 2008.

US General Accounting Office (USGAO). (1983). *Siting of Hazardous Waste Landfills and Their Correlation with Racial and Economic Status of Surrounding Communities*. Washington, DC: GAO/RCED.

Wu, S-S. 2006. *Incorporating GIS and Remote Sensing for Census Population Disaggregation*. ETD Collection for Texas State University. Paper AAI3221522. http://ecommons.txstate.edu/dissertations/AAI3221522

Chapter 9
Risk and Exposure to Extreme Heat in Microclimates of Phoenix, AZ

Darren M. Ruddell, Sharon L. Harlan, Susanne Grossman-Clarke, and Alexander Buyantuyev

Abstract As rapid urban development continues, the impacts of temperature extremes on human health and comfort are expected to increase as threshold temperatures of human tolerance are crossed more frequently and for longer periods of time. This study examined extreme heat as an urban hazard throughout the Phoenix (Arizona, USA) metropolitan area during a four-day 2005 summer heat wave. Utilizing the Weather Research and Forecasting (WRF) model to simulate 2 m air temperature variability throughout the region, the distribution of threshold temperatures and heat exposure was examined in 40 diverse neighborhoods. Neighborhood residents also responded to a social survey about perceived temperatures and heat-related health problems during the summer of 2005.

Results indicated that extreme heat was variably distributed throughout the neighborhoods; residents' perceptions of temperature and self-reported experiences with heat-related illnesses were related to environmental conditions; the highest risk of exposure to extreme heat was among elderly, minority, and low-income residents; and land use/cover characteristics exhibited strong relationships with local threshold temperatures. Research contributions include the development of a geotechnical analysis method that could help cities to prepare for and respond to the most vulnerable residents during periods of extreme heat as well as the interrelation of regional atmospheric model results with socio-economic data.

Keywords Climate · Hazard · GIS · Environmental justice · Urban heat island · Weather-forecasting

9.1 Introduction

Cities in most types of climate regimes are becoming warmer over time and, consequently, urban populations are increasingly vulnerable to the hazards of summertime heat. In cities, the effect of rising global temperatures is compounded by regional

D.M. Ruddell (✉)
School of Geographical Sciences, Arizona State University, Tempe, AZ 85287-0104, USA
e-mail: darren.ruddell@asu.edu

P.S. Showalter, Y. Lu (eds.), *Geospatial Techniques in Urban Hazard and Disaster Analysis*, Geotechnologies and the Environment 2, DOI 10.1007/978-90-481-2238-7_9,

climate change caused by large-scale, rapid urbanization. The global average temperature has risen 0.5°C since the 1970s (McMichael et al. 2006) but in roughly the same period, differences between temperatures in the city compared to surrounding rural areas have been measured ranging from 1 to 12°C (Aniello et al. 1995; Brazel et al. 2000; Voogt 2002). One study found that US cities, on average, experience 10 more hot summer nights than they did 40 years ago (DeGaetano and Allen 2002).

Urbanization affects physical processes that alter the surface energy balance, and therefore, near-surface air temperatures (Arnfield 2003; Oke 1982). For example, surface cooling is inhibited by reduced outgoing long-wave thermal radiation due to the vertical structure of buildings, and sources of anthropogenic heat (e.g., vehicles, air conditioners, and industry) exhaust heat into the air near the urban surface (Grossman-Clarke et al. 2005). High heat capacity and thermal conductivity of building materials lead to greater storage of heat in the city compared to the natural land covers and agricultural land uses that preceded urbanization. These changes produce what has been described as the urban heat island (UHI) effect, where cities experience higher nighttime temperatures and generally higher but more variable daytime temperatures than the surrounding less built-up areas (Lowry 1967; Oke 1997; Voogt 2002). However, data acquired through remote sensing, surface weather stations, and regional atmospheric modeling also indicate significant temperature variability within urban areas (Arnfield 2003; Voogt and Oke 2003; Grimmond 2005). It is likely that urban vegetation serves as a mitigating factor against warm temperatures for some areas of the city while exacerbating high temperatures for other areas (Stabler et al. 2005; Jenerette et al. 2007). Much of the intra-urban temperature variation is, therefore, driven by human decisions and resources that determine residential land use/land cover (LULC) within the urbanized region.

Not only are cities experiencing chronic temperature increases, but global warming and UHIs are jointly responsible for causing more extreme heat events in cities. Extreme (acute) heat events, defined as sustained high temperatures exceeding the normal range of temperature variability, occur throughout the world and are projected to become more intense, more frequent and longer lasting over the next century (IPCC 2007; Meehl and Tebaldi 2004).

There is ample evidence that prolonged exposure to excessively warm weather is a major human health hazard, especially at junctures when critical temperature thresholds in cities are abruptly crossed (Sheridan and Kalkstein 2004). Temperature-mortality relationships are evident in temperate as well as warmer climate regimes (Patz et al. 2005). More people die in the US from extreme heat than any other weather-related phenomenon (CDC 2006) and very hot weather increases mortality rates as well as hospital admissions for cardiovascular, respiratory, and other pre-existing illnesses (Semenza et al. 1999). The 1995 Chicago heat wave, for instance, claimed over 700 lives (Semenza et al. 1996). Between 22,000 and 52,000 Europeans died during the 2003 heat wave, many of them in large cities (Larson 2006). Less publicized cases of heat waves in India and other Asian cities also report high excess death rates (e.g., Choi et al. 2005). As rapid

urban development continues, the impacts of heat-related hazards on human health and comfort are also expected to increase as the threshold of human tolerance to rising temperatures are crossed more frequently and for longer periods of time (Kalkstein and Greene 1997). The Intergovernmental Panel on Climate Change (IPCC) projects with "medium confidence" a future increase in heat wave-related deaths worldwide (Confalonieri et al. 2007). The number of heat-related fatalities could double in the near future (Larson 2006 citing the World Meteorological Association).

Almost all epidemiological studies treat the city as a single entity in tallying the temperature-related mortality during and immediately after heat events (Braga et al. 2002; Curriero et al. 2002; Michelozzi et al. 2006; Smoyer et al. 2000). Recently, heat watch-warning systems have been developed to mitigate the health impacts of sudden heat events by providing advance notification of dangerously warm weather. The warning systems are sensitive to local synoptic weather variables that vary from city to city, but they rely on data from a single, centrally-located weather station in each city and the warnings are broadly applied to entire urban areas (Sheridan and Kalkstein 2004; Smoyer-Tomic and Rainham 2001). Thus, current heat watch-warning systems lack sensitivity to intra-urban microclimate variation and the precise locations where heat hazards are the greatest.

Heat-health studies often find that advanced age and some types of chronic illnesses and disabilities are associated with higher morbidity rates attributable to extremely hot weather (McGeehin and Mirabelli 2001; Kilbourne 2002). These variables are treated as individual characteristics that predispose people to physiological weaknesses which, in turn, increase their vulnerability to heat. Other high risk populations, such as racial minorities and people living in poverty, often have poorer general health and lack access to air conditioning and critical socioeconomic resources (O'Neill et al. 2003; Naughton et al. 2002). Klinenberg's (2002) study of the 1995 Chicago heat wave disaster found that deaths among the elderly were most numerous in a few neighborhoods with high concentrations of minority residents who lacked strong social networks and support systems. The associations between characteristics of urban residents and risk of heat-related health problems can also be caused by environmental conditions in the places where they live. In one study, affluent whites lived in neighborhoods that were several degrees cooler in the summer of 2003 than low-income and Latinos neighborhoods (Harlan et al. 2006, 2008; Jenerette et al. 2007). Residents in the warmest neighborhoods spent 20% of the entire summer in conditions that exceeded the "danger" threshold on a heat stress index.

9.2 The Study

One of the most effective ways to reduce the impacts of disasters that cause large scale environmental health problems is to obtain "accurate exposure assessments" (Patz 2005). Recent advances in the accuracy, resolution, and sensitivity of geospatial tools and weather simulation models have enhanced our ability to

identify the locations of the places and people that are most vulnerable to extreme heat within cities.

This study examined the spatial distribution of air temperature during an extreme heat event and the exposure of people to threshold temperatures (defined in Section 2.2.1) at a very fine spatial resolution in the Phoenix (Arizona, USA) metropolitan area. By means of combining remote sensing and GIS techniques, regional atmospheric modeling, and socioeconomic data, we developed a geospatial tool to analyze heat hazards for Phoenix. We applied the Weather Research and Forecasting (WRF) model developed by the National Center for Atmospheric Research (Shamrock et al. 2005) to simulate 2 m air temperatures in the Phoenix metropolitan area during a four-day heat event in July 2005 and subsequently to quantify the heat hazard by hours of human exposure to threshold air temperatures for 40 diverse neighborhoods throughout the urban region. The model showed marked contrasts in temperature across neighborhoods.

Social survey data on residents' perceptions of temperature and experiences with illnesses caused by heat stress were related to the results of the weather simulation model. To assess human risk, WRF model output was compared to US Census block group population characteristics, which showed how exposure to extreme temperature varied by socioeconomic status (household income), ethnicity, and age composition of the neighborhood. As far as we are aware this was the first time that socioeconomic data have been interrelated with output from a regional atmospheric model. Finally, the association of air temperature with LULC was examined to better understand the mitigating influence of landscapes on local microclimate variability.

The variable temperatures and landscapes within the Phoenix UHI create a thermal "riskscape" of heat hazards that are distributed unevenly over the city and impact people differently. During a period of elevated temperature (i.e., heat wave), the places inhabited by populations that were least likely to have key economic and natural resources were more exposed to hazardous conditions. This study provides information that may help to prevent health disasters related to extreme heat in cities by answering three important research questions: *(1) How are heat hazards distributed among places in the Phoenix metropolitan area? (2) How closely do residents' perceptions of temperature and experience with heat-related illnesses align with simulated air temperatures in their neighborhoods? (3) Within the study area, what types of residents were most at risk and can certain types of local landscape serve as mitigating influences on temperature?*

9.2.1 Research Methods

For the investigation of heat-related hazards in urban areas there is clearly a need to better understand the distribution of air temperatures in relation to residents' means to cope with extreme heat within a regional study area. Using a multi-method approach, we examine data on threshold temperatures, analyze the spatial distribution of the data, and interpret the results.

9.2.2 Study Area

Located in the Sonoran Desert of the southwestern United States, the Phoenix metropolitan area is an ideal setting for studying human vulnerability to high temperatures (Fig. 9.1). Encompassing over 1800 square miles in Central Arizona, metropolitan Phoenix is home to over 65% of the state's 6.1 million residents (Census Bureau 2006). The city has a naturally warm climate and over the past 50 years of population growth, the average daily temperature has increased by more than 3°C (Brazel et al. 2000). The 2005 summer season which began June 21st and ended September 22nd, witnessed record (16 records tied or broken) high temperatures in the day as well as the evening. The Center for Disease Control (CDC 2005) recently reported that Arizona led the nation in heat-related deaths from 1993–2002. Although Phoenix has experienced a steady rise in average daily temperature, human exposure to high temperatures varies widely throughout this region. For example, Hedquist and Brazel (2004) measured average nighttime maximum temperature variation on a rural to urban gradient equal to 7.3°C in 2001.

Within the metropolitan area, the present study concentrates on 40 diverse neighborhoods under study as part of the 2006 Phoenix Area Social Survey (PASS) project. These neighborhoods offer insight into the spatial distribution of temperature variability throughout the region during a summer heat event, in addition

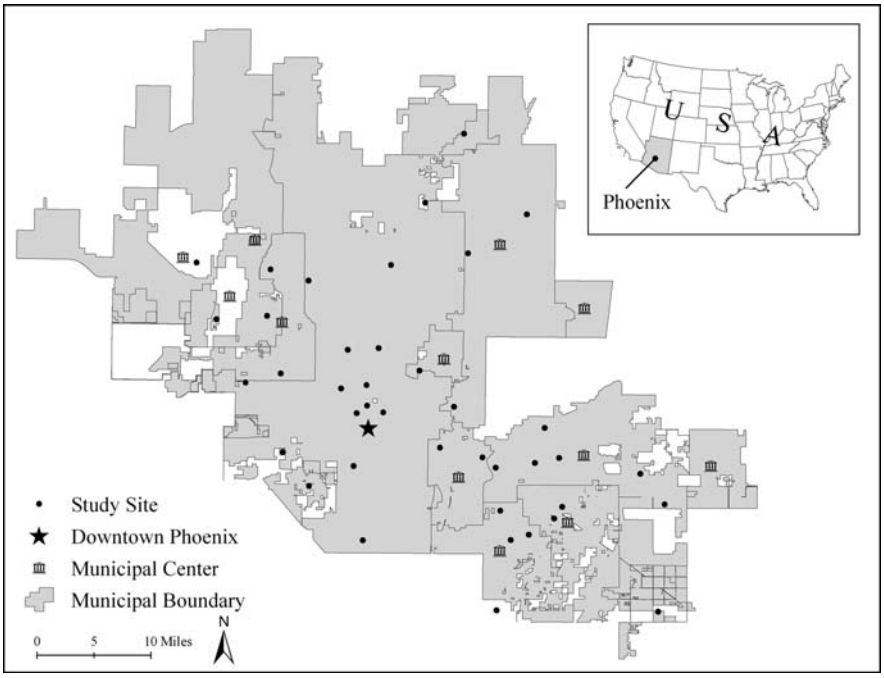

Fig. 9.1 Map of metropolitan Phoenix, Arizona

to a survey of residents' perceptions of and experiences with extreme heat. PASS employed a two-stage research design (Harlan et al. 2007). First, a systematic sample of 40 neighborhoods was selected from the 94 urban sites that are monitored by the Central Arizona-Project Long-Term Ecological Research CAP LTER project (Grimm and Redman 2004). Census data by block group were assembled for all 94 sites and classified by location (urban core, suburban, and fringe), median income, and ethnic composition. All types of neighborhoods in the Phoenix area were represented among the sample of 40. Second, a random sample of households within each neighborhood was selected to participate in a social survey, which is described in more detail below.

9.2.3 Extreme Heat Event Period

Following criteria used by Meehl and Tebaldi (2004), periods of extreme heat were identified in a three-step process. The first step was to examine National Oceanic and Atmospheric Administration (NOAA) temperature readings for Phoenix, AZ's Sky Harbor International Airport weather station, which is commonly used in climate studies (Brazel et al. 2000). This data set was used to determine normal historical (1961–1990) temperature variability in comparison to present day (2005) conditions. Second, using observed temperature readings, we calculated the distribution in percentiles for normal and present day summer temperatures. The third and final step to identify period(s) of extreme heat for the summer of 2005 was to compare the normal and present day conditions based on the three criteria of threshold temperatures (Threshold 1 [T1]: the 97.5 percentile of the observed distribution; and T2: the 81 percentile) identified by Meehl and Tebaldi (2004). Temporal periods satisfying all three of the following conditions are considered to be extreme heat events: (1) daily maximum temperature must be above T1 for at least three days; (2) average daily maximum temperature must be above T1 for the entire period; and (3) daily maximum temperature must be above T2 for the entire period.

After completing this process, the local threshold temperatures, based on normal conditions, were: T1 = 45°C (113°F); and T2 = 42°C (108°F). Comparing 2005 temperatures readings to normal conditions, there were three distinct heat events in the Phoenix metropolitan area on June 6–9; July 15–19; and August 1–3. The temporal period examined in this study is the four-day heat event from July 15–19, 2005, which represents the longest and most intense heat event during the year. The WRF model, described in the next section, was applied to simulate 2 m air temperature variability and exposure to threshold temperatures throughout the 40 neighborhoods.

9.2.4 WRF Modeling of Heat Event

An important step in the analysis of heat hazards in relation to human exposure is quantifying air temperature, usually at a height of 2 m, at appropriate spatial and

temporal scales. The spatial variability of temperatures in urban regions is more complex than a linear gradient from urban core to fringe, and an emerging theme of research on urban climate is to determine the factors that are associated with temperature variation. Current techniques to quantify air temperatures include measurements from weather stations and spatial information tools such as remote sensing or atmospheric models that simulate air temperature. Existing methods to quantify air temperature all possess various strengths and weaknesses. Surface meteorological stations, for example, offer precise information on air temperature changes over time at discrete sites in the urban area, but usually lack dense spatial coverage. Alternatively, remote sensing provides detailed spatially and temporally consistent information on surface temperature variability within urban areas, but it is limited to discrete temporal "snapshots" and surface temperatures are not necessarily an indicator of the magnitude of air temperature.

Modeling and simulation techniques continue to gain traction within the scientific community by offering new ways to study interactions of physical and social processes in urban areas where most humans live. The term model, as used in the context of meteorology and climate, refers to a complex computer code that numerically solves a set of differential equations that govern the evolution of the state of the atmosphere in space and time in terms of air temperature, pressure, specific humidity and wind speed. The evolution is determined in part through the interaction between the model variables, but also through external forcing (e.g. solar radiation) and interactions with the earth's surface through fluxes of heat, moisture and momentum. Physical properties of the earth's surface that influence the exchange with the atmosphere depend on land use/cover characteristics. The accurate characterization of LULC and corresponding physical properties therefore is an important input variable for meteorological models. The output of a global atmospheric model together with observations of the atmosphere are generally used to quantify initial and boundary conditions for the fine resolution regional model to determine atmospheric features that cannot be captured by the physical processes included in the regional model. Other methods for determining air temperature within urban areas are limited by the accuracy of regional atmospheric models that depend, among other factors, on limited knowledge of physical processes in the atmosphere and their mathematical description, as well as uncertainties in initial and boundary conditions as supplied by the global model.

Relatively recent developments in geocomputation have enabled advances in regional atmospheric models to resolve heterogeneity within urban areas, which, in turn, have inspired the development of model approaches that describe the energy exchange between the urban surface and the atmosphere by the climate community (Brown 2000; Masson 2006; Martilli 2007). The application of such schemes within atmospheric models have greatly improved the accuracy of urban air temperature simulations over the past 10 years, and today such models are widely employed to enhance scientific understanding of processes related to neighborhood scale climate and air quality (Taha 1997a, b; Civerolo et al. 2000; Seaman 2000; Lin et al. 2008).

This study combined WRF version 2 (Shamrock et al. 2005) together with the urban surface energy balance model by Kusaka and Kimura (2004) to simulate

2 m air temperatures for the period July 15–19, 2005. The model's spatial resolution of 1 km for horizontal model grid cells corresponds well with neighborhood block group data obtained from the Census. Since the average urban block group is about ¼ square mile, the model's spatial resolution of 1 km (or 0.39 square miles) roughly covers the same area. Grossman-Clarke et al. (2005, 2008) demonstrated that a well-tested mesoscale model is suited to simulate air temperature variability in the Phoenix metropolitan region.

The model run was started at 00 Coordinate Universal Time (1700 Local Standard Time, LST). Nested simulations with four domains and resolutions of 27 km (size east-west 3294 km; north-south 2700 km), 9 km (size east-west 1350 km; north-south 1080 km), 3 km (size east-west 594 km; north-south 414 km) and 1 km (size east-west 212 km; north-south 132 km), respectively and 51 vertical layers were performed with WRF. The innermost domain included the Phoenix metropolitan area, surrounding desert and agricultural land. Initial and boundary conditions were provided by the National Center for Environmental Prediction (NCEP) ETA grid 212 (40 km resolution) analysis. Every 6 hours the lateral boundary conditions were updated from the ETA analysis and NCEP/NCAR Reanalysis. Planetary boundary layer processes were included via the non-local closure Medium Range Forecast scheme (Hong and Pan 1996) in the version by Liu et al. (2006).

In order to evaluate the WRF model performance we compared National Weather Service temperature readings for 2 m air temperatures with the simulated data at Phoenix Sky Harbor Airport (Fig. 9.2). Generally the simulations are in close agreement with the measurements, although the simulated temperatures over-predict the peak measured observations for each day of the heat event by about 2°C. A complete agreement between observed and simulated air temperatures cannot be expected because of the complexity of the system, but also because the air temperature recorded at a weather station is a point measurement and is, therefore, conceptually different from the simulated air temperature that is the model grid cell

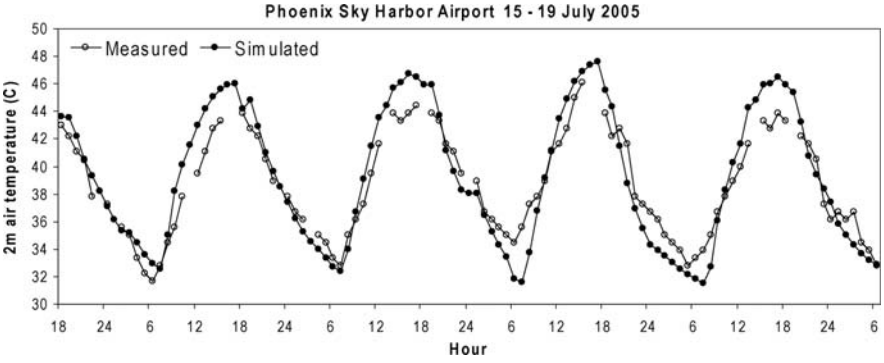

Fig. 9.2 Simulated and measured 2 m air temperature at the National Weather Service station at Sky Harbor Airport in the center of the Phoenix metropolitan region for the time period 15–19 July 2005

average temperature. The two are comparable if the station is placed in an extended homogeneous environment which is rare to find in an urban setting. Other possible reasons for the differences are an inaccurate assessment of the large scale synoptic weather conditions that are influencing the regional simulations through model boundary and initial conditions as provided from a global atmospheric model. These conditions hold true for all sites in the urban area and we assume, therefore, that the model captures differences between neighborhoods satisfactorily.

9.2.5 Land Use/Land Cover Classification System

The 24-category US Geological Survey (USGS) LULC system (Anderson et al. 1976) is the standard input for running WRF. Since the extent and heterogeneity of urban land use of the Phoenix metropolitan area are underrepresented in this dataset (Grossman-Clarke et al. 2005), we chose to use the 2005 12-category LULC classification available for Phoenix at the spatial resolution of 30 m, which is briefly described below.

The general reference LULC classification is based on the expert classification system (Stefanov et al. 2001) originally developed for use with Landsat Thematic Mapper (TM) data to monitor land cover changes in this rapidly expanding urban area. The system performs a posteriori sorting of classes initially derived using the supervised Maximum Likelihood classification. Such reclassification is implemented in the hypothesis-testing framework whereby all initially classified pixels are evaluated using sets of rules and by overlaying with co-registered auxiliary data layers. These layers originate from different sources or are computed directly from a Landsat image and include the county land-use map, image variance texture, water rights database, city boundaries, and Native American reservation boundaries.

The cloud-free Landsat TM image (path 37/row 37) used in the current classification was acquired on March 8, 2005. It was georeferenced and geometrically rectified using high resolution true color aerial photomosaic as a reference source. Raw digital numbers of image bands were converted into true surface reflectance values by applying an atmospheric correction. The final classification has a reported overall accuracy of 83% which is generally acceptable and common for Landsat-derived urban classification level of accuracy. User's accuracy for individual classes varies from 71 to 100% with the exception of commercial/industrial class (51%).

As described in detail in Grossman-Clarke et al. (2005), the derived 12-category LULC map was used to assign land cover class for each WRF 30-second grid cell by using majority rule to determine the highest associated fraction of land cover. We then used the revised land use/cover classifications as input into WRF, and coded the 30-second grid cells as one of the following categories: urban (commercial/industrial); xeric (urban residential draught resistant landscaping); desert (undisturbed natural land); or mesic (urban residential predominantly grass). The categories differed mainly by their type of vegetation and irrigation method (urban and desert – no irrigation; xeric – drought adapted vegetation with drip irrigation; mesic – well watered flood or overhead irrigated). The urban

(commercial/industrial) category was composed entirely of man-made surfaces with no significant vegetation or bare soil, while in the xeric and mesic residential categories, the fractional surface covers were, respectively, man-made (0.73/0.60), vegetation (0.10/0.23), and soil (0.17/0.17). Some peripheral neighborhoods, however, were located in undisturbed desert areas, so we also used the surface characteristics of this fourth classification to drive the model.

9.2.6 Household Survey on Sensitivity to Heat

One way to assess how well WRF simulations relate to human experience is to compare the WRF temperature output to the self-reports of 2006 Phoenix Area Social Survey (PASS) respondents about perceived temperatures and heat-related health problems in the summer of 2005. A comparison of model simulations with residents' reports has not been done before, probably because of the lack of social survey data that spatially corresponds to the model grids. In each of the 40 PASS neighborhoods, described above, 40 randomly selected households were recruited for participation in PASS until a minimum 50% response rate was achieved in each neighborhood. Overall survey response rate was 51% ($n = 808$). Data from the 2000 Census indicate variable numbers of dwelling units per neighborhood (minimum: 82; maximum: 3833; mean: 888). The percentage of households surveyed per neighborhood also varied from a minimum of 0.6 to a maximum of 24.4, with a mean of 4.4. Surveys were collected using a multi-modal approach (online, telephone, or personal interview), and the respondent who was 18 years or older with the most recent birthday was selected to participate in the study. The survey was administered by the Institute for Social Science Research (ISSR) at Arizona State University from April 29 through September 27, 2006.

As part of PASS, respondents answered the following two questions to gauge their sensitivity to heat: (1) During the summer of 2005, do you think your neighborhood was a lot cooler, a little cooler, a little hotter, or a lot hotter than most other neighborhoods in the Valley or do you think it was about the same temperature as other neighborhoods? (2) During last summer, did you or anyone else in your household have symptoms related to heat or high temperatures such as leg cramps, dry mouth, dizziness, fatigue, fainting, rapid heart beat or hallucinations? (Yes; No).

9.2.7 Neighborhood Demographics

The 2000 US Census Summary Files 1 and 3 for the sample neighborhoods were used to identify the following block group variables for comparisons: population per square mile, median income (US dollars), poverty rate (percent of population below the US government federal poverty guideline), ethnicity (percent minority), and age (median age and ages 65 and older). These variables were used in the analysis to show how different population groups experienced the heat event simulated by WRF.

9.3 Data Analysis

To investigate intra-urban variation in threshold temperatures, the data were analyzed in three phases. The first phase of analysis involved simulating threshold temperatures with the WRF model for the four-day (96 hours) heat event that occurred between July 15 and 19, 2005. Once the temperatures were simulated, GIS was used to map temperature variability for each study site throughout the area and neighborhoods' exposure to extreme heat was quantified. The severity of the heat hazard was calculated by determining the number of exposure hours for each study site to threshold temperatures at or above the 97.5 percentile for the heat event (Fig. 9.3). Exposure to threshold temperatures was then used to create three categories, herein referred to as Heat Intensity Classes. The Heat Intensity Classes were determined by calculating the mean hours of exposure for all 40 neighborhoods and using the difference of one standard deviation to establish each class (Table 9.1). The three levels of heat intensity are: low (less than 9 hours of exposure to temperatures at or above the 97.5 percentile for the 4-day heat event); medium (9–17 hours of exposure); and high (greater than 17 hours).

The final phase of analysis involved comparing the Heat Intensity Classes to household surveys, neighborhood demographics, and LULC types. We analyzed

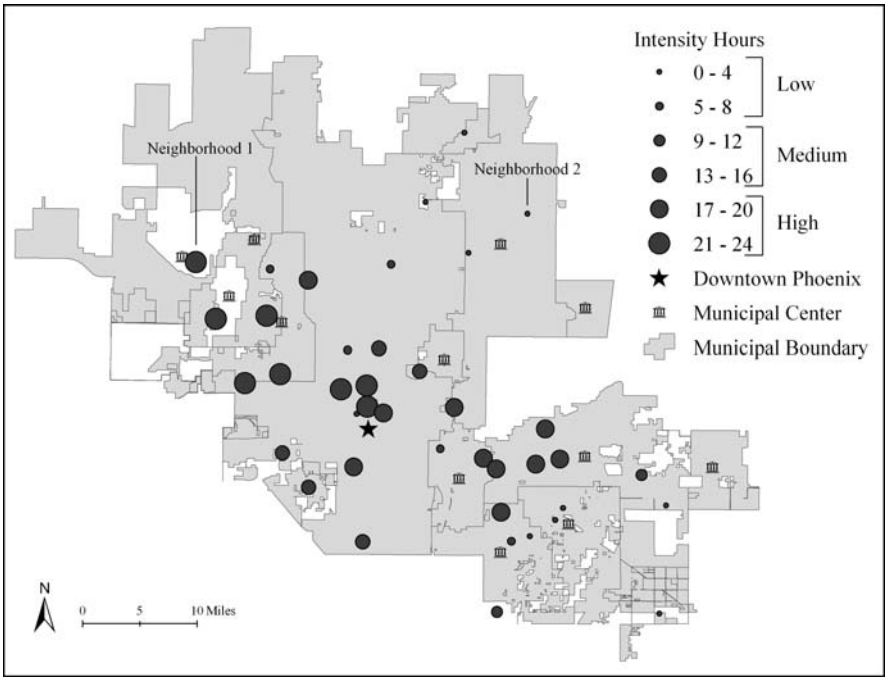

Fig. 9.3 Hours of Exposure to Threshold Temperatures at or above the 97.5 percentile from July 15–19, 2005 by Neighborhood

Table 9.1 Calculation of heat intensity classes based on hours of neighborhood exposure to threshold temperature

	Hours of exposure			Heat intensity classes		
Threshold temp	Range	Mean	SD	Low	Medium	High
97.5 percentile	24	12.6	7.9	<9 hours	9–17 hours	>17 hours

residents' perceptions of and experiences with extreme heat by conducting tests of significance on two measures of heat sensitivity, which serves as a validation of the WRF model. We also examined Census and LULC characteristics by Heat Intensity Class to better understand who is most vulnerable to extreme heat and what role vegetation may play in mitigating neighborhood exposure to threshold temperatures.

9.3.1 Results

9.3.1.1 Distribution of Heat Exposure Time

Tests for spatial autocorrelation presented in Table 9.2 report varying levels of statistical significance. Spatial autocorrelation permits statistical tests (e.g., Moran's *I*, Geary's *c*, Getis-Ord) which investigate spatial patterns by considering the presence of an attribute in space. Tests are based on correlation to neighbors whereby the pattern of a map is such that an area is similar (positive; aggregation) or dissimilar (negative; segregation) to adjacent areas (Burt and Barber 1996). The test both describes the structure of a spatial pattern and is also capable of detecting the presence of directional components (Legendre and Fortin 1989). Moran's *I* analyses on the distribution of simulated temperatures indicate that temperatures are not evenly distributed throughout the study area. While the mean four-day temperature reports modest temperature variation among the 40 neighborhoods (mean: 38.3°C; range: 4.9), hours of exposure to extreme temperatures varies significantly throughout the study area. Exposure to threshold temperatures at or above the 97.5 percentile, for instance, is significantly different among the 40 neighborhoods (mean: 12.6 hours;

Table 9.2 Spatial autocorrelation results for temperature simulations on the 40 neighborhoods

	Spatial autocorrelation			
Temperature simulations	Mean (sd)	Moran's *I*	Z-score	Significance
Mean four-day Temp ℃	38.3 (1.1)	0.03	1.73	0.10
Hours exposure: 81st percentile	29.4 (6.1)	0.04	2.37	0.05
Hours exposure: 97.5th percentile	12.6 (7.9)	0.08	3.1	0.01

range: 24). Results, therefore, indicate strong positive spatial patterns where adjacent neighborhoods in some areas are exposed to hazardous temperatures significantly more than other areas.

Figure 9.3 illustrates the varying levels of exposure to threshold temperatures throughout the 40 study sites. The circles represent the number of hours each neighborhood was exposed to threshold temperatures equal to or above the 97.5 percentile. The larger the circles, the greater the exposure to extreme conditions. Generally, the calculations exhibit the UHI pattern where neighborhoods near downtown centers are warmer with higher levels of exposure to threshold temperatures while neighborhoods on the fringe are cooler and have lower levels of exposure to threshold temperatures. However, the pattern of temperature gradients is more complex.

Physical and social processes may help to explain some of the variance in the distribution of air temperatures throughout the study area. Grossman-Clarke et al. (2005), for example, identified strong relationships between temperature and LULC, particularly the abundance of vegetation. In neighborhoods, residential landscapes are managed according to human preferences and availability of resources to cultivate vegetation (Larsen and Harlan 2006; Martin et al. 2004). Additionally, the Phoenix metropolitan region has an elevation gradient with increasing elevation to the north-east which causes differences in air temperature among neighborhoods with comparable land use. Air-flow patterns are influenced by the presence of mountains that typically cause upslope flows during the daytime towards the north and northeast. Downslope flow occurs during the night and is associated with cold advection that reaches various parts of the Phoenix metropolitan area at different times (Brazel et al. 2005). Depending on the location of a neighborhood, cooler or warmer air from areas with different land use/cover in the vicinity might occur. Finally, the current WRF version considers only four urban land use/cover classes and the predominant LULC type is assigned to a model grid cell but might not always be accurately representative, such as for mixed used areas.

Table 9.3 Neighborhood exposure to mean and threshold temperatures (Celsius) by heat intensity class

	Heat intensity class		
Temperature simulations	Low	Medium	High
N neighborhoods	15	10	15
Four-day heat event: Temp °C			
Mean average (sd)	37.2 (1)	38.5 (0.3)	39.2 (0.2)
Mean high (sd)	44.7 (0.9)	45.9 (0.2)	46.5 (0.2)
Mean low (sd)	29.8 (1.2)	30.9 (0.7)	31.8 (0.2)
Four-day heat event: Hours			
81st percentile (sd)	23.8 (6.9)	31.1 (0.9)	33.7 (0.9)
97.5th percentile (sd)	3.3 (2.5)	14.5 (2.6)	20.7 (1.9)

Note: A difference in 1°C = 1.8°F

Exposure to mean and threshold temperatures by Heat Intensity Class presented in Table 9.3 follow two distinct patterns. When considering mean temperatures (high, low, and average), there is a general positive linear relationship where temperatures increase modestly moving from low to high Heat Intensity Classes. Mean average temperature for the four-day heat event, for instance, increases from 37.2°C (Low) to 38.5°C (Medium) to 39.2°C (High), representing an increase of 2°C from the low to high classes. Exposure to threshold temperatures, however, reflects more pronounced differences among the three intensity classes. On average, neighborhoods in the high Heat Intensity Class were exposed to over six times the number of threshold hours that low intensity neighborhoods experienced during the four-day heat event. Among individual observations, three neighborhoods recorded zero hours of exposure to threshold temperatures in contrast to two neighborhoods that were exposed to twenty-four hours at or above threshold temperatures.

An analysis of the hourly temperature for the four-day heat event confirms variable levels of exposure to threshold temperatures among neighborhoods in the study area. Figure 9.4 presents the average temperature for all neighborhoods in addition to the temperature distribution of two particular neighborhoods. *Neighborhood 1* reported the warmest temperatures of the sample while *Neighborhood 2* reported the coolest temperatures. While the average temperature reached or exceeded the 97.5 percentile (45°C) each day during the heat event, Neighborhood 1 was exposed to considerably higher temperatures in the afternoon as well as the evening and early morning hours. Alternatively, Neighborhood 2 reported significantly cooler temperatures while remaining under 45°C for the duration of the four-day period.

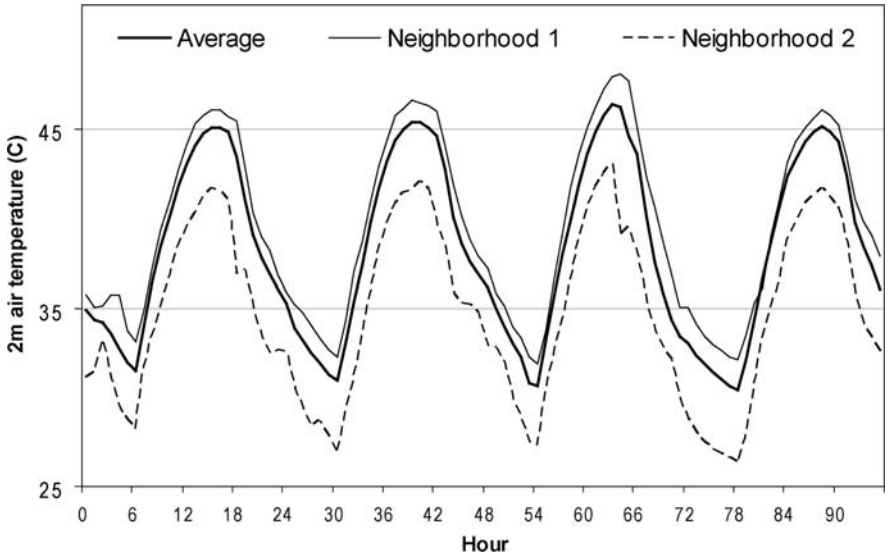

Fig. 9.4 Hourly Neighborhood Temperature (Celsius) Distribution for July 15–19, 2005 (45°C represents the 97.5 percentile)

The 65th hour of the four-day heat event produced the highest simulated temperatures. The temperatures ranged from 46.4°C (Average); 48.2°C (Neighborhood 1); to 43.1°C (Neighborhood 2), representing a difference of 5.1°C (or 9.2°F) between the warmest and coolest neighborhoods in the sample. Hourly neighborhood temperature, therefore, verifies significant variation in levels of exposure to extreme temperatures among the 40 neighborhoods.

9.3.1.2 Perceptions of and Experiences with Extreme Heat

Tests for global spatial autocorrelation analyses indicate the frequency and distribution of two social survey measures for residents' sensitivity to extreme heat are not statistically significant (Table 9.4). In other words, there is not a marked spatial pattern between location and residents' perceptions of and experiences with extreme heat. One explanation for this distribution is the fact that the survey responses reflect the average of 20 unique responses for each location. For instance, *Illness* was determined by coding individual survey responses (No heat-related household illness = 0; Yes = 1), and then we compared average scores at the neighborhood level. The aggregation of perceptions by neighborhood is subject to many influences which may explain the random distribution of the spatial autocorrelation analyses. In contrast to social perceptions, the 40 neighborhoods are variably exposed to threshold temperatures throughout the study area. In some cases, high intensity neighborhoods are adjacent to low intensity neighborhoods in both the urban core as well as residential suburban areas. Other considerations that could explain the spatial distribution of respondents' views include age and other demographics, housing quality, residential landscaping characteristics, and the availability of other resources that may influence individual residents' perceptions and experiences with extreme heat. Moreover, the question did not ask respondents where the heat incidents occurred, leaving open the possibility that incidents occurred outside their residential neighborhoods.

Analyses of local spatial autocorrelation, however, indicate that perception of risk and illness exhibit spatial clustering in some parts of the study area among adjacent

Table 9.4 Global spatial autocorrelation results for survey responses

	Global spatial autocorrelation		
Survey questions	Moran's *I*	Z-score	Significance
Perception of risk			
The temperature of your neighborhood compared to other neighborhoods for summer 2005	–0.05	−0.5	Random
Illness			
Experienced heat-related symptoms in household in summer 2005	−0.04	−0.2	Random

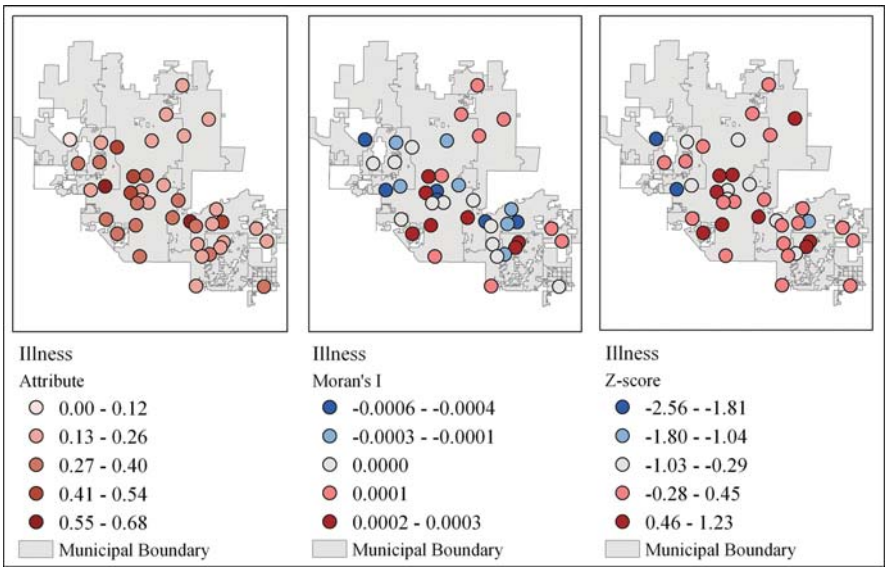

Fig. 9.5 Local spatial autocorrelation results for illness

neighborhoods. Aneslin's Local Index of Spatial Association (LISA) (Anselin 1995) for Moran's *I*, offers empirical insight into a spatial scale by measuring the similarity of an attribute and its spatial configuration to its neighbors. Figure 9.5 , for example, presents three maps illustrating the spatial distribution of self-reported illnesses associated with extreme heat. The first map shows the distribution of the attribute throughout the study area where lower attribute scores reflect fewer heat-related illnesses in the household while higher scores reflect a greater number of heat-related illnesses. The second map shows the distribution of the local Moran's *I* statistic which reports on similarity (low values reflect dissimilar neighbors and high values reflect similar neighbors). The third map presents Z-scores for each neighborhood where the dark red circles represent clustering 'hot spots' of statistically high morbidity (at the 95% confidence level) while the dark blue circles represent clusters of low morbidity. Notice LISA reports significant clustering of illness associated with extreme heat in neighborhoods in Central South Phoenix.

Organized by Heat Intensity Classes, Table 9.5 illustrates differences among residents' perceptions of and experiences with extreme heat. When considering perception of temperature, significantly more respondents in the high Heat Intensity Class reported that the temperature in their neighborhood was "hotter" compared to other Phoenix area neighborhoods for the summer of 2005. Likewise, illness, the second sensitivity measure, shows that almost 31% of respondents in the high Heat Intensity Class reported that someone in their household experienced a heat-related illness for the summer of 2005 in contrast to 24.1% and 24.2% for the low and medium Heat Intensity Classes, respectively. Although the distribution for illness is just outside the 0.10 significance level, results show variation among

Table 9.5 Perceptions of heat stress by heat intensity class

	Heat intensity class		
Survey questions	Low	Medium	High
N Neighborhoods	15	10	15
Perception of temperature			
Temperature in neighborhood compared to others: hotter*	19.0%	22.2%	30.6%
Illness			
Experienced heat-related symptoms: yes	24.1%	24.2%	30.9%

Chi-Square Test (2-sided): *p<0.01
Total number of respondents for Perception of Temperature n = 767; Illness n = 763.

residents' experiences with threshold temperatures. Respondents in high heat intensity neighborhoods, therefore, perceive and experience heat stress more than respondents in neighborhoods of medium and low Heat Intensity Class.

9.3.1.3 Neighborhood Demographics

The first two phases of the analysis found that threshold temperatures and residents' sensitivity to extreme heat are variably distributed throughout the 40 neighborhoods. This phase of analysis explored the types of people who live in the places that are most vulnerable to the exposure of extreme heat. Table 9.6 shows Census block group population characteristics for the following variables: density, income, ethnicity, and age. These variables are all highly related to Heat Intensity Class. Population per square mile, for instance, is roughly twice as high in the high Heat Intensity Class when compared to low and medium intensity classes. Median household

Table 9.6 Population characteristics of neighborhoods by heat intensity class

	Heat intensity class		
Demographics	Low	Medium	High
N neighborhoods	15	10	15
Density			
Population per sq mi	3569	3757	7550
Socioeconomic status			
Household income	$71,903	$62,669	$38,621
% in poverty	5.6	8.3	15.5
Ethnicity			
% minority	20.7	25.9	44.7
Age			
Median age	36.3	40.9	36.6
% ages 65 and over	9.8	20.4	17.5

Source: 2000 US Census, Summary Files 1 and 3

income for the high Heat Intensity Class was just over half the income of the low intensity class, and the percentage of minorities in the high intensity class was more than two times greater than the low class. Interestingly, neighborhoods in the high and medium Heat Intensity Classes had larger percentages of elderly residents, which is cause for concern because the elderly are one of the most vulnerable groups to extreme temperatures. Block groups in low heat intensity neighborhoods are characterized by low population density, higher income, and a relatively low presence of minorities or elderly. We expect that the people in these environments are the least vulnerable to extreme heat because they are likely to have more economic resources to buffer their exposure to threshold temperatures, which are the lowest and of shortest duration in these neighborhoods. Alternatively, high heat intensity class neighborhoods, in general, have high population densities, high percentage of minorities and elderly, and relatively low median household income. We expect that these people have fewer economic resources to buffer their exposure to many more hours of extremely high temperatures. Analyses, therefore, indicate that the urban residents most vulnerable to the risk of heat exposure live in the most hazardous environments.

9.3.1.4 LULC Characteristics

Tables 9.7 and 9.8 present results on the final phase of analysis which examines the relationship between local LULC characteristics, threshold temperatures, and Heat Intensity Classes. Table 9.7 shows that all six neighborhoods classified as urban are located in the high Heat Intensity Class while the eight mesic neighborhoods are all located in the low Heat Intensity Class. Of the 19 xeric neighborhoods, 3 are in the low Heat Intensity Class followed by 7 in the medium and 9 in the high Heat Intensity Class. Table 9.7 is consistent with previous research in showing that land-use patterns and land cover are significant drivers of air temperature differences within the urban area under conditions with weak synoptic forcing (Harlan et al. 2006; Stabler et al. 2005).

There are also some distinct patterns between LULC and simulated temperatures. One particular pattern is a bimodal trend where mesic and desert LULC classes report cooler temperatures when compared to the warmer xeric and urban classes

Table 9.7 Neighborhood LULC categories by heat intensity class

	Heat intensity class		
LULC	Low	Medium	High
N neighborhoods	15	10	15
LULC			
Urban	0	0	6
Xeric	3	7	9
Desert	4	3	0
Mesic	8	0	0

Table 9.8 Neighborhood exposure to threshold temperatures by LULC

	LULC class			
Temperature simulations	Urban	Xeric	Desert	Mesic
N neighborhoods	6	19	7	8
Four-day heat event: Temp °C				
Mean average (sd)	39.4 (0.2)	38.7 (0.5)	36.9 (1.3)	37.5 (0.6)
Mean high (sd)	46.6 (0.2)	46.0 (0.5)	44.6 (1.3)	44.9 (0.5)
Mean low (sd)	31.8 (0.2)	31.4 (0.4)	29.0 (1.1)	30.3 (0.6)
Four-day heat event: Hours				
81st percentile (sd)	33.8 (0.7)	31.5 (2.8)	22.4 (10)	26.9 (2.3)
97.5th percentile (sd)	21.8 (2.1)	15.8 (5.8)	6.0 (5.8)	4.1 (2.2)

(Table 9.8). The mean high, low, and average temperature of the xeric and urban classes all reported differences in temperature greater than 1°C when compared to mesic and desert classes. The hours at or above threshold temperatures reflect significant differences between the four LULC classes. Neighborhoods in the mesic class, for example, averaged 4.1 hours during the four-day heat event while urban and xeric neighborhoods averaged 21.8 and 15.8 hours at or above threshold temperatures, respectively. These analyses show that urban and xeric neighborhoods are exposed to warmer temperatures for much longer periods of time compared to mesic and desert neighborhoods. Thus, people who live in mesic neighborhoods or near natural desert landscapes have more natural resources in the form of vegetation that helps to lower the ambient temperature and thereby mitigate the impact of heat waves on people.

It is imperative to point out that WRF considers various physical processes in the governing temperature equation to calculate near-surface air temperature. Those physical processes include the strongly land use dependent vertical transport of heat between the atmosphere and the land surface as well as horizontal and vertical advection, horizontal diffusion, net radiative flux convergence and divergence, phase changes of water during fog and cloud formation, adiabatic warming and anthropogenic heating. While a relationship between land use characteristics and air temperature as mediated through vertical turbulent transport of heat can be expected, the strength depends on the synoptic conditions and the time of day and the other physical processes that might dominate temperature tendency near the surface. Using WRF's predecessor, MM5 (Mesoscale Meteorological Model), Grossman-Clarke et al. (2005) investigated the contribution of the different physical processes on the near-surface air temperature under typical summer conditions in Phoenix. Findings indicated that cooling through radiation fluxes accounted for the most significant contribution to changes in air temperature at night and that cooling is enhanced between sunset and midnight by horizontal advection while vertical turbulent transport of heat dominates the temperature tendency for most of the day leading to the reported relationship between land use characteristics and air temperature.

9.4 Discussion

This study offers three contributions to urban hazards and disaster analysis research. Unlike other studies that examine heat-related health disasters for entire cities, this study finds significant intra-urban variability for air temperature, exposure to threshold temperatures, human perceptions, and self-reported illnesses associated with extreme heat. Our first contribution, therefore, is to show that reliance on one climate station as a regional barometer to assess exposure to extreme heat will obscure significant climatic variation within a given urban area and, therefore, the locations and types of individuals who are most at risk from heat hazards.

A second contribution is the development of a methodology for simulating temperature variability for a given study area. Despite some limitations of climate models, which we discussed, we have established a baseline for modeling temperature variability which can be applied to any location. The methodological approach presented in this paper offers the ability to identify high risk urban areas, the areas that will be hit harder, earlier, quicker, and for longer periods of time during an extreme heat event when compared to other places within the same region. Identifying these places helps to enable efforts toward illness prevention and response.

Through the development of this methodology, a third contribution could be the application of this information via a disaster mitigation and response system. The large-scale health disasters caused by recent heat waves have prompted many cities to develop warning systems that alert people to the likely onset of dangerous weather conditions so that adaptive responses are possible. These systems are based on synoptic methods that use local weather data from a central location – such as the city airport – to record relevant variables, relate weather conditions to excess mortality, and create a synoptic analysis that forecasts dangerous heat conditions for a particular city (Kalkstein and Davis 1989; Kalkstein et al. 1996; Sheridan and Kalkstein 2004). While useful for anticipating an upcoming extreme heat event, current systems lack the spatial component reflecting which locations are the most vulnerable. The system developed in our study identifies spatially sensitive degrees of risk to threshold temperatures, based on historical records, to assist disaster efforts prior to a heat event. Benefits of this system are threefold: (1) to inform aid workers where to locate response units prior to the outset of a heat event; (2) to ensure staff and supplies are readily available to aid anyone requiring assistance during a heat event; and (3) to direct policy that may help reduce factors contributing to threshold temperatures (e.g., LULC, building codes) in high risk areas.

9.5 Conclusion

This study employs geospatial methods to investigate extreme heat as a human hazard in the Phoenix metropolitan area. Motivation for this study is to help prevent and reduce heat-induced illnesses, such as heat stroke, exhaustion, dehydration, cardiovascular, and respiratory problems, which strike suddenly and acutely during the warmest times of the year (ICLEI 1998; Semenza et al. 1999). Utilizing both

physical and social data, research findings indicate: (1) Exposure to threshold temperatures is variably distributed among places and people throughout the Phoenix metropolitan area; (2) Residents' perceptions of and experiences with extreme heat parallel simulated air temperatures; (3) The types of people most vulnerable to risk of exposure to extreme temperatures are minorities, elderly, and low income residents. (4) Neighborhoods with mesic landscaping or natural desert surroundings are significantly cooler than neighborhoods with urban or xeric yards. Public expenditures aimed at increasing outdoor amenities (e.g., vegetation, shade, public parks) would provide resources for people to cope during a heat wave event, while helping mitigate human exposure to threshold temperatures.

Simulations from the WRF climate model produced varying levels of mean temperature throughout the Phoenix region in general, and significantly distinct levels of exposure to threshold temperatures across the 40 neighborhoods in particular. While regional atmospheric modeling is currently the best available tool to assess air temperature variability within urban areas, there are limitations to the accuracy of the model output that must be considered when interpreting results. For instance, WRF only employed the predominant neighborhood LULC type as an input variable, which is not always representative in cases of mixed-use areas. Landscape classifications could be further improved in future modeling.

As extreme heat events are expected to increase in intensity, frequency, and duration throughout the world over the next century, monitoring regional weather stations is an insufficient system to mitigate human hazards to heat events. This study illustrates that temperatures vary significantly within the same urban area, and that some residents are at significantly greater risk of exposure to threshold temperatures than others. We applied advanced geotechnical methods to study extreme heat as an urban hazard, the results yielded theoretical, methodological, and practical contributions to disaster analysis research.

Acknowledgments This material is based upon work supported by the National Science Foundation under Grant Nos. DEB-0423704, ATM-0710631, and GEO-0816168. Any opinions, findings and conclusions or recommendation expressed in this material are those of the author(s) and do not necessarily reflect the views of the National Science Foundation (NSF). The authors would like to thank Drs. Pamela S. Showalter and Yongmei Lu for organizing this special issue, and the three anonymous reviewers for their constructive criticism.

References

Anderson, J. R., Hardy, E. E., Roach, J. T., Witmer, R. E., et al. 1976. A Land Use and Cover Classification System for Use with Remote Sensor Data. United States Geological Survey Professional Paper, 964, 36.

Aniello, C., Morgan, K., Busbey, A., Newland, L. et al. 1995. Mapping micro-urban heat islands using Landsat TM and a GIS. *Computer Geosciences*, 21, 965–969.

Anselin, L. 1995. Local Indicators of Spatial Association—LISA. *Geographical Analysis*, 27(2), 93–115.

Arnfield, A. J. 2003. Two decades of urban climate research: a review of turbulence, exchanges of energy and water, and the urban heat island. *International Journal of Climatology*, 23, 1–26.

Braga, A. L. F., Zanobetti, A., Schwartz, J., et al. 2002. The effect of weather on respiratory and cardiovascular deaths in 12 US cities. *Environmental Health Perspectives*, 110, 859–863.

Brazel, A. J., Selover, N., Vose, R., Heisler, G., et al. 2000. A tale of two climates—Baltimore and Phoenix urban LTER sites. *Climate Research*, 15, 123–135.

Brazel, A. J., Fernando H. J. S., Hunt, J. C. R., Selover, N., Hedquist, B. C., Pardviak, E., et al. 2005. Evening transition observations in Phoenix, Arizona. *Journal of Applied Meteorology*, 44(1), 99–112.

Brown, M. 2000. Urban parameterizations for mesoscale meteorological models. In Z. Boybeyi (Ed.), *Mesoscale atmospheric dispersion* (pp. 193–255). Southampton, UK: WIT Press.

Burt, J. E., and Barber, G. M. 1996. *Elementary statistics for geographers*. New York: The Guilford Press.

Census Bureau 2006. 2006 American Community Survey. www.census.gov; accessed October 26, 2008.

(CDC) Centers for Disease Control and Prevention 2005. Heat-related mortality – Arizona,1993–2002 and United States, 1979–2002. *Morbidity & Mortality Weekly Report*, 54 (25):628–630.

(CDC) Centers for Disease Control and Prevention 2006. Extreme heat: a prevention guide to promote your health and safety. http://www.bt.cdc.gov/disasters/extremeheat/heat_guide.asp; accessed 4/29/08.

Choi, G. Y., Choi, J. N., Kwon, H. J., et al. 2005. The impact of high apparent temperature on the increase of summertime disease-related mortality in Seoul: 1991–2000. *Journal of Preventive Medicine and Public Health*, 38, 283–290.

Civerolo, K. L., Sistla, G., Rao, S. T., Nowak, D. J., et al. 2000. The effects of land cover in meteorological modeling: implications for assessment of future air quality scenarios. *Atmospheric Environment*, 34, 1615–1621.

Confalonieri, U., Menne, B., Akhtar, R., Ebi, K. L., Hauengue, R. S., Kovate, B., Woodward, A., et al. 2007. Human Health. In M. L. Parry, O. F. Canziani, J. P. Palutikof, P. J. van der Linden and C. E. Hanson (Eds), *Climate Change 2007: Impacts, Adaptation and Vulnerability.* Contribution of Working Group II to the Fourth Assessment Report of the Intergovernmental Panel on Climate Change. Cambridge, UK: Cambridge University Press.

Curriero, F. C., Heiner, K. S., Samet, J. M., Zeger, S. L., Strug, L., Patz, J. A., et al. 2002. Temperature and mortality in 11 Cities of the eastern United States. *American Journal of Epidemiology*, 155, 80–87.

DeGaetano, A. T. and Allen, R. J. 2002. Trends in twentieth-century temperature extremes across the United States. *Journal of Climate*, 115, 3188–3205.

Grimm, N. B. and Redman, C. L. 2004. Approaches to the study of urban ecosystems: the case of Central Arizona – Phoenix. *Urban Ecosystems*, 7, 199–213.

Grimmond, C. S. B. 2005. Progress in measuring and observing the urban atmosphere. *Theoretical and Applied Climatology*. doi: 10.1007/s00704-00005-00140-00705.

Grossman-Clarke, S., Zehnder, J. A., Stefanov, W. L., Liu, Y., Zoldak, M. A. 2005. Urban modifications in a mesoscale meteorological model and the effects on near surface variables in an arid metropolitan region. *Journal of Applied Meteorology*, 44, 1281–1297.

Grossman-Clarke, S., Liu, Y., Zehnder, J. A., Fast, J. D., et al. 2008. Simulation of the Urban Planetary Boundary Layer in an arid metropolitan Area. *Journal of Applied Meteorology and Climatology*, 47(3), 752–768.

Harlan, S. L., Brazel, A. J., Prashad, L., Stefanov, W. L., Larsen, L., et al. 2006. Neighborhood microclimates and vulnerability to heat stress. *Social Science & Medicine*, 63, 2847–2863.

Harlan, S. L., Budruk, M., Gustafson, A., Larson, K., Ruddell, D., Smith, V. K., Yabiku, S. T., Wutich, A., et al. 2007. Phoenix Area Social Survey 2006 Highlights: Community and Environment in a Desert Metropolis. Central Arizona – Phoenix Long-Term Ecological Research Project, Contribution No. 4. Global Institute of Sustainability, Arizona State University.

Harlan, S. L., Brazel, A. J., Jenerette, G. D., Larsen, L., Jones, N. S., Prashad, L., Stefanov, W. L., et al. 2008. Made in the shade: The inequitable distribution of the urban heat island. *Research in Social Problems and Public Policy*, 15, 173–202.

Hedquist, B. C., and Brazel, A. J. 2004. Urban heat island (UHI) measures for the S.E. metropolitan area of the CAP LTER: transects versus fixed stations. Presented at the 6th Annual CAP LTER Poster Symposium, Tempe, AZ.

Hong, S. Y., and Pan, H. L. 1996. Nonlocal boundary layer vertical diffusion in a medium-range forecast model. *Monthly Weather Review*, 124, 2322–2339.

(ICLEI) International Council for Local Environmental Initiatives 1998. Cities at risk: assessing the vulnerability of United States cities to climate change. Toronto, Canada.

(IPCC) Intergovernmental Panel on Climate Change 2007. Climate Change 2007: Synthesis Report. http://www.ipcc.ch/pdf/assessment-report/ar4/syr/ar4_syr.pdf; accessed 4/29/08.

Jenerette, G. D., Harlan, S. L., Brazel, A. J., Jones, N., Larsen, L., Stefanov, W. L., et al. 2007. Regional relationships between vegetation, surface temperature, and human settlement in a rapidly urbanizing ecosystem. *Landscape Ecology*, 22, 353–365.

Kalkstein, L. S., and Davis, R. E. 1989. Weather and human mortality: an evaluation of demographic and inter-regional responses in the United States. *Annals of the Association of American Geographers*, 79, 44–64.

Kalkstein, L. S., and Greene, J. 1997. An evaluation of climate/mortality relationships in large US cities and the possible impact of a climate change. *Environmental Health Perspectives*, 105(1), 84–93.

Kalkstein, L. S., Jamason, P. P., Greene, J. S., Libby, J. Robinson, L., et al. 1996. The Philadelphia hot weather-health watch warning system: development and application, summer 1995. *Bulletin of the American Meteorological Society*, 77, 1519–1528.

Kilbourne, E. M. 2002. Heat-related illness: current status of prevention efforts. *American Journal of Preventive Medicine*, 22, 328–329.

Klinenberg, E. 2002. *Heat wave: A social autopsy of disaster in Chicago*. Chicago: University of Chicago Press.

Kusaka, H., and Kimura, F. 2004. Coupling a single-layer urban canopy model with a simple atmospheric model: impact on urban heat island simulation for an idealized case. *Journal of the Meteorological Society of Japan*, 82, 67–80.

Larsen, L., and Harlan, S. L. 2006. Desert dreamscapes: residential landscape preference and behavior. *Landscape and Urban Planning*, 78, 85–100.

Larson, J. 2006. Setting the record straight: more than 52,000 Europeans died from heat in summer 2003. *Earth Policy Institute*. Available at: http://www.earth-policy.org/Updates/2006/Update56.htm. Accessed October 19, 2007.

Legendre, P., and Fortin, M. J. F. 1989. Spatial pattern and ecological analysis. *Vegetation*, 80, 107–138.

Lin, C.-Y., Chen, F., Huang, J. C., Chen, W-C., Liou, Y.-A., Chen, W.-N., Liu, S-C., et al. 2008. Urban heat island effect and its impact on boundary layer development and land-sea circulation over northern Taiwan. *Atmospheric Environment*, 42, 5635–5649.

Liu, Y., Chen, F., Warner, T., Basara, J., et al. 2006. Verification of a Mesoscale Data-Assimilation and Forecasting System for the Oklahoma City Area During the Joint Urban 2003 Field Project. *Journal of Applied Meteorology*, 45, 912–929.

Lowry, W. 1967. The climate of cities. *Scientific American*, 217, 15–23.

Martilli, A. 2007. Current research and future challenges in urban mesoscale modeling. *International Journal of Climatology*, 27(14), 1909–1918.

Martin, C. A., Warren, P. S., Kinzig, A. P., et al. 2004. Neighborhood socioeconomic status is a useful predictor of perennial landscape vegetation in residential neighborhoods and embedded small parks of Phoenix, Arizona. *Landscape and Urban Planning*, 69, 355–368.

Masson, V. 2006. Urban surface modeling and the meso-scale impact of cities. *Theoretical and Applied Climatology*, 84(1), 35–45.

McGeehin, M. and Mirabelli, M. C. 2001. The potential impacts of climate variability and changer on temperature-related morbidity and mortality in the United States. *Environmental Health Perspectives*, 109, 185–189.

McMichael, A. J., Woodruff, R. E., Hales, S., et al. 2006. Climate change and human health: present and future risks. *Lancet*, 367, 859–869.

Meehl, G. A., and Tebaldi, C. 2004. More intense, more frequent, and longer lasting heat waves in the 21st century. *Science*, 305, 994–997.

Michelozzi, P., DeSario, M., Accetta, G., De'Donato, F., Kirchmayer, U., D'Ovidio, M., Perucci, C., et al. 2006. Temperature and summer mortality: geographical and temporal variations in four Italian cities. *Journal of Epidemiology and Community Health*, 60, 417–423.

Naughton, M. P., Henderson, A., Mirabelli, M. C. et al. 2002. Heat-related mortality during a 1999 heat wave in Chicago. *American Journal of Preventive Medicine*, 22, 221–227.

Oke, T. R. 1982. The energetic basis of the urban heat island. *Quarterly Journal of the Royal Meteorological Society*, 108, 1–24.

Oke, T. R. 1997. Part 4: The changing climatic environments: urban climates and global environmental change. In R. D. Thompson and A. Perry (eds.), *Applied Climatology Principals and Practice* (pp. 273–287). London: Routledge.

O'Neill, M. S., Jarrett, M., Kawachi, I., Levy, J. I., Cohen, A. J., Gouveia, N., Wilkinson, P., Fletcher, T., Cifuentes, L., Schwartz, J., et al. 2003. Health, wealth, and air pollution: advancing theory and methods. *Environmental Health Perspectives*, 111, 1861–1870.

Patz, J. 2005. Guest editorial: satellite remote sensing can improve chances of achieving sustainable health. *Environmental Health Perspectives*, 113, A84–85.

Patz, J., Campbell-Lendrum, D., Holloway, T., Foley, J. A., et al. 2005. Impact of regional climate change on human health. *Nature*, 438, 310–317.

Seaman, N. L. 2000. Meteorological modeling for air-quality assessments. *Atmospheric Environment*, 34, 2231–2259.

Semenza, J. C., Rubin, C. H., Falter, K. H., Selanikio, J. D., Flanders, W. D., How, H. L., Wilhelm, J. L., et al. 1996. Heat-related deaths during the July 1995 heat wave in Chicago. *American Journal of Preventive Medicine*, 16(4), 269–277.

Semenza, J. C., McCullough, J. E., Flanders, W. D., McGeehin, M., Lumpkin, J. R. et al. 1999. Excess hospital admissions during the July 1995 heat wave in Chicago. *American Journal of Preventive Medicine*, 16(4), 269–277.

Shamrock, W. C., Klemp, J. B., Dudhia, J., Gill, D. O., Barker, D. M., Wang, W., Powers, J. G., et al. 2005. A Description of the Advanced Research WRF Version 2. NCAR Technical Note.

Sheridan, S. C. and Kalkstein, L. S. 2004. Progress in heat watch-warning system technology. *Bulletin of the American Meteorological Society*, 85, 1931–1941.

Smoyer-Tomic, K. E., and Rainham, D. G. C. 2001. Beating the heat: Development and evaluation of a Canadian hot weather health-response plan. *Environmental Health Perspectives*, 109, 1241–1248.

Smoyer, K. E., Rainham, D. G., Hewko, J. N., et al. 2000. Heat-related stress mortality in five cities in southern Ontario: 1980–1996. *Institutional Journal of Meteorology*, 44(1809), 190–197.

Stabler, L. B., Martin, C. A., Brazel, A. J., et al. 2005. Microclimates in a desert city were related to land use and vegetation index. *Urban Forestry and Urban Greening*, 3, 137–147.

Stefanov, W. L., Ramsey, M. S., Christensen, P. R., et al. 2001. Monitoring urban land cover change: an expert system approach to land cover classification of semiarid to arid urban centers. *Remote Sensing of Environment,* 77, 173–185.

Taha, H. 1997a. Modeling the impacts of large scale albedo changes on ozone air quality in the south coast air basin. *Atmospheric Environment*, 31, 1667–1676.

Taha, H. 1997b. Urban climates and heat islands: albedo, evapotranspiration, and anthropogenic heat. *Energy and Buildings, 25*, 99–103.

Voogt, J. A. 2002. Urban Heat Island. In I. Douglas (ed.), *Encyclopedia of global environmental change* (pp. 660–666). Chichester: John Wiley and Sons.

Voogt, J. A., and Oke, T. R. 2003. Thermal remote sensing of urban climates. *Remote Sensing of Environment*, 86, 284–370.

Chapter 10
Wildfire Risk Analysis at the Wildland Urban Interface in Travis County, Texas

Yongmei Lu, Lori Carter, and Pamela S. Showalter

Abstract The term, "wildland urban interface" (WUI) refers to the area where structures and other human development meet or intermingle with undeveloped wildland or vegetative fuel. When development encroaches into wildland – areas that have been minimally impacted by human activities – the wildfire threat to life and property increases. A wildfire risk profile for the WUI in Travis County, Texas was created using a geographic information system (GIS). Historic wildfire records were linked to land cover types to identify the empirical relationship between fuels and ground cover. Topographical characteristics, land cover types, and housing density were combined to estimate wildfire risk. Risk levels for communities within and outside the WUI were compared. Analyses also compared wildfire risk levels for different types of WUI areas, which are distinguished based on vegetation coverage percentages and housing density. Findings indicate that in Travis County, TX, the wildfire risk is highest in high-density WUI areas, pointing to an urgent need for special fire control and fire regulations in this development zone. Vacant lands, which are likely future development sites, could be used by land managers to reduce wildfire risk if they can be managed as natural fire breaks or fuel free zones.

Keywords Wildland Urban Interface · Wildfire · Risk analysis · GIS · Texas

10.1 Introduction

The term "wildfire" refers to any unplanned or unwanted fire burning in forests, shrub lands, woodlands, or grasslands. Wildfire is one of the most destructive natural forces known to humanity. History is replete with episodes of notorious wildfires: the Miramichi fire in New Brunswick killed 160 people and burned three million acres (12,000 km^2) in 1825. The Peshitigo fire in 1872 killed over 1000 people

Y. Lu (✉)
Department of Geography, Texas State University-San Marcos, San Marcos TX 78666, USA,
e-mail: yl10@txstate.edu

P.S. Showalter, Y. Lu (eds.), *Geospatial Techniques in Urban Hazard and Disaster Analysis*,
Geotechnologies and the Environment 2, DOI 10.1007/978-90-481-2238-7_10,

in Wisconsin. California's 1991 Oakland Firestorm killed 25 people and destroyed 3469 homes and apartments. British Columbia's 2003 Okanogan Mountain Park Fire displaced 45,000 inhabitants, destroyed 239 homes, and threatened part of the City of Kelowna. That same year, San Diego County in Southern California suffered from a fire that took 15 lives and destroyed 2232 homes – that year California's total loss from wildfires neared $2 billion.[1]

Although most wildfires in Texas are of smaller scale, damages can be significant. For example, the Texas–Oklahoma wildfires of 2005–2006 caused enough damage to qualify for federal disaster relief funding. Higher than average precipitation rates during 2005 encouraged abundant vegetation growth. Subsequently, a period of extended drought with record high temperatures and high winds transformed the vegetation to dry fuel which, once ignited, sustained and spread the wildfire. In Texas, eleven people were killed and eight towns evacuated in early March of 2006. From late December 2005 until early April 2006, approximately five million acres (nearly 20,000 km^2) were burned and 423 homes destroyed (Lindley et al. 2007).

As pointed out by Dennison et al. (2007), fire presents the greatest hazard to land and life in the areas where humans and fire-prone vegetation meet. While vegetation fuel supply and weather conditions are major contributing factors to wildfire, continuing residential development in the wildland urban interface (WUI) – where structures and other human development meet or intermingle with undeveloped wildland or vegetative fuel (Cortner et al. 1990; Ewert 1993) – increases the possible occurrence of and subsequent damage from wildfires. Wildfires are often caused by human activities (Cardille et al. 2001; NIFC 2006). At the WUI, human activities occur where there are adequate fuel supplies, making it difficult to protect structures from wildfires (Cohen 2000; Winter and Fried 2001). The result: wildfire damage (as measured by both life and property loss) at the WUI tends to be greater than in other geographic locations.

The purpose of this study is to improve wildfire risk management by using a Geographic Information System (GIS) to perform wildfire risk analysis for one of the nation's fastest growing regions – Travis County, Texas (Fig. 10.1). Urban encroachment into wildland areas in the county has created a variety of "WUI communities"; the analyses reported in this paper took into account all of these communities. Spatial variation of vegetative fuel, county topography, and historic wildfire occurrences recorded by the Texas Forest Service were incorporated into the analysis. Using these criteria, statistical differences between the level of wildfire risk faced by each type of community were examined. Furthermore, because urban development is likely to move into vacant lands (which may, or may not, be within the WUI), the analysis also incorporated data regarding the county's vacant lands.

[1]More information about these and other notorious North American wildfires can be found at: http://en.wikipedia.org/wiki/List_of_wildfires

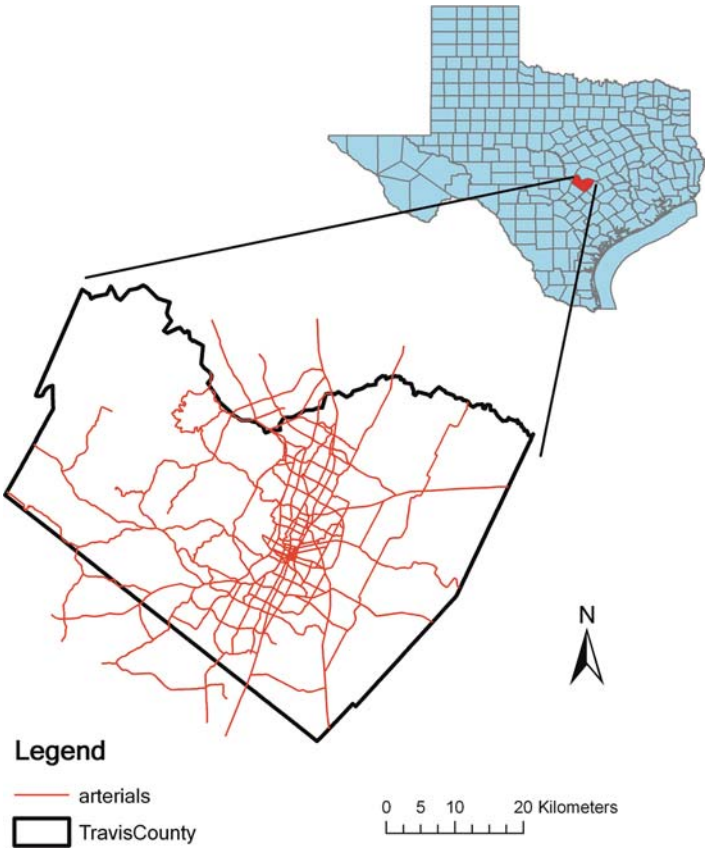

Fig. 10.1 Travis County, Texas

10.2 Risk Analysis and Wildfires

The concept of "risk" is as intriguing as it is multifaceted. Risk can be commonly accepted (e.g., driving a car), sought out (e.g., bungee-jumping from a bridge), or purposely avoided (e.g., refusing to fly). People perform "risk analysis" constantly as they go about their daily activities, while universities, companies, and governments study risk formally using scientific methods to better understand the dangers present in any given situation and how they can be effectively managed. Risk assessment requires both good science and good judgment (Keeney 1995) and can be either quantitative or qualitative. A risk assessment usually examines three items: hazard probability, expected loss, and loss mitigation (preparedness) (Finney 2005; Smith 2004). The risk assessment of wildfires in this study focuses on the first two items – probability and expected loss. The probability of wildfires is estimated by considering various factors that can contribute to the occurrence and sustenance of

wildfires throughout Travis County. These factors include vegetative fuel, topography, and the frequency with which different types of land cover have wildfires (as derived from historic fire records). The expected loss from wildfires in the WUI is determined by considering the size and density of population and housing units.

10.2.1 Natural Factors

Topography, weather conditions, and vegetative fuel loading play major roles in wildfire combustion potential (Cova et al. 2004). Fires that occur on larger slopes carry increased capacity to ignite fuels upslope (Thompson et al. 2000). Convective heat uplift from the fires down-slope (Pyne 2001) and longer flame lengths preheat vegetation above (Christiansen 2005; Davis 1990). On steep slopes, ignited materials can roll downhill with greater ease, spreading embers and flames. Aspect, or the direction that a slope faces, is also a significant factor. Slopes facing south and west in the northern hemisphere, patches of flat land, and very dry ridge tops have increased fire ignition potential because vegetative and soil moisture content decreases throughout the day due to longer exposure to solar radiation (Cova et al. 2004; Christiansen 2005; Johnson 2008; Perestrello de Vasconcelos et al. 2001; Thompson et al. 2000).

Climate and wind behavior can also contribute to the wildfire risk. Areas with temperate, moist climates have lower fuel ignition rates due to high retention of water within both vegetation and soil (Carapella 1996; Cardille et al. 2001). Areas subject to seasonal variations in moisture, such as much of the American West, Southwest, and Central Plains, have periods throughout the year when vegetative moisture retention is low. The low moisture retention is due to extended periods of lower than average rainfall coupled with higher than average temperature (Lawrimore 2005). The variables of high evaporation, low vegetation/soil moisture, and high vegetation density combine to create conditions most prone to wildfire ignition and spread. Under drier climatic conditions, areas with higher densities of vegetation are likely to have larger and more intense wildfires because of the increased fuel load. Without fuel breaks, wildfires can spread more rapidly and can be longer lived. Wind behavior further contributes to the wildfire risk because high wind speeds can carry firebrands or sparking embers of vegetation great distances[2] (Manzello 2007; Radeloff et al. 2005; Trembath 2005) while accelerating the drying process. Prolonged wind events can also "feed" existing fires by introducing more oxygen into the fire system (CSFS 2007).

[2]The California Forest Alliance estimates that firebrands from forest fires can be carried by winds or convective uplift for distances of up to 2.4 km (Radeloff et al. 2005).

10.2.2 Housing Density

Radeloff et al. (2005) considered housing density, vegetation type and density, and proximity to that vegetation as important variables for understanding wildfire risk. Other researchers have found that as the number of structures increases, the likelihood of anthropogenically-caused fire increases (Cardille et al. 2001; NIFC 2006; Perestrello de Vasconcelos et al. 2001; TFS 2007). Not surprisingly, denser residential developments tend to have greater loss of structures from wildfires (Trembath 2005) than those that are less dense. Communities that lack dense vegetation but are within reach of firebrands (Radeloff et al. 2005), overhanging branches, and contiguous grasslands (Trembath 2005) may be as vulnerable to wildfire as those with dense vegetation. In fact, the Texas Forest Service (TFS) recommends that structures be built more than 200 m from dense vegetation to prevent structural ignition from branch overhangs and grass fires (Cohen 2000; TFS 2007).

In conjunction with the wildfire problem faced by high density WUI areas, low density lands (including vacant lots) are commonly given insufficient attention when considering measures to reduce the wildfire threat. Given that urban growth commonly moves onto vacant lands, there are two important reasons for including these areas in wildfire risk analysis: (1) they represent future "built-up" areas, and (2) depending on how they are managed prior to development, they could serve as fire breaks, green buffers, or home ignition prevention zones (Cohen 2000; Ingalsbee 2003; IDL 2006); in short, they can behave either as a fire retardant or an accelerant, depending on how they are managed.

10.3 The Study Area

Located in Central Texas, Travis County is at the convergence of several distinct bioregions: the Edwards Plateau in the west, the Blackland Prairies toward the east and southeast, and the Cross-timbers and Prairies region toward the north (Travis County 2004). The county's varied topographical structure supports diverse vegetative communities. The Edwards Plateau's karst topography is characterized by plateaus and steep slopes dissected by waterways and supporting vegetation such as Ashe Juniper, Oak varieties and Mesquite. The Blackland Prairies region, whose deep rich soils are ideal for vegetative growth, supports agricultural endeavors and is experiencing considerable subdivision development. The Cross-timbers and Prairies region is characterized by rolling woodland savannah. At the southern tip of the Plains region, vegetation is characteristically grassy and interspersed with oak.

Occupying a transition zone between subtropical subhumid and subtropical humid climates, the County's average annual precipitation varies from 30 inches (71.2 cm) in the west to 36 inches (91.4 cm) in the east. Temperature range between an average January low of 39°F (3.89°C) and an average July high of 95°F (35°C). Major climatic hazards include straight line winds, lightning, flash floods, severe

heat, drought, and wildfires (Larkin and Bomar 1983). The County has recorded periods of extreme and prolonged rainfall followed by extended drought which has allowed wildfire fuel loads to collect and desiccate; towards the west, increased elevation and steep hill-slopes further exacerbate the risk of wildfire.

Travis County is one of the most rapidly growing counties in the US (TSDC/OSD 2006). Between 2002 and 2005, the population increased from 830,649 to 866,349 (TCHHS 2006), and by 2040 the population is projected to reach about 2 million (Travis County 2007). This growth is likely to increase the breadth of the WUI by converting lands that were formerly rural to those characterized by higher density development.

10.4 Data Utilized

To perform a wildfire risk assessment of Travis County, we combined vector data sets illustrating historic wildfires, ignition potential, and vacant lands in the study area with raster data sets containing information about elevation, slope, aspect, and vegetation/land cover at various resolutions. After identifying the related datasets, data extraction was performed followed by data cleaning, geocoding, registration, and other pre-processing where needed.

The Fire Reporting Database maintained by the Texas Forest Service Fire Department provided the data for wildfires occurring between January 1, 2005 and January 31, 2008 (for ease of discussion, referred to hereafter as between 2005 and 2007). After extracting, mapping, and cleaning the data, a total of 315 wildfires were identified (Fig. 10.2). Spatial distribution of the wildfires was used as a surrogate indicator of wildfire-prone areas, forming the foundation for further estimation of wildfire risk based upon historic records. Figure 10.2 displays the locations of these wildfires across Travis County, and reveals a clear association between the fires and urban areas. The term, “urban” in this paper follows the definition of the US Census Bureau. For Census 2000, “urban area” refers to all territory, population, and housing units located within an urbanized area or an urban cluster, which consists of core census block groups or blocks that have a population density of at least 1000 people per square mile and surrounding census blocks that have an overall density of at least 500 people per square mile.

Although Travis County’s annual precipitation varies spatially by about 6 inches (15.2 cm), for purposes of the study this variation was not included when modeling ignition potential. Spatial variation in temperature and moisture conditions for soil and vegetation was modeled by calculating surface exposure to solar radiation across the County. As wind pattern/wind speed data were unavailable for this study, the effect of wind for wildfire was not directly incorporated into the study. Rather, considering that wind tends to speed up as slope increases (Bradstock et al. 2002), relatively high wildfire potential was assigned to steeper slopes.

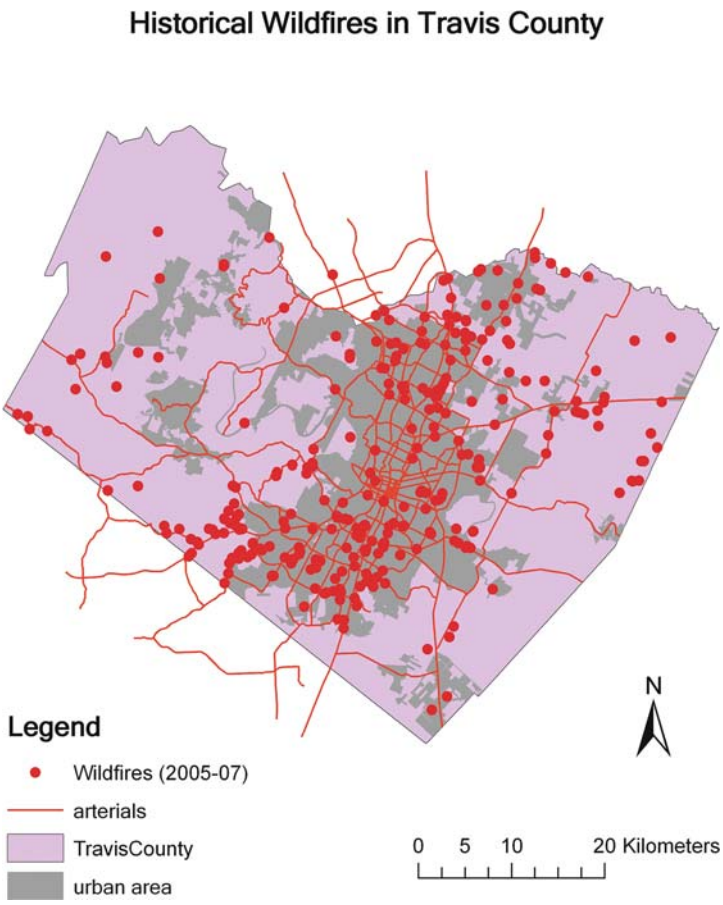

Fig. 10.2 Locations of Travis County wildfires between Jan. 1, 2005 and Jan. 31, 2008

Vacant land data were obtained from the Vacant Land Inventory (VLI) data set available from the Capital Area Council of Government (CAPCOG) Information Clearinghouse (CAPCOG 2008). The VLI was developed by CAPCOG to represent vacant lands identified through analysis of 2005 parcel and tax role information. These lands are normally five acres or lager in size and have improved value of $0.05 per square foot or less. Figure 10.3 displays the location of the 2005–2007 wildfires in relationship to vacant land in the County, and confirms the impression given by Fig. 10.2, that fewer fires occurred in or near vacant lands compared to "urban" areas.

The spatial extent of the WUI was defined by considering the spatial proximity of housing density and vegetation coverage. Travis County's WUI was defined

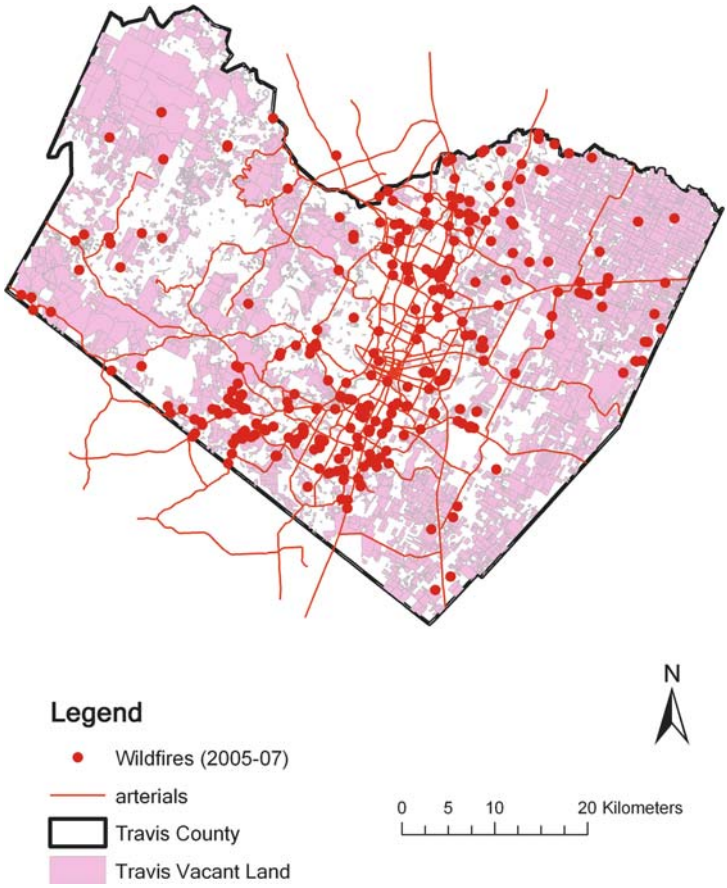

Fig. 10.3 Locations of the 2005–2007 wildfires in relation to Travis County's vacant land

following Radeloff et al. (2005) and Stewart et al. (2007). When vegetation covers over 50% of the land area, *High Density Intermix* refers to the blocks where housing density is higher than 741.3 housing units per km^2, *Medium Density Intermix* exists where housing density is between 49.2 and 741.3 units per km^2, and *Low Density Intermix* exists where housing density is between 6.2 and 49.2 units per km^2. In areas where vegetation covers less than 50% of the land but is within 2.4 km^2 of an area with 75% or more vegetation coverage, *High Density Interface* exists if the housing density is higher than 741.3 units per km^2, *Medium Density Interface* exists if the housing density is between 49.2 and 741.3 units per km^2, and *Low Density Interface* exists if the housing density is between 6.2 and 49.2 units per km^2(see Radeloff et al. [2005] for additional details). The WUI data set for Travis County was downloaded from Silvis Lab's webpage at the University of Wisconsin – Madison (Radeloff et al. 2005; Silvis Lab no date). Figure 10.4 displays

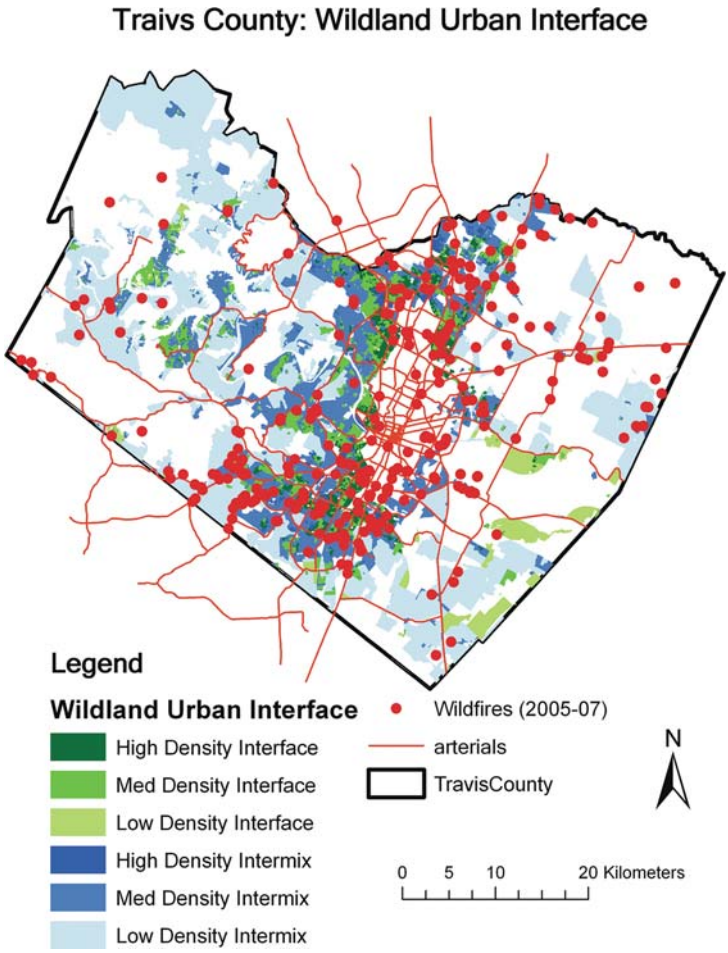

Fig. 10.4 Locations of the 2005–2007 wildfires in relation to Travis County's WUI

the location of the 2005–2007 wildfires in relation to the County's WUI. A clear spatial association appears to exist between the majority of the historical wildfires and human development, with fires apparently concentrated close to, or in, urban areas and the most high-density areas of the WUI.

Elevation was obtained via a digital elevation model (DEM) downloaded from the US Geological Survey's Seamless Data Distribution System (USGS no date). The National Elevation Dataset (NED) 1 arcsec is a raster product that has an approximate 30 m resolution. Both slope and aspect measurements for the study area were derived from this elevation dataset.

Vegetation and land cover data were obtained from the National Land Cover Dataset (NLCD) of 2001. To further refine the NLCD's 30 m spatial resolution and broad land cover/land use categories (e.g., forest, grassland, agricultural uses,

urban, and suburban development) the data was cross-referenced for regional variations using 1 m 2005 Digital Orthophoto Quarter Quadrangles (DOQQs) obtained through the Texas Natural Resource Information System (TNRIS 2008). By performing the cross-referencing, new subcategories of land cover/land use reflecting the local situation were created and their accuracy validated. Details of this process are reported in the following section.

10.5 Wildfire Risk Analysis of Travis County

Three factors that significantly influence and sustain wildfires are topography, fuel supply, and weather conditions. Travis County's wildfire risk was derived by analyzing aspect, slope, and fuel supply data in relationship to different land cover classes. Aspect, derived from DEM data, served as a surrogate for solar heating and vegetation moisture levels. Slope could be classified into different risk levels because uplift of heat along slopes causes wildfires to spread mainly uphill–steeper slopes facilitate the spread of wildfire more efficiently than gentle slopes (Perestrello de Vasconcelos et al. 2001). Since fuel supply data were limited, variation in topography was used to estimate micro-scale spatial variation in heating of fuels. Places receiving more sunshine tend to sustain well-grown vegetation with low moisture content, providing an ideal fuel supply for wildfires. Vacant land data were added to the analysis because they are typically un-cleared prior to development; they support vegetation, and thereby represent a source of fuel. Finally, wildfire risk was related to fuel supplies by generating a location quotient (LQ) of wildfire occurrence for different land cover classes. The latter item requires some explanation.

National Land Cover Dataset (NLCD) categories are generalized and do not reflect local characteristics such as vegetation density and vegetation ignition tendency – criteria that are critical for estimating wildfire risk. Therefore, the dataset underwent a two-step modification before it was used to create an LQ. First, the NLCD was reclassified to reflect local vegetation types. The new "Regional Land Cover Classes" (RLCC) were identified as:

- **H_2O**: Water bodies (not including intermittent and ephemeral streams)
- **MNT**: Maintained grasses (roadside grasses, parks, golf courses)
- **UT**: Urban Trees (groups of trees found in residential and commercial parks)
- **DVL**: Developed land (rooftops, driveways, commercial and residential)
- **ISC**: Impervious surface cover (roads, parking lots)
- **CMNT**: Cement and other artificial coverage (gravel, or not included in ISC)
- **JOP**: Juniper-Oak parks (groups of trees with interspersed grasses)
- **JOW**: Juniper-Oak woodlands (more dense canopies, less open grasses)
- **PR**: Prairie (Blackland Prairie open grasses–limited to eastern Travis County)
- **GRZ**: Grazing, rural (open grasslands–mostly found in western Travis County at higher elevations)

- **SPRS**: Sparse grasses (combined bare soil, rocky outcrops, and sparse grasses)
- **PRD**: Production (mainly agricultural–located near farming operations)
- **AGR**: Agricultural (open fields of continuous crops, visible farming implement footprints)
- **EVRG**: Evergreen (smaller groves of live oak, pine, higher canopies than ash juniper)
- **AQ**: Aquatic vegetation (found near or within water bodies, partial submersion)

Second, the accuracy of the reclassified NLCD data was evaluated to ensure the RLCC accurately reflect the true distribution of regional land cover in the study area. Using random sampling, 50 locations were selected within each of the 15 RLCCs created for the study area, creating 750 sampling sites. These sites were located on the 2005 DOQQs described earlier, and were examined to determine if the derived RLCC matched that found on the DOQQ. The numbers of correctly and incorrectly classified samples were recorded. The NLCD-derived RLCC was found to have an accuracy rate between 76% and 100% (Table 10.1), which was considered sufficient for the purposes of this study.

The LQ for wildfire was then derived by examining the spatial distribution of the RLCCs in relation to wildfire fuel supply. The RLCC was overlaid on a map showing the locations of historic wildfires, and the number of wildfires that occurred in each type of land cover/use recorded. The LQ was then calculated by dividing the percentage of wildfires occurring in each type of land cover/use by the areal percentage of the land cover/use over the entire study area (Table 10.2). The LQ thus reflects the tendency of each type of land cover/use to be impacted by wildfire. An LQ value equal to or less than one indicates that the percentage of wildfires occurring on that specific land cover is not greater than what would be expected given the spatial extent of that land cover within the study area. RLCC with LQ

Table 10.1 The accuracy of land cover classification from NLCD (based on 50 random samples obtained for each category)

Land Cover	Number of correctly classified samples	Accuracy
H_2O	50	1.00
MNT	48	0.96
UT	44	0.88
DVL	50	1.00
ISC	50	1.00
CMNT	50	1.00
JOP	39	0.78
JOW	44	0.88
PR	44	0.88
GRZ	39	0.78
SPRS	46	0.92
PRD	42	0.78
AGR	48	0.96
EVRG	38	0.76

Table 10.2 Wildfire risk: location quotient for different types of land cover based on historical wildfires (2005–2007)

Land cover	Areal percentage (%)	Fire_count percentage (%)	Location quotient (LQ)
H_2O	3.29	0.00	0.00
MNT	10.39	21.59	2.08
UT	6.46	16.19	2.51
DVL	4.10	15.87	3.87
ISC	2.00	13.97	6.99
CMNT	0.09	0.00	0.00
JOP	8.79	4.44	0.51
JOW	22.44	6.35	0.28
PR	0.65	0.32	0.49
GRZ	17.75	8.57	0.48
SPRS	11.64	7.94	0.68
PRD	4.15	0.63	0.15
AGR	6.37	2.86	0.45
EVRG	1.88	1.27	0.68
AQ	0.01	0.00	0.00
Total	100	100	n/a

values greater than one are therefore considered to be at greater risk than those equal to or less than one.

A wildfire risk ranking that combined aspect, slope, and LQ was created, representing each variable's relative contribution to wildfire risk. Slope, presented as a percent, reflects the escalating ability of wildfire to spread as slope increases. Aspect represents the different levels of sunshine a slope might receive. Finally, LQ, calculated as described above, represents the relative activity of wildfire on each land class. The five wildfire risk ranks were: None (0), Low (1), Medium-low (2), Medium-high (3), and High (4). Table 10.3 breaks down the fire risk rankings for the three variables and Figures 10.5, 10.6 and 10.7 utilize these ranks to illustrate the spatial patterns of wildfire risk in Travis County.

Table 10.3 Wildfire risk ranking based on slope, aspect, and Location Quotient for different types of land cover

Wildfire risk level: Reclassified	0 (None)	1 (Low)	2 (Medium-low)	3 (Medium-high)	4 (High)
Slope (%) (areal %)	n/a	0–4.99 (90.31)	5–9.99 (8.42)	10–14.99 (1.13)	≥ 15 (0.15)
Aspect (areal %)	n/a	Northeast, North (21.65)	Northwest, East (24.14)	West, Southeast (25.70)	Southwest, South, Flat (28.51)
Land cover LQ (areal %)	0 (3.38)	> 0 & ≤ 1 (73.67)	> 1 & ≤ 2 (0)	> 2 & ≤ 3 (16.85)	> 3 (6.09)

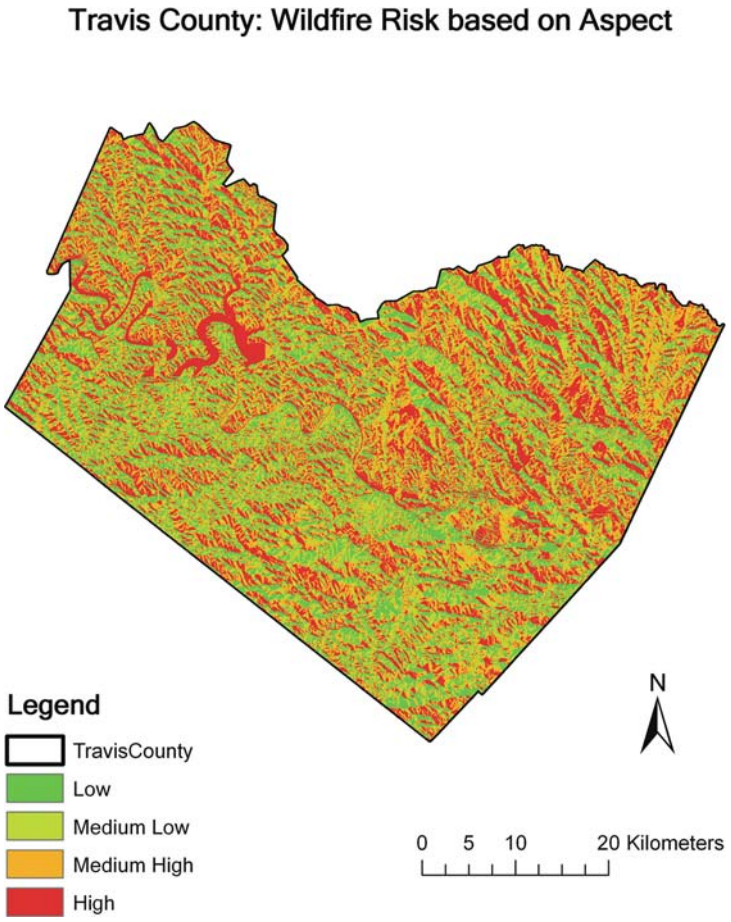

Fig. 10.5 Travis County wildfire risk ranking based on aspect

The fire risk rankings for aspect, slope, and land cover were then combined using GIS raster calculation, generating a data range between 0 and 12. The results were ranked into five categories, from Low to High (Table 10.4). The results indicate that the majority of the county (91.38%) falls in the Low to Medium level of wildfire risk (Fig. 10.8). However, a total of 8.7% of the County's land falls in the Medium-high to High levels of wildfire risk. Mapping this information reveals a clear pattern of High and Medium-high risk areas being prevalent in urbanized locations and in the WUI (Fig. 10.9).

As the population of Travis County continues to grow and developed areas expand, part of that growth is likely to occur on vacant lands. Consequently, vacant lands may indicate the direction of urban growth into the county's WUI. Among the 5548 vacant lots reported in CAPCOG's database, 1543 fall into the Medium-high to

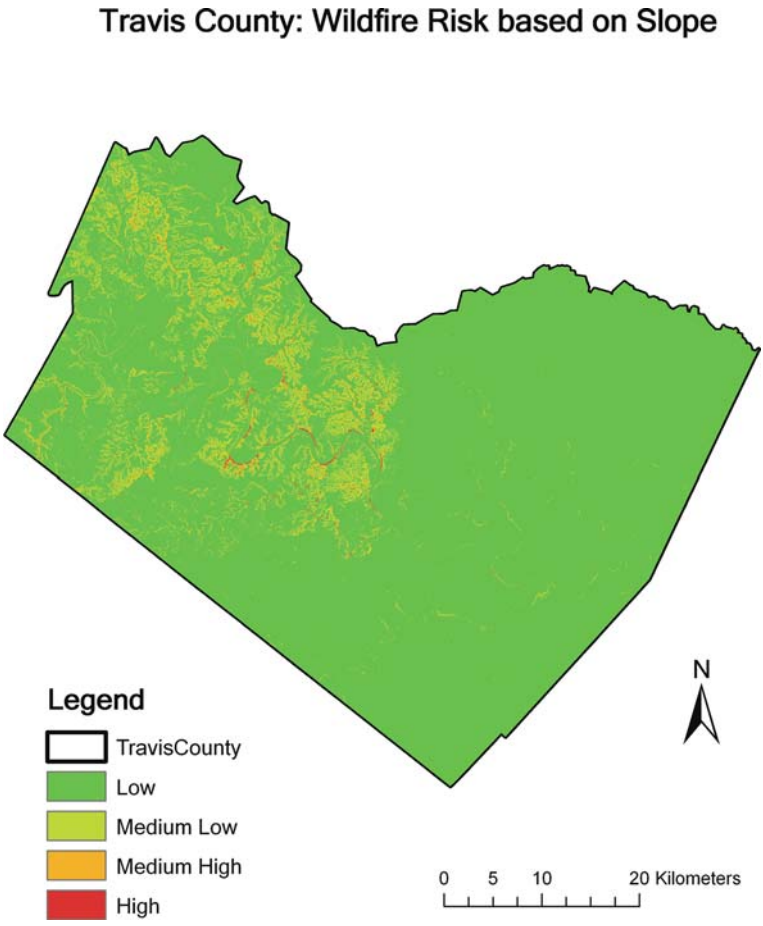

Fig. 10.6 Travis County wildfire risk ranking based on slope

High level for fire risk, with about 30% of the vacant lands located in relatively high fire risk zones. As population and housing move onto these lands, the potential loss from fire increases. Although new development on vacant lands may reduce vegetation density on the land parcel and the areas immediately surrounding it, the fire risk for a specific parcel is unlikely to change dramatically until significant change happens over a larger spatial extent. Thus, land use management designed to improve fire damage control on these vacant parcels, especially those located within the relatively high-risk zones for wildfire, is critical. Figure 10.10 provides a visual display of the spatial relationship between the vacant lands and their calculated fire risk levels.

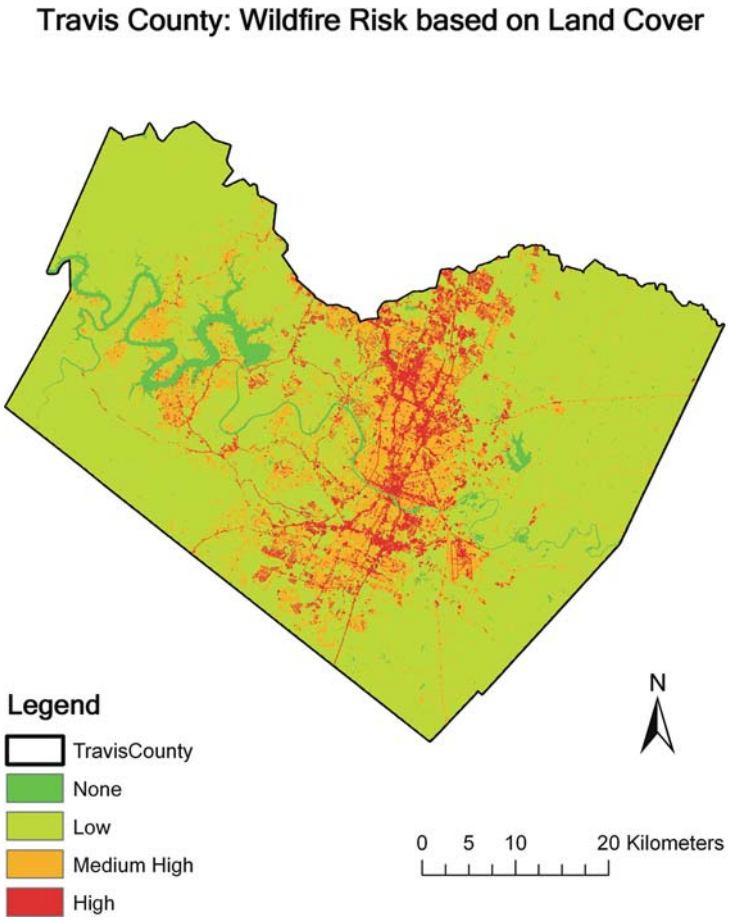

Fig. 10.7 Travis County wildfire risk ranking based on reclassified and cover

Table 10.4 Final wildfire risk ranking for the study area

Risk level	Low	Medium-low	Medium	Medium-high	High
Original combined risk value	2, 3	4, 5	6, 7	8, 9	10, 11, 12
New reclassified risk value	1	2	3	4	5
Areal percentage in Travis County (%)	15.12	42.72	33.46	8.64	0.06

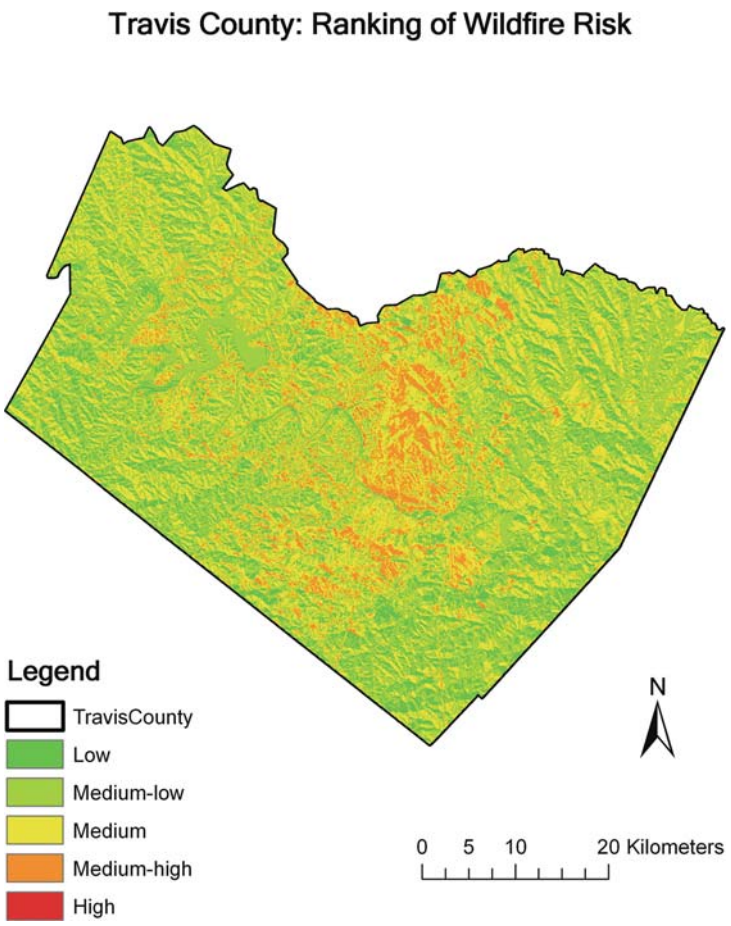

Fig. 10.8 Travis County wildfire risk ranking–overall

10.6 Risk of Wildfires in WUI Areas

As discussed earlier, wildland urban "Interface" and "Intermix" areas were defined following Radeloff et al. (2005) and Stewart et al. (2007). The definition groups all of the census blocks in Travis County into three different types: Interface, Intermix, and non-WUI blocks. Using the zonal statistics function in GIS, census block boundaries were used to define the zones belonging to the different types of WUI areas. The zonal statistics function calculates statistical indicators for all of the raster cells that are within the same zone – the same type of census block in this case. The wildfire risk level indicators derived for each type of census block are: minimum, maximum, mean, and median risk levels, standard deviation of the risk levels, and the majority of the risk levels. Due to space limitations, data for all 11,292 census

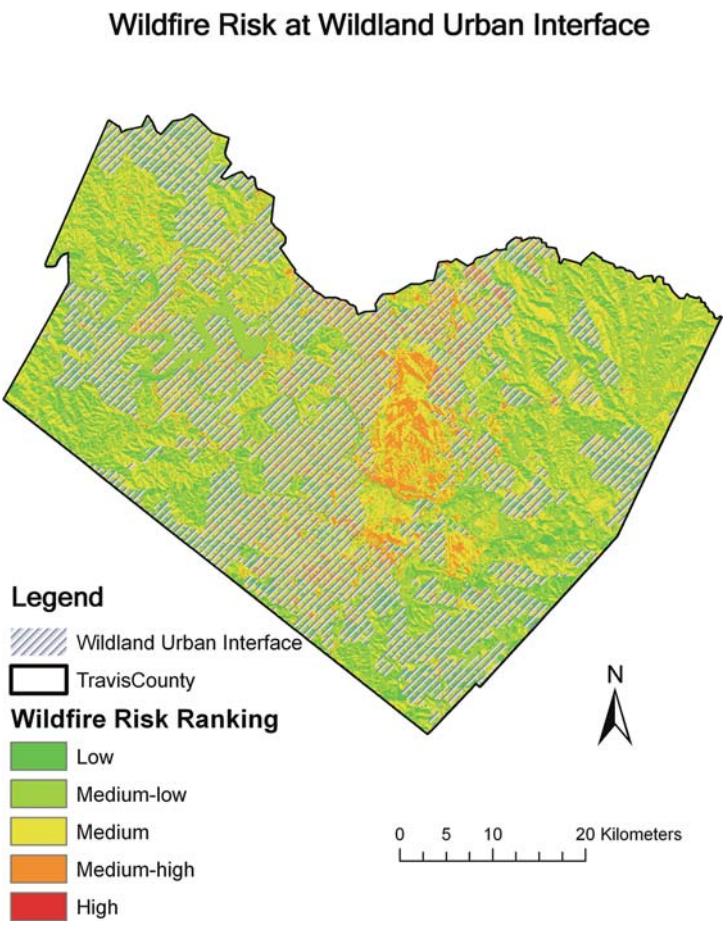

Fig. 10.9 WUI in Travis County and their wildfire risk

blocks are not reported here (but are available from the authors). Instead, Table 10.5 summarizes the different types of census blocks, classified according to their WUI status. Forty-six percent of the land in Travis County is in the WUI areas. More importantly for wildfire management and control, two-thirds of the county population and two-thirds of the housing units are within the WUI areas. These data illustrate that assessing wildfire risk for communities in the WUI is critical in order to appropriately prepare for, respond to, and contain wildfires.

The zonal statistics reported in Table 10.5 summarize the wildfire risk level for census blocks that belong to the same type of WUI category as *the average of the mean*, *the average of the median*, and *the average of the majority* risk levels. Table 10.5 reveals that the high-density WUI blocks (both Interface and Intermix) support more than 30% of the total population and more than 35% of the total

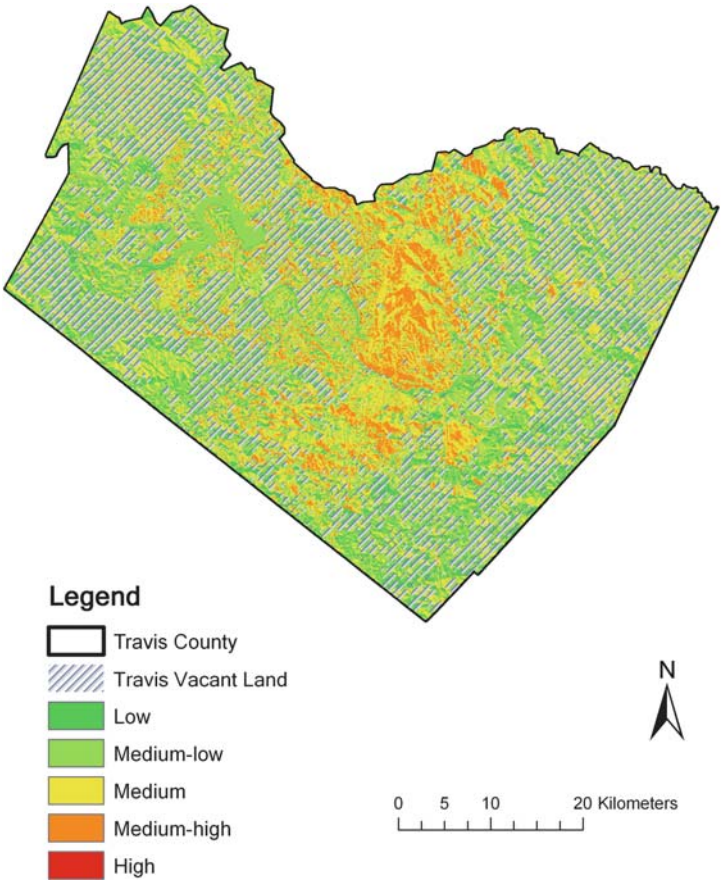

Fig. 10.10 Vacant lands in Travis County and their wildfire risk

housing units in the County. The Table also reveals that, despite the fact that the mean, median, and majority are different ways to represent fire risk for the many cells within each block, the average for the blocks belonging to the same WUI category can serve as an indicator of wildfire risk for each type of WUI area. It is a general trend that the wildfire risk increases from low-density WUI (both interface and intermix) through medium-density to high-density WUI blocks. This trend implies that within the WUI area, the higher the housing (and population) density, the higher the wildfire risk. In addition, compared to the non-WUI areas, blocks within low and medium density WUI areas are at lower risk for wildfire but the blocks within the high density areas are at much higher risk.

To confirm that the above observation was not spurious, further statistical analyses were applied to test for differences in fire risk levels in the different areas. Three statistical indicators for areal fire risk level were examined – the average

Table 10.5 Statistics for the different types of census blocks according to their WUI status

	WUI: interface			WUI: intermix				
	Low density	Medium density	High density	Low density	Medium density	High density	Not WUI	Total
Population size (%)	4463 (0.55)	102,631 (12.63)	209,856 (25.84)	28,137 (3.46)	127,520 (15.70)	65,522 (8.07)	274,151 (33.75)	812,280 (100)
Housing units (%)	1468 (0.44)	39,808 (11.85)	88,281 (26.28)	10,922 (3.25)	50,905 (15.16)	30,831 (9.18)	113,666 (33.84)	335,881 (100)
Number of blocks (%)	119 (1.05)	1665 (14.74)	1814 (16.06)	458 (4.06)	1127 (9.98)	437 (3.87)	5672 (50.23)	11,292 (100)
Area (km^2) (%)	1014 (3.56)	1295 (4.55)	707 (2.48)	6804 (23.91)	3126 (10.98)	252 (0.88)	15,259 (53.62)	28,456 (100)
Average mean risk level	2.80	2.92	3.11	2.41	2.71	3.20	3.04	
Average median risk level	2.80	2.95	3.12	2.41	2.73	3.27	3.04	
Average majority risk level	2.87	2.96	3.13	2.41	2.72	3.27	3.04	

of block mean fire risk, the average of block median fire risk, and the average of block majority fire risk. Non-parametric tests were conducted to compare the fire risk levels for: (1) WUI versus non-WUI areas, (2) high-density versus medium-density versus low-density WUI and non-WUI areas, and (3) high-density-interface versus medium-density-interface versus low-density-interface versus high-density-intermix versus medium-density-intermix versus low-density-intermix WUI and non-WUI areas. A Mann–Whitney (M–W) test and multiple Kruskal–Wallis (K–W) tests were conducted; the M–W test seeks to identify if there is a real difference between the scores of two samples. For example, if observations from two entirely different samples are ranked and mixed together, ranks from one sample should cluster on one end of a scale while ranks from the other sample should cluster on the other end. K–W is an extension of the M–W test to three or more groups of observations (Gravetter and Wallnau 1998; Ott 1984). The results from these two tests are reported in Table 10.6. All three indicators (mean, median, average of majority) are statistically different for the test groups at the 0.01 significance level. These non-parametric tests confirm that the fire risk levels in different types of WUI and non-WUI areas, as measured by each of the three tested indicators, are significantly different.

Examining Table 10.6, the M–W test comparing fire risk levels for WUI and non-WUI areas produced a low average fire risk within the WUI. This result may be due to the large number of Low- and Medium-density WUI blocks (with their associated relatively low fire risk) – 29.83% of the blocks classified as Low or Medium-density WUI, only 19.93% of the blocks classified as High.

Table 10.6 Results of the Mann-Whitney and Kruskal-Wallis tests

	Definition of groups	Average of the mean of risk levels	Average of the median of risk levels	Average of the majority of risk levels
Mann-Whitney	WUI blocks	5285.96	5413.35	5422.18
	Non-WUI blocks	6003.74	5877.51	5868.76
	Z value	−11.70*	−8.21*	−7.85*
Kruskal-Wallis (df = 3)	High-density WUI	6382.05	6293.05	6265.58
	Medium-density WUI	4853.50	5085.08	5106.15
	Low-density WUI	3102.48	3596.86	3661.20
	Non-WUI	6003.74	5877.51	5868.76
	Chi-Square	699.80*	511.44*	463.20*
Kruskal-Wallis (df = 6)	High-density interface WUI	6293.87	6177.63	6149.85
	Medium-density interface WUI	5278.81	5434.64	5470.03
	Low-density interface WUI	4728.34	4795.80	5066.68
	High-density intermix WUI	6748.08	6772.16	6745.97
	Medium-density intermix WUI	4225.15	4568.65	4568.55
	Low-density intermix WUI	2680.03	3251.33	3296.02
	Non-WUI	6003.74	5877.51	5868.76
	Chi-Square	814.22*	606.13*	569.08*

* Indicating significance level of 0.01.

In the K–W test for High versus Medium versus Low-density versus Non-WUI blocks, the Medium and Low-density WUI blocks show considerably lower fire risk than the Non-WUI blocks; but the High-density WUI blocks have much higher fire risk levels than the Non-WUI or other types of WUI blocks. More specifically, as the housing density in the WUI increases, the risk level for wildfire rises sharply. The fire risks in High-density Interface and High-density Intermix areas are significantly higher than all other types of blocks. Moreover, among all the different types of blocks, those in High-density Intermix WUI areas show the overall highest risk for wildfire, higher than those in the High-density Interface areas. Following the definition of High-density Intermix WUI, these blocks are in areas where vegetation covers more than 50% of the land and where the housing density is greater than 741 housing units per km^2. This finding confirms that the fire risk is highest where population and wildland are well-mixed. The large amount of vegetation in these High-density Intermix areas provides the fuel while the high density of housing units puts these blocks at high risk for property damage and loss of life from wildfires.

10.7 Limitations and Recommendations

The research presented here is not without its limitations. For example, wind speed/direction data are important elements when attempting to understand the potential for wildfire spread and duration. While we were able to locate county-wide data reporting monthly changes in wind direction and speed, we were unable to locate data regarding wind conditions at a finer resolution. In order to assess spatial variation in fire risk within/across the county, weather data at a higher spatial resolution is required. General weather conditions through time were also not incorporated into this study – if such information were included, it could add another layer of specificity to the findings.

While forest structure and canopy closure data are frequently incorporated into fire ignition models (Cova et al. 2004), they were not used here due to lack of availability. Other researchers have included road networks, distance to roads, and distance to agricultural fields in their research examining WUI wildfire potential (Perestrello de Vasconcelos et al. 2001). While the use of such data was outside the scope of this paper, they have the potential for revealing interesting spatial patterns if utilized in future research.

Two drawbacks concerning the use of census data must also be recognized. First, such data has limited spatial resolution in exurban areas (where census units can be very large). Second, the census is performed on a decadal basis, therefore has limited temporal resolution during which significant changes can occur (Cova et al. 2004).

The definition of WUI as used in this paper could also be flawed because it is not specific to Central Texas. The housing density criteria used to define the different types of WUI areas were developed based on the nationwide housing density situation in the US; the definition of WUI Interfaces as within 2.4 km of highly vegetation-covered area is based on the firebrand-carrying distance estimated from California data (Radeloff et al. 2005). Firebrands from grassland and bush fires, or from the less dense forest fires of Central Texas may behave differently than those on the west coast.

Given the above, it is recommended that future research consider incorporating the following data to further refine the results: (1) wind speed and direction at a scale finer than county-level, (2) meteorological data (e.g., humidity), (3) forest structure/canopy closure, (4) road networks, (5) distance to roads from ignition points, (6) distance to agricultural fields from ignition points, (7) finer resolution census data (perhaps by performing a survey of residents within their study area, or by processing recently acquired aerial imagery), and finally (8) a WUI definition specific to a study area.

10.8 Conclusion

The increased pace of development in fire-prone areas and exposure of new housing stock to wildfire poses a challenge for land use managers and emergency management officials (Cova et al. 2004). These managers need tools to help them plan for,

and thus mitigate, potential wildfires occurring in their areas of responsibility. With the goal of making new developments *disaster resilient*, it becomes imperative for decision makers to plan for the eventuality of wildfires, rather than simply responding to such fires when they occur (Godschalk et al. 1999).

This study assesses wildfire risk for Travis County, Texas. Historical wildfire data was linked to land cover to estimate the occurrence potential of wildfires on different types of land cover. The results were combined with the wildfire risk estimation derived from topographic characteristics. The final wildfire risk assessment was then related to Travis County's wildland urban Interface (WUI), an area recognized as being at higher risk for wildfire. Although the WUI blocks were not, as a group, subject to a higher fire risk level than the non-WUI blocks, it was confirmed that the high-density WUI areas have much higher fire risk levels than the medium- and low-density WUI blocks or the non-WUI blocks. This interesting pattern may signify the contribution of human activities to the ignition of wildfires – the high-density WUI areas are where sufficient vegetative supplies co-exist with more human activities while the low- and medium-density WUI areas lack human activities. This finding might indicate one "side-effect" of exurbanization in the study area. Exurbanization has been a trend in north America where many middle-class families move into areas that are outside of the city to be closer to nature but are still within commuting distance to the central city (Esparza and Carruthers 2000; Davies and Yeates 2008). Considering that the high-density WUI blocks (both Interface and Intermix) support more than 30% of the total population and more than 35% of the total housing units in Travis County, it is critical that appropriate measures be implemented in these areas to reduce the possibility of wildfire.

Further, the study discovered that the fire risk level in high-density-intermix WUI blocks is higher than that found in high-density-interface WUI blocks. Vegetation coverage is generally denser in WUI Intermix than WUI Interface areas. Therefore, in addition to human activity levels, the supply of fuel is an important factor when calculating fire risk. It can be concluded that as human activities rise in WUI areas (as indicated by increased housing density), controlling the vegetation supply might be an effective tool for fire risk management. Finally, with nearly 30% of the vacant land located in relatively high fire risk zones (especially when many of them are in the UWI areas) it is imperative to employ conscientious planning and preventive measures as development proceeds into these lands.

In 1999, Godschalk et al. wrote, "... geographic information systems and computer models ... [can] assist in guiding new development to safe locations ..." (p. 532). During the past two decades there has been an explosion in the use of GIS by private and governmental entities accompanied by enormous public exposure to maps and images produced by these systems. It is in this setting that we echo Franklin et al. (2000) who wrote that, "these types of analyses are [not only] essential for spatial decision support related to fire management, suppression, prevention, and land-use planning related to fire risk" (p. 1211), but are also becoming routinely expected from an increasingly sophisticated public.

Ultimately, effective mitigation programs must engage the participation of local governments, NGOs, private organizations and individual households (Godschalk

et al. 1999). Wildfire risk analyses such as the one demonstrated in this paper generate informative and compelling maps that can be used to encourage conscientious urban development, regulation of the WUI, scientific management of urban vacant lands, and the participation of local landowners in the protection of their property. These activities are integral necessities if Central Texas' communities are to be prepared for future wildfires.

References

Bradstock, Ross A., Jann E. Williams, and Malcom A. Gill (eds). 2002. *Flammable Australia: The Fire Regimes and Biodiversity of a Continent.* Cambridge University Press: Cambridge, United Kingdom.

Capitol Area Council of Governments (CAPCOG). 2008. Information Clearinghouse-Geospatial Data. http://www.capcog.org/Information_Clearinghouse/Geospatial_main.asp; last updated 2008. Accessed June 25, 2008.

Carapella, Ruth. 1996. Assessing fire risk using a GIS-based approach. *Earth Observation Magazine* 5(8): 22–24.

Cardille, Jeffrey A., Stephen J. Ventura, and Monica G. Turner. 2001. Environmental and social factors influencing wildfires in the Upper Midwest, United States. *Ecological Applications* 11: 111–127.

Christiansen, Julia. 2005. Calculating wildfire hazard levels: Algebraic raster construction using spatial analyst. Paper presented at *ESRI International User Conference,* San Diego, California, July.

Cohen, Jonathan D. 2000. Preventing disaster: Home ignitability in the wildland-urban interface. *Journal of Forestry* 98(3): 15–21.

Colorado State Forest Service (CSFS). 2007. Wildfire. Colorado State Forest Service, Colorado State University, Colorado Springs. http://csfs.colostate.edu/wildfire.htm; last updated October 8. Accessed April 14, 2008.

Cortner, Hanna J., Philip D. Gardner, and Jonathan G. Taylor. 1990. Fire hazards at the urban-wildland interface: What the public expects. *Environmental Management* 14(1): 57–62.

Cova, Thomas J., Paul C. Sutton, and David M. Theobald. 2004. Exurban change detection in fire-prone areas with nighttime satellite imagery. *Photogrammetric Engineering & Remote Sensing* 70(11): 1249–1257.

Davies, S. and Maurice Yeates. 2008. Exurbanization as a component for migration: A case study in Oxford County, Ontario. *Canadian Geographer* 35(2): 177–186.

Davis, James B. 1990. The wildland urban interface: Paradise or battleground? *Journal of Forestry* 88(1): 26–31.

Dennison, Philip E., Thomas J. Cova, and Max A. Mortiz. 2007. WUIVAC: A wildland-urban interface evacuation trigger model applied in strategic wildfire scenarios. *Natural Hazards* 41(1): 181–199.

Esparza, Adrian X. and John I. Carruthers. 2000. Land use planning and exurbanization in the rural mountain west. *Journal of Planning Education and Research* 21(1): 23–36.

Ewert, Alan W. 1993. The wildland urban interface: Introduction and overview. *Journal of Leisure Research* 25: 1–5.

Finney, Mark A. 2005. The challenge of quantitative risk analysis for wildland fire. *Forest Ecology and Management* 211(1–2): 97–198.

Franklin, Janet, Curtis E. Woodcock, and Ralph Warbington. 2000. Multi-attribute vegetation maps of forest service lands in California supporting resource management decisions. *Photogrammetric Engineering & Remote Sensing* 66 (10): 1209–1217.

Godschalk, David R., Timothy Beatley, Philip Berke, David J. Bower, and Edward J. Kaiser. 1999. Natural hazard mitigation: Planning for sustainable communities. In, *Natural Hazard Miti-*

gation: Recasting Disaster Policy and Planning, Chapter 13, pp. 525–552. Washington, DC: Island Press.

Gravetter, Frederick J. and Larry B. Wallnau. 1988. *Statistics for the Behavioral Sciences, 2nd Edition*. St. Paul, New York, Los Angeles, San Francisco: West Publishing Company.

Idaho Department of Lands (IDL). 2006. Summaries of risk and preparedness. *Jerome County WUI Wildfire Mitigation Plan*, Chapter 4, pp. 69–91. http://www.idl.idaho.gov/nat_fire_plan/county_wui_plans/jerome/jerome.htm; last updated November 11. Accessed June 25, 2008.

Ingalsbee, Timothy. 2003. Fuel breaks for wildland fire management: A moat or a drawbridge for ecosystem fire restoration? *Second Annual Wildland Fire Ecology and Fire Management Congress*, Orlando, FL, November 16–20, p. 1F.2. http://ams.confex.com/ams/FIRE2003/techprogram/paper_66008.htm; last update unknown. Accessed June 25, 2008.

Johnson, Angie. 2008. Mapping at local scale for CWPPs. Powerpoint presentation, 2008 Collaboration Workshop–Bringing it all Together, Reno, NV, March 3–4. Healthy Forests and Rangelands: Managing our National Heritage (US Department of Interior and Department of Agriculture). http://www.forestsandrangelands.gov/news/cwpp_workshop_2008.shtml; last updated April 15. Accessed June 25, 2008.

Keeney, Ralph L. 1995. Understanding life-threatening risks. *Risk Analysis* 15(6): 627–637.

Larkin, Thomas J. and George W. Bomar. 1983. *Climatic Atlas of Texas*. Texas Department of Water Resources, Austin, Publication No. LP-192, December. http://www.twdb.state.tx.us/publications/reports/GroundWaterReports/LimitedPublications/LP192.pdf, last update unknown. Accessed June 25, 2008.

Lawrimore, Jay. 2005. Climate of 2000- July Western U.S. wildfires. National Oceanic and Atmospheric Administration, National Climatic Data Center. http://lwf.ncdc.noaa.gov/oa/climate/research/2000/jul/west_fires.html; last updated June 25. Accessed May 3, 2008.

Lindley, T. Todd, Jared L. Guyer, Gregory P. Murdoch, Seth R. Nagle, Kenneth J. Schneider, and Gary D. Skwira. 2007. A Meteorological Composite of the 2005/06 wildfire outbreaks in the Southern Plains. Paper Presented at the Seventh Symposium on Fire and Forest Meteorology, Bar Harbor, ME, October 23–27, p. 10.4. http://ams.confex.com/ams/pdfpapers/126810.pdf; last update unknown. Accessed June 5, 2008.

Manzello, Samuel. 2007. Fires in the wildland-urban interface–experimental investigation of structural ignition in WUI fires. Project Information, Building and Fire Research Laboratory, National Institute of Standards and Technology. http://www2.bfrl.nist.gov/projects/projcontain.asp?cc=8662014000; last updated October 29. Accessed June 5, 2008.

National Interagency Fire Center (NIFC). 2006. Fire Information: Wildland fire statistics. National Interagency Fire Center, Boise, Idaho. http://www.nifc.gov/fire_info/historical_stats.htm; last update unknown. Accessed May 13 May, 2008.

Ott, Lyman. 1984. *An Introduction to Statistical Methods and Data Analysis*, 2nd Edition. Boston: Duxbury Press.

Perestrello de Vasconcelos, Maria José, Sara Silva, Margarida Tomé, and José Miguel Cardoso Pereira. 2001. Spatial prediction of fire ignition probabilities: comparing logistic regression and neural networks. *Photogrammetric Engineering & Remote Sensing* 67(1): 73–81.

Pyne, Stephen J. 2001. The fires this time, and next. *Science* 294: 1005–1006.

Radeloff, Volker C., Roger B. Hammer, Susan I. Stewart, Jeremy S. Fried, S.S. Holcomb, and Jason F. McKeefry. 2005. The wildland-urban interface in the United States. *Ecological Applications* 15(3): 799–805.

Silvis Lab (no date) Texas wildland-urban interface maps, statistics, and GIS data download. http://silvis.forest.wisc.edu/Library/WUI_state_download.asp?state=Texasandabrev=TX, accessed May 2008. Last update, unknown.

Smith, Keith. 2004. *Environmental Hazards: Assessing Risk and Reducing Disaster*, 4th edition. Routledge: London and New York.

Stewart, Susan, Volker C. Radeloff, Roger B. Hammer, and Todd J. Hawbaker. 2007. Defining the wildland-urban interface. *Journal of Forestry* 105(4): 201–207.

Texas Forest Service (TFS). 2007. Protecting your home against wildfires in Texas–everyone's responsibility. *Living on the Edge*, Texas Forest Service Urban Wildland Interface Publication. http://txforestservice.tamu.edu/main/article.aspx?id=1583; last updated September. Accessed May 17, 2008.

Texas Natural Resources Information System (TNRIS). 2008. National Agriculture Imagery Program (NAIP) and DOQQ Imagery. *Strat Map*, Texas Natural Resources Information System. http://www.tnris.state.tx.us/StratMap.aspx?layer=126; last update January 16. Accessed February 13, 2008.

Texas State Data Center and Office of the State Demographer (TSDC/OSD) 2006. New Texas State Data Center Population Projections from The University of Texas at San Antonio. Institute for Demographic and Socioeconomic Research (IDSER), College of Public Policy, University of Texas at San Antonio. http://txsdc.utsa.edu/tpepp/2006projections/summary/; last updated October 19; accessed June 23, 2008.

Thompson, William A., IIan Vertinsky, Hans Schreier, and Bruce A. Blackwell. 2000. Using forest hazard modeling in multiple use forest management planning. *Forest Ecology and Management* 134(1–3): 163–176.

Travis County. 2004. Travis County Parks. Travis County Transportation and Natural Resources Department. www.co.travis.tx.us/tnr/parks/climate.asp; last updated February 2. Accessed May 13, 2008.

Travis County. 2007. Section I: 2006–2010 Consolidated Plan, Amended August 2007.http://www.co.travis.tx.us/health_human_services/CDBG/August07Amendment/ConPlanAug07Amend_SectionI_Introduction.pdf; last updated August 2007; accessed October 15, 2008.

Travis County Health and Human Services and Veterans Service Department (TCHHS). 2006. American Community Survey, Travis County, Texas: Analysis of Trends 2002–2005. Research and Planning Division; http://www.co.travis.tx.us/health_human_services/research_planning/publications/ACS_2005_Report.pdf; last updated November; accessed October 15, 2008.

Trembath, Rick. 2005. Firebrands and long duration smoldering fires: What is the risk? How should we deal with them? *Wildfire News and Notes* 19(2): 2–8.

U.S. Geological Survey (USGS). No date. National Elevation Dataset. USGS Seamless Data Distribution System. http://seamless.usgs.gov/website/Seamless/viewer.htm; last update unknown. Accessed May 3.

Winter, Greg J. and Jeremy S. Fried. 2001. Estimating contingent values for protection from wildland fire using a two-stage decision framework. *Forest Science* 47(3): 349–360

Chapter 11
Early Warning of Food Security Crises in Urban Areas: The Case of Harare, Zimbabwe, 2007

Molly E. Brown and Christopher C. Funk

Abstract In 2007, the citizens of Harare, Zimbabwe began experiencing an intense food security crisis. Due to a complex mix of poor government policies, high inflation rates and production declines due to drought, the crisis produced a massive increase in the number of food-insecure people in the capital city. The international humanitarian aid response to this crisis was largely successful due to early agreement among donors and humanitarian aid officials as to the size and nature of the problem. This paper summarizes an analysis of MODIS NDVI which provided highly accurate estimates of corn production in Zimbabwe in 2007. The estimates enabled an early and decisive movement of resources, supporting the timely delivery of food aid to food insecure residents in Harare. Remote sensing data provided a clear and compelling assessment of significant crop production shortfalls, which gave donors of humanitarian assistance a single number around which they could come to agreement. This use of satellite data typifies how remote sensing may be used in early warning systems to identify food security crises in Africa.

Keywords Food security · MODIS · NDVI · Crop models · Zimbabwe · Early warning systems

11.1 Introduction

Africa has experienced rapid urbanization over the past three decades, but unlike many areas of the world, this transition has not been accompanied by strong economic growth. Over the 1970–1995 period, the average African country's urban population grew by 5.2% per annum while its GDP declined by 0.66% per year (Hicks 2002). Urban growth without increasing prosperity has failed to spur agricultural modernization. Supplying growing numbers of poor urban Africans with safe and affordable food will necessarily strain the food production and distribution

M.E. Brown (✉)
NASA Goddard Space Flight Center, Greenbelt, MD, USA
e-mail: molly.brown@nasa.gov

P.S. Showalter, Y. Lu (eds.), *Geospatial Techniques in Urban Hazard and Disaster Analysis*, Geotechnologies and the Environment 2, DOI 10.1007/978-90-481-2238-7_11,

system in Africa now and in the future, particularly in poorly managed economies. Zimbabwe, a country experiencing nine digit inflation, provides a compelling example. This chapter focuses on Zimbabwe's capital city, Harare, and the role that remote sensing has played in identifying and responding to food security crises in the city (Fig. 11.1). Driven largely by government policies, the economic crisis has transformed the country from a net exporter of food to a net importer. Extremely high rates of inflation have increased the vulnerability of the residents of Harare to climate-related food production declines by reducing their ability to import food from outside of the country to augment food grown locally. Although farmers are hard hit by inflation, wage earners in urban areas are particularly sensitive to the continued erosion of their income. In response to this crisis, regional food security organizations including the Famine Early Warning Systems Network (FEWS NET) set up a new monitoring program in Harare to monitor the ability of residents to access enough food.

Analysis of corn production in rural areas of Zimbabwe is central to the effort to determine how vulnerable urban residents are to food insecurity. Economic and policy changes by the Zimbabwean government in the past five years have caused significant declines in the productivity of farms, reducing the amount of land under cultivation, delaying the distribution of seed at the beginning of the season, reducing

Fig. 11.1 Digital Globe imagery of Harare, Zimbabwe, a city with approximately 2.8 million residents in the larger metropolitan area

the amount of fertilizer and pesticide available to farmers and greatly restricting the amount of fuel available for farm machinery. Remote sensing techniques that enable direct identification of cultivated land and its productivity and analysis that relates these to annual food requirements are critical tools in the effort to determine urban resident's vulnerability to hunger. Having a reliable, independent estimate of national grain production for the official United Nation's estimate was a critical element in determining the level of support that would be needed by the end of 2007.

This chapter first presents a description of the FEWS NET system and how it is used to collect data to determine residents' needs. A description of food security issues in urban areas (focusing on Harare) follows, examining the role remote sensing can play when dealing with issues concerning national and regional food production and urban food security. Finally, a description of how remote sensing was used to determining Harare's 2007 food aid needs is provided, along with the techniques used to estimate variations in agricultural production.

11.1.1 The Famine Early Warning Systems Network (FEWS NET)

FEWS NET is a program funded by the US Agency for International Development (USAID). FEWS NET is tasked with monitoring food security in 23 countries, and is composed primarily of local experts who work with specialists in the United States who coordinate their reporting. The organization estimates local food availability, access, and utilization with a wide variety of datasets, including remote sensing data, ground measurements of food production measuring "supply", and a wide range of other indicators meant to measure "demand" (the ability of a population to purchase food) in concert with political and economic pressures that may affect a region's food security (Brown 2008). FEWS NET's objective is to provide early and actionable information that can motivate intervention to break the link between climate extremes and famine (Davies et al. 1991; Wisner et al. 2004). This chapter describes how remote sensing provided the earliest possible estimate of a national-level food security problem and motivated a prompt and effective response from the humanitarian community to forestall a situation that could have severely affected Zimbabwe's residents.

Because FEWS NET usually focuses on rural areas, its food security monitoring system in Harare is unique. In the urban context, understanding how different economic groups earn income and gain access to food is the basis for evaluating food security. Urban consumers obtain most or all of their food from the market, and thus rely on regional and national food production and distribution systems to ensure there is sufficient food available for purchase. National production deficits can be compensated for with imports from other regions or from outside the country, but purchasing food from outside of the country requires foreign currency. If there is insufficient foreign currency, a lack of political will, or inadequate organization to move food from regions of surplus to regions of deficit, then urban areas are likely to experience scarcity and rapidly increasing food prices, resulting in food insecurity.

11.2 Background

In the 2006/2007 growing season, Zimbabwe's farmers produced less than expected, and significantly less than the long-term average. Land redistribution and other agricultural policies, in concert with the unavailability of, or poor access to, critical inputs such as fertilizers, improved seeds, fuel, electricity, labor and draft power (Fig. 11.2) aggravated the situation. Poor rainfall in the south exacerbated these larger problems, but it was unclear at the time exactly how much food was actually produced. Estimates suggested that the harvest provided 45% of Zimbabwe's cereal needs, which left the country with an estimated import requirement of over 610,000 metric tons (mt) for 2007. The extent of the problem in 2007 was difficult to determine because the government of Zimbabwe was blaming the crisis on hostile foreign governments, including the United States. Even if they were available, the likelihood that the Zimbabwean internal agricultural production figures were accurate and reliable was extremely unlikely. Since every province in the country faced a cereal deficit, urban residents were likely to find it a particularly difficult to access food due to extremely high inflation coupled with high international food prices and uncertain grain imports from other countries. Consequently, to determine the scope of necessary food aid interventions from the international community, remote sensing-based production estimates were critical.

In a rural setting, food security analysis focuses on sources of food and income for different wealth groups. This focus is appropriate because members of a particular wealth group generally share the same level of food security and a similar limited set of options for obtaining food and income. Members of these groups pursue similar strategies at different times of year. The relative homogeneity of rural livelihoods makes enquiry into sources of food and income the most efficient way to generate a rapid understanding of food security in a rural context (FEWS 2000b).

The same level of homogeneity within wealth groups is generally not found within an urban setting. Here, one source of food – the market – is usually predominant and so the focus of enquiry generally shifts towards questions of cash

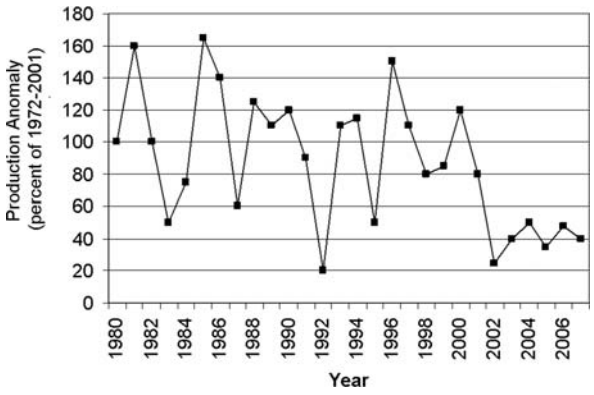

Fig. 11.2 US Department of Agriculture production statistics for Zimbabwe, expressed as a percentage of the 1972–2001 mean. Note the distinctly lower production from 2001 to 2007 as compared to before 2001

income and expenditure. Urban settings also offer a wider range of income sources for any one wealth group, and earnings are less regular than in the countryside. While incomes tend to be heterogeneous in urban settings, patterns of expenditure do not. Poor families tend to spend similar amounts of money on similar things, so that an enquiry into patterns of expenditure is often the most useful approach for establishing an effective baseline for food security monitoring in an urban setting. Since urban economies are primarily market-based, and many of life's essentials, often not paid for in a rural setting (i.e. accommodation, water, firewood) have to be purchased in the town, food security analysis thus focuses on these non-food elements (King et al. 2001).

During an initial assessment conducted in 2001, households were surveyed to determine issues that impact food consumption. Households were clear about the types of shocks that cause problems: inflation and the fact that residents are constantly battling to keep up with rising prices (Fig. 11.3), currency devaluation, increases in housing rents and electricity costs, and rising bus fares were all issues. Vulnerability to widespread scarcity in food due to drought is far higher when inflation is rampant.

In response to these types of shocks, households engage in a number of coping strategies. Most coping strategies are dependent on a household's own human and material resource base. To reduce expenditures, spending for, and consumption of all items is minimized, particularly for items considered non-essential. Cheaper, poorer quality food is purchased; walking or cycling is preferred to taking the bus; second-hand rather than new clothes are purchased; children and other dependants (including terminally ill people) are sent to rural areas to live with relatives; debt is accumulated on electricity, water and schooling payments; crops are cultivated; cheaper accommodation sought; and fewer meals per day con-

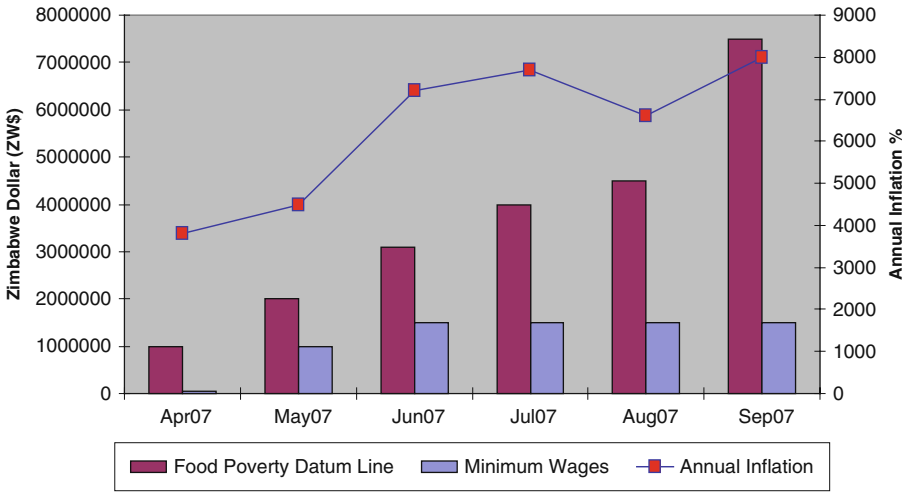

Fig. 11.3 Annual inflation compared to minimum wage of a low-income earner, indexed on the Food Poverty Line, which is calculated using market prices of a minimum basket of necessities

sumed. Attempts are made to maximize income from all sources. Those working in the formal sector initiate informal-sector activities to supplement income; children are sent out to work; gifts and loans sought from relatives; rooms rented; assets sold; and savings drawn down. Finally, as a last resort, some engage in undesirable, high-risk, or illegal activities such as begging, prostitution, or theft (King et al. 2001).

By September 2006 urban households had already exhausted food stocks from the spring growing season. After this point, the vast majority of the urban population became dependent on the market for maize and maize meal, with food access constrained by inflation, low incomes, rising unemployment, government price controls. The resultant shortages of food and other basic commodities in official markets were accompanied by exorbitant food prices in the "parallel" market, which is outside of authorized channels of trade. In November 2007, the Zimbabwean economy was stressed even further by foreign exchange shortages. As part of the monitoring that FEWS NET had been conducting in Harare, price trends of selected basic food items were recorded. Many goods had to be purchased on the parallel market, where prices had increased from 100 to 800% between October and December 2007, with little improvement anticipated until government policies change.

11.3 Food Availability in 2007

In April of 2007, the UN Food and Agriculture Organization (FAO) provided funds to Zimbabwe's Ministry of Agriculture to conduct a national multi-stakeholder crop assessment in May 2007. The assessment was required in order to move forward on appeals for assistance for the country. Immediately following the assessment the Government of Zimbabwe declared the drought a disaster and subsequently invited the joint FAO and WFP Crop and Food Supply Assessment mission (CFSAM) to verify the 2006/2007 crop production. After its in-country consultations and field work, the mission revised the government's cereal harvest estimates upwards because of improvements in crop performance prospects brought about by better than expected rainfall amounts and distribution towards the end of the 2006/2007 rainfall season.

The government's cereal production estimate for the 2006/2007 agricultural year was the lowest of the previous four years. The estimated production was about 59% of the average maize, sorghum and millet harvests for the past five years and 45% of the previous year's production estimate of the four staple crops. Taking the government's cereal estimate as the worst-case scenario, combined with carry-over stocks of 153,000 mt of maize, Zimbabwe faced a cereal deficit of 1,050,000 mt in the 2007/2008 consumption year. In terms of rainfall performance, the 2005–2006 season was a relatively good year, and although there were no reliable estimates of on-farm stocks from that harvest, anecdotal evidence showed that some on-farm carry-over stocks existed. The 2006 Zimbabwe Vulnerability Assessment Commis-

sion assessment estimated that only about 6% of rural households produced in that year than enough to take them to the current harvest (Table 11.1). Agricultural production in 2006/2007 was thus critical to national food security. Due to the relatively weak purchasing power residents of Harare, even small national deficits would have significant negative impact on the food security of those living in the capital city.

Table 11.1 Main cereal harvest estimates for 2006/2007 compared to recent seasons' harvests and their implications for national cereal availability, in thousands

Staple cereals balance sheet						
Year	2002	2003	2004	2005	2006	2007
Estimated cereal production	641	1172	1882	971	1648	739
Estimated national requirement	1897	1897	1905	1913	1923	1923
Estimated deficit	−1256	−725	−23	−942	−275	−1184
Percentage total Gap	−66	−38	−1.18	−49.24	−14.31	−61.57
Percentage gap human only	−58	−24	21.1	−37.9	4.8	−53.0

11.4 The Emergence of a Crisis

In the past, Zimbabwe as a whole coped well with rainfall fluctuations, even though they resulted in large variations in food production due to the predominance of rainfed agriculture. During the 1980s and 1990s, Zimbabwe was food self-sufficient and exported surpluses to its neighbors in southern Africa and beyond, producing significant export income. The country survived the droughts of 1982, 1987 and 1992 without substantial disruptions of economic activity (Mudimu 2002). Therefore, the rainfall deficit and drought currently being experienced in Zimbabwe does not explain the country's current vulnerability to food insecurity.

In 2000, Zimbabwe began implementing land reform policies that transferred farms from minority white commercial farmers to majority landless blacks. Although the policies were implemented to improve the equity of land ownership within the country, they have had a severely negative effect on the economy. Land redistribution caused a complete cessation of organized farming in formerly commercial farm areas that had produced enormous amounts of surplus food every year. Before land reform, organized commercial farmers utilized sophisticated technology and high levels of fertilizer and seed inputs to produce very high yields. The landless people who were resettled on the farms were not provided with the tools, seeds, or know-how needed to tend the farms properly and have been barely able to grow enough food to feed themselves. In 2005, the government exacerbated the economic crisis by demolishing illegal shantytowns on the outskirts of Harare. By demolishing swathes of informal urban settlements, Zimbabwe must now cope with an estimated population of 570,000 internally displaced people (IDP), as estimated by the Internal Displacement Monitoring Centre in 2007.

By the summer of 2007, Zimbabwe's inflation rate was the highest in the world, reaching more than 1000% per month (FEWS 2008). Erratic rainfall in the 2006/2007 growing season exacerbated production declines, forcing a larger por-

tion of the population to turn to markets for food, and greatly increasing prices in Harare and other urban areas. In March 2007, a meeting was held in Rome, Italy by the major partners concerned with food security in Zimbabwe (USAID, World Food Program [WFP], Southern African Development Council, US Department of Agriculture [USDA], the European Commission, European Global Monitoring for Food Security [EGMFS] and the European Union's Joint Research Council [JRC]) to come to a consensus about Zimbabwe's food security situation, what could be done to assist the country, and develop a general plan for how the humanitarian community should proceed. FEWS NET was able to provide meeting attendees an estimate of area planted, and maize yield/production estimates for the 2006–2007 growing season. The estimates showed that Zimbabwe's crop production was going to fall far below the levels necessary to provide adequate food for its citizens.

As it became clear that food aid would be needed in 2007, the question was how much assistance was appropriate. Zimbabwe's national government was unwilling to admit there was a food security problem or that its agricultural policies were unsuccessful, therefore the production/planting data released by the country in 2007 was suspect. Although crop areas in the north of the country had a very good rainy season that year, southern portions were experiencing drought and crop failure. Because of the agricultural production deficits, Zimbabwe needed to import grain, but how much grain was needed?

Having a reliable, independent estimate of national grain production for the Rome meeting was a critical element in determining the level of support that would be needed by the end of 2007.

11.5 Remote Sensing Data to Estimate Maize Production

FEWS NET routinely uses Normalized Difference Vegetation Index (NDVI) images to identify areas experiencing drought-related reductions in production, as well as poor pasture conditions (Field 1991; Hutchinson 1998; FEWS 2000a), malaria (Hays et al. 2002), epizootic diseases such as Rift Valley Fever (RVF) (Linthicum et al. 1999), and damaging pests such as locusts (Hielkema et al. 1986; Tucker et al. 1985). The NDVI is formed using the following equation, where NIR is near infrared light and VIS is visible light:

$$\mathrm{NDVI} = \frac{\mathrm{NIR} - \mathrm{VIS}}{\mathrm{NIR} + \mathrm{VIS}}$$

NDVI is related to vegetation vigor, because leaves that are photosynthesizing reflect 20% or less of light in the $0.5-7\ \mu$m range (green to red) but absorb light at about 60% in the $0.7-1.3\ \mu$m range (near infra-red). The value is then "normalized" to the range $-1<=\mathrm{NDVI}<=1$ to partially account for differences in illumination and surface slope.

Although NDVI is useful, FEWS NET usually calculates production with crop-specific models that enable estimates of yield reduction due to variations in rainfall (Senay and Verdin 2003). FAO studies have shown that rainfall can be related to

crop production using a linear yield reduction function specific to a crop (Doorenbos and Pruitt 1977; Frere and Popov 1986). More recently, Verdin and Klaver (2002) and Senay and Verdin (2003) demonstrated a regional implementation of this linear approach in a grid cell based modeling environment using FEWS NET's Rainfall Estimate (RFE) product. The spatially explicit water requirement satisfaction index (WRSI) is an indicator of crop performance based on the availability of water to the crop during a growing season (Verdin and Klaver 2002). The WRSI measures the reduction in yield per unit area due to water deficiencies at specific stages of crop development. It does not attempt to measure any other kind of yield reduction, of which there are many. FEWS NET has operational programs that calculate the WRSI for maize (corn), millet, sorghum and rangeland grasses in Africa and Central America.

In Zimbabwe, however, these methods were systematically overestimating the amount of food produced in the country. The WRSI does not incorporate variations in amount of crop planted, farming methods, use of inputs or other possible sources of variation in production. Because of the upheaveal in Zimbabwe during the previous five years, changes in farming methods, reduction in planted area and persistent rainfall deficits in the country resulted in a reduction in production since 2002 (see Fig. 11.2). These reductions confounded the models' normal assumptions of agricultural productivity and resulted in very poor ability to estimate production (Funk and Budde 2009).

In response to these problems, the Vegetation-Sum metric was developed as an analog to the WRSI by C. Funk (coauthor of this paper) with assistance from Michael Budde at the US Geological Survey, in order to improve FEWS NET's ability to predict maize production in Zimbabwe (Funk and Budde 2007). Because the metric was based on observed greenness in cropped areas correlated to actual recent production figures, it provided a much better ability to estimate production in current years than crop models. The Vegetation-Sum calculation incorporates a lag that combines delays associated with the temporal sensitivity of crops to length of the growing season and the delayed response of vegetation to rainfall during the first few weeks after sowing (Kerr et al. 1989; Richard and Poccard 1998; Potter et al. 1999; Ji and Peters 2003; Funk and Brown 2006). Inputs to the model include Moderate Resolution Imaging Spectoradiometer (MODIS) 250 m NDVI from the MOD13 product, a detailed, 30 m crop mask for the country and estimates of cereal production for the past 15 years.

While the WRSI estimates actual evapotranspiration (ET) via an extended moisture balance, it has also been shown that MODIS vegetation indices can be a good proxy for actual evapotranspiration (Chong et al. 1993). This finding suggests that the sum of NDVI increases over the mid-to-late season growing period should be a good indicator of crop evapotranspiration. Equation (11.1) thus summarizes the approach described in Funk and Budde (2009) to estimate production using vegetation data.

$$\sum_{onset}^{onset+LGP} ET_1 \alpha \sum_V = \sum_{onset+lag}^{onset+LAP+lag} (NDVI_t - NDVI_{onset}) \qquad (11.1)$$

The Σv calculation (Eq. 11.1) incorporates the lag described above. We also include a length of accumulation period (LAP), which estimates the length of growing period (LGP). LAP determines the length of the window over which the NDVI is summed. NDVI_{onset} is subtracted from Σv to remove the pre-onset influences associated with the previous dry and rainy seasons. The dates used in this study for the onset of rains were based on a simple rainfall accounting method defined as the first 10-day period in which at least 25 mm of rain fell, followed by two 10-day accumulation periods with a total of at least 20 mm of rain. These onset periods were then linked to the closest 16-day MODIS composite period (Funk and Budde 2009).

While the equation above is physically plausible there are a number of contamination sources that can confound the potential NDVI/ET and crop productivity relationship. Temporally, cloud and moisture contamination can influence the NDVI signal. Vegetation signals from before or after the season contain variations not related to grain filling. Thus an onset-of-rains temporal re-alignment to account for some of these effects was implemented. Finally, spatial filtering was used to minimize the influence of non-agricultural vegetation on the Vegetation-Sum results. Combined with a high-accuracy cropped area map based on 30-m Landsat Thematic Mapper data, the method provided a way to calculate relative production with high accuracy.

A major problem that FEWS NET encountered in implementing this method for the 2007 growing season was that the data upon which it relies, the MODIS NDVI, was affected by a change from one processing algorithm to another in January 2007. This change meant that data from one processing scheme (Collection 4) was available from 2000 to 2006 and from an improved scheme starting in January 2007 (Collection 5). Unfortunately, the Collection 4 and Collection 5 data are not compatible over cropped areas, and FEWS NET needed a complete time series from one or the other in order to conduct its analysis. To quickly process the data in March in time for the April meeting in Rome, FEWS NET appealed to the personnel who process NASA MODIS data to conduct a special processing using the defunct MODIS Collection 4 algorithm. By communicating the urgency of the situation in Zimbabwe to NASA officials, FEWS NET was able to receive 16-day composites for the four MODIS tiles over the region for the January–April 2007 period allowing the analysis to proceed in a timely manner.

The NDVI imagery was used to produce national 2006/2007 NDVI averages (Fig. 11.3), and Vegetation-Sum production estimates. A comparison of the USDA's Foreign Agriculture Service's Production Estimates and Crop Assessments Division (PECAD) cereal production estimates against Vegetation-Sum production estimates provided a way to transform the vegetation sum metric into actual production estimates. The Vegetation-Sum metric primarily measures yield variations associated with environmental drought. Using statistics from the Government of Zimbabwe and FEWS NET, an analysis shows that the 1999–2007 period production figures and yields are highly correlated ($R^2 = 0.85$), and Vegetation-Sum tracks with both these time-series (Funk and Budde 2007). The analysis showed that the 2006/2007 cereal production was estimated to be about 35% below that of last season. Varia-

tions in area harvested are not captured with this method. In 2006/2007 reductions in cultivated area were probably responsible for a further 15% reduction in cereal production (Reynolds 2007, Results from a USDA/USAID crop tour of Zimbabwe, Unpublished report to USDA).

11.6 Discussion and Conclusions

This chapter describes the use of remote sensing data to estimate reductions in food production in Zimbabwe in 2007. By combining information regarding how urban residents access food with national food production estimates based on remote sensing, the food security situation in Harare can be estimated. The price of food in the capital city in 2007 was highly dependent on production in the rest of the country, since inflation reduced the value of the currency and hence the ability to purchase food outside the country. Sharply reduced access to normal regional trade and dysfunctional markets in the capital city amplified the effect of production deficits on urban residents. This situation accentuated the normal role of markets in redistributing food within and between regions, demonstrating the interconnectedness of food markets in the region. When a market is isolated, it means much higher prices and more difficult access to necessary commodities for consumers.

Deficits in agricultural production in Zimbabwe during the 2006/2007 period appear fairly mild when examining the past two decades of rainfall variability. The vulnerability of Harare residents to food shortages during the period was caused by economic upheaval, not by variations in rainfall. Had the rainfall deficits that occurred in 2006/2007 happened ten years earlier, little or no response would have been required of the international community. It was due to the context in which the deficits occurred that made remote sensing data central to the effort to determine early estimates of food production so that plans could be developed to provide food aid to the regions most in need.

At the time of this writing, commodity prices are at a four-decade high. Such high prices have further focused aid organizations' efforts on accurately measuring the amount of food produced as each kilogram of grain is much more highly valued. This situation has reinforced the central role of remote sensing in the effort to detect and motivate early response to food insecurity. This chapter has shown that MODIS data and the Vegetation Sum analysis produced early maize production estimates, which provided a clear and direct way to understand the scope of the local food security problem.

The vegetation sum metric was developed as an alternative to the WRSI, but there are multiple other approaches to estimating food production over large areas, including systematic on the ground surveys, statistical analysis of wholesale agents, and complex crop models, which include multiple parameters that estimate the impact of temperature, fertilizer and seed varietals. These other approaches are often very expensive and time consuming, particularly in regions experiencing upheaval or conflict. The approach taken here is simple, rapid and completely independent of the local government. This independence makes the result

far more trustworthy for international aid organizations than an on the ground assessment where government officials would have much more control over the outcome.

The situation in Zimbabwe in 2007 was a complex economic, political and environmental problem, thus providing aid on the basis of national food production deficits instead of individual or household need was an expedient and effective way to rapidly provide assistance to region in turmoil. Remote sensing analysis provided humanitarian decision makers a single number that represented an estimate of food aid need around which all parties could come to agreement. This use of remote sensing data typifies how earth science data is used in early warning systems in Africa.

References

Brown, M. E. (2008) *Famine Early Warning Systems and Remote Sensing Data*. Heidelberg: Springer Verlag.

Chong, D. L. S., Mougin, E., Gastellu-Etchegorry, J. P. (1993) Relating the global vegetation index to net primary productivity and actual evapo transpiration over Africa. *International Journal of Remote Sensing*, 14, 1517–1546.

Davies, S. M., Buchanan-Smith, M., Lambert, R. (1991) *Early Warning in the Sahel and Horn of Africa: The State of the Art Review of the Literature.* Brighton, UK: Institute of Development Studies, University of Sussex.

Doorenbos, J. and Pruitt, W. O. (1977) Crop water requirements. *FAO Irrigation and Drainage Paper No. 24.* Rome, Italy: Food and Agriculture Organization.

Famine Early Warning Systems (FEWS). (2000a) Annual performance and monitoring report for the Year 2000: FEWS NET. Washington DC: Chemonics International.

Famine Early Warning Systems (FEWS). (2000b) Assessing Urban Food Security: Adjusting the FEWS Rural Vulnerability Assessment Framework to Urban Environments. Washington DC: FEWS/ARD.

Famine Early Warning Systems (FEWS). (2008) *Price Watch: Urban Food Markets in FEWS NET Countries*. Washington DC: US Agency for International Development′s Famine Early Warning Systems Network.

Field, J. O. (1991) Beyond relief: Toward improved management of famine. In Bohle, H. G., Cannon, T., Hugo, G. I., Ibrahim, F. N. (Eds.) *Famine and Food Security in Africa and Asia: Indigenous Response and External Intervention to Avoid Hunger.* Bayreuth: Verlag.

Frere, M. and Popov, G. F. (1986) Early Agrometeorological crop yield forecasting. *FAO Plant Production and Protection paper No. 73.* Rome: Food and Agriculture Organization.

Funk, C. and Budde, M. (2007) *National MODIS NDVI-Based Production Anomaly Estimates for Zimbabwe*. Santa Barbara: University of California.

Funk, C. C. and Brown, M. E. (2006) Intra-seasonal NDVI change projections in semi-arid Africa. *Remote Sensing of Environment*, 101, 249–256.

Funk, C. C. and Budde, M. E. (2009) Phenologically-tuned MODIS NDVI-based production anomaly estimates for Zimbabwe. *Remote Sensing of Environment,* 113, 115–125.

Hays, S. I., Cox, J., Rogers, D. J., Randolph, S. E., Stern, D. I., Shanks, G. D., Myers, M. F., Snow, R. W. (2002) Climate change and the resurgence of malaria in the East African Highlands. *Nature,* 415, 905–909.

Hicks, J. F. (2002) *Sub-Saharan Africa: Enhancing the Productivity of Urban Africa*. Washington, DC: World Bank.

Hielkema, J. U., Prince, S. D., Astle, W. L. (1986) Rainfall and vegetation monitoring in the Savanna zone of the Sudan using the NOAA AVHRR. *International Journal of Remote Sensing*, 7, 1499–1513.

Hutchinson, C. F. (1998) Social science and remote sensing in famine early warning. In Liverman, D., Moran, E. F., Rindfuss, R. R., Stern, P. C. (Eds.) *People and Pixels: Linking Remote Sensing and Social Science.* Washington, DC: National Academy Press.

Ji, L. and Peters, A. J. (2003) Assessing vegetation response to drought in the Northern Great Plains using vegetation and drought indices. *Remote Sensing of Environment*, 87, 85–98.

Kerr, Y. H., Imbernon, J., Dedieu, G., Hautecoeur, O., LaGouarde, J. P., Seguin, B. (1989) NOAA AVHRR and its uses for rainfall and evapotranspiration monitoring. *International Journal of Remote Sensing*, 10, 847–854.

King, A., Vhurumuku, E., Gough, N., Nyamutsamba, L., Kwenda, T. (2001) *Harare Urban Vulnerability Assessment*. Harare: FEWS Net and The Consumer Council of Zimbabwe.

Linthicum, K. J., Anyamba, A., Tucker, C. J., Kelley, P. W., Myers, M. F., Peters, C. J. (1999) Climate and satellite indicators to forecast rift valley fever epidemics in Kenya. *Science*, 285, 397–400.

Mudimu, G. (2002) Zimbabwe food security issues paper. London, Forum for Food Security in Southern Africa and the Overseas Development Institute.

Potter, C. S., Klooster, S., Brooks, V. (1999) Interannual variability in terrestrial net primary production: Exploration of trends and controls on regional to global scales. *Ecosystems*, 2, 36–48.

Richard, Y. and Poccard, I. (1998) A statistical study of NDVI sensitivity to seasonal and interannual rainfall variations in Southern Africa. *International Journal of Remote Sensing*, 19, 2907–2920.

Senay, G. B. and Verdin, J. (2003) Characterization of yield reduction in Ethiopia using a GIS-based crop water balance model. *Canadian Journal of Remote Sensing,* 29, 687–692.

Tucker, C. J., Vanpraet, C. L., Sharman, M. J., Van Ittersum, G. (1985) Satellite remote sensing of total herbaceous biomass production in the Senegalese Sahel: 1980–1984. *Remote Sensing of Environment*, 17, 233–249.

Verdin, J. and Klaver, R. (2002) Grid cell based crop water accounting for the famine early warning system. *Hydrological Processes*, 16(8), 1617–1630.

Wisner, B., Blaikie, P., Cannon, T., Davis, I. (2004) *At Risk: Second Edition*, Wiltshire: Taylor and Francis Books Ltd.

Part III
Earthquakes, Tsunamis, and International Applications

Chapter 12
Spatial Information Technologies for Disaster Management in China

Jing Li, Yunhao Chen, A-du Gong, and Weiguo Jiang

Abstract China's monsoon climate and special geographical and geological conditions leaves it vulnerable to frequent natural disasters, including floods, droughts, forest fires, and earthquakes. Because China's population density is high, these disasters often result in serious casualties and enormous economic losses. The problem becomes more and more severe as the frequency of natural disasters and related economic losses are expected to increase with global climate change. Therefore, disaster prevention and relief are considered as among the most important tasks facing the nation. A great deal of management and technical work (including spatial information technology for disaster reduction) has been performed to reduce losses from natural disasters. This chapter begins with an introduction to China's disaster management and emergency management systems. The "5.12" Wenchuan Earthquake and the application of spatial information technology to disaster relief in the earthquake area is then described. The chapter concludes by describing a new project in China, the "Small Satellite Constellation for Environment and Disaster Monitoring and Forecasting".

Keywords Spatial information technology · Wenchuan Earthquake · Disaster · Emergency management · UAV remote sensing

12.1 Introduction

Natural disasters cause serious casualties and losses every year and can sometimes lead to social and economic turbulence. Therefore, disaster prevention and relief are considered very important in most countries. China is subject to many severe natural disasters, and has been working to improve natural disaster relief and prevention.

J. Li (✉)
Academy of Disaster Reduction and Emergency Management, Beijing Normal University, Beijing 100875, China
e-mail: lijing@ires.cn

P.S. Showalter, Y. Lu (eds.), *Geospatial Techniques in Urban Hazard and Disaster Analysis*, Geotechnologies and the Environment 2, DOI 10.1007/978-90-481-2238-7_12,

Significant management efforts (such as the establishment of a nation-wide emergency management system) and technical achievements (such as the application of spatial information technology for disaster reduction) have been implemented in recent years to reduce loss from natural disaster. When responding to the "5.12" Wenchuan Earthquake, China's most severe disaster in 30 years, the national emergency management system and spatial information technologies both played a very important role in disaster relief.

12.2 Emergency Management System in China

Natural disasters threaten national economic development as well as people's lives. China is severely affected by multiple types of high frequency natural disasters (Li and Chen 2007). These natural disasters have caused increasing economic losses to the country, especially since the 1990s, with major impacts on economic growth and social stability. For example, in 1992, China's economic loss due to natural disasters was about $10 billion (US dollars). In 1994 losses increased to over $20 billion, and in 1996 to more than $30 billion (Li and Chen 2007). But these numbers are small when compared to losses from the Wenchuan Earthquake that occurred on May 12, 2008 in Sichuan Province. Direct economic loss from that single event reached more than $100 billion (WEEG 2008)!

As a response to its high frequency of natural disasters, China has taken a series of initiatives to set up official coordinators for management and research efforts related to disaster reduction and relief. In April 1989, the Ten-year International Disaster Reduction Committee of China (TIDRC) was founded at the recommendation of the United Nations. In October 2000, TIDRC was renamed the International Disaster Reduction Committee of China (IDRC), with a general office housed in the Ministry of Civil Affairs. More recently, the State Council of China approved changing IDRC to the National Committee for Disaster Reduction of China (NCDR), functioning as the nation's emergency coordinator for natural disaster relief (Fig. 12.1). NCDR's Board of Experts consists of many academicians and disaster reduction experts who serve as a "think tank" to provide recommendations for decision-making. The Ministry of Civil Affairs and the Ministry of Education have also co-founded the Academy of Disaster Reduction and Emergency Management (ADREM), based at Beijing Normal University. ADREM serves as a national research base and education center for disaster reduction and emergency management and includes four institutions: the Institute of Geo-information Science and Technology, the Institute of Disaster and Public Security, the Institute of Drought and Blown-sand Disaster, and the Chang-Cheng Institute of Integrated Risk Management. ADREM also supports a key laboratory of the Ministry of Education and seven research and teaching centers (No Author 2007).

In order to support disaster reduction and emergency response management, China established a National System for Disaster Emergency Response (NSDER). NSDER classifies natural disasters into four categories based on damage. When

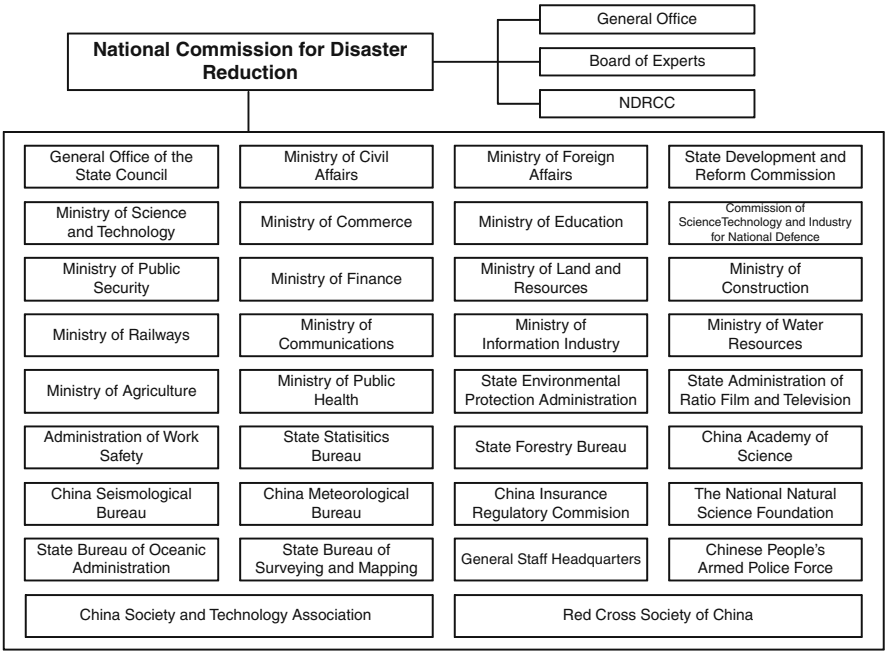

Fig. 12.1 The structure of National Committee for Disaster Reduction of China (NCDR)

a disaster occurs, depending on the category it occupies, a "project" designed to instigate the appropriate level of response is triggered. Therefore, during an emergent disaster situation, the system defines who is responsible for making the decision to instigate a project at each level as well as the tasks to be performed by every emergency response working group. Following this method, even if communication channels are interrupted (a common problem during large-scale disasters), all emergency response working groups continue functioning by following pre-defined procedures. This system minimizes delays as well as other issues that can arise due to communication problems. When a natural disaster situation initiates a national level project for disaster emergency response, the emergency response working group of the Central Government, following the procedure defined by NSDER, forms and arrives at the disaster area within 24 hours to manage relief activities.

NSDER also requires that a material reserve system for disaster relief be created. Consequently, ten national-level material reserve stations have been built in the cities of Shenyang, Harbin, Tianjin, Zhengzhou, Hefei, Wuhan, Changsha, Nanning, Chengdu and Xi'an. Furthermore, provincial-level material reserve warehouses have been created in 26 provinces, autonomous regions and municipalities. In some cities and counties that are especially vulnerable to disasters, local material reserve warehouses have been built as well. Currently, essential living materials such as tents, clothing and quilts are stored in these reserves. In the event of a disaster, these relief

materials can immediately be transported to the impacted area to provide necessities to the victims. In recent years, this national system for disaster emergency response has played a more and more important role in emergency response in China.

12.3 NSDER in Wenchuan Earthquake

The Wenchuan Earthquake (also referred to as the Si Chuan Earthquake, or on "Wikipedia" as the Sichuan Earthquake) occurred at 14:28 (Beijing Time) on May 12, 2008. Immediately, an NSDER first-level project for an earthquake disaster was launched with the Central and local government organizing rescue tasks. The emergency response working group of the Central Government, led by Prime Minister Wen Jiabao, arrived at the disaster area within hours of the quake. Within a short time frame various materials for disaster relief were also transported to the disaster area from central- and provincial-level material reserve warehouses. Simultaneously, a working group oversaw transport of the materials for disaster relief, evaluated the possible shortage of these materials in the reserve warehouses, and began the process of obtaining additional materials. For example, the normal yearly need for disaster-relief tents is 100,000–150,000, with 300,000–400,000 tents in material reserve warehouses. However, the intensity of Si Chuan Earthquake caused the destruction of so many houses that the working group estimated at least 1,000,000 tents were needed. Quickly announcing the increased need for tents resulted in the disaster area receiving a total of 1,600,000 tents within a short period of time. Another advantage of the NSDER response system became evident in terms of communication, as alluded to earlier. In the first few days after the earthquake, due to communication system damage, information and commands could not reach the various departments and working groups in a timely manner. However, these entities were still able to begin their work quickly after the quake, following the procedures that had been established for a first-level emergency response project. Time that may have been lost waiting for commands from the upper administration was therefore minimized, ensuring timely rescues.

During emergency response, it is very important to transmit timely and reliable information to support decision making. Because disasters can happen suddenly and affect a large area, developing events can be difficult to monitor using conventional means of communication, especially during a severe event such as an earthquake. The destruction of communication instruments and information collecting/transmitting facilities in a disaster can cause serious problems for emergency response and damage relief efforts. In an effort to address this problem, various new information technologies are being employed (e.g., remote sensing, GIS, satellite navigation systems, satellite communications) to ensure communication and information collection is not interrupted. Collectively referred to as geographic information technologies (GIT) for the purposes of this paper, such an information collection, analysis and sharing system was established by NSDER and has become an integral part of the national disaster and emergency management system. From

the day the Wenchuan Earthquake occurred, this system was used several times a day to send situation reports to disaster relief headquarters as well as to all NCDR members.

12.4 Spatial Information Technologies in Emergency Response

When the Wenchuan Earthquake occurred, all regular communication systems ceased functioning. The Central and local governments immediately dispatched many satellite communication vehicles and more than 3000 satellite telephones to the region, creating a satellite communication network in the earthquake area. Simultaneously, the Chinese satellite navigation system (BeiDou-1), which has both navigation and communication functionality, was pressed into use. More than 1000 BeiDou-1 terminals were dispatched to the disaster area to support the satellite communication system, representing the first time that a satellite-based communication system was extensively used for disaster relief on such a large scale in the country. During the first two weeks after the quake, almost all important communications in the disaster area were transmitted by this satellite-based system, ensuring that the disaster relief headquarters could get fast and accurate information regarding activities and make timely decisions. Because most of the disaster area is located in mountainous terrain, repairing the regular communication system is a difficult and time-consuming enterprise. Under these circumstances the satellite communication system was an essential component of the response to, and relief activities of, the 5.12 Quake for a long period of time.

One role of disaster risk analysis is to monitor and analyze the risks posed by various hazards and assess a location and its population's relative vulnerability to diasaster. GIT plays an important role in disaster risk assessment and development of early warning techniques by integrating physical data derived from scientific observation of the atmosphere, land, and ocean with socio-economic data. A spacegound integrated monitoring network further improves risk analysis and early warning efforts, increasing the accuracy of models and analyses.

Together with the satellite communication system, remote sensing technology is widely used for disaster response in China. Remote sensing fosters the collection of data over large spatial areas and from various portions of the electromagnetic spectrum. Images can be obtained from great distances and some satellites that utilize RADAR imagery can provide all-weather imaging capability. Analyzing remote sensing data can help identify the occurrence of a natural disaster, monitor its development, and provide timely and reliable information that assists in determining the spatial extent of the disaster and estimating losses. In China, remote sensing technology has been used widely in all phases of disaster management, including during the preparation, early warning, emergency response, and recovery phases.

Prior to a disaster, remote sensing's primary role is in the preparation and early warning phases. In the preparation phase, remote sensing (in concert with GIS and satellite navigation systems) data can be used to establish a background database, including natural and social economic data. A background database is very

important for each phase of disaster management and also offers needed parameters to support early warning efforts.

When a disaster occurs, remote sensing is normally used to monitor the impact area with a focus on collecting information regarding type of event, its location and scope, whether it is localized or has a moving path, and its duration. When monitoring a natural disaster, visualization and fast evaluation of the disaster-affected area are two of the most useful contributions remote sensing can supply to those tasked with disaster management. Satellite images can be used to extract information about trends and changes in the area affected by the disaster; analyzing these images, policy recommendations for disaster prevention can be made and measures to improve disaster relief practice designed.

Under the right circumstances (e.g., no cloud cover), remote sensing can quickly perform initial disaster impact assessment in the emergency response phase. An integrated system containing images, land use/land cover, and GIS layers (e.g., socio-economic, pre-disaster imagery) can be used to model the scope of a disaster, the number of people affected in a disaster area, and the total population that may need to be relocated. Based on the results of an impact assessment, measures and countermeasures can be implemented in improve efficiency when making arrangements for affected populations and planning for recovery.

After a disaster, remote sensing can be used for loss assessment, including analyzing the extent and intensity of damage (including economic loss), damage to utilities (e.g., transportation, power, water, gas) telecommunications, housing, and environmental pollution. Such technology can also be used to evaluate the effect of disaster relief efforts.

12.5 Remote Sensing Applied in Response to the Wenchuan Earthquake

As summarized above, remote sensing can provide a great deal of information to support disaster relief decision-making during crisis situations, and has been successfully used for disaster reduction in China (Li and Chen 2007). During the "5.12" Wenchuan Earthquake, remote sensing technologies played a very important role in the disaster management effort.

Shortly after the earthquake, many government agencies (e.g., National Remote Sensing Center of China, National Committee for Disaster Reduction of China), universities, and research institutes began to collect and analyze satellite images from the disaster area. Agencies in China that had remote sensing satellite data were contacted in an effort to obtain updated imagery. Also contacted for additional imagery was the "International Charter", whose membership seeks to provide "... a unified system of space data acquisition and delivery to those affected by natural or man-made disasters ..." (International Charter 2008). The request was supported by all agencies, both inside and out of China, and a large amount of imagery delivered on a daily basis – more than 1300 images acquired by at

least 23 different satellites were provided to disaster response agencies free of charge. Meanwhile, the remote sensing working group of the National Remote Sensing Center of China arrived in the disaster area on May 13, after which aircraft were also used to collect data and monitor progress. More than 20 aircraft were used, acquiring visible, infrared (IR), Synthetic Aperture Radar (SAR), and laser imagery.

More than 20 terrabytes of imagery were collected and experts from many agencies worked together to analyze the data. Information and analysis results were produced and shared with the disaster relief management headquarters and various government agencies. Based on a rough survey conducted in mid-June of 2008, about 2000 disaster analysis maps were made based on remote sensing images and 50 Atlases (in 3 series) compiled (SECWE 2008). Through image analysis, 5776 new landslides, 935 destroyed roads, and 143 new "barrier lakes" were identified. These analyses were compiled into 400 analysis reports provided to the State Council. The results of the image analysis and the related reports provided updated and accurate information to decision makers regarding the disaster situation, and greatly improved disaster relief efforts. For example, on May 14, 2008, the National Remote Sensing Center of China (NRSCC) analyzed a satellite image and discovered a new lake (named Tangjiashan Barrier Lake) had formed in a mountainous area due to landslides caused by the earthquake. Analysis revealed that the lake's water level was rising quickly and posed a severe threat to earthquake victims temporarily housed downstream. The NRSCC monitored the new lake on a daily basis using satellite and aircraft remote sensing images (Fig. 12.2), regularly reporting any observed changes to the Central Government.

Fig. 12.2 Dynamic change map of Tangjiashan Barrier Lake in BeiChuan County, based on satellite optical images (May 14, 16, 19, 22, and 26); the various colors show change in water area on different days
Source: State Expert Committee of Wenchuan Earthquake 2008

These reports provided critical information to disaster relief headquarters, leading to decisions regarding the lake's management and the related downstream evacuation plan.

Disaster monitoring efforts also received immense support from international agencies and experts who not only provided updated satellite images free of charge, but also shared their analysis results in a timely manner. For example, Professor Linlin Ge from the University of New South Wales, Australia, and Professor Yifang Ban from the Swedish Royal Institute of Technology worked closely with the authors of this chapter, obtaining the newest images (including visible and SAR data), processing them quickly, and providing the results to us as rapidly as possible.

In addition to the conventional collection devices discussed above, an Unmanned Aerial Vehicle (UAV) was employed in order to obtain images with much higher resolution (0.1−0.2 m) beneath cloud coverage. While UAVs have been widely used in China, this was the first time they have been used to monitor a disaster situation. On May 15, 2008, more than 100 images in Beichuan Town were collected using a mini-UAV (Fig. 12.3). Beichuan Town is the most damaged location in the entire disaster area, with most houses destroyed. During the first week after the earthquake, cloud cover forced the aircraft to fly at an altitude lower than 300 m to stay beneath the clouds. High quality and high resolution images were collected in this manner and immediately sent to the Central Government in Beijing and the disaster relief headquarters through the satellite communication

Fig. 12.3 Unmanned Aerial Vehicle (UAV) image, Beichuan County; house damage in the disaster area can be clearly seen
Source: Photograph by Jing Li, May 15, 2008.

system. More than 20 pilotless aircraft were used in the disaster area, collecting many high resolution images which could be used to monitor changes in the disaster situation and to make various maps to support relief and recovery plans. These images are considered to be among the most valuable data collected following the earthquake.

12.6 Conclusion and Discussion

Over the past 20 years, GIT has been widely used for natural disaster management in China, serving in the capacity of disaster monitoring, loss evaluation, risk analysis, and in the creation of maps and reports to disaster management agencies. In the aftermath of the "5.12" Wenchuan Earthquake, GIT again provided invaluable data to aid disaster relief efforts and decision making. Application of the UAV during the disaster monitoring stage was also very successful due to its ability to obtain high resolution imagery on cloudy days. Research is continuing to improve UAV capabilities so that it can function more efficiently in future disaster situations.

Remote sensing imagery greatly aided disaster management during the aftermath of the "5.12" Wenchuan Earthquake. However, current Chinese satellites were not designed for disaster monitoring, nor can the total number of satellites owned by China meet the country's needs for disaster management. This fact was recognized before the Wenchuan Earthquake, when in February 2003, the State Council of China approved creation of the "Small Satellite Constellation for Environment and Disaster Monitoring and Forecasting" (called the "HJ-1 satellite constellation"). Consisting of four optical and four SAR satellites, the HJ-1 is designed to fly sun

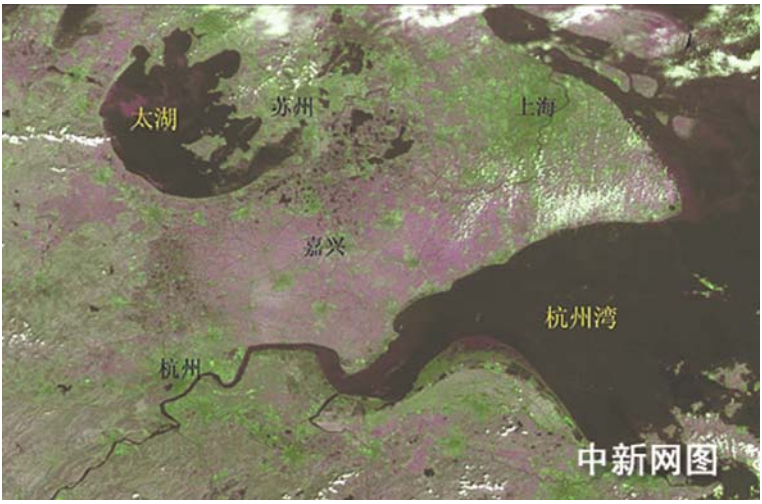

Fig. 12.4 HJ-1A Wide Field CCD Camera Color composite image, Hangzhou Bay Area, September 8, 2008 (http://mil.news.sina.com.cn/s/2008-10-21/0943526303.html)

synchronous orbits, and after all 8 satellites are launched the constellation will provide country-wide disaster monitoring capabilities on a 12-hour basis (Li and Chen 2007). Two of the optical satellites, HJ-1A and HJ-1B, were launched on September 6, 2008. HJ-1A carries a Wide Field Charge-coupled Device (CCD) camera and a Hyperspectral Imager. HJ-1B satellite carries the same CCD camera and an IR camera. The CCD cameras collect information from four bands (0.43−0.52 μm, 0.52−0.60 μm, 0.63−0.69 μm, and 0.76−0.90 μm) with 30 m resolution and a 720 km swath (Fig. 12.4). The infrared scanner collects information from four IR bands (0.75−1.10 μm, 1.55−1.75 μm, 3.50−3.90 μm, and 10.5−12.5 μm) with 150∼300 m resolution and a 720 km swath. The hyperspectral imager, China's first such satellite, collects information at 110 bands (5 nm radio) with a 100 m spatial resolution and a 50 km swath. The launch of these satellites and use of their sensors for disaster mitigation, planning, and response will greatly improve China's future disaster management practices and policy making.

Acknowledgments This work is supported by the Hi-tech research and development program of China (2006AA120102, 2007AA120306, 2007AA120205), the Key Technologies R&D Program (2006BAJ09B06, 2006BAJ09B03, 2006BAJ05A01), and the International Scientific and Technological Cooperation Program (2007DFA20640).

References

No Author. 2007. Academic Exchange. Academy of Disaster Reduction and Emergency Management. Ministry of Civil Affairs and Ministry of Education. http://adrem.org.cn/English/index.html; last update unknown, accessed December 18, 2008.

International Charter. 2008. International Charter: Space and Major Disasters. http://www.disasterscharter.org/about_e.html; last updated April 11; accessed December 19, 2008.

Li, Liguo and Weilan Chen. 2007. *Emergency Response and Disaster Reduction*, Peking University Press, Beijing, China.

State Expert Committee of Wenchuan Earthquake (SECWE). 2008. *Earthquake and Geological Disaster Atlas of Wenchuan Earthquake Disaster Area*, China Map Press, Beijing, China.

Wenchuan Earthquake Expert Group (WEEG). 2008. *Earthquake Disaster: Analysis and Evaluation*. Wenchuan Earthquake Expert Group of NCDR and MOST.Science Press, Beijing, China.

Chapter 13
A Cybercartographic Tool for Supporting Disaster Prevention Planning Processes and Emergency Management in Mexico City

Elvia Martínez-Viveros and Fernando López-Caloca

Abstract Researchers at Mexico's CentroGeo have developed a cybercartographic tool under the acronym Geodisplat. The objective of this chapter is to present this tool and its potential to support processes of disaster prevention planning and emergency management in Mexico City. Geodisplat is an interactive-computerized tool that allows the fusion of pieces of information and data from multiple sources and the modeling of systems that interact in the disaster cycle. Navigation in Geodisplat is guided by a conceptual model with vulnerability serving as the central concept for the spatial analysis of disaster, and planning as the process with the capacity to diminish vulnerability. Disasters are approached in stages that comprise "before", "during", and "after" a natural or technological catastrophe occurs at a certain place and time. Planning groups need to understand factors that increase human and system vulnerabilities at different times during the disaster cycle and, in a procedural sense, to adapt their activities to the decision-making environment in which they find themselves operating. The tool's main contribution lies in its capacity to support the decision maker's information needs during the different stages of the disaster cycle, and to do so in an efficient and timely way.

Keywords Vulnerability · Disaster · Cybercartography · Planning

13.1 Introduction

Mexico City is a megalopolis full of complexities including highly accelerated demographic growth with an enormous part of the population inhabiting areas prone to disasters. The city's urbanization has been characterized (amongst other processes and factors) by a large population density in poverty-stricken and marginal neighborhoods, frail housing concentrated in irregular settlements, stress placed on

E. Martínez-Viveros (✉)
Centro de Investigación en Geografía y Geomática "Ing. Jorge L. Tamayo A.C.", Contoy 137, Lomas de Padierna, Tlalpan 14240, México D.F.
e-mail: emartinez@centrogeo.org.mx

P.S. Showalter, Y. Lu (eds.), *Geospatial Techniques in Urban Hazard and Disaster Analysis*, Geotechnologies and the Environment 2, DOI 10.1007/978-90-481-2238-7_13,

marginal soils by displaced rural migrants, inefficient and oversaturated transport and roadway systems barely able to support the massive daily commute of the city's inhabitants, irregularities in the enforcement of construction norms and use of soil regulations, and the building of structures that impede natural drainage patterns and water flow.

In the basin of the Valley of Mexico, where this megalopolis is situated, there are a number of natural hazards that can cause a disaster, including: earthquakes, volcanic activity, floods and landslides (these last two can affect different areas within the city limits during the rainy season, causing multiple minor disasters). The possibility of a technological disaster is also quite relevant due to the concentration of intense industrial activity and the storage of hazardous materials that are transported and discarded, often without complying with strict safety regulations. This situation increases the vulnerability of not only the city's inhabitants but also the systems on which they depend, such as water, electrical supply, distribution of staples, and access to health care.

Recently, international consensus has developed regarding the value of geospatial information and tools when used for disaster prevention and emergency management. Consequently, a series of Mexican government and academic institutions have produced geospatial data including landmarks from the city's geographic surface to be used as spatial reference points for data relevant to disaster prevention and emergency management, thematic data to help visualize the geographic context, and hazard-related data considered useful during the response/recovery phase or to generally reduce the impact of disasters. Models to analyze dangerous scenarios posed by different hazards have also been developed, and spatial differentiation between social group vulnerability (mainly using housing characteristics) and the city's infrastructure are being explored. These efforts result in a wide variety of relevant scientific information and knowledge pools. Unfortunately, they are often stored in incompatible formats, represent diverse geographic scales and attribute accuracies, and are dispersed across multiple agencies and organizations with little culture of information-sharing. Limited diffusion of this existing geospatial data impedes user access and thus its incorporation into decision making, monitoring and analytic processes.

To address the problem described above, a "cybercartographic" tool was developed by a research group at CentroGeo. The main objective of this tool is to integrate and fuse spatial information and knowledge within a systematic perspective in order to support prevention planning processes aimed at mitigating risk and reducing vulnerability in Mexico City. This geo-disaster-planning-tool (Geodisplat) performs salvaging, updating, visualization and analysis of geospatial data produced by different sources regarding Mexico City's risks and vulnerabilities. Geodisplat also performs spatial analysis of population vulnerabilities, fusing spatial patterns of vulnerability and hazard in order to create risk maps. The system builds upon a cybercartograpic model and architecture proposed by Reyes et al. (2006), which takes into consideration the process of communication and the role of these tools in conveying spatial information and knowledge by means of different languages and media.

Users interact with Geodisplat by navigating through cartographic products, geospatial information, and multimedia files (e.g., text, audio, video). A viewer that responds to queries from the multimedia platform was created to display geospatial information. Scenarios presented in the geospatial viewer can be examined or enriched by users who can add spatial, statistical, or qualitative information or build new maps using Geodisplat's tools. The cartographic layer can accept diverse file formats such as: html, pdf, doc, or xls, allowing inclusion of text, photographs, videos or graphics. Geodisplat can also build algebraic indicators using variables included in the data base. These indicators can be displayed as thematic maps for visualization and analysis or intersected for more complex analyses.

Geodisplat development is supported on ESRI MapObjects; therefore it includes all basic tools of a Map Viewer (e.g., zooming in or out, panning, measuring). Geodisplat also includes tools programmed in Microsoft Visual Basic for: saving in a database digitized points, lines or polygons; buffering the affected areas; hyperlinking information in multimedia files such as text, audio or video; identifying population, buildings and infrastructure by means of spatial operations, such as maps intersections; and using network analysis for the location of intersecting roads.

To better understand the functions of Geodisplat, consider the following example: an emergency first responder or dispatcher (e.g., a 911 operator) starts by opening a case file related to the emergency at hand. The emergency is located on a map and Geodisplat automatically links this location to all relevant information, including images, text, and maps. The operator can retrieve information about the area's characteristics, the number of inhabitants, the size of groups with certain vulnerabilities, the services and infrastructure exposed and the assets useful for delivering response services such as hospitals, police departments or fire stations located inside or near the impacted area. Geodisplat compiles all of the information generated and incorporates it into the event response protocol. This information supports the emergency response management teams' field tasks.

Two models guide the organization of information in Geodisplat. The first is a conceptual model of vulnerability and risk approached from a spatial, systemic and multidimensional perspective. The second is of a procedural nature relative to planning processes that seek to reduce risk. The tool discussed in this chapter will be presented from the perspective of these two models, as well as how they link and integrate geospatial information used in support of planning activities during different stages of the disaster cycle.

13.2 The Conceptual Model: Vulnerability as the Core Concept in Disaster Analysis

"Vulnerability" represents the fragility or weakness of the unit under consideration, be it a building, a place, a person, a group or a human settlement. Physical vulnerability is related to the unsafe characteristics of places, buildings or infrastructure that can be impacted by a disaster. Social vulnerability is associated with a lack

of resources to prevent, cope with, or recover from disaster. According to Voguel (1998), vulnerability can be approached from two dimensions: internal and external. The internal dimension focuses on individual and/or group abilities to face, resist and overcome (mitigate) disaster impacts. The external dimension views vulnerability as a process, a product of socio-economic and political dynamics that, over time, result in the exposure of people and groups to danger.

Brooks (2003) states, "... we can only talk meaningfully about the vulnerability *of a specified system to a specified hazard or range of hazards*" (p. 3). Hazard implies the presence of a disturbing or dangerous threat, be it natural or technological in origin, with the ability to cause such damage to a system that the damage would constitute a disaster (Guevara et al. 2006). Consequently, hazard is a probabilistic function of danger, exposure and vulnerability; while "... disaster as measured in human terms (lives lost, people affected, and economic losses) is the *outcome* of a hazard, mediated by the properties of the human system that is exposed to and affected by the hazard" (Brooks 2003: 3).

The traditional approach to disaster research focused on the "triggering" event, whether natural or artificial. More recently, such events are considered to be, "... the result of a huge violent rupture in the correlation between humans and their environment, a serious or sudden event; of such a scale that the community struck requires extraordinary efforts to face it and frequently needs external or international aid" (Noji 2005). This "rupture" has also been expressed as "... the susceptibility or propensity of exposed systems to be affected or damaged by the effect of a disturbing phenomenon ..." (Guevara et al. 2006: 16–17). Thus, vulnerability under this approach is seen as the result of the impact of a disaster in terms of victims, economic losses and injuries.

However, a number of researchers believe that the impact of disasters must be interpreted as a consequence of different structural situations that expose people and systems to danger (Blaikie et al. 1995). These authors believe natural events, as determining factors of disaster, play a secondary role when compared to the social, political and economical environment. Consequently, and following García (1993), vulnerability becomes the "active agent" in a disaster, not the natural phenomenon, which only serves to ignite preexisting, critical situations. This approach to vulnerability stresses the way systems operate to generate disasters and increase vulnerability.

Increased vulnerability increases the probability of disaster for the unit under analysis (e.g., people, places, social groups, systems); it exists in time and space in a dynamic process where different factors and variables interact (Wilches-Chaux 1993). Political and socioeconomic dynamics combine in a process that increases vulnerability and leaves people, individually or in groups, exposed to danger as they travel, live or work in risky areas, construct insecure buildings and infrastructure, or utilize unsound transport and roadways. Vulnerability is acutely connected to people's ways of life, as individuals or in groups, and is related to their assets, access to resources (e.g., productive, natural, managerial, organizational) and

their capacity to prevent, face, organize and adapt to disastrous events (Kasperson and Kasperson 2001: 13). As recommended by the Interagency Secretariat of the International Strategy for Disaster Reduction, it is necessary "... to shift the primary focus from hazards and their physical consequences to emphasize more the processes involved in incorporating physical and socio-economic dimensions of vulnerability into the wider understanding, assessment and management of disaster risks" (IAS-ISDR 2004: 14). While some authors counsel not to assume a direct relationship between vulnerability and poverty, the connection cannot be entirely ignored. The IAS-ISDR report indicates that although natural disasters theoretically threaten everyone equally, their impacts are far greater on the poverty–stricken because they outnumber the wealthy and are more likely to dwell in substandard housing in more densely populated environments on more hazard-prone land (IAS-ISDR 2004).

Vulnerability is also related to options – or lack of same – due to economic, social and political restrictions. A lack of options is common among those who have limited choices regarding where "to live." Urban areas are not, by nature, more vulnerable to disasters. Instead, the structural processes occurring in an urban area can accelerate urbanization and concentrate population in places within the city that increase vulnerability. Consequently, vulnerability needs to be examined in relationship to changes in socio-spatial patterns that occur in urban systems (Hamza and Zetter 1998).

13.3 Geospatial Data and Tools to Analyze Vulnerability in Mexico City

Mexico City and its metropolitan area lie within the Valley of Mexico and is integrated by the Federal District, 58 municipalities in the state of Mexico and one in the State of Hidalgo (Fig. 13.1). According to the Emergency Research Data Base from the Centre for Research on the Epidemiology of Disasters, from 1975 to 2005 this area experienced 24 disasters: 13 natural and 11 technological. Of these, two are outstanding because of their impact and intensity: a natural gas explosion on 19 November 1984 in San Juan Ixhuatepec (452 killed, 4248 injured, 4000 homeless, and an estimated 703,000 otherwise affected), and an earthquake on 17 September 1984 (9500 killed, 30,204 injured, approximately 100,000 homeless, and more than two million otherwise affected [EM-DAT 2008]). These two disasters illustrated the enormous vulnerability of the city.

Disasters of such intensity and magnitude are relatively rare. However, the dynamic processes present in Mexico City increase the probability that a dangerous event (natural or technological) will be converted into a disaster of great magnitude. Among those factors and processes are the size of the city, the characteristics of its settlements, the cultural and economic capacities of its inhabitants, the

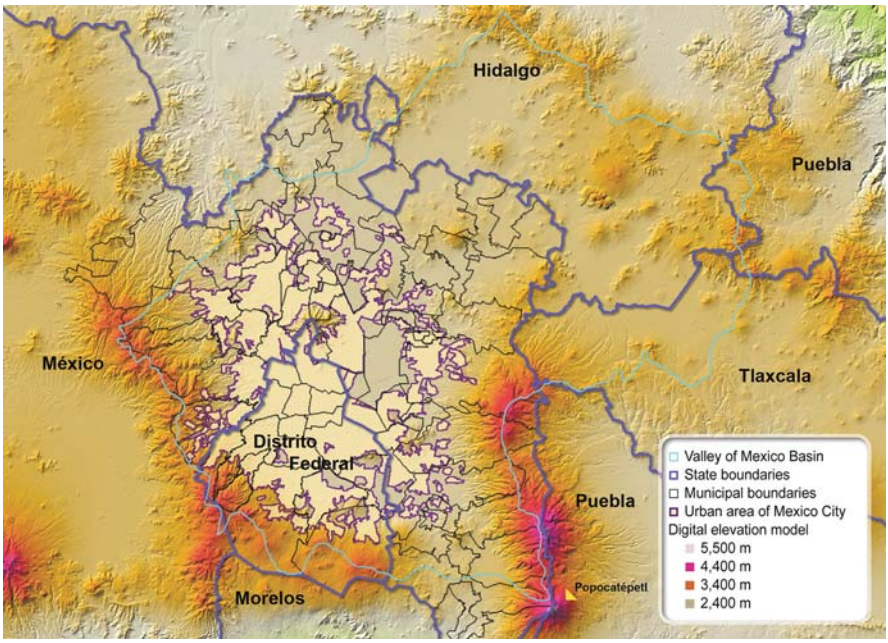

Fig. 13.1 Map of Mexico City and its surroundings (source material: Shuttle Radar Topography Mission (SRTM) data processed at the Jet Propulsion Laboratory and distributed through the US Geological Survey's EROS Data Center)

socio-economic gaps between the different social groups and other demographic and urban dynamics. The city is exposed to natural disasters of seismic origin, hydro-meteorological origin (which can cause landslides, flooding, subsidence), and volcanic origin (because of the proximity of Popocatépetl volcano (Fig. 13.1). Added to these natural hazards are dangers derived from human activities, which can cause technological accidents.

The organized and systematic process of generating geospatial information on the subject of risk and vulnerability in Mexico City is still very rudimentary. The National Center for Disaster Prevention has created a National Risk Atlas which displays spatial danger scenarios for volcanic or earthquake hazards. This atlas can be consulted on-line through a cartographic viewer available at: http://www.atlasnacionalderiesgos.gob.mx/metadataexplorer/index.html (SIIRIDE -ANR-1).

More highly developed cartographic products simulate danger scenarios through spatial modeling that make use of historic and geographic information. Geodisplat displays the spatial aspect of events that have the highest probability of occurring or recurring and/or causing major damage to exposed systems and social groups in Mexico City. The tool includes research from Universidad Nacional Autónoma de México (UNAM), which has published maps for Popocatépetl volcano representing danger scenario caused by lava flows, falling ash or other particles, and landslides as well as scenarios representing seismic risks in Mexico City for buildings and

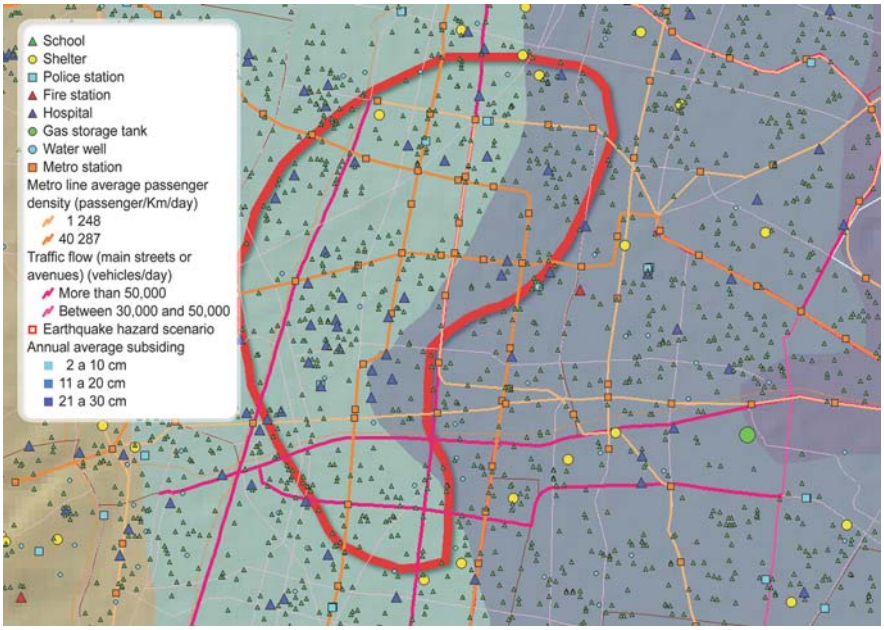

Fig. 13.2 Earthquake hazard scenario displaying vulnerable infrastructure. The red border encircles the area of Mexico City most affected by past earthquakes

households of different quality (SIIRIDE-ANR-2). Geodisplat also includes a map of hydro-meteorological dangers that indicates zones likely to be affected by inundation resulting from heavy rains with different return periods (Tapia-Silva et al. 2007).

Geodisplat allows the visualization of systems and infrastructure exposed to damage under different spatial scenarios. For example, Fig. 13.2 portrays a zone historically affected by earthquakes of magnitude up to 8.2 on the Richter scale. The map displays points representing critical infrastructure (e.g., schools, hospitals, police stations, fire stations) as well as the layout of the metro lines and main roads and their average daily travel density.

While Geodisplat can construct spatial scenarios of disasters, expressing spatial patterns of population vulnerability is difficult. Indicators must be constructed using information that directly references specific weaknesses of groups exposed to different threats at specific stages of the disaster cycle. Unfortunately, the information available for determining these levels of weaknesses is quite poor.

The most vulnerable groups are those who, prior to a disaster, are most exposed to danger, during a disaster are limited in their ability to react, and after a disaster have more difficulty recovering to a "normal" state and reconstructing their means of subsistence. Historically these groups have been identified by variables such as social class, ethnic background, religion, disability, age, or economic status. Vulnerability varies spatially because the natural environment, housing schemes, and social

structure varies spatially and because people carry out their daily activities in space. It is in time and space where physical threats, social relationships and individual choice converge.

To represent and analyze the spatial distribution of vulnerable social groups in Mexico City, Geodisplat's capabilities were expanded so it could construct and display indicators dealing with vulnerable groups' characteristics. This effort uses official data from 2005 of: population density, age, gender, home management, access to health public services, schooling, housing characteristics, services, migration, disability and ethnic background. These data, while limited, are a first step in constructing indicators that can reveal the relative vulnerability of different population groups. As a result, the tool provides the opportunity to construct indices of vulnerability expressed in mathematical formulas. The spatial distribution of these indices can be displayed on thematic maps of census areas (Fig. 13.3).

To summarize, Geodisplat provides the ability to simultaneously identify and display areas of Mexico City that are exposed to hazards, the spatial distribution of various infrastructure and installations, and populations grouped according to characteristics that express vulnerability. The system also contains accurate georeferenced data for schools, markets, hospitals, fire/police stations, landmarks, public buildings, and reservoirs, among others. The visualization and analysis of this

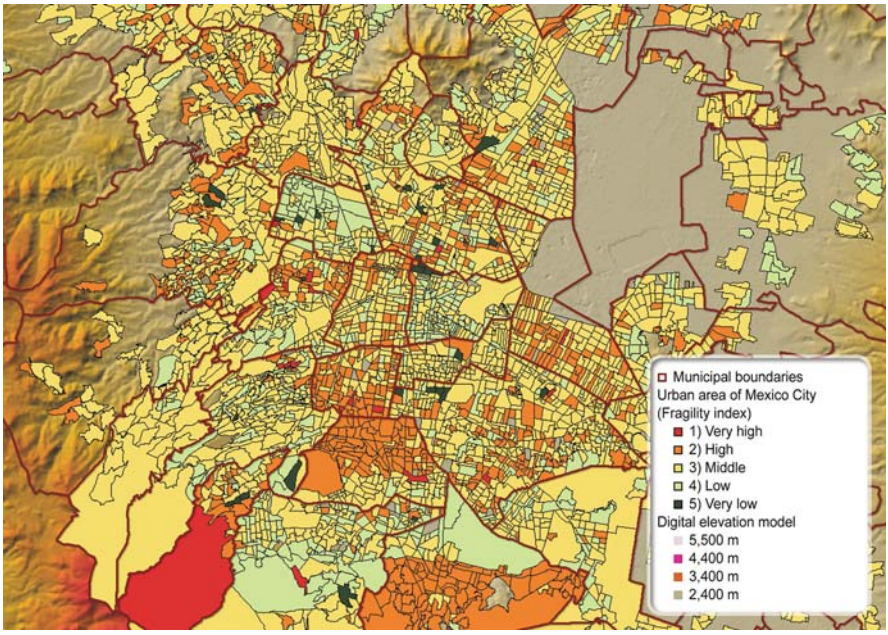

Fig. 13.3 Thematic map displaying a vulnerability index at census area scale. This example is a weighted linear equation involving population with no access to public health services, young children, elders, and the illiterate population

spatial information can be divided into diverse scales that span the metropolis and its geographic surroundings (e.g., limits of municipalities, census areas, sectors, street blocks).

13.4 Vulnerability and the Disaster Cycle

While an event that creates a disaster can be classified as limited in time and space, it is in reality a process. This process of disaster has been divided into stages that can be studied, planned and managed. Most authors agree on a four-stage model: preparedness, response, recovery and mitigation (Committee on Planning for Catastrophe 2007). The conceptual model in the cybercartographic tool includes five overlapping stages, beginning with prevention followed by emergency (focusing on survival, rescue and attention to victims and damages). Recovery follows, during which capacities are generated to cope with the crisis, then reconstruction, during which efforts are made to "return to normal". The final stage is "back to normal", which overlaps the reconstruction and prevention stages of the next cycle (Fig. 13.4). Components within the five overlapping stages of Geodisplat's conceptual model are further elaborated, below, and displayed in Fig. 13.5.

Fig. 13.4 The disaster cycle, conceptualized in four overlapping stages: prevention, emergency, recovery, reconstruction and back to normal

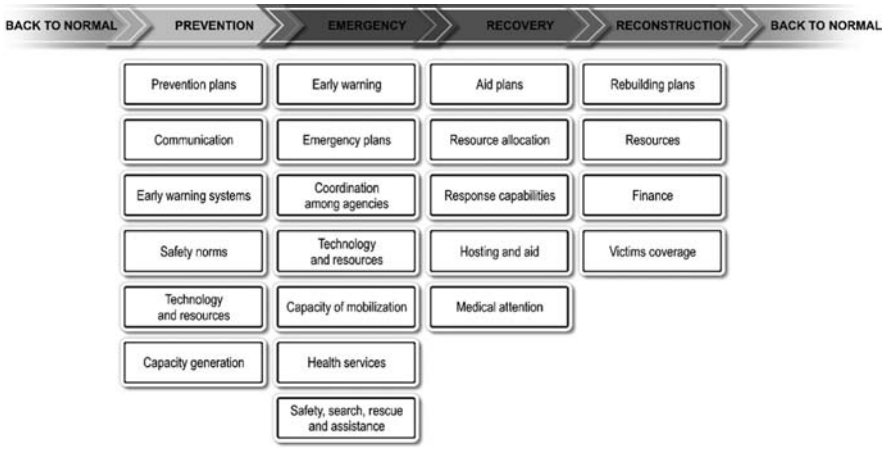

Fig. 13.5 Public issues in the disaster cycle includes the main issues identified in the National Program of Civil Protection (SEGOB/SNPC 2008)

13.4.1 Prevention

Prevention provides exposed groups access to information, knowledge, technology and resources to learn about their exposure and how best to react in case an event occurs. Prevention also helps these groups understand the information and knowledge and manage the technology.

There are a large number of issues that prevention should address. Among these are: processes of early warning, construction of infrastructure to lessen the impact of dangerous events, training of emergency responders, relocation of people to safe places, installation of shelters, and effective diffusion of information and knowledge regarding what places are insecure, what may happen during a disaster and which is proper behavior when facing these events. In essence, people exposed to danger need to know what must be done, where to go, and who to help in an emergency.

Prevention should also address structural factors embedded in the construction of social vulnerability. Structural factors must be considered in long term programs that deal with social or economic development, urbanization, or education. Therefore, disaster prevention should be at the core of public policy, reflected in laws and public institutions as well as in the planning of national and local governments. While costly, the benefits of effective prevention exceed their costs. A culture of prevention requires the development of creative social communication techniques and the adoption of new technologies that allow people access to the information and knowledge they need the moment it is needed.

13.4.2 Emergency

The emergency stage occurs immediately after an event. During this stage, buildings can be destroyed; people can die or be trapped or wounded. Secondary disasters

can also occur (e.g., fires or explosions caused by gas leaks). During this stage, pre-existing vulnerabilities can limit response. For example, small children and the elderly may lack the ability to escape from danger. Poverty can increase vulnerability if people must bear the cost of being transported to safe havens. In addition, the physical attributes of buildings can increase vulnerability if they are constructed of sub-standard materials or improperly maintained. The time of day, day of the week, or month of the year an emergency occurs can also increase or decrease vulnerability (e.g., causing displaced individuals to be exposed to extremes of heat or cold).

13.4.3 Recovery

During the recovery stage people attempt to regain physical, emotional and financial equilibrium. In this stage the dead are buried and physical wounds healed; temporary housing and food are provided; aid is delivered to victims; public services (e.g., electricity, telephone) restored. However, "... recovery does not entail simple clean-up and restoration operations to get a community back on its feet, but requires long-term rehabilitation processes that are affected by prevailing socio-economic conditions and structural constraints" (Tobin 1999: 15). A disaster ruptures the social system; survivors face stress and anxiety that can be overcome only when a state of equilibrium at the family and community level is regained.

In this effort, resilience plays a major role. The ability to undergo stress and recover varies from person to person and from one community to another. The level of stress that young people with economic resources face is different than for the elderly living in poverty. Community social cohesion is also a factor. During recovery, networks of support woven by the community and social mobilizations help to overcome the tragedy. At this stage, the affected groups' vulnerability is sensitive to factors such as access to information, knowledge, technology, representation and politicians with the power to deliver resources. Resilience can be improved when exposure and vulnerabilities are lowered; when the level of support from responsible agencies and political leaders is high and when different governmental levels and social networks work together.

13.4.4 Reconstruction and Back to Normal

On a longer-term basis, different actions are taken in an attempt to re-establish pre-event conditions for affected communities. These actions include repairing or rebuilding damaged infrastructure and housing facilities. Reconstruction programs encompass public as well as private property and must consider several complex issues, such as: economic feasibility, environmental fitness (urban harmony, availability of communications and roads, public services), safety from probable future hazards and acceptance by the affected people. A major source of disruption for a household is the loss or damage of their residence; research has found that people

so affected want to return to their pre-event location and that, even during recovery, they resist relocation to temporary shelters (Miller and Nigg 1993).

Reconstruction involves very complex programs which, according to the US Federal Emergency Management Agency (FEMA) are often subject to pressure by residents from disaster-stricken communities who wish to be quickly restored to their pre-disaster form and condition. However, public safety and economic recovery should be driving factors behind any plans for post-disaster reconstruction (FEMA 2005). In this context, while reestablishing the conditions of every day life may be important, it is equally important to reduce as much as possible the vulnerabilities that preexisted the event. Otherwise, the cycle of vulnerability is simply renewed. Because it is not possible to alter the course of nature by deviating hurricanes or preventing earthquakes the most viable method for society to reduce risk is to address vulnerability. Therefore, after a tragic event, reconstruction must provide victims with better resources: to strengthen institutional, social and individual capacities.

13.5 The Planning Process

Some of the main variables we propose as appropriate for planning models implemented during different disaster stages include: social vulnerability rate of change, stability/maintenance of processes that reduce vulnerability, response time for effective decision making, and decision-making control nodes and their centralization/decentralization (Table 13.1).

Table 13.1 Planning environment characterization

Stage/capacities to build	Social vulnerability rate of change	Stability of processes that reduce vulnerability	Response time for effective decision making	Decisión making control nodes
Prevention/ anticipation	Slow	Dynamic equilibrium	Medium and long	Defined, maybe strongly centralized
Emergency/ resistance	Very fast and accelerated	Loss of the stable state, chaos	Very short	Diffuse, usually multiple
Recovery/coping	Fast	Some process are stabilized while others remain in disequilibrium	Short	Fragmented, usually multiple
Reconstruction/ recovery	Medium	Tendency towards stability	Medium	Defined, maybe various
Back to normal/ adaptation	Slow	Dynamic equilibrium	Medium and long	Defined, maybe strongly centralized

During the prevention stage, the rate of change in vulnerability is slow; exposed social systems maintain a dynamic equilibrium, co-evolving with the complex socio-economic and urban processes that converge in the construction of a disaster. In this kind of environment there is enough time for planning groups to design medium- or long-term strategies geared towards anticipating a disaster, thereby reducing vulnerability. Decisions and actions can be controlled from nodes defined in a clear-cut decision chain.

In the emergency stage there is a loss of stability and chaos prevails. The processes involved in vulnerability experience an exponential change; decision makers have to respond fast and with high levels of autonomy, since control of the situation is dispersed in the social system and the line of command becomes fuzzy. The ability to resist is what needs to be improved among affected people or communities.

During the recovery phase some processes stabilize while others remain out of equilibrium; however, the rates of change of the processes that build vulnerability remain accelerated. The time-span for responding is short and control of the situation remains fragmented and dispersed among multiple agencies and social actors. At this point, affected people or communities need to develop an ability to cope with the situation.

As reconstruction takes place, rate of change slows and stability is gradually regained. There is a steady definition of functions and action domains among stakeholders and control becomes more proscribed although it may be dispersed among different public agencies or community organizations.

The circle comes to a close with a return to normality. Depending on the extent of the disaster's impact, people and communities need to adapt to new locations and housing facilities, new social or family environments, and new living conditions based on post-disaster economic or health situations.

Once it is accepted that vulnerability is a social process, not a matter of fate, it becomes possible to generate capacities to diminish it and better anticipate not only the likely occurrence but the potential impact of disasters. Planning is a purposeful process that links knowledge to action in order to induce changes geared toward desired future outcomes.

Generally, the spatial changes evident in Mexico City have not been the product of planning. Rather, rural-urban migration and the quest for employment opportunities brought about chaotic growth and the generation of irregular settlement. Immediate demands for services (streets, sidewalks, transport, water, electricity, drainage) prevented coordinated and participatory planning. This situation is exacerbated by the relative autonomy of federal entities, municipalities and delegations that make up the city, each with its own administration and identity. The authorities responsible for urban planning have largely been unable to deal with the spatial impacts of the city's demographic expansion. And, most of these agencies are involved in some manner with disaster response functions and need to perform coordinated actions in this domain. Geodisplat contains information about government agencies and processes involved in the disaster planning environment of Mexico City. The tool includes a section that synthetically identifies these agencies and functions and links them on the Web with detailed information regarding their rules and regulations,

attributes, functions of the different institutions from the civil protection system, relief plans, and disaster programs.

Friedmann (1973) defined planning as "the process by which scientific and technical knowledge is joined to organized action" (246). The use of scientific knowledge in the planning process may seem to put planning in the arena of rationality; however, planning is mainly about human decision making and does not necessarily reflect optimal choices. Fortunately, both science and technology permit us to reduce or at least manage uncertainty through the construction of probabilistic disaster scenarios that estimate impact. These estimations can steer the processes of planning and it is within this framework that Geodisplat exists.

13.6 Geospatial Data and Planning for the Disaster Cycle

All planning models adapted to the decision environment of disaster stages can benefit from adopting a geospatial perspective. According to the National Research Council, "... geospatial data and tools should be an essential part of all aspects of emergency management – from planning for future events, through response and recovery, to the mitigation of future events. Yet they are rarely recognized as such because society consistently fails to invest sufficiently in preparing for future events, however inevitable they may be" (Committee on Planning for Catastrophe 2007: 2). In this section we explore Geodisplat's role in supporting "disaster cycle planning" through its ability to integrate, combine, and deliver geospatial data currently dispersed among multiple agencies in largely incompatible formats.

During the prevention stage it is possible to perform detailed diagnostics and design proposals to better anticipate disaster issues. These plans should account for structural factors that increase the vulnerability of people, systems and infrastructure. Geodisplat delivers information services to support risk mitigation and vulnerability reduction. The geospatial information includes identifying: places containing human settlements exposed to hazards, the characteristics of such places, infrastructure needed to reduce physical vulnerability, the spatial distribution of vulnerable groups, and others. Geodisplat also provides the ability to perform spatial analysis on internal population vulnerabilities in a friendly and efficient manner. This ability allows planning groups to experiment with different vulnerability indexes and to perform sensitivity analyses useful for disaster prevention.

Prevention planning also involves the generation of plans to handle emergencies. Such planning begins by using geospatial information to identify hazards and group vulnerabilities, to design strategies for emergency management, and to support training of first responders (whether public or private). Geodisplat delivers geospatial information such as the layout of places likely to be affected, the spatial distribution of internal vulnerabilities within such places, and the location of critical infrastructure, shelters or available resources. Planners and responders need this geospatial information in order to know the specific characteristics of the places for which they be making decisions during an emergency.

Emergency management plans must be known not only by those tasked with executing those plans, by those likely to fill the role of first responders, as well as by vulnerable groups. For example, during the emergency evacuation phase, first responders need geospatial information regarding streets and the location of shelters, police/fire stations and the like because rescue is followed by transport to a safer area or medical facility. Geodisplat can support the decision-making processes of first responders by providing appropriate hard copy maps or by use of laptops. In terms of the latter, Geodisplat is available on DVD and can be installed on any computer with Windows XP or Vista, with a minimum of 512 MB RAM and 50 MB HD.

Under the right circumstances, post-disaster remote sensing imagery can be quickly acquired to help identify damaged traffic networks or critical infrastructure (e.g., hospitals, fire stations). Such aerial images can be used to help guide effective mobilization of rescuers and relief. Geodisplat can integrate aerial imagery with cartographic georeferences, providing a way to identify and track immediate damage as well as later recovery efforts.

During reconstruction, Geodisplat can support negotiations by generating alternative spatial scenarios that provide the public the reconstruction proposal, its characteristics, and its spatial relationship within the environment of the city. The tool allows users to layer cartographic products, compare different scenarios and the spatial distribution of diverse variables; to construct, display and interact with thematic maps to carry out analyses, ultimately facilitating reflection and dialogue.

To mitigate population vulnerability, special tools are needed to diffuse critical information to individuals and social groups so that they are aware of local hazards. Geodisplat serves that role because people and affected groups can locate where they live and work, and the routes they frequently use, and learn about the hazards to which they are exposed.

13.7 Conclusion

Geodisplat, the cybercartographic tool presented in this chapter, is supported by a conceptual model by which the disaster process is produced and reproduced by social, economic and political structural factors. The process is cyclic and its conceptualization divided in four stages: prevention, emergency, recovery and reconstruction. Rather than using physical events as the focal point, in this model vulnerability is considered to be the active agent that unleashes the disaster or increases its impacts.

Following MacFarlane (2005), the development and application of geospatial data and tools in disaster management should address issues of strategic purposes shared among stakeholders, coordination among actors and local responders, preparation and definition of roles and responsibilities among them, response grounded on the current functions of the agencies involved, communication, cooperation and ongoing risk identification, analysis and mitigation. We believe that Geodisplat's information/knowledge content and ability to interact with and between individuals and groups shows great promise for improving hazard and disaster decision making.

The utility of Geodisplat can be appreciated in three ways. First, it allows the merging or combination in space and time of pieces of information and data from multiple sources (e.g., digital cartography, satellite images, texts, videos). Such information and data are useful in planning processes aimed at disaster prevention, emergency response, victim support and reconstruction efforts. The current dispersal of these data among different government agencies, research institutions, and non-governmental organizations, obstructs their timely and efficient accessibility, comparability and integration. Merging geospatial data allows the user to visualize spatial trends and relationships, as well as to approach the subject of disaster from a variety of perspectives (e.g., local, regional). The tool does not attempt to store and process huge data bases, but to fuse relevant information and data (in the form of vectors, points, raster, texts, and so on) in order to produce holistic images of the hazard or disaster problem. This function may, perhaps, be the main quality that distinguishes Geodisplat from a standard geographic information system.

Second, besides the visualization and querying capabilities, Geodisplat can create risk maps based on a population's vulnerabilities (e.g., lack of access to health services, lack of mobility). And, third, the tool is a stand-alone desktop product that guarantees prompt delivery of geospatial information (e.g., affected areas, shelter location, obstructed roads, emergency telephones, institutions in charge of distributing aid, institutions responsible for evacuation).

Geospatial data and tools have great potential to aid in hazard/disaster planning and to diminish vulnerability and risk in Mexico City. However, its use (at present) is very limited. Geodisplat may change this situation due to its ability to efficiently support decision makers at a variety of levels during different stages of the disaster cycle. As a public research center, CentroGeo can freely distribute the tool to interested relevant agencies.

Acknowledgments Geodisplat was developed by CentroGeo with the support of Agencia Española de Cooperación Internacional and the Consejo Nacional de Ciencia y Tecnología de México.

References

Blaikie, P., Cannon, T., David, I., and Wisner, B. 1995. *Vulnerabilidad: El entorno social, político y económico de los desastres*. Perú: Red de estudios sociales en prevención de desastres en América Latina (La Red).

Brooks, N. 2003. Vulnerability, risk and adaptation: A conceptual framework. Tyndall Centre for Climate Change Research. Working paper 38. www.tyndall.ac.uk/publications/working_papers/wp38.pdf. Accesed 4 september 2008.

Committee on Planning for Catastrophe, Mapping Science Committee, Board on Earth Science and Resources. 2007. *Successful response starts with a map: Improving geospatial support for disaster management.* Division on Earth and Life Studies. National Research Council of the National Academies. Washington D.C.: The National Academy Press.

EM-DAT Emergency Research Data Base. The International Disaster Database, Centre for Research on the Epidemiology of Disaster, Université Catholique de Louvain, Brussels, Belgium: http://www.emdat.be/. Accessed 27 October 2008.

Friedmann, J. 1973. *Retracking America. A theory of transactive planning*. New York Garden City: Anchor Press/Doubleday.

Federal Emergency Management Agency 2005. *Planning for post-disaster recovery and reconstruction.* FEMA 421.

García, A.V. 1993. Enfoques teóricos para el estudio histórico de los desastres naturales. In A. Maskrey (Ed.), *Los desastres no son naturales* (pp. 128–137). Red de Estudios Sociales en Prevención de Desastres en América Latina http://www.desenredando.org/public/libros/1993/ldnsn/LosDesastresNoSonNaturales-1.0.0.pdf. Accessed 27 October 2008.

Guevara, E., Quaas, R., and Fernández, G. 2006. *Guía básica para la elaboración de atlas estatales de peligros y riesgos. Conceptos básicos sobre peligros, riesgos y su representación geográfica.* Serie Atlas Nacional de Riesgos. Centro Nacional de Prevención de Desastres y Secretaría de Gobernación. México. http://www.atlasnacionalderiesgos.gob.mx/metadataexplorer/index.html. Accessed 25 April 2008.

Hamza, M. and Zetter, R. 1998. Structural adjustments, urban systems and disaster vulnerability in developing countries. *Cities*, 15(4), 291–299. Great Britain: Pergamon.

IAS-ISDR, The Inter-Agency Secretariat of the International Strategy for Disaster Reduction. 2004. *Living with risk. A global review of disaster reduction initiatives*, UN/ISDR. http://www.unisdr.org/eng/about_isdr/bd-lwr-2004-eng.htm. Accesed 24 February 2008.

Kasperson, J. and Kasperson, R. 2001. International Workshop on vulnerability and global environmental change. A workshop summary. 17–19 May 2001, Stockholm Environmet Institute, SEI Risk and Vulnerability Program, Report 2001–01. Stockholm, Sweden.

MacFarlane, R. 2005. *A Guide to GIS Applications in Integrated Emergency Management*. Emergency Planning College, Cabinet Office. http://www.ukresilience.gov.uk/~/media/assets/www.ukresilience.info/gis_guide_acro6%20pdf.ashx. Accesed 27 October 2008.

Miller, K. and Nigg, J. 1993. Event and consequence vulnerability: Effects on the disaster recovery process. http://www.udel.edu/DRC/preliminary/217.pdf. Accesed 4 May 2008.

Noji, E.K. 2005. Public health disasters. Consequences of disasters, Second Annual John C. Cutler Global Health Lecture and Award. University of Pittsburg. 29 September. http://www.publichealth.pitt.edu/supercourse/cutlerlecturefullversion.pdf. Accessed 27 October 2008.

Reyes, C., Taylor, F., Martínez, E., and López, F. 2006. Geo-cybernetics: A new avenue of research in geomatics? *Cartographica* 4(1), 7–20.

SEGOB/SNPC. 2008. Programa Nacional de Protección Civil 2008–2012. *Diario Oficial,*México 19 September.

SIIRIDE-ANR-1. 2008. Sistema Integral Sobre los Riesgos de Desastres en México, Atlas Nacional de Riesgos, Centro Nacional de Prevención de Desastres. http://atl.cenapred.unam.mx/website/RiesgosGeologicos/Volcanes/Popocatepetl/viewer.htm; http://atl.cenapred.unam.mx/website/RiesgosGeologicos/RiesgoSismicoDF/viewer.htm. Accessed 27 October 2008.

SIIRIDE-ANR-2. 2008. Sistema Integral Sobre los Riesgos de Desastres en México, Atlas Nacional de Riesgos. Programa Interactivo de visualización. Centro Nacional de Prevención de Desastres.http://www.cenapred.unam.mx/es/Atlas/.Accessed 27 October 2008.

Tapia-Silva, F.O., Nuñez, J.M., and López-López, D. 2007. Using SRTM DEM, Landsat ETM+ images and a distributed rainfall-runoff model to define inundation hazard maps on urban canyons. *Proceedings 32nd International Symposium on Remote Sensing of Environment*. San Jose, Costa Rica, June 25–29.

Tobin, G.A. 1999. Sustainability and community resilience: The holy grail of hazard planning? *Environmental Hazards. Elsevier Pergamon* 1, 13–25.

Voguel, C. 1998. Vulnerability and global environmental change. *World Commission on Environment and Development. Our Common Future.* Oxford: Oxford University Press.

Wilches-Chaux, G. 1993. La vulnerabilidad global. In A. Maskrey (Ed.) *Los desastres no son naturales* (pp. 11–44). Red de Estudios Sociales en Prevención de Desastres en América Latina http://www.oei.es/decada/portadas/Desnat.pdf. Accesed 2 March 2008.

Chapter 14
Integration of Tsunami Analysis Tools into a GIS Workspace – Research, Modeling, and Hazard Mitigation efforts Within NOAA's Center for Tsunami Research

Nazila Merati, Christopher Chamberlin, Christopher Moore, Vasily Titov, and Tiffany C. Vance

Abstract The National Oceanic and Atmospheric Administration's (NOAA) Center for Tsunami Research (NCTR) uses geospatial data and GIS analysis techniques in support of building an accurate tsunami forecasting system for the US Tsunami Warning Centers. The resulting forecast products can be integrated into applications and visualizations to assess hazard risk and provide mitigation for US coastal communities ranging from small towns to large urban centers. NCTR also conducts basic research on the nature of tsunami propagation and inundation, which relies on accurate geospatial information. In this chapter, we discuss how we have used both open source and commercially available geospatial technologies to address issues in tsunami research and hazard mitigation – including model visualization, data delivery, and emergency management products. Additionally, we discuss the development and coupling of tsunami model results with coastal risk, vulnerability, and evacuation models, raising the issues of integration, visualization, proliferation of mapping applications, and the ease of use and intended audience of these products.

Keywords Tsunami · GIS · Modeling · Inundation · Hazard assessment · Data management · Bathymetry · Mapping · Emergency management · Coastal processes

14.1 Introduction

The December 26, 2004 Sumatran event showed the world the devastating impact of a large-scale tsunami. Geographic Information System (GIS) and remote sensing information was integral to the rapid assessment of the situation and was later used to support recovery and rebuilding efforts. National Oceanographic and Atmospheric Administration (NOAA) scientists delivered rapid assessments of this event

N. Merati (✉)
NOAA/PMEL/NCTR/JISAO, Seattle, WA 98115, USA
e-mail: nazila.merati@noaa.gov

P.S. Showalter, Y. Lu (eds.), *Geospatial Techniques in Urban Hazard and Disaster Analysis*, Geotechnologies and the Environment 2, DOI 10.1007/978-90-481-2238-7_14,

using GIS to compare tide gauge and buoy measurements, for field surveying of damaged sites, and to make comparisons with model output (Venturato et al. 2005).

At NOAA's Center for Tsunami Research (NCTR) geospatial information such as imagery, digital elevation models (DEM), LIDAR, and GIS data are applied and integrated into the tsunami research and forecasting workflow. Currently we are expanding our use of techniques for analyzing inundation model output and rapid visualization of forecast events through the use of spatially enabled databases, the use of Python and model building capabilities in ArcGIS™, creating Google Earth™ KML, and integrating the GeoTools (an open source JAVA GIS toolkit; GeoTools 2008) library into desktop and web based applications.

It is well known that models do not operate independently of their data. In the case of hazard mitigation, modelers need to integrate real-life data into their workflow. The integration of GIS into disaster response and mitigation has proven invaluable as shown for Hurricane Katrina and other large-scale disaster recovery efforts (Eveleigh et al. 2006; Merati et al. 2007; Vance et al. 2007).

14.2 Tsunami Research and GIS

NCTR is located at the Pacific Marine Environmental Laboratory in Seattle, Washington. NCTR evolved from NOAA and state-funded programs, including the National Tsunami Hazard Mitigation Program (NTHMP). The NTHMP started as a joint effort by NOAA, USGS, FEMA, and the states of Hawaii, Washington, California, Alaska, and Oregon to prepare US coasts and coastal urban centers for tsunami events. Through the efforts of the NTHMP program, the Pacific Marine Environmental Laboratory (PMEL) became the home of the Tsunami Inundation Mapping Efforts (TIME) program, whose aim was to integrate geospatial data and techniques to support tsunami research and hazard mitigation. The 2004 Indonesian Sumatra event elevated GIS efforts at PMEL and led us to better incorporate geospatial information and technologies into our data processing and into the generation of products for researchers and our clients – the tsunami warning centers and emergency managers. The NTHMP has now been expanded to include all US coastal states, territories, and possessions.

NCTR's mission is three-fold. First, NCTR works to design and develop tsunami detection devices and build monitoring systems. Second, NCTR provides research, development, and implementation of numerical models to increase the speed and accuracy of operational tsunami forecasts and warnings provided by the NOAA Tsunami Warning Centers (TWC). Third, NCTR conducts research and development to improve methods of predicting tsunami impacts on populations and the infrastructure of coastal communities (http://nctr.pmel.noaa.gov/tsunami-forecast.html). All three mission goals require some dependence on geospatial infrastructure – whether we are building a site suitability map or designing a model to determine at-risk population within an inundation zone. Examples include buoy siting optimization studies, producing static maps for briefings and updates, building database applications for data dissemination and storage, and

development of stand-alone analysis and visualization tools. Additionally, GIS data and technologies are currently integrated into the NCTR development of the Short-term Inundation Forecasting for Tsunamis (SIFT) software used locally for analysis and deployed to NOAA Tsunami Warning Centers for operational use. NCTR has long recognized the need to provide information in a GIS format to emergency managers and state partners. In this chapter, we outline how NCTR integrates geospatial technologies in the daily workflow for data access, for modeling support and error checking, and for producing products used by our partners.

NCTR uses geospatial techniques, information, and applications to directly support two of three of our mission goals – the development and implementation of numerical models to increase the speed and accuracy of tsunami operational forecasts and warnings, and research and development to improve methods of predicting tsunami impacts on population and infrastructure of coastal communities. ArcGIS™ is used for grid development, bathymetric error checking, scripting, and basic GIS analysis capability. NCTR uses Python to script our tsunami model output and perform data conversions as well as for geoprocessing routines. Data management procedures utilize OpenGIS Consortium standards using PostgresSQL and PostGIS. Our data warehouse relies on web mapping services using the Minnesota Map Server (MapServer 2008).

Model integration and functionality is achieved by using GeoTools, an open source library that allows us to build GIS functionality and products into the MOST inundation web interface (http://geotools.codehaus.org/). A standalone GIS application called Tsunami GIS uses ESRI's™ ArcEngine and Java to visualize inundation and to analyze results.

New tools developed by the atmospheric and modeling community to integrate netCDF file types into the ESRI™ suite, including time series analysis and rapid automation of animations, increases the use of GIS by the modeling community. While not necessarily replacing the functionality of products such as MATLAB®, these new tools add the ability to interrogate layers for a given point or adding other layers of information.

14.3 Tsunami Modeling – MOST Model

A tsunami is a series of waves generated in a body of water by a disturbance that vertically displaces the water. These disturbances push water upwards, sideways, or downwards to create tsunami waves. The waves have extremely long wavelengths and periods and can propagate across the oceans, inundating coastal areas. Most often caused by earthquakes and landslides, tsunamis can also be caused by volcanic eruptions (NCTR 2008b).

PMEL uses the Method of Splitting Tsunami (MOST) numerical model for tsunami research and software development to develop faster and more accurate tsunami forecasts. The MOST model is a finite difference model that simulates, in three distinct phases, tsunami behavior due to underwater earthquakes – generation of the earthquake, transoceanic propagation of the earthquake, and inundation of

dry land (Titov and González 1997). The MOST model is currently being refined to create products for NOAA's Tsunami Warning Centers forecasting operations as well as products for inundation modeling of coastal communities. The model is used to determine wave height, arrival time and inundation extent and depth for tsunami events. This effort requires pre-processing of propagation data so that, as real time data from the Deep-ocean Assessment and Reporting of Tsunami (DART) buoys come in, the warning centers and tsunami modelers are able to determine more precisely the coastal forecast (Percival et al. forthcoming; Venturato et al. 2007). These forecasts are output as netCDF files. Geospatial technologies and products, such as accurate bathymetric and topographic models, source data, and archived historical records are all available to the MOST model. Inundation of coastal areas, using pre-selected scenarios based on past events and simulations, are used to develop tsunami inundation maps used by emergency managers to plan evacuations. Currently, MOST is being expanded by NCTR personnel to allow for desktop use by the warning centers for real-time forecasting and for post-event analysis (Denbo et al. 2007).

As part of the tsunami forecast system, NCTR is building Stand-by Inundation Models (SIMs) for 75 US coastal communities. The work is to be completed by the end of 2011. SIMs are pre-calculated 4-hour simulations of tsunami wave inundation, run-up, and created using high-resolution bathymetric and topographic data covering a specific community or harbor area. They are implemented into the tsunami forecast system (SIFT) and optimized to run within a few minutes during an tsunami event (Wei, in prep.). The SIMs model scenarios using likely earthquake source locations for the area in question and earthquakes at a variety of probable magnitudes. Historical observations are used to validate the model results. To date, 35 communities have been completed. The urban areas for which SIMs has been completed include San Diego, San Francisco, and Los Angeles (the Harbor area), California; Honolulu, Hawaii; and San Juan, Puerto Rico.

14.4 DEM Development

The MOST model relies on accurate bathymetric and topographic information, especially for near-shore environments. GIS techniques have proven effective for building seamless DEMs of bathymetry and topography at finely scaled resolutions. An abundance of new data, including LIDAR, multibeam sonar, and other remotely sensed imagery, plus rapid dissemination of these data make the development of DEMs faster and more accurate. Since 1995, NCTR has developed merged bathymetric and topographic grids at varying scales for areas of interest, from basin-wide to cities and coastal communities. DEMs are built using the best available data including shorelines, bathymetry, and topography from a variety of sources. Stringent quality checking is performed as each DEM is developed. Of particular concern is the transition between edges – along and between the data sources of varying quality and resolution, which could cause a grid mismatch. Developing a bathymetry grid that has been error checked and standardized to one vertical datum

using GIS software insures the MOST model will run smoothly (NCTR 2007). For inundation modeling, output grid cell spacing ranges from 1/3 to 1 arcsec (approximately 10−30 m) depending on the source data.

In the past, NCTR performed in-house development of grids for areas of interest. As the number of areas undergoing modeling increased, we contracted with NOAA's National Geophysical Data Center (NGDC) to develop DEMs for tsunami modeling (NGDC 2008a). To develop a DEM, NGDC acquires data from federal, state, and local sources, then quality-checks the data using ArcGIS™. Careful vertical datum adjustments are necessary as bathymetric and topographic data may be measured relative to differing vertical datums. Data are edited to remove outliers and clipped to the correct dimensions. If the data are sparse, which can be the case for older single beam bathymetric surveys, NGDC uses Generic Mapping Tools (GMT) to interpolate or infill these data sets. Data are finally gridded using MB-System software to extract the xyz data from ESRI™ shapefiles and to assign weighting in order to use the best data value for each cell value. A spline is used to interpolate data and assign a value to each DEM grid cell.

While NCTR and NGDC strive to create the best DEM for each area, issues commonly encountered during processing include geomorphologic and anthropogenic coastline change that occurs between the time the data were collected and the time they are used, data mismatches, and data quality errors. Tools such as Google Earth™ and satellite imagery allow for rapid validation of features that are in question. In addition, ArcGIS 3D Analyst™ and Spatial Analyst tools (e.g., hill shading, slope calculations) allow scientists to view DEMs in perspective and note outliers that may need to be regridded and edited (NGDC 2008b).

14.5 Community Model Interface for Tsunami (ComMIT)

The Second Session of the Intergovernmental Coordination Group for the Indian Ocean Tsunami Warning and Mitigation System (ICG/IOTWS II; December 2005) in Hyderabad, India recommended establishing a web-based community model for tsunami modeling. It was envisioned that the Community model and associated tools would be the primary avenue to transfer modeling expertise and capabilities to and between Indian Ocean countries. Funding was provided by the United Nations Educational, Scientific, and Cultural Organization (UNESCO) and the United States Agency for International Development (USAID). NCTR was tasked with developing the Community Model Interface for Tsunami (ComMIT). It was quickly apparent that ComMIT would have applicability not only in the Indian Ocean, but world-wide as a tool for web-based modeling, elementary forecasting, model development, education, and emergency management.

The framework of ComMIT is based on the Short-term Inundation Forecasting for Tsunamis (SIFT) forecast system designed at NCTR. The Standby Inundation Models (SIMs) from SIFT give very accurate results for inundation and current velocity in the area of interest. Typical SIMs cover several kilometers of shoreline and extend inland to cover densely populated urban areas (Wei, in prep.). Running a

SIM requires the modeled propagation results, combined in such a way that they best match the deep-ocean buoy measurement of the incoming tsunami wave. The propagation model (a linearized version of MOST), outputs two velocity components, as well as sea-surface height, in three netCDF files covering an entire ocean basin. It became apparent that there was a need to quickly create a subset of the propagation model output, perform the scaling and combination, feed them to the inundation model, and track the output. ComMIT was designed to address that need.

ComMIT is written in the Java programming language and accesses a database of propagation model netCDF output files using the OPeNDAP interface (NCTR 2008a). ComMIT allows the user to easily select among these files according to the deep-ocean buoy measurement, launch the MOST code, and monitor the inundation. Figure 14.1 shows the ComMIT application main window. The window has a map (upper left) of the ocean basin, with rectangular seismic fault planes covering subduction zones. Each rectangle represents a single propagation model run (approximately 5.5 Gb each, for a total database size of 1.5 terabytes). In the example, four fault planes have been selected (in red) near the Aleutian Islands, and the Crescent City SIM has been selected as the at-risk community. ComMIT downloads subsets of these propagation model files, sized to cover the outermost of the three nested grids that the inundation MOST model requires, and launches the computational code.

Figure 14.2 shows the ComMIT wave amplitude window with inundation output for the Crescent City harbor. This model has been optimized to run in a very short period of time (typically less than 10 min), allowing the Tsunami Warning

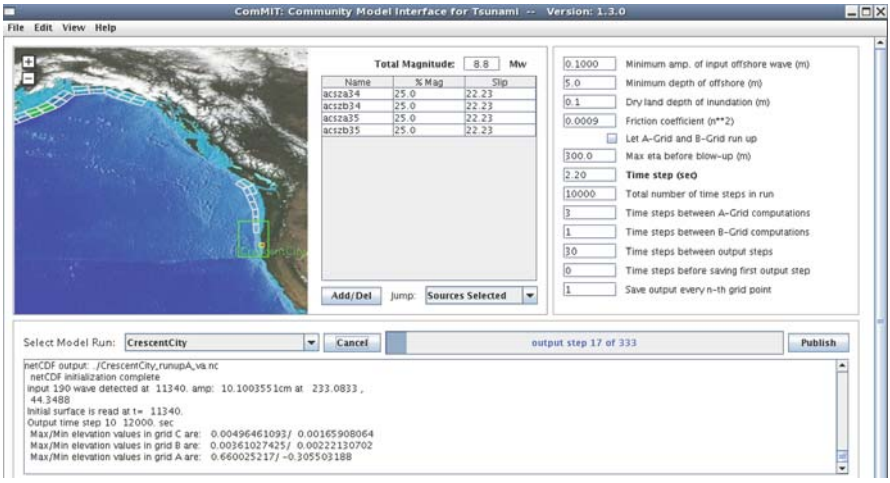

Fig. 14.1 The Community Model Interface for Tsunami (ComMIT) showing a hypothetical Mw = 8.4 seismic event generating a tsunami in the Aleutian Islands and a Standby Inundation Model (SIM) of the at-risk community, Crescent City, CA

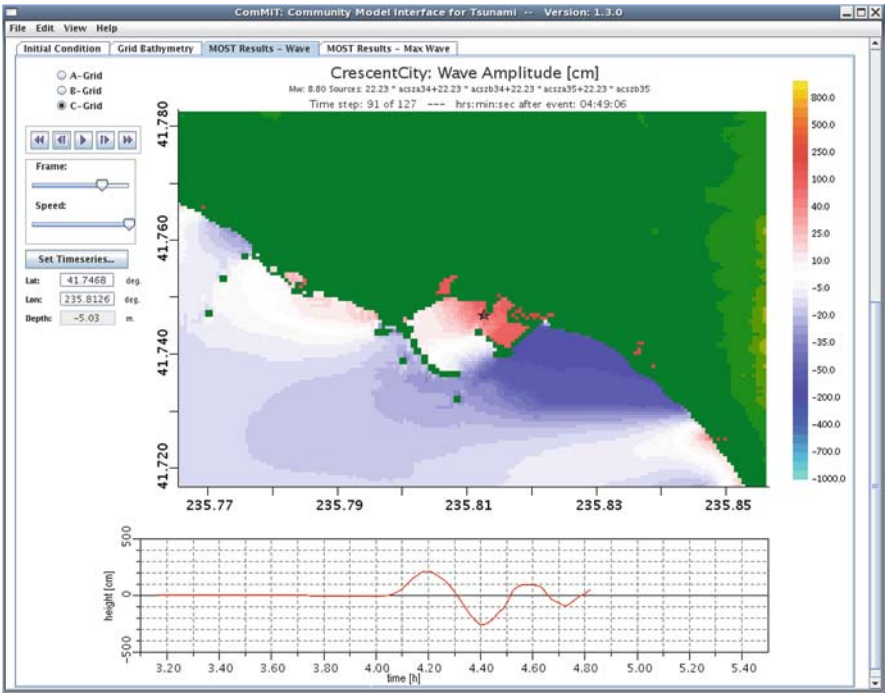

Fig. 14.2 Wave amplitude window showing MOST model results of Crescent City harbor inundation using hypothetical Aleutian Island forcing files. Note the time series location marked by the *star*

Centers to not only issue a detailed warning, but to provide detailed images and animations to emergency managers. Since the FORTRAN-based computational code outputs inundation results in netCDF format, ComMIT can return snapshots of maximum amplitude, sequences of geo-referenced images, files in standard GIS formats (e.g. netCDF for native read, shapefiles, ASCII raster) or Google Earth™ files (Fig. 14.3).

ComMIT allows control of all of the MOST model input parameters, and access to the model output files for analysis. Selecting the scaling of the propagation files requires using a data assimilation inversion technique as part of the NCTR forecast system. ComMIT interfaces with the forecast system to receive this inversion information, and can perform the scaling automatically, allowing ComMIT to act as a forecast model during an event.

ComMIT has been found valuable both in developing SIMs, validating for historical accuracy, and as an educational tool to teach the basics of tsunami modeling and the NOAA tsunami forecast system. During 2007, four courses to teach how to use ComMIT were held in Melbourne, Australia (January), Bangkok, Thailand (June), Seattle, Washington (July), and Jakarta, Indonesia (September). Three courses were been offered in 2008 in Mahe, Seychelles (January), Cadiz, Spain (April), and Valparaiso, Chile (May).

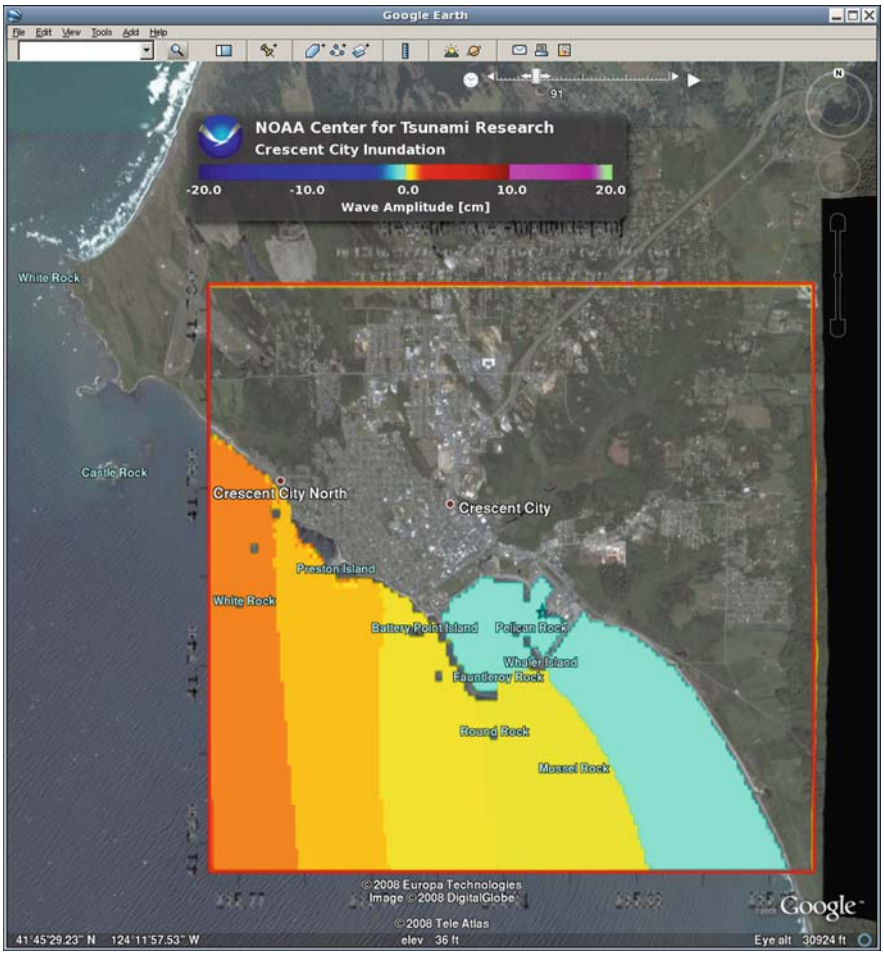

Fig. 14.3 Results from the Crescent City wave amplitude plot showing the height of a tsunami wave at a time slice during an inundation event. The amplitude is the height of the wave from mean sea level. In this case, at the current time step, the leading wave coming into the shoreline is in the trough part of its phase, thus showing a lower amplitude that the off shore amplitude which is positive. Geospatial formats such as GeoTIFFs of ComMIT output overlaid in Google Earth^{TM} provide users a way to integrate model results into an easily navigated and useable format

14.6 NCTR Atlas

The NCTR Atlas is an internal web application used to store and display information about the modeling locations and data used by NCTR for tsunami forecasting. The Atlas stores relevant metadata for the sites planned for inundation modeling, the bathymetric grids used as input to the models, and records of historic tsunami events used to validate the models. Design requirements included web accessibility for attractive, simple maps, integration with GIS and mathematical applications, and

ease of use for data producers and consumers. At NCTR, the Atlas is used by scientists to discover and download the data they need for their work, by data managers to ensure that collected data are complete, and by management to track the progress of modeling efforts. The Atlas also operates as a data service, providing information in an XML-based format to other applications.

The Atlas web interface is focused around maps of the current area of interest. Users of the Atlas are presented with a map view of the area in which they are interested. The maps can be customized to display bathymetric and topographic contours of the area, extents of bathymetric modeling grids, areas of urbanization, population density, and similar layers. The Atlas tracks the progress of modeling, including initial development, testing, and documentation, and produces reports summarizing current model status by fiscal year and assigned personnel.

Grid details, including grid extents, resolution, content, relevant population centers, and type are displayed on each map view. Users can download the source grids for use in GIS applications and as source inputs for the MOST model. Written reports, documentation, and metadata are stored for each model and grid, and can be downloaded from the web interface. Model locations and grid extents are also exported as a Web Feature Service (WFS), an open GIS standard that can be read into many applications, including ArcGIS^{TM} using the Interoperability Extension.

The Atlas stores historical and recent tsunami event information including seismic source information for each event, and recorded tide gauge and bottom-pressure recorder time series. This information is essential for validation of newly developed site-specific inundation models, and for testing potential changes to the numerical modeling codes. The Atlas can import time series data in several formats, present simple graphs of the data automatically, and export the data in text-based or netCDF formats for further analysis.

Recent work on the Atlas has focused on integration with NCTR's other software systems. In this capacity, the Atlas serves as a central database for tsunami model and event data, providing a consistent set of data to NCTR's diverse users. Through its XML-based web application service interface, the Atlas allows external software to query and update the database. For example, tsunami events are automatically added to the database as soon as they are broadcast by the tsunami warning centers; these events are then passed to the WebSIFT real-time modeling interface.

The Atlas is implemented with custom software written in the Python programming language, using the Django web framework. The application is backed by a PostgreSQL database with the PostGIS spatial extension. Mapping is done by the UMN MapServer, an open-source mapping toolkit.

14.7 Coordinated Efforts with State partners – Inundation Mapping

If one draws a buffer overlay from the shoreline to approximately one kilometer inland of the West Coast of the United States, over 1.2 million people could be affected by tsunami inundation (González et al. 2005). Inundation mapping is useful

for communities and emergency managers in determining the extent of coastal storm events and tsunami inundation. Mitigation efforts include physical maps that are distributed to communities as brochures, open file reports, and evacuation routes that are found in the public service section of local phone books. Inundation maps are also available via the Internet. While to some they appear off putting, having an inundation line mapped with proximity to roads, infrastructure, and evacuation routes puts many minds at ease. Inundation maps require model runs as input along with a good level of knowledge of local landmarks and hazards that may hamper or inhibit evacuations. In the past, inundation maps had been developed by the states with little input from tsunami modelers. One of the major foci of the NTHMP was to create tsunami evacuation maps for affected coastal areas based on the threat of a near-field tsunami triggered by an event in the Cascadia Subduction Zone off the northwestern coast of the United States and other far-field earthquake sources in the Pacific Ocean.

Inundation and hazard mapping was undertaken by PMEL's TIME Center. The Center was tasked to develop an infrastructure to support tsunami inundation modeling in support of the NTHMP Program and to create tsunami inundation maps using model output. The mapping effort focused on the five states associated with the NTHMP steering committee and produced inundation maps and products useful to the states and their local emergency managers. TIME scientists worked to derive the best available bathymetry, shoreline, and topographic data to create gridded bathymetric products to run inundation models (Bernard 2005). While the best available data are used for shoreline derivation and shoreline changes, the development of a seamless DEM is not trivial. TIME scientists worked to develop a methodology to describe tidal datum distributions that use tidal harmonic constants for each tide station within Washington State's Puget Sound region to derive an accurate tidal datum for the area of interest (Mofjeld et al. 2004). The Puget Sound region is home to over 4 million people; as with other coastal urban areas, small errors in DEM interpolation could translate into miscalculating the population at risk. Numerical model results, including resulting maximum wave heights and velocities, were used to develop inundation products for the NTHMP partners. ArcGIS^{TM} products were used for grid development and error checking of these grids (Titov et al. 2003).

In all, 22 inundation maps were developed for the 113 communities identified as at risk. Figure 14.4 is an example of a typical inundation map in the event of a near-field Seattle Fault Earthquake of moment magnitude (Mw) of 7.3 showing areas around Elliott Bay that would be inundated according to output from MOST model runs.

More sophisticated levels of hazard assessment incorporate land use and land cover with inundation mapping to assess what landscape features will be adversely affected by a tsunami event. While the MOST model requires bald earth topography, incorporating wave height, velocities, and amplitudes into a GIS system can assist in understanding how and where populations and structures may be impacted by tsunami events.

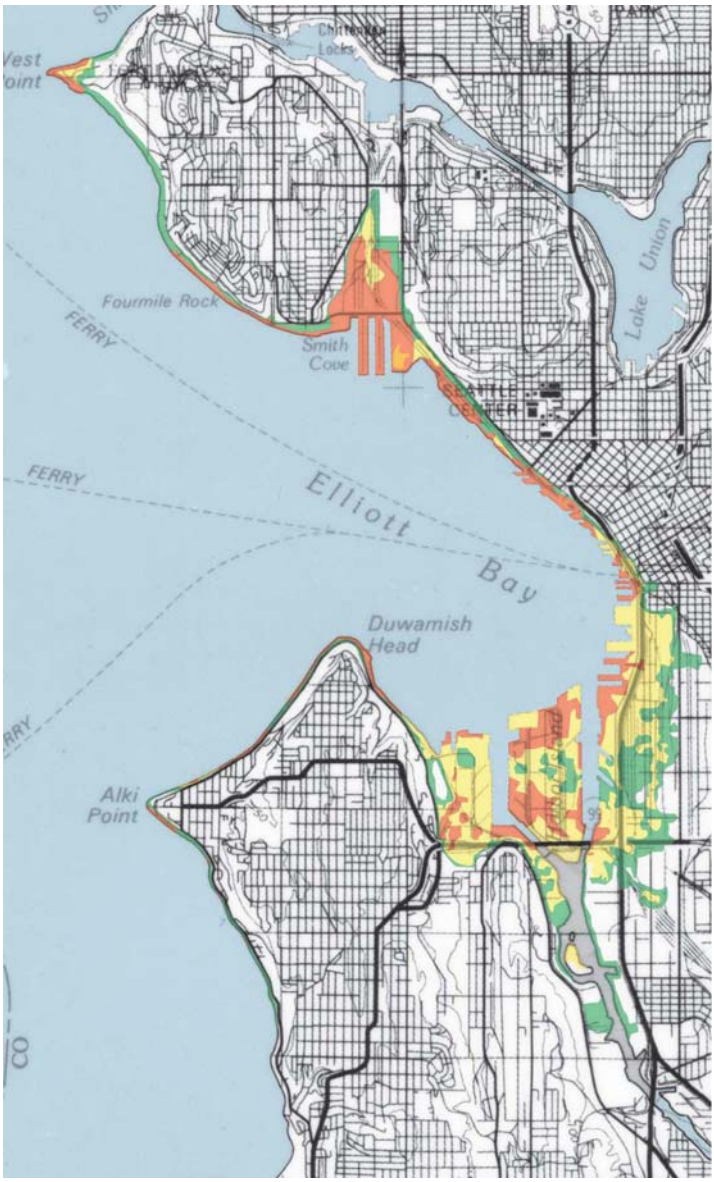

Fig. 14.4 Blow up of Tsunami Hazard Map of Elliott Bay Area, Seattle, WA: Modeled tsunami inundation from a theoretical moment magnitude (Mw) 7.3 along the Seattle Fault (not pictured). Green areas are inundated 0–0.5 m, yellow areas 0.5–2 m and orange from 2 to 5 m in depth (Source: Walsh et al. 2003)

In 2006, NCTR was asked to evaluate the suitability of Ford Island at Pearl Harbor, HI, which is under construction as the new home for the Pacific Tsunami Warning Center, in relation to the likelihood of tsunami inundation. Modeling scenarios used far field tsunami sources to model the impact of a tsunami affecting Oahu and the site of the new building. Model results demonstrated that historical and modeled scenarios produced no inundation higher than 1.5 m above mean high water. The proposed building height is at 3 m above mean high water. While GIS was not used for the suitability analysis, GIS software and the building of detailed bathymetry, topography, and satellite imagery was used to ground truth the data (Tang et al. 2006). Subsequent research to improve our methods is described in the following section.

14.8 Technical Aspects

The geoprocessing functions in ArcGIS™ simplify the process of selecting, projecting, processing, buffering, and converting data into formats that work well with each other. Models are created in Python and run in batch form using scripting formulas for converting from census information to the correct format and correcting for the area of each block group that is affected by inundation. Modifications can be made to the code to allow users (emergency managers or GIS analysts) to rerun the population-at-risk calculations for areas that may not have been analyzed yet or to adjust the parameters of the algorithm to better suit their area of interest. For example, by using the likely maximum wave height for tsunami events developed from each SIM area, we were able to build an accurate assessment tool for coastal areas of interest (Merati et al. 2007).

Recently, ESRI has supported the use of Python as a scripting language. Python is an object-oriented programming language that is widely used for a variety of applications. Its simple syntax and flexible, dynamic nature make it easy to learn, and there are libraries available to support many scientific analysis tasks (van Rossum 2006). The use of Python allows GIS programmers to create models and scripts that can run within ArcGIS™ or stand alone to provide geoprocessing and batch scripting for file configuration, model iteration, or complex modeling actions.

Python's base level of code and libraries is extensive and extendible. In ArcGIS™, anyone can write Python scripts to call different functions and interact with data. The ability to call scientific Python to do more complicated spatial functions provides a level of functionality beyond standard GIS processing that makes it more appealing to the modeling community. NCTR has created Python scripts to convert between model native formats and ArcGIS™ formats (ESRI™ grids and xyz triplets, commonly used by modelers) and for grid resampling. The scripts are used as stand alone scripts or as ArcToolbox add-ins.

Using ArcGIS™ Model Builder and integrating multidimensional tools into ArcGIS™ allows NCTR modelers to add their data to ArcMap, build a model

to grid and resample their data, create rasters and interpolate the results, and then display their data. The addition of iteration, feedback loops, and automation allows researchers to process their data using ArcGIS™. Outputting Model Builder results into Python and adding code to place the output into specific directories and clean-up temporary files makes processing and creation of tsunami output more efficient. Using Modelbuilder to automate the generation of images from MOST model results utilizes the Animation toolbox in ArcGIS™. Resulting animations can be played as standalone visualizations of scenarios or embedded within other applications

The resulting images or raster data sets can easily be added to raster catalogs and animated to display the results of tsunami wave propagation or inundation for different scenarios Creating a 3-D view of the inundation or propagation event and combining this with building footprints, topographical features, and hazardous areas enhances planning and mitigation efforts. The ability to perform geoprocessing on raster layers, add vector data such as shorelines, population centers and hazards, and critical infrastructure, then interact with the data makes this a much richer application than standard 2-D animations and static maps. One drawback is that it takes longer to generate than a MATLAB animation, which reduces its utility in real-time situations, but it is still useful for post-event processing and scenario testing. An added benefit is that placing the animation into ArcGlobe provides researchers the opportunity to show the public and policy makers a powerful visualization of the global impact of historic tsunami events (Merati et al. 2007).

For emergency management purposes, model output needs to be integrated with socio-economic and infrastructure data, as well as evacuation routes and the location of vulnerable populations. These types of data are easily accessible in GIS formats. A prototype application containing such types of data was developed using ESRI's ArcEngine, providing a way to visualize results and perform common analysis functions found in a GIS but often difficult to run in modeling software packages. ArcEngine is an ESRI developer product for creating and deploying ArcGIS™ solutions that can be customized for the user community. The product is a simple API-neutral cross-platform development environment for ArcObjects – the C++ component technology framework used to build ArcGIS™. ArcObjects is at the core of ArcGIS™ functionality and includes tools such as: intersect, proximity (buffer or point distance), surface analysis (aspect, hillshade, or slope), and data conversion (shapefile, coverage, or DEM to geodatabase) (Vance et al. 2007). Using ArcEngine, solutions can be built and deployed to users without requiring that ArcGIS™ Desktop applications (ArcMap, ArcCatalog) be present on the same machine. This product is a developer kit as well as a deployment package for ArcObjects technology. Desktop deployment of ArcGIS™ is not required to run these scenarios, which eases deployment of this tool in field situations or to developing countries (Vance et al. 2007).

14.9 GIS Case Study Illustrating the NCTR Workflow

14.9.1 Seaside, Oregon – Probabilistic Modeling and Modernization of Flood Hazard Maps

Probabilistic modeling has been used to estimate flood inundation, landslide hazard and hydrodynamic modeling. Integration of these models with GIS is reviewed in the literature (Martin et al. 2005; Zerger and Wealands 2004; Zerger 2002).

The US Federal Emergency Management Agency (FEMA) has developed flood insurance maps for areas within traditional flood prone areas (e.g., low-lying flood plains). Flood Insurance Rate Maps (FIRM) serve as the official FEMA document marking flood hazard zones and the resulting insurance premium zones for each community mapped. Hydrological models and meteorologists use long time series of river gage data to determine the probability of flood risk within a given area. The same concepts were applied in a pilot study to determine if predictive inundation mapping could be used to map the probability of tsunami inundation at 100- and 500-year levels. One hundred and 500-year flood levels are defined as the possibility that the (average) water elevation would be exceeded 1% or 0.2% of the time in any year (Wong et al. 2006).

The community of Seaside, Oregon was selected for testing for a variety of factors, including the availability of paleotsunamic and seismic records, recent tsunami flooding, earthquake source recurrence, and excellent availability of baseline data for tsunami modeling. Probabilistic Tsunami Hazard Analysis (PHTA) was used in this study to model the magnitude of tsunami flooding from a variety of sources at different recurrence rates (Wong et al. 2006). The development of the hazard analysis required development of a DEM for the area in question for use by the MOST model. Near-field sources (the Cascadia Subduction Zone) and far-field sources (Kuril-Kamchatka, Aleutian/Alaska, and Chilean Subduction zones) were also used to run the MOST model at various earthquake magnitudes. Maximum wave heights from the MOST model were input into the PTHA model. These data were combined with tidal data and inundation data for each grid point to determine if a grid cell would exceed a given flooding threshold and become flooded or not. The grid cells were contoured to create the 1% and 0.2% contours that translate to the 100- and 500- year occurrences. Figure 14.5 compares the 100 and 500 year tsunami inundation line for Seaside using probabilistic analysis using a combination of near and far source scenarios modeled.

Results from the 100-year study showed that a small area of the study site would be flooded. However, in the event of a 500-year inundation, a large area of Seaside was flooded with wave heights exceeding 4 m. This study demonstrated that model data were easily integrated into a probabilistic GIS model to create hazard curves for assessing risk. The results of this study were later used by Dominey-Howes et al. to assess vulnerability to Seaside structures using tax parcel information and the US multi-hazard loss estimation software (HAZUS-MH) database (Dominey-Howes et al., submitted).

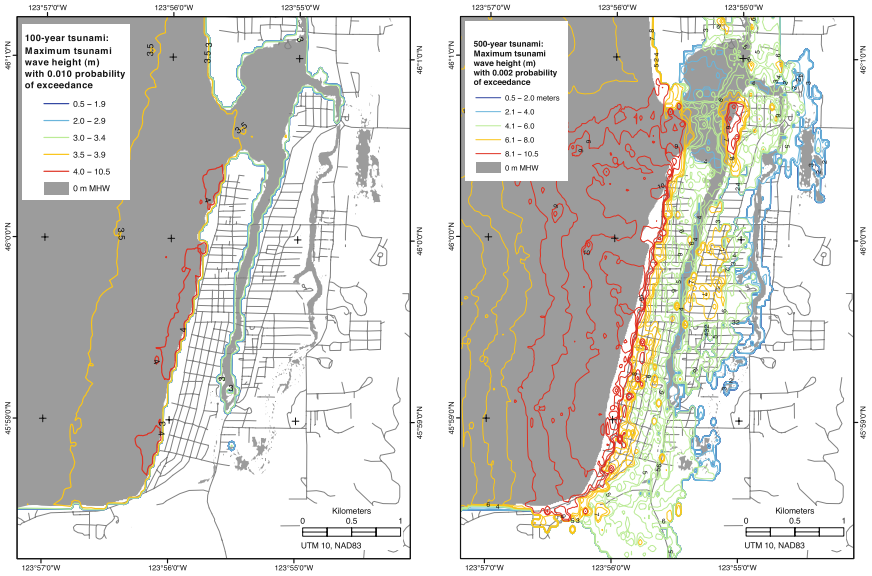

Fig. 14.5 Tsunami wave heights (in meters) of the 1% (*left-hand panel*) and .2% (*right-hand panel*) probability of exceedance for Seaside, Oregon (Source: Wong et al. 2006)

14.10 Tools for Use by Emergency Managers and Urban Planners

14.10.1 Tsunami GIS

While we have focused on the use of geospatial tools and analysis by tsunami modelers, the information we produce must ultimately be used by planners and emergency managers to prepare for and mitigate the impact of tsunamis. Scenario testing and collaborative GIS use by emergency personnel, city managers, and first responders requires a streamlined GIS application that is portable and customizable with newly created data, especially in the case of rapid response.

Tsunami GIS is an application that allows users to create inundation scenarios for pre-calculated near-shore and off-shore sources for a tsunami event in a selected region. The ArcEngine development environment lets us build a stand-alone GIS application that has the look and feel of a standard ArcGIS™ desktop, but with tsunami-specific menus added to the standard ArcGIS™ functionality and editing capabilities. The geoprocessing application programming interface (API) operates in the backend to merge the gridded inundation result with census information for the area of study to create a new polygon of affected areas. Users are able to edit their own data and add new information as necessary. Census data are used to calculate estimates of populations at risk including the elderly or handicapped. Critical infrastructure – hospitals, schools, bridges, and emergency centers – within the inundation

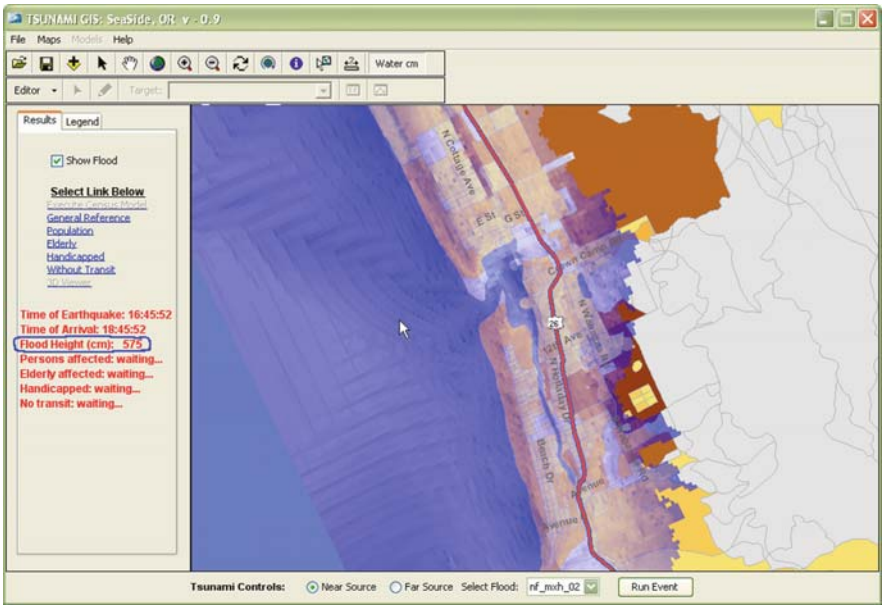

Fig. 14.6 Tsunami GIS interface shows the result of a near shore event inundating Seaside, Oregon. The census blocks covered with the inundation polygon (*blue*) (nf_mxh2) are affected by this event. The ArcEngine framework allows customization of the ArcMap window such that new tools can be added – in this case, a cursor hovers over the inundation polygon and returns a water height for the inundated area on the left hand panel of the application (*circled in blue*)

zone can be highlighted and standard geoprocessing functions such as proximity analysis run to determine mitigation strategies. Users are able to print maps and reports and export map images to be used in operation manuals and reports.

The final product is a map of inundated areas and estimates of affected population in the inundation zone. The tsunami height modeling application shown in Fig. 14.6 is an example of modeling the inundation phase for the city of Seaside, Oregon; data were derived from the probabilistic tsunami analysis work done in Seaside, and it uses both near-shore and far-field sources and the resulting inundation grids (Merati et al. 2007).

ArcEngine's framework allows users to add their own data sets (e.g., inundation grids, evacuation routes, and infrastructure) as well as links to live data feeds and servers to add current and derived data products "on the fly". The ability to customize the application using the ArcObjects modules will allow developers to implement additional models and algorithms as they are developed, from elevation data and distance from the shoreline to the calculation of populations at risk. The ability to run the tool and change parameters such as the height of the tsunami also supports scenario testing.

Tsunami GIS has made it easier to combine modeling results with related socioeconomic data in support of emergency management. Being able to link models

with socio-economic data provides planners with a powerful tool to plan for and mitigate the impacts of tsunamis.

14.11 Discussion

GIS packages are starting to share software code and objects to allow closer coupling of core GIS functionality and analytical/modeling tools. Through the use of Java-based APIs and connectors, a GIS front-end is directly linked with models. The Python scripting language, the proliferation of PostGIS and the PostGIS and PostgresSQL databases, native data readers (netCDF, HDF4), and visualization tools are making it easier to integrate model output into GIS. Outputting model results as Google Earth™ KML enhances products for hazard mitigation by giving the end user a visual reference – an updated map or context for decision making.

The lack of standard data formats can make integrating model output with GIS difficult. Many scientific modeling outputs are in netCDF and HDF formats with time steps for all runs in a single file. File sizes may be very large, irregularly spaced, or unstructured, and file management can be unwieldy. This issue is changing as the advent of multidimensional tools in ArcGIS™ products provides direct reading of netCDF files. These new input mechanisms allow NCTR propagation and inundation data to be easily imported into GIS, opening up new methods of analysis and visualization.

The ability to take propagation or inundation results and overlay them on infrastructure data has long been desired by stakeholders. While the majority of hydrodynamic models are visualized in custom code or visualization analysis packages that allow for post processing. In the past modelers have had to use MATLAB and other tools such as "Ferret" (Ferret 2008) (see http://ferret.pmel.noaa.gov/Ferret, an in-house visualization package) to visualize model output. To improve upon this situation, NCTR modelers and programmers developed custom code to streamline output and to visualize model results in animations and static images. This ability is especially critical during an actual tsunami event when fast response is crucial. While MATLAB and Ferret are excellent for building animations and creating 2-D maps, the results are static because it is not possible to interrogate the data, add data in real time, or perform any analysis "on the fly" (Merati et al. 2007). GIS provides a more interactive way to create and analyze data.

Emergency managers and coastal planners recognize the risk posed by near-and far-field tsunami events that can inundate coastal areas. Developers at NCTR are building at-risk community tsunami tools, working with state partners and emergency managers to determine the level of risk posed by a tsunami to coastal communities. The tools will allow us to use parameters such as distance to shoreline, elevation, and time of day to determine affected populations (Fig. 14.7).

NCTR, Tsunami Warning Centers, and the NOAA Tsunami program have identified sites for further study and inundation modeling in the United States and its territories, and are working on establishing criteria that can define what determines

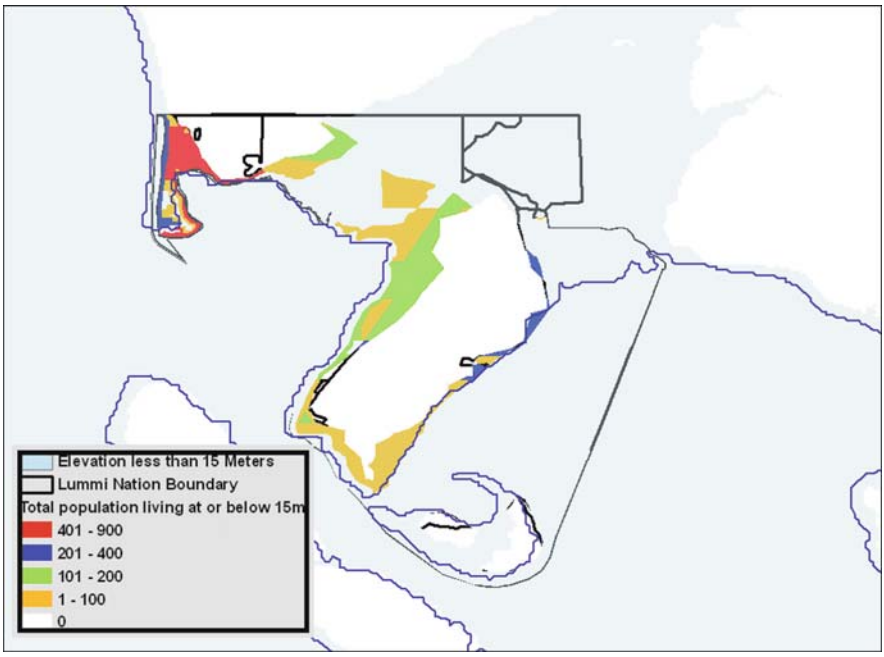

Fig. 14.7 Results of running the at-risk population tool for Washington State coastal communities, describing populations within 2 km of the shoreline at elevations lower than 15 m that would be inundated in a near field tsunami scenario

an "at-risk" population. Currently, age, mobility, access to transport, and income level are included as well as seasonal factors (especially in resort areas).

Data management is an important component for getting information into the hands of coastal managers and scientists at the time an event occurs. Development of the NCTR Atlas project, whose initial goal was to house static maps of modeled sites, has proven to be an invaluable tool for data display, management, and organization of all event data. Additionally, the housing of seismic and water level data in a GIS format in one location promotes more efficient retrieval of data for model validation. Extensions of the Atlas to work with ArcGIS™ desktop applications and with NCTR's WebSIFT real-time modeling application will improve its utility for modelers and data managers as events are updated in real time and assigned standardized event names and data structures, thus making data integration and management easier.

Data integration and data formats have often been a stumbling block to the acceptance of GIS to the hydrological and oceanographic community (Martin et al. 2005). The recognition of netCDF as the de facto standard of the hydrological and modeling community by ESRI™ and the move to make native file readers available to the standard mapping toolkit (ArcView™ GIS) made the integration of netCDF rasters and features much simpler for GIS analysts and scientists wishing to directly analyze their model output in ArcGIS™. Python scripting language – for stand-alone

applications or for creating geoprocessing scripts within ArcGIS™ – makes transformation of data formats, batch processing of large files, and integration of spatial operators much easier by taking model output and visualizing and placing it within a GIS framework. Simple tools that NCTR programmers have written to convert data between formats in Python make data interchange smoother. While the hydro modeling community has been a large proponent of these tools, the ability to integrate irregularly time-stepped or meshed-gridded datasets outputted by inundation models is largely due to work by the atmospheric community. Integration of time series tools for visual analysis and animation are also crucial to understanding coastal inundation and its impact on communities. GIS community-based tools are beginning to address the most accurate and effective way to display this information.

14.12 Conclusion

GIS and geospatial technologies have been critical to the success of NCTR's modeling efforts and the dissemination of products to its stakeholders. Development of mapping standards and techniques to create merged bathymetric and topographic models for inundation modeling, with corrections for tidal variations, have been used successfully for inundation modeling. DEM products are available to the public and are used for coastal storm modeling, fisheries studies, and estuarine habitat modeling. The use of the best available data and standard methods has streamlined the creation of the DEMs, which serve as one of the critical inputs to running the MOST model and generating accurate results. Methods of DEM development, including the accessibility and availability of current data, the use of satellite altimetry and imagery, and efforts to improve the accuracy of vertical datum adjustments for Alaska and other parts of the United States coast, will enhance the DEMs scheduled for creation in the next few years.

While we have not discussed mitigation strategies for tsunami preparedness, NCTR recognizes the importance of using model output, wave heights, amplitudes and time-of-first-wave as important parameters that localities will need to create disaster preparedness plans. Tools to assess where vulnerable populations exist, factoring in age, race, gender, income level, and access to transportation are crucial for long-term planning for coastal evacuation. The same information is useful for planning development restrictions in coastal areas. Dominey-Howes et al.'s (2009) integration of vulnerability analysis with building types for Seaside, Oregon, begins to address these issues. While NCTR has focused on providing at risk estimates based on elevation, probable maximum inundation heights, and potential flooding areas at various periods of the day, we are working on determining what factors are needed to make accurate estimates of vulnerable populations. Census information and spatial statistics along with up to date tax parcel information for city and county jurisdictions will assist in making more accurate estimations. Land cover and land change over time, especially in coastal areas, are especially subject to change. Integration

of standby inundation outcomes such as a maximum inundation line could be used to build predictive models that use MOST parameters with GIS analysis.

Acceptance of GIS as a framework for emergency planning and decision making is not new in terms of hazard planning, but the tools for bringing model output to GIS requires changing the way we look at model output and how we visualize these data. The Tsunami GIS project demonstrated that gridded model output can be added to a stand-alone GIS application and used to assess the level of damage and vulnerability without having a full suite of ArcGIS™ on the user's desktop. A run-time license of the Tsunami GIS application means that we can deploy this application as part of a suite of training tools to developing nations that may not currently have a full GIS laboratory. Stand alone tools that can be extended using Java, that can read native GIS file formats, and that can produce products useful to first responders, are important for rapid assessment and response in disaster scenarios.

Adding full GIS capability and visualization tools, as seen in the ComMIT interface, has brought GIS to the forefront of hazard assessment in the Indian Ocean. Imagery that can be geo-referenced and placed on an inundation zone to provide real-time display and output into a GIS is critical for bringing modeling results into the hands of the emergency manager in a timely manner (Titov et al. 2005). The option of putting inundation results output (e.g., KML) in a Google Map™ application with the option of adding additional information makes the application more powerful and more easily delivered to the end user. Mapping mashups, while not a new technology, permit some user-based content to be placed on an image, and have also proven useful for recovery efforts.

Ideally, the MOST model could be directly integrated into ArcGIS™ or any GIS enabled package, but as others have noted model integration is not simple, nor straightforward (Eveleigh et al. 2006; Martin et al. 2005). Research is ongoing to create an interface that is user friendly to both the scientist whose model output is being used and the end user who must interpret the model's results.

The creation of a 2-D evacuation map for state hazard mitigation and the need for accurate bathymetric data for model input provided the initial foundation for the use of GIS for tsunami research, modeling, and hazard mitigation efforts at NCTR. The ability of ArcGIS™ to handle native file formats used by the MOST model and development of the Python scripting language helped move NCTR to adopting GIS as a tool to help display, analyze, and disseminate information. New research linking evacuation models with hydrodynamic models through the use of GIS have strengthened our commitment to this research. With the recent proliferation of Google Earth™ imagery and mapping applications that do not require a desktop GIS application, NCTR looks forward to many opportunities to expand its suite of geospatial products.

References

Bernard, E.N. 2005. The U.S. National Tsunami Hazard Mitigation Program: A successful state–federal partnership. *Natural Hazards*, 35(1), Special Issue, U.S. National Tsunami Hazard Mitigation Program, 5–24.

Denbo, D.W., McHugh, K.T., Osborne, J.R., Sorvik P., Venturato, A.J. 2007. NOAA tsunami forecasting system: Design and implementation using service oriented architecture. In *23rd Conference on Interactive Information Processing Systems (IIPS) for Meteorology, Oceanography, and Hydrology*, 87th AMS Annual Meeting, San Antonio, TX, 14–18 January 2007, Paper 3A.9.

Dominey-Howes, D., Dunbar, P., Varner, J. (2009). 'Estimating probable maximum loss from a Cascadia Tsunami' *Natural Hazards.*

Eveleigh, T.J., Mazzuchi, T.A., Sarkani, S. 2006. Systems engineering design and spatial modeling for improved natural hazard risk assessment. *Disaster Prevention and Management*, 15(4), 636–648.

Ferret. 2008. Users Guide. http://ferret.pmel.noaa.gov/Ferret/documentation/user-guide. Accessed April 15, 2008.

GeoTools. 2008. GeoTools: The Open Source Java GIS Toolkit. http://geotools.codehaus.org/. Accessed April 28, 2008.

González, F.I., Titov, V.V., Mofjeld, H.O., Venturato, A., Simmons, S., Hansen, R., Combellick, R., Eisner, R., Hoirup, D., Yanagi, B., Yong, S., Darienzo, M., Priest, G., Crawford, G., Walsh, T. 2005. Progress in NTHMP hazard assessment. *Natural Hazards*, 35(1; Special Issue): U.S. National Tsunami Hazard Mitigation Program, 89–110.

MapServer. 2008. Welcome to MapServer. http://mapserver.gis.umn.edu/. Last modified May 12. Accessed April 28.

Martin, P.H., LeBoeuf, E.J., Dobbins, J.P., Daniel, E.B., Abkowitz, M.D. 2005. Interfacing GIS with water resource models: A state of the art review. *Journal of the American Water Resources Association*, 41(6), 1471–1487

Merati, N., Gica, E., Chamberlin, C. 2007. Building Tsunami tools into a GIS workspace. In*ESRI International User Conference Proceedings (UC1889)*, 18–22 June 2007, San Diego, CA.

Mofjeld, H.O., Venturato, A.J., González, F.I., Titov, V.V., Newman, J.C. 2004. The harmonic constant datum method: Options for overcoming datum discontinuities at mixed-diurnal tidal transitions. *Journal of Atmospheric and Oceanic Technology*, 21, 95–104.

National Geophysical Data Center (NGDC). 2008a. NGDC Tsunami Inundation Gridding Project: http://www.ngdc.noaa.gov/mgg/inundation/tsunami/inundation.html. Last updated October 22. Accessed April 29, 2008

National Geophysical Data Center (NGDC). 2008b. NGDC Tsunami Inundation Gridding Project: Tsunami DEM Development.. http://www.ngdc.noaa.gov/mgg/inundation/tsunami/general.html. Last updated July 23. Accessed April 29, 2008.

NOAA Center for Tsunami Research (NCTR). 2007. *Method of Splitting Tsunami (MOST) Software Manual*, Seattle, WA: NOAA.

NOAA Center for Tsunami Research (NCTR). 2008a. Community Model Interface for Tsunami (ComMIT). http://nctr. pmel.noaa.gov/ComMIT. Accessed April 29, 2008.

NOAA Center for Tsunami Research (NCTR). 2008b. Tsunami Modeling and Research. http://nctr.pmel.noaa.gov/model.html. Accessed April 29, 2008.

Percival, D.,Arcas, D., Denbo, D.W., Eble, M.C., Gica, E., Mofjeld, H.O., Spillane, M.C., Tang, L., Titov, V.V. 2009. *Extracting Tsunami Source Scaling Factors via Inversion of DART Buoy Data*. NOAA Tech Memo., Seattle, WA: NOAA.

Tang, L., Chamberlin, C., Tolkova, E., Spillane, M., Titov, V., Bernard, E., Mofjeld, H. 2006. *Assessment of potential tsunami impact for Pearl Harbor, Hawaii*. NOAA Tech. Memo. OAR PMEL-131, Seattle, WA: NOAA.

Titov, V., González, F. 1997. *Implementation and testing of the Method of Splitting Tsunami (MOST) model*. NOAA Tech. Memo. ERL PMEL-112 (PB98-122773), NOAA/Pacific Marine Environmental Laboratory, Seattle, WA: NOAA.

Titov, V., González, F., Bernard, E., Eble, M., Mofjeld, H., Newman, J., Venturato, A. 2005. Real-time tsunami forecasting: Challenges and solutions. *Natural Hazards*, 35(1), Special Issue, U.S. National Tsunami Hazard Mitigation Program, 41–58.

Titov, V., González, F., Mofjeld, H., Venturato, A. 2003. *NOAA TIME Seattle Tsunami Mapping Project: Procedures, data sources, and products*. NOAA Tech. Memo. OAR PMEL-124, NTIS: PB2004-101635.

van Rossum, G. 2006. Python Tutorial. Python Software Foundation, http://docs.python. org/tut/. Accessed April 28, 2008.

Vance, T.C., Merati, N., Mesick, S., Moore, C.W., Wright, D. 2007. GeoModeler: Tightly linking spatially-explicit models and data with a GIS for analysis and geovisualization. In *15th ACM International Symposium on Advances in Geographic Information Systems (ACM GIS 2007)*, Seattle, WA, 7–9 November 2007.

Venturato, A.J., Denbo, D.W., McHugh, K.T., Osborne, J.R., Sorvik, P., Moore, C. 2007. NOAA tsunami forecasting system: Using numerical modeling tools to assist in tsunami warning guidance. In *23rd Conference on Interactive Information Processing Systems (IIPS) for Meteorology, Oceanography, and Hydrology*, 87th AMS Annual Meeting, San Antonio, TX, 14–18 January 2007, Paper 3A. 8.

Venturato, A.J., Titov, V., Arcas, D., González, F., Chamberlin, C. 2005. Reducing the impact: U.S. Tsunami forecast modeling and mapping efforts. In *ESRI International User Conference Proceedings*(UC2471), 25–29 July 2005, San Diego, CA.

Walsh, T.J., Titov, V., Venturato, A., Mofjeld, H., González, F. 2003. *Tsunami hazard map of the Elliott Bay area, Seattle, Washington—Modeled tsunami inundation from a Seattle fault earthquake*. Washington State Department of Natural Resources Open File Report 2003–14, 1 plate, scale 1:50,000.

Wei, Y. (No Date).Development of the Stand-by Inundation Model (SIM) and its Application in Tsunami Hazard Assessment for Unalaska, Alaska. NOAA Tech. Memo. Seattle, WA: NOAA. In Preparation.

Wong, F.L., Venturato, A.J., Geist, E.L. 2006. *Seaside, Oregon, tsunami pilot study—Modernization of FEMA flood hazard maps: GIS Data*: U.S. Geological Survey Data Series 236 (http://pubs.usgs.gov/ds/2006/236/).

Zerger, A. 2002. Examining GIS decision utility for natural hazard risk modeling. *Environmental Modelling and Software*, 17, 287–294.

Zerger, A., Wealands, S. 2004. Beyond modelling: Linking models with GIS for flood risk management. *Natural Hazard*s, 33, 191–208.

Chapter 15
Utilizing New Technologies in Managing Hazards and Disasters

Ronald T. Eguchi, Charles K. Huyck, Shubharoop Ghosh, Beverley J. Adams, and Anneley McMillan

Abstract This chapter introduces new and emerging technologies that have proven effective in disaster management or show promise in future deployments. These technologies are discussed in the context of the four major phases of disaster management: preparedness, response, recovery and mitigation. Examples of some technologies discussed in detail include real-time hazard warning or monitoring systems; advanced loss estimation methodologies and tools; remote sensing for response and recovery; and field data collection and visualization systems, especially those that are GIS and/or GPS-based. The chapter concludes with a brief discussion of research or implementation issues, focusing specifically on the above technologies, and including issues related to real-time event monitoring; privacy protection; and information sharing and trust management.

Keywords Remote sensing · Disaster management · Damage assessment · Loss estimation · Reconnaissance · Warning and monitoring

15.1 Introduction

Often, disasters act as catalysts for the adoption of new and emerging technologies. Spawned by the need to rapidly collect vital information for disaster management, technical innovations have helped emergency responders more efficiently and rapidly assess the impact of large disasters, and track and monitor progress in critical response and recovery operations. For example, after Hurricane Andrew struck Florida (1992), the lack of rapid damage or situation assessment tools hindered the

R.T. Eguchi (✉)
ImageCat, Inc., Long Beach, CA 90802, USA
e-mail: rte@imagecatinc.com

Any opinions, findings, and conclusions or recommendations expressed in this publication are those of the authors and do not reflect the views of the National Science Foundation, the US Department of Transportation, the University at Buffalo, or the University of California.

P.S. Showalter, Y. Lu (eds.), *Geospatial Techniques in Urban Hazard and Disaster Analysis*, Geotechnologies and the Environment 2, DOI 10.1007/978-90-481-2238-7_15,

deployment of federal resources and thus identified the need for near real-time loss estimation methodologies. Following the 1994 Northridge California earthquake, use of geographic information systems (GIS) during the initial response and recovery periods provided important visual and spatial information about critical operations (Eguchi et al. 1997a). New York City's World Trade Center attacks (2001), demonstrated the potential use of remote sensing technologies for damage assessment and recovery (Huyck and Adams 2002). And, shortly after Hurricane Charley struck Florida in 2004, deployment of global positioning system (GPS)-based survey technologies helped to "freeze" in time the storm's damage and destruction so researchers could study the effects of significant wind hazards in a more comprehensive and complete manner. All these events underscore the opportunities that emerge when time-critical information can be more efficiently delivered to users who are making critical decisions during a disaster.

The last decade has witnessed technological innovations in numerous areas, including data collection and management, information visualization, smart sensors, robust communication systems (including wireless platforms), loss estimation, GIS, personal digital assistant (PDA) solutions, GPS-based technologies, and remote sensing, often collectively referred to as geographic information technologies (GIT). In many cases, these technologies have existed for many years, however, their application or deployment for disaster response or management has been nonexistent or slow. Part of the reason for the delay in their utilization is the long lead time required for response organizations to understand and embrace the efficacy of these solutions for facilitating response and recovery operations. In almost all cases, implementing these new technologies necessitates replacing "old, but tried and true" solutions. Attempts to replace these solutions, particularly during an actual disaster, are often met with extreme resistance especially if the newer solutions are not problem-free from the outset.

This chapter introduces technologies that have either proven to be effective in disaster management or are considered important components in future deployments. We begin by discussing each technology from the perspective of its maturity level, benefits, and potential drawbacks. In addition, we suggest future directions for incorporating these technologies into different phases of disaster management, i.e., preparedness, response, recovery and mitigation. We also discuss some of the barriers that exist in their deployment and utilization. One of the biggest challenges is overcoming the resistance that typically accompanies the introduction of new technologies. The chapter concludes with a discussion of other issues, some ironically caused by the availability of more powerful information technologies, e.g., privacy protection, information sharing, and trust management.

15.2 Applications to Emergency Management

The following sections describe how advanced and emerging technologies are being used to enhance disaster mitigation, preparedness and response efforts.

15.2.1 Mitigation and Preparedness

While working towards the long-term goal of disaster prevention, in the shorter term, contemporary emergency management is concerned with minimizing the extent and effects of extreme events (Garshnek and Burkle 2000). Mitigation measures serve to reduce or negate the impact of an event, while preparedness efforts facilitate a more effective response once the disaster has occurred.

Hazard Assessment. Hazard identification is a pre-event research activity where remote sensing and GIS play important roles. For example, MIKE21[1] has been used to create detailed digital elevation maps to identify areas at risk of flooding in the event of a dam break (DHI 2007); similarly fluvial and coastal flooding have been modeled using MIKE21 and HAZUS®MH (FEMA 2008). Elevation data are routinely derived from interferometric[2] synthetic aperture radar (IfSAR[3]) (e.g., Galy and Sanders 2000) and Light Detection and Ranging (LIDAR) data. Hazard maps showing landslide potential can be directly created using remotely-sensed detailed elevation readings from such instruments, and indirectly through geological, soil and moisture information from optical and radar coverage (CEOS 2002). Interferometry has also been used to track changes in topography associated with volcanic activity (JPL 1995; Lu et al. 2003), and glacial movement (JPL 2003).

Optical data are particularly useful for the visual assessment of hazards. Monitoring patterns of vegetation growth, identified through classification techniques (Campbell 1996), provides a means of detecting encroachment around energy transportation pipelines (DOT/NASA 2003). Such monitoring ensures adequate access to pipelines in case of needed repairs and/or maintenance. This process is most successful when "supervised" by an analyst, whereby a user identifies "areas of interest" to guide subsequent image-wide categorization. Multi-spectral coverage extending to longer wavelengths of the electromagnetic spectrum offers the unique opportunity to inspect features that are invisible to the naked eye. In terms of wildfire risk, the Southern California Wildfire Hazard Center (SCWHC 2003) documents the quantification of chaparral fuel content using multi-spectral data (c.f., CEOS 2002; Roberts et al. 1998).

Figure 15.1 shows how satellite imagery was used to map the extent of flooding in New Orleans after Hurricane Katrina (2005). The flood boundary shown in Fig. 15.1 was created using expert interpretation of high-resolution imagery provided by DigitalGlobe (QuickBird image captured on September 3, 2005; see Womble et al. 2006 for details on flood boundary determination). This flood boundary was visually compared with an automatically-generated spectral classification of

---

[1]MIKE 21 is a professional engineering software package for the simulation of flows, waves, sediments and ecology in rivers, lakes, estuaries, bays, coastal areas and seas; http://www.dhigroup.com/Software/Marine/MIKE21.aspx

[2]Interferometry is a widely used technique where an object is observed from several angles and then digitally reconstructed as a single, more detailed image.

[3]IfSAR, or InSAR, is an aircraft-mounted sensor designed to measure surface elevation, which is used to produce topographic imagery.

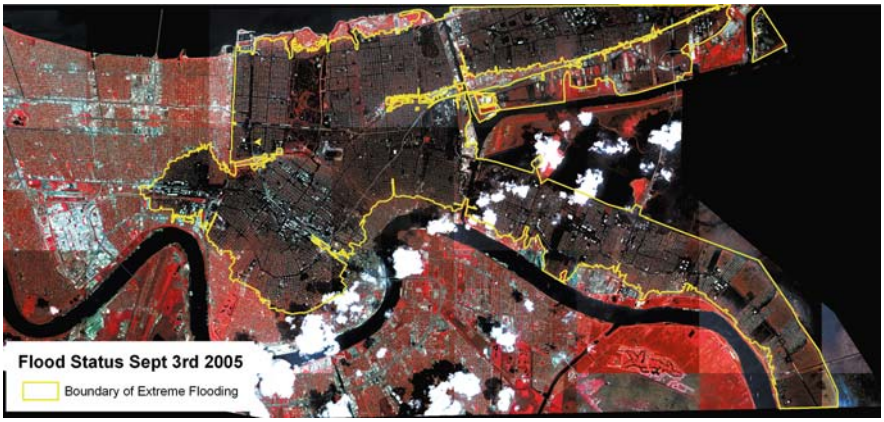

Fig. 15.1 Expert interpretation of September 3, 2005 flood limit (*yellow lines*) overlaid onto DigitalGlobe QuickBird "false color" composite of New Orleans after Hurricane Katrina
Source: Womble et al. 2006

the inundated area obtained from moderate-resolution (30 m) Landsat 5 coverage, captured on 30 August 2005 by the National Aeronautics and Space Administration (NASA), and posted by the USGS on 03 September 2005. Although comparison was precluded in some areas due to cloud cover, the degree of correspondence between the QuickBird flood line and the Landsat 5 spectral classification was generally high.

In addition to mapping the extent of flooding in New Orleans, other remote sensing technologies were used to estimate the height or depth of the flooding. The National Oceanographic and Atmospheric Administration's (NOAA) flood depth map for 31 August 2005 was developed using a combination of satellite imagery from the National Geospatial Intelligence Agency and LIDAR (Light Detection and Ranging) data from Louisiana State University and the State of Louisiana. This map (Fig. 15.2) shows that most of New Orleans was covered by at least 7–9 ft of water, with some areas exceeding 20 ft. The extent of surface flooding shown in this Figure visually appears to correspond well with the flood boundary delineations shown in Fig. 15.1.

Inventory Development. Compiling a comprehensive and accurate database of existing critical infrastructure is a priority in emergency management, since such data provide the basis for simulating probable effects through scenario testing, and set a baseline for determining the extent of damage and associated losses once an event has occurred. In the context of mitigation and preparedness, demand is increasing for accurate inventories of the built environment, in order to perform vulnerability assessments, estimate losses in terms of repair costs (RMSI 2003), assess insurers liability, and for relief planning purposes (Sinha and Goyal 2001; RMSI 2003). In lesser developed regions of the world, such inventories are often scarce. The Committee on Earth Observation Satellites (CEOS 2002) documents a program to compile comprehensive records of urban settlements at risk in the event of an earthquake. This effort is being driven by the experience of the 1998 Afghanistan

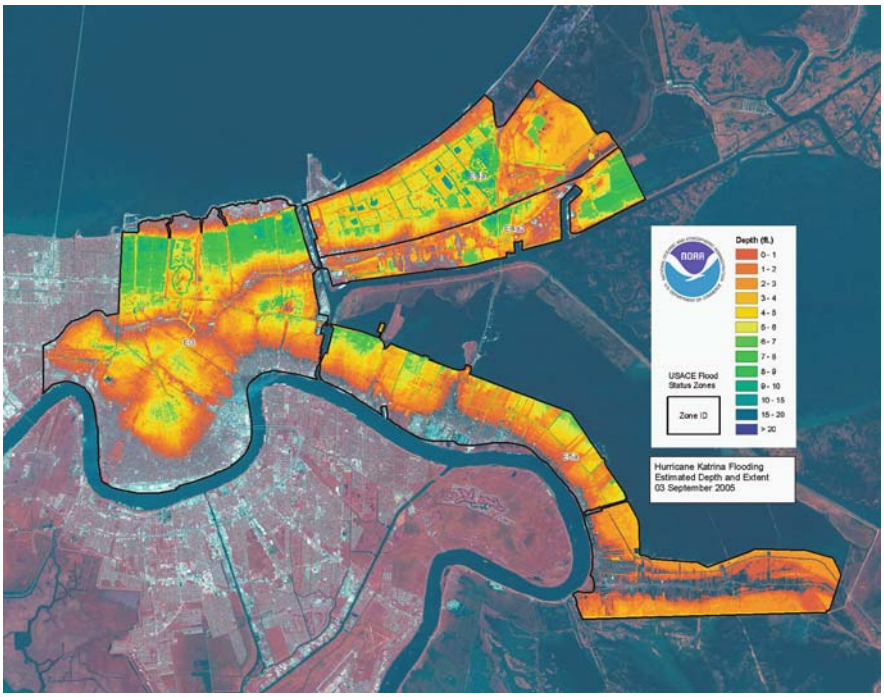

Fig. 15.2 August 31, 2005 flood depth estimation for New Orleans after Hurricane Katrina Source: No Author 2005

earthquake, when due to the unavailability of even simple maps or images, relief workers experienced extreme difficulty locating affected villages.

Because building inventories are the primary data input into loss estimation models such as the Federal Emergency Management Agency's (FEMA) HAZUS®MH and California's Early Post-Earthquake Damage Assessment Tool (EPEDAT), the more detailed the inventory the more reliable the model output. These models are used as planning tools prior to an event and as response tools once an event has occurred. Measures of interest include: building height, square footage, and occupancy (use). To a large degree, the accuracy of loss estimates depends on the quality of input data. Default datasets are often based on regional trends, rather than local data. Research being undertaken at the Multidisciplinary Center for Earthquake Engineering Research (MCEER), suggests that remote sensing data offer a detailed inventory of both height and square footage, which, through supplementing existing datasets, may lead to more accurate loss estimates.

For example, building height and square footage information can be obtained from a combination of IfSAR and optical imagery (Eguchi et al. 1999; Huyck et al. 2002; Adams and Huyck 2005). The efficacy of this methodology has been tested on case study areas in Los Angeles, where the values for building height and coverage correspond closely with independently derived tax assessor data (Eguchi et al., in

press). Methodological procedures are under development to use these results to update existing inventories within the HAZUS®MH program.

A significant advantage of remotely-derived inventories is the relative ease with which they can be updated. This attribute is particularly important at the city scale, where the overview offered by satellite imagery can be used by planning departments to track urban growth (DOT/NASA 2002, 2003). Classifying image features into vegetation, concrete, and buildings is a common task, readily applied to multitemporal images. Growth or contraction of those features can be detected by examining change between the scenes.

In addition to using active sensors (e.g., IfSAR), new building inventory development techniques are emerging from the use of high-resolution optical satellite data. Research at Stanford University and ImageCat, Inc. has focused on the development of an approach using rational polynomial coefficients (RPC) as a camera replacement model to quickly obtain spatial and structural information from a single high-resolution satellite image (Sarabandi et al. 2005; Chung and Sarabandi 2006). Geometric information that defines the sensor's orientation is used in conjunction with the RPC projection model to generate an accurate digital elevation model (DEM). The methodology described in Sarabandi et al. (2005) shows how the location and height of individual structures are extracted by measuring the image coordinates for the corner of a building at ground level and at its corresponding roof-point coordinates, and using the relationship between image-space and object-space together with the sensor's orientation to arrive at these parameters. Figure 15.3 shows a 3-dimensional model of Long Beach, California developed using this methodology, called the Mono-Image Height Extraction Algorithm (MIHEA).

Loss Estimation. Although loss estimation studies were conducted in the 1960s, only in the 1990s did such methodologies become widely used. A major factor in this development was the emergence of GIS technology that allowed users of

Fig. 15.3 Three-dimensional building inventory model of Long Beach, California Source: Chung and Sarabandi 2006

information technology to easily overlay hazard data or information onto maps of various systems (e.g., lifeline routes, building data, population information).

Loss estimation methodologies are now a vital part of many hazard mitigation studies. These methods are typically used to forecast the potential impacts of different hazard scenarios (typically used for planning), to project losses in an actual event (when used in conjunction with near real-time sensor systems, such as the ShakeMap system deployed by the US Geological Survey), and to assess the benefits of a mitigation activity such as structural retrofit. A National Research Council report, *Impacts of Natural Disasters* (NRC 1999), also discusses the importance of relying on loss estimation modeling as a means of tracking and monitoring the costs of natural disasters. Because current government accounting systems are inadequate when it comes to totaling the costs of a disaster, the NRC report suggests that loss estimation modeling could provide a surrogate means of tracking these costs.

The Federal Emergency Management Agency (FEMA) has recognized the value of loss estimation modeling as a key hazard mitigation tool. In 1992, FEMA began a major effort (which continues today) to develop standardized loss estimation models that could be used by non-technical hazard specialists. The resulting tool, HAZUS®MH, currently addresses earthquake, flood, and wind.

HAZUS®MH is built on an integrated GIS platform composed of seven major interdependent modules. The connectivity between the modules is conceptualized by the flow diagram in Fig. 15.4. The following discussion provides a brief description of each module; detailed technical descriptions can be found in the HAZUS®MH Technical Manuals (NIBS/FEMA 2003a, b, c).

Potential Hazards (1) - This module estimates expected intensities, or the severity of, three hazards: earthquake, flood, and wind. For each of these the software estimates ground motion and ground failure potential from landslides, liquefaction, and surface fault ruptures; flood heights or depths; and wind speeds and wind-born debris. If probabilistic analysis is needed, frequency or probability of occurrence can be included.

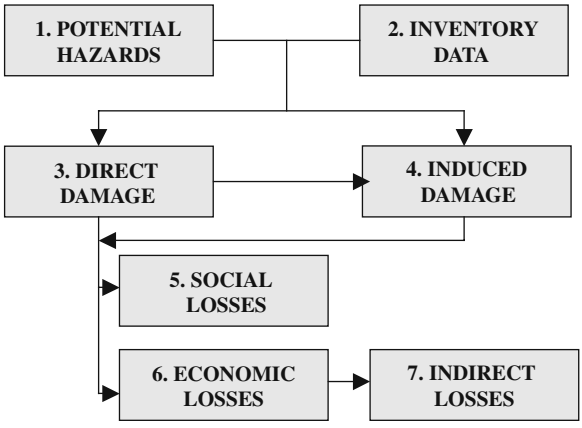

Fig. 15.4 HAZUS®MH modules
Source: (FEMA 2008)

Inventory Data (2) - HAZUS®MH provides a national-level built environment exposure database that allows preliminary analysis without the necessity of collecting local data. This database includes general building stock, essential facilities, transportation systems, and utilities. General building stock data are classified by occupancy (e.g., residential, commercial, industrial) and by model building type (structural system, material of construction, roof type, and height). State-specific mapping schemes are provided for single-family dwellings, and region-specific schemes for all other occupancy types (in all cases, the schemes are age and building-height specific).

Direct Damage (3) - Based on the level of exposure and the vulnerability of structures at different hazard intensity levels, this module estimates property damage in each of the four inventory groups (general building stock, essential facilities, transportation, and utilities).

Induced Damage (4) - Estimates are also calculated for "induced damage", which is secondary property damage occurring as a consequence of an event (e.g., fire following an earthquake).

Social Losses (5) - These losses are estimated in terms of casualties, displaced households, and short-term shelter needs. Casualties are calculated at four levels (minor injury to death), during three times of day (2:00 a.m., 2:00 p.m., and 5:00 p.m.), for four population groups (residential, commercial, industrial, and commuting). Displaced households are calculated from the number of uninhabitable structures, estimated by examining the relationship between damage to residential building stock and utility service outages.

Economic Losses (6) - Direct economic losses are estimated in terms of structural and nonstructural damage, contents damage, costs of relocation, losses to business inventory, capital-related losses, wage and salary income losses, and rental losses.

Indirect Economic Losses (7) - This module evaluates region-wide, longer-term effects by examining changes in sales, income, and employment by sector (i.e., commercial, industrial, retail).

The various modules of the HAZUS®MH software have been calibrated using existing literature and damage data from past events. Pilot studies have been conducted to assess and validate the credibility of estimated losses. Recently, the system was used to assess savings from FEMA-sponsored mitigation activities; the conclusion was that a ". . . dollar spent on mitigation saves society an average of $4" (MMC 2005, p. 5).

Another example of a loss estimation modeling effort is illustrated by the Early Post-Earthquake Damage Assessment Tool (EPEDAT), which was used during the 1994 Northridge Earthquake (Eguchi et al. 1997b). EPEDAT's use as a loss estimation technique in the immediate post-event context was a key development, marking a significant departure from conventional applications. Beforehand, earthquake loss studies largely addressed the pre-earthquake planning needs of utility operators, the insurance industry and government emergency response agencies. The needs of these entities generally required modeling events that would have the greatest impact on local population and economies (e.g., worst-case scenarios). Technological advances in high-speed computing, satellite telemetry and GIS altered

the modeling landscape, making it possible to generate multiple-scenario loss estimates, provide nearly unlimited mapping capability, and (perhaps most importantly) develop near real-time estimates given the source parameters of the event (i.e., magnitude and location). For years, real-time broadcasts of earthquake data including magnitude, location, depth, time of occurrence, and in some cases, ground motion maps or contours, have been available in California and other western states. Access to such data in conjunction with the availability of powerful GIS-based loss estimation tools has made near real-time loss estimates a reality in many seismically-active regions of the world.

Logistical Support. In addition to inventory development, databases of critical infrastructure provide a baseline for determining the extent of damage and associated losses once an event has occurred. For example, remote sensing and GIS technologies played an important role in response efforts at Ground Zero following the 9/11 World Trade Center attack. A pre-existing very detailed base map of New York City, compiled from aerial photos and GIS data, depicted building footprints, roads, and lifelines (Cahan and Ball 2002; Huyck and Adams 2002) – data that underpinned subsequent mapping efforts.

Following the 9/11 attack, it was recognized that several remote sensing technologies were underutilized during response efforts (Huyck and Adams 2002; Huyck et al. 2003). For example, calibrated temperature readings would have been valuable for firefighters, but were unavailable until early October. To facilitate the collection of appropriate and timely data for extreme events occurring within the US, FEMA and NASA have established a Remote Sensing Consultation and Coordination Team (Langhelm and Davis 2002). This team is tasked with identifying suitable data, coordinating its acquisition, and distributing the resulting imagery (Langhelm 2002, personal communication, FEMA Region X GIS Coordinator). To support data collection through the RSCCT system, it is important to have contractual agreements in place before an event occurs. Prior agreements between the New York State Office for Technology and EarthData facilitated overflights of Ground Zero in the aftermath of the terrorist attack (Huyck and Adams 2002).

15.2.2 Response and Recovery

Following the onset of an extreme event, assessing the nature, extent, and degree of damage are priorities. Accomplishing these tasks can be problematic due to the distributed nature of natural disasters, and limited accessibility when transportation routes are disrupted. After the initial chaos has subsided, emergency efforts turn to monitoring activities and the provision of logistical support. In terms of response, advanced technologies (especially remote sensing and GIS) offer a number of distinct advantages over traditional ground-based techniques (Puzachenko et al. 1990; Garshnek and Burkle 2000).

Damage Detection. Damage detection provides information needed to: (a) prioritize relief efforts, (b) direct first responders to critical locations, thereby optimizing

response times (Sinha and Goyal 2001) and ultimately saving lives, (c) compute initial loss estimates (RMSI 2003; Tralli 2000), and (d) determine whether the situation warrants national or international aid. In urban areas, building and infrastructure damage (e.g., roads, pipelines, bridges) are of particular interest. This section describes remote sensing damage detection methodologies developed from recent earthquake events and the World Trade Center attack.

The vast US transportation network includes over 500,000 bridges and four million miles of road (Williamson et al. 2002). When a disaster strikes, effective incident response demands a rapid overview of damage sustained by numerous elements, spread over a wide geographic area. Given the magnitude and complexity of transportation systems, near-real time field-based assessment is not an option. For example, during the recent Indian Ocean earthquake and tsunami (2004) centered near Sumatra, the media reported damage to roads and bridges, with a number of villages cut off. Considering the critical 48 hour period that urban search and rescue teams have to locate survivors, accessibility must be quickly and accurately determined in order to reroute response teams and avoid life threatening delays. Earth orbiting remote sensing devices such as IKONOS and QuickBird can present a high-resolution, synoptic overview of the highway system, which can be used to monitor structural integrity and rapidly assess the degree of damage.

A DOT/NASA initiative promoting remote sensing applications for transportation (Morain 2001; DOT/NASA 2002, 2003) has developed preliminary damage detection algorithms termed "Bridge Hunter" and "Bridge Doctor" for highway bridges (Adams et al. 2002). Bridge Hunter locates and compiles a catalogue of remote sensing imagery together with attribute information from Federal Highway Administration (FHWA) databases. Bridge Doctor diagnoses the "health" of bridges, determining whether catastrophic damage has been sustained by quantifying differences in the before-and-after images (Adams et al. 2002). The Northridge earthquake served as a testbed for these algorithms due to widespread damage sustained by the transportation network. Six examples of bridge collapse were available for model calibration and validation. SPOT imagery indicated substantial change between the "before" and "after" earthquake images of the bridges. A bivariate damage plot quantified the visual impression by producing a low correlation/high difference for collapsed bridges, and high correlation/low difference for undamaged bridges (Adams et al. 2002).

The use of remotely-sensed data for assessing building damage offers significant advantages over ground-based survey. Where the affected area is extensive and access limited, remote sensing presents a low-risk, rapid overview of an extended geographic area. A range of assessment techniques are documented in the literature, including both direct and indirect approaches.

Direct approaches attempt to quantify building damage in terms of the extent or density of collapsed structures (for a useful review, see Yamazaki 2001). Research by Matsuoka and Yamazaki (1998), Chiroiu et al. (2002) and Chiroiu and Andre (2001) suggests that collapsed and extensively damaged buildings have distinct spectral signatures. Unfortunately, moderate and minor damage states are currently indistinguishable from undamaged states.

Direct approaches to building damage assessment may be categorized as multi- and mono-temporal. Multi-temporal analysis determines the extent of damage via spectral change between images acquired at several time intervals, typically before and after an extreme event. Figure 15.5 outlines the methodological process that has been employed at city-wide and regional scales for various earthquakes, using optical and Synthetic Aperture Radar (SAR) imagery.

At a city-wide scale, comparative analysis of Landsat and Earth Resources Satellite (ERS) imagery collected before and after the 1995 Hyogoken-Nanbu (Kobe) earthquake, suggested a trend between spectral change and ground truth estimates for the concentration of collapsed buildings (Aoki et al. 1998; Matsuoka and Yamazaki 1998, 2000a, 2000b; Tralli 2000; Yamazaki 2001). Similar qualitative and quantitative methods were used to evaluate damage in various cities affected by the 1999 Marmara earthquake in Turkey (Eguchi et al. 2000a, b) and the 2003 Bam earthquake in Iran (Yamazaki et al. 2005; Hutchinson and Chen 2005; Chiroiu 2005; Gusella et al. 2005; Rathje et al. 2005; and Saito et al. 2005). Visual comparison between SPOT scenes in Figs. 15.6a, b for the town of Golcuk, demonstrates changes in reflectance due to earthquake damage (see also Estrada et al. 2001a, b). Areas of pronounced change are highlighted by circles. Figure 15.6c, f shows measures of change such as difference, correlation and block correlation (see also Eguchi et al. 2003), overlaid with the zones where ground truth data were collected (AIJ 1999). Graphing the concentration of building damage by each measure generates the damage profiles in Fig. 15.7 (see also No Author 2000; Huyck et al. 2002; Eguchi et al. 2002, 2003). There is a clear tendency towards increased offset between before and after scenes as the percentage of collapsed structure rises from class A–E.

This methodology has also been implemented for ERS synthetic aperture radar (SAR) coverage (Eguchi et al. 2000b), offering 24-hour all-weather viewing, and an additional index of change termed "coherence" (Matsuoka and Yamazaki 2000a; Yamazaki 2001; Huyck et al. 2002; Eguchi et al. 2003). Matsuoka and Yamazaki (2002, 2003) recently generalized this approach to show consistency in the trend between building collapse and remote sensing measures for the earthquakes that occurred in Hokkaido and Kobe, Japan (1993 and 1995, respectively), Marmara, Turkey (1999), and Gujarat, India (2001). The authors detected damaged settlements within the Marmara and Gujurat provinces following those earthquakes. Regional approaches using SAR as a data source provide a quick-look assessment of damage extent and can direct responders to severely impacted areas. Further details of multi-temporal damage detection following the Gujurat event are available in Yusuf et al. (2001a, b, 2002), Chiroiu et al. (2002, 2003) and Chiroiu and Andre (2001).

Mono-temporal analysis detects damage from imagery acquired after a disaster has occurred and is useful where "before" data is unavailable. The methodology relies on direct recognition of collapsed structures on high-resolution coverage, through either visual recognition or diagnostic measures. As with the multi-temporal approach, mono-temporal analysis is most effective for extreme damage states, where buildings have collapsed or are severely damaged (Chiroiu et al. 2002; Chiroiu 2005; Saito et al. 2005).

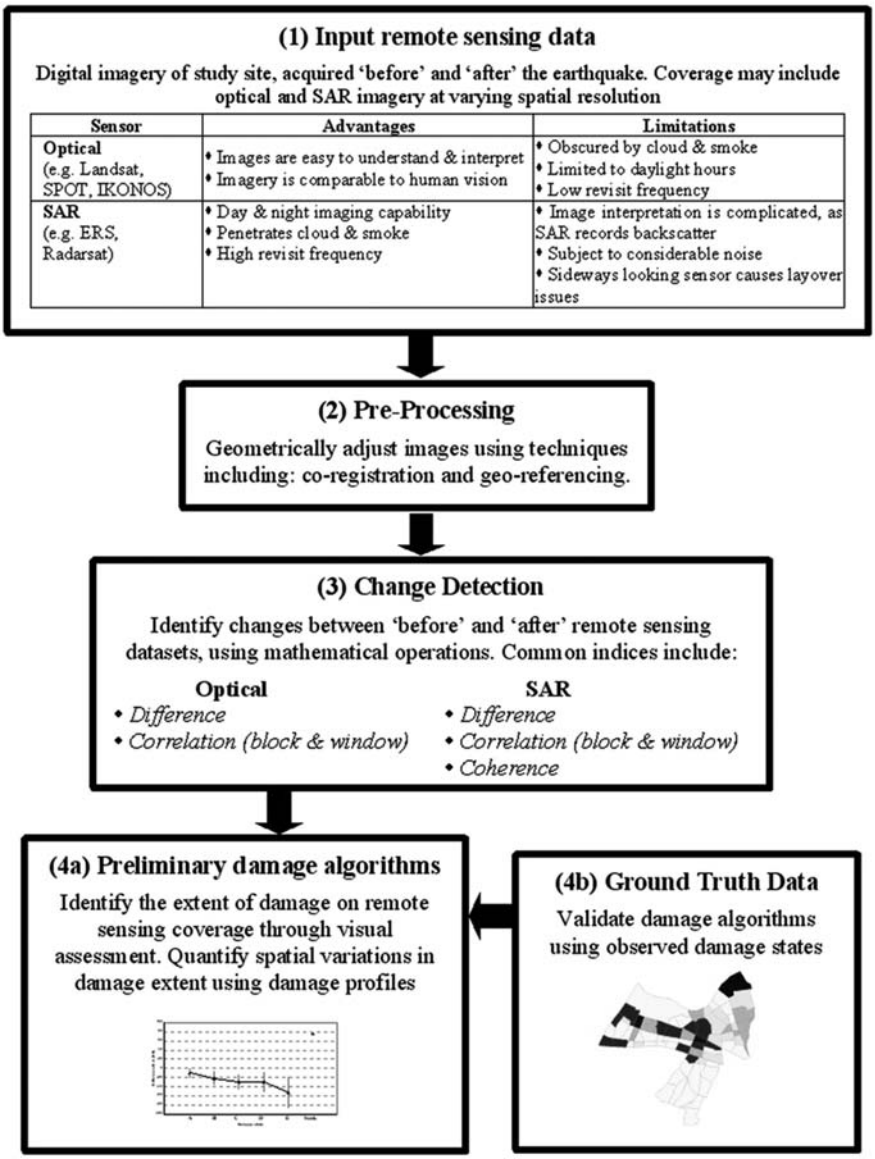

Fig. 15.5 Damage detection methodology employed for buildings and urban settlements, using multi-temporal remote sensing imagery
Source: Adams and Huyck 2005

Ogawa et al. (1999) and Ogawa and Yamazaki (2000) employ mono- and stereoscopic photo interpretation of vertical aerial photography to determine the damage sustained by wooden and non-wooden structures after the 1995 Hyogoken-Nanbu (Kobe) earthquake. A "standard of interpretation" was devised to

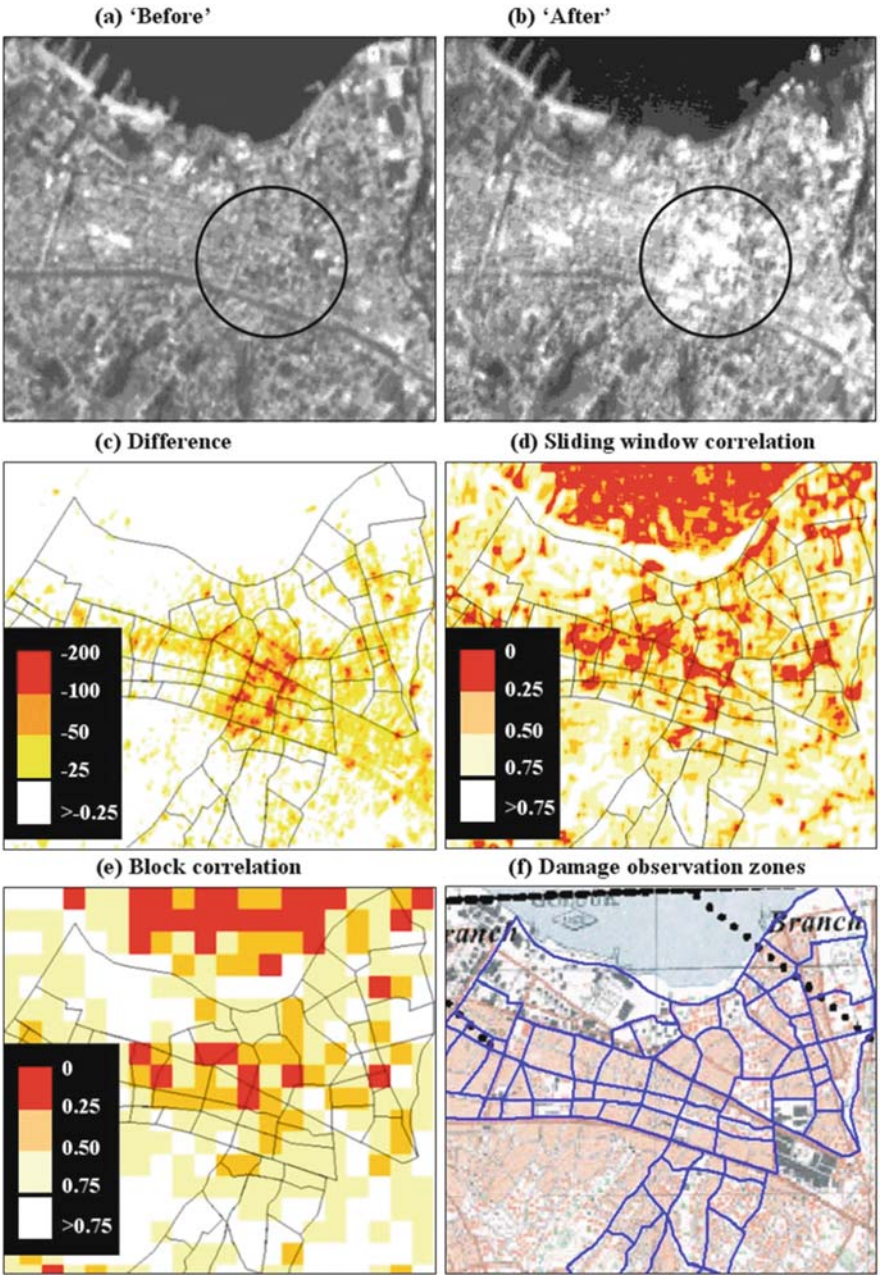

Fig. 15.6 Panchromatic SPOT4 coverage of Golcuk, Turkey (1999 Marmara, Turkey Earthquake) showing "before" image (**a**); "after" image (**b**); difference values (**c**); sliding window correlation (**d**); block correlation (**e**); and ground truth zones (**f**), where the percentage of collapsed buildings was observed (Data courtesy of the European Space Agency, NIK and Architectural Institute of Japan.)
Source: Huyck et al. 2004

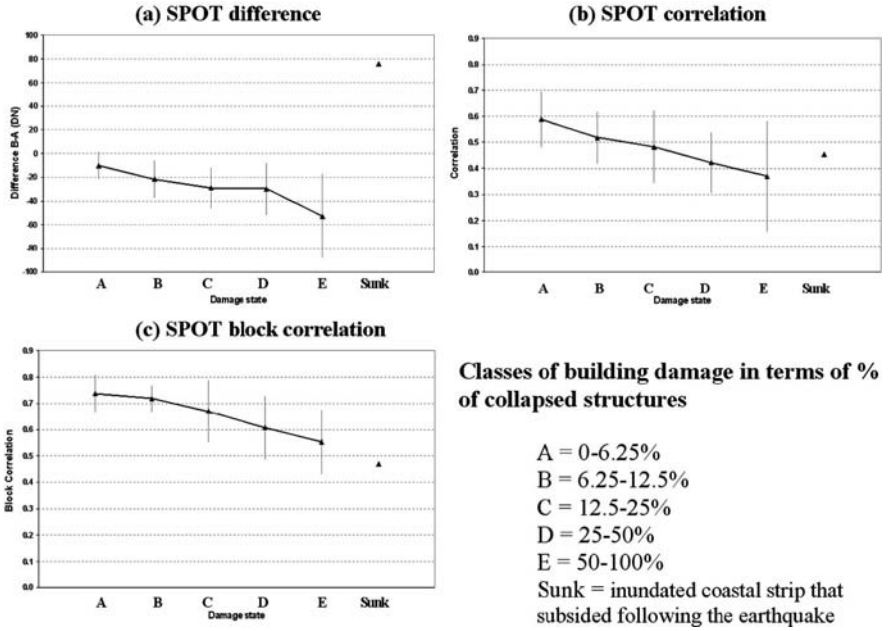

Fig. 15.7 Damage profiles for Golcuk, Turkey (1999 Marmara, Turkey Earthquake) showing how values recorded in the 70 sample zones for each SPOT index of change varies with the concentration of collapsed buildings (a–e). Error bars represent 1 standard deviation about the mean
Source: Huyck et al. 2004

distinguish between collapsed, partially collapsed, and undamaged structures based on: occurrence of debris, level of deformation, and degree of tilt. Success of this methodological approach was judged in terms of correspondence with ground truth observations. Chiroiu and Andre (2001), as well as Chiroiu et al. (2002) used similar criteria to interpret building damage from high-resolution IKONOS satellite imagery of the city of Bhuj following the 2001 Gujurat earthquake, and similar work was performed by Saito et al. (2005) after the Bam, Iran earthquake.

High speed automated aerial television is also emerging as a useful tool for mono-temporal damage assessment. Ogawa et al. (1999) and Hasegawa et al. (2000) inventoried Kobe building collapse from visual inspection of HTTV imagery. Diagnostic characteristics of debris and structural building damage are expressed quantitatively by Hasegawa et al. (1999) and Mitomi et al. (2002) by recognizing collapsed and non-damage scenarios in terms of color, edge and textural information. Multi-level slice and maximum likelihood classifiers determined the spatial distribution of these classes (Mitomi et al. 2001b, 2002). This methodology has been successfully used to detect collapsed buildings from the Marmara (Turkey), Chi Chi (Taiwan) (Mitomi et al. 2000, 2001b), and Gujurat (India) earthquakes (Mitomi et al. 2001a; Yamazaki 2001).

Indirect methods of mono-temporal building damage assessment can also be inferred using a surrogate measure. Theoretically, for example, urban nighttime

lighting levels should diminish in proportion to urban damage (CEOS 2002). Hashitera et al. (1999) and Kohiyama et al. (2001) compared night-time lighting levels in US Defense Meteorological Satellite Program Operational Linescan System (DMSP-OLS) imagery acquired before and after the Marmara and Gujurat earthquakes. In both cases, areas exhibiting the greatest reduction in intensity corresponded with damaged settlements, supporting the hypothesis that fewer lights shine where buildings are severely damaged (Chiroiu and Andre 2001). Operating under the cover of darkness, this damage assessment tool is a useful supplement to optically-based methodologies that are limited to daylight hours.

In addition to the earthquake events described above, damage detection from remotely sensed imagery proved useful following the World Trade Center attack (Cahan and Ball 2002; Hiatt 2002; Huyck and Adams 2002; Logan 2002; Thomas et al. 2002; Williamson and Baker 2002; Huyck et al. 2003). IKONOS coverage acquired on 12th September 2001 and posted on the Internet provided an early visualization of the damage at Ground Zero. The first detailed pictures were captured the following day when the Fire Department of New York (FDNY) recorded oblique shots from a circling helicopter, and Keystone Aerial Surveys took vertical photographs of the area for the New York State Emergency Management Office. From the 15–16th September until mid October, EarthData systematically acquired orthophotographs, thermal and LIDAR data (for a full timeline of data acquisition, see Huyck and Adams 2002). While these datasets were initially used to detect damage, they also played an important role in post-event monitoring.

Another example of a damage map, this time prepared following the 2004 Indian Ocean earthquake and tsunami, is shown in Fig. 15.8. This map was created for the town of Ban Nam Khem in Thailand using expert interpretation of high-resolution pre- and post-tsunami imagery. Of the 761 structures sampled, 449 (59%) were classified as collapsed, with 312 sustaining a lesser damage state. The degree of damage is most extreme bordering the open coast and inlet where 50–100% of the houses were destroyed. The degree of damage rapidly diminishes inland, reaching 0–30% at approximately 500 m from the shorelines (Chang et al. 2006).

Early Warning. For events such as a hurricane where ample time is available before the hazard affects an urban area, tracking or monitoring the progress of the hazard is crucial. Satellite systems have long been used to identify hurricanes and estimate when they will make landfall and where significant damage may occur. NOAA/National Weather Service has recently added "strike probabilities" – with respect to landfall – as well as projected wind speeds for all major hurricane events. This information, when used with simulation models (loss estimation) can provide important data for planning response and recovery efforts.

Several years ago, the feasibility of an early warning system for earthquakes was studied by a research team led by ABS Consulting (ABS 2000, 2001a, b, 2002). The study consisted of four phases: (a) identification of potential users of an earthquake early warning system within selected institutional sectors using a structured telephone survey; (b) review of the risk communication and hazard warning literature to identify relevant findings that apply to the design of warning systems and to the issuance of real-time and near real-time warnings, with a special emphasis

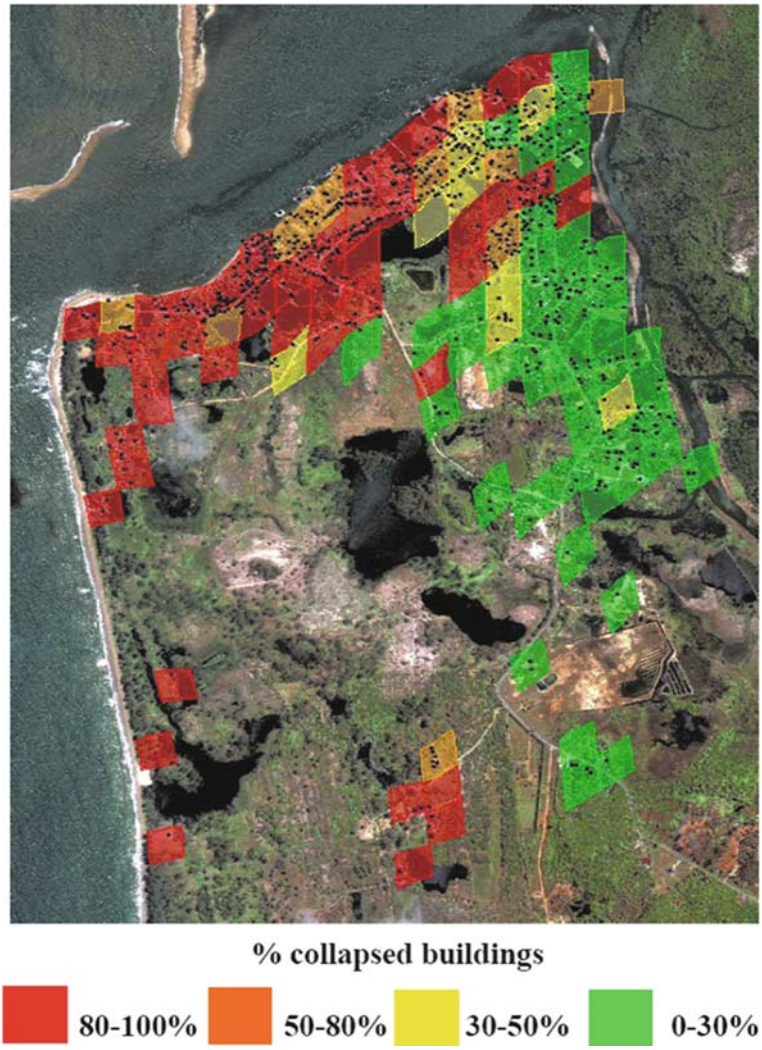

Fig. 15.8 Damage map using high-resolution QuickBird and IKONOS imagery for Ban Nam Khem, 2004 Indian Ocean Earthquake and Tsunami. The percentage of collapsed buildings is computed within zones at 100 m intervals from the open coast and inlet shores
Source: Chang et al. 2006

on the challenges associated with the dissemination of very short-term warnings; (c) identification and analysis of public policy issues associated with the earthquake early warning system; and (d) proposal to design a pilot project to introduce an earthquake early warning system to southern California. The basis for the Seismic Computerized Alert Network (SCAN) was that during an event, seismic sensors located throughout the southern California basin would detect ground motion and earthquake source information early enough to alert areas expected to experience

significant ground motions. While this type of early warning system has been successfully deployed in Japan, it has yet to be implemented in the US. A key issue is whether the system provides sufficient time to prepare for impending ground motions. At best it can supply only 1 min of warning between the occurrence of a large San Andreas earthquake near the Salton Sea to the time it would reach the Los Angeles basin.

Post-Event Monitoring. As response efforts unfold following an extreme event, remote sensing is an important source of logistical support. The following section presents selected instances where remote sensing has aided response efforts in the aftermath of man-made and natural disasters (see also Mileti 1999).

In terms of man-made disasters, remote sensing data was of value following the recent explosion of the Columbia Space Shuttle. A combination of airborne COMPASS and radar satellite imagery was used to show the distribution of the debris field (No Author 2003; Oberg 2003). After the World Trade Center attack, LIDAR, thermal imagery and aerial photography acquired by EarthData gave a detailed overview of Ground Zero. Multi-temporal analysis enabled the monitoring of cleanup operations and volumetric analysis using LIDAR elevation data (Fig. 15.9) tracked progress clearing the debris pile. In several instances, the fusion of key datasets provided responders with valuable new information (Huyck and Adams 2002; Huyck et al. 2003). For example, overlaying the 3D LIDAR representation of the debris pile with a map of hazardous materials and fuel sources enabled firefighters to assess what was happening underneath the ground. The correlation between voids and the position of fuel and Freon tanks presented a focus for firefighting efforts, possibly preventing explosions that would have released toxic gases. When thermal data was overlaid with a two-dimensional 75×75 ft transparent reference grid established by the FDNY, it provided a common system for tracking objects and remains amongst the debris. And when fused with an orthophotograph, it facilitated strategic planning needed to consider the location of hotspots within the pile (Rodarmel et al. 2002). The thermal data were also used to evaluate firefighting strategies, by visually noting differences in a time series of images during which various chemicals were tested. Aerial photographs were also widely employed as a base-map. Applications included overlay with CAD models of floor plans for the Twin Towers, enabling search and rescue teams to pinpoint specific infrastructure, such as stairwells and elevator shafts.

Remote sensing is also increasingly employed to track oil spills. Danish and Norwegian agencies use satellite and airborne surveillance to perform reconnaissance on detected slicks. CEOS (2002) and Fingas and Brown (1997) note that optical, SAR and laser flurosensor devices are particularly useful for detecting and monitoring oil slicks. Tracking pollution and particulate debris is another emerging application. Atmospheric pollutants are recorded through increased absorption at specific wavelengths of the electromagnetic spectrum. Following the World Trade Center attack, hyperspectral imagery was recorded by the JPL Advanced Very High Resolution Imaging Spectrometrer (AVIRIS). Through studying absorption patterns in narrow bands, it was possible to map the concentration of airborne particulates surrounding Ground Zero, including concrete, cement and asbestos (Clark et al.

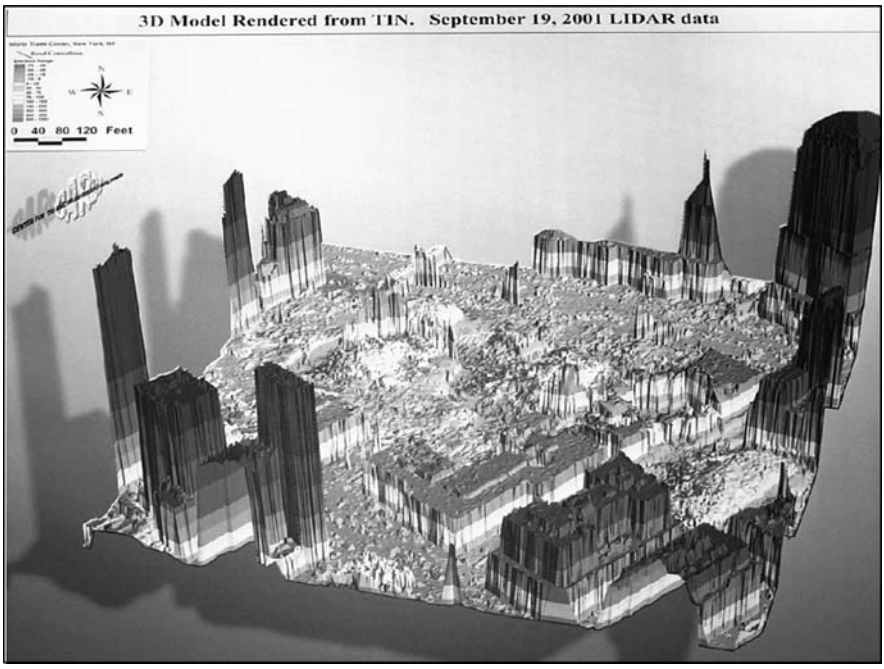

Fig. 15.9 Map showing a 3D terrain model for Ground Zero, produced from LIDAR data acquired by EarthData on September 19th 2001
Source: Adams and Huyck 2005

2001). The Airborne LIDAR Pipeline Inspection System (ALPIS) uses an infrared laser to monitor gas plumes at ground surface level (LaSen 2003). Together, these examples clearly point towards the potential application of spatial technology in response to bioterrorism, and the detection of airborne contaminants (Brown 2002).

For natural disasters, remote sensing applications typically focus on tracking the location and extent of a given hazard, using a temporal sequence of images. In the case of wildfires, the online GEOMAC service (GEOMAC 2003) integrates MODIS thermal imagery (see also Ahern et al. 2001; CEOS 2002). GEOMAC offers a reasonably timely visualization at a regional scale, but until a constellation of low earth orbiting satellites (LEOS) comes online (see Sun and Sweeting 2001), the ultimate target of real-time detection with 15 min updates (CEOS 2002) remains out of reach. For tracking floods, optical imagery has been widely used (Sharma et al. 1996; Laben 2002), despite the persistent challenge posed by cloud cover. A number of authors illustrate all weather capability through integrating optical and SAR imagery (Profeti and MacIntosh 1997; Tholey et al. 1997; Wang et al. 2003). Volcanic eruptions also represent a considerable challenge, creating a range of land- and air-based hazards. Kerle and Oppenheimer (2002) describe the use of optical and radar imagery to track fast flowing lahars. Monitoring the spread of atmospheric ash clouds is a further application area (CEOS 2002; Francis and Rothery 2000), which promises to reduce risk to aviators.

Field Reconnaissance. GPS-based technologies are one of the reasons field reconnaissance efforts after major disasters have improved. Before this technology became available to the general public, documentation of field reconnaissance activities was cumbersome and time consuming. Now, with GPS-systems offering positional accuracies of about 1–3 m anywhere in the world, it is possible to link photos and videos with actual points on the earth. This capability becomes even more important when this technology is integrated with GIS systems.

One of the field-based systems that has emerged in recent disasters is the VIEWS system developed for MCEER. VIEWS is a laptop-based portable field data collection and visualization system used during disaster reconnaissance missions to collect geo-referenced: (i) damage observations, (ii) photographs, and (iii) video footage. The system has been deployed from a moving vehicle, boat, aircraft and on foot. Through a real-time GPS feed, the geographic location of every record is overlaid on "before" and "after" remote sensing images and damage base maps. Through inbuilt GIS functionality, the field team uses the high-resolution satellite scenes to prioritize field survey activities, plan and track their route, and pinpoint damaged structures and features of interest. Traditional methods of post-disaster damage assessment typically involve walking surveys, whereby damage indicators together with the overall damage state are manually logged on a spreadsheet. VIEWS significantly increases the rate at which survey data is collected (Adams et al. 2004b). VIEWS has previously been used in reconnaissance activities following the 2003 Bam, Iran earthquake (Adams et al 2004a), Hurricane Charley and Hurricane Ivan (US Gulf coast 2004) (Adams et al. 2004b, c), the Niigata, Japan earthquake in October 2004 (Huyck et al. 2005), and Hurricanes Katrina and Rita in 2005 (Womble et al. 2006).

The Indian Ocean tsunami event constituted the first deployment of VIEWS and high-resolution satellite imagery for post-tsunami field reconnaissance (Ghosh et al. 2005). The system was deployed to study several key sites from August 16–25 2005, in order to "ground truth" the preliminary remote sensing results. VIEWS was equipped with layers including a Landsat landuse classification, a mangrove change/loss map, and QuickBird and IKONOS satellite imagery. The damage survey of impacted areas (Fig. 15.10) was conducted by a three member team from a moving vehicle, on foot, and by boat depending on vehicular access and type of landuse (e.g., mangrove). Fourteen (14) hours of geo-referenced digital video footage were recorded along the reconnaissance survey route covering about 75 miles (50 miles from a moving vehicle, 20 miles from a boat, and 5 miles walking tour). A library of approximately 550 digital photographs was also collected by the team.

15.3 Challenges

Ironically, the emergence of new technologies – especially, information technologies – has created a number of challenges that are only now being addressed by researchers and practitioners in disaster management. Whereas, the norm several decades ago was to have sophisticated modeling solutions to disaster management problems with little or no empirical data, the situation today is quite the reverse.

Fig. 15.10 VIEWS interface showing "before" and "after" high-resolution imagery and part of the GPS route (*yellow and red dots*) followed by the field team in Ban Nam Khem – Indian Ocean Earthquake and Tsunami. The upper photograph shows an example of the rapid reconstruction that is occurring, and the lower digital video shows remaining building damage
Source: Chang et al. 2006

Because of widespread field sensors and other data (e.g., remote sensing), the disaster management community has access to much more data than it can possibly handle. Some of the issues now arising because of the overabundance of data and information are real-time event monitoring, privacy protection, information sharing and trust management.

Real-Time Event Monitoring. As discussed earlier, some hazards are monitored through extensive field networks where information on an event as it is occurring can be sent back to some central site where the data can be analyzed. An example of this type of network is the California Integrated Seismic Network (CISN) which monitors earthquake occurrences in California and uses this data to create real-time ground motion intensity maps (http://earthquake.usgs.gov/resources/software/shakecast/). Ideally, the ground motion maps are imported into GIS-based loss estimation tools like HAZUS®MH and the impacts caused by the event can be approximated within a matter of minutes. Similar tools are available for monitoring and tracking significant hurricanes. One of the major issues arising from this process is how to disseminate this information to emergency management officials and the public. One solution being explored is providing information through online systems. By showing maps of heavily shaken areas, emergency management officials can assess where resources are needed first and eventually determine

whether outside resources will be needed during the initial response period, mainly to address life safety issues. Furthermore, if these online systems are able to overlay different information layers (e.g., location of hospitals, initial damage reports, location of shelters) onto hazard or damage maps, the public can use this information to decide how best to plan for their own recovery. Some possible applications for an online GIS system include a family re-unification system, guides for where to obtain assistance or supplies, locations of highway closures, locations of hazardous conditions (e.g., fire-following, hazardous materials release; possible dam failure), and locations of utility outages.

Privacy Protection. With increasing amounts of georeferenced data available to the public, privacy protection becomes an issue. Satellite images or aerial photos of workplaces and residences are commonly accessible on the internet. Some internet applications provide photos or video at street levels, potentially capturing images of individuals without their knowledge. While there is no current law prohibiting companies or individuals from taking these photos or videos, there should be general guidelines that either limit the types of photos that can be taken, seeks authorization from individuals included in these images, or follows some protocol to obscure the identification of specific individuals in the images.

Information Sharing and Trust Management. The sharing of data between organizations has always been problematic, either because the mechanism to do so has not been developed or because the information that could be shared is either proprietary or protected under some privacy measure or law. During an emergency, certain types of data should be shared between government agencies so that effective decision-making can take place. For example, sharing damage assessment or repair information between utility companies and transportation agencies because utility companies attempting repairs need to know which roads and highways are still operational. In addition, system-wide repairs for a particular utility system may benefit greatly by coordinating the timing of these repairs with other utilities that may also have experienced damage. In this way, the restoration process can proceed in more systematic and efficient manner. Such coordination is being facilitated through Emergency Operations Centers (EOC), however, joint access to this information on a more real-time basis may provide significant benefits. In order to facilitate this type of collaboration, information sharing technologies that allow organizations to retain control over their information and to ensure the proprietary nature of some data must be developed (e.g., trust management systems).

15.4 Final Remarks

While much progress is evident from the examples given above, remote sensing and GIS technologies are not yet institutionalized into current and future emergency response programs. Disaster experts continually warn governments and the public about the possibility of "worst-case" natural hazard scenarios and their overwhelming impacts. Yet, planning for the occurrence of these events has fallen far short of need. The large earthquake that occurred off the coast of Sumatra, which resulted

in one of the deadliest tsunamis ever recorded, was a painful reminder that living in some of the most desirable areas of the world includes risks.

Although predicted some years ago, the disaster in New Orleans after Hurricane Katrina seemed to surprise many, including some key government agencies. While the calamity may have been caused by the "perfect storm," the response by key government organizations tasked with providing emergency support to New Orleans and other areas affected by the hurricane was neither timely nor effective. Whether the government's emergency response system was overtaxed to the point where it became dysfunctional will be discussed for many years. It is hoped that such discussion will result in significant changes that will prevent such catastrophic failure from occurring again. Proper use of geospatial technologies could have alleviated some of the confusion and suffering of New Orleans' citizens; properly applied, such technologies can help response teams alleviate, and even prevent, similar suffering in the future.

In the case of both Katrina and the Indonesian tsunami, new benchmarks were met in terms of the use of GIT to mitigate the effects of these disasters. The 2004 Indian Ocean earthquake and tsunami were among the first events where satellite and airborne imagery of all types was being captured and studied. The commercial high-resolution satellite data provider DigitalGlobe captured and immediately released images of the tsunami wave train hitting the shores of Sri Lanka. Sobering before-and-after images of Banda Aceh showed the world the level of devastation that had occurred. Had such images been captured all along Indonesia, Thailand, India and Sri Lanka in the first few days after the earthquake, a much better situational assessment could have been made and, perhaps assisted in providing a more rapid and coordinated response to the most severely affected areas. More rapid response may not have saved the majority of individuals killed in the tsunami, but could have alleviated much of the suffering and perhaps some lingering health issues that occurred weeks and months after the disaster.

Similarly, a more rapid response after Hurricane Katrina – especially understanding the extent of flooding in New Orleans and inundation areas along the Mississippi – could have provided a more realistic assessment of needs and priorities in the first few days and weeks after Katrina's landfall. While there were many useful images of these areas taken quickly after the hurricane's initial onslaught, these images would have been more useful if geo-referenced to a GIS.

In order for GIT to more effectively respond to the next wave of disasters, it must address the following issues or requirements:

- First-responders, and those who provide them with technical support, must have timely access to all images collected after an event. This access is especially pertinent for sensors operated at all levels of government. In addition, there must be adequate training and education for first-responders to enable them to appropriately interpret and use such information for response and recovery.
- Damage detection methodologies must become more robust, capable of working with various levels of data resolution or sensor types. Data fusion should be emphasized, and conclusions based on independent assessments.

- Emphasis needs to be placed on integrating post-event imagery and data into models that predict damage or impacts. Taking model results as the initial a priori estimate of impacts and revising or calibrating this estimate with real, post-event data should provide the basis for model re-calibration and improved output.
- Post-event imagery and event analysis should be posted on the internet as quickly as possible. Access to these data will not only improve response but provide the opportunity for additions and corrections from additional sources.
- Success and failure with respect to the use and adoption of GIT must be documented for every event, to improve its application and implementation for disaster response.
- Finally, government support is critical, especially in terms of research to design, develop and test methodologies, systems, platforms, and other components so that robust disaster response GIT can be developed and deployed not only throughout the US, but around the world.

Acknowledgments Much of the research presented in this chapter was conducted at ImageCat and was supported in whole or in part by the Earthquake Engineering Research Centers Program of the US National Science Foundation under award number EEC-9701471 to the Multidisciplinary Center for Earthquake Engineering Research, MCEER. Additional grants awarded to ImageCat are also acknowledged here. They include: US Department of Transportation Grant No. DTRS56-01-T-0013; NSF Grant No. CMS-0454564; NSF Grant No. CMMI-0806874; and the Responding to Crises and Unexpected Events (RESCUE) NSF Grant No. IIS-0331707 made to the University of California at Irvine.

References

No Author (2000). Report on the Kocaeli, Turkey Earthquake of August 17, 1999. The 1999 Turkey Report, Volume 1, Earthquake Disaster Mitigation (EDM) Technical Report No. 6. Earthquake Disaster Mitigation Research Center. The Institute of Physical and Chemical Research (RIKEN). Miki, Hyogo Prefecture.

No Author (2003). Weather radar appears to show shuttle debris. Publication date February 1. http://spaceflightnow.com/shuttle/sts107/030201columbia/radarimage.html, last update 2008; accessed December 13, 2008.

No Author (2005). NOAA aerial mapping assisting U.S. Coast Guard, FEMA shows flood waters receding in regions affected by Hurricane Katrina. *NOAA Magazine*, http://www.noaanews.noaa.gov/stories2005/s2503.htm, last update unknown, accessed December 13, 2008.

ABS Consulting (ABS). 2000. *TriNet Studies and Planning Activities in Real-Time Earthquake Early Warning: Task 2 – Lessons and Guidance from the Literature on Warning Response and Warning Systems*, UCLA Center for Public Health and Disasters/Disaster Research Center, University of Delaware. Prepared for the California Institute of Technology, ABS Project No. 1033753, November.

ABS Consulting (ABS). (2001a). *TriNet Studies and Planning Activities in Real-Time Earthquake Early Warning: Task 1- Survey of Potential Early Warning System Users*, UCLA Center for Public Health and Disasters/Disaster Research Center, University of Delaware. Prepared for the California Institute of Technology, ABS Project No. 1033753, March.

ABS Consulting (ABS). (2001b). *TriNet Studies and Planning Activities in Real-Time Earthquake Early Warning: Task 3 – Identification and Analysis of Policy Issues,* UCLA Center for Public Health and Disasters/Disaster Research Center, University of Delaware. Prepared for the California Institute of Technology, ABS Project No. 1033753, October.

ABS Consulting (ABS). (2002). *TriNet Studies and Planning Activities in Real-Time Earthquake Early Warning: Task 4 – Development of Plans and Options for Pilot Project,* UCLA Center for Public Health and Disasters/Disaster Research Center, University of Delaware. Prepared for the California Institute of Technology, ABS Project No. 1033753, January.

Adams, B.J., and Huyck, C.K. (2005). The emerging role of remote sensing technology in emergency management. In *Infrastructure Risk Management Processes: Natural, Accidental, and Deliberate Hazards*, Monograph 1, C. Taylor and E. VanMarcke (eds), American Society of Civil Engineers: Reston, Virginia, pp. 95–117.

Adams, B.J., Huyck, C., Mansouri, B., Eguchi, R., and Shinozuka, M. (2002). Post-disaster bridge damage assessment, *Proceedings of the 15th Pecora Conference: Integrating Remote Sensing at the Global, Regional, and Local Scale*, Denver, Colorado.

Adams, B.J., Huyck, C.K., Mio, M.Z., Cho, S., Eguchi, R.T., Womble, A.J., and Mehta, K. (2004c). Streamlining post-disaster data collection and damage assessment, using VIEWS (Visualizing Impacts of Earthquakes With Satellites) and VRS (Virtual Reconnaissance System), *Proceedings of 2nd International Workshop on Remote Sensing for Post-Disaster Response,* Newport Beach, California, October 7–8.

Adams, B.J., Huyck, C.K., Mio, M., Cho, S., Ghosh, S., Chung H., Eguchi, R.T., Houshmand, B., Shinozuka, M., and Mansouri, B. (2004a). The Bam (Iran) Earthquake of December 26, 2003: Preliminary reconnaissance using remotely sensed data and the VIEWS (Visualizing the Impacts of Earthquakes with Satellite Images) System. *MCEER Earthquake Reconnaissance Investigation*, 10 pp. http://mceer.buffalo.edu/research/Reconnaissance/Bam12-26-03/bam.pdf, last update unknown; accessed December 13, 2008.

Adams, B.J., Womble, J.A., Mio, M.Z., Turner, J.B., Mehta, K.C., and Shubharoop, G. (2004b). Field report: Collection of satellite-referenced building damage information in the aftermath of Hurricane Charley. *MCEER/NHRAIC Response*, September 15. Multidisciplinary Center for Earthquake Engineering Research (MCEER), University at Buffalo, The State University of New York, New York.

Ahern, F., Goldammer, J.G., and Justice, C. (2001). *Global and Regional Vegetation Fire Monitoring from Space: Planning a Coordinated International Effort*, SPB, The Hague.

Architectural Institute of Japan (AIJ). (1999). Hague*Report on the Damage Investigation of the 1999 Kocaeli Earthquake in Turkey*, Architectural Institute of Japan in Connection with Bogazici University, Istanbul Technical University and Middle East Technical University, AIJ, Tokyo.

Aoki, H., Matsuoka, M., and Yamazaki, F. (1998). Characteristics of Satellite SAR images in the damaged areas due to the Hyogoken-Nanbu Earthquake, *Proceedings of the 19th Asian Conference on Remote Sensing*, November 16–20, Manila. http://www.gisdevelopment.net/aars/acrs/1998/ts3/ts3007.shtml, last update unknown; accessed December 13, 2008.

Brown, S.F., (2002), Building America's anti-terror machine how infotech can combat homeland insecurity. *Fortune*, July 22: 99–104.

Cahan, B., and Ball, M. (2002). GIS at ground zero: Spatial technology bolsters world trade center response and recovery. *GEO World*, January 1. http://findarticles.com/p/articles/mi_hb4311/is_200201/ai_n15030288?tag=content;col1; last update unknown, accessed December 13, 2008.

Campbell, J.B. (1996). *Introduction to Remote Sensing*, 2nd ed., Taylor & Francis, London.

Committee on Earth Observation Satellites (CEOS). (2002). *The Use of Earth Observing Satellites for Hazard Support: Assessments & Scenarios.* Final Report of the CEOS Disaster Management Support Group, published by the US National Oceanic and Atmospheric Administration and Department of Commerce, November. http://www.ceos.org/pages/DMSG/pdf/CEOSDMSG.pdf

Chang, S.E., Adams, B.J., Alder, J., Berke, P.R., Chuenpagdee, R., Ghosh, S., and Wabnitz, C. (2006). Coastal ecosystems and tsunami protection. *Earthquake Spectra* 22(53): S863–S887.

Chiroiu, L., 2005. Damage assessment of the 2003 Bam, Iran using IKONOS imagery. *Earthquake Spectra* 21(S1): S219–S224.

Chiroiu, L., and Andre, G. (2001). Damage assessment using high resolution satellite imagery: Application to 2001 Bhuj, India Earthquake, *RiskWorld*, November, pp. 1–13,

http://www.preventionweb.net/english/professional/publications/v.php?id=2966; accessed December 13, 2008.

Chiroiu, L., Andre, G., and Bahoken, F. (2003) Earthquake loss estimation using high resolution satellite imagery. *GIS Development*, www.gisdevelopment.net/application/natural_hazards/earthquakes/nheq0005.htm, last update unknown, accessed December 13, 2008.

Chiroiu, L., Andre, G., Guillande, R., and Bahoken, F. (2002). Earthquake damage assessment using high resolution satellite imagery, *Proceedings of the 7th U.S. National Conference on Earthquake Engineering*, Boston.

Chung, H., and Sarabandi, P. (2006). Remote sensing for building inventory updates in disaster management, *Proceedings of the Smart Structures and Materials and NDE for Health Monitoring and Diagnostics Conference,* San Diego, February 26–March 2.

Clark, R.N., Green, R.O., Swayze, G.A., Hoefen, T.M., Livo, K.E., Pavi, B., Sarcher, C., Boardman, J., and Vance, J.V. (2001).*Images of the World Trade Center Site Show Thermal Hot Spots on September 16 and 23.* Open File Report OF-01-405, U.S. Geological Survey.

DHI. (2007). Sample case from Spain. *The Network* – A community newsletter for DHI Software users. DHI Water Environment Health, Norway. http://www.dhi.no/Programvare/TheNetworkNyhetsbrev/TheNetWorkApril2007.aspx; last updated April. Accessed December 13, 2008.

DOT/NASA. (2002). *Achievements of the DOT-NASA Joint Program on Remote Sensing and Spatial Information Technologies. Application to Multimodal Transportation*, US Department of Transportation and National Aeronautics and Space Administration, April. http://www.ncgia.ucsb.edu/ncrst/synthesis/; last update unknown; accessed December 13, 2008.

DOT/NASA. (2003). *Remote Sensing and Spatial Information Technologies Application to Multimodal Transportation. Developing and Implementing Advances to Transportation Practice*, US Department of Transportation and National Aeronautics and Space Administration, May. http://www.ncgia.ucsb.edu/ncrst/synthesis/; last update unknown; accessed December 13, 2008.

Eguchi, R.T., Goltz, J.D., and Seligson, H.A. (1997a). Applications of new technologies. In *Northridge Earthquake: Lifeline Performance and Post-Earthquake Response*, A.J. Schiff (ed), Technical Council on Lifeline Earthquake Engineering, American Society of Civil Engineers, NIST GCR 97-712. Report to U.S. Department of Commerce, Technology Administration, National Institute of Standards and Technology, Building and Fire Research Laboratory, April.

Eguchi, R.T., Goltz J.D., Seligson, H.A., Flores, P.J., Blais, N.C., Heaton, T.H., and Bortugno, E. (1997b). Real-time loss estimation as an emergency response decision support system: The Early Post-Earthquake Damage Assessment Tool (EPEDAT), *Earthquake Spectra*, 13(4): 815–832.

Eguchi, R., Houshmand, B., Huyck, C., Shinozuka, M., and Tralli, D., (1999), A new application for remotely sensed data: Construction of building inventories using synthetic aperture radar technology, MCEER Research and Accomplishments 1997–1999, MCEER, Buffalo.

Eguchi, R., Huyck, C., and Adams, B., (in press), *Advanced Technologies for Loss Estimation: Construction of Building Inventories Using Synthetic Aperture Radar and Optical Imagery*, MCEER Technical Report, MCEER, Buffalo.

Eguchi, R., Huyck, C., Adams, B., Mansouri, B., Houshmand, B., and Shinozuka, M. (2002) Earthquake damage detection algorithms using remote sensing data – Application to the August 17, 1999 Marmara, Turkey Earthquake, *Proceedings of the 7th US National Conference on Earthquake Engineering*, Boston.

Eguchi, R., Huyck, C., Adams, B., Mansouri, B., Houshmand, B., and Shinozuka, M. (2003) Resilient disaster response: Using remote sensing technologies for post-earthquake damage detection, *MCEER Research and Accomplishments 2001–2003*, MCEER, Buffalo.

Eguchi, R., Huyck, C., Houshmand, B., Mansouri, B., Shinozuka, M., Yamazaki, F., and Matsuoka, M. (2000a). The Marmara Earthquake: A view from space, *The Marmara, Turkey Earthquake of August 17, 1999: Reconnaissance Report,* Section 10, Technical Report MCEER-00-0001, MCEER, Buffalo.

Eguchi, R., Huyck, C., Houshmand, B., Mansouri, B., Shinozuka, M., Yamazaki, F., Matsuoka, M., and Ulgen, S., (2000b), The Marmara, Turkey Earthquake: Using advanced technology to conduct earthquake reconnaissance, *MCEER Research and Accomplishments 1999–2000*, MCEER, Buffalo

Estrada, M., Kohiyama, M., Matsuoka, M., and Yamazaki, F. (2001a). Detection of damage due to the 2001 El Salvador Earthquake using landsat images, *Proceedings of the 22nd Asian Conference on Remote Sensing*, Singapore.

Estrada, M., Matsuoka, M., and Yamazaki, F. (2001b). Digital damage detection due to the 1999 Kocaeli, Turkey Earthquake, *Bulletin of the Earthquake Resistant Structure Research Center*, 34: 55–66.

Federal Emergency Management Agency (FEMA). 2008. HAZUS: FEMA's Software Program for estimating potential losses from disasters. http://www.fema.gov/plan/prevent/hazus/; last updated August 20. Accessed December 13, 2008.

Fingas, M.F., and C.E. Brown, (1997), Review of oil spill remote sensing. *Spill Science and Technology Bulletin*, 4(4): 199–208.

Francis, P., and D. Rothery, (2000), Remote sensing of active volcanoes. *Annual Review of Earth and Planetary Sciences*, 28: 81–106.

Galy, H.M., and Sanders, R.A. (2000). Using SAR imagery for flood modeling, *Proceedings of the RGS-IBG Annual Conference*, Brighton.

Garshnek, V., and Burkle, F.M. (2000). *Communications and Information Tools for the 21st Century: Changing the Face of Disaster Response and Humanitarian Assistance*. SSGRR 2000—International Conference on Advances in Infrastructure for E-Business, Science, and Education on the Internet; L'Aquila, Rome, Italy, July 31-August 6. Session G2-7. http://www.internetconferences.net/pastattendees/Italija2000/Welcome.pdf; last update unknown; accessed December 13, 2008.

Ghosh, S., Huyck, C.K., Adams, B.J., Eguchi, R.T., Yamazaki, F., and Matsuoka, M. (2005). Preliminary field report: Post-tsunami urban damage survey in Thailand, Using the VIEWS Reconnaissance System. *MCEER Earthquake Reconnaissance Investigation*, 9 pp.;http://mceer.buffalo.edu/research/Reconnaissance/tsunami12-26-04/Tsumani-Dec2004new.pdf, last update unknown; accessed December 13, 2008.

GEOMAC. (2003). *GEOMAC Wildland Fire Support: Geospatial Multi-Agency Coordination*. US Department of the Interior; http://www.geomac.gov/, last update March 1, 2007; accessed December 13, 2008.

Gusella, L., Adams, B.J., Bitelli, G., Huyck, C.K., and Mognol, A. (2005). Object oriented image understanding and post earthquake damage assessment for Bam, Iran, Earthquake. *Earthquake Spectra*, 21(S1): S225–S238.

Hasegawa, H., Aoki, H., Yamazaki, F., and Sekimoto, I. (1999). Attempt for automated detection of damaged buildings using aerial HDTV images, *Proceedings of the 20th Asian Conference on Remote Sensing*, Hong Kong. www.gisdevelopment.net/aars/acrs/1999/ts3/ts3097.shtml, last update unknown, accessed December 13, 2008.

Hasegawa, H., Yamazaki, F., Matsuoka, M., and Seikimoto, I. (2000). Determination of building damage due to earthquakes using aerial television images, *Proceedings of the 12th World Conference on Earthquake Engineering*, Aukland. http://ares.tu.chiba-u.jp/~papers/paper/WCEE/1722Hasegawa.pdf, last update unknown, accessed December 13, 2008.

Hashitera, S., Kohiyama, M., Maki, N., and Fujita, H. (1999). Use of DMSP-OLS images for early identification of impacted areas due to the 1999 Marmara Earthquake disaster, *Proceedings of the 20th Asian Conference on Remote Sensing*, Hong Kong, 1291–1296.

Hiatt, M. (2002). Keeping our homelands safe. *Imaging Notes*, May/June: 20–23.

Hutchinson, T.C., and Chen, Z. (2005). Optimized estimated ground truth for object-based urban damage estimation using satellite images. *Earthquake Spectra*, 21(S1): S239–S254.

Huyck, C.K., and Adams, B.J. (2002). *Emergency Response in the Wake of the World Trade Center Attack: The Remote Sensing Perspective*, MCEER Special Report Series, Volume 3, MCEER, Buffalo.

Huyck, C.K., Adams, B.J., Cho, S., Eguchi, R.T., Mansouri, B., and Houshmand, B. (2004). *Methodologies for Post-Earthquake Building Damage Detection Using SAR and Optical*

Remote Sensing: Application to the August 17, 1999 Marmara, Turkey Earthquake, Technical Report MCEER-04-0004, June 15.

Huyck, C.K., Adams, B.J., and Kehrlein, D.I. (2003). An Evaluation of the Role Played by Remote Sensing Technology Following the World Trade Center Attack. *Earthquake Engineering and Engineering Vibration*, 2(1): 1–10.

Huyck, C.K, Eguchi, R., and Houshmand, B. (2002). *Bare-Earth Algorithm for Use with SAR and LIDAR Digital Elevation Models*, MCEER-02-0004 Technical Report, MCEER: Buffalo.

Huyck, C.K, Mansouri, B., Eguchi, R.T., Houshmand, B., Castner, L., and Shinozuka, M. (2002). Earthquake damage detection algorithms using optical and ERS-SAR satellite data – Application to the August 17, 1999 Marmara, Turkey Earthquake, *Proceedings of the 7th US National Conference on Earthquake Engineering*, Boston.

Huyck, C., Scawthorn, C., Bardet, J.-P., Kayen, R., Kawamata, Y., Olshansky, R., Somerville, P., Mori, J., Rathje, E., Bay, J., Jibson, R., Kelson, K., Pack, R., and Nishi, N. (2005). Preliminary observations on the Niigata Ken Chuetsu, Japan, Earthquake of October 23, 2004, *EERI Newsletter*, January 2005, 39(1).

Jet Propulsion Laboratory (JPL). (1995). *The SRL Volcano Exhibit,* http://southport.jpl.nasa.gov/volcanopic.html, last updated March 30, 1995; accessed December 13, 2008.

Jet Propulsion Laboratory (JPL). (2003). *Glaciers and Ice Sheets in a Changing Climate*, http://www-radar.jpl.nasa.gov/glacier/; last update unknown, accessed December 13, 2008.

Kerle, N., and Oppenheimer, C. (2002). Satellite remote sensing as a tool in Lahar disaster management. *Disasters*, 26(2): 140–160.

Kohiyama, M., Hayashi, H., Maki, N., and Hashitera, S. (2001). *Night Time Damage Estimation*, GIS Development. http://www.gisdevelopment.net/magazine/gisdev/2001/mar/ntde.shtml; last update unknown, accessed December 13, 2008.

Laben, C. (2002). Integration of remote sensing data and geographic information system technology for emergency managers and their applications at the pacific disaster center, *Optical Engineering*, 41: 2129–2136.

Langhelm, R., and Davis, B. (2002). Remote sensing coordination for improved emergency response, *Proceedings of the 15th Pecora Conference: Integrating Remote Sensing at the Global, Regional, and Local Scale*, Denver, Colorado.

LaSen, Inc. (2003), *ALPIS: Airborne LIDAR Pipeline Inspection System*. LaSen, Las Cruces, New Mexico.

Logan, B. (2002). The Lessons of 9/11, *Geospatial Solutions*, September: 26–30.

Lu, Z., Wicks, C., Dzurisin, D., Power, J., Thatcher, W., and Masterlark, T. (2003). Interferometric synthetic aperture radar studies of Alaska Volcanoes, *EOM*, 12(2): 8–18.

Matsuoka, M., and Yamazaki, F. (1998). Identification of damaged areas due to the 1995 Hyogoken-Nanbu earthquake using satellite optical images, *Proceedings of the 19th Asian Conference on Remote Sensing*, Manila.

Matsuoka, M., and Yamazaki, F. (2000a). Interferometric characterization of areas damaged by the 1995 Kobe Earthquake using satellite SAR images, *Proceedings of the 12thWorld Conference on Earthquake Engineering*, Auckland.

Matsuoka, M., and Yamazaki, F. (2000b). Satellite remote sensing of damaged areas due to the 1995 Kobe Earthquake, In *Confronting Urban Earthquakes, Report of Fundamental Research on the Mitigation of Urban Disasters Caused by Near-field Earthquakes*, K. Toki (ed), pp. 259–262.

Matsuoka, M., and Yamazaki, F. (2002). Application of the damage detection method using SAR intensity images to recent earthquakes, *Proceedings of the IGARSS*, Toronto.

Matsuoka, M., and Yamazaki, F. (2003). Application of a methodology for detection building-damage area to recent earthquakes using SAR intensity images, *Proceedings of the 7th EERI US Japan Conference on Urban Earthquake Hazard Reduction*, Maui.

Mileti, D. (1999) *Disasters by Design: A Reassessment of Natural Hazards in the United States*, National Academies Press: Washington.

Mitomi, H., Matsuoka, M., and Yamazaki, F. (2001a). Automated detection of buildings from aerial television images of the 2001 Gujurat, India Earthquake, *Proceedings of the IEEE International Symposium on Geoscience and Remote Sensing*, Sydney.

Mitomi, H., Matsuoka, M., and Yamazaki, F., (2002), Application of automated damage detection of buildings due to earthquakes by panchromatic television images, *Proceedings of the 7th U.S. National Conference on Earthquake Engineering*, Boston.

Mitomi, H., Yamazaki, F., and Matsuoka, M. (2000) Automated detection of building damage due to recent earthquakes using aerial television images, *Proceedings of the 21st Asian Conference on Remote Sensing*, Taipei.

Mitomi, H., Yamazaki, F., and Matsuoka, M. (2001b). Development of automated extraction method for buildings damage area based on maximum likelihood classifier, *Proceedings of the 8th Conference on Structural Safety and Reliability*, Newport Beach.

Multihazard Mitigation Council (MMC). (2005). *Natural Hazard Mitigation Saves: An Independent Study to Assess the Future Savings from Mitigation Activities, Volume 1-Findings, Conclusions, and Recommendations*. National Institute of Building Sciences, Washington, D.C.

Morain, S. (2001). Remote sensing for transportation. safety, hazards and disaster assessment, *Proceedings of the International Conference on Urban Geoinformatics*, Wuhan.

NIBS/FEMA. (2003a). *Multi-Hazard Loss Estimation Methodology, Earthquake Model,* HAZUS® MH *Technical Manual,* National Institute of Building Sciences and Federal Emergency Management Agency, Washington, D.C., 690 pp.

NIBS/FEMA. (2003b). *Multi-Hazard Loss Estimation Methodology, Hurricane Model,* HAZUS® MH *Technical Manual,* National Institute of Building Sciences and Federal Emergency Management Agency, Washington, D.C., 557 pp.

NIBS/FEMA. (2003c). *Multi-Hazard Loss Estimation Methodology, Flood Model,* HAZUS® MH *Technical Manual,* National Institute of Building Sciences and Federal Emergency Management Agency, Washington, D.C.

National Research Council (NRC). (1999). *Impacts of Natural Disasters*, NRC Committee on Assessing the Costs of Natural Disasters.

Oberg, J. (2003). *High-Tech Sensor in the Shuttle Search*. MSNBC, March 30. http://www.msnbc.com/news/891627.asp?0sl=-13; last update 2008; accessed December 13, 2008.

Ogawa, N., Hasegawa, H., Yamazaki, F., Matsuoka, M., and Aoki, H. (1999). Earthquake damage survey methods based on airborne HDTV, photography and SAR, *Proceedings of the 5th US Conference on Lifeline Earthquake Engineering, ASCE*, 322–331.

Ogawa, N., and Yamazaki, F. (2000). Photo-interpretation of buildings damage due to earthquakes using aerial photographs, *Proceedings of the 12th World Conference on Earthquake Engineering*, Auckland.

Profeti, G., and MacIntosh, H. (1997). Flood management through landsat TM and ERS SAR data: A case study, *Hydrological Processes*, 11(10): 1397–1408.

Puzachenko, Y.G., Borunov, A.K., Koshkarev, A.V., Skulkin, V.S., and Sysuyev, V.V. (1990). Use of remote sensing imagery in analysis of consequences of the Armenian Earthquake, *Mapping Sciences and Remote Sensing*, 27(2), 89–102.

Rathje, E., Crawford, M., Woo, K., and Neuenschwander, A. (2005). Damage patterns from satellite images from the 2003 Bam, Iran Earthquake, *Earthquake Spectra*, 21(S1): S295–S307.

Roberts, D., Gardner, M., Regelbrugge, J., Pedreros, D., and Ustin, S. (1998). Mapping the distribution of wildfire fuels using AVIRIS in the Santa Monica mountains, *Proceedings of 7th AVIRIS Earth Science Workshop JPL 97-21*, Pasadena.

Rodarmel, C., Scott, L., Simerlink, D., and Walker, J. (2002). Multisensor fusion over the World Trade Center Disaster Site, *Optical Engineering*, 41(9): 2120–2128.

RMSI. (2003). *Application of GIS for Regional Earthquake Loss Estimation*. www.rmsi.com/PDF/regionalearthquake.pdf, last update unknown, accessed December 13, 2008.

Saito, K., Spence, R., and De C Foley, T.A. (2005). Visual damage assessment of Bam, Iran using high-resolution satellite images following the Bam Earthquake on 26th December 2003, *Earthquake Spectra*, 21(S1): S309–S318.

Sarabandi, P., Adams, B., Kiremidjian, A.S., and Eguchi, R.T. (2005). Infrastructure inventory compilation using single high resolution satellite images, *Proceedings of the 3rd International Workshop on Remote Sensing for Post-Disaster Response,* Chiba University, Japan, September 12–13.

Southern California Wildfire Hazard Center (SCWHC), 2003. *The Role of Remote Sensing*, http://www.crseo.ucsb.edu/resac/; last update unknown, accessed December 13, 2008.

Sharma, P.K., Chopra, R., Verma, V.K., and Thomas, A. (1996). Flood management using remote sensing technology: The Punjab (India) experience, *International Journal of Remote Sensing*, 17(17): 3511–3521.

Sinha, R., and Goyal, A. (2001). Lessons from Bhuj Earthquake. GIS development, March. http://www.gisdevelopment.net/magazine/gisdev/2001/mar/lbe.shtml, last update unknown, accessed December 13, 2008.

Sun, W., and Sweeting, M. (2001). An international disaster monitoring constellation with daily revisit employing advanced low-cost earth observation microsatellites, *Proceedings of the 22nd Asian Conference on Remote Sensing*, Singapore.

Tholey, N., Clandillon, S., and DeFraipont, P. (1997). The contribution of spaceborne SAR and optical data in monitoring flood events: Examples in Northern and Southern France, *Hydrological Processes*, 11(10): 1409–1413.

Thomas, D.S.K., Cutter, S.L., Hodgson, M., Gutekunst, M., and Jones, S. (2002). *Use of Spatial Data and Geographic Technologies in Response to the September 11 Terrorist Attack*, Quick Response Report No. 153, Natural Hazards Research and Applications Information Center, University of Colorado, Boulder.

Tralli, D.M. (2000) *Assessment of Advanced Technologies for Loss Estimation*, MCEER, Buffalo.

Wang, Q., Watanabe, M., Hayashi, S., and Murakami, S. (2003). Using NOAA AVHRR data to assess flood damage in China, *Environmental Monitoring and Assessment*, 82(2): 119–148.

Williamson, R.A., and Baker, J.C. (2002). Lending a helping hand: Using remote sensing to support the response and recovery operations at the World Trade Center, *PE&RS*, 68(9): 870–896.

Williamson, R., Morain, S., Budge, A., and Hepner, G. (2002). *Remote Sensing for Transportation Security, Report of the Washington NCRST Workshop,* NCRST-H, Albuquerque.

Womble, A.J., Ghosh, S., Friedland, C.J., and Adams, B.J. (2006). Hurricane Katrina – Advanced Damage Detection: Integrating Remote Sensing Images with VIEWS Field Recon. MCEER, Buffalo.

Yamazaki, F. (2001). Applications of remote sensing and GIS for damage assessment, *Proceedings of the Joint Workshop on Urban Safety Engineering*, Asian Institute of Technology, Bangkok.

Yamazaki, F., Yano, Y., and Matsuoka, M. (2005). Visual damage interpretation of buildings in Bam City using QuickBird images, *Earthquake Spectra*, 21(S1): S329–S336.

Yusuf, Y., Matsuoka, M., and Yamazaki, F. (2001a). Damage assessment after 2001 Gujurat Earthquake using Landsat-7 satellite images, *Journal of the Indian Society of Remote Sensing*, 29(1), 233–239.

Yusuf, Y., Matsuoka, M., and Yamazaki, F. (2001b). Damage detection from Landsat-7 satellite images for the 2001 Gujurat, India Earthquake, *Proceedings of the 22nd Asian Conference on Remote Sensing*, Singapore.

Yusuf, Y., Matsuoka, M., and Yamazaki, F. (2002). Detection of building damage due to the 2001 Gujurat, India Earthquake, using satellite remote sensing, *Proceedings of the 7th US National Conference on Earthquake Engineering*, Boston.

Part IV
Hurricane Response/Recovery

Chapter 16
Remote Sensing and GIS Data/Information in the Emergency Response/Recovery Phase

Michael E. Hodgson, Bruce A. Davis, and Jitka Kotelenska

Abstract Based on popular images and scientific literature discussing geographic information science (GIScience) approaches for hazard analysis, it might be assumed that GIScience is a core element in the response and recovery phases of the disaster cycle. Findings from our research suggest that the use of GIScience in disaster response/recovery is: (1) in an evolutionary phase and (2) timing and coordination are major impediments. In Spring 2005 (prior to Hurricane Katrina), a survey was conducted of all state-level emergency preparedness offices to determine geographic information system/remote sensing use (hereafter referred to as geographic information technologies, or GIT) and spatial data needs. While a few states had five to seven staff educated in GIT, 23% had no spatial analysts in early 2005. Thus, for many states the adoption of GIT is still in its infancy. This finding also indicates that many state emergency management agencies (EMAs) would benefit from external (e.g., state/local/federal agency, private, university) expertise in order to utilize GIT during a hazard event. With a focus on remote sensing, we use three hurricane events to illustrate the federal government's work to change procedures associated with GIT during response/recovery efforts. Concrete and anecdotal information on the role of GIT in Hurricanes Andrew (1992), Floyd (1999), and Katrina (2005) are provided. Acceptance of GIT must be based on timeliness of data/information, awareness by the user community, and appropriate application to response/recovery endeavors.

Keywords Response phase · Remote sensing · Institutional · Coordination · Survey · Hurricane

16.1 Introduction

The primary phases of the disaster cycle are event, response, recovery, mitigation, and warning, followed by a future event. Remote sensing and geographic

M.E. Hodgson (✉)
Department of Geography, University of South Carolina, Columbia, SC 29208, USA
e-mail: hodgsonm@sc.edu

P.S. Showalter Y. Lu (eds.), *Geospatial Techniques in Urban Hazard and Disaster Analysis*, Geotechnologies and the Environment 2, DOI 10.1007/978-90-481-2238-7_16,

information systems (GIS) (hereafter referred to collectively as geographic information technologies, or GIT) have been and continue to be used in all phases of the disaster cycle. GIS is primarily used during the mitigation phase. Remote sensing, through daily use of geostationary and polar orbiting satellites, is primarily utilized in the mitigation and warning phases. While GIT (which includes global positioning systems) is increasingly used for *practical* disaster event applications, *research* focused on overall issues regarding the use of GIT in disaster analysis is lacking. The majority of research using GIT in hazard analysis appears to be focused in three areas: (1) the development of algorithms, (2) example applications, and (3) summaries of what these technologies could offer in the future. While these topics are of interest, the goal of this chapter is to describe, discuss, and encourage additional research examining social/institutional and logistical issues regarding the integration of GIT into the emergency *response phase* of the hazard cycle.

Considerable research has been conducted regarding the use of GIT during the mitigation phase of disasters (Cova 1999; Hodgson and Cutter 2001; Jensen and Hodgson 2006; Cutter et al. 2007) as well as during the response/recovery phase (Hodgson and Davis 1998; Zlatanova and Li 2008). Applied studies are not uncommon (e.g., Ambrosia et al. 2003), as well as scholarly "lessons-learned" studies examining the use of GIT after a disaster event (NOAA 2001; Langhelm and Davis 2002; Williamson and Baker 2002; Huyck and Adams 2002; Bruzewicz 2003; Thomas et al. 2003; Parrish et al. 2007). The information provided in this chapter is unique because the data presented here are from the first nationwide survey conducted to establish the level of use of GIT during all phases of the hazard/disaster cycle (as opposed to conducting such a survey at the state-wide or sub-state level; see Parrish et al. 2007).

In the 1970s, GIS was used to model and estimate populations at risk from nuclear power plant accidents (Durfee and Coleman 1983) or nuclear attacks. In the next decade, after the Federal Emergency Management Agency's (FEMA) flood insurance rate maps (FIRM) were produced, the use of GIS expanded as it was used to estimate population and infrastructure exposure to flood events. That expansion continues to the present. While the role of GIS in the disaster cycle may not be formalized, it has become such an important component of the mitigation and recovery phases for some agencies (e.g., FEMA post-Hurricane Andrew in 1992) it is difficult to conceive of recovery or mitigation studies being performed without its use.

The launch of the Television Infrared Observation Satellite (TIROS) satellite in April 1960 initiated the systematic observation of major weather systems over the United States. Many other weather satellites followed TIROS, and today geostationary operational environmental satellites (GOES) transmit nearly continuous (every 30 min) images of the Atlantic and Pacific oceans, providing early warning of hurricanes, tropical cyclones, and other weather systems. In addition to providing warnings of approaching events, there are numerous examples of the use of remote sensing during the mitigation phase of the disaster cycle (Hodgson and Davis 1998; Zlatanova and Li 2008; Bresnahan 1998).

While much has been written about the use of GIT in the hazard-cycle phases described above, little research, and few protocols or methods of practice formally

describe its use during the *response* and *recovery* phases. In addition, there are essentially no formal discussions (outside of the post-event lessons-learned workshops) dealing with societal or institutional issues although such issues were made a short term research priority by the University Consortium for Geographic Information Science (UCGIS) in 2002 (Hodgson et al. 2002). One exception is found in the National Research Council report on geospatial support for disaster management (Committee on Planning for Catastrophe, National Research Council 2007).

It is unknown why there is so little evidence of academic research examining adoption of GIT approaches, or exploring logistical issues that must be addressed when attempting to incorporate GIT into the response/recovery phase of the hazard cycle. Research that has been conducted largely seems to focus on analytical methods, such as extracting information from imagery. GIT has great potential to assist those who are engaged in emergency response and recovery – but only with a clear understanding of the severe constraints under which data and information are collected, processed, information extracted, and output produced and delivered to the users. The extraordinary demand for rapid data acquisition/processing and information delivery is foreign to most GIScientists. For example, during response to the World Trade Center attacks in 2001 several technologies were provided to first responders including personal digital assistants (PDAs). While some devices were used, the size and durability of the PDAs was generally inadequate under those extreme conditions (firefighters found them nearly impossible to use while wearing heavy gloves). Similarly, attempting to collect aerial imagery following a disaster is made more difficult due to circumstances such as airport closures, lack of flight crew lodging, and/or difficulties establishing ground monument control. The GIScience community is generally unprepared to collect or process data under such unusual conditions.

In this chapter we offer objective data and information on the use of GIT, focusing on remote sensing, by state-level emergency management offices during the response and recovery phases. Our framework for the discussion is US federal, state, and supporting agency/company response to disaster events in the United States. Much of the data are derived from a systematic national survey of state offices conducted during Spring 2005, just prior to Hurricane Katrina's landfall along the US Gulf Coast. While the data and information provided here are from a US perspective, viewpoints from other countries can be found in publications such as Varstappen (1995) and Visser and Dawood (2004). Seventeen years of active US disaster response, participation in post-disaster GIScience "lessons-learned" workshops, and having conducted numerous post-event interviews with individuals (private, academic, state, and federal participants) has provided insight into how and why remote sensing was or was not utilized in the three hurricane disasters used as case studies in this chapter. The chapter closes with a discussion of five research challenges in the use of remote sensing during response/recovery phases:

(1) coordination and planning of image acquisition,
(2) knowledge of and access to available imagery,
(3) the need to collect imagery within 1–3 days,

(4) availability and access to ancillary spatial information,
(5) the need for trained GIS/remote sensing staff.

16.2 Survey of State Emergency Management Agencies

16.2.1 Survey Context

GIT and associated resource support (monetary, personnel, equipment) may be provided by numerous entities – state emergency preparedness offices, other state agencies, local counties/cities, federal agencies, private companies/non-governmental agencies, and religious institutions. However, response to natural and technological disasters is initially managed at the state or county level rather than the federal level. The state is in charge of emergency response operations and the federal government plays a supportive role unless the state requests emergency assistance because the disaster is beyond the state's ability to respond. When a disaster declaration is made, FEMA is usually the lead federal agency which can then draw on other agencies (e.g., US Corps of Engineers [USCOE], National Aeronautic and Space Administration [NASA], National Oceanic and Atmospheric Administration [NOAA], Department of Energy) through a Mission Assignment process.

Because the state has primary responsibility for disaster response, it is appropriate to examine the use and coordination of GIT from the state's perspective. Prior to the survey results presented here, no nationwide survey focusing on the use of GIT by state-level emergency management agencies had been conducted. Assessments for a specific hazard event have occasionally been performed but these only addressed the single state that "hosted" the event (e.g., Williamson and Baker 2002; Thomas et al. 2003). In the spring of 2005, the Department of Geography at the University of South Carolina, under NASA sponsorship, conducted a survey of GIT use and spatial data needs in all state-level emergency preparedness offices (Hodgson et al. 2005). This section describes some key findings from this survey that relate to geospatial data collection and coordination during the disaster response and recovery phases of a disaster event.

16.2.2 Survey Design

This study followed Dillman's (2000) *Tailored Design* for establishment surveys, which is an extension of the *Total Design Method.* A "tailored design" utilizes procedures to increase respondent cooperation and response rates to mail and Internet surveys by recognizing the differences between individual and "establishment" respondents. Development of the survey instrument was guided by discussions with a focus group as well as individuals. A pilot test of the survey was performed by experts and researchers in hazard management, GIS, and remote sensing, resulting in further refinements. The survey instrument was administered via Internet by

the University of South Carolina. Access to the survey was by "invitation only" and password controlled. Six steps were used to elicit and clarify responses (Table 16.1):

Table 16.1 Survey responses received

	Letter 1. (Jan. 14th)	Email 1. (Jan. 24th)	Letter 2. (Feb. 3rd)	Email 2. (Feb. 14th)	Letter 3. (Feb. 20th)	Phone calls (Mar. 3rd–19th)
Responses	6	16	12	6	3	2
Cumulative responses	6	22	34	40	43	45

- 1st Mailing of invitation letter through surface mail,
- 1st Email,
- 2nd Mailing of invitation letter through surface mail,
- 2nd Email,
- 3rd Mailing of invitation letter through surface mail,
- Personal telephone call.

As can be seen from the above list, the survey data gathering method was performed using two approaches: mail/email and telephone. The first phase gathered fundamental information common to most states using a web-based survey form. The second phase used a telephone interview with agency staff, which served three purposes: (1) to gather less common, elusive information, (2) to validate the respondent's understanding of the survey questions, and (3) to increase response rates through direct contact.

The target population for the survey was each state Emergency Management Agency (EMA) in the United States. Responses were sought from either a Director or an Assistant/Deputy Director from each state EMA as well as the District of Columbia and the Commonwealth of Puerto Rico (remaining US territories were not included due to possible language barriers and the different structure and division of emergency management responsibilities between the local, state, and federal levels). Due to the limited target population size and the directors' demanding schedules it was challenging, yet important, to secure a high response rate. If directors were unable to complete the survey instrument they were encouraged to appoint their assistant, deputy directors, or other designees to complete all or part of the survey (where appropriate) on the agency's behalf.

The survey's purpose was used to systematically explore the following general questions:

(1) What spatial data/information do EMAs need, when do they need them, and how are these data obtained?
(2) Are EMAs utilizing GIT in their operations (particularly in the response phase?

(3) If EMAs are not utilizing GIT, what limiting factors are slowing/preventing its use?
(4) What is the organizational and coordination structure within which GIT is applied in state EMAs?

Additional questions were included to identify lessons learned or perceived limitations, which are particularly important data if the goal is to reduce resistance of state-level staff to the use of GIT. These additional questions broadly addressed the following issues:

(1) What current methods are used to acquire these kinds of information/data?
(2) For emergency response applications, when is the information/data collection "too late"?
(3) Does your agency currently have the technical expertise to collect/process imagery for hazard applications?

The first invitation letter to participate in the survey was mailed to the entire survey population (52 EMAs) on January 14th, 2005. The mail/telephone steps outlined above were followed and completed in nine weeks with a response rate of 45 agencies (Table 16.1), or 87% – considerably more than anticipated. An addition to the steps outlined above was a short follow-up telephone survey conducted to clarify issues raised after the initial evaluation of responses and to encourage respondents to forward their recommendations to the supporting agencies (NASA and FEMA). The survey data collection efforts were completed by Spring, 2005; Hurricane Katrina made landfall later that summer.

Forty-two states completed the survey, while three states partially completed the survey (Fig. 16.1). The percentage of states responding to any particular question will be used in the following discussion of survey response rates. (Note: due to rounding, some percentages may sum to 99 or 101.)

16.2.3 Survey Findings

Within many EMAs there are few spatial analysts (i.e., someone with GIS or remote sensing expertise); 23% had none and only 43% more than one (Fig. 16.2). Eighty-six percent of EMAs had no staff trained exclusively in remote sensing, which helps explain why remote sensing is so little used by state agencies during the emergency response phase (discussed in more detail, later).

Prior to Hurricane Katrina's landfall in August of 2005, use of GIS at state EMAs could be characterized as fairly high; 88% of respondents considered GIS to be very beneficial to the agency (Fig. 16.3). However, only 40% of states considered remote sensing to be very beneficial to the agency.

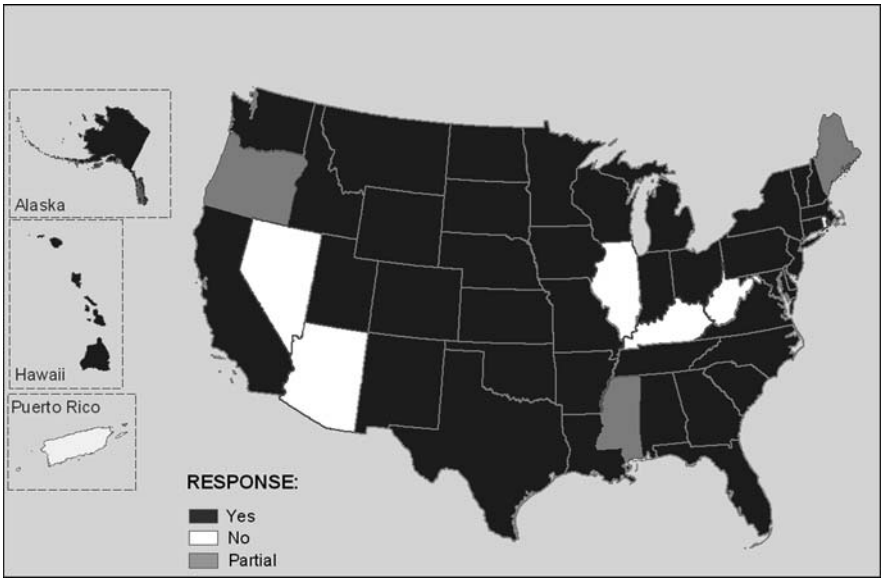

Fig. 16.1 Spatial distribution of survey responses from state EMAs

Fig. 16.2 Number of GIS or remote sensing analysts within state EMAs

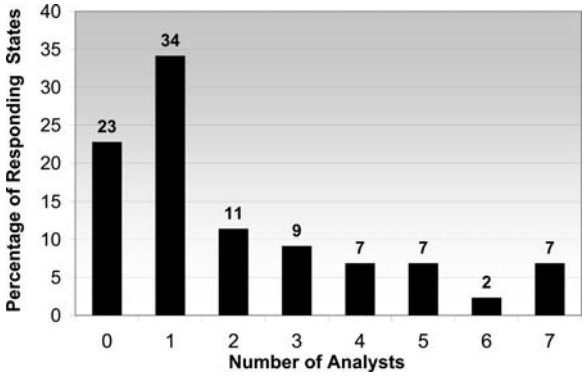

The majority of states (about 60%) considered remote sensing to be of none, or only moderate benefit to their agency. Interestingly, no state considered GIS to be of no benefit.

In contrast to the low perceived value of remote sensing found in Fig. 16.3, over 90% of states indicated they would (if resources were available) use remotely sensed imagery for mapping fire extent, flood inundation, crop/vegetation damage, debris characteristics, and damaged buildings during response and recovery phases following a disaster (Fig. 16.4). Interestingly, the data indicate that while perception of the benefit of remotely sensed imagery to the states is low (Fig. 16.3), when the survey offered specific applications for which remote sensing might provide valuable

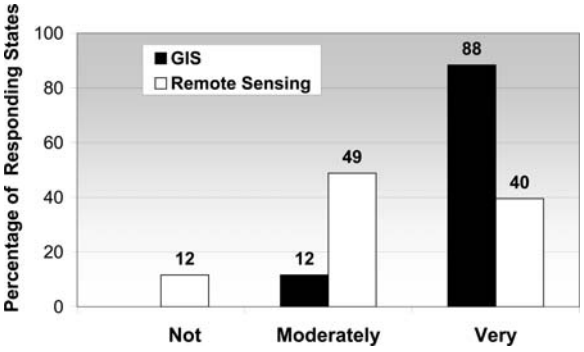

Fig. 16.3 EMA assessment of the benefits of GIS versus remote sensing to their agency

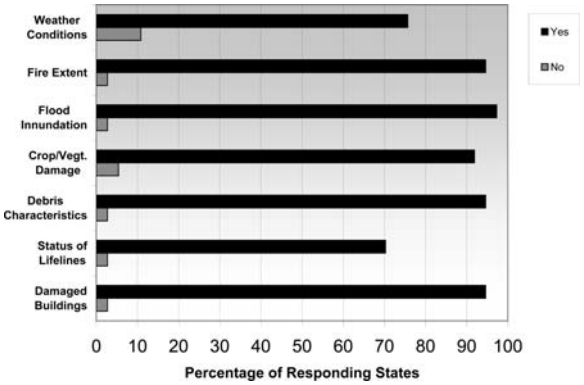

Fig. 16.4 Perceived utility of remote sensing for different phenomena, post-disaster, if resources were available for collecting imagery

information during two critical phases of the hazard cycle the response was very positive. This finding indicates that respondents may individually lack familiarity with how remote sensing data can be applied, but when specific uses are offered respondents can recognize the technology's potential.

Given that 1) few states are using remotely sensed imagery during the response phase but 2) respondents indicate the imagery could be used if resources were available, what are the limiting factors slowing/preventing its use? Cost of image acquisition and collection time constraints were identified as issues by 68 and 66% of states, respectively (Fig. 16.5). Processing time (49%) and staff technical skill limitations (47%) were also identified as problems. Accuracy was considered a limitation by only about one-fifth of the states. This finding implies that in early 2005, accuracy was considered to be less of a problem than price and collection time. In other words, obtaining imagery quickly and cheaply during the response phase was considered a higher priority than obtaining highly accurate imagery. The finding may also reflect the confidence of potential users in the data providers' ability to conduct adequate quality control.

Acquiring and extracting information from spatial data sources in a timely manner is critical during the emergency response phase. The lag-time between

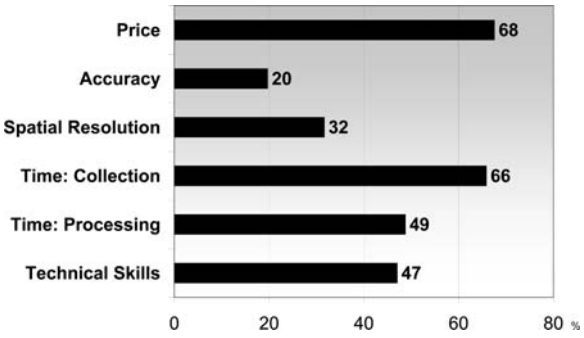

Fig. 16.5 Limitations to using remotely sensed imagery during the response phase

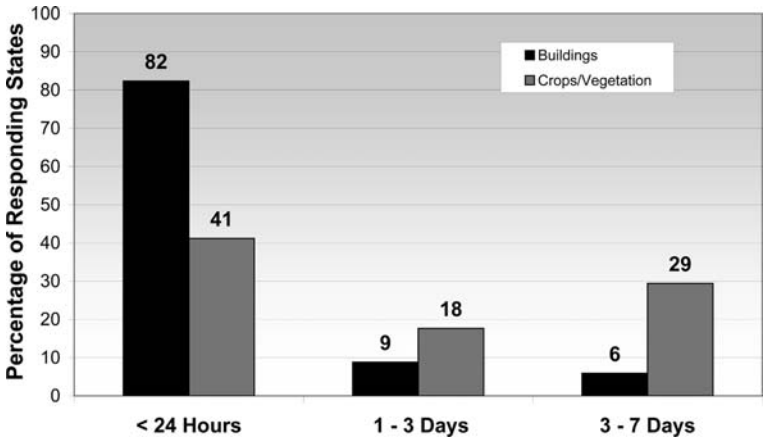

Fig. 16.6 Information regarding damage to buildings or crops/vegetation needed within a specified time period after a disaster event

an event and an agency's need for spatial disaster impact data can be very short (Fig. 16.6). When posing this question, states were asked to indicate data needs within a temporal context ranging from hours to days. Spatial data regarding damage to crops and vegetation were not considered urgent necessities. However, for infrastructure (e.g., building, bridge) damage, most agencies (82%) indicated a need for information within 24 hours of the event as opposed to the "3-day window" suggested by others (Zhang and Kerle 2008, p. 97). Expanding the time frame to 3 days after an event only increases the percentage to 91 (an additional 9%). One explanation for this finding may be that remote sensing-derived information is only one source of post-event spatial photographic data being gathered, others being ground-level or windshield surveys. As days pass and information from these other sources becomes available there is less reliance on remote sensing data. In addition, while remotely sensed imagery may be useful for some response/recovery applications (e.g. as a "backdrop" for a recovery mapping need), as time progresses its usefulness for identifying damaged features wanes as other sources become available.

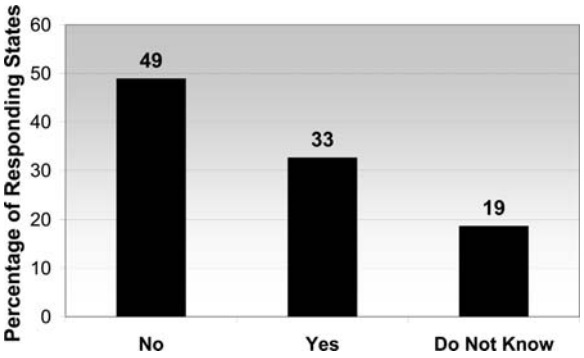

Fig. 16.7 Percentage of states that collect remotely sensed data through a coordinating authority

Designing image requirements (e.g. spatial/spectral resolutions, coverage area, acquisition time, sensor type) and coordinating image collection within the response community has long been problematic. The survey found that in early 2005, remote sensing data gathered by stakeholders (e.g. state agencies, counties, councils of governments) was only collected through a coordinating authority by 33% of the states and nearly half stated that they did not coordinate collection of such data (Fig. 16.7).

An effort was made to ascertain the use of predictive models (e.g., Hazards United States, or "HAZUS"). Because HAZUS and consequences assessment (CATS) are two commonly used models, respondents were asked to specifically consider those two in their answers as well as the general concept of models. For all three types, the major limiting factor in their use was input data (Fig. 16.8). Technical skills (needed to work with the models), processing time, and accuracy were the next most commonly cited limitations, while spatial resolution and cost were generally the least problematic.

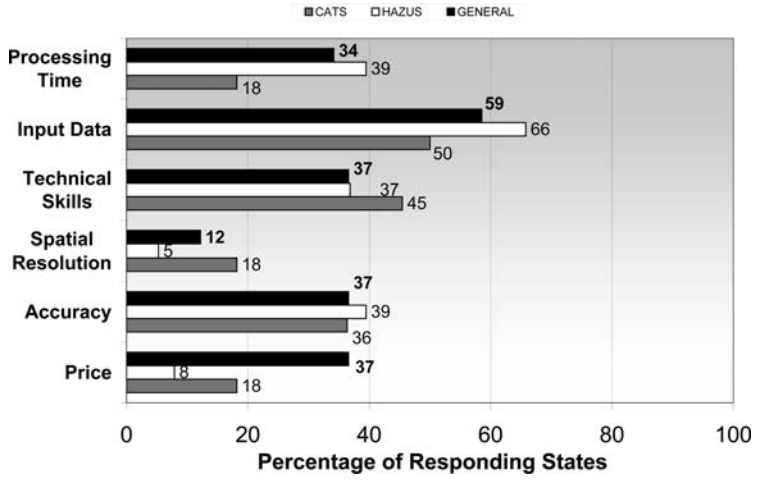

Fig. 16.8 Percentage of EMAs indicating a specific limitation for using a hazard predictive model

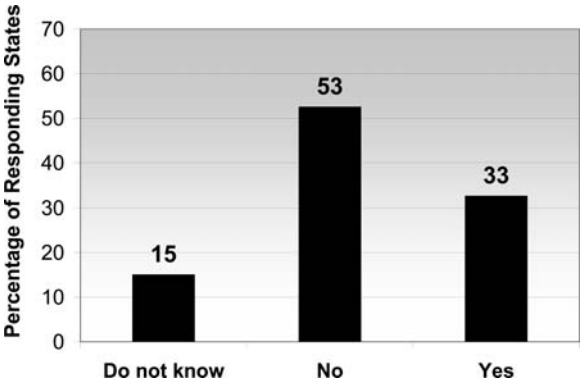

Fig. 16.9 Percentage of EMAs that validated the performance of a predictive model

Validating a model's performance requires comparing predictions to observations, and remotely sensed imagery can play an important role in the validation process. However, because collecting evidence for model validation is not a post-event priority (compared to task such as response/recovery, debris removal) we expected few, if any states, to validate models. While 68% either did not validate, or did not know if they validated, the finding that 33% did validate the performance of a predictive model exceeded our expectations (Fig. 16.9).

16.3 Remote Sensing Data/Information Use in Three Major Hurricanes

In this section, concrete and anecdotal information on the role of GIT in hurricanes Andrew (1992), Floyd (1999), and Katrina (2005) are presented. Remote sensing was used as a response and damage assessment tool following each storm, and each experience produced a set of recommendations.

Under normal conditions, incorporating remote sensing into a project generally follows systematic steps:

(1) define mapping requirements and platform-sensor type,
(2) identify platform-sensor availability/provider (e.g., a satellite or aeroservice company) and desired collection period,
(3) ferry platform, collect imagery, download, and repeat as per contract,
(4) post-process data (e.g. scan, download, geometrically rectify, duplicate) and ferry,
(5) assess image quality and conformance to contract (e.g., accuracy assessment), and
(6) extract information.

In most non-disaster settings many of these steps are considered "inconsequential", for example, post-collection download and ferry time. If using an aerial film

camera, the film canister must be ferried to a photographic laboratory with 9" × 9" film processing capabilities (particularly for processing color imagery) and the processed film/prints ferried back to the client. Due to the popularity of digital cameras finding such a laboratory today (2008) has become problematic – the only aerial image color processing laboratory in the country is located in Dayton, Ohio.

Processing of aerial digital imagery has its own challenges, including the fact that the data must be downloaded from special camera disks and a backup copy created. The hard drives for these aerial sensors are expensive, pressurized, and engineered to older technology specifications for purposes of stability and durability. For example, a typical Zeis DMC camera being used on a four-hour mission carries hard drives worth approximately $300,000 (2008 dollars). While moderate size solid state drives have recently become available, many aeroservice companies using standard technology experience significant delays in the delivery of image data due to lengthy data download speeds – each hour of mission time results in an hour of download time (Aslaksen, NOAA National Geodetic Survey, Acting Chief, Remote Sensing Division, personal communication 2008, April 30). However, advances in parallel data extraction techniques are slowly improving this situation, with some aeroservice companies able to download a four-hour mission in 20-minutes (Allen, Vice President, PhotoScience, Inc., personal communication 2008, November 4).

Airborne collection of imagery and supporting logistics becomes increasingly complicated in disaster situations. Many remote sensing aircraft have a fuel/flight limitation of about four hours. Flying a full collection event requires one or two four-hour missions followed by refueling, data download, and flight crew rest. Other hurdles commonly encountered under such circumstances include:

- small airports closed,
- larger airports restricted,
- flight crew lodging severely restricted (one flight crew collecting data following Hurricane Katrina had to fly to Tennessee and Arkansas for lodging/refueling),
- restricted airspace caused by Presidential visits,
- recovery of monuments used for horizontal/vertical imagery control during the mission hampered by landscape change and lack of ground access, and
- non-operational National Geodetic Survey (NGS) differential correction stations (Allen, Vice President, PhotoScience, Inc., personal communication 2008, November 4).

Aerial digital data files can be enormous (e.g., 500 GB to terrabytes). Consequently, it can be more efficient to send the data to the client via airborne courier than over the Internet, especially if operating out of a disaster area where infrastructure has been impacted and bandwidth is crowded with other communications. Bandwidth and online storage space in a federal/state Joint Field Office (JFO) responding to a disaster can also become scarce as additional geographic data are required. One factor that increases the speed of data delivery during a crisis is that quality control (Step 5, in the list presented at the beginning of this section) is essentially abandoned.

Following are observations derived from surveys, interviews, personal experience with, and discussions regarding how GIT was used following three powerful hurricanes that struck the US. This information is not presented as a comprehensive accounting, but to illustrate how technology has changed, awareness of application potential has improved, and how implementation of GIT has increased over a 17-year period.

16.3.1 Hurricane Andrew 1992

When Hurricane Andrew struck Florida, few satellite sensors were available for use during the emergency response. Two high spatial resolution (~1 m) systems were in development by commercial vendors, but no commercial satellite data provider was in orbit. The highest resolution government satellites were Landsat 5's Thematic Mapper (spatial resolution ~30 m) and France's SPOT (10 m panchromatic and 20 m multispectral). Most aerial photogrammetric firms were using 9" × 9" inch mapping cameras with black-white, true-color, or color infrared film. Some scanning sensor systems were in use primarily by government research and development groups. Automatic georectification or orthorectification on board aircraft was not widely available or operational. Image processing software was available from commercial off-the-shelf (COTS) and government agencies for digital data analysis.

Coordination of remote sensing resources at a national level for natural disaster response was not well developed. Federal agencies involved in remote sensing largely operated independently (with respect to remote sensing missions), with little communication.

User awareness of remote sensing's utility for natural disaster response was also very limited. Emergency Operations Center's were primarily focused on "boots on the ground" work, endeavoring to deliver critical resources and services to sustain life and mitigate further property loss. Remote sensing was not formally incorporated into the state Emergency Operations Center (EOC) or the Disaster Field Office (DFO).

Consideration of remote sensing by the state was in the context of information needed by Florida's governor regarding:

- How big is the disaster and how bad is the damage?
- How many resources are needed to respond/recover and does the state have such resources?

Post-Andrew, a few remote sensing-based damage assessments were conducted – all independently. The US Army Corp of Engineers (USCOE) mapped and estimated debris amounts. NASA and the State of Florida assessed total damage by functional categories. A local utility company contracted with Pan American to acquire aerial photographs to use to determine infrastructure damage. And, the US Air Force flew local missions for undisclosed military purposes.

The USCOE was, and still is, responsible for estimating debris volume and removal after natural disasters. The Corps had a practice of collecting post-disaster aerial imagery to estimate damage and had contracts in-place to ensure rapid mobilization and mission execution in the event of a hurricane. Thus, as Hurricane Andrew was moving across south Florida on August 24, 1992, an aircraft from East Tennessee was enroute to the damage area to begin photo acquisitions. For several days the aircraft few out of Alcoa, Tennessee to collect black-white imagery across the damage area, then flew back to Tennessee to deliver the film to the photographic lab.

Through professional contacts made during a pilot project designed to acquaint state and local governments with remote sensing, the state of Florida contacted NASA'S Stennis Space Center and requested assistance acquiring imagery over the impacted area to assess damage. Approximately ten days after the hurricane impacted Florida, NASA dispatched its Lear 23 aircraft to the state, equipped with a Zeiss RC-10 camera and the Calibrated Airborne Multispectral Scanner (CAMS) (while other scanners available at Stennis were better suited for analysis of disaster phenomena, the CAMS was already installed and changing to a different scanner would have resulted in an unacceptable delay in departure). The Stennis team took direction by phone from Florida officials to construct initial flight lines. The altitude assignment by the FAA for the acquisition mission produced a spatial resolution of 5 m for the CAMS data, and the resulting scale of the photography was 1:13,200. Florida officials wanted to develop pre- and post-event images to illustrate storm impact (they had pre-event Landsat satellite imagery for the whole state as well as selected photography over portions of the state).

NASA flew remote sensing acquisition missions on a daily basis, weather permitting. At the end of each mission the color-infrared (CIR) film was loaded into shipping canisters and placed aboard a commercial aircraft for processing by a professional aerial photography firm under contract to Stennis, located in Dayton, OH. Conversations with this firm revealed that approximately one year prior to Andrew's landfall another CIR mission for the same area had been completed and the firm had the film positives. Because the photographic scale of the earlier imagery was similar to that being flown by Stennis, the firm was able to construct similar-scale pre- and post incident photographs of the same area for selected portions of the storm-damaged region (Fig. 16.10).

State officials were very interested in the high resolution photography and the opportunity to construct pre- and post-event images. Products developed as a result of the remote sensing analysis consisted of estimated dollar value lost for four broad land cover categories (commercial/industrial, residential, natural resources, and agriculture). Through the use of enlargements from aerial photographs, the Governor of Florida was able to show federal officials examples of storm damage with estimated dollar values, effectively conveying Andrew's impact. While these products helped Florida convince Congress that federal relief funds were needed, there is no record of remote sensing data being used for emergency response, situational awareness, or incorporation into a common operating picture shared throughout the incident command structure.

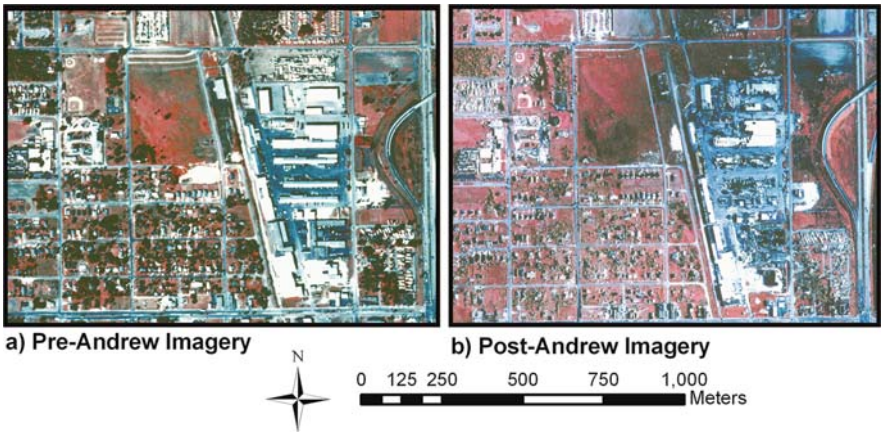

Fig. 16.10 Examples of pre- (**a**) and post-hurricane Andrew (**b**) CIR imagery near Homestead, FL

16.3.2 Hurricane Floyd 1999

Remote sensing's use for disaster response had matured greatly by September 16, 1999 when Hurricane Floyd impacted much of the lower third of North Carolina. While Florida's 1992 experience with Andrew prompted some hurricane-prone states to further develop their GIT capabilities, in the mid-1970s North Carolina had already begun pursuing aggressive development of a state-wide geographic database through the North Carolina Geographic Information and Analysis (NCGIA) agency. This commitment to comprehensive geographic information was a great boon for the hurricane response effort in 1999, with NCGIA able to provide hundreds of maps to the state EOC in a timely manner. Although very competent in the use of GIS, NCGIA was not using remote sensing on a regular basis at this time although there was an understanding of its value for numerous state applications.

As North Carolina responded to Hurricane Floyd, commercial airborne data providers were increasing their use of digital remote sensing scanners, but the bulk of such imagery was still collected on film. Satellite imagery was available from Landsat's Enhanced Thematic Mapper Plus (ETM+), the seventh version of the US' primary land remote sensing satellite. This instrument, launched earlier in the year, included a 15 m panchromatic channel, six 30 m multispectral channels, and a 60 m thermal channel. The first high spatial resolution (~1 m) imagery from Ikonos, a US commercial satellite, had yet to be produced. And, sophisticated commercial image processing software was more available as well as compatible with GIS software used by many states.

Shortly after Floyd's landfall, NASA Administrator Dan Goldin asked representatives from NASA Headquarters and Stennis to travel to North Carolina and assist with response efforts. These representatives worked out of the state EOC advising

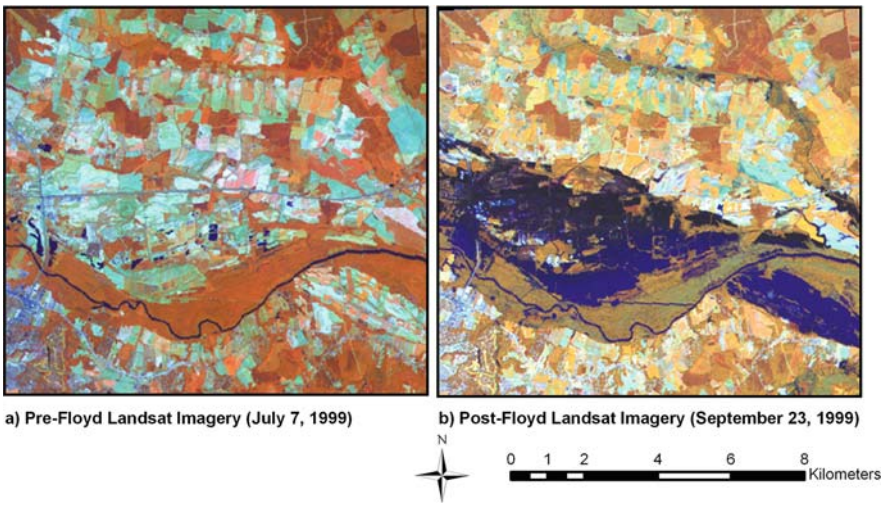

Fig. 16.11 Pre- (**a**) and post- (**b**) Hurricane Floyd Landsat ETM+ imagery acquired July 7 and September 23, 1999, respectively (residential and commercial buildings are *bright blue*, flooded land and existing water bodies are *dark blue*)

what remote sensing data were appropriate to address specific issues. RADARSAT data were used for overall flood delineation, while Landsat data were used to define flooding problems in specific regions. An aerial photography mission was also flown using panchromatic film to map specific areas. A recently acquired cloud-free Landsat image was used as the pre-incident base image for a change detection product requested by EOC officials (Fig. 16.11). The 15 m panchromatic channel provided adequate, but not optimal delineation of urban/suburban development, and was merged with the 30 m multispectral data. Image enhancement techniques were used to emphasize flooded areas in the post incident image. Throughout the response phase, deciding which sensor system to use was not problematic, but scheduling imaging opportunities and acquiring relatively cloud-free data was more difficult. At this time, coordination of remote sensing for disaster response was in its early stage of development. A Technical Services Branch was in place within FEMA to provide predictive modeling, mapping services and GIS capability, and remote sensing tasking and analysis. Unfortunately, the remote sensing data acquired for use in response to Hurricane Floyd was not delivered in time for actual implementation into the decision process. These data did, however, provide backup and verification for visual observation of damage extent and severity and were used to assist land use planning and redevelopment.

One of the legacies of Hurricane Floyd was that the State of North Carolina undertook an ambitious statewide mapping project. LiDAR data have been acquired from two commercial aerial mapping firms to develop digital elevation data critical for enhancing the state's understanding of flood risks.

16.3.3 Hurricane Katrina 2005

On August 29, 2005, Hurricane Katrina made landfall along the Louisiana/Mississippi Gulf Coast causing catastrophic damage and over 1500 deaths. In the interim between Floyd and Katrina, GIT had been incorporated on the federal level into a GIS Unit of FEMA's Hurricane Concept of Operations (placed under Emergency Support Function #5, Planning and Information). This Unit replaced the Technical Services Branch that had been the initial effort to coordinate and use GIT for disaster response and provided the same technical functions. For each GIS Unit a standard set of computer hardware and software was configured for delivery to the JFO housing both federal and state response officials. This GIS suite, as it was called, contained several laptops with GIS software, plotters, color printers, and geographic data for the area as well as a server connected into the FEMA Intranet of the JFO.

Another important development to disaster response was that by 2005 the US had three commercial high spatial resolution (~1 m panchromatic) satellites in orbit. Because these satellites had already been employed in response to several previous hurricanes, some of the contractual problems associated with government purchase of products and services from the private sector had been identified and solved. Furthermore, the wealth of data provided by these instruments imagery for a wide variety of natural disasters was expanding general understanding of their applicability in disaster response. Consequently, in 2005 the federal government had standing contracts with several commercial satellite companies to provide imagery in the event designated disasters occurred.

In addition to the commercial satellites, Landsat was still in orbit as well as newer satellites such as Aqua (carrying six sensors) and Terra (five sensors). The synoptic view provided by these sensors' wide swath widths and the availability of several useful spectral channels complimented data available from higher resolution satellites. The ability of the MODIS sensor, which was on board both Aqua and Terra, to image the same location twice each day provided valuable information regarding the environmental impact of the disaster despite a fairly course spatial resolution of 250 m.

Figure 16.12 illustrates the time frame during which several entities collected airborne data immediately after Katrina through the end of 2005. The day after landfall, NOAA began flying its Cessna Citation jet, carrying a digital frame camera (Fig. 16.13), to collect data. After two to three collections per day, the images were ferried to Panama City, FL for conversion to JPEG form and Internet transfer to the Washington, DC office. Gulfcoast Aerial Mapping also began flying the day after landfall and, in two days, flew the entire Mississippi coast using panchromatic film they were able to process locally. Photoscience was already under contract with the USGS to fly the Louisiana Gulf Coast for the purpose of wetlands mapping/monitoring, so they collected data of the impact area under a pre-existing contract. The USCOE set up a contract with the firm 3001, Inc. to fly imagery in support of their response and recovery efforts, which included debris removal and "Operation Blue Roof" (IG 2006). Although some of the aerial photography services shown in Fig. 16.12 used film-based cameras, several had incorporated digital frame

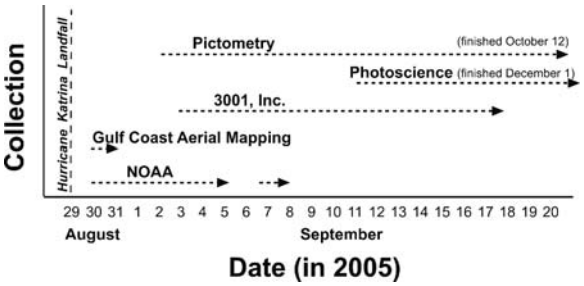

Fig. 16.12 Time envelopes indicating post-Katrina acquisition of airborne imagery

Fig. 16.13 Example of natural color airborne vertical imagery collected by NOAA one day after Katrina's landfall; a debris line near Long Beach, MS is visible (http://ngs.woc.noaa.gov/storms/katrina/24330996.jpg)

cameras that usually contained three-band visible and near-infrared imaging capability with the capacity to capture very high resolution multispectral images over large geographic areas. For example, Pictrometry flew oblique imagery with very high geometric fidelity to allow mensuration (Fig. 16.14).

While the acquisition of remotely sensed imagery occurred in a more timely manner than in previous disasters, some issues contributing to inefficiencies were identified. For example, although at the time Katrina hit the Gulf Coast the federal government did have standing contracts with several of the digital airborne remote sensing data providers, those contracts did not allow the companies to pre-position aircraft prior to hurricanes for early data acquisition. Aerial acquisition missions such as those described above can also produce extremely large data files, on the order of a terabyte or more. Furthermore, standard data product specifications were not uniformly applied resulting in the variety of products being delivered to the

Fig. 16.14 Post-Katrina oblique high spatial resolution black and white aerial imagery (Courtesy, Pictometry)

JFO with varying degrees of image quality (e.g., some products were geometrically rectified while others were not).

Despite some coordination problems and specification issues, numerous GIT-based efforts began developing "products" for use during the response/recovery phase. Many response/recovery staff considered a product as simply a hardcopy map showing, for instance, the locations of roads and road names along the coast (most signage near the coast was removed by the storm surge). Because in-car navigation systems were not commonly used or available to the recovery teams, simply finding a route between debris sites and disposal sites was challenging. To other staff a product might be an estimate of the location and magnitude of debris, such as was needed by the JFO in Biloxi, MS. Such products were based on analytic work using airborne imagery and field verification (Figs. 16.16 and 16.17).

The survey finding discussed earlier (Fig. 16.4), that only 20% of states considered accuracy to be a limitation when using remotely sensed data, was reconfirmed in the post-Katrina environment. *Access* to remote sensing data by the JFO determined if those data would be used for decision-making purposes, regardless of whether or not the sensor system used to collect the data was an appropriate choice. In the immediate aftermath of an event, disaster response managers are eager to take advantage of GIT information as long as it is available when needed. Decisions can not wait until imagery is delivered or processed–in those cases decision makers default to whatever information is available because the provision of critical resources or services to sustain life can not be delayed.

In retrospect, it appears that when compared to previous disaster response efforts progress has been made both in the *quality* of the information and the *speed* at which it is delivered.

As indicated at the beginning of this section, FEMA began the process of establishing its JFO containing a GIS Unit as Katrina made landfall. The hurricane's

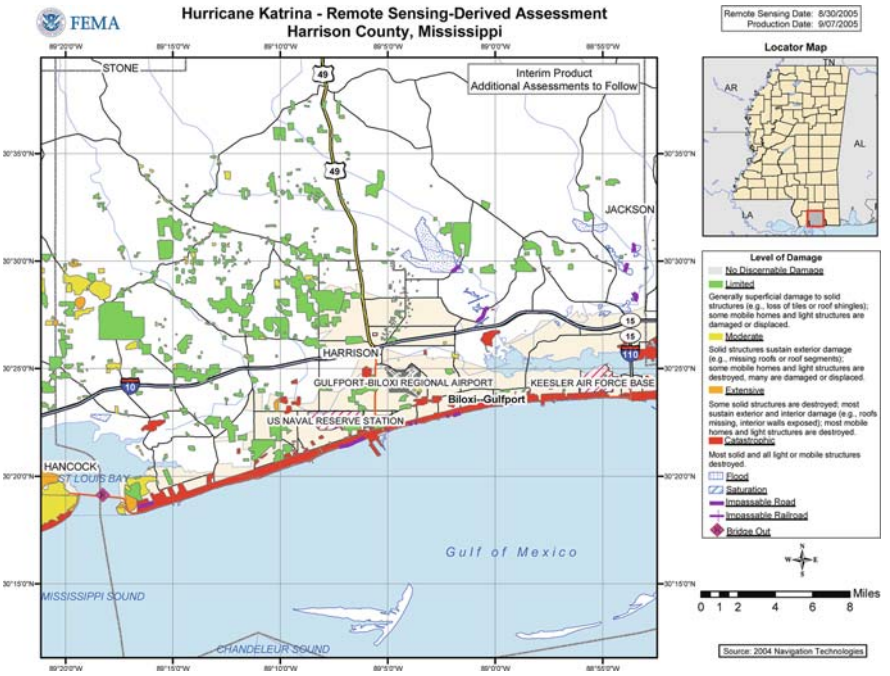

Fig. 16.15 Example of an NGA/FEMA map of damage intensity, coastal Harrison County, MS (FEMA 2008)

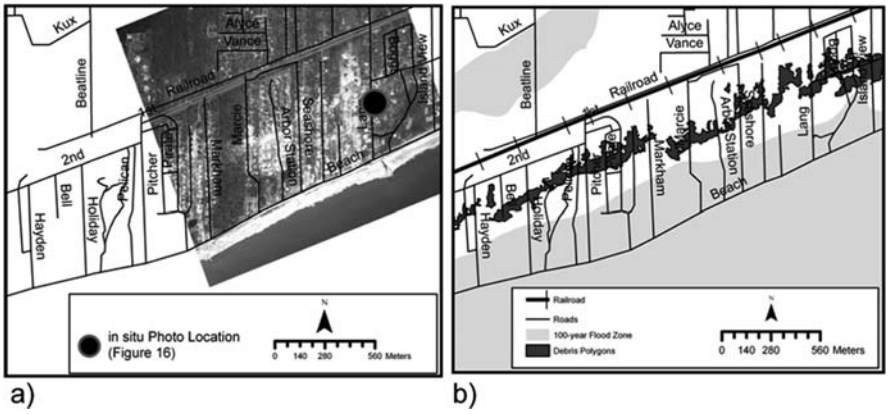

Fig. 16.16 NOAA digital aerial imagery (**a**) used to map debris polygons (**b**)

impact was so geographically immense that FEMA ultimately established two JFOs, onein Baton Rouge, LA and the other in Jackson, MS. Personnel from other regions were added to support the operation, including the initial task of developing situational awareness maps for the impacted area to understand what resources had been

Fig. 16.17 Ground view of debris line, Long Beach, MS (Source: Bruce A. Davis)

delivered and what were outstanding. Early in the response phase standard maps were developed for fairly static reporting purposes such as location of disaster relief shelters, population by jurisdiction in shelters, and jurisdiction maps showing city and county limits. Maps delineating flooding, major debris sites (Fig. 16.18), and structural damage are additional examples of products developed during this phase. Road network maps were some of the most valuable initial products because all landmarks had been destroyed along a large portion of the coast.

By the middle of October (recovery phase) over 80,000 map products had been produced for use by the Eastern Division of the response group. Most of these maps were created to answer a specific question pertinent at the time of response, and to establish the relative, as opposed to absolute, location of features. As the recovery phase progressed, GIS Unit representatives presented additional mapping options to personnel for addressing then-current issues and questions. The GIS Unit's "evangelism" for the use of GIT slowly created additional demand from various segments of the response community, many of whom had not previously experienced the opportunity of having a custom product developed for their needs. After initial exposure some of the JFO response offices came to depend on the GIS Unit's products, managing their programs on a daily basis with maps developed by the Unit.

In terms of local community emergency response offices, along the Gulf Coast of Mississippi there were varying levels of incorporation and use of GIT for response activities. Larger jurisdictions (e.g., cities, counties) generally had more-developed GIT capabilities and data protection plans in place. Unfortunately, in several smaller

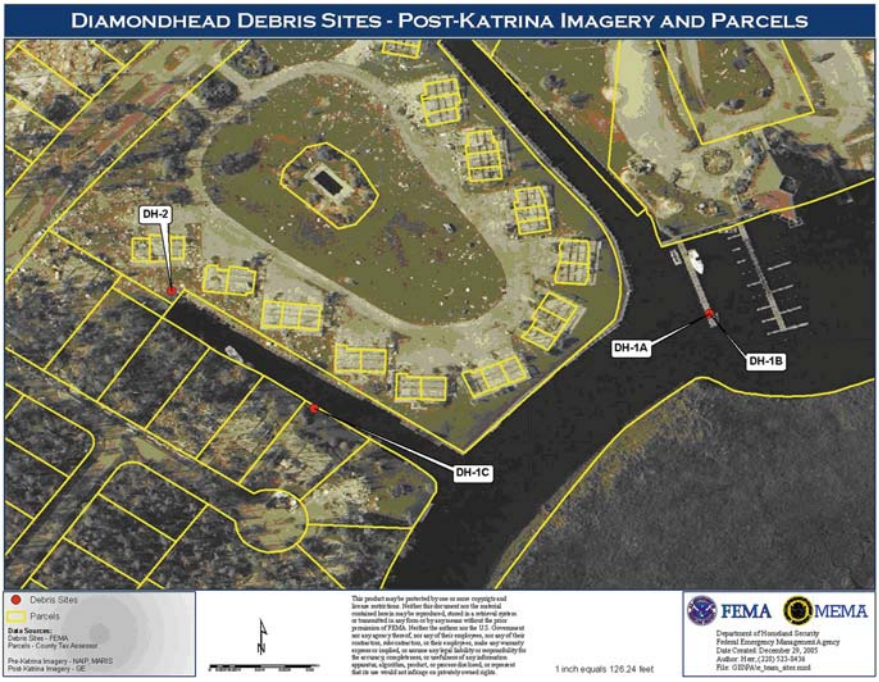

Fig. 16.18 Aerial view of the home locations (building footprints and parcel boundaries) in Diamond Head, Mississippi

jurisdictions the computer containing critical geographic data or imagery may simply have been powered down the Friday before Katrina's landfall. Post-Katrina, many of these were under salt water for hours and therefore rendered useless, if found at all. After the storm considerable time and effort was spent recovering or replacing computer systems, reloading copies of data held off line (if they existed), sharing data held by adjacent jurisdictions or regional authorities, and reconstructing the geographic database.

Both the 2005 pre-Katrina survey described earlier and a more recent study (Parrish et al. 2007) confirm that at the time of Katrina, GIT-trained staff were largely lacking in state-level EOCs. To address that problem, GIS volunteers came to the stricken area from many other states as well as from ESRI (DeCapua 2007). In some jurisdictions emergency response agreements with adjoining states were used to bring in outside GIS and remote sensing expertise to construct a geographic database and produce initial maps for local response. In other jurisdictions the GISCorps, an organization whose membership volunteer their expertise with GIT to aid humanitarian causes (GISCorps 2008), provided initial database development and map generation. Such efforts provided critical products to local groups for functions ranging from search and rescue to infrastructure restoration.

16.4 Conclusion

Our research consistently led to five key issues related to the use of remotely sensed data/information in the response phase of the hazard cycle:

(1) coordination and planning of image acquisition,
(2) knowledge of and access to available imagery,
(3) collection of imagery within 1–3 days,
(4) availability and access to ancillary spatial information, and
(5) trained GIS and remote sensing staff.

16.4.1 Coordination and Planning of Image Acquisition

Pre-existing contracts and plans between federal (and possibly state) agencies should exist prior to disaster events. These contracts should clearly state requirements regarding the imagery, its collection time/processing, and delivery expectations. The need for such contracts is not a new concept for disaster event planning, but these may not be pursued for a variety of reasons. For example, federal and state agencies must reestablish and rewrite each contract with every change in federal/state response plans, which are continuously being modified. Pre-existing contracts must also be continuously renegotiated as technology changes (e.g., new imaging systems, delivery methods) and as agency responsibilities change. Relying on a contract with a single provider (satellite or airborne) may also be untenable because there is no guarantee that provider will be able to respond under such conditions while, conversely, companies that provide such services need pre-existing commitments in order to schedule aircraft, flight crew, and ground-support. At least in terms of satellite imagery one web-based solution to help pre-determine sensor collection opportunities from multiple satellite providers is in development – the Remote Sensing Hazard Guidance System (Hodgson 2008) part of a NASA REASoN project at the University of South Carolina. The goal of this system is to assist hazards managers by automatically determining the optimum sensors available for specific events, geographic areas, as well as time frames and ultimately to predict the area of impact (Hodgson and Kar 2008).

16.4.2 Knowledge of and Access to Available Imagery

Over ten years ago, it was noted that while technology development is needed, the most serious challenge to successful use of remote sensing for emergency response is the coordinated use of this resource throughout the incident command structure (Hodgson and Davis 1998). The utility of GIT in disaster analysis is perceived differently by different emergency response/recovery staff. Those familiar with the use

of these technologies in prior events are typically very interested in the establishment and generation of related map products. Staff unfamiliar with these geographic approaches either do not know that this capability can assist them or are less receptive to their use during the response phase. While individuals in state agencies may lack familiarity with how remote sensing data can be applied, when specific uses are offered they are capable of recognizing the technology's potential. As familiarity with remote sensing grows, its use will expand into additional areas of emergency response. For example, FEMA now has a remote sensing (as well as a GIS) coordinator.

Communicating information regarding the availability of remotely sensed imagery to stakeholders, particularly local agencies, is problematic. Federal agencies with a need for, and resources to obtain, imagery will do so, and it is often assumed that this imagery (or its availability) will be shared with state and local agencies. While state agencies may be aware of the imagery through direct communication with the FEMA regional coordinator, local agencies may not. This communication roadblock occurred during each of the hurricanes described above. Therefore, while the incorporation of remotely sensed imagery into the decision making process of the response phase has improved, evidence indicates that communication about, and access to, such data could still be improved.

16.4.3 Collection of Imagery Within One to Three Days

All of the states indicated a need for geospatial data representing disaster impacts on building and other man-made infrastructure within three days of an event (most indicated 24-hours was preferable). Responses (e.g., from surveys, interviews, observations during events) suggest a theoretical curve relating the value of remote sensing derived information to the passage of time after the event (Fig. 16.19). For example, the inherent value of remote sensing derived information about damaged buildings may be very short (e.g., 24–72 hours) because as other sources of information (e.g., ground surveys) become available these may be perceived as more reliable or efficient uses of time. Remotely sensed imagery can provide valuable damage information over longer time frames about phenomena that are either less accessible (e.g., forests) or perceived as less critical (e.g., crops). Responders mapping structural damage to somewhat inaccessible natural environments (e.g., wetlands) will value remote sensing with longer lag times. And, for environmental research, remotely sensed imagery will be highly valued even if it is not collected for weeks after the event (Wakimoto and Black 1994; Ramsey et al. 2001; Kupfer et al. 2008).

The immediate need for data can only be met with a standardized approach to collecting the imagery, an approach that must also be well established among state EMAs so that procedures can immediately be set in motion during an event. Unfortunately, very few states have staff trained in the use of remote sensing analysis embedded within their operational agencies. However, almost all states indicated remote sensing would be beneficial during the response and recovery phases. To

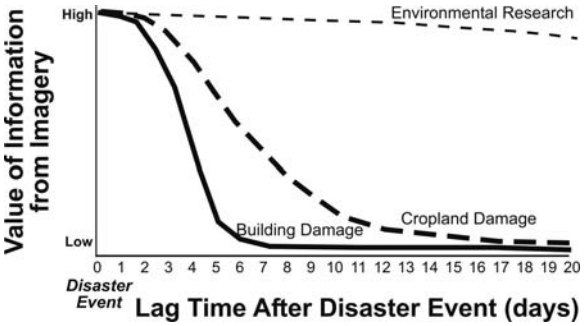

Fig. 16.19 Theoretical curve relating value of information (for responders) derived from remotely sensed imagery to lag time after the event when the information (or imagery) becomes available

improve collection of such data, federal agencies and the states need better coordination, funding, and access to remote sensing expertise in order to produce useful products in the immediate aftermath of a disaster. And, even with improved coordination, implementing collection activities can be problematic due to challenges presented by the event's impact (e.g., lack of accommodations, closed airports, destroyed monumentation).

16.4.4 Availability and Access to Spatial Information

Today, the recognition of spatial data needs for response and the fact that these may be addressed by existing data used for planning, mitigation, or other governmental activities exists at many levels of government. Since Katrina several national studies (e.g. National Research Council 2007b) have identified common geographic data existing in most communities that are critical for incident response. Most notable among these are current imagery for the jurisdiction, parcels, building footprints, and locally derived digital elevation model data. Due to the high cost of acquisition and the fear of misuse there is resistance by many local governments to share these data outside their immediate governmental agencies. While local communities are aware of the value of these data for a variety of local governmental functions it is uncertain whether these data are appreciated as critical information for emergency response that should be protected from loss in a catastrophic incident. In a recent NRC study on the need for a national cadastral system (National Research Council 2007a) it was noted that while some local governments provide free access to such data, others charge a fee. This issue was demonstrated during response to Katrina when, eight weeks into the response, the FEMA JFO was still seeking local parcel data. However, it should also be noted that at the time of Katrina few state or national systems maintained current geographic information shared by local government agencies or acquired from state and/or federal agencies. Notable exceptions are the USGS' efforts to develop the National Map, and the National Aerial Photography program conducted by the US Department of Agriculture. The ability and willingness to share locally developed data critical for emergency response remains an issue. In an effort to improve the sharing and analysis of all forms of information,

including geographic data, the Department of Homeland Security has established State Data Fusion Centers in each state. While this effort does not solve the issue of securing *locally* shared data for use during disaster response, it initiates the process of sharing information and critical data on a *national* basis.

16.4.5 Trained GIS and Remote Sensing Staff

The increasing use of GIS and supporting staff in state EMAs is, from a hazard perspective, encouraging because five years ago the use of GIS and availability of educated staff in the EMAs was very low. While a few states had five to seven educated staff in the GISciences, many states (23%) had none in early 2005. Realistically, however, the adoption of GIT is still in its infancy for many states, which means many state EMAs will continue to need external expertise (e.g., other state, local agencies, federal, private, or university) to utilize GIT during a hazard event. Except for the efforts of FEMA and a few states, there are almost no formal plans/agreements (e.g. a memorandum of understanding) to assimilate trained GIT staff from other agencies, private companies, or universities into EMAs during the first few days of an event.

Immediately following a catastrophic incident there is a critical need for information on the extent and severity of damage. This critical need is and has been present with every catastrophic incident. With the emergence of remote sensing as a means of quantifying land cover change on a regional basis the opportunity exists to use this technology to provide rapid assessment to decision makers. The emergence of this technology to assist emergency response has led to a demand for human skills and other supporting technologies not previously envisioned. The lag in the development and implementation of the supporting technologies (e.g., real-time receipt of image data, data coordination across a spatially diverse incident management command chain, appropriate data fusion and exploitation tools) has reduced the effectiveness of remote sensing for disaster response and affected the way remote sensing is perceived in local and federal emergency response centers and other incident management facilities. As a technically sophisticated civilization with tools to respond to natural disasters, reduce their impact, and speed recovery it is important to abandon the view that remote sensing is simply an interesting and potentially valuable piece of information. Instead, efforts should be made to ensure that this technology is fully incorporated into the fabric of our incident management systems.

References

Ambrosia, V.G., Wegener, S.S., Sullivan, D.V., Buechel, S.W., Dunagan, S.E., Brass, J.A., Stoneburner, J., Schoenung, S.M. (2003). Demonstrating UAV-acquired real-time thermal data over fires, *Photogrammetric Engineering and Remote Sensing* 64(10), 391–402.

Bresnahan, P. (1998). Identification of potential hazardous waste sites using aerial radiological measurements, *Photogrammetric Engineering and Remote Sensing* 64(10), 995–1001.

Bruzewicz, A.J. (2003). Remote sensing imagery for emergency management. In *The Geographical Dimensions of Terrorism*, S.L. Cutter, D.B. Richardson, T.J. Wilbanks (eds), New York: Routledge, pp. 87–97.

Cova, T.J. (1999). GIS in emergency management. In *Geographical Information Systems: Principles, Techniques, Applications, and Management*, P.A. Longley, M.F. Goodchild, D.J. Maguire, D.W. Rhind (eds), New York: John Wiley & Sons, pp. 845–858.

Cutter, S.L., Emrich, C.T., Adams, B.J., Huyck, C.K., Eguchi, R.T. (2007). New information technologies in emergency management, *Emergent Management: Principles and Practice for Local Government*, 2nd edition, W.L. Waugh and K. Tierney (eds), Washington: International City/County Management Association, pp. 280–297.

DeCapua, C. (2007). *Applications of Geospatial Technology in International Disasters and During Hurricane Katrina*. Gulfport, MS: Mississippi State University Coastal Research and Extension Center. http://www.gri.msstate.edu/research/katrinalessons/Documents/GeoSp_Tech_Applications.pdf; last downloaded November 4, 2008, 29p.

Dillman, D.A. (2000). *Procedures for Conducting Government-Sponsored Establishment Surveys: Comparisons of the Total Design Method (TDM), a Traditional Cost-Compensation Model, and Tailored Design*, URL: http://survey.sesrc.wsu.edu/dillman/papers.htm, (last date accessed: May 22, 2005).

Durfee, R.C., Coleman, P.R. (1983). *Population Distribution Analyses for Nuclear Power Plant Siting*. Oak Ridge, TN: Oak Ridge National Laboratory.

Federal Emergency Management Agency (FEMA) (2008). Mapping and Analysis Center, http://www.gismaps.fema.gov, last updated November 4, accessed December 10. Navigating to: http://www.gismaps.fema.gov/2005graphics/storms/Katrina/downloads/NGA_Graphics_%2006–09Sept.hld, causes a zip file to appear that contain Figure 15 under the filename, "Harrison_county_07sep05.pdf".

GISCorps. (2008). Publications. GISCorps: GIS Professionals Volunteering for a Better World, http://www.giscorps.org/index.php?option=com_content&task=view&id=23&Itemid=60; accessed December 11.

Hodgson, M. (2008). Remote Sensing Hazard Guidance System. http://ww2.rshgs.sc.edu/; last updated November 11. Accessed December 11.

Hodgson, M.E., Cutter, S.L. (2001). Mapping and the spatial analysis of hazardscapes. In *American Hazardscapes: The Regionalization of Hazards and Disasters*, S.L. Cutter (ed.), Washington, DC: Joseph Henry Press, pp. 37–60.

Hodgson, M.E., Cova, T.J., Goodchild, M.F. (2002). *Emergency Data Acquisition and Analysis: Short Term Research Priority*. Washington, DC: University Consortium for Geographic Information Science.

Hodgson, M.E., Davis, B.A. (1998). Foreword, Special Remote Sensing, GIS and Hazards, *Photogrammetric Engineering & Remote Sensing* 64(10), 976.

Hodgson, M.E., Davis, B.A., Kotelenska, J. (2005). *State-Level Hazard Offices: Their Spatial Data Needs and Use of Geospatial Technology*, Final Research Report to NASA-Stennis Space Center (University of South Carolina), 71p.

Hodgson, M.E., Kar, B. (2008). Modeling the Potential Swath Coverage of Nadir and Off-Nadir Pointing Remote Sensing Satellite-Sensor Systems, *Cartography and Geographical Information Science* 35(3): 147–156.

Huyck, C.K., Adams, B.J. (2002). Emergency response in the wake of the world trade center attack: the remote sensing perspective, Volume 3, *Engineering and Organizational Issues Related to the World Trade Center Terrorist Attack,* http://mceer.buffalo.edu/publications/sp_pubs/WTCReports/02-SP05-screen.pdf

Inspector General (IG) (2006). US Army Corps of Engineers' "Operation Blue Roof" Project in Response to Hurricane Katrina. US Department of Defense, Report No. D-2007-038; December 22.

Jensen, J.R., Hodgson, M.E. (2006). Remote sensing of natural and man-made hazards and disasters. In *Manual of Remote Sensing*. Bethesda: MD American Society for Photogrammetry and Remote Sensing, pp. 401–429.

Kupfer, J.A., Myers, A.T., McLane, S.E., Melton, G. (2008). Factors associated with forest damage in a South Mississippi landscape following Hurricane Katrina. *Ecosystems* 11:45–60.

Langhelm, R.J., Davis, B.A. (2002). Remote sensing coordination for improved emergency response, *Pecora 15/Land Satellite Information IV/ISPRS Commission I/FIEOS 2002 Conference Proceedings*, November 10th–15th, 2002, Denver, CO, USA, URL: http://www.isprs.org/commission1/proceedings/paper/00083.pdf, (last date accessed: May 22, 2005).

National Research Council (2007a). *National Land Parcel Data: A Vision for the Future*. Committee on Land Parcel Databases. Washington, DC: National Academies Press, 172p.

National Research Council (2007b). *Successful Response Starts with a Map: Improving Geospatial Support for Disaster Management.* Committee on Planning for Catastrophe. Washington, DC: National Academies Press, 184p.

NOAA, Coastal Services Center (2001). *Lessons learned regarding the use of spatial data and Geographic Information Systems (GIS) during Hurricane Floyd*. U.S. National Oceanic and Atmospheric Administration, NOAA/CSC/20119-PUB, Charleston, SC: NOAA Coastal Service Center, 48p.

Parrish, D.R., Breen, J.J., Dornan, S. (2007). *Survey Development Workshop for the Southeast Region Research Initiative (SERRI) Project*. Gulfport, MS: Mississippi State University Coastal Research and Extension Center, 29p.

Ramsey, E.W., Hodgson, M.E., Sapkota, S.K., Laine, S.C., Nelson, G.A., Chappell, D.K. (2001). Forest impact estimated with NOAA AVHRR and Landsat TM data related to a predicted Hurricane Windfield distribution, *International Journal of Remote Sensing* 77(3), 279–292.

Thomas, D.S.K., Cutter, S. L., Hodgson, M., Gutekunst, M., Jones, S. (2003). Use of spatial data and geographic technologies in response to the September 11th terrorist attack on the World Trade Center. In *Beyond September 11th: An Account of Post-Disaster Research*, Publication no 39. University of Colorado, Boulder: NHRAIC, pp. 147–162.

Varstappen, H.Th. (1995). Aerospace technology and natural disaster reduction, *Advanced Space Research* 15(11), 3–15.

Visser, S.J., Dawood, A.S (2004). Real-time natural disasters detection and monitoring from smart Earth observation satellite, *Journal of Aerospace Engineering* 17(1), 10–19.

Wakimoto, R.M., Black, P.G. (1994). Damage survey of Hurricane Andrew and its relationship to the eyewall, *Bulletin of the American Meteorological Society*75(2), 189–200.

Williamson, R.A., Baker, J.C. (2002). Lending a helping hand: using remote sensing to support the response and recovery operations at the World Trade Center, *Photogrammetric Engineering and Remote Sensing* 68(9), 870–875.

Zhang, Y., Kerle, N. (2008). Satellite remote sensing for near-real time data collection, *Geospatial Information Technology for Emergency Response*, ISPRS Book Series, Vol. 6, Zlatanova and Li (eds), London: Taylor & Francis, ISBN978-0-415-42247-5, 382 pp.

Zlatanova, S., Li, J. (2008). *Geospatial Information Technology for Emergency Response*, ISPRS Book Series, Vol. 6, London: Taylor & Francis, ISBN978-0-415-42247-5, 382 pp.

Chapter 17
Investigating Recovery Patterns in Post Disaster Urban Settings: Utilizing Geospatial Technology to Understand Post-Hurricane Katrina Recovery in New Orleans, Louisiana

Steven M. Ward, Michael Leitner, and John Pine

Abstract This chapter seeks to improve upon current disaster research in the discipline of geography by expanding the geographic study of hazards beyond the event and into the recovery process. A review of current disaster based literature in geography illustrates a lack of comprehensive research by geographers in the arena of disaster recovery. It appears as if established researchers in this field are content to focus their efforts on the issues preceding disasters, as well as the immediate response to, and physical results of disaster events. The responsibility of understanding the topic of recovery has thus far been the primary focus of researchers in the fields of social science and public administration. This study will utilize Geographic Information Technology (GIT) to assess the level of recovery, determine the most appropriate scale to study the spatial aspects of recovery, and identify spatial indicators of recovery in New Orleans, Louisiana as of February 2008.

Keywords Disaster recovery · Recovery index · Spatial model · Hazards geography · Program evaluation

17.1 Introduction

In order to improve current disaster research in the discipline of geography, it is necessary to expand upon existing research paradigms in the field. Currently this means extending the geographic study of hazards beyond the event and into the recovery process. The lack of substantial empirical studies of spatial recovery patterns on record means that no established academic backbone or definition for the context of this study exists (Cutter et al. 1996; Reed et al. 2006). This project has attempted to address the lack of research focused on disaster recovery by utilizing geospatial technologies, qualitative analysis, geoprocessing procedures, spatial

S.M. Ward (✉)
Department of Geography and Anthropology, Louisiana State University, Baton Rouge, LA 70803, USA
e-mail: sward2@lsu.edu

P.S. Showalter, Y. Lu (eds.), *Geospatial Techniques in Urban Hazard and Disaster Analysis*, Geotechnologies and the Environment 2, DOI 10.1007/978-90-481-2238-7_17,

modeling, and geostatistics to develop a greater understanding of the geographic variables guiding recovery in a post-disaster urban environment. Using the City of New Orleans, Louisiana as the overall project area, this study attempted to interpolate the recovery fabric of the entire city through the use of traditional and non-traditional indicators of recovery. The purpose of this study was to provide decision makers and planners with a one-stop-shop for assessing the spatial distribution of recovery, and identifying geographic indicators that contribute to improved recovery in post-disaster environments.

In order to keep this study firmly entrenched in geographic concepts and avoid reproducing a social assessment of recovery, social demographics were purposely avoided in the indexing and modeling stages. Rather than utilize social metrics to assess recovery, this research has focused on the relationship between the ability of a community to recover and variations in proximity to social institutions within the built environment. The spatial assessment of recovery in New Orleans has permitted the identification of spatial indicators of recovery, offered insight into the issues associated with scale that are commonly associated with spatially based evaluations, and produced a tool which demonstrates potential for use within a local program evaluation framework. From a broader disaster management perspective, the tools and results of this study have also offered further support to the systems theory approach to disaster research (Cutter 1994; Mileti 1980).

This chapter highlights the initial segment of a study that is anticipated to extend into the spring of 2009. During this timeframe, the authors hope to utilize emerging datasets, multiple iterations of the model, varying statistical techniques, and groundtruthing in order to develop and calibrate an unbiased and transparent methodology of quantifying spatial patterns in recovery and identifying those geographic variations that guide its progress. Due to the difficulties in conducting multivariate analysis with multiple temporal scales, the initial portion of this study highlighted in this chapter has focused on a static measurement of recovery through February of 2008.

17.1.1 Study Area

The City of New Orleans is an ideal candidate for this type of study. The impacts of Hurricane Katrina coupled with the social dynamics and vulnerable geographic setting offer a living laboratory for empirical study. Being more than two years removed from the disaster of Hurricane Katrina, the city of New Orleans has had sufficient time to progress and recover to a quantifiable degree; thus making it an appropriate candidate for a case study (Wilbanks and Kates 1999). The transformations occurring on a daily basis in New Orleans are not biased by the observer or researcher and offer a truly organic view of post disaster recovery. Although, a ten parish region was heavily impacted by this storm, the City of New Orleans was selected as the focal area. The geographic boundaries of this study area are limited to Orleans Parish. The city is bordered by Lake Pontchartrain to the north, Jefferson Parish to the west and southwest, St. Bernard Parish to the east, and Plaquemines

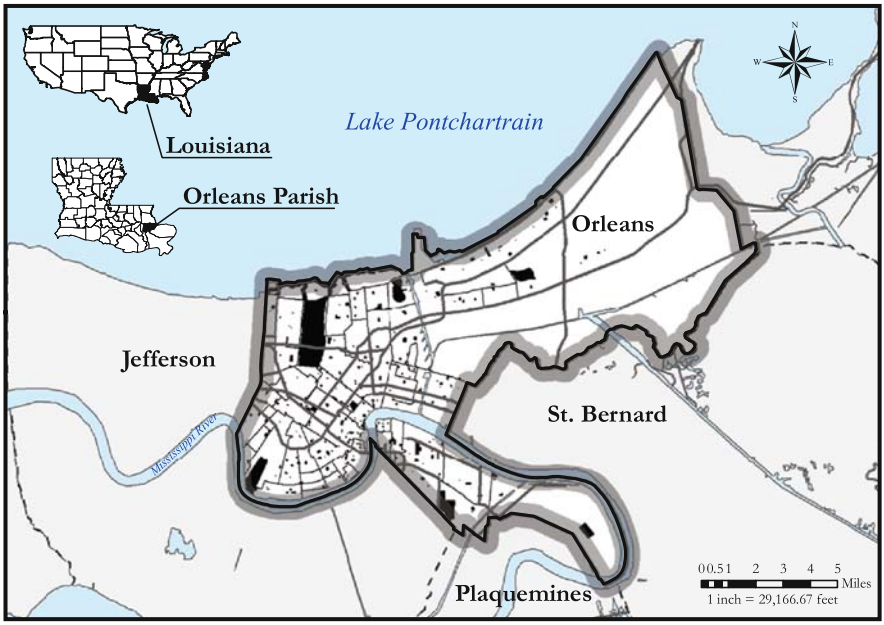

Fig. 17.1 Orleans Parish study area detail

Parish to the south and southeast. Orleans Parish and its surrounding region are depicted in Fig. 17.1.

In order to conduct this research using a case study methodology, sub segments of the city were used to spatially divide recovery rates. The smallest areas employed in this study are neighborhoods. Due to the scale of available input data, as well as the use of the neighborhood boundaries by the Greater New Orleans Community Data Center (GNOCDC) and New Orleans Regional Planning Commission (NORPC), it was determined that neighborhoods represented the most discrete level of measurement practical for this study. Each neighborhood will be considered a case for the purpose of this study. The value of a case study lies in the fact that it seeks to explain the observable fact in question (recovery), within the context of the real world through the use of empirical investigation and multiple sources of supporting evidence (Swaroop 2000). Kates has also suggested that the use of neighborhoods in the study of urban areas is the most appropriate level of measurement due to the diverse characteristics of the human use system seen at the parcel, tract, and block level (Kates 1971). Wu et al. (2002) and Cutter (1996, 2001) also suggest the importance of the neighborhood level of measurement through the application of the idea of Hazards of Place. Focusing the study on areas that are too small will mask overall issues of recovery and emphasize opportunistic recovery patterns that do not sustain themselves for the entire recovery period (Kates 1971). Careful consideration of this issue will help resolve the modifiable areal unit problems which often plague this type of study (Cutter et al. 1996).

The neighborhood boundaries used for this study were defined by the city in the late 1970s and early 1980s. This original dataset has been further refined by the Brookings Institute for data analysis purposes. There are 73 distinct neighborhood areas in the city based on this current dataset (GNOCDC 2007). These boundaries are useful because they are coincident with census tracts throughout the city, making it easier for future studies to identify demographics associated with each area (GNOCDC 2007). For the purpose of this study, two neighborhood areas were dropped from consideration. The north eastern portion of Little Woods and entire Lake Catherine neighborhood units are located at the extreme northeastern end of the parish and represent large areas of wetlands that have never been developed. These areas were largely unpopulated prior to the storm and have little use beyond recreation and outdoor sports. It was determined that leaving these large areas within the study boundary could potentially skew the results of any future analysis due to lack of data, population, or social activity in the region. In addition to removing the undeveloped neighborhoods in the extreme north eastern portions of the parish, this study also excluded all areas representing parks, green spaces, ponds, lakes, canals, and wetlands. It was determined that leaving these areas in the study would also bias the results of any interpolation techniques used to standardize datasets prior to analysis. From this point, the study took on a broader focus and analyzed the same results based on the boundaries of the 18 different zip code areas in the city. While the neighborhoods in this study area were expected to be somewhat homogenous, the boundaries for zip codes in the city appear to be more arbitrary in nature. The final level of measurement used in this study was the Planning Districts boundary file. These boundaries are based on the neighborhood distinctions and represent generalized areas of the city for management purposes. These Planning District boundaries were designated in 1999 and are the same recovery districts being used by the Unified New Orleans Plan group (UNOP) studying and guiding the recovery of the city (UNOP 2007).

17.1.2 Defining the Problem

When viewed through a systems theory approach, a disaster event is in reality a series of complexly intertwined components whose actions at any level have measurable repercussions system-wide (Cutter 1994). In turn, vulnerability can be seen as a component of recovery while the ability to recover can be seen as a component of vulnerability. Therefore, it is not appropriate to measure vulnerability without accounting for a community's ability to recover. Moreover, recent disaster events in the United States have demonstrated an increased need for the study of vulnerability/recovery science due to the insubstantial contributions provided to disaster management by predictive science (Weinberg 1985; Cutter 2001). These current inadequacies point to the distinct need for a recovery index within the sphere of hazards research in geography.

When assessing the recovery of a particular region after a disaster event, one must look to various qualitative and quantitative indicators in order to evaluate the level of

improvement which has been achieved. The indicators in this study were selected in order to assess recovery of different portions of New Orleans, as well as determine whether discrete vagaries in spatial settings and vulnerabilities of these devastated communities have any influence on their ability to recover. These spatial variants or spatial indicators will be helpful in reducing the weight placed on traditional social indicators in future recovery studies, offering a more comprehensive and less biased approach to post disaster management. With this being said, it was important that this tool be developed as a dynamic instrument that could be altered and amended based on the temporal and physical context of its application.

17.1.2.1 Parameters

The general indicator groups utilized in this study have been based on those outlined by the United Nations (UN) in the 2005 Tsunami Recovery project. The categories used by the UN to assess recovery in the countries affected by the tsunami were designed to be used from a regional perspective and include; shelter, finance, infrastructure, health, education, and livelihoods (UN 2005). While these basic categories are too general for direct application to this particular study, they were used as a guide for the development of indicator categories more appropriate for a study at a finer resolution. The UN study also offers strong support to the use of spatial datasets and indicates the importance of geography in the recovery process (UN 2005). A wealth of hazards literature has focused on the recovery after the 1995 earthquake in Kobe, Japan. Recovery studies in this area have utilized a more detailed and dynamic set of indicators in order to assess recovery. These include land use planning, social support networks, housing, physical and mental health, economic and financial situations, government assistance policy, and social infrastructure/preparedness (Takeda et al. 2003).

Importantly, none of the recovery studies referenced in the development of this index have focused on a direct measure of population as an indicator of recovery. To simplify the idea of recovery, one may be inclined to simply rely on the measure of change in population from a pre-disaster environment to the post-disaster environment. Due to concerns expressed by the NORPC and GNOCDC, over the soundness of early population estimates, as well as data availability, it was determined that this model would maintain integrity by not using population as a direct measure of recovery. In addition to this, work by Takeda et al. (2003) notes that population alone cannot be relied upon as a sound metric for recovery. Despite the return of a significant population to Kobe, Japan after the 1995 earthquake, "life recovery" has not been fulfilled (Takeda et al. 2003).

In order to organize the parameters for this study into logical groups, a modified principal components analysis was employed through the framework of the Land Use Conflict Identification Strategy (LUCIS) developed by Carr and Zwick (2007). The LUCIS model offers a proven data organization framework for application within this model. The use of utility assignments and organized grouping of data in the LUCIS model were uncomplicated to apply to the development of the Spatial Recovery Index for this study. Guided by empirical analysis and the framework set

forth in literature, the parameters incorporated into this study represent social institutions within the built environment which lend themselves to the recovery of social networks across the city as well as spatial vulnerability metrics which have recovery implications. These parameters include churches, childcare, healthcare, education facilities, infrastructure, economic activity indicators, flood depth, elevation, proximity to transportation/contraflow corridors, municipal services, recreation activity, and proximity to flood control structures.

17.2 Methodology

This study utilized Geographic Information Systems (GIS) technology and qualitative analysis to determine if the geographic characteristics of the City of New Orleans have had an influence on the rate, level, and distribution of recovery (Scott and Cutter 1996; McCarthy et al. 2006). The GIS based Spatial Recovery Index (SRI) developed by this study looks beyond the literature based on social vulnerability and assists in the development of a methodology to study geographic patterns of recovery (Scott and Cutter 1996). Quantitative assessment has long been a preferred choice of disaster geographers attempting to assess risk and vulnerability, thus it makes sense to apply this technique to measuring recovery (Weinberg 1985; Freudenburg 1988). It is important that the model developed for this analysis and datasets employed are flexible (Carreno et al. 2007). This type of spatial modeling requires large sums of diverse datasets to be standardized and digested in a relatively short period of time. The multi-layered data management techniques inherent in the typical functions of GIS packages meant that a spatial model was in fact the most appropriate approach to employ when considering the scale and focus of this study (Lloyd 2007). Utilizing this index will allow public officials to make informed decisions about funding of recovery projects and resource allocation, while also acting as a complimentary tool to other social vulnerability assessments.

The model developed for this study utilized a progressive raster based approach to integrate all of the variables into a single coded index value. Utilizing a simple index to visualize and quantify the final outcome of this model was important for interpretations and analysis by independent parties. The progressive raster based process starts with a few base data elements and incrementally adds data layers to the model. As these data sets were added to the model their categorical values were recoded to represent levels of measurement on a recovery scale. This recoding process is precarious and presents one of the most difficult steps in the entire development process. The challenge is to objectively standardize all of the parametric variables into a single quantitative level of measurement in a transparent and justifiable manner.

The framework of the model was based on the LUCIS model developed by Carr and Zwick (2007) to assist in the identification of land-use conflicts, and was developed within the modeling environment of Environmental Systems Research Institutes (ESRI®) ArcGIS 9.2® Platform. The model developing tool within ArcGIS® was used to document the generic backbone of the model prior to integrating any

data layers. This backbone provided an abridged schematic of the model which visualized the process steps into a logical organizational structure. Based on the LUCIS data management schema, the data used in this study were generalized into Single Utility Assignments (SUAs), Multiple Utility Assignments (MUAs), and Complex Multiple Utility Assignments (CMUAs) (Carr and Zwick 2007). Each SUA represented a raw dataset such as hospital locations, health clinics, and elder care facilities. These SUAs were then grouped into a general category and combined through a raster calculation process into a MUA such as Health. All of the MUAs can then be combined into a single CMUA to represent Recovery Indicators for the City of New Orleans. The ranking and calculation processes are discussed in detail in subsequent portions of the methodology section. Utilizing this stepwise raster based approach to develop the final spatial index was important in the analysis of the results. By organizing each input variable into separate SUAs, MUAs, and CMUAs, it was easy to measure the level of influence each component had on the final outcome of the index through the comparison and analysis of standardized raster files.

The model was organized into two main CMUA components that fed into the final Spatial Recovery Index CMUA. The first component was a measure of Recovery Indicators (RI) that included MUAs for Health (hospitals, health clinics, elder care facilities), Education (schools, after school programs, and libraries), Economy (banks, gas stations, and grocery stores), Municipal Services (fire, police, emergency medical services, and post offices), and Social Activity (churches, child care facilities, and recreation facilities). The second CMUA was a measure of Spatial Vulnerability Indicators (VI) which contribute to recovery. Spatial Vulnerability can also be considered to be a measure of the ability of an area to recover based on measurements of proximity and level of damage sustained during the storm. This CMUA included MUAs representing Katrina Flood Depth (flood depth grid and flood mask), Geographic/Topographic Variables (LiDAR elevations, and navigable water), Flood Control Variables (levees, pump stations, and canals), and Transportation Variables (highways, interstates, evacuations routes, contra-flow corridors). It is important to include these spatial vulnerability metrics in the assessment of recovery as they are important in dictating the ability of a particular area to recover.

Due to the fact that this is the first segment of a long term study with subsequent data sets and input variables yet to be determined and acquired, each input into this system was assigned an equal weight. The raster grid utilized in this study was based on 5 meter grid cells coincident with those from the Light Detection and Ranging (LiDAR) Digital Elevation Models (DEM) for the city. This grid was selected because it was the same one utilized after the storm in raster data depicting elevation, flood depth, flooded areas, and flood duration. Each of the original vector based SUA datasets was converted to raster format using a Euclidean Distance interpolation technique. Based on the theory of distance decay this study assumed that the contribution of a particular facility or structure to overall recovery declined as the distance from it increased due to the increased likelihood of an individual using a facility in close proximity. Past studies have supported this validation by looking at the relationships between homestead location and visits to hospitals, clinics and other service facilities based on distance (Muller et al. 1998; Lin 2002). The

selection of Euclidean distance over Manhattan (rectilinear) measurements is due to the difficulty in obtaining detailed and accurate network data for the City of New Orleans. Research has indicated that Euclidean measurements commonly offer distances in the order of 20% less than real network distances, making them an adequate indexing tool based on the scale of the input data (Lin 2002; Francis et al. 1992). The Euclidean distances are classified into five categories using a natural break classification method. This index ranged from 1 to 5 and represented, low, medium-low, medium, medium-high, and high levels of recovery suitability. Those input variables that were already in raster format (i.e. flood depth and elevation) were reclassified to created recovery suitability index using the same classification method. For example, areas with the highest elevation were assigned a value of five, while those with the lowest elevation were assigned a value of one. The location where a facility or institute is operating at the time of this study is assigned a value of 5 for recovery suitability for the specific category. As distance from the facility increases, a place receives decreasing values for its recovery suitability index for the same category. Figure 17.2 represents the data for schools (Fig. 17.2a) and the reclassified raster data ready for input into the model (Fig. 17.2b).

Once calculted, each of these CMUAs was input into the final model step in order to produce a raster file with values representing the SRI. This final SRI provides a visual representation of the distribution of recovery across the entire city based on traditional indicators of recovery (RI) combined with spatial vulnerability (VI). While it is not expected that the results of these CMUAs will accurately depict real world conditions within every discrete cell in the final raster output, it is believed that each of these CMUAs will provide planners with an enhanced perspective of recovery throughout the city. Furthermore, the CMUAs will also allow planners to identify those areas of the city that have yielded unconventional results, and in turn, require more in-depth qualitative analysis to understand the dynamics driving recovery.

In order to advance the usefulness of this study beyond ESDA and visual analysis, spatial analysis techniques were applied to describe the spatial distribution of the recovery from Katrina in the study area. Due to the scale of this study, local statistics were a more appropriate choice than global statistics owing to the latter's tendency to mask subtle spatial relationships and patterns (Fotheringham et al. 2000). The study began with a generalized assessment of the significance of recovery index patterns through autocorrelation and hot spot analysis. In accordance with this assessment, Local Moran's I, and $G_i$were calculated to identify the hot spots/cold spots of the RI, VI, and SRI. Moreover, Geographically Weighted Regression (GWR) analyses were conducted on the RI, VI, and SRI results to explore the relationship between the input variables and the indices. While it is common in more generalized studies to utilize Spearman's Rank Correlation Coefficient to assess the relationship between variables and results when datasets are not assumed to be linear and are measured on an ordinal scale, this approach fails to take into account the spatial vagaries of these relationships. Utilizing GWR is more appropriate than traditional Global Regression analyses as it has the ability to account for heterogeneous relationships between variables and results as they are distributed across the entire city

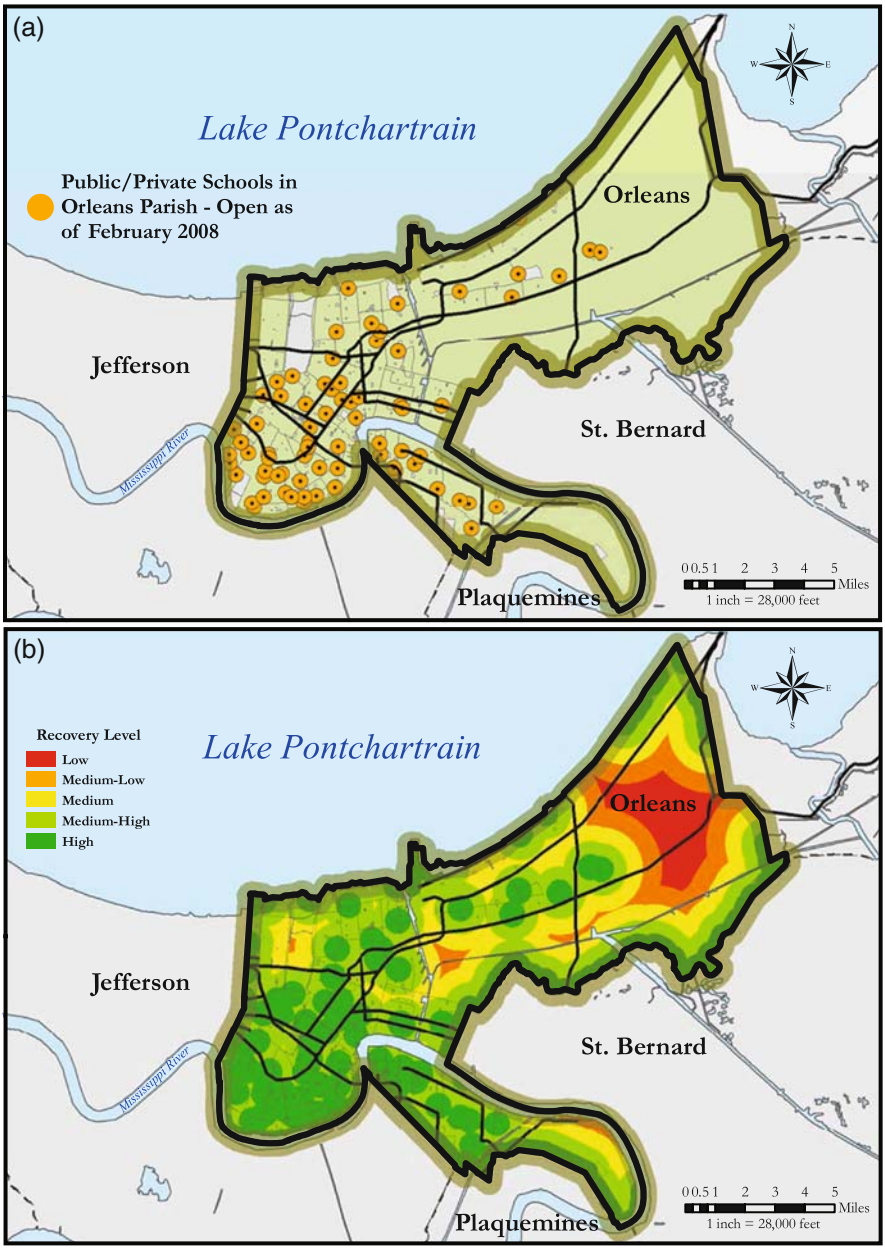

Fig. 17.2 Orleans Parish schools open as of February 2008 – represented as point data (**a**) and interpolated raster (**b**)

(Fotheringham et al. 2002). In addition, the use of GWR permits easy visualization of the regression coefficients. The use of GWR was vital to determine the variance in recovery explained by the model (coefficient of determination) as well as the relative influence each parameter has on the final SRI value. Although each input variable is receiving a rank based on Euclidean Distance and natural breaks in the data, there is still subjectivity in this approach and as a result, the index can not be assumed to be an interval level of measurement.

To facilitate increasing the value and interpretability of the model, a zonal analysis of the study area at the neighborhood, zip code, and planning district levels was conducted. This portion of the study collapsed the detail of the initial model results into statistics that were tied to specific study areas. The new output correlated the statistics of the model input and results to each study area and identified the diversity of limiting factors, median and mean of the suitability index, as well as a number of other exploratory aspects of the data. These results were visualized in cartographic and tabular format for ease of interpretation. The final results of the zonal analyses can be used to assess the most appropriate scale at which recovery should be studied. It was important that the results of this study were produced and analyzed at the same scale management decisions are being made (Carreno et al. 2007; Wilbanks and Kates 1999; Clark et al. 2000; Cash and Moser 2000). Analyzing this data at different geographic divisions also helped determine if recovery trends appear to project themselves on surrounding areas (Cutter 2001).

17.3 Results

Analysis of the Recovery Indicators portion of the model indicates that the highest level of recovery in the city has been achieved in the areas surrounding the Broadmoor and Audubon neighborhoods in a concentric pattern. These neighborhoods are located in the south central portion of the city and experienced varied levels of flooding. Broadmoor sits at a considerably lower elevation than Audubon and experienced low to moderate flood depths while Audubon increases in elevation as it approaches the river to the south. As a result it only experienced flooding on the extreme northern end of the neighborhood. The recovery of these areas may result from a combination of higher elevation, low flood levels, and proximity to the increased financial stability of the Central Business District and French Quarter. These results are consistent with the Spatial Vulnerability outputs for the most extreme portions of the southwestern part of the parish but diverge from the vulnerability data to the north central and southeastern portions of the parish. The lowest level of recovery appears to be consistent with a highly vulnerable swath that runs from the extreme northeastern portion of the parish just south of the lake to the western border. Some discrepancy is seen in this pattern as you approach the Lake View and Fillmore areas in the extreme northwestern end of the parish. These neighborhoods are highly vulnerable according to the VI analysis but are experiencing moderate to high levels of recovery. Some might argue that the high level of damage in these areas coupled with the higher number of insured homeowners

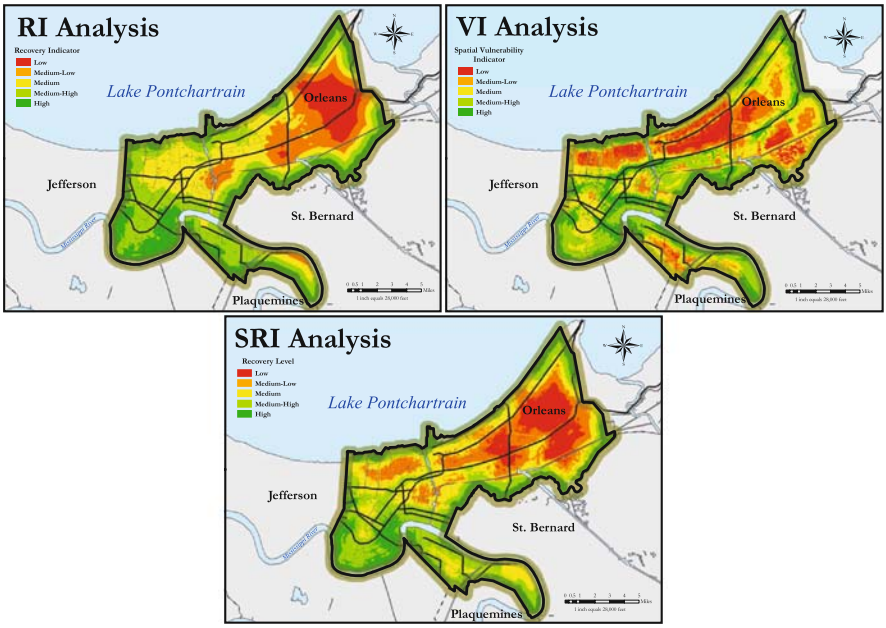

Fig. 17.3 Recovery Indicator (RI), Spatial Vulnerability Indicator (VI), and Spatial Recovery Index (SRI) analysis results

is offering a greater opportunity for recovery to flourish. Further analysis will have to be conducted in order to support this argument. In general there seems to be an inverse consistency between the RI and VI outputs, while the combined SRI output depicts a city with a large area undergoing moderate to slow recovery interrupted by isolated areas of high and low recovery. Figure 17.3 shows the results of all three CMUAs visualized using a red to green color ramp representing low to high levels of recovery or recovery suitability, respectively.

17.3.1 Recovery

A more detailed analysis of the results produced constructive conclusions. Even with each variable being considered equally during the initial study, the statistical analysis of the RI, VI, and SRI CMUAs still provided significant results. The Local Moran's I (SPAC) calculated for the spatial recovery output variable indicated highly significant clustering of data at a 95% confidence interval with a Moran's I Index value of 0.28 and Z Score of 16.9. Furthermore, the results of the Getis-Ord General G High/Low Cluster analysis indicate moderate to highly significant hot-spots or clustering of high spatial recovery values across the city with a General G Index of 0.000181 and Z Score of 2.13 at the 95% confidence interval. Figure 17.4 a demonstrates the recovery pattern associated with the results of the P-Values from the hot spot analysis. This figure demonstrates a significant pattern associated with the

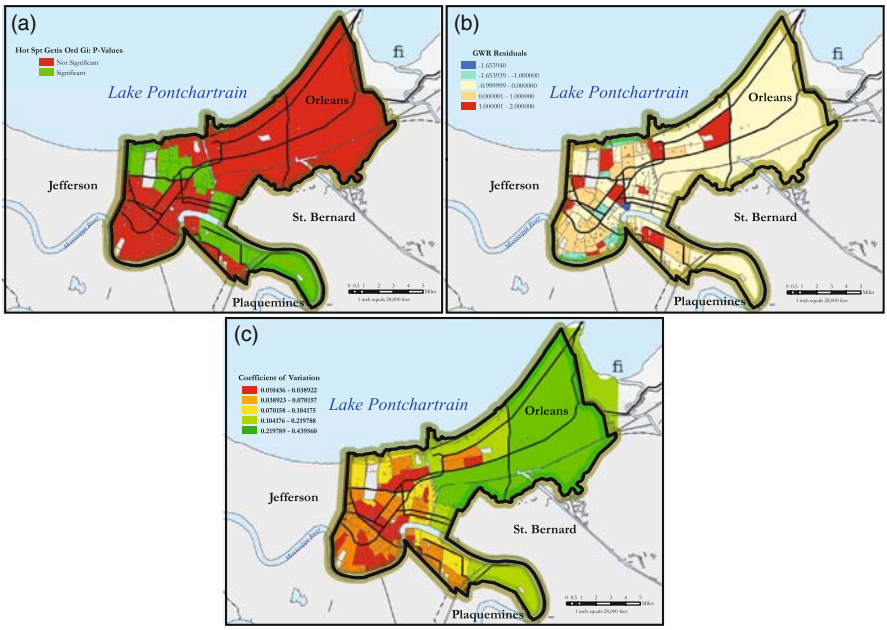

Fig. 17.4 Results of hot spot analysis (**a**), GWR Analysis (**b**), Č Zonal analysis (**c**)

recovery indicator results extending from the extreme northwestern portion of the parish through the southeastern edge of the parish. These results appear to suggest that there is an uneven distribution of recovery occurring across the city. While not groundbreaking in nature, these results provide an easily interpreted visual representation of recovery throughout the city. This visualization also presents planners and government officials with a new instrument for identifying those areas that do not follow recovery projections or trends. This ability will, in turn, justify the implementation of comprehensive studies of these locales in order to identify those factors driving recovery in these discrete settings.

In order to determine the salient factors and spatial variation contributing to this heterogeneous distribution of recovery, a GWR analysis was conducted. Initial results of this analysis are limited in value due to an apparent over estimation of the significance by both the global and local models. There is some indication of low to moderate significance in spatial variation of recovery across the city, as well as evidence of limited influence on the model by a number of the MUAs. The GWR results also indicate that the level of variance in recovery explained by the local GWR model diverges only slightly from the global model, with the coefficients of determination falling in the 99% range for each. This finding could be attributed to the limited number of input variables being considered at this time. Despite this slight discrepancy, the decrease in the Akaike Information Criterion (AKC) from 633.31 in the Global Model to 631.9 in the local GWR, in spite of the varied degrees of freedom, suggests that the local GWR analysis offers an improvement over the

results of the global model. The Analysis of Variance (ANOVA) results from the same procedure coincide with these conclusions, offering an F-Value from the GWR Residuals of 2.314, demonstrating only slightly significant improvement from the global model. Figure 17.4b visualizes the spatial distribution of the standardized residuals from the GWR analysis.

Both the global and local models resulted in high coefficients of determination (99% range), suggesting that both approaches offer a significant explanation of the variance in recovery across the city. A coefficient of determination this high was unexpected and may also be an indicator of the need for more data in the model or the result of issues associated with multicollinearity. It is believed that this high level of inference will be reduced as more consequential datasets become available in the future. In addition, spatial indicators began to emerge from the GWR results. The Monte Carlo significance test was utilized to assess the significance in spatial variation associated with each input variable. This portion of the GWR analysis indicates proximity to education facilities, social institutions, and municipal structures as primary indicators of recovery. The P-Values associated with each of these variables were 0.87, 0.62, and 0.75 correspondingly. Additionally, proximity to education facilities and social institutions were identified as significant contributors to spatial recovery values by a linear regression analysis. These factors had R-Squared values of 0.88 and 0.86 respectively when using the SRI values as the dependent variable. No single variable positively correlated with recovery stands out significantly above the rest, but the results of this initial study do suggest that the availability of education facilities and social institutions lend themselves to increased recovery in post disaster situations. This result may indicate a need to include more variables in the model or investigate multicollinearity effects. At this stage of research, the variance in recovery associated with other factors such as economic, municipal, and health services appear to be occurring more by chance. This trend seems to be indifferent to the level of damage or depth of flooding during the storm, though an explicit analysis to determine this relationship was not conducted. Consequently, these results also suggest that the socio-economic status and race of an area prior to a disaster event may have less impact on that area's ability to recover than previously thought. This impression is supported by the similar level of overall recovery seen in the Lakeview area when compared to areas of lower income and greater racial variation (e.g., the Desire and Pines Village areas near the eastern edge of the parish).

17.3.2 Scale

In order to assess the influence of scale on the interpretation of recovery throughout the city, a zonal analysis was conducted. The first portion of the zonal analysis of this study was based on the neighborhood level. Due to a lack of data collected at the census tract and block level, this study did not subdivide the city at a smaller scale. Future research will seek to address the best way to approach this task. By aggregating the data from the SRI CMUA to the neighborhood level, one gets a better sense of the broader geographic influences on recovery than the previous discussion

focused on individual parameters. While not as detailed as the GWR results in terms of identifying primary variables contributing to recovery, the results of the zonal analysis do demonstrate the overall trends in recovery seen throughout the city. The coefficient of variation associated with the zonal analysis at the neighborhood levels is illustrated in Fig. 17.4c. This map demonstrates a high level of variance in results for the eastern side of the parish while little variation is seen in those areas demonstrating high levels of recovery in the central and southwestern portions of the parish. This analysis suggests that recovery can be better understood when interpreted over a larger area. The ability to compare generalized recovery estimates from neighborhood to neighborhood over a larger region offers city planners a generalized view spatial of variations in recovery across the city. In turn, this can lead to valuable understanding of the scale at which management decisions should be made throughout the recovery process. This trend also supports the idea that there may be subtle issues associated with multicollinearity of parameters being used in this study. Viewing the results of this study at the neighborhood level reveals a direct relationship between high level of recovery and proximity to undisturbed/flooded parishes and proximity to the river levees. Proximity to internal levees subdividing the city appears to have limited influence on recovery patterns, regardless of their integrity throughout the storm event. As the zonal analysis is conducted with larger and more stochastic delineations at the zip code and planning district level, one begins to see an overgeneralization of the recovery process. Trends seen at the five meter grid and neighborhood level appear to be lost at these scales. In general, overall recovery of the city appears to be at a much higher level when viewed at these scales. This variation in results further demonstrates the problems associated with artificial masking of data through variations in scale, in addition to the importance of conducting these studies at the local level. A SPAC analysis of all three zone studies demonstrates moderately significant clustering at the neighborhood level with low significance at the zip code and planning district level. The data at these scales are too homogeneous in nature to draw any significant conclusions. Further analysis will seek to assess the progression of recovery at varying scales, most importantly the delineations of leveed areas utilized by the United States Army Corps of Engineers (USACE) and Federal Emergency Management Agency (FEMA) to conduct hydrologic studies and manage policy development in New Orleans.

17.3.3 Sensitivity

The results of this study offer support to the hypothesized program evaluation benefits of a Spatial Recovery Index. The results of the Spatial Recovery Index confirm mild significance in the variability of the recovery process and spatial vulnerability at the neighborhood level while also offering insight into those factors which influence recovery rates as well as the ability of an area to recover. These results would certainly lend value to a program evaluation as well as program development if used appropriately. These are not stand alone decision-making tools and should be used in conjunction with qualitative assessments and subjective evidence. Nevertheless,

this study offers planners and policy makers the ability to see quantitative measures of recovery at the same scales that management decisions are being made. By using a zonal analysis to aggregate the data based on any jurisdictional delineation throughout the city, planners have the ability to make more informed decisions about resource allocation, mitigations measures, and policy decisions. Of equal importance may also be the application of this type of analysis to pre-disaster planning and vulnerability analysis. Simple modification of this analysis would allow for a proactive assessment of spatial vulnerability and recovery potential distributed across at-risk populations. The ability to quantify the recovery potential of a discrete area has indisputable value in the planning and resource allocation stages of local emergency operation and mitigation centers.

17.4 Conclusion and Recommendations

In general the model development and geoprocessing procedures incorporated in this study were successful and required little editing given the user friendly work environment provided by ESRI's® model builder application. One issue that will have to be addressed in future studies is associated with edge effects. The city of New Orleans spans multiple parishes and those individuals living on the extreme edge of Orleans Parish undoubtedly utilize facilities and infrastructure located in neighboring parishes. In order to account for these, it may be necessary to buffer the study area and include data within a larger region during the SUA, MUA, and CMUA development phase. The analyses could then be conducted on just Orleans Parish to facilitate accounting for these neighboring influences. Simple visual ESDA of the results of the RI CMUA, VI CMUA, and SRI CMUA demonstrate consistency between model results and did not draw any attention due to overly skewed data or potential outliers. It is projected that the general distribution of recovery throughout the city will see variation with the incorporation of future datasets.

The GNOCDC has indicated that the United State Postal Service (USPS) activity data may be the best indicator of long term population available in the city of New Orleans. Once available, this data will be used to assess the quality of the model results as well as act as a baseline for model calibration. It is believed that a population approaching pre-Katrina numbers will not be reached in New Orleans in the near future. As a result, it is not appropriate to utilize pre-storm population numbers as a measure of the accuracy of this model in assessing recovery.

Given the multi-layered nature of most spatial modeling techniques, it has been reasonable to make use of GIS technology to aid in the development of a recovery index for the City of New Orleans (O'Brien et al. 2004; ESRI 2006). Utilizing a modeling based approach to this study has allowed for easy adaptability and assessment of recovery in Orleans Parish, regardless of the heterogeneity and non-stationarity of the recovery process as it is dispersed throughout the city (Lloyd 2007). While many researchers will point out that quantitatively based indices suffer from a variety of fallacies and are victims of poor science and subjectivity, most literature suggests that this approach is still a relevant and acceptable spatial analysis

technique (Wilson and Crouch 1987; Freudenburg 1988; Weinberg 1985). Recovery datasets generally have important temporal and spatial dimensions. This means that the collection time and scale are very important in assessing data suitability. This limiting factor means that a GIS based approach is limited to the obtainable data rather than the best data (Cutter 2001). "Fuzzy Sets" should be coupled with change detection in order to justify the quantitative assessment of qualitative parameters (Carreno et al. 2007).

Recovery from hazards is not only social in nature. GIS and geotechnologies have opened the door to a new chapter in hazards geography that will unquestionably improve upon existing theories and understanding of the spatial aspects of hazards and disasters. This type of study can only improve as data are collected at a finer resolution, in a timelier manner, and more comprehensively. Orleans Parish has not only been guided by the traditional social and economic indicators long thought of as the main contributors to recovery. The results of the early portions of this study appear to suggest that geography does in fact play a role in post disaster recovery. Furthermore, it is important to consider these spatial factors in future management practices and policy decisions as this tool offers leaders another instrument to assess the success of recovery programs. Currently, the recovery program in New Orleans is not working homogeneously. This lack of homogeneity indicates that management decisions regarding recovery in the city are not being addressed at the proper scale. Proactive application and exposure to the results of this type of study may help guide decision makers in a different direction. Every future recovery initiative is a unique entity that will reveal new issues and trends that were not previously predicted. This study demonstrates that allocation of resources and management focus in post-disaster urban settings should operate within an integrated context of spatial and social variables in order to achieve optimum understanding of the erratic nature of the recovery process.

Abbreviations

AKC	–	Akaike Information Criterion
ANOVA	–	Analysis of Variance
CMUA	–	Complex Multiple Utility Assignments
DEM	–	Digital Elevation Model
ESDA	–	Exploratory Spatial Data Analysis
ESRI®	–	Environmental Systems Research Institute
FEMA	–	Federal Emergency Management Agency
GIS	–	Geographic Information System
GIT	–	Geographic Information Technology
GNOCDC	–	Greater New Orleans Community Data Center
GWR	–	Geographically Weighted Regression
LiDAR	–	Light Detection and Ranging
LUCIS	–	Land Use Conflict Identification Strategy

MOGA – Multi-Objective Genetic Algorithm
MUA – Multiple Utility Assignments
NORPC – New Orleans Regional Planning Commission
RI – Recovery Indicators
SPAC – Spatial Autocorrelation
SRI – Spatial Recovery Index
SUA – Single Utility Assignments
UNOP – Unified New Orleans Plan
USACE – United States Army Corps of Engineers
USPS – United State Postal Service
VI – Vulnerability Indicators

References

Carr, M.H., and Zwick, P.D. (2007). *Smart Land-Use Analysis: The LUCIS Model*. Redlands, CA: ESRI Press, 1–100.

Carreno, M.L., Cardona, O.D., and Barbat, A.H. (2007). A Disaster Risk Management Performance Index. *Natural Hazards*, 41(1), 1–20.

Cash, D., and Moser, S.C. (2000). Linking Global and Local Scales: Designing Dynamic Assessment and Management Processes. *Global Environmental Change*, 10, 109–120.

Clark, W., Jaeger, J., Corell, R.W., Kasperson, R.F., McCarthy, J.J., et al. (2000). Assessing Vulnerability to Global Environmental Risks. *Discussion Paper 2000–2012, Environmental Natural Resource Program,*Cambridge, MA: Belfer Center for Science and International Affairs, Kennedy School of Government, Harvard University.

Cutter, S. (1996). Vulnerability to Environmental Hazards. *Progress in Human Geography*, 20, 529–539.

Cutter, S. ed. (1994). *Environmental Risks and Hazards*, Upper Saddle River. NJ: Prentice-Hall Inc.

Cutter, S. ed. (2001). *American Hazardscapes*. Washington, DC: Joseph Henry Press.

Cutter, S., Holm, D., and Clark, L. (1996). The Role of Geographic Scale in Monitoring Environmental Justice. *Risk Analysis*, 16(4), 517–526.

ESRI. (2006). GIS and Emergency Management in Indian Ocean Earthquake/Tsunami Disaster. *ESRI White Paper*, 1–40.

Fotheringham, A.S., Bunsdon, C., and Charlton, M. (2000). *Quantitative Geography: Perspectives on Spatial Data Analysis*. London: Sage Publications Ltd.

Fotheringham, A.S., Chris, B., and Martin, C. (2002). *Geographically Weighted Regression: The Analysis of Spatially Varying Relationships*. Chichester, England: John Wiley and Sons, Ltd., 1–64, 83–102.

Francis, R.L., McGinnis, L.F., and White, J.A. (1992). *Facility Layout and Location: An Analytical Approach*. Cliffs, NJ: Prentice Hall Englewood.

Freudenburg, W.R. (1988). Perceived Risk, Real Risk: Social Science and the Art of Probabilistic Risk Assessment. *Environmental Risks and Hazards,* Ed. Cutter, S.L., Upper Saddle River, NJ: Prentice-Hall Inc., 1994, 244–256.

Greater New Orleans Community Data Center (GNOCDC) Website. 2007. October 21, 2007. http://www.gnocdc.org/. Accessed August 7, 2008.

Kates, R.W. (1971). Natural Hazard in Human Ecological Perspective Hypotheses and Models. *Environmental Risks and Hazards,* Ed. Cutter, S.L., Upper Saddle River, NJ: Prentice-Hall Inc., 1994, 78–93.

Lin, G. (2002) *A GIS Method to Assess Distance Effects on Hospitalizations*. Research Paper #2002–15. West Virginia University Regional Research Institute 2002 Working Papers. http://www.rri.wvu.edu/pdffiles/linwp2002-15.pdf. Accessed August 7, 2008.

Lloyd, C.D. (2007). *Local Models for Spatial Analysis*. Boca Raton, FL: CRC Press, 1–26, 61–86, 195–198.

McCarthy, K., Peterson, D.J., Sastry, N., and Pollard, M. (2006). The Repopulation of New Orleans after Hurricane Katrina. RAND Corporation. ISBN:0-8339-3940-7.

Mileti, D.S. (1980). Human Adjustment to the Risk of Environmental Extremes. *Environmental Risks and Hazards*, Ed. Cutter, S.L., Upper Saddle River, NJ: Prentice-Hall Inc., 1994, 178–193.

Muller, I., Smith, T., Mellor, S., Rare, L., and Genton, B. (1998). The Effect of Distance from Home on Attendance at a Small Rural Health Centre in Papua New Guinea. *International Journal of Epidemiology*, 27, 878–884.

O'Brien, K., Leichenko, R., Kelker, U., Venema, H., Aandahl, G., et al. (2004). Mapping Vulnerability to Multiple Stressors: Climate Change and Globalization in India. *Global Environmental Change*, 14, 303–313.

Reed, D., Preuss, J., and Park, J. (2006). Assessing Vulnerability of Social Environmental Systems. *Annual Review of Environmental Resources*, 31, 365–394.

Scott, M., and Cutter, S. (1996). GIS and Environmental Equity: An Analysis of the Assumptions, National Center for Geographic Information and Analysis (NCGIA). Position paper, Initiative 1–19.

Swaroop, D.R. (2000). Factors Influencing the Incorporation of Hazard Mitigation During Recovery from Disasters. *Natural Hazards*, 22(2), 185–201.

Takeda, J., Tamura, K., and Tatsuki, S. (2003). Life Recovery of 1995 Kobe Earthquake Survivors in Nishinomiya City: A Total-Quality-Management-Based Assessment of Disadvantaged Populations. *Natural Hazards*, 29, 565–583.

Unified New Orleans Plan (UNOP) Website. (2007). October 21, 2007. http://unifiedneworleansplan.com/home3/. Accessed August 7 2008.

United Nations (UN) (2005). *Tsunami Recovery Status Report Summary*, Document prepared for the United Nations Information Management Service and Reconstruction Agency for Aceh and Nias. October 21, 2007. http://www.humanitarianinfo.org/sumatra/reference/indicators/docs/UNIMS%20Recovery%20Indicators%20Summary_20051214.pdf. Accessed August 7 2008.

Weinberg, A.M. (1985). Science and Its Limits: The Regulators Dilemma. *Environmental Risks and Hazards*, Ed. Cutter, S.L., Upper Saddle River, NJ: Prentice-Hall Inc., 1994, 257–268.

Wilbanks, T.J., and Kates, R.W. (1999). Global Change in Local Places: How Scale Matters. *Climate Change*, 43, 601–628.

Wilson, R., and Crouch, E.A.C. (1987). Risk Assessment and Comparisons: An Introduction. *Environmental Risks and Hazards*, Ed. Cutter, S.L., Upper Saddle River, NJ: Prentice-Hall Inc., 1994, 236–243.

Wu, S.Y., Yarnal, B., and Fisher, A. (2002). Vulnerability of Coastal Communities to Sea-Level Rise: A Case Study of Cape May County. New Jersey, USA, *Climate Research*, 22, 255–270.

Chapter 18
Space and Time Changes in Neighborhood Recovery After a Disaster Using a Spatial Video Acquisition System

Andrew J. Curtis, Jacqueline W. Mills, Timothy McCarthy, A. Stewart Fotheringham, and William F. Fagan

Abstract This chapter uses the case of Hurricane Katrina to show how an advance in geospatial data collection initially used to improve damage assessment can also provide utility throughout other phases of the emergency management cycle. A spatial video acquisition system (SVAS), employed as a disaster assessment tool because of Katrina-related response deficiencies, is described in terms of its genesis, and its application in the ongoing recovery phase of the disaster. The SVAS is discussed conceptually as a new approach for capturing the spatially and temporally dynamic urban environments of a post-disaster neighborhood; for example, collecting data that can be used as a proxy for disaster-related health vulnerability, especially psychopathology. The ability to collect such a dynamic data set has previously been lacking in post-disaster health research.

Keywords neighborhood recovery · spatial video · GIS · post–disaster health · health · vulnerability

18.1 Introduction

Geospatial support is important in any disaster situation, whether terrorist attack (e.g., the World Trade Center in 2001), or a major hurricane such as Katrina (Curtis et al. 2006a; Huyck et al. 2003; Mills 2008). No matter how much preplanning occurs, Geographic Information System (GIS) users must be flexible and able to engage in ingenuity in order to adapt to the fluid nature of emergency response using available data and data collection strategies. Extreme events may occur at a scale that exceeds existing plans, requiring adaptations and modifications while executing a response (Curtis et al. 2006a, b). Given this need for flexibility, it is not surprising that there are advances in geospatial technologies involving data

A.J. Curtis (✉)
Department of Geography, University of Southern California, Los Angeles, CA 90089-0255, USA
e-mail: ajcurtis@usc.edu

P.S. Showalter, Y. Lu (eds.), *Geospatial Techniques in Urban Hazard and Disaster Analysis*, Geotechnologies and the Environment 2, DOI 10.1007/978-90-481-2238-7_18,

collection and dissemination centered on response operations, particularly search and rescue (e.g., use of Unmanned Aerial Vehicles). The protracted recovery period from Katrina along the Gulf Coast, especially in Orleans Parish, has resulted in the need for this same type of geospatial ingenuity to extend into the recovery phase. This chapter focuses on one such geospatial advance, a spatial video acquisition system (SVAS), which has been successfully employed to gauge the status of neighborhood-level recovery and to link these data to the issue of post-disaster health vulnerability.

18.2 Developing the Spatial Video Acquisition System

Although remotely sensed data will always be important for post-disaster assessment, the costs involved, as well as the distance of the sensor from its subject limits neighborhood-level data collection. Conventional remotely sensed image data are generally acquired by satellite or airborne platforms looking down at the area of interest. These sensor platforms image large areas at resolutions typically measured in meters. While capable of providing synoptic map-like views of damage, there are shortcomings in terms of resolution, re-visit time, and viewing geometries (Huyck et al. 2003). Even off-nadir, oblique imagery will miss the human-scale or "door-to-door" data typically collected by damage assessment teams. The need for house level data extends beyond cataloguing the amount of damage, and includes checking for the presence of looting or, in the case of Katrina, recording flood heights. In the recovery phase domicile aggregation data is also important, not only to gauge returning/rebuilding, but also to find correlates for local crime levels or health outcomes. If a video recorder could be incorporated into the data collection framework, its non-specialist nature would enable anyone capable of operating a camcorder to become part of the mapping team. Using technology that is easy to use and relatively inexpensive, users could decide where and when they would like to collect data unimpeded by weather or operational restrictions. In addition, while damage assessment is the goal of most door-to-door post-disaster data collection efforts, a SVAS would have the potential to add into existing models more geographically informed data on the recovery process.

Possibly the largest damage assessment team in the US is comprised of volunteers with the American Red Cross (ARC), who fly into the impacted areas of most disasters in the country. ARC volunteers perform several duties, one of which is to assess the amount of damage per residence so that temporary financial relief can be distributed to victims. Two to three person teams drive to the impacted area and collect these data by visually inspecting each property (essentially a "windshield survey") to determine how much damage has occurred. Their assessments are recorded on "street sheets" which are filed as paper records – they are not turned into a digital format resulting in the loss of this valuable spatial resource (Curtis et al. 2007a).

The low-tech ARC data collection approach was described in 2006 at a *GIS in Practice Symposium* held in Ireland and organized by theNational Centre for Geocomputation (NCG). Serendipitously, a presentation by researchers from the

National University of Ireland, Maynooth, followed that described a video-linked-to-GPS approach to collecting similar data, although designed mainly for use in transportation applications. Spatially encoded video first came to prominence in the 1980s (Meisner 1986) but not until the 1990s was it possible to merge image data with positional information at time of collection (McCarthy et al. 2007; Toth and Grejner-Brzezinska 1998). The development of GPS encoders allows geographic information to be attached to the video capture, either directly on the image or through an audio channel. The quality (and cost) of these systems varies from engineering grade components to simple and relatively inexpensive camcorder systems. We refer to the system described in this chapter as a SVAS, but it has alternatively been called a Mobile Mapping System. GPS-encoded camcorder systems have been applied to a number of projects, from road-surveys to ecological mapping (Lirman and Deangelo 2008; McCarthy et al. 2007, 2008) and its potential usefulness for collecting post-disaster-related data is compelling.

The system used for data collection in this case study is small, simple to use, and relatively inexpensive. Its equipment consists of two to three window-mounted cameras and a central GPS unit (not much bigger than a camera), all of which can easily be stored in a backpack. The system itself works as follows: the GPS encoder records a continuous signal onto the audio track of each video camera. These tapes are then processed using a frame capture card and the decoding setting of the GPS unit, which in effect attaches a unique ID to each image. The next step in processing links these images to a coordinate file which has also been generated; this is the path of the SVAS vehicle. Once processed the user can navigate this coordinate path within the software to move to any point of the data collection route. The coordinate file is in a GIS format that allows the SVAS path to be overlaid with other geographic layers, such as high-resolution aerial photography, or building footprints.

A relationship was established with the NCG and a team from Louisiana State University (LSU) took the system into the field to perform a damage assessment proof-of-concept data collection exercise in the Lower 9th Ward (Curtis et al. 2007a). Figure 18.1 displays the SVAS browser with three images taken during this trip using a single camera. The left section of the browser shows the car's route, in this case overlaid onto flood imagery from immediately after Katrina's landfall; the image in the main screen displays the video. The video can be stopped, sped up, or reversed, adding additional flexibility by allowing the user to "jump" to any part of the video track. In addition, a database allows information to be extracted from any image, for example populating the attribute table "does the house appear salvageable?" In the uppermost image two severely damaged houses are seen with a car overturned between them. Examining the accompanying aerial photograph, the breach in the Industrial Canal is visible as is the barge (the reddish rectangular object) connected with that breach incident. The houses have been heavily damaged by the force of the water. The middle image of Fig. 18.1 displays one of the many small churches that can be found in the Lower 9th Ward. The doors are broken inwards and search and rescue messages are evident, while on the brick wall at the corner animal rescue messages are spray painted in yellow. The lower image of Fig. 18.1 also shows a scene of destruction – a house and car have apparently

Fig. 18.1 Spatial Video Acquisition System (SVAS) browser for three images taken from the Lower 9th Ward

Fig. 18.2 Spatial Video Acquisition System (SVAS) as a damage assessment tool in a post-tornado environment

"collided"; in the background (top left side of the image) one of the major bridges crossing the Industrial Canal is visible.

One of the benefits of this system is that a windshield survey can be replicated at any time in the future, allowing new information to be extracted, visualized and analyzed. For example, Fig. 18.1 was generated for this chapter – in effect creating an historical record of an urban settlement that no longer exists – but these data can be "called up" repeatedly, allowing for both qualitative investigations and GIS-based analyses as Geographic Information Technologies improve.

The original rationale for using the SVAS was as a damage assessment tool. Figure 18.2 demonstrates its use in such an environment; in this case for the community of Huntersville, Tennessee after the Super Tuesday tornadoes of February 2008 (Mills et al. 2008). This image illustrates the three-camera version (left, right and front facing) of the SVAS, which allows users to switch between any of the three views by simply clicking on a "thumbnail" image.

18.3 The Spatial Video Acquisition System as a Recovery Assessment Tool

A common challenge for post-disaster researchers is that data collection often proves to be extremely difficult. Specifically, this challenge includes a lack of baseline data for comparison, the stressful situation impacting both data collectors and

those being studied, and the lack of resources to collect good quality dynamic (in terms of both space and time) data (Gibbs 1989; Ginexi et al. 2000). In addition, the lack of a clearly defined time frame associated with recovery can also cloud decisions regarding when to begin and end the data collection process.

As of the third anniversary of Katrina's landfall, entire neighborhoods seem to be re-establishing themselves at a very slow rate, while others appear to be permanently abandoned, with residences being overtaken by vegetation. Tens of thousands of people are still displaced, houses vacant, and communities in disarray. Due to these circumstances, it was decided that all field-testing of the SVAS would occur within Katrina-impacted neighborhoods as any data collected might still prove useful. During 2006 and 2007, Louisiana State University students conducted field-tests to gauge various data collection tolerances, including the impact of atmospheric conditions (affecting the GPS signal), vehicle speeds, camera placements and ideal crew numbers. Neighborhoods were chosen by virtue of their exposure during the disaster (e.g., proximity to levee breaches) or due to their stagnation in recovery. These initial trips provided baseline data to which subsequent trips in 2008 could be compared.

The SVAS approach provides a solution to many of the previously described disaster-related data collection challenges. A neighborhood can be driven, the data processed and archived, and then re-driven several months later to gauge how much change has occurred. For example, Fig. 18.3 compares the same stretch of road for the 29th August 2006, and again on the 1st of July 2007. In the upper-most part of the image the owner has painted his/her contact information across the garage doors of the abandoned building. Obviously at this point the owner had not returned to live on this street. The bottom image reveals that almost a year later, the house remains abandoned with the painted contact information still visible, though faded and now hidden by vegetation that has grown unchecked. Interestingly, additional video reveals more information about conditions in the vicinity of this house via the thumbnail at bottom left, which shows the plot across the road as empty due to its building having been removed.

Figure 18.4 compares three additional buildings, this time over the shorter time frame of two months: 21st April 2007 (left side) and 30th June 2007 (right side). These frames were selected from the same small stretch of road to illustrate how even over this relatively short time frame the decline of a neighborhood is noticeable.

The uppermost frame shows an abandoned home next to a property where people have returned (at least to a trailer on the premises). Two months later the abandoned home to the left shows evidence of further decline, while the family still resides in the trailer. Interestingly, in both images the trash bin can be seen in front of the house, which is an indicator used to identify possible returnees. The leftmost middle image is of a house with extensive roof damage but a flag hangs at the front entry indicating some level of activity. Two months later the roof shows evidence of additional damage, and the flag is gone. The left thumbnail image beneath this picture is of the home across the road where a family has returned and is living in a trailer. Of the bottom two images, the left is of a home with boarded windows,

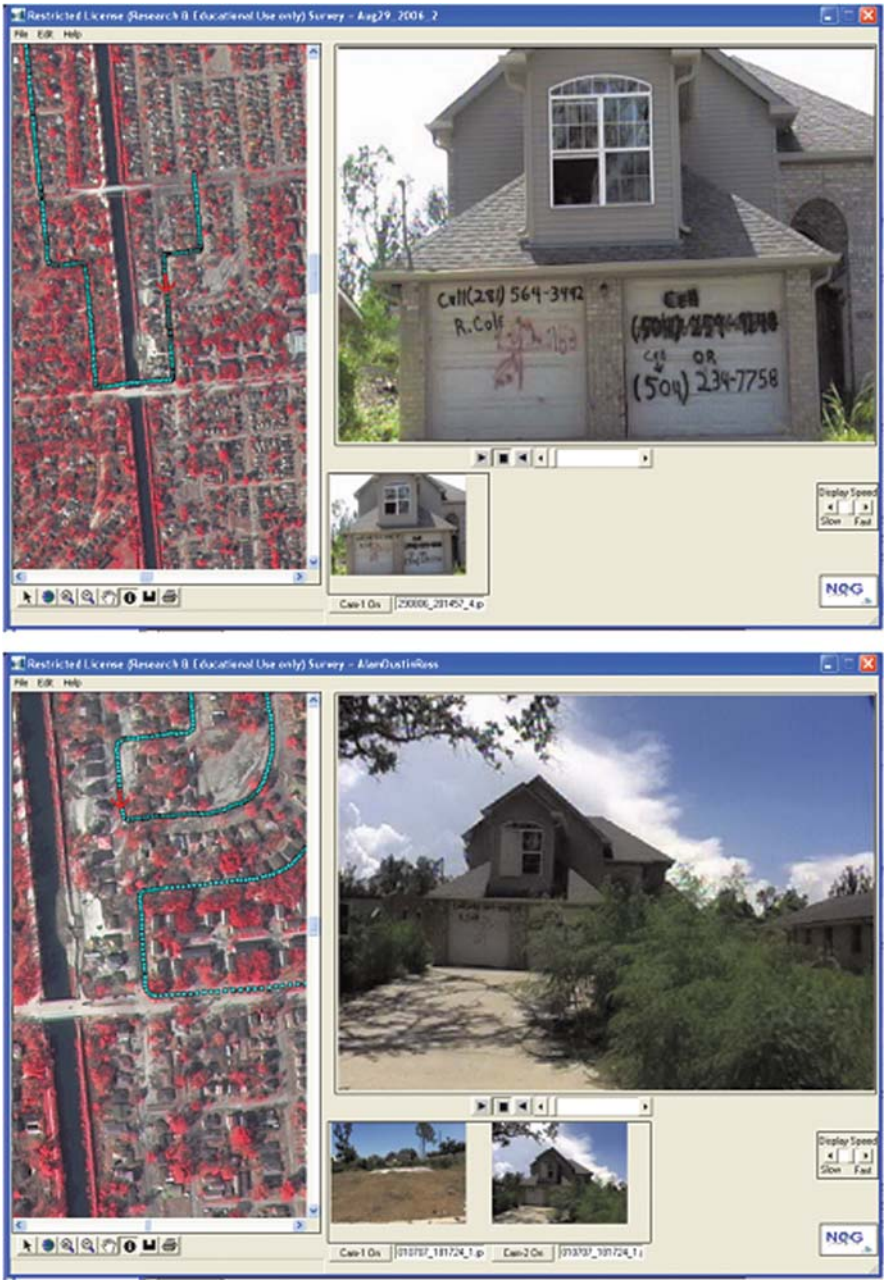

Fig. 18.3 Temporal neighborhood change (in years) captured with the Spatial Video Acquisition System (SVAS)

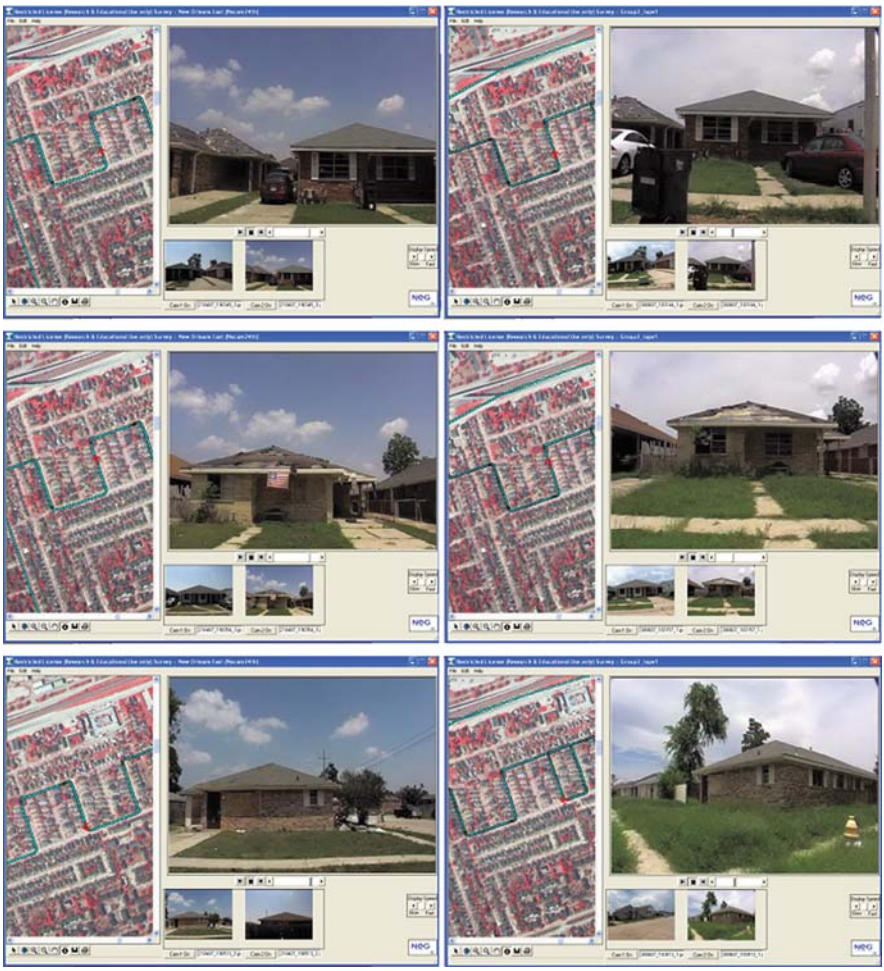

Fig. 18.4 Temporal neighborhood change (in months) captured with the Spatial Video Acquisition System (SVAS)

but with potential rebuilding activity outside due to the presence of materials on the right of the building. Two months later (right image), there are no signs of rebuilding and the lawn is unkempt (the different angle captures the amount of vegetation growth by using the fire hydrant as a frame of reference). Data such as these can be used to create more realistic models of recovery that capture the nonlinear nature of the process; evidence such as this demonstrates that recovery is not necessarily positively associated with time.

These examples show how SVAS provides a dynamic tool to collect data that have never before been recorded, providing a more accurate gauge of levels of neighborhood recovery or abandonment. SVAS not only serves to collect post-disaster geographic data, it facilitates re-collection and comparison of those

data. Typically, post-disaster data can be highly perishable. Fortunately, the cost-effectiveness of SVAS allows researchers to gather field data under arduous circumstances before they may have developed a formal research question. Although collecting data without a research question "in mind" violates the tenets of hypothesis-driven research, the fluidity of disaster and post-disaster environments can demand a different modus operandi.

18.4 Linking the SVAS to a GIS

In order to spatially analyze SVAS data, information from the spatially encoded images needs to be extracted into a GIS. One approach is to capture attribute information from each building (or other geographic feature such as a park, or even a trash pile) and link these to a GIS layer. For example, existing pre-Katrina building footprints and "heads-up" digitizing of building outlines from post-Katrina imagery, have both been used to hold SVAS information. Attributes can be added to each footprint by progressing the video frame by frame, with the analyst entering what is seen into the attribute table of the GIS layer. In addition, if standard architectural frames of reference are used (e.g., door height, number of floors/partial floors), SVAS can provide enough information to construct a three-dimensional rendering of the neighborhood. The GIS environment also enables spatial video to be integrated with existing remote sensing data. Wide-area patterns or anomalies visible on synoptic remote sensing images and resulting from an unknown process can be investigated using the very high resolution spatial video data. Conversely, remotely sensed image data can be used as a reference to explain phenomena visible in the spatial video frames.

To illustrate, Fig. 18.5 is a three-dimensional rendering of the Holy Cross neighborhood on 18 January 2008. The darker colored houses identify returnee homes. The dotted line shows the path of the SVAS. Above this scene floats an inverted kernel density cloud that shows high intensities of rebuilding activity. The darker contours point down to areas of rebuilding as defined by a variety of variables (Curtis 2008). A scale was created to represent the amount of rebuilding, from wooden planks sitting outside a home (score of 1) to teams of builders working on the property (score of 10). The resulting density surface has been raised above the neighborhood and then inversely projected downwards to identify those sections with the most activity – in effect, showing where recovery is progressing. This figure is only a snapshot of patterns that can be more fully explored in three dimensions through rotating the map in Environmental Systems Research Institute's (ESRI) ArcScene software.

The preceding description of SVAS has been in terms of a data collection tool for post-disaster environments and several examples have been provided of physical information that can bee seen and extracted from SVAS. However, the true power of SVAS may lie in its ability to expand broader research investigations. For example, the geographic pattern of building abandonment may represent a geography of potential antisocial behavior (Fullilove 2003; Greenberg et al. 1992; Greenberg

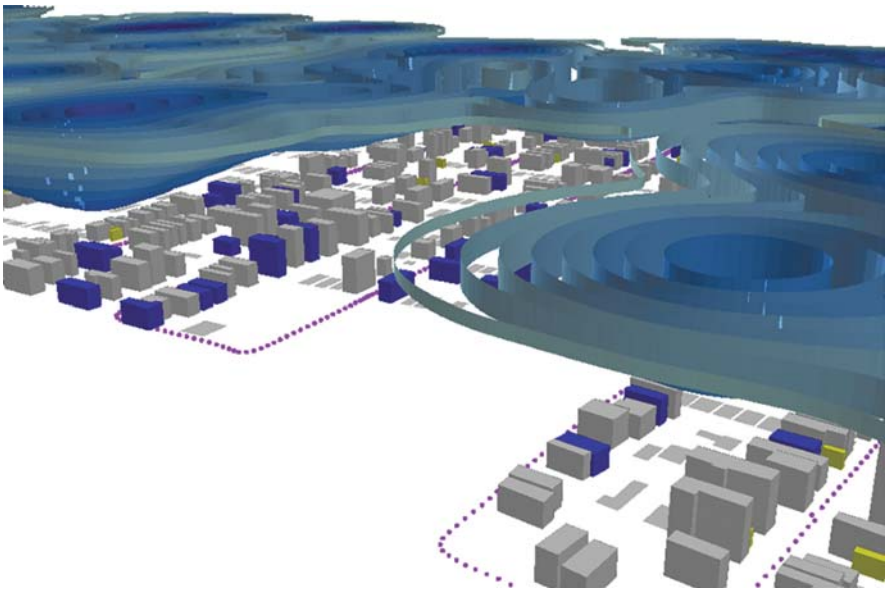

Fig. 18.5 Three-dimensional visualization of neighborhood rebuilding status

and Schneider 1994). Returnees might be used in an analysis that better gauges post-disaster health and public safety issues. A social justice investigation might be interested in which neighborhoods have received poor service provision from the city, or where local infrastructure is degrading. To examine these types of issues further, a conceptual approach is offered for how SVAS could be used to monitor post-disaster health vulnerability, especially mental health outcomes.

18.5 Post-Katrina Psychopathology

Full recovery of a community after a disaster depends on many factors such as the severity of the event, the ability of residents to financially buffer themselves from the shock, the ability to navigate government and non-profit assistance, and whether they have a political champion (Blaikie et al. 1994; Cutter et al. 2003; Ginexi et al. 2000). Until community conditions "revert to normal", it can be argued that in some fashion the disaster is still occurring (Pastor et al. 2006). Unfortunately a prolonged recovery exacerbates existing health problems and creates new-public health challenges. For example, in early 2008 both the Centers for Disease Control and Prevention (CDC) and the Substance Abuse and Mental Health Services Administration (SAMSHA) issued warnings about Katrina illnesses, including formaldehyde exposure in trailers, and the potential for developing psychopathology (FEMA/CDC 2008; SAMHSA 2008). These are only two of many possible Katrina health-legacies; indeed it is unlikely the true cost of this ongoing disaster

will ever be known. This situation is partly a result of the complexities involved in understanding secondary and tertiary impacts with a root cause in the disaster, for example poor birth outcomes occurring several years later to women who either live in the devastated communities or are still among the diaspora (Antipova and Curtis 2007; Xiong et al. 2008). Just as with all post-disaster research, there are considerable challenges to collecting health data, especially dynamic data that include both space and time attributes.

The health vulnerability of the pre-Katrina Orleans Parish population has now been well described, with the largely poor urban African American population carrying high rates of what are commonly accepted as typical inner city health problems: diabetes, hypertension, and obesity (Curtis et al. 2007b). Many of these conditions are linked to the day-to-day living conditions of the inner city, for example, poor access to service provision and poor access to/availability of healthy lifestyle options including nutritious food and recreation opportunities (Krieger 1996, 2003; Krieger et al. 2003). The post-disaster consequences of these health vulnerabilities are complex – the conditions themselves may have resulted in a decision not to evacuate (Eisenman et al. 2007). For returnees, the added stress of experiencing the storm, a lack of medication, the stress of returning to an uncertain future, and poor medical service provision in the devastated city only lead to intensifying existing health conditions (Cefalu et al. 2006; Curtis et al. 2007b; Galea et al. 2007).

Possibly the most commonly described problems are psychosocial including-Post Traumatic Stress Disorder (PTSD) and associated negative coping strategies used to moderate the ongoing stressful situation (Freedy et al. 1992; Norris et al. 2002a, 2002b). There may be a linear initial relationship between event and health outcome – the event and its aftermath are stress causing, and stress (including grief) may lead to mental health problems (Gibbs 1989), but this is an oversimplification. The vulnerability of someone to psychopathology is not only attributed to the acuteness of the actual event (e.g., being stranded on a roof top, or having to experience poor conditions in a shelter) (CDC 2006b Ginexi et al. 2000; Melick 1978), but also to what was happening to the person before the disaster – had they a previous history of mental health problems, or were they living in an environment of high stress close to a "tipping" point (Asarnow et al. 1999; Gibbs 1989; Lonigan et al. 1994; Resnick et al. 1992)?

The stress associated with living conditions commonly faced in poor and/or minority neighborhoods often increases the potential for mental health problems (Rehner et al. 2000). The external shock of a disaster, combined with several other post-disaster stresses (such as having to deal with the loss of home, friends and family) compounds this vulnerability. For example, even if a Katrina-displaced resident returned to the city in the months or years after the storm, it is likely the neighborhood is very different. Key focal points of social capital – the church, the store, places of employment – would likely be closed or in disrepair. The neighborhood infrastructure (e.g., health care, schools) would not be accessible and the combination of a reduced police force and abandoned buildings would increase the potential for crime. Neighborhood streets might display multiple examples of abandonment; search and rescue markings are likely to still be evident. From a human and social

perspective neighbors may still be gone and in general terms there is a loss of "community" on which economically disadvantaged African Americans are often dependent. Given all of these stressors, it is hardly surprising that many returnees run the risk of suffering mental health collapse.

The challenge is this: the impact of Katrina is ongoing, with many neighborhoods still in recovery, even regressing. It is likely that a high proportion of returnees are vulnerable to developing mental health problems, especially because the area suffered high pre-Katrina health vulnerabilities. But how to identify who is at risk and spatially target where the need is greatest to best distribute resources? Data collected from before Katrina have little relevance. The population has changed, even the urban fabric is different – pre-Katrina buildings have closed or lie in disrepair while post-Katrina habitats (trailers) are now scattered throughout the landscape. Post-Katrina datasets such as those provided by the Brookings Institution's Katrina Index (Brookings Institution 2007) or the Center for Social Inclusion's (CSI) Recovery Report Card (CSI 2007) that detail various measures of recovery are at the wrong geographic scale (Mills 2008). When psychological impact is felt at the residence scale there is little point in mapping mental health vulnerability by census tract and especially not by zip code. There is a need to record what the returnee faces every day in terms of sight-line from his/her window and the state of the neighboring buildings.

Previous post-disaster psychopathology research has been limited when considering the aspect of space and even time, with data being collected in (infrequent) discrete phases rather than as a continuum (Norris 2002). Given the prolonged Katrina-situation it is unlikely that recovery (both in terms of community or individual health) will progress at a steady rate (Kimhi and Shamai 2004; Marshall et al. 2007; van den Berg et al. 2005).

The SVAS provides a geospatial approach that can help redress over-reliance on static data. Ideally SVAS data would be used in conjunction with other health data, either collected via surveys or through biometric recorders. However, as it is likely that evidence of continuing neglect in the built environment will cause returnee stress, it is reasonable to use the SVAS to identify where health vulnerability is likely to be greatest based on the geography of abandonment and return. By using this proxy measure of blight to identify areas of potential health vulnerability, health workers can collect invaluable data that can be used to spatially allocate relevant healthcare resources to neighborhoods in need, regardless of the workers' GIS skill level.

18.6 Using the SVAS as a Proxy for Psychopathology Vulnerability

Information about the built environment has previously been used as either a causative factor or a proxy for health conditions (Tibbetts 2002). Built environment factors can include housing density, proximity to heavily trafficked roads, or evidence of trash surrounding a domicile. In a post-disaster environment, information

that can be collected using SVAS is limited to the field of view from the data collection vehicle. A sports utility vehicle provides the necessary ruggedness to cope with debris-littered streets, while its additional height allows for more information to be captured by the camera setup. The superior image quality of new generation camcorders also allows for subsequent "drilling into" the image to extract housing details. Given these parameters, and recognizing that environmental conditions are often visible (vehicles parked in the road, buildings obscured by vegetation), a considerable amount of detail can be captured and mapped using the SVAS. The type of information captured can be broadly described as being positive (signs of return/rebuilding) and negative (signs of damage and/or abandonment). Following is a detailed example of how these negative and positive attributes can be found in geographic proximity as well as speculation regarding how these environments might impact those who have returned.

There are a number of negative attributes originating from the storm: damage, evidence of the search and rescue effort (e.g., search and rescue markings on homes), evidence of abandonment (boarded-up doors and windows, overgrown yards), loss of social capital (closed churches, schools, and clinics, community playgrounds falling into disrepair), and evidence of declining community infrastructure (e.g., broken street signs replaced by hand-drawn ones), and closed neighborhood stores. There is also the possibility of further decay through abandonment or post-event damage (e.g., uncontrolled fires burning due to lack of firefighter services) during the period after the disaster.

Positive neighborhood attributes involve signs of return: neatly manicured front yards, "wheely" trash bins, people sitting on porches, cars in driveways, curtains in windows, all of which are useful indicators – especially when used in combination. If a fully returned home presents one end of this positive spectrum, then along the continuum are families who are apparently rebuilding – as evidenced by home gutting, construction materials in the yard, and workers climbing ladders and hammering nails. Occasionally the SVAS captures activity of a positive nature that originates outside the community. On one trip into the Holy Cross neighborhood (March 2008) that coincided with Spring Break (a general university holiday), scores of young people were seen in the streets helping residents to rebuild.

There are also many variables that prove difficult to classify as either negative or positive. For example, presence of a trailer indicates that a family has returned to their neighborhood – but at the same time this type of residence does not provide a "healthy" living situation for that family (DeSalvo et al. 2007; FEMA and CDC 2008) The trailers, especially those with elaborate construction around the frame (e.g., zigzagged wooden ramps, white skirting, roofs designed to resemble a "house") may also act as reminders of the disaster and how the neighborhood has been physically changed.

Positive and negative attributes also present different patterns when space and time are considered. For example, a house that is neglected and abandoned on one SVAS run may be on the brink of a rebuilding project. A returnee's home may be abandoned not because of direct storm damage but because of wider neighborhood factors (lack of services, employment or neighbors). Building materials in a front

yard may never be used – or the framing of a house may never extend beyond that phase, either because volunteer workers leave or the homeowner runs out of money (Rose et al. 2008). Even a sign placed in the garden or a window acting as a rallying cry to rebuild can have a positive effect when first posted – but if that sign remains for too long, it may revert to being yet another negative symbol of inactivity. Recovery is temporally complex, and this complexity increases when the relationship of space is added. During any single time period it is impossible to ascertain whether the whole neighborhood is recovering or not – for on every street the pattern of these negative and positive indicators will vary both in terms of an aggregate rate (number of abandoned buildings per all homes) or in terms of the sight-line of what a family walks by every day, or looks out on from a dining room window, or while preparing food in the kitchen, or closing the curtains before going to sleep at night. More research is needed to understand how this spatial complexity affects developing psychopathology – is it a function of the street, the sight line, the immediate neighboring house? Similarly, is there a spatial pattern to recovery – is it a process akin to evolution or diffusion? Is the likelihood of a house being returned to partly a function of whether the neighboring house has been reoccupied? SVAS has the potential to contribute to better understanding of such questions due its inexpensive and easy-to-use data collection capabilities. For example, Figs. 18.6 and 18.7 represent one section of road in Holy Cross imaged 18 January 2008 (Fig. 18.6) and 11 March 2006/12 September 2007 (Fig. 18.7). The underlying three-dimensional streetscape is taken from an SVAS run in 2008.

The buildings are color coded according to their amount of destruction and abandonment (reds), as well as whether or not they are returnee homes (blues). A black frame in the middle of each figure is used to focus the discussion. In Fig. 18.6, six buildings with considerable destruction and abandonment face three buildings occupied by returnees. Such a situation may present a mental health challenge for the returnees as these residents have invested time, effort and probably money in rebuilding, while across the road a series of apartment buildings lie boarded up, with search and rescue markings still evident.

Figure 18.7 presents two scenes from March 2006, and then again on September 2007. In 2006 and 2007, the windows in the apartment building were still glassed, and someone is actually looking out of the window in the bottom left image (2006). Search and rescue markings are visible on the walls and windows, but as of this date the building still appears to have hope of recovery. In 2008, however, the building has been boarded-up. More dramatic still is the white frame house at the top of the map. A search and rescue marking is evident in 2006, and the vegetation has grown higher by 2007, but the building looks intact and salvageable, and there are even shades in the window. Compare that to Fig. 18.6 (2008) which shows the same house overgrown with vegetation, with open and charred windows, discolored paint, and through the windows the sky is visible because the roof is missing. A fire has reduced the building to a shell. This side of the street has actually *regressed*.

These examples provide an illustration of why the SVAS is important to this type of research. Firstly, only at this geographic scale (the house and street level) can

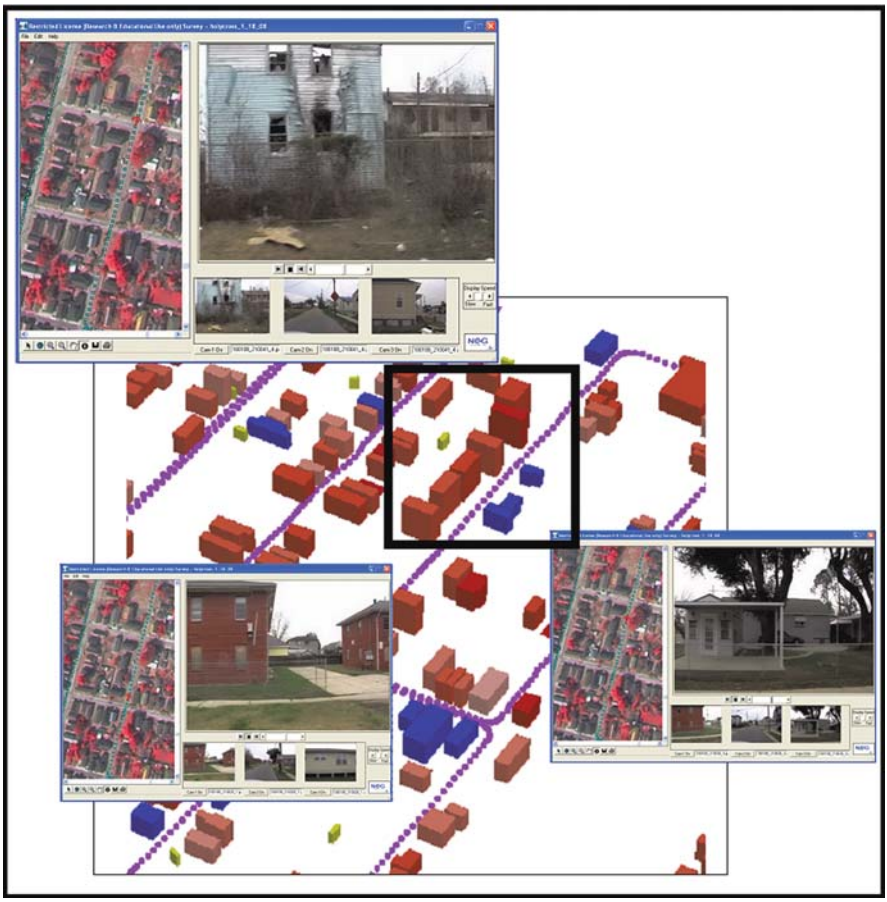

Fig. 18.6 Street segment in the Holy Cross neighborhood of New Orleans (1/18/2008)

judgments be made regarding possible environment stresses surrounding a returnee, which means that only at this scale can geographic prioritization of outreach be determined. Secondly, each Orleans Parish neighborhood contains hundreds of these examples – a potentially overwhelming situation for understanding the on-the-ground environment for either researchers or health providers. However, the SVAS collects data for all neighborhoods, quickly and efficiently, and informs fine scale investigations. Consequently, irrespective of the resources available, the SVAS can be used to target these resources where they may be most effectively used.

As spatial scientists, we can further refine this process by identifying patterns of return and abandonment within a GIS environment, so that in future disasters SVAS data collection could be matched with spatial pattern matching to automatically recognize areas needing prioritization. The archival quality of data collected using the SVAS again allows this to be a research possibility, and represents a significant improvement over the paper street sheets collected by ARC.

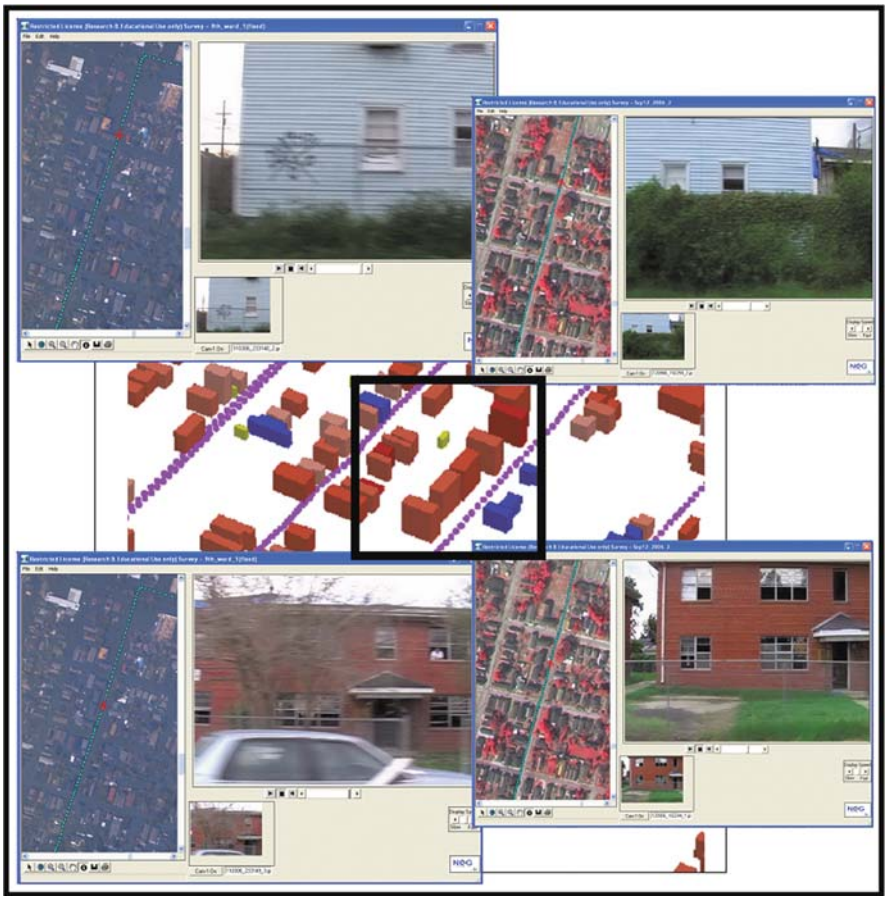

Fig. 18.7 Street segment in the Holy Cross neighborhood of New Orleans (3/2006 and 9/2007)

18.7 Discussion and Conclusion

Spatial video technology has proven that it is a useful geospatial tool in post-disaster scenarios. The challenge lies in making this technology accessible to a wider, global audience, and cell-phones with video capability may represent the next "frontier" for this tool. Based on current population projections, over half of the world's population (approximately 3.3 billion people) will own a cell phone in 2008 (ITU 2008). Many of these mobile devices now have the ability to capture video as well as the user's geographic position. The new geotechnology center StratAG (www.StratAG.ie), based at the National University of Ireland, Maynooth, is researching the next generation of spatial video technology based on cell phones. A prototype system will be tested within various post-disaster recovery scenarios together with the University of Southern California (USC) research team. This

development will enable anyone to collect spatial video and seamlessly transmit these data to a central server. This spatial video will be automatically integrated with existing geospatial databases for further processing and made available over the Internet or as a Location Based Service (LBS). This technology will empower ordinary citizens to play a useful role during recovery and in doing so, become a new generation of remote sensors armed with relatively simple geosensors, i.e., cell phones.

Spatial video technology may be considered similar to Google Earth Street View where users can act as virtual pedestrians, but SVAS provides greater flexibility in what data can be captured and the ease of extracting these data into a GIS. Though Google Earth Street View has data for most of New Orleans, these views are static. Such technology may be useful for displaced residents who wish to see the recovery occurring in their neighborhood, but unless these data are updated regularly they will misrepresent the current neighborhood status and they do not capture the dynamic recovery landscape. In addition, the SVAS browser enables easy extraction of data from the video into a GIS, a task Google Earth Street View is not designed to address. For these reasons, spatial video technology is preferable for neighborhood data collection in a post-disaster environment.

Post-disaster recovery at the neighborhood level, especially the geography of recovery, has previously received scant attention in the literature. This state of affairs is mainly due to technical and conceptual constraints in collecting data. All phases of the disaster cycle are characterized by continually changing situations, and dynamic geographic data have always been difficult to capture. In addition, there is little tradition in terms of collecting such ephemeral data, even though there are obvious advances that could be made by understanding how people and their neighborhoods institute "return" after a disaster.

The post-Katrina situation in New Orleans has provided an opportunity for researchers to focus on the recovery phase of the emergency management cycle due to how geographically extensive the damage was, and how long it is taking for communities to rebound. This recovery is important not only in terms of rebuilding what has been lost, but also from an individual health perspective because until normalcy is reached, there is the potential, indeed the likelihood, that secondary disaster-related illnesses will manifest, especially psychopathology. A geospatial approach that was initially conceived and field-tested as a result of "ride-alongs" with American Red Cross damage assessment teams, has evolved into a dynamic space-time data collection tool that can be used to accurately assess neighborhood recovery.

Ideally, all damage assessment vehicles could incorporate a SVAS which would reduce the number of human "ride-alongs", speed damage assessment data collection trips, and allow windshield surveys to be "virtually" performed at ARC headquarters. The benefit is obvious; more oversight and less subjectivity, and the generation of a digital data set that can be archived, revisited, and even distributed to officials in the Emergency Operations Center (EOC).

Interestingly this approach is now being used to not only consider other aspects of the post-Katrina environment, such as the spatial risk for crime, but also in

non-disaster related urban research. For example, several USC pilot projects are attempting to provide a link between the built environment and accelerometer and multimodal biometric readings for young girls in an investigation of activity and obesity, and are studying urban "markings" associated with gang activity in Los Angeles. However, it is as a recovery assessment tool, especially within the post-Katrina neighborhoods of New Orleans, that SVAS best demonstrates its utility, and where its need is greatest.

Acknowledgments The authors would like to thank the following colleagues who have been involved on different data collecting trips and processing: Barrett Kennedy, Farrell Jones, Chelsea Core, Felixcia J. Mendoza-Jones, J.P. Michael, John Pine and the many students of Geog 4047 – Introduction to GIS.

In addition, research contributions presented in this paper by Stratag (www.stratag.ie) were funded by a Strategic Research Cluster grant (07/SRC/I1168) by Science Foundation Ireland under the National Development Plan.

References

Antipova, A. and Curtis, A. (2007). *Public Health and Disasters: The Relationship Between Pregnancy Outcomes and Hurricane Andrew*. Saarbrucken, Germany: VDM Verlag Dr. Muller e. K (VDM Publishing House).

Asarnow, J., Glynn, S., Pynoos, R., Nahum, J., Guthrie, D., Cantwell, D., Franklin, B. (1999). When the earth stops shaking: Earthquake sequelae among children diagnosed for pre-earthquake psychopathology. *Journal of the American Academy of Child and Adolescent Psychiatry*, 38(8), 1016–23.

Blaikie, P., Cannon, T., Davis, I., Wisner, B. (1994). *At Risk: Natural Hazards, People's Vulnerability, and Disasters*. London: Routledge.

Brookings Institution. 2007. The New Orleans Index: Tracking Recovery in the Region. http://www.brookings.edu/reports/2007/08neworleansindex.aspx.

Cefalu, W., Smith, S., Blonde, L., Fonseca, V. (2006). The Hurricane Katrina aftermath and its impact on diabetes care: Observations from "ground zero": Lessons in disaster preparedness of people with diabetes. *Diabetes Care*, 29(1), 158–160.

Center for Social Inclusion (CSI). (2007). Katrina Recovery Report Card. Available at: http://www.centerforsocialinclusion.org/racetorebuild.html.

Centers for Disease Control (CDC). (2006). Illness surveillance and rapid needs assessment among Hurricane Katrina evacuees – Colorado, September 1–23, 2005. *(MMWR) Morbidity and Mortality Weekly Report*, 55(9), 244–247.

Curtis, A. (2008). Three-dimensional visualization of cultural clusters in the 1878 yellow fever epidemic of New Orleans. *International Journal Health Geographics*, 7(47). http://www.ij-healthgeographics.com/content/7/1/47. Accessed 14 September 2008.

Curtis, A., Mills, J., Blackburn, J., Pine, J. (2006a). Hurricane Katrina: GIS response for a major metropolitan area. *Quick Response Research Report 180*. Boulder: University of Colorado Natural Hazards Center.

Curtis, A., Mills, J., Blackburn, J., Pine, J., Kennedy, B. (2006b). Louisiana State University Geographic Information System Support of Hurricane Katrina recovery operations. *International Journal Mass Emergencies and Disasters*, 24(2), 203–221.

Curtis, A., Mills, J., Kennedy, B., Fotheringham, A.S., McCarthy, T. (2007a). Understanding the geography of post-traumatic stress: An academic justification for using a spatial video acquisition system in the response to Hurricane Katrina. *Journal of Contingencies and Crisis Management*, 15(4), 208–209.

Curtis, A., Mills, J., Leitner, M. (2007b). Katrina and vulnerability: The geography of stress. *Journal of Health Care for the Poor and Underserved*, 18(2), 315–330.

Cutter, S., Boruff, B., Shirley, W. (2003). Social vulnerability to environmental hazards. *Social Science Quarterly*, 84(2), 242–261.

DeSalvo, K., Hyre, A., Ompad, D., Menke, A., Tynes, L., Munter, P. (2007). Symptoms of posttraumatic stress disorder in a New Orleans workforce following Hurricane Katrina. *Journal of Urban Health*, 84(2), 142–152.

Eisenman, D., Cordasco, K., Asch, S., Golden, J., Glik, D. (2007). Disaster planning and risk communication with vulnerable communities: Lessons from Hurricane Katrina. *American Journal of Public Health*, 97(S1), S109–S115.

Federal Emergency Management Agency/Centers for Disease Control (FEMA/CDC). (2008). CDC Releases Results of Formaldehyde Level Tests, Joint Press Release, Centers for Disease Control and Prevention. http://www.cdc.gov/media/pressrel/2008/r080214b.htm. Accessed 14 September 2008.

Freedy, J., Shaw, D., Jarrell, M., Masters, C. (1992). Towards an understanding of the psychological impact of natural disasters: An application of the conservation resources stress model. *Journal of Traumatic Stress*, 5(3), 441–454.

Fullilove, M. (2003). Neighborhoods and infectious diseases. In I. Kawachi and L. Berkman (Eds.), *Neighborhoods and Health* (pp. 211–222). New York: Oxford University Press.

Galea, S., Brewin, C., Gruber, M., Jones, R., King, D., et al. (2007). Exposure to Hurricane-Related stressors and mental illness after Hurricane Katrina. *Archives of General Psychiatry*, 64(12), 1427–1434.

Gibbs, M. (1989). Factors in the victim that mediate between disaster and psychopathology: A review. *Journal of Traumatic Stress*, 2(4), 489–514.

Ginexi, E., Weihs, K., Simmens, S., Hoyt, D. (2000). Natural disaster and depression: A prospective investigation of reactions to the 1993 midwest floods. *American Journal of Community Psychology*, 28(4), 495–518.

Greenberg, M. and Schneider, D. (1994). Violence in American Cities: Young black males is the answer, but what was the question? *Social Science and Medicine*, 39(2), 179–187.

Greenberg, M., Popper, F., West, B., Schneider, D. (1992). TOADS go to New Jersey: Implications for land use and public health in mid-sized and large US cities. *Urban Studies*, 29(1), 117–125.

Huyck, C., Adams, B., Kehrlein, D. (2003). An evaluation of the role played by remote sensing technology following the World Trade Center attack. *Earthquake Engineering and Engineering Vibration*, 2(1), 159–168.

International Telecommunication Union (ITU). (2008). January Report. http://www.itu.int/itunews/manager/main.asp?lang=en&iYear=2008&iNumber=01. Accessed 14 September 2008.

Kimhi, S. and Shamai, M. (2004). Community resilience and the impact of stress: Adult response to Israel's withdrawal from Lebanon. *Journal of Community Psychology*, 32(4), 439–451.

Krieger, N. (1996). Inequality, diversity, and health: Thoughts on "race/ethnicity" and "gender". *Journal of American Medical Women's Association*, 51(4), 133–136.

Krieger, N. (2003). Place, space, and health: GIS and epidemiology. *Epidemiology*, 14(4), 384–385.

Krieger, N., Chen, J., Waterman, P., Rehkopf, D., Subramanian, S. (2003). Race/ethnicity, gender, and monitoring socioeconomic gradients in health: A comparison of area-based socioeconomic measures – the public health disparities geocoding project. *American Journal of Public Health*, 93(10), 1655–1671.

Lirman, D. and Deangelo, G. (2008). Geospatial video monitoring of benthic habitats using shallow-water positioning system. *Oceans*, 2007, 1–5.

Lonigan, C., Shannon, M., Taylor, C., Finch, A., Salleee, F. (1994). Children exposed to disaster: II. Risk factors for the development of post-traumatic symptomatology. *Journal of American Academy of Child & Adolescent Psychiatry*, 33(1), 94–105.

Marshall, G., Schell, T., Elliott, M., Rayburn, N., Jaycox, L. (2007). Psychiatric disorders among adults seeking emergency disaster assistance after a wildland-urban interface fire. *Psychiatric Services*, 58(4), 509–514.

McCarthy T., Fotheringham A.S. and O'Riain G. (2007). Compact Airborne Image Mapping System (CAIMS). The International Archives of the Photogrammetry, Remote Sensing and Spatial Information Sciences, Padua, Italy, Vol. XXXVI, Part 5/C55, pp. 198–202.

McCarthy, T.M., Farrell R.J., Fotheringham, S., Curtis, A. (2008). Integrated remotely sensed datasets for disaster management. *Remote Sensing for Environmental Monitoring, GIS Applications, and Geology VIII*, SPIE Europe Security+Defence and SPIE Europe Remote Sensing Conferences, University of Wales Institute, Cardiff, Wales, UK, September.

Meisner, D. (1986). Fundamentals of airborne video remote sensing. *Remote Sensing of Environment*, 19, 63–79.

Melick, M. (1978). Life change and illness: Illness behavior of males in the recovery period of a natural disaster. *Journal of Health and Social Behavior*, 19(3), 335–342.

Mills, J. (2008). Understanding disaster: GI Science contributions in the ongoing recovery from Katrina. *Transactions in GIS*, 12(1), 1–4.

Mills, J., Curtis, A., Fagan, W. Core, C. (2008). The Spatial Video Acquisition System as an approach to capturing damage and recovery data after a disaster: A case study from the Super Tuesday Tornadoes. *Quick Response Research Report* Boulder: University of Colorado Natural Hazards Center.

Norris, F. (2002). Disasters in urban context. *Journal of Urban Health*, 79(3), 308–314.

Norris, F., Friedman, M., Watson, P., Byrne, C., Diaz, E., Kaniasty, K. (2002a). 60,000 disaster victims speak: Part I. An empirical review of the empirical literature, 1981–2001. *Psychiatry*, 65(3), 207–239.

Norris, F., Friedman, M., Watson, P., Byrne, C., Diaz, E., Kaniasty, K. (2002b). 60,000 disaster victims speak: Part II. Summary and implications of the disaster mental health research. *Psychiatry*, 65(3), 240–260.

Pastor, M., Bullard, R., Boyce, J., Fothergill, A., Morello-Frosch, R., Wright, B. (2006). *In the Wake of the Storm: Environment, Disaster, and Race After Katrina* (pp. 1–52), New York: The Russell Sage Foundation.

Rehner, T., Kolbo, J., Trump, R., Smith, C., Reid, D. (2000). Depression among victims of South Mississippi's Methyl Parathion Disaster. *National Association of Social Workers*, 25(1), 33–40.

Resnick, H., Kilpatrick, D., Best, C., Kramer, T. (1992). Vulnerability-stress factors in development of posttraumatic stress disorder. *Journal or Nervous and Mental Disease*, 180(7), 424–430.

Rose, K., Clark, A., Duval-Diop, D. (2008). *A Long Way Home: The State of Housing Recovery in Louisiana in 2008*. PolicyLink report. http://www.policylink.org/threeyearslater/index.html. Accessed 14 September 2008.

Substance Abuse and Mental Health Services Administration (SAMSH). (2008). *The NSDUH Report: Impact of Hurricanes Katrina and Rita on Substance Use and Mental Health*. Rockville, MD: Substance Abuse and Mental Health Services Administration, Office of Applied Studies.

Tibbetts, J. (2002). Building awareness of the built environment. *Environmental Health Perspectives*, 110(11), A670–A672.

Toth, C. and Grejner-Brzezinska, D. (1998). Performance analysis of the airborne integrated mapping system (AIMS). *International Archives of Photogrammetry and Remote Sensing*, 32(2), 320–326.

van den Berg, B., Grievink, L., Yzermans, J., Lebret, E. (2005). Medically unexplained physical symptoms in the aftermath of disasters. *Epidemiologic Reviews*, 27, 92–106.

Xiong, X., Harville, E., Mattison, D., Elkind-Hirsch, K., Pridjian, G., Buekens, P. (2008). Exposure to Hurricane Katrina, post-traumatic stress disorder and birth outcomes. *The American Journal of the Medical Sciences*, 336(2), 111–115.

Part V
Evacuation Studies

Chapter 19
Pre-evacuation Trip Behavior

Melany Noltenius and Bruce A. Ralston

Abstract Evacuation models, which seek to calculate evacuation time estimates (ETEs) and evaluate evacuation strategies, are based on assumptions concerning human behavior. One of the most consistent assumptions is that once an evacuation order is given, people will proceed to an evacuation point. ETEs are further assumed to be a function of network congestion along arcs. We test these assumptions through a survey of residents of Key West, Florida who experienced evacuation orders associated with Hurricane Wilma in 2005. Of particular interest are the trips residents made between the time the evacuation order was given and the deadline for evacuation, what we call pre-evacuation trips. Such trips were made by people who evacuated as well as by those who waited out the storm. That is, traffic on the transportation network is not solely limited to people seeking to evacuate. Survey data indicate three important aspects of pre-evacuation trip making behavior that run counter to common evacuation modeling assumptions. First, trip delays at stops are longer than delays on links. Second, trip delays are associated with trip purposes, which often are not to evacuate an area, and there is evidence of trip chaining. Finally, patterns of pre-evacuation trips show a dispersal of origins and destinations resulting in pre-evacuation trips that flow in many directions, not just toward evacuation points.

Keywords Pre-evacuation trips · Trip chaining · Evacuation time estimates · Hurricane Wilma

19.1 Introduction

Events of the past decade have highlighted the importance of understanding how people respond to large scale disasters. The logistical problems associated with Hurricane Katrina and the terrorist attacks of September 11, 2001 have made

M. Noltenius (✉)
Department of Geography, University of Tennessee, Knoxville, TN 37996-0925, USA
e-mail: mnolteni@yahoo.com

P.S. Showalter, Y. Lu (eds.), *Geospatial Techniques in Urban Hazard and Disaster Analysis*, Geotechnologies and the Environment 2, DOI 10.1007/978-90-481-2238-7_19,

clear the need to improve both the techniques used to model human response to hazards and our understanding of human behavior in the face of large scale disasters. Modeling advances have included more realistic transportation models, particularly advances in microsimulation and agent based approaches (e.g., Axelrod 1997; Ben-Akiva et al. 1998; Chen 2008; Chen and Zhan 2008; Cova and Johnson 2002). Studies on human response to impending natural disasters provide some understanding of who will or will not evacuate an area (e.g., Alsnih et al. 2005; Cutter 2006; Mei 2002; Wilmot and Mei 2004; Wolshen et al. 2005). While advances on both these research fronts should lead to better planning, they are based on certain assumptions. Evacuation models, in particular, usually assume away non-evacuation trips made after an evacuation order is given but before the evacuation deadline is reached, what we call pre-evacuation trips. Because pre-evacuation trips can be made by residents who evacuate an area as well as those who stay behind, both types of behavior can affect traffic patterns and congestion. That is, knowledge of the pre-evacuation trip making behavior by those who leave and by those who stay is important in order to refine evacuation models. The purpose of this paper is to describe pre-evacuation trip behavior with an emphasis on the implications of such trips for existing evacuation models. In respect to that goal, this study examines the response of Key West, Florida residents to the mandatory evacuation order associated with Hurricane Wilma in October, 2005. Key West was an appropriate research site for two reasons. First, the city was evacuated four times in 2005. Second, similar to the strategy employed by Chen (2008) in her microsimulation of the evacuation of Galveston (Texas), there exists only one road leading out of the city – US Highway #1 (Fig. 19.1).

The time it takes for the residents to evacuate an area is calculated as an evacuation time estimate (ETE). These estimates are based on a number of inputs, including clearance time, the impact of traffic management techniques, and the time for the public to prepare to evacuate (Dow and Cutter 2000). Evacuation models such as WITNESS (Farahmand 1997), OREMS (Franzese 2003), CEMPS (Pidd et al. 1993), and MASSVAC (Hobeika and Jamei 1985), can calculate clearance times, as well as incorporate the temporal impact of traffic management techniques (e.g., contra-flow traffic). However, these models do not include delays associated with pre-evacuation trips. Because these trips are not well represented in hurricane evacuation models, the evacuation time estimate may be miscalculated (Wilmot and Mei 2004).

In order to capture pre-evacuation trip behavior, an online survey of residents' responses to the evacuation order associated with Hurricane Wilma in 2005 was conducted. The survey was designed primarily to gather sociodemographic data such as gender, age, marital status, trip purpose, trip stops and delays. These variables were chosen based on the literature describing evacuee attributes. Trip stops were determined by capturing respondents' mouse clicks on a street map of Key West. The survey also contained areas in which respondents could relate their own personal stories. Further details of the survey and sampling strategy are discussed in Noltenius (2008).

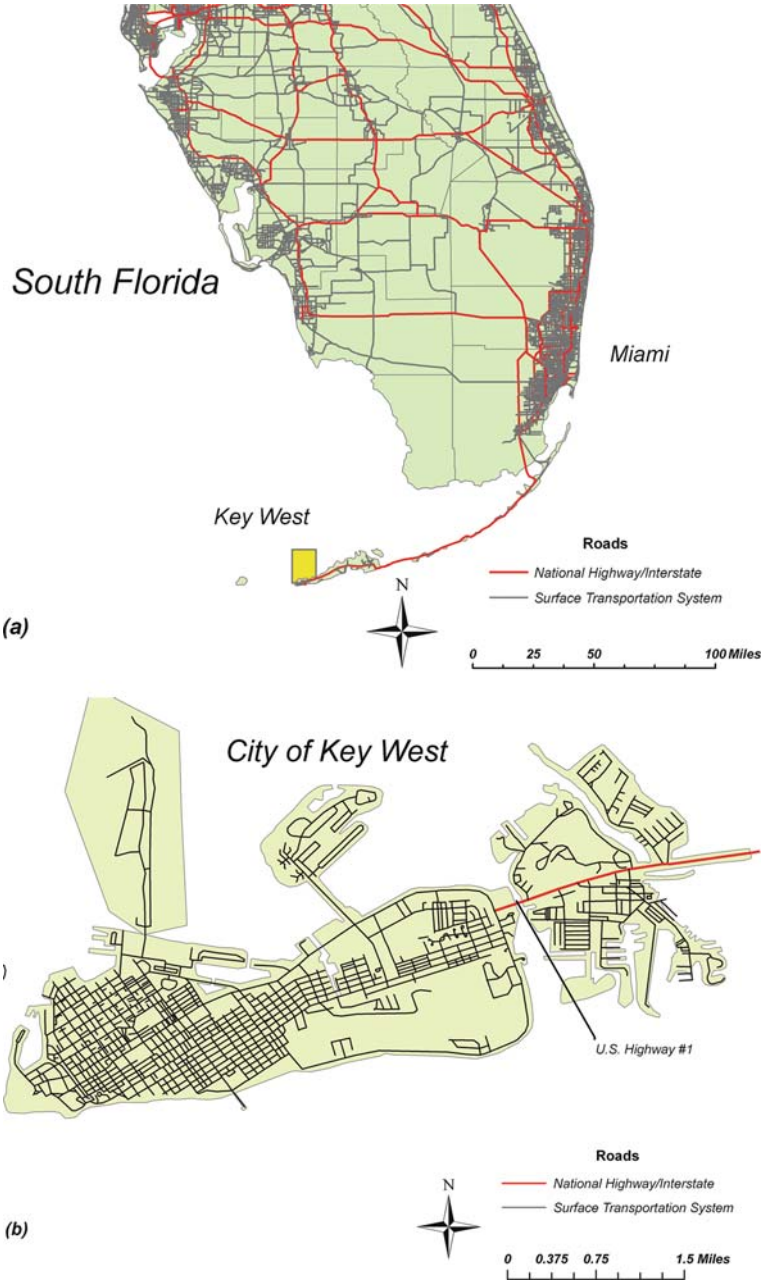

Fig. 19.1 The geographic location of Key West, Florida; **(a)** Key West, the western most Florida Key; **(b)** The City of Key West, Florida

Survey data gathered from the residents of Key West indicate three important aspects of pre-evacuation trip making behavior. First, not all residents evacuate during a mandatory evacuation; some residents make trips but stay in the evacuation zone to "ride out" the storm. Second, residents who evacuated for Hurricane Wilma did not travel from a single origin point directly to an evacuation point, but rather made various pre-evacuation trips that included traveling toward as well as away from the city. Finally, pre-evacuation trips, which include those made by residents who did not evacuate, caused delays not only in the time spent traveling from an origin to a destination, but also resulted in significant delays associated with trip purpose. These delays were usually longer than the delays associated with route traversal.

Our survey gathered data regarding pre-evacuation trips made by Key West residents before either evacuating or "waiting out" Hurricane Wilma in October 2005. Respondents who made pre-evacuation trips were asked to identify origin nodes, which were intersections located nearest the start of their trips, and destination nodes, which were intersections located nearest the end of their trips. A total of 349 respondents filled out the survey, but 62 were eliminated because they did not live in Key West in October 2005, were below 18 years of age at that time, or did not fully complete the survey. Of the remaining 287 respondents, 81 (28%) reported making pre-evacuation trips. Of those who reported pre-evacuation trips, 77 provided usable information regarding the trips they made, the time it took to makes those trips, and the time it took to complete the trip's purpose.

19.2 Pre-evacuation Trip Behavior

Evacuation models make a number of assumptions when calculating ETEs. One of these assumptions is that residents evacuate, and that only evacuating residents make trips. Another assumption is that trips made after an evacuation order is given are solely for the purpose of evacuating. In fact most models rely on this assumption in order to calculate route congestion effects on ETEs. Information collected in Key West suggests that only about half of the residents evacuated during the approach of Hurricane Wilma, and that residents participated in pre-evacuation trips regardless of whether or not they actually evacuated. Trips were often made in directions that were not toward the evacuation point.

A total of 132 origin-destination pairs were reported for the 77 respondents who provided complete information about at least one origin and destination pair. Of these 77 respondents, a total of 35 respondents evacuated the city and 42 respondents waited out the storm. Forty-two respondents made only one trip; of these, 18 evacuated the city in their first trip (they left from an origin node in the city and identified a destination node either inside or outside the city, but reported that they evacuated). Thirty-five of the 77 respondents made at least two trips, and of these 20 only made two trips. Of the respondents that only made two trips, twelve evacuated the city and eight waited out the storm. Fifteen respondents made at least three trips, and ten of these only made three trips. Of the ten respondents that made three

Table 19.1 Trips made and evacuation

Respondents making at least one trip	77
Respondents who made only one trip	42
Respondents who evacuated on their first trip	18
Respondents who waited out the storm	24
Respondents making at least two trips	35
Respondents who made only two trips	20
Respondents who evacuated on their second trip	12
Respondents who waited out the storm	8
Respondents making at least three trips	15
Respondents who made only three trips	10
Respondents who evacuated on their third trip	4
Respondents who waited out the storm	6
Respondents making four or more trips	5
Respondents who evacuated	1
Respondents who waited out the storm	4

trips, four evacuated in their third trip and six did not. The remaining five respondents made four or more trips, and one of those respondents evacuated, while the remainder waited out the storm (Table 19.1).

19.2.1 Trip Flows, Origins, and Destinations

A common assumption in evacuation modeling is that the traffic flow during the evacuation period follows the shortest path to a designated evacuation point. Further, the only trip purpose considered is that people want to evacuate the area as quickly as possible without making any stops along the way. Key West survey data for Hurricane Wilma does not support this assumption.

Evacuation models usually assume trips are solely for evacuation, so the "trip purpose" issue was examined. The Key West survey data discovered that there were a variety of trip purposes (Table 19.2). The majority of purposes (36%) for the first trip are represented in the "Other" category, which includes trips to "purchase water and food", "park a vehicle above the flood stage", "take DVDs to Blockbuster", "[leave] town after getting gas", " [participate in a military] base evacuation", "eat at a restaurant", "go to dinner", "catch a flight in Fort Lauderdale", "[go to the] grocery store," and "look around". The second most common trip purpose was "Go to Work" (34%). The remainder of the respondents took their first trip to perform tasks such as gathering medicines or money, pick up others or protect property (Table 19.2).

The most frequently chosen trip destinations were store (27%) and work (27%). The "Other" category (26%) follows next, and includes "P.T.'s Restaurant", "bar", "boat dock", "parking garage", and "hotel" (Table 19.3). For six respondents, the first trip destination was a local Home Depot.

Thirty-five respondents made a second trip. Similar to the results for the first trip, most respondents (39%) fell into the "Other" category and includes "[attending an] AA meeting", "[moving] to a guest house", "going to a friend's house to ride out the

Table 19.2 Trip purpose

	First trip		Second trip		Third trip		Fourth trip	
	Respondents		Respondents		Respondents		Respondents	
Trip purpose	Number	Percentage	Number	Percentage	Number	Percentage	Number	Percentage
Other	28	36	14	39	7	62	4	80
Go to work	26	34	6	17	1	9	0	0
Pick up person	11	14	4	12	2	14	0	0
Get medicines	6	8	4	12	0	0	1	20
Get money	3	4	6	17	0	0	0	0
Get property protection materials	3	4	1	3	1	9	0	0
Total	77	100	35	100	11	100	5	100

Table 19.3 Trip destination

	First trip		Second trip		Third trip		Fourth trip	
	Respondents		Respondents		Respondents		Respondents	
Trip destination	Number	Percentage	Number	Percentage	Number	Percentage	Number	Percentage
Store	21	27	13	37	3	28	2	40
Work	21	27	10	28	1	9	0	0
Other	20	26	1	3	4	36	0	0
Friend's house	14	18	3	9	2	18	3	60
Home	1	2	8	23	1	9	0	0
Total	77	100	35	100	11	100	5	100

storm", and "[taking] a 13-mile ride on a bike around [the] island." Unlike the first trip, however, getting money and going to work tied for the second most popular trip purpose for the second trip.

The destination for the second trip was also different than the first trip. During their second trip, more respondents traveled to a store (37%), while the percentage traveling to work (28%) was nearly unchanged (Table 19.3). Interestingly, unlike the first trip when 2% of respondents traveled home, 23% of respondents traveled home during their second trip. Also, 12 respondents reported evacuating on their second trip.

As with the first and second trips, most "three trip" respondent purposes (62%) fall in the "Other" category, which includes "[dropping] the car off at above flood", "golfing", "going to the high school", and "[eating at a] restaurant." Four respondents evacuated on their third trip. Four other respondents did not provide adequate information regarding their trip purposes or destinations, and are not included in the trip purpose or trip destination tables. For the 11 respondents who made three trips and provided adequate information, most chose "Other" as the destination (Table 19.3).

Similar to the respondents who made less than four trips, all but one of the five respondents who made four or more trips chose "Other" as the trip purpose. The other trip purposes included "[going to my] mother's trailer", "[going] to friends' house for dinner", and "[helping] a friend close up house." Only one respondent reported getting medicines as the trip purpose. The trip destinations for all remaining trips were either to a friend's house or to the store. Of the four or more trips taken by five respondents, only one respondent evacuated, and this respondent evacuated on his sixth trip.

19.2.2 Trip Direction

Of the 77 respondents making their first trip, nearly an equal number traveled westbound toward the center of the city (38), or eastbound toward US Highway #1 (36; the evacuation point). Three traveled north-south along the roadways or remained in the same location (Fig. 19.2). Of those who traveled eastbound, twenty-four respondents stopped at a destination short of the evacuation point. Thus, traffic flowed in many directions, not just toward an evacuation point.

Unlike the first trip, respondents making at least two trips did not travel in nearly equal numbers east- and westbound. During the second trip, three times as many respondents reported traveling eastbound toward US Highway #1 than westbound toward the city center. Twenty-four respondents traveled eastbound, eight respondents traveled westbound, and three respondents either traveled north-south or identified the same location for their origin and destination pair for the second trip (Fig. 19.3).

A third trip was taken by 15 respondents. Like the first trip, the respondents making a third trip traveled nearly equally eastbound and westbound. Eight respondents traveled toward US Highway #1, and six respondents traveled toward the city. One

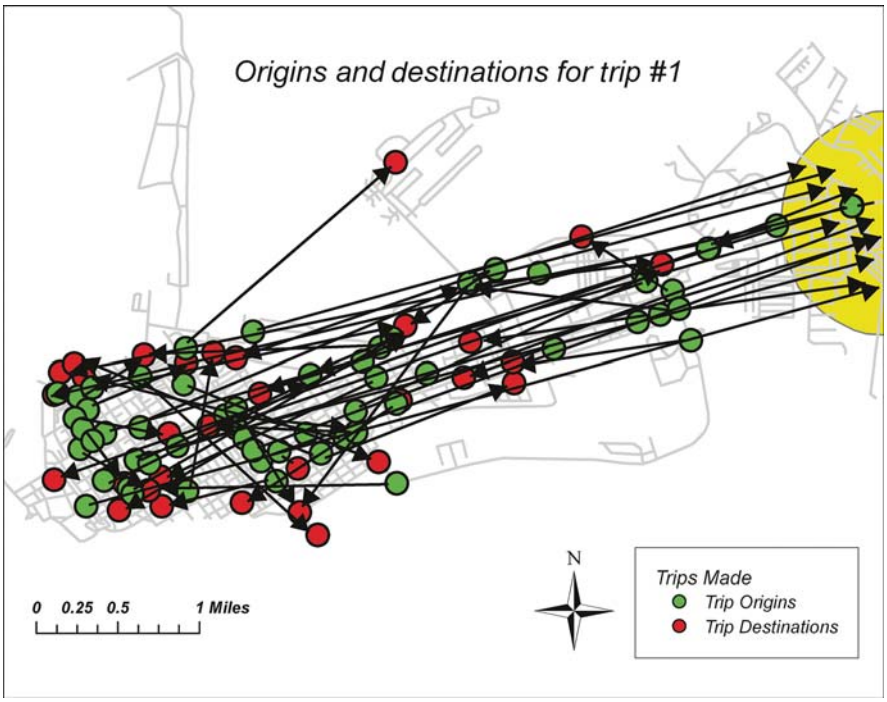

Fig. 19.2 Origins and Destinations for Trip #1

respondent chose the same intersection as both the origin and destination node (Fig. 19.4).

Four or more trips were taken by five respondents. Like the first and third trips, the respondents traveled east and westbound in nearly equal numbers. Three respondents traveled eastbound, and two traveled westbound (Fig. 19.5).

For the first trip, respondents did not report traveling directly toward an evacuation route, but instead traveled both to and away from an evacuation point. Many of the respondents who did travel toward an evacuation point, stopped before actually evacuating the city. Respondents who made a second trip were more likely to head toward the evacuation point; whereas, respondents who made a third or fourth trip reacted like the first trip respondents – traveling in almost equal numbers both eastbound and westbound. Proportionally, more respondents evacuated on their second trip (almost 35%) than respondents who made first (23%), third (26%) or fourth (20%) trips.

Based on the survey data gathered in Key West regarding the trips made in conjunction with the Hurricane Wilma evacuation, residents do not proceed directly to an evacuation point, but rather travel around town before evacuating or waiting out the storm. Of the 77 survey respondents who provided origin and destination node information, 35 respondents eventually evacuated. Respondents reporting pre-evacuation trips primarily traveled either eastbound toward the evacuation point

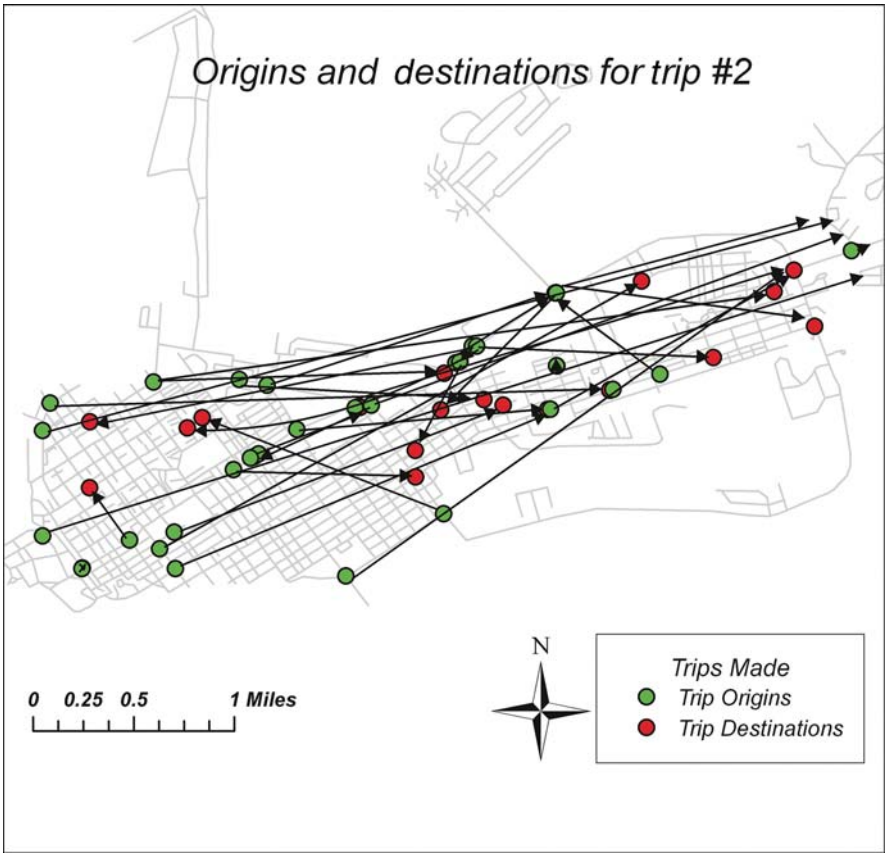

Fig. 19.3 Origins and Destinations for Trip #2

or westbound toward the portion of the city known as Old Town, which is where the original city of Key West was located. For the most part, respondents traveled in equal numbers either east or west. This finding counters the underlying assumption in evacuation models that residents will use the shortest path to travel to an exit point as soon as the evacuation order is issued. In addition, trip purpose and destination were not concentrated solely on evacuation issues. Trips commonly associated with evacuation behavior, such as obtaining medications, money or property protection materials, were few when compared to trips made for "other" causes or work-related trips. Trip destinations did concentrate on trips made to a store, supporting the idea that people are gathering supplies regardless of evacuation intentions.

19.2.3 Trip Chaining

Of the 77 survey respondents reporting pre-evacuation trips, just under half (35) engaged in 'trip chaining" to accomplish their trip purposes. Trip chaining is an important part of pre-evacuation trip making behavior. An example of such behavior

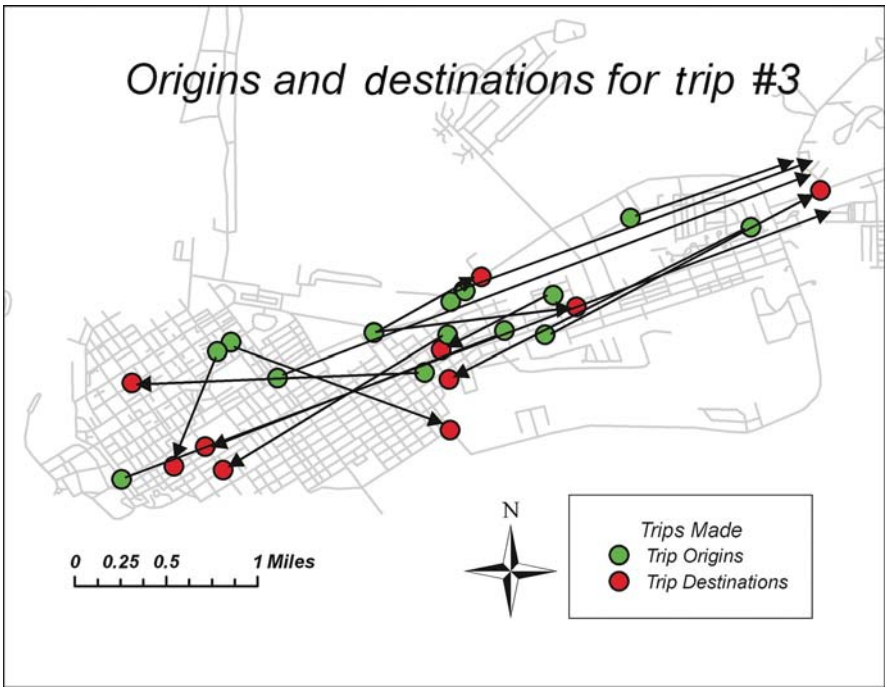

Fig. 19.4 Origins and Destinations for Trip #3

is provided in Table 19.4, which illustrates one survey respondent's actions. This person's pre-evacuation trip chaining demonstrates the relationship between trip purpose, destination, and delay.

This particular respondent is a married, Hispanic, female, 60–74 years old, responsible for children, or the caretaker for others. A high school graduate with an income of $100,000–$149,000, she owns a single family home and has two cars at her disposal. At 12:00 PM on Saturday, October 22, 2007, she left an origin near the intersection of 15th and Flagler Avenues, and traveled 15 min to a destination near the intersection of 10th and Flagler Avenues where she picked up a passenger (Table 19.4). According to the respondent, the trip from origin to destination took 15 min, and it took 45 min to complete the purpose for the trip – to pick someone up. The respondent then reported that she departed on her second trip at 1:30 PM. There is an unexplained delay of 30 min between the time the respondent reported leaving her origin at noon, and the hour it took for the respondent to drive to the destination and complete her task. At 1:30 PM, she and her passenger traveled 20 min to Walgreens on Roosevelt Avenue to pick up some medications. The delay associated with this stop was about an hour. At 2:50 PM she started her evacuation of the city; it took her 30 min to exit to US Highway #1 at approximately 3:20 PM. The longest delays for this respondent were associated with trip purpose, not en-route delays. For both entries in Table 19.4, the ratio of trip purpose delays to en-route delays is 3–1.

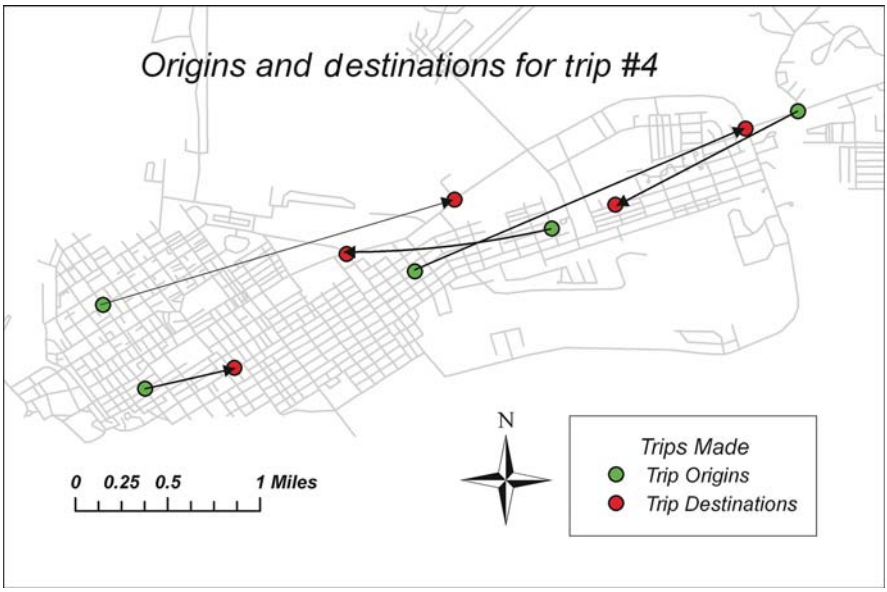

Fig. 19.5 Origins and Destinations for Trip #4

Table 19.4 Trip chaining example for repondent #201

Origin	Start time	Trip purpose	Destination	Travel time	Purpose time	Ratio of purpose:travel delay times
15th and Flagler	12:00 PM	Pick-up	10th and Flagler	15 min	45 min	3:1
Unexplained 30 minute delay between end of Trip 1 and beginning of Trip 2						
10th and Flagler	1:30 PM	Medicine	Walgreens on Roosevelt	20 min	60 min	3:1
Unexplained 20 minute delay between end of Trip 2 and beginning of Trip 3						
Walgreens on Roosevelt	2:50 PM	Evacuate	U.S. Hwy 1	30 min		

Figure 19.6 illustrates the trips taken by the 17 respondents who engaged in trip chaining before evacuating (the 18 respondents who evacuated on their first trip and did not engage in trip chaining are not mapped). The grey origin and/or destination nodes are located throughout the city. The evacuees' first trip is identified by a solid black line, and the second trip is identified by a hatched line. Twelve respondents made two trips before evacuating Key West. Of these, six reported that they

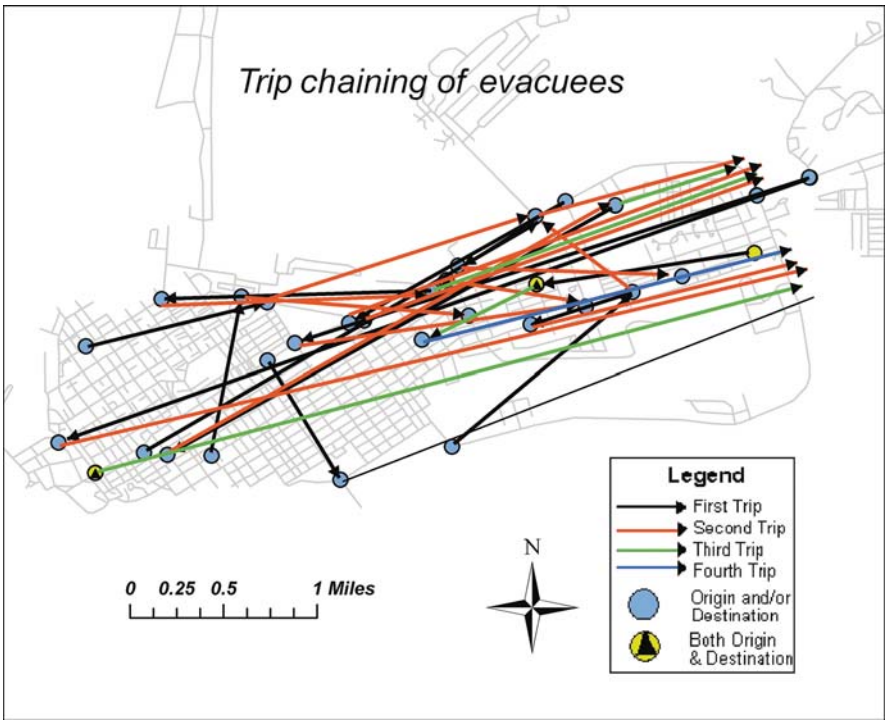

Fig. 19.6 Trip chaining of evacuees

evacuated the city of Key West, but identified a node inside the city as their final destination location before evacuating. One possible reason for these seemingly contradicting replies could be the lack of realization that a journey from the last identified inner-city destination to someplace outside the city is considered a trip. Four respondents took at least three trips before evacuating; these trips are identified by black lines within grey backgrounds. Of these respondents, two reported that their first and second trips occurred at the same intersection (the black nodes within circles identify locations where respondents reported the same intersection as origin and destination nodes). Three respondents evacuated on their third trip, and one evacuated on the fourth trip; the fourth trip is identified by the dashed line.

Trip chaining, a result of multipurpose trip making, is a well established area of study in transportation geography (Pipkin 1995; Thill and Thomas 1987; Noland and Thomas 2005; Wallace et al. 2000; Krizek 2003). The literature on trip chaining clearly indicates that chains reflect the spatial structure of an area and the locations of intervening opportunities. In our study, opportunities included the location of pharmacies, banks and ATMs, and grocery, convenience, and hardware stores. In a study of trip chaining and evacuation behavior, Murray-Tuite and Mahmassani (2003) found that trip chaining takes place as families attempt to gather and evacuate together. The obvious implications from that work and ours are that future

evacuation models should identify common opportunity sets, locate them in a space, and incorporate behavioral modules that allow the affected population to make trips with multiple purposes, not just direct evacuation. Moreover, the delays at stops are significant and should be incorporated into evacuation time estimates. Agent based models, such as those by Chen (2006) and Chen and Zhan (2008), offer a promising method for incorporating such behavior.

19.2.4 Temporal Delays

Evacuation models usually assume that delays take place along links. For example, when faced with link congestion some of the models force agents to take links with underused capacity. Survey data collected for both respondents who evacuated and respondents who did not suggest that delays do occur during the travel from origin to destination; however, longer delays are associated with trip purpose. As derived from the survey, the average travel time from origin to destination for the first trip was about 16.5 min for all respondents, and for respondents who did not evacuate on the first trip, the average delay associated with trip purpose was 44 min. Unlike the first trip, the average travel time from origin to destination for the second trip was about 10 min longer (about 25.5 min), and the average delay associated with trip purpose was the same as the first trip (about 44 min). The average travel time from origin to destination for the third trip was about 10 min long, and the average delay associated with trip purpose was longer than the first or second trip delay at slightly less than one hour. Finally, the average travel time from origin to destination for the fourth, fifth, and sixth trips was about 8.5 min long, and the average delay associated with trip purpose was the longest of all at 74 min.

Though some evacuation models can mimic a delay in respondent evacuation by categorizing respondents into specific groups, and then coding each group to begin evacuation at different times during the simulation, the models do not take into account the delay caused by trip purpose. Based on this research, the longest delays are associated with trip purpose. Indeed, one respondent reported a delay of four hours at the local Home Depot store.

19.3 Implications for Evacuation Models

The evacuation models used to calculate evacuation time estimates do not inherently include an option to incorporate various pre-evacuation trips and time delays into the evacuation time calculation. The models also do not provide options for traveling toward an evacuation zone (i.e., away from the evacuation point) and pausing to complete a trip. The focus of these models is on delays associated with congested links, not on delays associated with stops and trip purpose. Many models assume that residents evacuate directly from an origin to an exit point at a particular time and, though there may be delays based on link congestion, the evacuees do not make other trips.

One of the reasons that models do not accurately reflect pre-evacuation trip delays may be that pre-evacuation trip data are not readily available. A second reason may be that the calculation of evacuation time estimates becomes more complex and computationally demanding when one attempts to incorporate data regarding delays associated with trip purpose. In either case, evidence of trip chaining makes questionable the assumption by evacuation models that evacuees always choose the shortest travel path from origin to destination.

To establish how the findings from this study could inform current evacuation models, several existing models have been reviewed. This review provides a basis for further research into the extension of model attributes to allow for the incorporation of pre-evacuation trips and delays made before evacuating an area or returning home to wait out a storm.

One method for depicting evacuation scenarios is through simulation (Axelrod 1997). Simulation models incorporate the actions of agents, which can either represent a single element (one vehicle) or an aggregated number of elements (more than one vehicle). Traffic movements on a road network are simulated through a series of behavioral rules linked with each agent's attributes (Axtell 2000). Unfortunately, current evacuation models limit the types of behavior each agent can reflect. For example, some models allow agents to be categorized, and each category is then allowed to evacuate at different times to reflect a staged evacuation (Chen 2008). However, the number of categories is limited and each agent must act in the same way. None of the agents can stop mid-way in the evacuation process to perform a trip purpose. Further, Noltenius (2008) found that many residents ignore staged evacuation orders.

Some models can assign each agent a route, a speed, and the probability of a vehicular break-down. Each agent then moves in the traffic stream with one car following another in an orderly fashion (Mei 2002). In microsimulation models such as this, the large numbers of agents make the processing of each evacuation computationally demanding and time-consuming (Pidd et al. 1993). This problem can be addressed through advances in computer hardware and software, and in the use of high performance computing clusters. Another approach is meso-simulation (Chen 2008) where traffic flow is composed of each agent representing a platoon of vehicles where movement is guided through speed, flow and density (Mei 2002). This approach prohibits the simulation of individual agent delay based on trip purpose, where one vehicle leaves at a different time to travel to a location and then waits for the trip purpose to be completed. As a result, the resulting evacuation time estimate values in these more aggregated models are more unreliable than in disaggregated models (Chen 2006). Another issue with the aggregate approach occurs when each aggregated agent passes an exit point – the assumption is that two, three, four or even more vehicles pass the exit point at exactly the same time, a phenomena that probably is rare.

Evacuation models also can be differentiated based on those that use dynamic versus static road network assignment. In dynamic models, road demand changes at each time interval. This process allows agents entering the network to choose a path to an exit point based on updated travel times and congestion. However, these

models also assume that agents always choose a different path when congestion occurs, and will take the shortest path to travel to the nearest exit point. There is also an assumption that agents have perfect knowledge of the road network, which is unlikely during an evacuation. On the other hand, static assignment models assume that road capacity is constant. In such models, agents do not change routes nor are they affected by other agents (Wilmot and Mei 2004).

In order to gain a fuller understanding of evacuation models with regards to conducting future research, a discussion of some currently used Hurricane and nuclear evacuation models is appropriate. Our purpose is to gather information regarding the specific inputs of these models to evaluate the limitations each has with respect to integrating pre-evacuation trips in the calculation of the evacuation time estimate.

Though the WITNESS evacuation model provides evacuation times that take into account delays based on either bi-directional or unidirectional traffic flows, evacuation times are calculated on the accident rate and evacuation start time (Farahmand 1997). Evacuation times are based on the aggregated agents being assigned to the "resident" or "tourist" category. Only two different start times are allowed based on category designation. Additional categories would allow for many more groups to be represented. There are three road types: primary, secondary, and other, and different links on the road network are assigned different road capacities. As the model is run, demand decreases as road capacity is met (Farahmand 1997). However, no agent category allows for delays based on trip purpose or allows an agent to travel toward the evacuation zone. Agents that do not participate in evacuation are assumed to remain stationary and do not make any trips. Furthermore, WITNESS results have been known to calculate that higher demand, delays and late evacuees do not affect evacuation times when 100% of residents are evacuated (Farahmand 1997).

Unlike WITNESS, the Configurable Emergency Management and Planning System (CEMPS) model allows for multiple evacuation destinations to be created, and the geographic region is divided in zones, which dictate the phasing of the evacuation (Pidd et al. 1993). Link choice is based on link capacity (Alsnih and Stopher 2004), which also assumes perfect knowledge of the network. Evacuation times incorporate not only population evacuation, but the time needed to get relief vehicles into the affected area. The model can include delays and congestion based on vehicle break-downs, and re-routing based on link capacity (Pidd et al. 1993). However, the model assumes that all agents that are activated at the beginning of the evacuation are constantly active throughout the calculation of the evacuation time estimate. No agents are allowed to "wait" in order to simulate the time it takes to complete a trip task, and no vehicles are allowed to travel and then stop without evacuating in order to mimic an evacuee making an inner city pre-evacuation trip (Pidd et al. 1993).

The Network Emergency Evacuation Model (NETVAC) uses a GIS platform to display the movement of vehicles, and estimate network clearance times. Agents can replicate behaviors of three different categories: resident, transient and special facility populations. These evacuees are assigned to the evacuation network at varying times based on a particular category (Earth Tech, 2006). Each of the three categories

is also given attributes pertaining to evacuation notification; preparation and mobilization times. Different traffic flows are simulated based on road type (rural, residential, or city) and each road type is assigned a lane width, speed limit and traffic control device (stop sign, signal light, etc.) (Earth Tech, 2006). Each agent's route choice is determined at each node based on the shortest path to the exit point and link congestion. When run in the normal mode, the model assumes that agents have delays based on existing traffic control devices. When in the override mode, the model does not make these assumptions. However, the model will only calculate the time needed for 100% evacuation. The model does not incorporate the concept that some residents will make trips without evacuating, nor does the model allow for delays at nodes in order to simulate trip purpose completion times. In addition, the model has some inherent difficulty calculating accurate evacuation times for hurricane evacuation because it moves agents away from one single point of danger (Alsnih and Stopher 2004). Although the model can track from a single origin point to a single destination point, it cannot track multiple origins to multiple destinations (Southworth 1991).

Finally, the Oak Ridge Evacuation Modeling System (OREMS) is a disaggregate model that simulates traffic demand, response and flow in a staged evacuation. The geographic region is divided into three types of evacuation zones: Immediate Response (the area closest to the disaster), Protective Action (an area slightly farther away), and the Precautionary (the area where no adverse effect is expected). Links represent unidirectional roadways, which do not allow for the agents to backtrack or travel away from the exit node using the same link; however, parallel unidirectional links can be incorporated to represent roadways leading away from the exit. Nodes represent entry or exit points along the network. Unlike the other models, entry into the network can take place at either links or nodes. Characteristics are assigned to each link and node, including road capacity and traffic controls. Agents are assigned entry onto a link or node, at each node turn percentages force agents onto certain links, and road closures and signal timings add evacuation delay. Evacuation start delays are based on household characteristics, the time-of-day, and the evacuee's location (Franzese 2003). OREMS also assumes the agent chooses the shortest route to evacuate (Franzese 2003). All of the evacuation models described above assume evacuation will take place using personal vehicles – none take into consideration public transit.

19.4 Conclusions

Events of recent years, and in particular the plight of the US Gulf Coast during Hurricane Katrina, have made it clear that a fuller understanding of human response to evacuation orders is needed. While there have been advances in agent based evacuation models, we believe the findings reported here and elsewhere (Noltenius 2008) are the first empirically-based studies of pre-evacuation trip making behavior. The survey findings have implications for evacuation planners, evacuation modelers, and social scientists wanting to better understand how individuals and communities may

react to impending natural disasters. In particular, many of the assumptions incorporated into current models regarding trip purpose, trip direction, and route delays appear too simplistic. More effort is needed to incorporate delays associated with trip purposes, trip directions that lead away from (not toward) evacuation points, as well as trip chaining behavior. Incorporating these criteria should produce model output that more accurately reflects traffic congestion and delays during evacuation.

References

Alsnih, R. and Peter, S. (2004). *A Review of the Procedures Associated with Devising Emergency Evacuation Plans.* Institute of Transport Studies: The Australian Key Centre, University of Sydney.

Alsnih, R., John, R., and Peter, S. (2005). Understanding Household Evacuation Decisions Using a Stated Choice Survey – Case Study of Hurricanes. Paper presented at the Transportation Research Board (TRB) 84th Annual Meeting.

Axelrod, R. (1997). Advancing the Art of Simulation in the Social Sciences. In R. Conte, R. Hegelsmann, and P. Terna (Eds.), *Simulating Social Phenomena*. (pp. 21–40). New York: Springer.

Axtell, R. (2000). Why Agents? On the Varied Motivations for Agent Computing in the Social Sciences. Center on Social and Economic Dynamics Working Paper No. 17.

Ben-Akiva, M., Bowman, J., Ramming, S. and Walker, J. (1998). Behavioral Real-ism in Urban Transportation Planning Models. http://people.bu.edu/joanw/JW_BREAL.pdf. Accessed on January 30, 2007.

Chen, X. (2006). Microsimulation of Evacuation Strategies. Unpublished Ph.D. Dissertation. Department of Geography, Texas State University – San Marcos.

Chen, X. (2008). Microsimulation of Hurricane Evacuation Strategies of Glaveston Island. *The Professional Geographer* 60(2), 160–173.

Chen, X. and Zhan, F.B. (2008). Agent-based Modeling and Simulation of Urban Evacuation: Relative Effectiveness of Simultaneous and Staged Evacuation Strategies. *Journal of the Operations Research Society* 59, 25–33.

Cova, T.J. and Johnson, J.P. (2002). Microsimulation of Neighborhood Evacua-tions in the Urban-Wildland Interface. *Environment and Planning A* 34(12), 2211–2229.

Cutter, S. (2006). The Geography of Social Vulnerability: Race, Class, and Ca-tastrophe. Social Science Research Council. http://understandingkatrina.ssrc.org/Cutter/. Accessed 20 July 2006.

Dow, K. and Cutter, S.L. (2000). Public Orders and Personal Opinions: HouseholdStrategies for Hurricane Risk Assessment. *Environmental Hazards* 2, 143–155.

Earth Tech. (2006). ASG at Earth Tech: EPS Computer Models – NetVac 2 Overview. http://www.calpuff.net/ep/netvac/netvac2.htm. Accessed 7 June.

Farahmand, K. (1997). Application of Simulation modeling to Emergency Population Evacuation. *Proceedings of the 1997 Winter Simulation Conference*. 1181–1188.

Franzese, O. (2003). OREMS 2.6 User's Guide. Oak Ridge National Laboratory.

Hobeika, A.G. and Jamei, B. (1985). MASSVAC: A Model for Calculating Evacuation Times Under Natural Disasters. *Emergency Planning, Simulation Series* 15(1), 23–28.

Krizek, K. (2003). Residential Relocation and Changes in Urban Travel: Does Neighborhood-Scale Urban Form Matter? *Journal of the American Planning As-sociation* 69(3), 265–281.

Mei, B. (2002). Development of Trip Generation Models of Hurricane Evacua-tion. Louisiana State University. Department of Civil and Environmental Engi-neering, A Thesis. http://etd.lsu.edu/docs/available/etd-0612102-192601/unrestricted/Thesis.pdf. Accessed 20 July 2006.

Murray-Tuite, P.M. and Hani, S.M. (2003). Model of Household Trip chain Sequencing in Emergency Evacuation. *Transportation Research Record* 1831, 248–257.

Noland, R. and Thomas, J. (2005). Multivariate Analysis of Trip Chaining Behaviour. *European Regional Science Association Conference Papers*. http://www.ersa.org/ersaconfs/ersa05/papers/541.pdf. Accessed 27 July 2006.

Noltenius, M.S. (2008). Capturing Pre-evacuation Trips and Associative Delays: A Case Study of the Evacuation of Key West, Florida for Hurricane Wilma. Dissertation, University of Tennessee.

Pidd, M., de Silva, F.N., and Eglese, R.W. (1993). CEMPS: A Configur-able Evacuation Management and Planning System Progress Report. *Proceedings of the 1993 Winter Simulation Conference*. The Management School Regional Research Laboratory. Department of Management Science: Lancaster University, United Kingdom.

Pipkin, J.S. (1995). Disaggregate Models of Travel Behavior. In S. Hanson (Ed.), *The Geography of Urban Transportation*, Second Edition. (pp. 188–218). New York: Gilford.

Southworth, F. (1991). Regional Evacuation Modeling: A State of the Art Review, Centre for Transportation Analysis, Oak Ridge National Laboratory, A Report Prepared for the U.S. Department of the Army.

Thill, J.C. and Thomas, I. (1987). Toward Conceptualizing Trip chaining Behav-ior. *Geographical Analysis* 19:1–17.

Wallace, B., Barnes, J., and Rutherford, G. (2000). Evaluating the Effects of Trav-eler and Trip Characteristics on Trip Chaining, with Implications for Transporta-tion Management Strategies. *Transportation Research Record* 1718:97–106.

Wilmot, C.G. and Bing, M. (2004). Comparison of Alternative Trip Gen-eration Models for Hurricane Evacuation. *Natural Hazards Review* 6(3):170–178.

Wolshon, B., Urbina, E., Wilmot, C. and Levitan, M. (2005). Review of Policies and Practices for Hurricane Evacuation. I: Transportation Planning, Preparedness, and Response. *Natural Hazards Review* 6(3):129–142.

Chapter 20
Micro-Level Emergency Response: 3D Geometric Network and an Agent-Based Model

Jinmu Choi and Jiyeong Lee

Abstract This chapter discusses a micro-scale emergency response model that integrates GIS with an agent-based model. The first part of the chapter explains 3D geometric network construction for buildings using GIS. Computer-aided design data used commonly for building blueprints have been converted to a 3D geometric network through wall extraction and 3D topology construction. Two wall extraction methods (vector-based medial-axis transformation and raster-based thinning) are tested. The resulting 3D geometric network provides agent-based models with routing information to determine the shortest path to outer exits of a building. The second part explains what an agent-based model for building evacuation entails. In the building evacuation simulation, the only moving agents considered are human beings. To model human behavior, we adopted a generalized force model to incorporate a mixture of socio-psychological and physical forces of human-to-human and human-to-wall interactions influencing agents' behavior. We tested two simple evacuation scenarios: evacuation with and without a jamming situation by enforcing different numbers of people in a room. As expected, the results showed that the average rate of evacuation increased continuously before jams, decreased during jams, and eventually increased again as individuals escape from the jams.

Keywords 3D geometric network · 3D topological structure · Medial-axis transformation · Thinning · Agent-based model · Building evacuation

20.1 Introduction

Emergency services are relying increasingly heavily on Geographic Information System (GIS) (Kevany 2003). This chapter discusses the use of micro-level GIS for emergency response. Since the World Trade Center attacks, interest in micro-level

J. Choi (✉)
Department of Geosciences, Mississippi State University, MS 39762-5448, USA
e-mail: jc778@msstate.edu

P.S. Showalter, Y. Lu (eds.), *Geospatial Techniques in Urban Hazard and Disaster Analysis*, Geotechnologies and the Environment 2, DOI 10.1007/978-90-481-2238-7_20,

emergency response has increased. These interests are critically related to national security concerns. The ultimate emergency management system would function on a macro scale (such as, urban areas with low levels of detail), but also be able to "zoom in" and provide detailed information about the world on a micro scale (such as, an individual building or room). For example, an emergency response GIS in a large city might route responders to a building through the quickest path, and then route them to the room providing emergency shelter through the quickest path once they arrive at the building's entrance (Lee and Kwan 2005). Therefore, emergency response in a building depends upon information regarding the internal structure of the building and the situation can be simulated by multi-agent modeling in order to visualize possible results and help decision-makers avoid disastrous situations.

While the technology to model and analyze two-dimensional (2D) geometric networks is well developed, the technology for the generation of three-dimensional (3D) geometric networks to represent the internal structure of buildings in a micro-level urban environment is still nascent. The first part of this chapter deals with building a 3D geometric network. The discussion includes data conversion from computer-aided design (CAD) files and scanned blueprints to 3D vector data, 3D topology construction using 3D vector data, and 3D geometric network structure from 3D topology data.

A model is a simplified representation of reality (Longley and Batty 2003). A model can be dynamic if the output represents a later point in time than the input and represents time steps in the operation of a dynamic process (Goodchild 2005; Longley et al. 2005). Dynamic models are used to assess different management scenarios by attempting to project quantifiable impacts into the future (Castle and Crooks 2006). As a dynamic model, agent-based modeling has become one of the key computational approaches to simulate collective outcomes from complex geographic phenomena based on individual decisions. Therefore, the second part of this chapter discusses a multi-agent model as a dynamic model for geospatial simulation in a micro-level urban environment. Using the 3D geometric network, two building evacuation cases (with and without jamming) will be simulated using a multi-agent model. Among various multi-agent modeling tools (such as Swarm, MASON, RepastPy, StarLogo, NetLogo, OBEUS, AgentSheets and AnyLogic), Agent Analyst based on RepastPy is used here since it is tightly coupled with ArcGIS® for data input, storage, and visualization.

In Section 20.2, 3D geometric network structure is discussed and used to create the shortest path information for the agent-based model in order to simulate the building evacuation process. The third section presents two simple building evacuation models with Agent Analyst. Finally, several issues are identified in Section 20.4 and the findings are summarized in Section 20.5.

20.2 3D Geometric Network for Internal Structure of a Building

As GIS continues to mature, there is increasing demand by various disciplines, including cadastre management and emergency services, for 3D modeling (Zlatanova et al. 2002; Coors 2003; Zhou and Zhang 2003; Benhamu and Doytsher

2003; Kevany 2003). For example, if there is an emergency situation in a room in a building, 3D GIS can provide the quickest path for evacuation. 3D modeling has become a tool for GIS analysis with varying levels of success (Zlatanova 2002). However, most current commercial GIS typically do not provide tools to model 3D sub-unit structures. They only include surface-based 3D representation methods.

20.2.1 3D Topological Models

Most commercial GIS systems are primarily concerned with 3D visualization. The Environmental Systems Research Institute, Inc. (ESRI®) provides 3D Analyst, which allows users to generate surfaces, compute volume, and perform viewshed analysis. ArcScene is another product from ESRI®, which emphasizes visualization through texture mapping and fly-throughs. The Earth Resources Data Analysis System (ERDAS®) Imagine VirtualGIS™, Intergraph® GeoMedia®, and PAMAP™ GIS Topograph tool from PCIGeomatics® also provide the ability to perform 3D fly-throughs over terrain. These systems do not provide tools for modeling and analyzing the internal structure of buildings (Zlatanova et al. 2002).

Boundary-based representations (B-Rep) are the most popular method for storing details of 3D internal structures for analysis. B-Rep models describe objects in terms of three boundaries: faces, edges, and nodes. Coors (2003) has proposed an Urban Data Model based on the B-Rep model that is query-oriented and allows the querying of relationships between rooms. However, these relationships are implicit and some processing power is needed to interpret them. Billen and Zlatanova (2003) have proposed a Dimensional Model that considers objects to be composed of "dimensional elements," whereby relationships between objects are defined by the type of dimensional elements the objects share. This system allows for topographical associations between any combination of one, two, and three-dimensional objects to be analyzed. The Dimensional Model is intended to handle complex 3D relationships; however, it would also be resource intensive when applied to an entire building.

While B-Rep models provide the level of detail needed for 3D analysis, most require a large volume of data and considerable power to process. To address these issues, Lee and Kwan (2005) proposed a simple 3D topological data structure called a Combinatorial Data Model (CDM). The structure of a CDM does not represent the volume or shapes of objects but their relationships (e.g., adjacency and connectivity). CDM consists of node-relation structure (NRS) and hierarchical network structure (HNS). In an NRS, a node represents a room and an edge connects two nodes if they share a wall horizontally or vertically, therefore providing adjacency information. An HNS, which is a subset of an NRS, stores an edge and connects two nodes *only* if they are connected through a door or a stairway, therefore providing connectivity information. While this type of 3D topological structure may not be useful for cadastral purposes, it supports fast processing 3D analysis using the concise data structure of the internal sub-units of buildings. Which raises the question: how can we acquire detailed information about the sub-units (rooms) found within buildings?

3D topological data for many buildings are already available. CAD has been widely used since the 1980s (Marion 2004), and today, CAD building data are widely available in the form of construction blueprints. Unfortunately, while CAD data contain details regarding the internal structure of buildings, they lack topological information for 3D analysis (Stevens and Choi 2006). Therefore, because the agent-based evacuation model proposed in this chapter requires connectivity information to determine the shortest path from an occupant's location to outer exits, it is necessary to construct 3D topological data from the CAD files.

20.2.2 Conversion Algorithm from CAD Data to 3D Topological Data for Buildings

A geometric network for 3D sub-units of buildings can be created using two steps: 3D topological data extraction and geometric network construction. In this chapter, we tested both a vector-based (Stevens and Choi 2006) and raster-based wall extraction method for 3D topological data from CAD data. While a vector-based wall extraction method can extract wall structure from CAD data, a raster-based method is required for wall extraction from the scanned images of the paper-based blueprints. We adopted Lee's (2004) method to build a 3D geometric network from the extracted 3D topological data for further evacuation simulation.

3D topological data extraction requires wall extraction and topological node-relation extraction. To extract wall structure, raster-based or vector-based approaches can be applied. Stevens and Choi (2006) have developed a vector-based wall extraction method (Fig. 20.1a) using a simple medial-axis transformation (MAT). The MAT algorithm requires three steps. First, bisectors of the inner angles at each vertex of the wall polygon are created. Second, terminal and junction nodes are extracted. If two inner bisectors meet inside of a wall polygon, the intersecting point is a terminal node. Alternatively, if an inner bisector meets a vertex or a line segment of the wall polygon, a junction node is located halfway between the origin of the inner bisector and the meeting point. In the third step, all terminal nodes are connected through the junction nodes. While useful, the MAT algorithm only works for simple rectangular sub-unit structures in a building. If the building's sub-units are complex, a different MAT algorithm such as straight MAT (Prasad and Rao 1998; Eppstein and Erickson 1999; Haunert and Sester 2004) or the ArcGIS® THIN operator should be considered for extracting the walls of such sub-units. Of particular interest is the ArcGIS® THIN operator, which can extract skeletons of walls from raster data after vector (CAD data) to raster conversion (Fig. 20.1b). The thinned raster data then needs to be converted to vector line segments. Although skeleton lines may not represent the exact medial-axis, they are appropriate for representing walls and identifying rooms in a building.

The topological node-relation (TNR) algorithm builds a 3D topological node-relation structure, in which a node represents a room and a relationship (e.g., adjacency and connectivity) is represented by an edge. The TNR algorithm is applied to each floor to construct horizontal topological information (Fig. 20.1c), and it

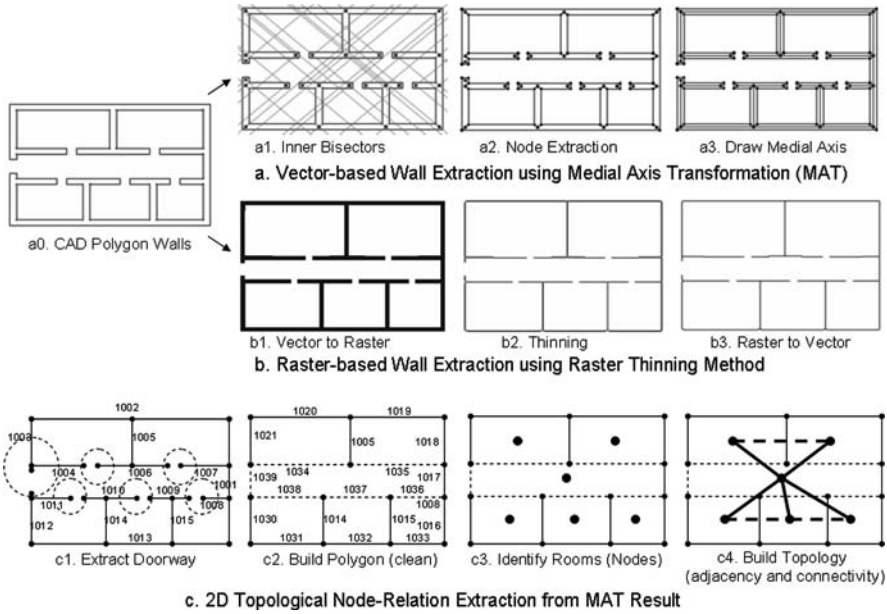

Fig. 20.1 Wall extraction and topological data construction for each floor from CAD data

requires four steps. First, doorways are closed using a user-defined circle at each end node in order to create a room polygon. The circle's radius represents the maximum door size, and the doorway data are stored separately for later use in building connectivity. Second, the ArcGIS® Build (or Clean) operator is used to split any line segments shared by three rooms (the assumption is that a wall is only shared by two rooms). Third, a node is created for each room. Fourth, the nodes are connected by edges in order to build 3D topology information. All edges represent adjacency, and some of the edges represent connectivity if they pass the wall that has a doorway. Consequently, horizontal TNR data for each floor can be linked by vertical connectivity if the sub-unit represents a stairway (Fig. 20.2). If the sub-unit is a room, the room is vertically adjacent to the rooms found above and below.

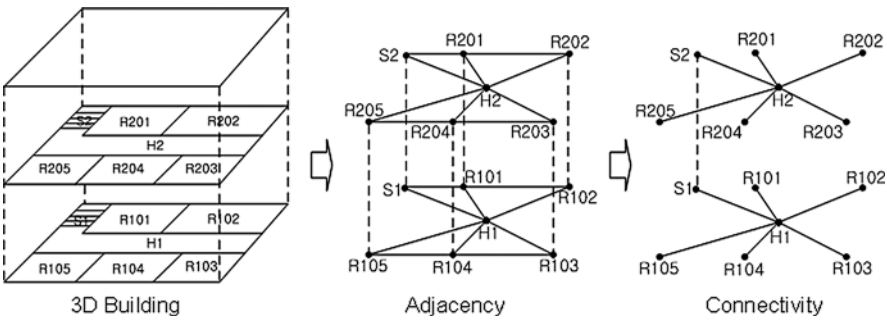

Fig. 20.2 3D topological data structure

20.2.3 3D Geometric Network for Evacuation Model

To perform shortest path analysis, 3D topological data should be converted to a 3D geometric network structure. In 3D topological data, hallways are represented by nodes that actually represent rooms. Since hallways are spaces for moving, they should be recognized as edges that connect rooms for navigation. Building 3D geometric network from a 3D topological data structure (TDS) requires two steps (Lee 2004) (Fig. 20.3). First, nodes that represent hallways are converted to edges, which is an easy process because each node in TDS has its own room ID. Hallway nodes need to be removed and hallway polygons should be converted to edges using the MAT algorithm in the TDS construction tool. Second, all edges from the other nodes need to be adjusted perpendicularly to the hallway edges in order to maintain the shortest connectivity between nodes.

In the next section, an agent-based model is described for the evacuation simulation of a building. Each agent (e.g., human) in the evacuation simulation utilizes the shortest path to reach the nearest outer exit from his or her location in a building. To adopt the shortest path information, the 3D geometric network (see Fig. 20.3) that was originally created from the CAD data is used during the evacuation modeling.

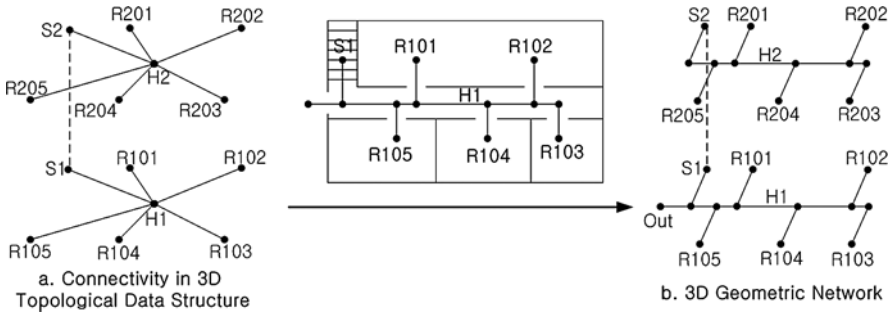

Fig. 20.3 3D geometric network from 3D topological data structure (Lee 2004)

20.3 Geospatial Modeling Using Multi-Agent Model

20.3.1 Agents and Agent-Based Models

The concept of agent depends on the application domain. Any type of independent component (i.e., software, model, individual) can be an agent. Nonetheless, there are several features that are common to most agents (Wooldridge and Jennings 1995; Frankline and Graesser 1996; Epstein 1999; Torrens 2004; Macal

and North 2005). First, agents are autonomous units who can process and exchange information for independent decisions. Second, agents permit the development of autonomous individuals. Groups of agents are simply amalgamations of similar autonomous units. Third, agents are active because they exert independent influence in a simulation. Agents can have goals to achieve, a sense of their surroundings, the ability to solve complex problems, the ability to communicate, mobility in the space within a model, and can adapt by altering their state (Castle and Crooks 2006).

Agent-based models are comprised of multiple, interacting agents situated within a model or simulation environment. The elements of an agent-based model include agents, relationships, and environments. Agents have their own states and behaviors. The behavior of agents can be synchronous or asynchronous according to the action schedule. That is, the behavior of agents depends on whether every agent performs actions in the same time step or if agent actions are scheduled by the actions of other agents. The results of the behavior modify their own and/or others' status. Relationships between agents are specified by linking agents and by linking agents with other entities within a system. Environments define the space in which agents operate, serving to support their interaction with the environment and other agents.

In this chapter, the agent-based simulation of a building requires five types of input information: walls, rooms, doors (or exits), a geometric network, and human beings. Among these input data, humans and rooms are agents. Human beings are moving agents that navigate to exit the building according to their own decisions derived from their own states and behaviors. Human data need to be created manually and have Room ID information based on their locations. Rooms are static agents that update their own states according to the states of neighboring rooms and provide a state (or, type of situation) that can be encountered by moving agents. For example, if a room has an emergency situation such as a fire, that situation represents the "state" provided to the human beings (moving agents). Room data are created after the third step of the TNR algorithm during CAD data conversion process (see Section 20.2.2). Doors and walls are environments that provide human beings with a specific location against which to assess their exit strategy for building evacuation. Door data are created after the first step of the TNR algorithm and wall data are created after the second step of the TNR algorithm during the CAD data conversion process. Geometric network data provide an evacuation route based on the connectivity of rooms.

In the Agent Analyst extension of ArcGIS®, there are two types of agents: vector agents and generic agents. A generic agent is a non-spatial agent such as an emergency announcement and a vector agent is a spatial agent that is captured in each feature of a shapefile. In our evacuation model, both human beings and rooms are modeled as vector agents. Human beings change their locations through evacuation and rooms change based on neighboring room situations such as fire expansion and toxic gas diffusion. The details of agents' attributes and behavior are discussed in the next section.

20.3.2 Agent Attributes and Behaviors

Agents mimic real world entities. Although real world entities must be simplified for the purposes of simulation, agents should include the fundamental characteristics of those entities in order to represent them and simulate their actions and reactions as accurately as possible. The main components that construct an agent are attributes and behaviors. Agent data are current states that include the agent's internal state and relationship with other agents. Agent behaviors include perception, action, and interaction. Perception gives the agent the capability to analyze its surroundings in order to avoid collisions and to choose what actions to adopt. The agent's states are also modified depending on what the agent perceives in its interactions with other agents.

For the building evacuation model presented in this chapter, the two agents (humans and rooms) have attributes and behaviors. The data represent the states of an agent in a given time. Human agents have five types of data: LOCATION, SIZE, ROOMID, SITUATION, SPEED, and DIRECTION. LOCATION stores the current absolute location of an agent and is updated according the agent's movement. SIZE stores each agent's physical size. ROOMID stores the agent's presence in a specific room, which is a relative location and connects human actions with the situation in the room. SITUATION stores the awareness of an emergency situation in a building and is the trigger for action. SPEED and DIRECTION store each agent's desired speed and direction, respectively. In an emergency situation, an agent's speed will increase rapidly and decrease in a jamming situation. Room agents have four types of data: ROOMID, STATE, NEIGHBOR, and SHORTPATH. ROOMID is a room number. STATE stores the situation of the room. NEIGHBOR stores the adjacency information of each room, which is built from 3D geometric network information. Finally, SHORTPATH stores the shortest path to outer exits based on the 3D geometric network.

Behaviors rule the actions that change an agent's location and update an agent's status. In the evacuation modeling presented in this chapter, human beings are the only moving agents. Therefore, the paradigms for building evacuation can be derived from those related to pedestrian movement. Studies of pedestrian movement analyze and try to explain the circulation of people (Jiang 1999; Schelhorn et al. 1999; Therakomen 2001; Helbing et al. 2002). Pedestrian movement is influenced by personal motivation, spatial configuration, and areas of attraction. For building evacuation, we assume that personal motivation is limited to following the shortest path in order to exit the building, spatial configuration is limited to the internal structure of the building, and "attraction" is not relevant.

To simulate the crowd dynamics of pedestrians in a panic situation, Helbing et al. (2000) provide a generalized force model. The model is based on the acceleration equation (Newton's second law of motion) and assumes a mixture of socio-psychological and physical forces influencing the behavior (Equation 20.1).

$$m_i \frac{dv_i}{dt} = m_i \frac{v_i^0(t)e_i^0(t) - v_i(t)}{\tau_i} + \sum_{j \neq i} f_{ij} + \sum_w f_{iw} \tag{20.1}$$

Here, each pedestrian (i) of weight (m_i) likes to move with a certain desired speed ($v^0{}_i$) in a certain direction ($e^0{}_i$) through time (t), and tends to correspondingly adapt his or her actual velocity (v_i) with a certain reaction time (τ_i). Therefore, the first part of Equation (20.1) represents socio-psychological force. The second and third parts represent human interaction (f_{ij}) (Equation 20.2) and human to wall interaction (f_{iw}) (Equation 20.3) forces.

$$f_{ij} = \{A_i \exp[(r_{ij} - d_{ij})/B_i] + kg(r_{ij} - d_{ij})\}n_{ij} + \kappa g(r_{ij} - d_{ij})\Delta v^t{}_{ji} t_{ij} \qquad (20.2)$$

In Equation (20.2), the first part $f_{ij} = A_i \exp[(r_{ij} - d_{ij})/B_i]n_{ij}$ is a repulsive interaction force that represents the psychological tendency of two pedestrians i and j to stay away from each other. d_{ij} denotes the distance between the pedestrians. A_i and B_i are constants that can reproduce the distance kept at normal desired velocities. Higher A_i produces greater repulsive forces if two agents, P_i and P_j, are overlapped within the range of B_i. r_{ij} is $(r_i + r_j)$ of their radii r_i and r_j of $\mathrm{P_i}$ and $\mathrm{P_j}$, respectively. $\mathrm{n}_{ij} = (\mathrm{P}_i - \mathrm{P}_j)/d_{ij}$ is the normalized vector pointing from point j to i. If $d_{ij}$is smaller thanr_{ij}, body compression $kg(r_{ij} - d_{ij})n_{ij}$ and relative tangential motion $\kappa g(r_{ij} - d_{ij})\Delta v^t{}_{ji} t_{ij}$ are considered. k and κ determine the obstruction effect in cases of physical interactions. $g(x)$is zero if the pedestrians do not touch each other.

$$f_{iw} = \{A_i \exp[(r_i - d_{iw})/B_i] + kg(r_i - d_{iw})\}n_{iw} + \kappa g(r_i - d_{iw})(v_i t_{iw})t_{iw} \qquad (20.3)$$

Equation (20.3) captures the interaction between human beings and walls. d_{iw} means the distance to wall (w). n_{iw} denotes the direction perpendicular to the wall. t_{iw} is the direction tangential to the wall.

To implement Equation (20.1) for human movement, six behaviors of human agents have been taken into account: MYSTATE, MYROOM, MYEXIT, MAINFORCE, P2PFORCE, P2WFORCE, MOVE, and UPDATE. The MYSTATE action checks an agent's states. MYROOM checks the current room situation that decides the agent's desired speed ($v^0{}_i$). MYEXIT checks the current exit to decide the desired direction ($e^0{}_i$) of the agent. MAINFORCE calculates the socio-psychological force (first part) in Equation (20.1). P2PFORCE calculates the human interaction force using Equation (20.2). P2WFORCE calculates the human to wall interaction force using Equation (20.3). MOVE changes the agent's location using the calculated velocity of Equation (20.1) and modifies its state. Finally, UPDATE updates the agent's location and state. Room agents are static and only change if the situation of the room changes. Therefore, for rooms, the "behavior" of ROOMSTATE is used to change the situation of each room through time.

20.3.3 Simulation: Building Evacuation

Helbing et al. (2000) have summarized the characteristics of escape efforts motivated by panic as follows:

(1) people move or try to move considerably faster than normal;
(2) individuals start pushing each other, and interactions among people become physical in nature;
(3) moving and, in particular, passing through a bottleneck becomes uncoordinated;
(4) at exits, arching and clogging are observed;
(5) jams build up;
(6) the physical interactions in the jammed crowd add up and cause dangerous pressures up to 4450 N/m^2 (Elliott and Smith 1993; Smith and Dickie 1993) which can bend steel barriers or push down brick walls;
(7) escape is further slowed by fallen or injured people acting as "obstacles";
(8) people show a tendency towards mass behavior, that is, to do what other people do; and,
(9) alternative exits are often overlooked or not efficiently used in escape situations.

For building evacuation, we tested two cases: evacuation with and without jamming. Therefore, we simplified the situation by using only the first five characteristics listed above. We assume that all people in the building know its structure so that they know where the nearest exit is and how to reach it. Each room in the simulation building has shortest path information created from the 3D geometric network. Although 3D shortest path information is given, the simulations in this study only consider the first floor situation for simplicity. Since floors are connected by stairways, evacuation simulation for each floor can be easily extended to the multi-floor simulation using stairways. In the multi-floor evacuation simulation, jamming situations in stairways should be considered.

To run the generalized force model (see Equation 20.1), we have specified the parameters as follows: a mass of m averages 60 kg; the initial desired speed ($v^0{}_i$) is 5 m/s; the initial desired direction ($e^0{}_i$) is toward the exit; distributed pedestrian diameters $2r_i$ in the interval [0.5 m, 0.8 m] are considered to be shoulder widths; the constant A_i is 250 and B_i is 0.08 m; the parameter k is 250 kg s^{-2} and κ is 500 kg/ms. The first case considers an (N) of ten people in a room to produce evacuation with a jamming situation. The second case considers an (N) of three people in the room for evacuation without jamming.

The first simulation revealed jamming at the room door during building evacuation because agents follow the shortest path to the outer exit through the door of the room they occupy. Figure 20.4a–f display the evacuation situation in the building. The number of moving people and the average speed are shown in Fig. 20.4 g. When people start to jam, the number of movements and the average speed starts to decrease (Figs. 20.4b and g). Physical interaction among the jammed agents accumulates, further reducing movement (Figs. 20.4c and g). As agents nearest the door exit the room, movement and average velocity increase again (Figs. 20.4d–g). Overall, if there are many people in a room wanting to evacuate at the same time, jams occur at the door, decreasing the average speed of evacuation and making more distant people take even longer to evacuate.

The second simulation shows evacuation without jamming (Fig. 20.5). In this scenario, there are only three agents in a room and their distances to the door are

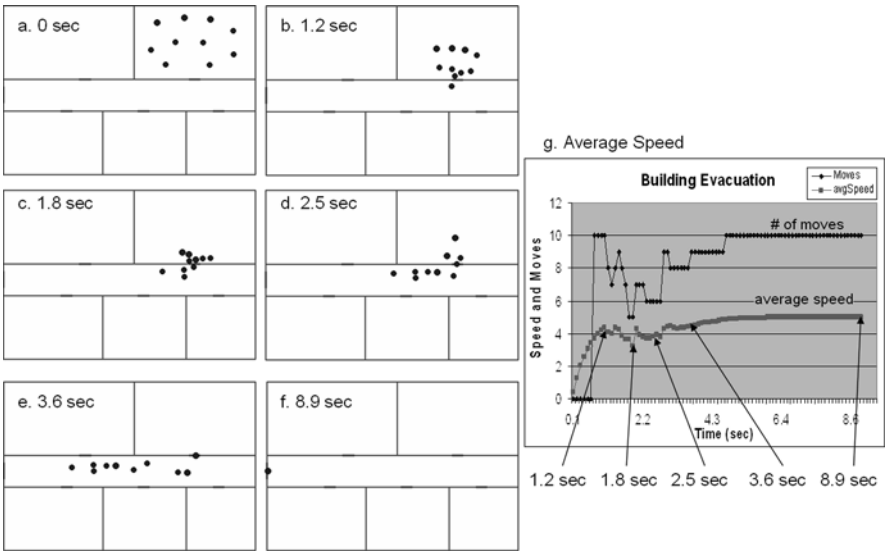

Fig. 20.4 Building evacuation with jamming

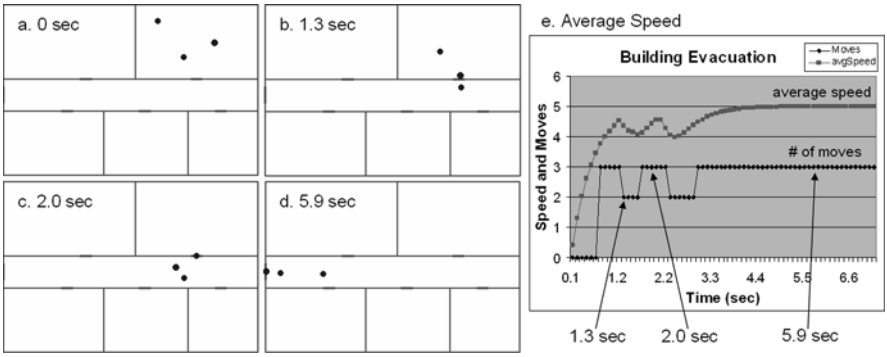

Fig. 20.5 Building evacuation without jamming

different from each other. As in the previous simulation, agents also follow the shortest path to the outer exit. Figures 20.5a–e illustrate that there is no jamming situation. All agents keep moving and their average speed increases continuously (Fig. 20.5e). The average speed is only slightly reduced when an agent leaves a room because they turn to adjust their direction to the next door (Figs. 20.5b and e). Therefore, we can simulate the evacuation model with different numbers of agents in each room to determine the maximum number of occupants before significant jamming would occur during an evacuation situation.

20.4 Discussion: Integration of GIS and Agent-Based Model for Building Evacuation

Agent-based modeling attempts to capture spatial complexity. Spatial data structures for agent-based modeling, however, inevitably over-simplify the complex nature of geographic space because of the need for efficiency in computation. Agent-based modeling mostly operates on cell-, lattice-, or network-based data structures (Batty 2005; Andersson et al. 2006; Bithell and Macmillan 2007). These confined data structures restrict neighborhood geometry and possible locations, as well as spatial actions and interactions. Since GIS representation can capture the complex structure of geographic phenomena, GIS can empower agent-based modeling in two significant ways: by hierarchical observation of phenomena for rule setting and by yielding a spatiotemporal database for storage of modeling results (Yuan 2007).

First, rules applicable to different levels of geographic scale can be incorporated into agent-based modeling. In a building evacuation model, individuals in a room can be regarded as fine-grain agents, and, comparably, groups of people in different rooms can be treated like coarse-grain agents that are aggregates of individuals (fine-grain agents). GIS data representing a lower level of geographic dynamics (such as doors and walls of each room and room situation) provide the basis for individual agent behavior (finer grains). GIS data representing a high level of geographic dynamics (such as building structure and 3D geometric network) offer different conditions to a group of people (coarser grains) in each room. While reality may or may not be hierarchical, hierarchical structures of geographic dynamics facilitate observations and understanding (Allen and Starr 1982). Therefore, agent-based modeling needs to incorporate the hierarchical nature of geographic phenomena supported by GIS, in order to build rule sets of agents' behaviors from any complex system in the world.

Second, GIS can provide empirical support for agent-based modeling. Since the results from agent-based modeling can be stored into a spatiotemporal database for query, retrieval, and analysis, comparison of model output and observations are used to validate the results of simulation from agent-based modeling. Further, comparison between modeling results from different scenarios or rule sets will help decision makers consider all possible situations.

An integration of agent-based modeling and GIS offers improvements to understand complex spatial phenomena. With spatiotemporal GIS data, agent-based modeling can effectively represent the distributed nature of actions and reactions at the individual level to the aggregated level under conditions of spatial complexity. With agent-based models, GIS can represent feature dynamics such as temporal changes in spatial patterns for further time-series spatial analysis.

Urban planners or building designers may be especially interested in utilizing human evacuation simulations for planning purposes or during building design. The locations of doorways and stairways in a building may have critical impacts on egress time during an emergency situation in a building. By running evacuation simulations that incorporate possible doorway locations in a room, the most efficient

doorway location for evacuation purposes can be identified. Such analysis could be used in a backcasting approach by taking existing building configurations, envisioning possible future situations such as a fire, and using the results to modify current locations of doorways and stairways to minimize egress time. Models such as the one described here can also be used to analyze whether GIS-based "shortest distance to doorways" findings actually ensure minimum egress time during a building evacuation simulation. The simulation could show that following the shortest paths actually causes considerably large jams. If that were the case, new paths could be computed that might not be the shortest but would be faster. Another application would be route optimization for dispatching response units to a disaster, such as a fire in a building, as analyzed by integrating GIS, agent-based models, and optimization models (Huang and Pan 2007).

20.5 Summary and Conclusion

In this chapter, we have tried to model a building evacuation scenario using 3D geometric network data and an agent-based model. A 3D geometric network was been created from CAD data through wall extraction and 3D topology construction. We tested two wall extraction methods: vector-based MAT and raster-based thinning. If the internal structure of a building is complex, the thinning method is preferred. 3D topology was built by converting rooms (3D space) to nodes and the adjacency of rooms to edges. If adjacent rooms had doors, the edges represent connectivity. 3D topological structure was then converted to a 3D geometric network by converting spaces (nodes) for movement such as hallways or stairways to edges for navigation in a building. Using 3D geometric network data, we extracted the shortest path information from each room to the outer exits of a building.

Using the agent-based model, a building evacuation was simulated in a GIS environment. In the simulation, building data (including a 3D geometric network) were generated and used to build rule sets for updating agents' states and behaviors. To model human evacuation behavior, we adopted a generalized force model (Helbing et al. 2000) to incorporate a mixture of socio-psychological and physical forces of human-to-human and human-to-wall interactions that would influence agents' behaviors. We tested two simple evacuation scenarios: evacuation with and without jamming, with different numbers of room occupants. As expected, the results showed that average velocities increase continuously before jams, decrease during jams, and eventually increase again as individuals escape from jams. Without jams, average velocity increased continuously, allowing individual agents to evacuate the building in increasingly shorter time spans.

As emphasized above, integration of GIS with an agent-based model provides a more advanced methodology for observing and understanding complex real world phenomena. In this chapter, we integrated GIS with an agent-based model by providing the agent-based model with spatial data and the GIS with the results of the simulation to generate a dynamic visualization of the spatial process. The research

is ongoing, as we attempt to improve our evacuation model with the inclusion of realistic variables such as injuries and determining the desired direction of a group during rising levels of panic. We are also experimenting with simulating complex emergency evacuation scenarios such as a bombing/fire in micro-scale spatial environment such as a stadium and switching between alternate evacuation strategies.

Acknowledgments This research was supported by a grant from "Seoul R&BD Program (10592)" funded by the City of Seoul, South Korea.

References

Allen, T.F.H. and Starr, T.B. (1982). *Hierarchy: Perspectives in Ecological Complexity*. Chicago: University of Chicago Press.

Andersson, C., Frenken, K., and Hellervik, A. (2006). A complex network approach to urban growth. *Environment and Planning A*, 38(10), 1941–1964.

Batty, M. (2005). Agents, cells, and cities: New representational models for simulating multiscale urban dynamics. *Environment and Planning A*, 37(8), 1373–1394.

Benhamu, M. and Doytsher, Y. (2003). Toward a spatial 3D cadastre in Israel. *Computers, Environments and Urban Systems*, 27, 359–374.

Billen, R. and Zlatanova, S. (2003). 3D spatial relationships model: A useful concept for 3D cadastre? *Computers, Environment and Urban Systems*, 27, 411–425.

Bithell, M. and Macmillan, W.D. (2007). Escape from the cell: Spatially explicit modeling with and without grids. *Ecological Modelling*, 200, 59–78.

Castle, C.J.E. and Crooks, A.T. (2006). Principles and Concepts of Agent-Based Modeling for Developing Geospatial simulations. *UCL Working Papers Series: Paper 110*. Resource document. http://www.casa.ucl.ac.uk/working_papers/paper110.pdf. Accessed 21 July 2008.

Coors, V. (2003). 3D-GIS in networking environments. *Computers, Environment and Urban Systems*, 27, 345–357.

Elliott, D. and Smith, D. (1993). Football stadia diasters in the United Kingdom: Learning from tragedy? *Organization and Environment*, 7(3), 205–229.

Eppstein, D. and Erickson, J. (1999). Raising roofs, crashing cycles, and playing pool: Applications of a data structure for finding pairwise interactions. *Proceedings of the 14th Annual ACM Symposium on Computational Geometry* (pp. 58–67), Minneapolis, Minnesota.

Epstein, J.M. (1999). Agent-based computational models and generative social science. *Complexity*, 4(5), 41–60.

Frankline, S. and Graesser, A. (1996). Is it an agent, or just a program? a taxonomy for autonomous agents. *Proceedings of the Third International Workshop on Agent Theories, Architectures, and Languages*, Springer-Verlag.

Goodchild, M.F. (2005). GIS, spatial analysis, and modeling overview. In D.J. Maguire, M. Batty, and M.F. Goodchild (Eds.), *GIS, Spatial Analysis and Modeling* (pp. 1–17). Redlands, California: ESRI Press.

Haunert, J.H. and Sester, M. (2004). Using the straight skeleton for generalization in a multiple representation environment, *Proceedings of the ICA Workshop on Generalization and Multiple Representation*, Leicester.

Helbing, D., Farkas, I.J., and Vicsek, T. (2000). Simulating dynamical features of escape panic. *Nature*, 407, 487–490.

Helbing, D., Farkas, I.J., Molnar, P., and Vicsek, T. (2002). Simulation of pedestrian crowds in normal and evacuation situations. In N. Waldau, P. Gattermann, H. Knoflacher, and M. Schreckenberg (Eds.), *Pedestrian and Evacuation Dynamics* (pp. 21–58). Berlin: Springer-Verlag.

Huang, B. and Pan, X. (2007). GIS coupled with traffic simulation and optimization for incident response, *Computers, Environment and Urban Systems*, 31, 116–132.

Jiang, B. (1999). SimPed: Simulating pedestrian flows in a virtual urban environment. *Journal of Geographic Information and Decision Analysis*, 3(1), 21–30.

Kevany, M.J. (2003). GIS in the World Trade Center attack-trial by fire. *Computers, Environment and Urban Systems*, 27, 571–583.

Lee, J. and Kwan, M. (2005). A combinatorial data model for representing topological relations among 3D geographical features in micro-spatial environments. *International Journal of Geographical Information Science*, 19(10), 1039–1056.

Lee, J. (2004). A spatial access-oriented implementation of a 3-D GIS topological data model for urban entities. *GeoInformatica*, 8(3), 93–113

Longley, P.A, Goodchild, M.F., Maguire, D.J., and Rhind, D.W. (2005), *Geographical Information Systems and Science*, Hoboken, NJ: John Wiley and Sons

Longley, P.A. and Batty, M. (2003). Advanced spatial analysis: Extending GIS, In P.A. Longley and M. Batty (Eds.), *Advanced Spatial Analysis: The CASA Book of GIS* (pp. 1–20). Redlands, California: ESRI Press.

Macal, C.M. and North, M.J. (2005). Tutorial on agent-based modeling and simulation. In M.E. Euhl, N.M. Steiger, F.B. Amstrong, and J.A. Joines (Eds.), *Proceedings of the 2005 Winter Simulation Conference*, Orlando.

Marion, B. (2004). The History of CAD. *MB Solutions*. Resource document. http://mbinfo.mbdesign.net/CAD-History.htm. Accessed 21 July 2008.

Prasad, L. and Rao, R. (1998). Morphological analysis of shapes. Resource document. http://citeseer.ist.psu.edu/18235.html. Accessed 21 July 2008.

Schelhorn, T. and O'Sullivan, D., Haklay, M., and Thurstain-Goodwin, M. (1999). STREETS: An agent-based pedestrian model. *Working paper*. Centre for Advanced Spatial Analysis UCL, London, UK. Resource document. http://www.casa.ucl.ac.uk/working_papers/paper9.pdf. Accessed 21 July 2008.

Smith, R.A. and Dickie, J.P. (1993). *Engineering for Crowd Safety*, Amsterdam: Elsevier.

Stevens, M. and Choi, J. (2006). CAD Data conversion to a node-relation structure for 3D sub-unit topological representation. *Journal of the Korean Geographical Society*, 41(2), 188–194.

Therakomen, P. (2001). *Mouse.Class – the Experiment for Exploring dynamic Behaviors in Urban Places*, Master Thesis, University of Washington, Washington.

Torrens, P.M. (2004). *Simulating Sprawl: A Dynamic Entity-Based Approach to Modeling North American Suburban Sprawl Using Cellular Automata and Multi-Agent Systems*, Ph.D Thesis, University College London, London.

Wooldridge, M. and Jennings, N.R. (1995). Intelligent agents: Theory and practice. *Knowledge Engineering Review*, 10(2), 115–152.

Yuan, M. (2007). Temporal GIS for Agent-Based Modeling of Complex Spatial Systems. Resource document. http://www.ncgia.ucsb.edu/projects/abmcss/docs/yuan_paper.pdf. Accessed 21 July 2008.

Zhou, Q. and Zhang, W. (2003). A preliminary Review on 3-dimensional City Model. *Asia Geographic Information System Association 2003 Conference.* Resource document. http://www.hku.hk/cupem/asiagis/fall03/Full_Paper/Zhou_Qiming.pdf. Accessed 21 July 2008.

Zlatanova, S. (2002). Advances in 3D GIS. *Quarterly Review of Disegno Digitale e Design*, 1(4), 24–29.

Zlatanova, S., Rahman, A.A., and Pilouk, M. (2002). 3D GIS: Current status and perspectives. *Proceedings of ISPRS*, Ottawa, Canada. Resource document, http://www.gdmc.nl/zlatanova/thesis/html/refer/ps/SZ_AR_MP02.pdf. Accessed 21 July 2008.

Chapter 21
A Planning Support System for Terror-Resistant Urban Communities

Xinhao Wang, Joshua S. Belhadj, and Heng Wei

Abstract The shocking terrorist attacks that took place in New York (2001) and London (2005) have raised serious concerns about the safety of cities and the need for identifying potential threats and preparing preventive measures. There is a gap in the literature, where on the one hand, planning for terror is discussed at the federal level (large scope), and on the other hand, at a site-specific level (small scope). The fact is that there is very little planning research at the urban community level (medium scope). The research presented here aims to start to fill this gap by developing a Community Evacuation Planning Support System (CE-PSS) to aid urban communities identify likely community terror targets and shelters. The CE-PSS was developed using ArcGIS® 9.2 and two extensions – ESRI's® Network Analyst and Placeways'™ CommunityViz®. By comparing the capacity and location of potential targets with that of potential shelters, shortcomings in a community's readiness for terror attacks can be detected. With such knowledge, planners, citizens, and community leaders can address these issues in revising their comprehensive plans. As planners are charged with paying special attention to the long-term and interrelated implications of their decisions, preparing for possible terror attack is an essential consideration in today's planning paradigm.

Keywords Planning support system · Target · Shelter · Terrorism hazard · Community · Evacuation

21.1 Introduction

Compared to natural disasters, man-made disasters are more likely to occur in dense urban areas, have a higher degree of centrality, and a smaller degree of predictability. The realities of events such as the 2005 terrorist attack on transit lines in London and the 2001 World Trade Center tragedy in New York have raised serious concerns

X. Wang (✉)
School of Planning, University of Cincinnati, Cincinnati, OH 45221-0016, USA
e-mail: xinhao.wang@uc.edu

P.S. Showalter, Y. Lu (eds.), *Geospatial Techniques in Urban Hazard and Disaster Analysis*, Geotechnologies and the Environment 2, DOI 10.1007/978-90-481-2238-7_21,

about the safety of cities and the need for identifying potential threats and preparing preventive measures (Light 2004).

Over the history of urbanization, the safety of a city has always been closely related to its urban form. For example, walls and moats surrounded ancient Chinese cities to protect against infantry and cavalry attacks (Ke 1994), likewise, urban sprawl in America can be partly attributed to fear of atomic bomb attacks on city centers (Dudley 2001). Making communities safer places has become a major focus of planners and urban designers. In many cases, limiting access to key infrastructure may not be feasible or desirable and the cost of implementing high security measures could be exorbinate. Further, security strategies could degrade cities by reducing pedestrian traffic, discouraging mixed land uses, and encouraging more facilities to move away (Holzheimer 2004; Krohe 2005; Goodno 2005; Flint 2005). In 2004, the American Institute of Certified Planners held a symposium on Safe Growth and prepared a Safe Growth America Checklist to improve the safety situations in neighborhoods (APA 2004). Building upon those efforts, this chapter presents a study aimed at achieving a more desirable future through a planning process that makes an effort to acknowledge potential targets, shelters, and the routes connecting them.

The word "community", as used in this chapter, refers to any local municipality which undergoes planning activities. In particular, the focus of this chapter is on urban communities (in contrast to suburban or rural communities) since man-made disasters are most likely to occur in urban areas. The Planning Support System described in this chapter aims to arm a community with the tools to assess the readiness of its infrastructure, evaluate its resources, and incorporate preparation for possible urban evacuation into its community plan. The system employs an automated geographic information system (GIS) model to provide a framework for community-level building-based assessment in order to identify potential targets. Once the targets are identified, shelters are identified based on capacity and proximity to targets.

The chapter is organized as follows: first, a literature review of man-made disaster mitigation is performed. This review is followed by discussion of the development of the Community Evacuation Planning Support System. The next two sections describe the system's operation, and demonstrate its application. The chapter ends with a discussion of the contributions of the study to the literature and provides recommendations for further research.

21.2 Background

The enabling legislation for communities to engage in disaster planning is the Disaster Mitigation Act of 2000 that provides an impetus for state and local governments to undertake mitigation planning. The policy encourages and rewards state and local communities' pre-disaster planning as a strategy for reducing the effects of disasters (FEMA 2003).

An "all-hazard" approach has been a cornerstone of the Federal Emergency Management Agency 's (FEMA) response program since the agency was first established

(Smith 2006). The approach integrates various emergency plans and activities into a "life cycle" of mitigation, preparedness, response and recovery (the four principles of emergency management). The approach also provides a template for inter-agency coordination, as a foundation for making evacuation management plans.

FEMA defines hazard mitigation planning as "the process of determining how to reduce or eliminate the loss of life and property damage resulting from natural and man-made hazards" (FEMA 2003, i). According to FEMA, there are two subcategories under the label of man-made hazards: terrorism hazards and technological hazards (FEMA 2003). Terrorism hazards differ from technological hazards in that they are intentional and malicious, while technological hazards arise from unintentional human errors. In the context of this study, the prefix "man-made" is used to refer to intentional and malicious acts of terrorism.

In the United States, FEMA has developed specific criteria to identify a community's target s that are prone to attack. FEMA's definition of critical infrastructure is the "systems whose incapacity or destruction would have a debilitating effect on the defense or economic security of the nation", including the categories of agriculture/food, water, public health, emergency services, defense bases, telecommunications, energy, transportation, banking/finance, chemicals/hazardous materials, postal/shipping (FEMA 2003, 2–8).

"Shelter" refers to the use of existing structures in a jurisdiction to temporarily house and provide services to evacuees. A shelter can only be available if it is both suitable and accessible. Suitability refers to the shelter's ability to meet the immediate needs of evacuees in the most convenient and comforting way possible. Identifying suitable shelters requires assessment of their occupancy capacity and their proximity to water, electricity, and other essential utilities (Laefer et al. 2006). Schools and churches are examples of potential shelters due to their traditional roles as venues for community gatherings and places of public support under harsh situations (Gursky 2004). Accessibility refers to the availability of a building to function as a shelter and the distance or time required traveling to that shelter from a target.

Shelters prepared for different disasters have different characteristics and methods for access and traffic analysis vary significantly. Gall (2004) conducted a GIS-based shelter analysis for floods in Mozambique. The shelter analysis employed a two-step process determining access for vulnerable communities first, followed by a suitability analysis for additional emergency shelter sites. Yazici and Ozbay (2007) studied the location and effectiveness of hurricane evacuation shelters with a stochastic programming model. Their analysis focused on determining the desirable location and capacity of shelters. They extended a cell transmission–based system to an optimal dynamic traffic assignment (SO-DTA) formulation which was first proposed by Ziliaskopoulos (2000) by introducing probabilistic capacity constraints. The study found that accounting for flood probabilities and links that are not used by all evacuees can change the system-optimal flows and performance measures as well as the favorable shelter locations and capacity requirements. Kongsomsaksakul et al. (2005) used the Stackelberg Game Model to assess the interaction between a planning authority and evacuees. The problem was modeled using a bi-level programming formulation. The planning authority determines

the number and locations of shelters that minimize total network evacuation time, whereas evacuees simultaneously decide which shelter to use and the route to take within the capacity constraints and location of the shelter. While these studies have been informative, none have attempted to perform shelter accessibility analysis by integrating roadway network configuration, roadway categories, traffic control, and other environmental factors.

Evacuation planning for the most part is meant to optimize the effectiveness of an evacuation operation (Han et al. 2007). Efforts preparing and executing evacuation plans are often based on knowledge of existing urban infrastructure such as potential targets, shelters, and roadway networks (Zepeda and Sol 2007) to achieve the most efficient pattern for evacuation within the shortest time (Lin et al. 2008). Various computer technologies have been used to simulate these patterns (Chen et al. 2007; Liu et al. 2007; Mól et al. 2008; Patterson and Apostolakis 2007; Zerger and Smith 2003).

The lack of research for community-level systems may well reflect difficulties in developing an over-arching framework that acknowledges variability in community character. Varying community characteristics demand flexible and dynamic systems that are adaptable to the community's priorities and circumstances.

A planning support system is a computerized system that organizes data and provides an interactive interface for its users to actively participate in the planning process of assessing alternative scenarios (Klosterman 2001). The power of a planning support system lies in its ability to provide a planning context and to enhance the effectiveness of planning (Geertman and Stillwell 2004; Hopkins et al. 2005). The rest of this chapter describes Community Evacuation Planning Support System (CE-PSS), a planning support system we developed to provide a platform to meet the needs of preparing a community for man-made disaster evacuation.

21.3 Development of CE-PSS

The first question a community must attempt to answer regarding possible man-made disaster is, "What types of assets are potential targets?" Buildings, which are considered potential terrorism targets by FEMA, should be classified by a typology that represents terrorism motivation. For example, a terrorist motivated to hinder the economy is more likely to attack buildings associated with government, corporations, or businesses. Similarly, a terrorist motivated to cause human casualties may attack stadiums, airports, or theaters. The system prompts the user to specify types and sizes of buildings as potential target selection criteria.

The second question to address when preparing for man-made disaster is, "Which buildings will be collaterally damaged?" Buildings that may be damaged secondarily as a byproduct of the terror attack on primary targets are in this category. The identification of collaterally damaged buildings depends upon the identified targets and the type of attack. The system provides a prompt to the user to specify a buffer distance in order to select collateral damage buildings.

The third question is, "Where are the shelters which can be used as temporary places for evacuees to stay before they go home or places where medical care can be administered?" Similar to the identification of targets, the system prompts the user to specify types, sizes and other features of buildings as shelter selection criteria. Only buildings which have not already been identified as target or collateral damage buildings can be considered as shelters.

The fourth and last question is, "Considering the existing street network, are there enough shelters within an acceptable travel distance to accommodate the people in the target buildings in case of a disaster?" Again, the user is able to answer the system prompt with a definition of "acceptable" travel distance.

Accordingly, CE-PSS consists of the following five steps as shown in Fig. 21.1: (1) database development and pre-processing – building and street data are collected and added to a GIS database; (2) identification of targeted buildings – building

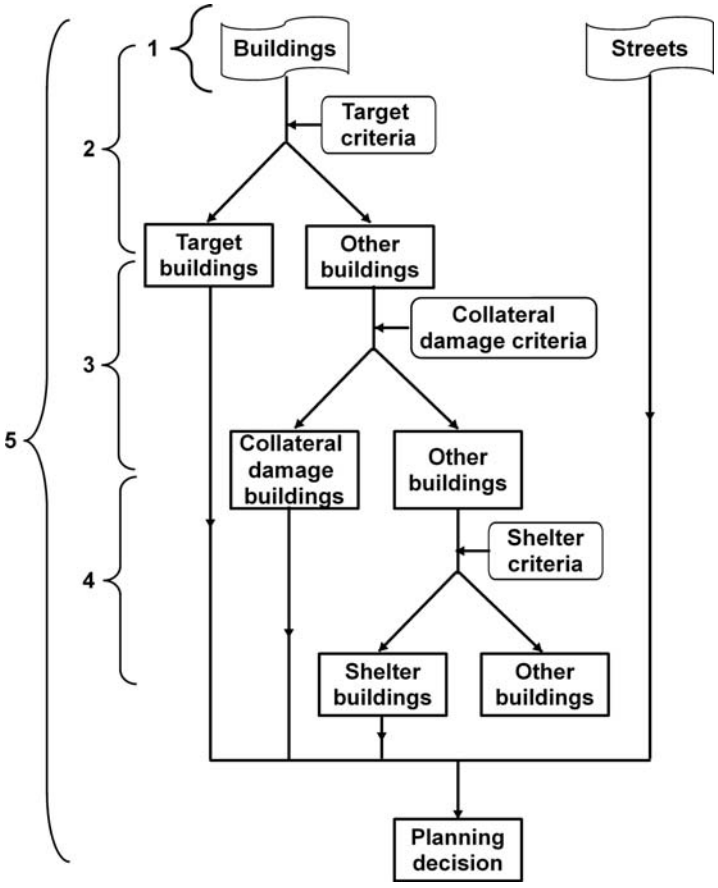

Fig. 21.1 The community evacuation planning support system

characteristics are compared with the user-specified target criteria to select potential target buildings; (3) identification of collateral damage buildings for each target – after target selection, the remaining buildings are compared with collateral damage criteria to select potential collateral damage buildings; (4) identification of shelter buildings – after target selection and collateral damage identification, the remaining buildings are compared with shelter criteria to select potential shelter buildings; and (5) assessment of shelter and target key performance indicators for community planning – the capacity and relative location of targets and shelters are analyzed in reference to the existing street network to assess the readiness of the community for the user-specified threat.

CE-PSS is developed using Network Analyst (ESRI®, Redlands, CA) and CommunityViz® (CV; Placeways™, Boulder, CO), both are extensions of ArcGIS® (ESRI®, Redlands, CA). CV provides an interactive scenario analysis interface with which a user specifies factors to be considered in the planning process and interactively assigns the factor values to dynamically review the analytical results or change the factor values and review the outcome of the changes.

Although there are many different infrastructures that can be potential targets of terrorists, only buildings are used as potential targets in this study. Once CE-PSS is fully developed, other types targets can be added to the database. The building footprint data layer contains a "building type" attribute field. The building type values are prepared based on the literature regarding terrorism motivation and the potential for use as shelters as part of the data pre-processing phase. Other attribute fields of the building layer are building size and occupancy capacity.

The power of a planning support system is that the user is in charge during the planning process. A graphic user interface (GUI) provides a platform for users to specify desired input values for the analysis. In identifying targets, the user specifies building types and the minimum building size. In addition, the user specifies the search distance for identifying collateral damage buildings. The criteria for shelter selection include building type, the maximum acceptable evacuation distance and the minimum building size.

For each target that has been identified, the distance between targets and shelters are calculated by way of street network distance.[1] To represent the worst case scenario, the number of people in a target building is assumed to be equal to the building's capacity. The evacuation population is compared to the capacity of the shelters within the maximum acceptable evacuation distance. If the capacity of the target is greater than that of the nearest shelter, the system will continue to find the next closest shelter for evacuation. The search will continue until all the evacuees are allocated or the number of shelters reaches five (a limit of five has been placed on

[1] Distance was chosen as the travel impedance rather than time. We assume that under evacuation conditions, travel time, which is dependent on street speed limits, becomes irrelevant, as speed limits would be ignored for the purpose of timely evacuation.

this iterative process for processing purposes). We assume that if the total capacity of the five shelters is still not enough for the target, that there is an evacuation deficit.

Modeling results are presented as target-specific or community-wide indicators. The six community-wide indicators are calculated to provide a descriptive picture of how well a community is prepared for handling a potential evacuation.

1. *Number of Targets* – The total number of buildings that have been identified as targets.
2. *Number of Shelters* – The total number of buildings that have been identified as shelters.
3. *Underprepared Targets* – The number of targets that require more than five close-by shelters. This indicator represents the number of targets lacking adequate shelter capacity for the evacuees.
4. *Average Distance to the Nearest Shelter* – The average distance from all targets to their nearest shelters.
5. *Maximum Distance to the Nearest Shelter* – The maximum evacuation distance from any of the targets to the nearest shelter.
6. *Minimum Distance to the Nearest Shelter* – The minimum evacuation distance from any of the targets to the nearest shelter.

In addition, four target-specific indicators measure the level of vulnerability of each target. This value is based on evacuee travel distance in relation to the user defined maximum acceptable evacuation distance.

1. *Average Evacuee Travel Distance* – For each target, the average distance evacuees must travel to a shelter. This indicator is calculated to measure the degree to which each target is prepared for a man-made disaster.
2. *Unaccommodated Evacuees* – For each target, the number of evacuees who cannot be accommodated by the five closest shelters.
3. *Evacuees Traveling Too Far* – For each target, the number of evacuees who are assigned to a shelter that is further than the user-specified "Maximum Acceptable Evacuation Distance".
4. *Proportion of Adequate Evacuation* – For each target, the proportion of evacuees who are assigned to shelters which are less than or equal to the user-specified "Maximum Acceptable Evacuation Distance".

21.4 System Operation

The usefulness of illustrative scenarios, including an alternative "Harm to Economy" scenario have been explored by Belhadj (2008). To illustrate how CE-PSS works, a hypothetical "Harm to People" scenario is presented here. A user first specifies the selection criteria for targets, collateral damage buildings, and shelters.

Fig. 21.2 Parameter input interface of CE-PSS building type selection criteria for targets

The building type selection criteria for potential targets are chosen as: Emergency Services, Food and Water Services, Gathering Places, and People Transportation (Fig. 21.2). Similar designation is required for shelter identification. In this case, buildings of type Churches, Conference, Schools, Theaters, Hotels, and Parking Structures are candidates for shelters (Fig. 21.3).

Building size is another criterion for selection. The minimum building sizes for targets and shelters are chosen as 20,000 m^2 and 10,000 m^2, respectively. The Maximum Acceptable Evacuation Distance is set to 2.5 km and the Collateral Damage Distance is set to 300 m (Fig. 21.4).

After processing, a map is generated that shows potential targets, potential shelters, and potential collateral damage buildings (Fig. 21.5). There are four potential targets and two buildings can be used as shelters. There is a concentration of potential targets located in the southern portion of the community.

Fig. 21.3 Parameter input interface of CE-PSS building type selection criteria for shelters

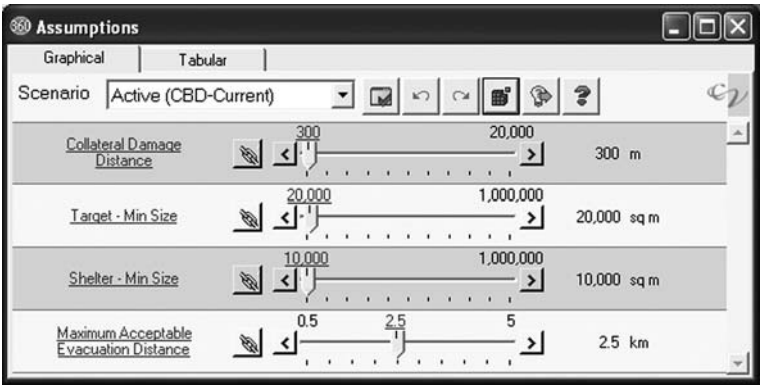

Fig. 21.4 Parameter input interface of CE-PSS additional planning support criteria

Table 21.1 shows that the evacuation distance from the targets to the nearest shelter, on average, is about 1.26 km. The shortest distance between a target and the nearest shelter is 0.90 km and the longest distance between a target and the nearest shelter is 1.68 km. Both shelters are within the user-defined maximum acceptable evacuation distance from any of the four potential targets.

Examination of the individual target indicators (Table 21.2) shows that the average evacuee traveling distance from any of the four potential targets to the two shelters is within the user-specified maximum acceptable travel distance (2.5 km). However, only one of the potential targets (Target ID = 1198) can be expected to

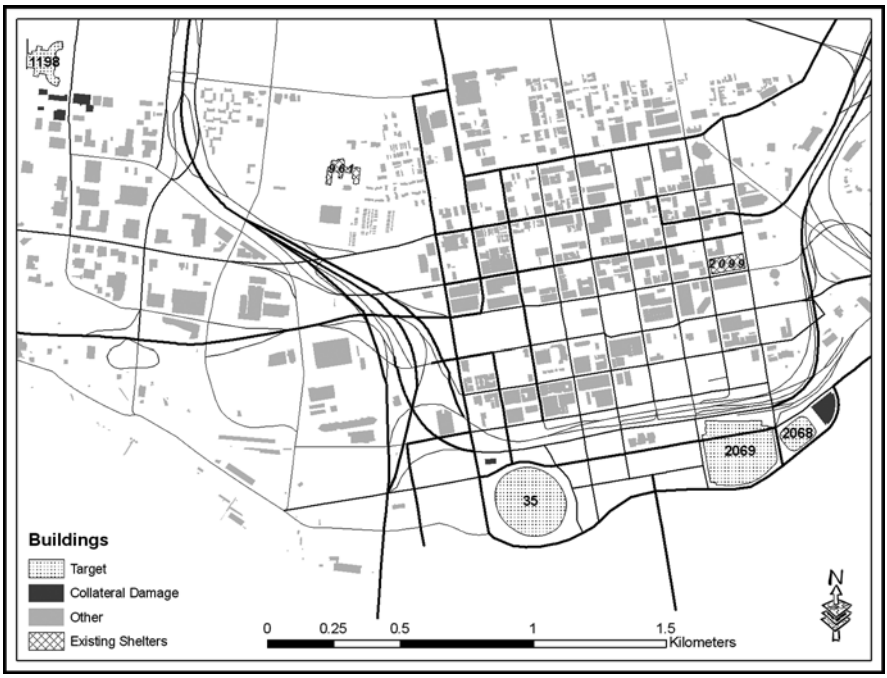

Fig. 21.5 Identified targets and shelters: current scenario

Table 21.1 Distance between Targets and Shelters (km), Current Scenario

Shelter ID \ Target ID	35	1198	2068	2069
961	1.60	1.68	2.76	2.34
2099	1.47	3.22	1.01	0.90
Distance to the nearest shelter	1.47	1.68	1.01	0.90
Minimum distance to the nearest shelter			0.90	
Maximum distance to the nearest shelter			1.68	
Average distance to the nearest shelter			1.26	

Table 21.2 Target level evacuation indicators, current scenario

Target ID	Potential evacuees	Average evacuee traveling distance (km)	Evacuees traveling too far	Unaccommodated evacuees	Proportion of adequate evacuation
35	65335	1.52	0	60805	7%
1198	2621	2.26	0	0	100%
2068	17000	1.62	0	12270	28%
2069	43000	1.4	0	38270	11%

have adequate shelter. The other three potential targets need additional shelter space since the two shelters can only accommodate 7–28% of the potential evacuees. The results indicate that there is a need for more shelters in better proximity to the buildings that are currently considered as potential targets.

21.5 Planning Scenario: Improvement for Emergency Evacuation

Future development planning for the community can utilize the results generated above to improve sheltering options by suggesting the addition of new buildings on vacant lots, the conversion of existing incompatible uses, or the expansion of existing buildings that do have compatible uses. In this example, it is proposed that five new buildings be added on currently vacant lots (Fig. 21.6). Developers would be encouraged to place on these lots shelter-compatible uses such as churches, schools, hotels, or parking facilities.

After interactively adding these proposed shelter-compatible uses, the scenario is recalculated and CE-PSS shows that all the shelters are now within the user-specified maximum acceptable travel distance (Table 21.3). While the minimum, average, and maximum distances to the nearest shelter do not change much,

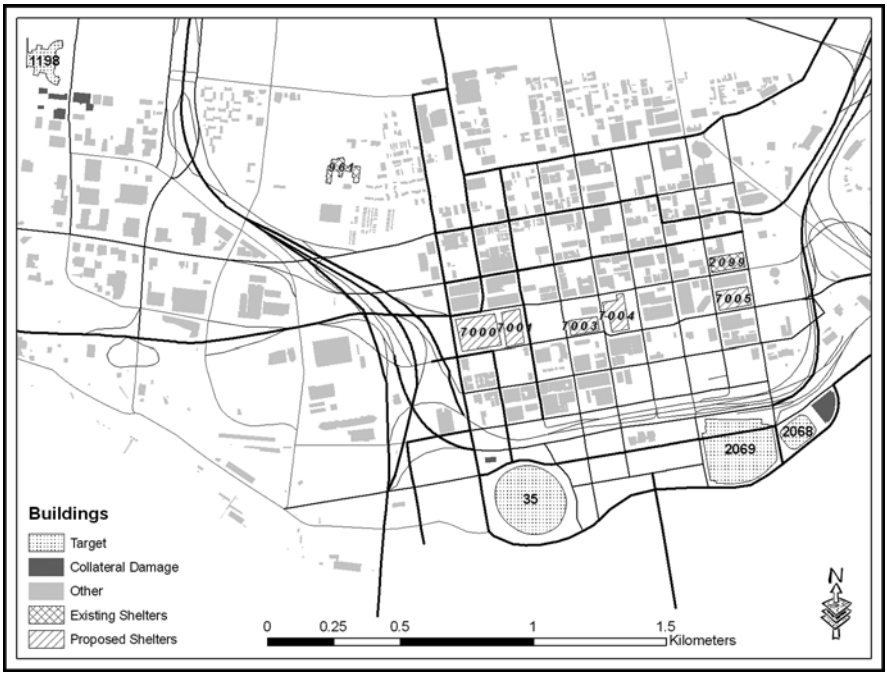

Fig. 21.6 Identified targets and shelters: improved scenario

Table 21.3 Distance between targets and shelters (km), improved scenario

Shelter ID \ Target ID	35	1198	2068	2069
961		1.68		
2099			0.90	
7000	0.58	2.34		
7001	0.75			
7003	0.71			
7004	0.84			0.93
7005	1.26		0.79	0.68
Distance to the nearest shelter	0.58	1.68	0.79	0.68
Minimum distance to the nearest shelter			0.58	
Maximum distance to the nearest shelter			1.68	
Average distance to the nearest shelter			0.93	

Table 21.4 Target level evacuation indicators: improved scenario

Target ID	Potential evacuees	Average evacuee traveling distance	Evacuees traveling too far	Unaccommodated evacuees	Proportion of adequate evacuation
35	65335	1.15	0	18872	71%
1198	2621	1.93	0	0	100%
2068	17000	0.79	0	0	100%
2069	43000	0.71	0	0	100%

comparing the individual target indicators in Table 21.2 (Pre-improvement Indicators) to Table 21.4 (Post-improvement Indicators) reveals other benefits from adding the new shelter-compatible buildings. The average evacuee traveling distance from all potential targets has been reduced. The most significant improvement is that all evacuees from three of the four potential targets are evacuated to a shelter within the acceptable distance. Only one potential target still faces the problem of not enough shelter space, but even for that target, the proportion of adequate evacuation improved from 7 to 71%."

21.6 Conclusion

The Community Evacuation Planning Support System (CE-PSS) described in this chapter is intended to provide a framework for evaluating planning opportunities to mitigate evacuation impacts from terror events. Increasing shelter capacity or decreasing proximity to shelter can and should be considered when making community development plans. Areas that are deficient in shelter capacity ought to be

given priority when new shelter-compatible uses, such as churches, schools, parking structures, hotels, and community centers are proposed.

Perhaps the most critical first step towards better preparation for emergency evacuation is the integration of all critical components into a comprehensive GIS database. Such components would include adding building attributes that could lead to a more vigorous facilitation of the selection process for shelters (e.g., number of bathrooms, existence of large congregational rooms, cooking facilities) as well as identification of potential targets (e.g., whether there are chemical agents on site, level of accessibility, occupancy). The key is getting critical data into a central database in order to maximize the usefulness of the system. The success of any such system depends upon the ability to access a highly detailed level of information (Laefer et al. 2006). The City of Los Angeles learned this lesson while developing its critical asset management system (Operation Archangel), during which it was discovered that much of the city's asset data were stored in paper format in many locations (Amur 2005).

Another data need is increased temporal and spatial resolution. The model in this chapter uses static target and shelter capacity values. More robust models would include real-time data about who is where and when, based on time of day, day of week, and season of the year. A baseball park, for example, may hold up to 40,000 guests on a "game night", however game nights only take place a few times per week and only during the baseball season between April and October. Estimating that the maximum capacity of a baseball park would require evacuation in December would result in a gross miscalculation.

Other studies have explored the network functionality offered in CommunityViz®, finding it to be very limited, only allowing identification of the closest features between two data layers, such as between targets and shelters (Belhadj 2008). Future research may use more effective methods for traffic generation and assignment, for instance, the ArcGIS Network Analyst extension that allows a user to specify that the optimal evacuation traffic routing cannot pass through collateral damage areas. Traffic passing through collateral damage areas both puts evacuees at additional risk and further complicates traffic that is originating in collateral damage areas.

The spatial distribution of targets and shelters may also play a role in laying out new surface transportation infrastructure. Surface transportation infrastructure improvements can include capacity increases, and creation of new intra-urban connectors. The interrelationships between planning decisions can be demonstrated if new roads were built not only taking into account conventional variables related to criteria such as traffic flow but also those related to emergency evacuations.

Researchers are still trying to understand more completely what efforts can be put forth to mitigate the possible consequences of acts of terrorism. Much of the effort is comprised of evacuation simulation models, dynamic route assignment models, and intelligent transportation systems, to name a few. However, Bronzini and Kicinger (2006) find current analytical tools are lacking. This project attempts to address this perceived lack. Because there is a need for a community-wide integration of evacuation preparation and development planning, CE-PSS's ability to assess the spatial

relationships between possible targets, shelter sites, and evacuation under current conditions helps planners anticipate the needs of emergency evacuation before they occur. Given that man-made disasters are external forces which cannot be controlled at the community level, planners can use intelligence reports and knowledge about the characteristics of their community to anticipate what would be the most likely targets. Once potential targets are identified, communities can prepare for the potential evacuation by choosing their own acceptable parameters, such as the types of buildings that can act as shelters, and acceptable distances traveled for evacuation.

These inputs can be put together in maps, tables, and charts that can be analyzed to show areas requiring planning action. By anticipating these likely evacuation circumstances, planners can consider these evacuation improvement scenarios when making traditional planning decisions. We believe that evacuation circumstances should be considered a factor in planning decisions that seek to lead to the best long-term health of a community. Because planners need to pay special attention to the long-term implications and interrelationships of their decisions, preparing for possible terror attack is an essential consideration in today's planning paradigm.

References

American Planning Association (APA). (2004). *Safe Growth America Checklist*. Washington, DC: American Planning Association.

Amur, N.T. (2005). Homing in. *The American City & County* 120(5), 50–55.

Belhadj, J.S. (2008). Anticipating urban evacuations: a planning support system for impact reduction. University of Cincinnati, College of DAAP, School of Planning. http://www.ohiolink.edu/etd/view.cgi?acc_num=ucin1203967246. Accessed September 24, 2008.

Bronzini, M., Kicinger, R. (2006). Conceptual model of a self-organizing traffic management hazard response system. *Transportation Research Board 85th Annual Meeting Compendium of Papers*.

Chen, M., Chen, L., Miller-Hooks, E. (2007). Traffic signal timing for urban evacuation. *Journal of Urban Planning & Development*, 133(1), 30–42.

Dudley, M. (2001). Sprawl as strategy: city planners face the bomb. *Journal of Planning Education and Research*, 21(1), 52–63.

Federal Emergency Management Agency (FEMA). (2003). Integrating manmade hazards into mitigation planning. Version 2.0. FEMA. http://www.fema.gov/library/viewRecord.do?id=1915 . Accessed 20 July 2007.

Flint, A. (2005). Both safe and sorry? *Planning*, 71(6), 4–9.

Gall, M. (200). Where to go? strategic modeling of access to emergency shelters in Mozambique. *Disasters*, 28(1), 82–97.

Geertman, S., Stillwell, J. (2004). Planning support systems: an inventory of current practice. *Computers, Environment and Urban Systems*, 28, 291–310.

Goodno, J.B. (2005). Saying no to sabotage. *Planning*, 71(7), 10–15.

Gursky, E. (2004). Schools as shelters: anticipating 21st-century terrorist threats: how schools may be used to shelter and serve communities in times of need. *HPAC Engineering*, 49–53.

Han, L.D., Yuan, F., Urbanik II, T. (2007). What is an effective evacuation operation? *Journal of Urban Planning & Development*, 133(1), 3–8.

Holzheimer, T. (2004). Planning in an era of heightened security: making communities safer places. *Practicing Planner*, 2(1), http://www.planning.org/practicingplanner/member/04spring/feature.htm . Accessed September 21, 2008.

Hopkins, L.D., Nikhil, K., Varkki, G.P. (2005). Representing urban development plans and regulations as data: a planning data model. *Environment and Planning B: Planning and Design*, 32, 597–615.

Ke, M. (1994). Ancient wall in Xian. *Beijing Review*, 37(13), 26–27.

Klosterman, R. (2001). Planning support systems: a new perspective on computer-aided planning. In: R.K. Brail and R.E. Klosterman (Eds), P*lanning support systems: integrating geographic information systems, models, and visualization tools.* (pp. 1–25). Redlands, CA: ESRI Press.

Kongsomsaksakul, S., Yang, C., Chen, A. (2005). Shelter location-allocation model for flood evacuation planning. *Journal of the Eastern Asia Society for Transportation Studies*, 6, 4237–4252.

Krohe Jr., J. (2005). It′s dangerous out there, *Planning*, 71(5), 24–29.

Laefer, D.F., Pradhan, A.R., Koss, A. (2006). GIS-based disaster management systems: a cogent data framework. *Transportation Research Board 85th Annual Meeting Compendium of Papers*.

Light, J. (2004). Urban planning and defense planning, past and future. *Journal of the American Planning Association*, 70(4), 399–410.

Lin, P., Lo, S.M., Huang, H.C., Yuen, K.K. (2008). On the use of multi-stage time-varying quickest time approach for optimization of evacuation planning. *Fire Safety Journal*, 43(4), 282–290.

Liu, H.X., Ban, J.X., Ma, W., Mirchandani, P.B. (2007). Model reference adaptive control framework for real-time traffic management under emergency evacuation. *Journal of Urban Planning & Development*, 133(1), 43–50.

Mól, A.C.A., Jorge, C.A.F., Couto, P.M. (2008). Using a game engine for vr simulations in evacuation planning. *IEEE Computer Graphics & Applications*, 28(3), 6–12.

Patterson, S.A., Apostolakis, G.E. (2007). Identification of critical locations across multiple infrastructures for terrorist actions. *Reliability Engineering and System Safety*, 92, 1183–1203.

Smith, S.D. (2006). Inter-agency collaboration and consequence management: an all-hazard approach to emergency incident response. Website: http://www.respondersafetyonline.com/500/.Issue/Article/False/17938/.Issue. Accessed 8 August, 2008.

Yazici, M.A., Ozbay, K. (2007). Impact of probabilistic road capacity constraints on the spatial distribution of hurricane evacuation shelter capacities. *Transportation Research Record: Journal of the Transportation Research Board*, 2022, 55–62.

Zepeda, C., Sol, D. (2007). Planning using answer set programming: an initial approach. *Engineering Letters*, 15(2), 240–249.

Zerger, A., Smith, D.I. (2003). Impediments to using GIS for real-time disaster decision support. *Computers, Environment & Urban Systems*, 27(2), 123–141.

Ziliaskopoulos, A.K. (2000). A linear programming model for the single destination system optimum dynamic traffic assignment problem. *Transportation Science*, 34(1), 37–49.

Index